Cape Peninsula
University of Technology

VOLTAGE STABILITY ASSESSMENT AND WIDE AREA PROTECTION/CONTROL USING SYNCHROPHASOR MEASUREMENTS

by

ADEYEMI CHARLES ADEWOLE

Thesis Submitted in fulfilment of the requirements for the degree

Doctor of Engineering: Electrical Engineering

in the Faculty of Engineering

at the Cape Peninsula University of Technology

Supervisor: Prof R. Tzoneva
Co-supervisor: Prof. A. Apostolov

Bellville
May 2016

DECLARATION

I, Adeyemi Charles Adewole, declare that the contents of this dissertation/thesis represent my own unaided work, and that the dissertation/thesis has not previously been submitted for academic examination towards any qualification. Furthermore, it represents my own opinions and not necessarily those of the Cape Peninsula University of Technology.

Signed **Date**

ABSTRACT

Electric power systems are being operated closer to their designed stability limits due to the constraints caused by the continuous increase in system loading, and the lack of new power stations and transmission network infrastructure to support this increase in system loading. This coupled with the practice of long distance bulk power transmission and cascading contingencies, makes system instability and consequently blackouts inevitable. In such scenarios, system instabilities like voltage instability becomes a serious threat to the secure operation of the power system, and voltage collapse (system-wide blackouts) are prone to occur. This is often compounded by the unavailability of real-time system measurements for situational awareness from the existing Supervisory Control and Data Acquisition (SCADA)/Energy Management System (EMS) platforms which are usually based on unsynchronized SCADA measurements with a slow reporting rate of 1 measurement every 2-10 seconds.

This Doctoral thesis proposes non-iterative algorithms and methods of solution based on the IEEE C37.118 synchrophasor measurements from Phasor Measurement Units (PMUs) with a high reporting rate of up to 200 measurements every second (200 fps) for voltage stability assessment and automated wide area Centralised Protection/Control (CPC) against catastrophic voltage instabilities/blackouts in power systems. Extended formulations are proposed for the Optimal Placement of PMUs (OPP) in power systems with respect to voltage stability assessment. The impact of zero injection buses, critical buses, and PMU redundancy is considered in the formulation of the OPP problem solution. The extended formulations made use of Binary Integer programming (BIP) and Modal Participation Factors (MPFs) derived from the eigenvalues of the power flow Jacobian.

Three generator-derived wide area Real-Time Voltage Stability Assessment (RVSA) indices for large interconnected power systems were formulated. The RVSA indices were used for online voltage stability assessment based on accurate and reliable synchrophasor measurements obtained from widely dispersed time-synchronized PMUs. The voltage stability assessment task involves the monitoring of the operating state of the power system, the prediction of the system's margin to voltage collapse, and the identification of the critical areas in the power system. In the event that the transition of the power system from a stable/alert state to an emergency/*in extremis* state is detected, protection and control countermeasures are initiated to restore the system to an acceptable operating state.
Also, the research applies the proposed voltage stability assessment index as one of the inputs to the system protection element for arming/disarming the proposed response-based

centralised System Integrity Protection Schemes (SIPSs) designed to automatically enhance system reliability and prevent voltage collapse.

The first countermeasure designed and implemented is a SIPS algorithm based on the automatic blocking/unblocking of transformer Under-Load Tap Changers (ULTC-SIPS) using synchrophasor measurements, and control signals transmitted using the IEC 61850 Generic Objected Oriented Substation Events (GOOSE) messages. The second SIPS algorithm was designed and implemented as a last resort countermeasure to prevent the transition of the system into an *in extremis*/voltage collapse state through the use of an adaptive Under-Voltage Load Shedding scheme (UVLS-SIPS). The amount of reactive power load to be shed was predicted in real-time using the Least Squares (LS) curve fitting algorithm. A methodology is presented for the calculation of the amount of load to shed using a proposed reactive power mismatch method. Also, the calculated total amount of load to shed is distributed among the Voltage Control Areas (VCAs) in the interconnected power system based on an adaptive weighted summation RVSA (vcaRVSA) index proposed in this thesis. Furthermore, the candidate load buses for load shedding within each respective VCA were ranked and selected using their voltage dip information. In particular, the proposed adaptive UVLS-SIPS method is suitable for application in power systems where the synchronous generators are controlled by governors with a fixed mechanical torque set-point. In this case, the existing UVLS methods based on the load-to-generation real power mismatch will fail since the real power produced by the generators will be constant.

A lab-scale Wide Area Monitoring, Protection, and Control (WAMPAC) 'proof-of-concept' testbed implemented with 'state-of-the-art' industrial-grade equipment comprising of the Real-Time Digital Simulator (RTDS), hardware and software-based PMUs, Phasor Data Concentrators (PDCs), Programmable Logic Controller (PLC), and Protective Intelligent Electronic Devices (PIEDs) was developed in this research. The WAMPAC testbed was used for real-time hardware-in-the-loop simulations with the 10-bus multi-machine test system and the New England 39-bus test system respectively. Performance analyses have been carried out for various system dynamics involving increased loading condition, line contingencies, generator contingencies, generator Over-Excitation Limiters (OXLs) operation, and Under-Load Tap Changers (ULTCs) actions. Experimental results obtained demonstrate the simplicity, efficiency, reliability, and the practicability of the proposed algorithms and methods of solution.

Key words: IEEE C37.118, IEC 61850, phasor measurement units, real-time digital simulation, synchrophasors, substation automation, system integrity protection scheme, under-voltage load shedding, voltage stability, wide area monitoring, protection and control.

ACKNOWLEDGEMENTS

This Doctoral thesis is the outcome of the research carried out at the Centre for Substation Automation and Energy Management Systems (CSAEMS) at the Cape Peninsula University of Technology (CPUT). This would not have been possible without the help and support of a couple of people.

My profound gratitude goes to my Supervisor, Professor R. Tzoneva for her guidance, encouragement, and support over the years. This accomplishment would not have been possible without her. I could not have wished for a better Supervisor.

I would like to thank Dr. A. Apostolov for serving as my Co-Supervisor. His comments, insights, advice, and wealth of experience did go a long way in activating some positive thought process.

Many thanks to my colleagues at CSAEMS for all the interesting discussions we had, and for contributing to a pleasant work environment. I also wish to acknowledge the friendship and support of everyone who stood by me in the course of this journey.

Lastly, but by no means the least, my sincere gratitude goes to the entire members of my immediate family for their boundless love, encouragement, understanding, and support throughout my years of studies. This thesis is dedicated to them.

Gloria in Excelsis Deo!

Adeyemi Charles Adewole
Bellville, May 2016

TABLE OF CONTENTS

LIST OF FIGURES

LIST OF TABLES

Abbreviations	Definition/Explanation
BIP	Binary Integer Programming
BrPF	Branch Participation Factor
CART	Classification and Regression Tree
CCT	Channel Components Transform
CHC	Calinski-Harabasz Criterion
CPF	Continuation Power Flow
CT	Current Transformer
D/A	Digital to Analog
DSA	Dynamic Security Assessment
DT	Decision Tree
EDT	Ensembles of Decision Tree
EGFCR	Effective Generator Field Current Reserve
EGRPR	Effective Generator Reactive Power Reserve
EGSCR	Effective Generator Stator Current Reserve
EMS	Energy Management System
FCR	Field Current Reserve
FE	Frequency Error
FVSI	Fast Voltage Stability Index
GOOSE	Generic Object Oriented Substation Event
GPC	Giga-Processor Card
GPF	Generator Participation Factor
GPS	Global Positioning System
GTAI	Giga Transceiver Analog Input
GTAO	Giga Transceiver Analog Output
GTFPI	Giga Transceiver Front Panel Interface
HIL	Hardware-in-the-Loop
HV	High Voltage
IEC	International Electro-Technical Committee
IED	Intelligent Electronic Device
IEEE	Institute of Electrical and Electronics Engineers
I/O	Input/Output
ISI	Impedance Stability Index
LCPI	Line Collapse Proximity Index
LIM	Local Impedance Matching
LV	Low Voltage
MISO	Midwest Independent System Operator
MPF	Modal Participation Factors
mVSM	minimum Voltage Stability Margin
NASPI	North American Synchrophasor Initiative
NERC	North American Electric Reliability Corporation
OPP	Optimal PMU Placement
OXL	Over-Excitation Limiter
PDC	Phasor Data Concentrator
PLC	Programmable Logic Controller
PMU	Phasor Measurement Unit
POUs	Programme Organisation Units
PTSI	Power Transfer Stability Index
RFE	Rate of Change of Frequency Error
RLS	Recursive Least Square
ROCOF	Rate of Change of Frequency
RPR	Reactive Power Reserve

RPRB	Reactive Power Reserve Basin
RTDS	Real Time Digital Simulator
RTU	Remote Terminal Unit
RVSA	Real-Time Voltage Stability Assessment
SCADA	Supervisory Control and Data Acquisition
SCE	Southern California Edison
SCR	Stator Current Reserve
SEL	Schweitzer Engineering Laboratories
SM	Stability Margin index
SOC	Second of Century
SVD	Singular Value Decomposition
SVIMI	Synchrophasor-Based Voltage Instability Monitoring
SVP	Synchronous Vector Processor
TCP/IP	Transmission Control Protocol/Internet Protocol
TEPCO	Tokyo Electric Power Company
TGRPR	Technical Generator Reactive Power Reserve
TSO	Transmission System Operator
TVE	Total Vector Error
ULTC	Under-Load Tap Changers
ULTC-SIPS	Under-Load Tap Changers-SIPS
UTC	Coordinated Universal Time
UVLS-SIPS	Under-Voltage Load Shedding-SIPS
VCA	Voltage Control Area
VCPI	Voltage Collapse Proximity Index
VIP	Voltage Instability Predictor
VMI	Voltage Margin Indicator
VSI	Voltage Stability Index
VSM	Voltage Stability Margin
VT	Voltage Transformer
WAMPAC	Wide Area Monitoring, Protection and Control
WAMS	Wide Area Measurement System
WECC	Western Electricity Coordinating Council
ZIBs	Zero Injection Buses

Λ	diagonal eigenvalue matrix of $\mathbf{J_R}$
P_{ki}	bus participation factor of bus k for the ith mode
Φ_{ki}	kith element of the right eigenvector matrix of $\mathbf{J_R}$ for the bus k, ith mode
Γ_{ik}	ikth element of the left eigenvector matrix of $\mathbf{J_R}$ for the bus k, ith mode
$\mathbf{J_R}$	reduced Jacobian matrix
$\mathbf{J_{P\theta}}$	Jacobian matrix for the active power sensitivities wrt voltage angles
$\mathbf{J_{PV}}$	Jacobian matrix for the active power sensitivities wrt voltage mag.
$\mathbf{J_{Q\theta}}$	Jacobian matrix for the reactive power sensitivities wrt voltage angles
$\mathbf{J_{QV}}$	Jacobian matrix for the reactive power sensitivities wrt voltage mag.
$\overline{E}_{th}$	Thevenin equivalent voltage
$\overline{Z}_{th}$	Thevenin equivalent impedance
*	complex conjugate
$\overline{Z}_{app}$	apparent load impedance
$CHC(k)$	Calinski-Harabasz criterion
SS_{Bk}	overall variance between the clusters
SS_{Wk}	overall variance within the cluster
N_o	number of observations
Q_{gi0}	reactive power output of the ith generator at the initial operating point
P_{gi0}	real power output of the ith generator at the initial operating point
I_{fdi0}	field current of the ith generator at the initial operating point
$Q^c_{g\max}$	generator maximum reactive power at the point of voltage collapse
$Q^c_{g\max i}$	maximum reactive power of the ith generator at the voltage collapse
P_{gik}	real power of the ith generator at the kth operating time
Q_{gk}	generator reactive power at the current operating time k
Q_{gki}	reactive power of the ith generator at the kth operating point
$I^c_{fd\max}$	generator maximum field current at the point of collapse
$I^c_{fd\max i}$	maximum field current of the ith generator
I_{fdk}	generator field current at the kth operating time
I_{fdik}	field current of the ith generator at the kth operating time
I_{fdm}	generator field current margin from the current operating point
I_{fdmi}	effective generator field current margin on the ith generator
I_{fdki}	field current of the ith generator at the kth operating point
P_{ga}	generator real power computed using stator winding parameters
Q_{ga}	generator reactive power computed using stator winding parameters
$\lvert I_a \rvert$	generator stator current phasor magnitude
Q_{gamax}	maximum generator reactive power using stator winding parameters
P_{gamax}	maximum generator real power using stator winding parameters
$\lvert I_{amax} \rvert$	maximum generator stator current phasor magnitude
$\lvert I_{ak} \rvert$	stator current at the kth operating time phasor magnitude
$\lvert I_{aki} \rvert$	stator current of the ith generator phasor magnitude
P_{gak}	generator real power at the kth operating time
I_{ami}	effective generator stator current margin on the ith generator
$I^c_{a\max i}$	maximum stator current of the ith generator
$RVSA_Q$	computed $RVSA$ index using generator RPR
$RVSA_{Ifd}$	computed $RVSA$ index using generator field current
$RVSA_{Ia}$	computed $RVSA$ index using generator stator current

N	number of areas in the interconnected power system
n_r	total number of generators in the rth RPRB
$vcaRVSA$	weighted summation of the $RVSA$ in the RPRB
$vcaRVSA_{Q,r}$	weighted summation of the $RVSA$ in the RPRB using RPR
$vcaRVSA_{Ifd,r}$	weighted summation of the $RVSA$ in the RPRB using FCR
$vcaRVSA_{Ia,r}$	weighted summation of the $RVSA$ in the RPRB using SCR
w_i	generator weights for the weighted-summation index
w_{ik}	individual generator weight
$RVSA_{Q,rk}$	computed $RVSA_{Qik}$ index using the RPR
ϕ	impurity function for Decision Tree (DT) classifiers
c_i	object class for DT-classifiers
$p(c_i)$	prior probability associated with the ith class C_i of DT-classifiers
$p(c_i \mid t)$	conditional probability associating a given object with DT class C_i
$\Delta I(s,t)$	decrease in impurity for a given split denoted by s for a node t
P_{shed}	minimum amount of load that needs to be shed
ΔQ_{gik}	reactive power mismatch at the kth operating time
Q_{gi0}	synchronous machine MVAr output at an initial steady-state condition
Q_{gik}	synchronous machine MVAr output at the kth operating time.
ΔQ_{gTk}	MVAr deficit from all the synchronous machine in the system
$\lvert V_{gj} \rvert$	terminal voltage phasor magnitude of the ith generator
X_{si}	synchronous reactance of the ith generator
ΔQ_{Lk}	change in the reactive power demand
$\Delta Q_{shed,VCA_{jk}}$	amount of loads to be shed in the jth *VCA*
N_l	load buses where load can be shed
$\Delta Q_{shed,jBp}$	amount of load to shed at the pth load bus $\Delta Q_{shed,jBp}$ within the jth *VCA*
N_{bj}	number of load buses in the jth *VCA*
$W_{j\Delta V_{Bpk}}$	weighted voltage deviation at the pth bus at the operating time k
$\lvert \Delta V_{Bjk} \rvert$	voltage phasor magnitude deviation at the pth bus at the operating time k
$\lvert V_{j0} \rvert$	reference voltage phasor magnitude at an initial steady-state condition
$\lvert V_{jpk} \rvert$	pth load bus voltage phasor magnitude at the kth operating time for the jth *VCA*

CHAPTER ONE
INTRODUCTION

1.1 Introduction

Power systems are continuously being operated in their stressed state. This is as a result of the continuous growth in the load demand without a concomitant growth in the power generation, transmission, and distribution infrastructures respectively. One implication of this is that the system security is reduced and the system might not survive the N-1 criterion used in power system design, planning and operation.

One of the phenomena which can reduce the system security in the power system is voltage instability. Voltage stability is the ability of the power system to maintain an acceptable voltage profile and security before a disturbance, and to regain an acceptable level of voltage profile and security after being subjected to a disturbance (Van Cutsem and Vournas, 1998; Kundur, 1994).

Voltage instabilities usually occur as a result of a sequence of events. A couple of system dynamics have been identified to cause voltage instability. These include the following (Ajjarapu, 2006; Aumuller and Saha, 2003; Schlueter, 1998; Van Cutsem and Vournas, 1998; Kundur, 1994; Taylor, 1994):

- High reactive power consumption at heavy loads.
- Large distance between the generated power and the system load leads to the difficulty in the transmission of reactive power under heavy load condition.
- Lack of coordination between the various control and protective schemes in the systems.
- Occurrence of line contingencies, leading to a decrease in the maximum loadability of the transmission lines.
- Limitation in the amount of reactive power generated due to the action of generator Over-Excitation Limiters (OXL), the operation of the generators at their maximum capability point, or generator contingencies.
- Operation of transformer ULTCs leading to clogging voltage instability.

In (Aumuller and Saha, 2003; Schlueter, 1998), the mechanism of voltage collapse was identified to be mainly as a result of the loss of voltage control and clogging voltage instability. The voltage instability caused by the loss of voltage control is due to the constraints resulting from the exhaustion of the reactive power produced by the reactive power sources in the system (synchronous generators, synchronous

condensers, and shunt capacitors). The loss of voltage control within a Reactive Power Reserve Basin (RPRB), for instance, increases the reactive power losses in the system. These reactive power losses prevent the reactive power supply from reaching the reactive power deficit areas of the Voltage Control Area (VCA) comprising of load buses with similar voltage collapse problem. The transmission and the sub-transmission systems are the most affected.

The other type of voltage instability identified in the literature (Aumuller and Saha, 2003; Schlueter, 1998) is the clogging voltage instability. This is caused by the I^2X series reactive losses, the limitations due to the transformer ULTCs reaching their maximum tap-limit, and the limitations due to the switchable shunt capacitors reaching their maximum susceptance limit respectively. The clogging voltage instability inhibits the reactive power sources from delivering reactive power to the specific VCA experiencing voltage instability by choking off the reactive power flow to the reactive power deficit VCA. The affected areas are usually the distribution and sub-transmission networks. However, it could also affect the transmission network (Aumuller and Saha, 2003; Schlueter, 1998).

Power systems around the world are being operated in their constrained state, and there is the need for improved real-time monitoring and assessment methods. The monitoring and assessment methods should be capable of the following:

- Giving real-time voltage stability-related information and situational awarenesss from a system-wide perspective.
- Identification of the weak and critical areas in the power system.
- Providing information regarding the mechanism of voltage instability occurring under various system dynamic conditions.
- Recommendation of the remedial measures that can be used in the mitigation of voltage instability and voltage collapse.
- Capable of mitigating voltage instability due to the loss of voltage control and that caused by clogging voltage instability irrespective of the time scale of the disturbance (short-term and long-term voltage instabilities) or the level of the disturbance (small disturbance and large disturbance voltage instabilities).

The use of the measurements from the existing Supervisory Control and Data Acquisition (SCADA) systems implemented in various utility companies might fail for real-time voltage stability monitoring and assessment. This is because some of the system dynamics that occur especially during short-term voltage instabilities might not be captured by the SCADA system due to its slow reporting rate of about 1

measurement every 2-10 seconds. Also, SCADA measurements from the various segments of the power system when collected at the control centre might correspond to different time instants because these measurements are not time-synchronized or time-tagged at the point of acquisition.

One way of capturing fast events/system dynamics over a wide area is through the use of synchrophasor measurements from Phasor Measurement Units (PMUs), time-synchronized to the reference time from the Global Positioning System (GPS). These synchrophasor measurements have faster reporting rates up to 200 measurements per second (200 fps) for a 50 Hz system (up to 240 fps for a 60 Hz system), and can be effectively applied to overcome the challenges associated with SCADA measurements.

Although, many synchrophasor-based methods have been proposed in the literature for voltage stability assessment, most of these methods do not make use of actual synchrophasor measurements from PMUs. Rather, assumptions are made that the measurements from time-domain power system simulation packages (DIgSILENT PowerFactory, MATLAB/Simulink, PSCAD, SIMPOW®, DSA-PowerTools) are equivalent to synchrophasor measurements from PMUs. However, synchrophasor measurements are unique and distinguished by the type of estimation algorithms used in their computation, the type of filters, reporting rates, data transfer/communication media, compliance to the IEEE C37.118 standard, and performance requirements for steady-state and dynamic conditions.

Similarly, the countermeasures against voltage instability/voltage collapse should be based on inputs obtained from synchrophasor measurements. These countermeasures would act as wide area-based protection and control schemes designed to timely detect abnormal system-wide conditions and initiate corrective actions to prevent voltage collapse/system-wide blackouts.

This Chapter discusses the awareness of the problem considered in this thesis, the research questions to be answered, and the hypotheses relating to the respective research questions. Also, the research aim and objectives, the research methodology used, and the contribution of the research are presented and discussed in detail.

1.2 Awareness of the Problem

Although, wide area blackouts are infrequent, their after-effects are usually devastating with far reaching socio-economical consequences. Often times, they are the result of randomly occurring series of events emanating from a local area until they cascade and become system-wide.

The existing unit/local protection schemes based on N-1 protection philosophy are not capable of preserving the integrity of large interconnected grids during wide area disturbances. Wide area system protection schemes which are based on N-2, N-3, or N-k protection philosophies, designed to preserve and improved the security of the power system are required for contingencies when the power system is severely constrained (stressed) by wide area disturbances, and is transitioning towards instability or cascading blackouts.

The depletion of the Reactive Power Reserves (RPRs) in the system directly impacts the voltage stability margin of the system (Leonardi and Ajjarapu, 2013; Ajjarapu, 2006; Van Cutsen and Vournas, 1998; Taylor, 1992). There are many contributing factors with respect to voltage instability. These include the type of load, reactive power sources, load tap-changers, limitation in generation due to OXL operation, and power transfer capability of transmission systems. Most of these factors have a significant effect on the reactive power produced, transmitted, and consumed by the system.

There have been several studies focused on methods to accurately predict system conditions relating to voltage stability and control actions to avoid voltage collapse. However, most of these methods are computationally intensive and the online real-time practical implementation is often difficult. Also, the type of measurements used is usually local measurements or non-synchronized measurements from SCADA systems. Thus, there is the need for research aimed at the development of real-time accurate algorithms and methods for system stability monitoring and countermeasures against system instability using high-speed synchrophasor measurements from PMUs.

It is required that in the course of analysing the voltage instability problem, essential factors that contribute to voltage instability be identified and investigated. Also, the physical nature of the resulting instability, the size of the disturbance, and time span should be considered. Through this, the appropriate monitoring/prediction index and methods for improving the stability of the system can be formulated.

Investigations on the voltage collapse problem usually comprise of the determination of the system's proximity to voltage instability and the mechanism of the voltage instability (Kundur, 1994). The proximity to voltage instability determines the current operating state of the power system and estimates the distance to voltage instability by means of physical quantities. The second aspect examines the reason and the contributing factors, the voltage weak/critical areas, and the factors causing/leading to the voltage collapse.

The mechanism of voltage instability provides information useful in the identification of the operating strategies which could be used to prevent voltage instability/voltage collapse. Some countermeasures against voltage instability include the switching of shunt capacitors, blocking of tap-changing transformers, dispatching of generations, rescheduling of generators, secondary voltage regulations, and load shedding.

1.3 Problem Statement

As power systems continue to be operated beyond their design specifications, voltage instability is inevitable. When voltage instability is left unchecked or not timely attended to, it eventually degenerates and leads to voltage collapse or blackouts in a significant part of the system.

Thus, there is the need for fast, accurate, online voltage stability assessment, protection and control methods in order to mitigate voltage instability. This research proposes, develops, and implements algorithms and methods of solution for online real-time voltage stability assessment and wide area protection/control in power systems. The research contributes to new areas pertaining to wide area monitoring, protection, and control using time-tagged synchrophasor measurements from widely dispersed PMUs.

Real-Time Voltage Stability Assessment (RVSA) indices derived from the Reactive Power Reserve (RPR) margin of synchronous machines are applied and implemented in a centralised Programmable Logic Controller (PLC) for real-time monitoring, assessment, and prediction of the system operating state. Also, automated wide area centralised protection and control schemes are applied as countermeasures. These algorithms are executed as Programme Organisation Units (POUs) in the PLC. The RVSA indices developed are applied as one of the inputs to the system protection element to arm the response-based centralised System Integrity Protection Schemes (SIPSs) developed as countermeasures against voltage instability/voltage collapse.

1.4 Research Aim and Objectives

1.4.1 Aim

The aim of this research is the design, development, and implementation of algorithms and methods of solution for synchrophasor-based wide area voltage stability assessment, and Systems Integrity Protection Schemes (SIPSs) using transformer tap-changer control and undervoltage load shedding.

1.4.2 Objectives

The main objective of this research is the development of algorithms and methods for real-time voltage stability assessment and response-based centralised SIPSs using IEEE C37.118 synchrophasor measurements, and control signals based on IEC 61850-8-1 messages.

The objectives of this research are further sub-divided into theoretical derivations and practical implementation respectively:

1.4.2.1 Objectives: Theoretical Analysis

- To conduct literature review on the existing methodologies for voltage stability assessment and wide area protection/control.
- To review the industry's standards on synchrophasor measurements.
- To formulate an Optimal Placement of Phasor Measurement Units (OPP) problem using the critical bus information computed from the eigenvalues and eigenvectors of the Jacobian matrix of the power system's load flow, and the impact of zero injection buses.
- To implement a synchrophasor-based voltage stability assessment method through indices derived from synchronous machine parameters. The assessment includes the prediction of the operating state of the power system, the prediction of the power system's proximity to voltage instability, and the critical/weak areas (mechanism) of the instability.
- To formulate an adaptive weighted-summation approach for voltage stability assessment in large interconnected power systems with multiple coherent synchronous machines within a local area.
- To design a transformer tap changer control SIPS method based on synchrophasor measurements and control signals using IEC 61850-8-1 Generic Object Oriented Substation Event (GOOSE) messages.
- To formulate and design a non-threshold adaptive Under-Voltage Load Shedding (UVLS-SIPS) algorithm and method based on the reactive power mismatch at the reactive power sources. The reactive power mismatch is

applied in the prediction of the amount of load to shed in real-time using the Least Squares (LS) algorithm.

1.4.2.2 Objectives: Practical Real-Time Implementation

- Modelling of two study networks in RSCAD software.
- Real-time Hardware-In-The-Loop (HIL) simulations.
- Configuration of hardware-based and software-based Phasor Measurement Units (PMUs), Phasor Data Concentrator Units (PDC), and their integration for real-time computation.
- Development of a data acquisition method for parameter and simulation results exchange between the Real Time Digital Simulator® (RTDS) and the computation platform.
- Implementation of the proposed methods and algorithms for real-time voltage stability assessment using external hardware interfaced to the RTDS®.
- Implementation of the proposed methods and algorithms for wide area protection/control using external hardware interfaced to the RTDS®.
- Real-time lab-scale implementation and integration of a synchrophasor-based wide area monitoring, protection, and control scheme using the RTDS®. Real-time synchrophasor measurements from PMUs are to be used in capturing the state of the system and the various system dynamics like the increase in system loading, topology changes, contingencies, transformer Under-Load Tap Changer (ULTC) action, and the operation of the generator Over-Excitation Limiters (OXLs).

1.5 Research Questions

The research questions arising from the above stated objectives include the following:

- **Question 1:** What are the best real-time indicators of the proximity of a power system to voltage instability and voltage collapse points?
- **Question 2:** Would reactive power/reactive power reserve provide good indication of voltage instability using synchrophasor measurements?
- **Question 3:** What are the effects of different load models on the proposed synchrophasor-based voltage stability index?
- **Question 4:** How accurate or effective are synchrophasor measurements when applied for wide area protection and control?
- **Question 5:** Can an adaptive undervoltage load shedding scheme based on synchrophasor measurements be coordinated to provide better power system security?

1.6 Hypotheses

- **Hypothesis 1:** The state of the system can be evaluated using synchrophasor measurements from widely dispersed PMUs.
- **Hypothesis 2:** The voltage stability assessment indices from the field currents and stator currents of synchronous generators can successfully be used to replace the existing index derived from the reactive power reserve.
- **Hypothesis 3:** The predictive capability of the proposed RVSA indices could accurately reflect the system state and condition irrespective of the load types.
- **Hypothesis 4:** Power system control and protection actions need to be executed in a timely manner. The use of real-time synchrophasors from PMUs would allow high-speed measurement and control functions to be applied in the mitigation of voltage instability/voltage collapse.
- **Hypothesis 5:** The proposed RVSA indices allow for the real-time determination of the amount of load to shed in the interconnected system and per voltage control area.

1.7 Delimitation of Research

1.7.1 Within Scope

- Optimal location of Phasor Measurement Units (PMUs).
- Derivation of RVSA indices from synchronous machine parameters for wide area voltage stability assessment.
- Comparison of the performance of the derived wide area RVSA indices.
- Design and implementation of System Integrity Protection Schemes (SIPSs) for mitigating voltage instability/voltage collapse.
- Design, implementation, and integration of the proposed algorithms and methods using a real-time Hardware-in-the-Loop (HIL) platform.

1.7.2 Beyond Scope

- State estimation using synchrophasor measurements is regarded as out of the scope of this research.
- Development of a wide area visualization tool using Geographic Information System (GIS) or contour maps would not be covered in the research.
- The research does not include the impact of reactive power sources like switchable shunt capacitors, series capacitors, and Flexible Alternating Current Transmission System (FACTS) devices.
- Other power system stability issues like rotor angle stability and frequency stability are regarded as beyond the scope of this research.

- Post event analysis and bad data detection on the synchrophasor measurements are considered as out of the scope of this research.

1.8 Motivation for the Research Project

Power systems are being operated closer to their security limits and the need for long distance power transfer has increased significantly. This is aggravated by environmental and economical constraints restricting the expansion of the existing transmission networks and the building of new power stations. These power system infrastructures continue to be operated beyond their designed capability, thereby leading to contingencies and system instability. Voltage instability is a major threat to grid reliability and has resulted to a couple of blackouts around the world (Van Cutsem and Vournas, 2008; Kosterev *et al.,* 1999; Taylor and Erickson, 1997; Taylor, 1994). Information on the performance of the system and the system's response to contingencies can be obtained through voltage stability monitoring and assessment.

The need for real-time measurements for system monitoring and situational awareness was emphasized in (NERC, 2004) on the August 14, 2003 North America blackout. In pursuance of this, the North America Synchrophasor Project Initiative (NASPI) was established. Consequently, several utilities in North America set out their roadmaps for the adoption of synchrophasor-based applications. Figures 1.1-1.2 show the direction of the research being carried out in the industry for various synchrophasor-based applications (MISO, 2010; SCE, 2010).

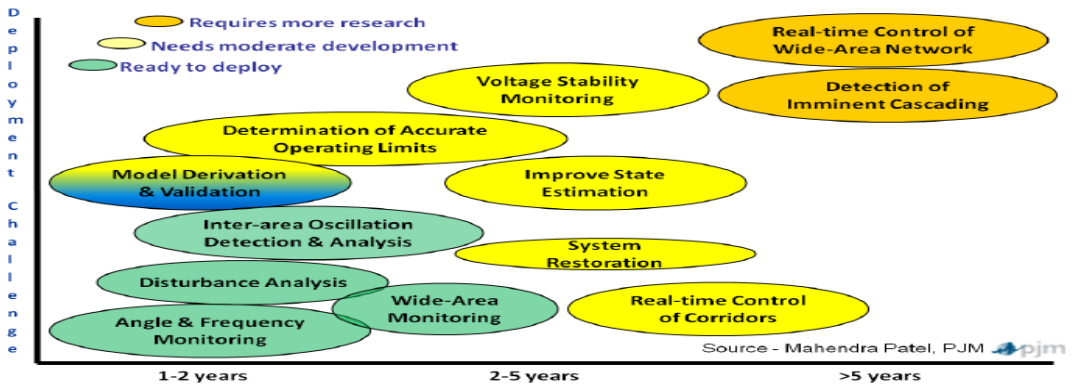

Figure 1.1: **Midwest ISO synchrophasor deployment project (MISO, 2010)**

From Figures 1.1-1.2, it can be seen that most of the research efforts at the moment are for addressing mainly oscillation detection, rotor angle stability and frequency stability respectively. Voltage stability assessment and real-time protection/control applications have a delivery date beyond 2017. From the foregoing, it is clear that the methods and algorithms proposed in this thesis are way ahead of the forecasted delivery dates for similar research activities around the world.

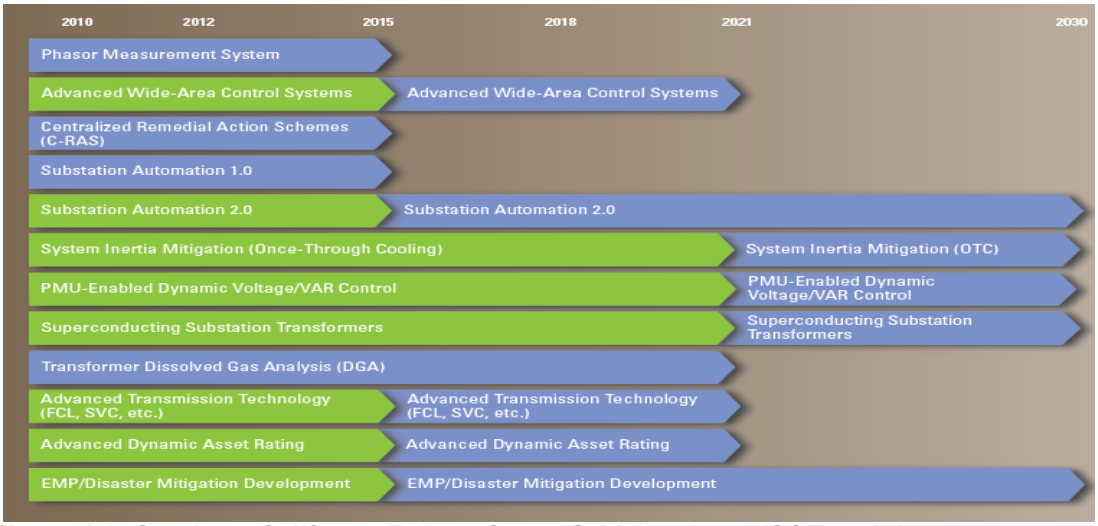

Figure 1.2: Southern California Edison Smart Grid Roadmap (SCE, 2010)

1.9 Assumptions

The following are assumed in the course of the research relating to this thesis:

- For the proposed generator-derived RVSA indices, the only requirement needed is the siting of PMUs at the generator buses in the system.
- The measurements obtained from the PMUs are without any bad data.
- Reactive power compensation from shunt capacitors and FACTS devices are assumed to have been applied prior to the arming of the proposed SIPS.
- For practical systems, it is assumed that the stator currents can be obtained from the generator Current Transformers (CTs), while the field currents can be obtained using Hall effect current sensors which can be non-intrusively mounted at the excitation system either during the manufacturing stage (for new generators) or retro-fitted in existing generators.
- The dependability and security of the Decision Tree (DT) classifier proposed for predicting the system operating state will mainly depend on the training method used, the operating scenarios considered in the generation of the training dataset, and the periodic update using new cases. The availability of an online updating system for retraining the DT-classifier is assumed.

1.10 Contributions of the Research Project

The main contributions of this research are given below:

- The review of methodologies for voltage stability assessment, wide area monitoring, protection and control.
- The optimal placement of PMUs in power systems for complete system observability based on critical buses derived from modal participation factors, zero injection buses, and binary integer programming.
- The derivation of Wide Area Real-Time Voltage Stability Assessment (RVSA) indices for the prediction of the system operating state and the quantification of the system's margin to voltage instability from the current operating point.

- The development of methods and algorithms for real-time wide area voltage stability assessment based on synchrophasor measurements.
- The design and development of a System Integrity Protection Scheme (SIPS) for transformer tap-changer control (blocking/unblocking) using synchrophasor measurements and control signals based on IEC 61850 GOOSE messages.
- The design and development of an adaptive wide area undervoltage load shedding SIPS for large interconnected power system.
- The integration and implementation of a wide area voltage stability assessment, protection/control lab-scale testbed for hardware-in-the-loop simulation with the RTDS® and industrial-grade equipment.

The developmental stages involved in the implementation of the above-mentioned research contributions are as shown in Figure 1.3.

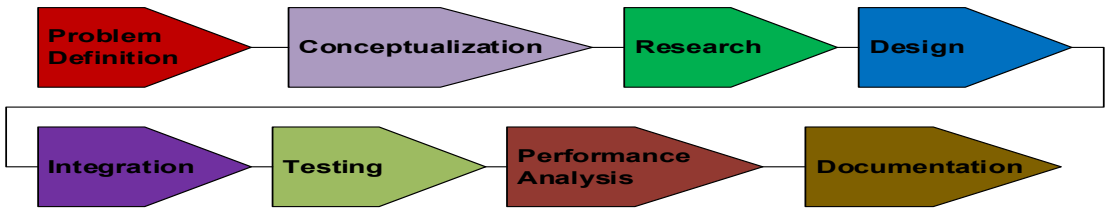

Figure 1.3: **Block diagram of the developmental stages of the proposed algorithms**

The first stage of the developmental process required in the design and implementation of the proposed voltage stability assessment and wide area protection/control algorithms and methods of solution is the definition of the problem and the hypothesized solution. The conceptualization of the ideas in the proposed method involves the formulation of the various concepts and phases of the proposed methods and algorithms. The research stage has to do with the investigation of the various existing methodologies and platforms available with respect to the subject-matter. Also, suitable techniques and possible modifications/improvements are identified.

The design and development of the various algorithms are implemented after the research study. This involves the design, modifications, and implementation of the software/hardware components intended to improve the existing methods. Afterwards, both components are integrated to form a complete package. The testing stage involves the evaluation of the individual algorithms and the testing of the complete method. The performance analysis of the method is carried out after the testing stage. Lastly, related documentation on the proposed algorithms and methods is prepared.

1.11 Outline of the Thesis

This thesis is made up of nine chapters. Chapter One presents the introduction to the doctoral thesis, the awareness of the problem, research problem, research questions arising, and hypotheses. Also, the research aim and objectives, the scope of the research, the assumptions made in the course of the research, and the contributions of the research are described therein.

Chapter Two provides a general overview of power system stability with emphasis on voltage stability in power systems. Also, the causes of voltage instability, voltage stability incidents around the world, and the various classification of the voltage instability problem are presented. Furthermore, an extensive review of previous work done in the area of voltage stability assessment is carried out for a span of 35 years from 1980-2015. The Chapter classified voltage stability assessment into three methodologies. These are the methodology based on load flow calculations, the methodology based on local measurements, and the methodology based on wide area measurements respectively.

Chapter Three introduces and reviews System Integrity Protection Schemes (SIPSs), the various SIPSs classification, the functional elements, and the implementation of SIPSs in power systems. Similar to the process followed in Chapter Two, a thorough literature review on wide area protection and control using SIPSs is carried out for a span of 35 years from 1980-2015 for transformer tap-changer control, and for under-voltage load shedding. Industrial use cases are further presented for the latter.

Chapter Four presents the proposed methods and algorithms for voltage stability assessment using synchrophasor measurements from PMUs. Three types of generator-derived indices were formulated. The proposed indices were further extended for wide area application comprising of various voltage control areas. This also included the derivation of an adaptive weighting factor for calculating the contribution of the individual generators to the reactive power support of their respective voltage control areas.

Chapter Five describes the implementation of the proposed methods and algorithms using a Wide Area Monitoring, Protection, and Control (WAMPAC) 'proof-of-concept' testbed. The developed testbed comprising of industrial-grade equipment is set up at the Centre for Substation Automation and Energy Management Systems (CSAEMS) laboratory, Cape Peninsula University of Technology, for real-time hardware-in-the-loop implementation with the RTDS®. Performance testing and validation of the proposed algorithms and methods are carried out using benchmark models of typical power system networks modelled in the RSCAD software, and by real-time hardware-in-the-loop simulations of several operating scenarios. The aim of the extensive

scenarios is to cover all possible operating conditions that are likely to occur in a typical power system network experiencing voltage instability.

Chapter Six presents the results obtained for the proposed voltage stability assessment methods and algorithms. These include the results for the generator and load bus clustering, and the proposed voltage stability assessment indices. Machine learning-based classification and prediction for real-time voltage stability assessment are discussed. Also, the procedure for the generation of the dataset for the training and testing of the decision trees/ensembles of decision trees is given. Furthermore, the results for the training and testing of the decision trees and ensembles of decision trees are elucidated.

Chapter Seven provides details on the implementation of the proposed real-time voltage stability assessment method, and the methods and algorithms for the System Integrity Protection Schemes (SIPSs). Two SIPSs algorithms based on transformer tap changer control and under-voltage load shedding are considered. The algorithms are designed to be adaptive and are based on synchrophasor measurements from actual PMUs. In particular, the formulation for the under-voltage load shedding covers the calculation of the amount of load to shed and the distribution of the amount of load to shed in a large interconnected power system. Also, a least squares fitting algorithm is proposed for the real-time calculation of the amount of load to shed.

Chapter Eight presents the investigation carried out on the structure of the synchrophasor measurements obtained from actual PMU devices, and their comparison with the specification provided in the IEEE C37.118 standard. Also, the impact of various communication conditions on the measurements is investigated.

Chapter Nine highlights the conclusions drawn from the research, the deliverables of the research, the publications emanating from this research, and the direction for future work. The references and the appendices are presented immediately after.

1.12 Chapter Summary

This Chapter presented the background to this research work, the research aim and objectives, research questions arising from these, hypotheses, and the delimitation of the research. Also, the motivation behind the research, the assumptions made, and the contribution of the research were discussed.

Chapter Two gives a comprehensive review of previous work done in the areas relating to voltage stability assessment. Research work from reputable journal publications/conferences are presented and discussed. The literature review carried out spanned a period of 35 years covering publications from 1980-to-2015.

CHAPTER TWO
VOLTAGE STABILITY ASSESSMENT IN POWER SYSTEMS

2.1 Introduction

Power systems around the world are continuously being operated beyond their design limits. This may be attributed to the increase in system loading without a concomitant increase in generation and transmission capacities, thereby resulting in the operation of the power systems in their stressed states. The operation of a power system in its stressed/weakened state leaves the system vulnerable and unable to fulfill the N-1 criterion required for secure power system operation. The occurrence of a system disturbance during such operating conditions would certainly drive the system to an alert/emergency state where instabilities and system collapse are inevitable.

A study of the majority of blackout incidences around the world has shown that blackouts occur as a result of cascading actions triggered by a single or multiple events such as increased system loading, transmission line faults, generator outages, and operation of protection/control devices. In the mitigation of voltage instability and blackouts, there is the need to have in place efficient monitoring and assessment tools capable of giving real-time situational awareness of the system operating state at any given instant.

In order to achieve this, synchrophasor measurements from Phasor Measurement Units have been recommended to be best suited for this as reported in (NERC, 2004) on the 2003 North American blackout. However, very few publications actually exist on the use of synchrophasor measurements from actual PMUs in the area of real-time voltage stability assessment.

This Chapter presents an overview of power system stability and power system operating states. In particular, voltage stability in power system is further discussed. Also, the causes of voltage instability, voltage stability incidents around the world, and the various classification of voltage instability are presented. Furthermore, a literature survey spanning 35 years was carried out. In addition, the theoretical background of some commonly used voltage stability assessment methods was evaluated and presented alongside an extensive review of the literature relating to voltage stability assessment.

2.2 Power System Stability

The operating state of a power system can be categorised into five states (Kundur, 1994; Fink and Carlsen, 1978). These include: normal, alert, emergency, *in extremis*, and restorative states. Figure 2.1 (Kundur, 1994) shows the interconnection and the transition between these various operating states.

An electric power system is said to be in the normal operating state when generation is adequate for supplying the load demand, and no equipment is being overloaded. In this operating state, all the power system quantities are within their technical nominal values, and the system is able to withstand an equipment outage (contingency). This is referred to as the fulfilment of the N-1 criterion.

The system proceeds to the alert state if the security level drops below a certain limit or if a contingency occurs. In this state, a further increase in system loading or another contingency may threaten the secure operation of the power system and remedial actions must be implemented to restore the system to its normal (acceptable) operating state. If the disturbance is sustained, then the system enters the emergency state. The emergency state is characterized by low voltages and equipment overload. A power system may proceed to the emergency operating state directly from the normal operating state following severe contingencies like multiple faults. However, the system would still be intact, and emergency remedial actions could be initiated in order to restore the system back to the alert operating state and then to normal operating conditions.

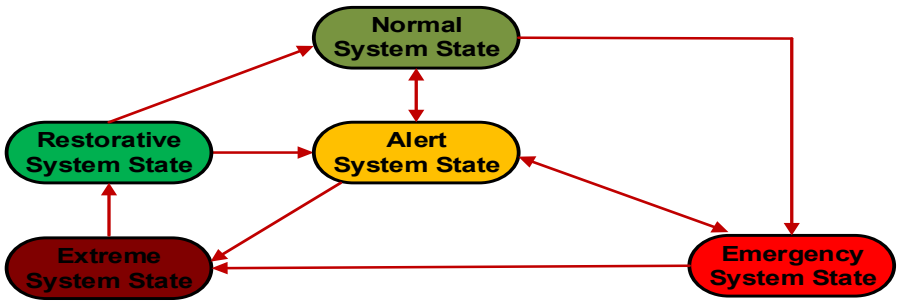

Figure 2.1: **Power system operating states (adapted from Kundur, 1994)**

Power systems can degenerate into the *in extremis* state from the emergency state if no corrective actions were implemented or if the corrective action implemented was ineffective. The result of which is cascading outages and possibly blackout. The next state after the system collapse is the restorative state in which remedial actions are implemented to reconnect a lost load or system, and transfer the system to either the alert state or to the normal state (Kundur, 1994; Fink and Carlsen, 1978).

Power system stability is the ability of an electric power system to operate under normal operating conditions with acceptable system variables, and regain a state of operating equilibrium after a system disturbance with most of the system variables being within acceptable limits such that the entire power system continues to remain in equilibrium (Kundur *et al*., 2004; Kundur, 1994).

Although, power system instability is a single subject, it would be impractical to consider it as such when studying it. This is because it may take many forms and can be affected by various factors, such as the system variables affected and the power system conditions leading to the instability. The various types of instability in power systems can be broadly classified into rotor-angle instability (transient and small signal), frequency instability, and voltage instability. The first two phenomena are mainly related to active power control, while voltage stability is influenced by the reactive power control in the power system. The abovementioned classification is illustrated in Figure 2.2 (Kundur *et al*., 2004).

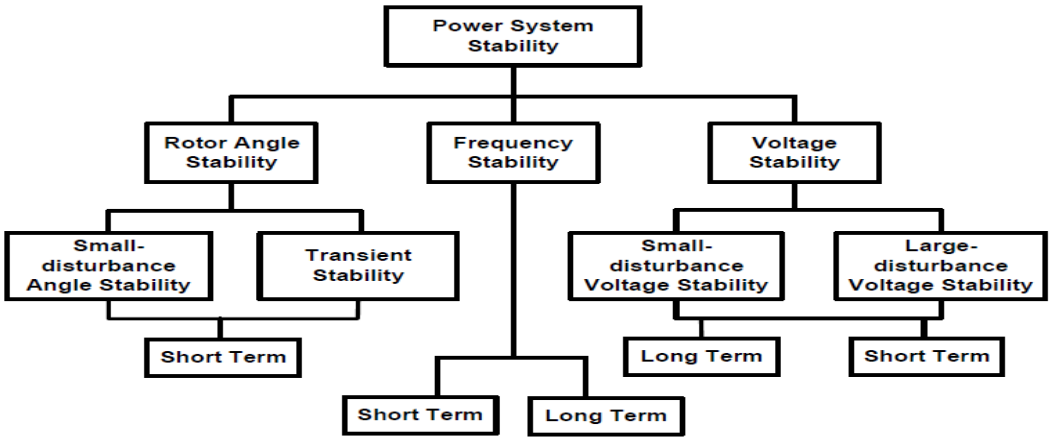

Figure 2.2: Classification of power system stability (Kundur *et al*., 2004)

2.2.1 Rotor Angle Stability

Rotor angle stability is directly related to the rotor angles of the synchronous machines in a power system. It is the ability of these synchronous machines to remain in synchronism following a disturbance. The time frame of the rotor angle stability phenomenon is a few seconds (Cutsem and Vournas, 1999; Kundur, 1994).

From Figure 2.2, it can be seen that rotor-angle stability is further sub-divided into small-signal (small-disturbance) angle stability and transient stability. Small-signal rotor angle stability refers to the ability of a power system to remain in synchronism during small disturbances caused by insufficient damping of oscillations, insufficient

synchronizing torque, changes in scheduled generation, or small increase in the system load.

Transient stability is defined as the ability of a power system to remain in synchronism during a severe disturbance. The post-disturbance stability of the power system would depend on the initial operating state of the system as well as the severity/level of the disturbance. The period of interest for transient stability analysis is usually about 3 to 5 seconds after the disturbance (Kundur, 1994).

2.2.2 Frequency Stability

Frequency stability is related to long-term rotor angle instability and it is the ability of a power system to sustain a steady system frequency after a severe system disturbance with a significant imbalance between generation and load.

The period of interest for analysis of the frequency ranges from fraction of seconds to several minutes (Kundur, 1994). For a short-term phenomenon lasting a time span of seconds, the devices used as countermeasures are generator control/protection and under-frequency load shedding. For long-term frequency stability, the devices involve Automatic Generator Control (AGC). The time span ranges from a couple of seconds to several minutes.

2.2.3 Voltage Stability

Voltage stability is the ability of the various segments of a power system to maintain acceptable voltage profile during normal system operating conditions and after being subjected to a disturbance.

Generally, this could be as a result of the inability of the combined generation and transmission capacities to meet with the system demand at the load centres. This causes the power system to proceed into a state of voltage instability when a disturbance results in a progressive and uncontrollable voltage decline in a major part of the system.

2.3 Voltage Stability Assessment in Power Systems

Several definitions for voltage stability, voltage instability, and voltage collapse have been proposed in (Leonardi and Ajjarapu, 2013; Van Cutsem and Vournas, 2008; Ajjarapu, 2006; Kundur, 1994; Taylor, 1994). A power system is voltage stable if following a disturbance, the load bus voltages are close to the pre-disturbance values in all the segments of the power system. This implies that there is an existence of a

considerable margin from an operating point to the point of voltage collapse (or the maximum loadability point) following credible contingencies.

In contrast, voltage instability is the lack of voltage stability, and it is manifested as a progressive and uncontrollable drop in voltage in a major part of the system after a power system disturbance. This could be as a result of the increase in the load demand, equipment outage(s), or loss of voltage control especially in a stressed power system. A power system which is subjected to a voltage stability related disturbance undergoes voltage collapse if the post-disturbance parameters are below acceptable limits.

Voltage stability assessment involves the determination of the voltage stability level of a power system at the current operating point and for the anticipated system operating conditions. This involves the analysis of the system's proximity to voltage collapse, the driving force(s) behind the voltage instability/collapse, why it occurred, where the voltage critical (weak) areas are, and the effective countermeasures to implement in order to restore the system to an acceptable operating state.

2.3.1 Causes of Voltage Instability

The main cause of voltage instability is the inability of the power system to meet the reactive power demand from the various components in the system. This could be as a result of the electrical distance between the generation and load centres, due to the lack of investments in generation/transmission infrastructures close to the load centres, or as a result of operating the power system closer to it stability limits (Ajjarapu, 2006; Kundur, 1994; Taylor, 1994;). Table 2.1 describes the classification of voltage instability according to the time-scale of operation and the dominant system components driving these instabilities.

Table 2.1: Voltage instability based on time-scale

Time-scale	System component	Type of load
Instantaneous	Network	Static loads
Short-term	Generators, capacitors/reactors switching, Flexible Alternating Current Transmission System (FACTS), Static VAR Compensator (SVC).	Induction motors
Long-term	ULTC, Over-Excitation Limiter (OXL)	Thermostatically controlled loads

The main factors that influence voltage stability other than the strength of the transmission network and the maximum loadability limit are the generator reactive power/voltage control limits, the load characteristics, the characteristics of the

reactive power compensation devices, and the action of the control devices such as transformer Under Load Tap-Changers (ULTCs) and generator Over-Excitation Limiters (OXLs).

2.3.1.1 Impact of Loads on Voltage Stability

The operation of a power system within its operating capacity at acceptable margins depends on the ability of the system to continuously match the load demand by the appropriate rescheduling of the generator output. However, system loading depends on the load class, load mix, and load characteristics. These vary and are highly stochastic. System loading is also influenced by the time of the day (base or peak load), season (summer or winter), and the prevailing weather conditions (hot or cold).

Generally, power system loads are modelled using static and dynamic load models. Static load models are expressed using algebraic functions of the bus voltage and system frequency. For voltage stability analysis, the frequency dependency characteristic is negligible (Cutsem and Vournas, 1998; Kundur, 1994; Taylor, 1994).

Thus, the characteristic of a load with respect to its voltage dependency can be given by the exponential load model as follows (Kundur, 1994; Taylor, 1994):

$$P = P_0 \left(\frac{V}{V_0} \right)^{\alpha} \tag{2.1}$$

$$Q = Q_0 \left(\frac{V}{V_0} \right)^{\beta} \tag{2.2}$$

where P and Q are the real and reactive powers of the load after a time t when the load bus voltage is V. P_0, Q_0, and V_0 are the real power, reactive power, and load bus voltage at the initial operating state respectively.

The α and β coefficients given in Equations (2.1)-(2.2) represent the particular characteristics of the load with respect to its real and reactive powers. For constant power, constant current, and constant impedance loads, $\alpha = \beta = 0, 1, 2$, respectively (Kundur, 1994).

This implies that the power demanded by constant power loads remain constant irrespective of the changes in bus voltages. Similarly, the power demanded by constant current loads is linearly proportional to the bus voltages, while the power demanded by constant impedance loads is proportional to the square of the bus voltages.

Aside exponential load models, the voltage dependency of loads can be represented using the polynomial load models or ZIP models. These are made up of three components comprising of constant impedance (Z), constant current (I), and constant power (P).

The polynomial load is given as (Kundur, 1994; Taylor, 1994):

$$P = P_0\left[p_1\left(\frac{V}{V_0}\right)^2 + p_2\left(\frac{V}{V_0}\right) + p_3\right] \tag{2.3}$$

$$Q = Q_0\left[q_1\left(\frac{V}{V_0}\right)^2 + q_2\left(\frac{V}{V_0}\right) + q_3\right] \tag{2.4}$$

The coefficient of these components must satisfy the following conditions:

$$p_1 + p_2 + p_3 = 1 \tag{2.5}$$

$$q_1 + q_2 + q_3 = 1 \tag{2.6}$$

The proportions of each of the ZIP components are given by the p *and* q coefficients (p_1-p_3 and q_1-q_3) in Equations (2-3)-(2.4) respectively.

Unlike static load models, induction motors have dynamic characteristics with shorter time constants. Therefore, it is necessary to model their short-term dynamic behaviour. Induction motor loads are similar to constant power loads, and will continue to demand constant power even as their bus voltages drop as a result of a disturbance. As the voltage decline increases and the reactive power supplied by the system is constrained, the induction motor would stall and draw a high current in the process. This further aggravates the voltage collapse problem.

Also, the impact of thermostatically-controlled loads (water heaters, process heating, space heating/cooling, and refrigeration) can be seen in long-term voltage stability. Typically, thermostatically-controlled loads draw full power until the reference temperature is reached before switching off. They remain off until their temperature drops again below the preset reference temperature. Thermostatically-controlled loads are constant resistance loads, the drawn power are proportional to the square of the bus voltages. This implies that they will operate longer during low-voltage circumstances.

The average power P_{avg} drawn by a thermostatically-controlled load is given by (Kundur, 1994):

$$P_{avg} = \frac{t_{on}}{t_{on} + t_{off}} P_{\max} = \frac{t_{on}}{t_{on} + t_{off}} GV^2 \tag{2.7}$$

where t_{on} and t_{off} represent the duty cycle of the thermostatically-controlled load, P_{max} is the maximum power demanded, G is the conductance of the load, and V is the bus voltage.

Discharge lamps are constant current loads, and the real and reactive powers vary linearly with their bus voltages. Usually, discharge lamps are extinquished when their bus voltages go below a minimum voltage level, and will restart after a few seconds delay when the bus voltage recovers.

2.3.1.2 Impact of System Components on Voltage Stability

System components like transformer ULTCs, generator OXLs, and generator Armature Current Limiters (ACLs) are very important in long-term voltage stability studies. The load restorative effect of a transformer ULTC occurs when the voltage of the regulated (usually Low Voltage (LV)) side of the transformer falls below the reference voltage as a result of a disturbance. The transformer ULTC acts in order to restore this voltage to its reference voltage. This effectively reduces the impedance seen by the system, and makes the load connected to the LV side to appear as a constant power load.

Typically, as the voltage of the LV side rises, the voltage of the unregulated (High Voltage (HV)) side drops as a result of the increase in reactive power demand. Once sufficient time has passed and the reactive power required on the network still exceeds the reactive power generated, the voltage will decline further and could lead to a total voltage collapse.

Generators are usually protected from overheating by OXLs and ACLs. The OXL limits the excitation voltage when the maximum acceptable field current is exceeded. ACLs are used to protect the generator stator windings. These limiters ensure that the capability limits of the generator exciter and stator windings are not exceeded. When they act, they keep the generator output constant at the acceptable maximum limit. This could further exacerbate the voltage instability condition due to the lack of reactive power supply and the consequent loss of voltage control.

A power system network is constrained by its transfer capability indicating the maximum power which the transmission system can carry without failure. The Available Transfer Capability (ATC) will determine if the loads at the load centre will continue to get the much needed reactive power support from the generators located far from the loads without the need for local reactive power compensation. Also, the

operation of the protection equipment can result to the disconnection of major transmission corridors and generators. This results in an increase in transmission losses and the lack of reactive power support, thereby triggering a series of cascading events which inevitably could lead to voltage collapse.

2.3.2 Voltage Stability-Related Incidents

Several voltage stability incidents have been reported in several countries over the past decades. These incidents are usually as a result of cascading events which are at first local, before becoming system-wide.

Some of these incidents are further discussed below in terms of their impact, the pre-event conditions, triggering events, and pre-collapse events.

2.3.2.1 Voltage Instabilities Resulting From Contingencies/Protection Operation

The 1965 blackout in North America occurred on the 9th of November, 1965. It affected the Northeastern states of Connecticut, Massachusetts, New Hampshire, Rhode Island, Vermont, New York, and New Jersey. 20000 MW of load was lost for about 13 hours and over 30 million people were affected. The prevailing weather was mild and the system loading was normal. The blackout was triggered by a faulty setting in an overcurrent relay. A power surge around the generating station in New York caused the operation of an overcurrent relay thereby tripping the main transmission line to Southern Ontario in Canada. This resulted in an overload in the other transmission lines. Four 230 kV transmission lines tripped in quick succession within a couple of minutes (Kundur, 1994).

A description of the blackouts which occurred in the Western Electric Coordinating Council (WECC) on the 2nd of July, 1996 and on the 10th of August, 1996 is found in (Kosterev *et al.,* 1999; Taylor and Erickson, 1997). According to several post-mortem reports, the lack of proper reactive power support and loss of voltage control was the primary cause of the voltage collapse. A tree flashover triggered the voltage collapse experienced on the 2nd of July, 1996, and was aggravated by a relay mis-operation. The 10th August, 1996 instability problem was as a result of inadequate trimming of trees and lack of adequate instructions to dispatchers. The temperature before the collapse was 38°C, and loading was heavy as a result of the increase in load from air conditioners and chillers.

A voltage instability condition was experienced in the Northern part of the Eskom grid in South Africa in 1999 (van der Merwe *et al*., 2005). The incident was triggered by

the operation of the line protection on the 275 kV Witkop-Tabor power line within the network. The protective relays operated correctly, but the auto-reclose function failed. The loss of the line resulted in an overloaded and weakened system. The power transfer requirement of the rest of the network pushed the system beyond its maximum loadability limit (bifurcation point), causing the voltage collapse.

The most recent large-scale voltage stability incident occurred in North America on the 14th August, 2003. A detailed investigation of the event showed that it was caused by a combination of failures, leading to cascading events (NERC, 2004). Chiefly among which was the contact of an overloaded transmission line with vegetation. 5716 MW of load was lost as a result of the shutdown of 508 generators in 265 power stations. The blackout affected the Northeastern United States, Midwestern United States, and Ontario-Canada. A total of 10 million people in Ontario and 4 million people across 8 states in the US were affected.

A voltage instability incident occurred on the 23rd of September, 2003 in Europe and it affected the Southern part of Sweden and Eastern Denmark. Prior to this incident, the Swedish power system was moderately loaded with a total consumption of approximately 15000 MW which is almost half of the maximum yearly consumption (Larrson and Danell, 2006). The consumption in the southern part of Sweden was approximately 3000 MW. Two 400 kV transmission lines and four nuclear units taken out for maintenance caused a double bus fault. This caused a N-3 generator event comprising of the loss of a 1200 MW nuclear unit in south-eastern part of Sweden, and the loss of two 900 MW nuclear unit. This resulted in a voltage instability condition with system separation into islands 97 seconds later (Larrson and Danell, 2006).

2.3.2.2 Voltage Instabilities Resulting From Increased Loading Condition

The voltage collapse incident in Japan occurred on the 23rd of July, 1987 resulting in the loss of most of the 500 kV system of the Tokyo Electric Power Company (TEPCO), as well as the loss of 8000 MW of load with almost three million customers affected for about three hours (Ohno and Imai, 2006). The event was as a result of an increase in demand because of the prevailing summer heat. The 500 kV voltages dropped to 460 kV (0.92 p.u.), and eventually, lines were tripped by the overcurrent protective relays.

Large disturbances involving three-phase faults occurred in Southeastern Florida on the 18th August, 1988 (de Leon and Taylor, 2002). Voltage recovery was slow, taking

about ten seconds. Similarly, a voltage instability incident was reported in Phoenix, Arizona on 29th July, 1995 (de Leon and Taylor, 2002). The prevailing temperature was high at 112°F (44°C), with the system operating in a stressed state as a result of the air conditioning loads. The voltage instability condition was caused by a fault on the 230 kV capacitor bank with delayed clearing. Consequently, five 230 kV transmission lines tripped. After 3 seconds, two 230/69 kV transformers also tripped. This resulted to the stalling of air conditioning motors with a loss of about 2100 MW of load. It took 20 seconds for voltage recovery. High reactive power output from generators at the Palo Verde nuclear plant prevented a total voltage collapse.

A voltage instability incident occurred on the Greek power system network on the 12th of July, 2004 (Savulescu, 2014). In the Greek interconnected system, the main generation is located in the Northern and Western part of the country respectively, while the main consumption is located in the metropolitan area of Athens in the South eastern part of Greece. Voltage instability was triggered by the loss of 300 MW of generation at the Lavrio power station near Athens. This resulted to the loss of about 9160 MW of load, and the system voltages dropped to about 0.9 p.u. Further tripping of generators resulted to the loss of more loads with a voltage collapse and uncontrolled separation of the Greek system occuring.

A system collapse affecting over 620 million people occurred on the Northern and Eastern Indian regional grids on the 30th and 31st of July, 2012. Although, the exact cause of the blackout is unknown, high temperatures, overloading, weak interconnections, and increased system loading as a result of motor loads at the irrigation fields resulted to the tripping of the breakers at the 220 kV and 400 kV transmission lines. This resulted to the cascading failures experienced throughout the grid (Indian Blackout Report, 2012). The zone-3 distance protection relay operation due to load encroachment further aggravated the blackout on the 31st of July, 2012, thereby causing a higher reactive power flow and decline in system voltages. A total of 36000 MW of load was lost on the 30th of July, 2012, while 48000 MW was lost on the 31st of July, 2012. The loads were finally restored on the 1st of August, 2012.

The literature on voltage stability is quite extensive. Further information on power system stability and voltage stability may be obtained from (Ajjarapu, 2006; Taylor, 1998; Van Cutsem *et al*., 1998; Kundur, 1994).

2.3.3 Classification of Voltage Stability

Voltage stability has been discussed in the preceding section, and was defined as the ability of a power system to sustain acceptable voltages at all system buses under normal system operating condition and after being subjected to a disturbance.

Various types of dynamics are associated with the voltage instability problem. The critical ones are equipment contingencies, load dynamics, the generator reactive power limits, and the response of the protection/control devices in the system. Voltage instability often starts in a local network and gradually extends to the whole system.

Voltage instability can be classified based on the scale of disturbance and the time frame as shown in Figure 2.2. Large disturbance voltage stability relates to the ability of a power system to sustain acceptable voltages following large disturbances comprising of system faults, loss of generators, or loss of transmission lines. It is determined by the characteristics of the loads and controls. The period of interest could be from a couple of seconds to tens of minutes.

Small-disturbance voltage stability is the ability of the power system to maintain acceptable voltages when subjected to small perturbations such as increase in system loading. This is typically influenced by the characteristics of the loads, the type of continuous controls, and the discrete controls at a given instant of time. Small disturbance voltage instability lasts for a few seconds (Ajjarapu, 2006; Cutsem and Vournas, 1999; Kundur, 1994).

Short-term voltage stability encompasses the dynamics of fast acting load components. Examples include induction motors, electronically-controlled loads, and HVDC converters. The period of interest is in the order of 0 to 10 seconds.

Long-term voltage stability is influenced by slower acting equipment such as tap-changing transformers, thermostatically-controlled loads, and generator current limiters. The period of interest may extend to several or many minutes (Ajjarapu, 2006; Cutsem and Vournas, 1999; Kundur, 1994).

Section 2.4 presents a review of the various methodologies used in voltage stability assessment. Some methods based on curve analysis, modal analysis, sensitivity analysis, and Thevenin equivalent are discussed. Also, an extensive review of the publications relating to voltage stability was categorized and discussed under three

headings. Namely: (i) load flow calculation-based methodologies; (ii) local measurements-based methodologies; and (iii) wide area measurements-based methodologies.

It should be noted that the last category mentioned above are focused on methods based on synchrophasor measurements from PMUs. Such systems for wide area monitoring, situational awareness, protection, and control are currently the subject of research in the academics and also in the industry.

2.4 Review of Methodologies for Voltage Stability Assessment in Power Systems

2.4.1 Literature Survey

The voltage profile at different locations in a system after a disturbance has generally been used as an indication of voltage instability. For heavily compensated systems, the voltage level might not change much even with an impending voltage collapse. Therefore, voltage magnitude by itself alone is not a good indicator of instability. It is necessary to carry out assessments by means of other scalar magnitudes or indices. The system operator needs indices either in the online or offline modes to determine how close the system is to voltage collapse, and the appropriate control actions to implement as countermeasures to the instability.

Voltage stability analysis generally involves the investigation of the proximity of the power system to voltage instability and the mechanism of the voltage instability/collapse. The proximity to voltage instability determines how close the power system is to its voltage instability point. This can be measured in terms of the load level, the real power flow, and the available reactive power reserve. The mechanism of voltage instability investigates how the instability occurs, the reasons why they occur, and the key factors that caused the instability (Kundur, 1994; Taylor, 1994). Other analyses of the mechanisms of voltage instability are the determination of the critical or voltage weak areas, and the most effective countermeasures for improving the voltage stability of the system (Cutsem and Vournas, 1999; Kundur, 1994; Taylor, 1994).

A literature survey was carried out using Elsevier's 'Engineering Village' database. The Engineering Village database provides a platform for accessing authoritative contents from renowned sources. The survey carried out spanned a period of 35 years (1980-2015).

Generally, the procedure followed in this review was to select, review, and analyze articles seen as representative of the various existing techniques and methods from reputable journals only. However, conference proceedings from renowned authors in this field were also included in the review.

Figure 2.3 shows the analysis per year for published research articles when the search parameters were 'voltage stability assessment'. A total of 1185 articles were reported. These articles comprised of conference proceedings, journal articles, and report reviews. Out of which only 483 (40.8%) articles were journal publications as shown in Table 2.2.

When the search parameters were changed to 'voltage stability assessment using measurements from phasor measurement units', only 27 articles were returned. However, a total of 55 articles were returned when the search parameters were 'voltage stability analysis using measurements from phasor measurement units' as shown in Figure 2.4 and Table 2.3 respectively.

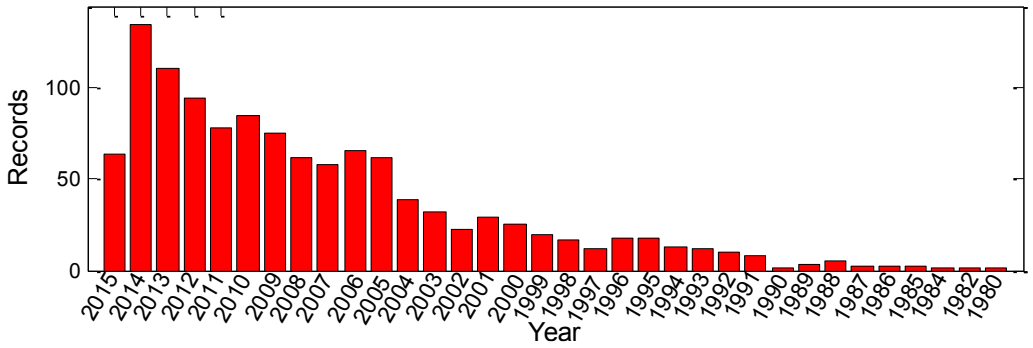

Figure 2.3: **Survey of published articles per year for 'voltage stability assessment' from 1980-2015**

Table 2.2: **Survey of published articles according to document-type for 'voltage stability assessment' from 1980-2015**

Type of Document	Number of Articles
Conference article	594
Journal article	483
Conference proceeding	79
Article in press	22
Report review	5

Table 2.3 shows the analysis per type of document for the published research articles, out of which only 16 (29.1%) articles were journal publications. Although, the search years were from 1980-to-2015, no article was reported for 1980-to-2000. Figures 2.3-2.4 show a rising trend in the subject-matter from the year 2010 as

demonstrated by the increase in the number of the published articles. This demonstrates the increasing interest in this subject.

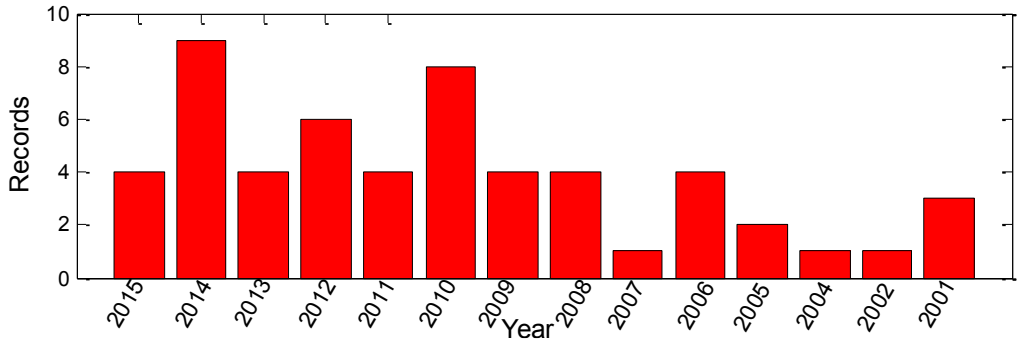

Figure 2.4: **Survey of published articles per year for 'voltage stability assessment using phasor measurement units' from 2001-2015**

Table 2.3: **Survey of published articles according to document-type for 'voltage stability assessment using phasor measurement units' from 2001-2015**

Type of Document	Number of Articles
Conference article	36
Journal article	16
Conference proceeding	1
Article in press	2

2.4.2 Review of Methodologies

Several traditional methods have been presented in the existing literature for voltage stability assessment. Some of these methods are based on the analyses of the mathematical models of the power system (Ajjarapu, 2006; Ajjarapu and Christy, 1992). Others are based on the analysis of the margin to the voltage collapse point using the curve analysis method (Kundur, 1994; Taylor, 1994). Aside these, the eigenvalues of the load flow Jacobian have been applied in the sensitivity analysis of power systems (Ajjarapu, 2006; Kundur, 1994; Ajjarapu and Christy, 1992).

These traditional methods for voltage stability assessment can be broadly classified into (Ajjarapu 2006; WECC, 2006; Cutsem and Vounas, 1998; Barquin *et al*., 1995; Kundur, 1994; Lof *et al*., 1993; Ajjarapu and Christy, 1992):

- Curve analysis methods
- Modal analysis methods
- Sensitivity-based methods
- Thevenin-based methods

These traditional methods for voltage stability assessment are further elucidated below.

2.4.2.1 Curve Analysis Methods

The voltage stability analysis of a power system can be carried out by using P-V and V-Q curves at selected load buses to characterize the capability of the transmission system and the reactive power compensation required at the respective load buses.

The P-V curve is a plot showing the relationship between the active power P and the voltage V at a bus. That is, it captures the voltage response at a particular bus due to load (real power) increase at the bus or at other buses in the power system.
This can be further explained by using the 2-bus system shown in Figure 2.5. The system is made up of a load connected to a voltage source via a transmission line. The P-V curve for this 2-bus system can be generated by increasing the real power demand of the load and running a series of load flow calculation until the load flow calculation fails to converge.

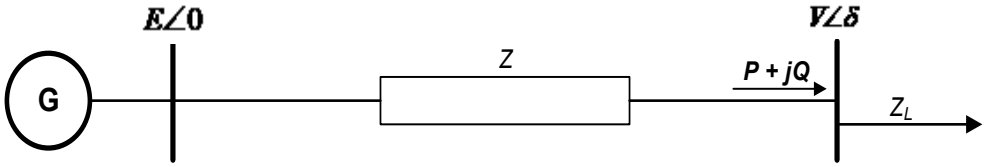

Figure 2.5: Single line diagram of a 2-bus system

The maximum load that can be supplied by the system before it reaches the nose point or voltage collapse point is known as the maximum loadability margin. The P-V curve plotted for the 2-bus system is given in Figure 2.6.

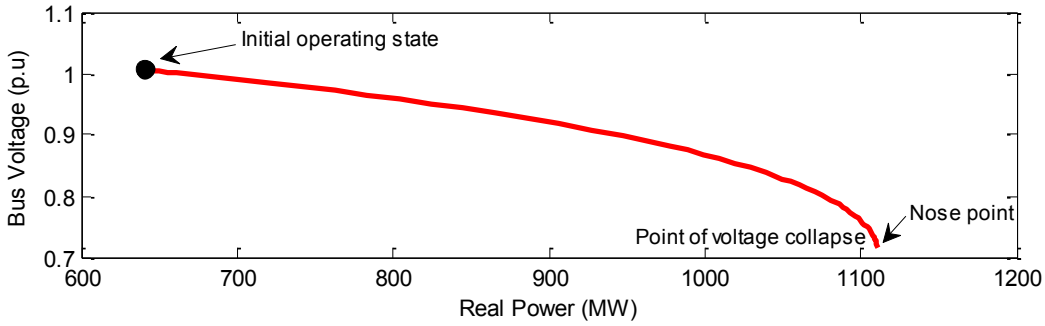

Figure 2.6: P-V curve for a simplified 2-bus system

Similarly, the V-Q curve is a plot showing the relationship between the reactive power support from a fictitious synchronous condenser Q_c with zero real power, and the voltage V at a given bus. The reactive power Q_c produced when the terminal voltage is varied is recorded and plotted against the bus voltage. The V-Q curve shows the amount of reactive power required to achieve a specified voltage level.

One of the information that can be accessed from the V-Q curve is the sensitivity of the loads to the reactive power sources. While varying the reactive power requirements of a bus, the generators that deplete their reactive reserves the most, form the reactive power sources responsible for voltage control at that bus.

Figure 2.7 shows the V-Q curve obtained for the 2-bus system. The right hand side of the curve before the minimum point (bottom point) shows that the system is stable since an increase in the reactive power injection Q is accompanied by an increase in voltage V. The left hand side of the curve is unstable, since an increase in Q represents a decrease in V.

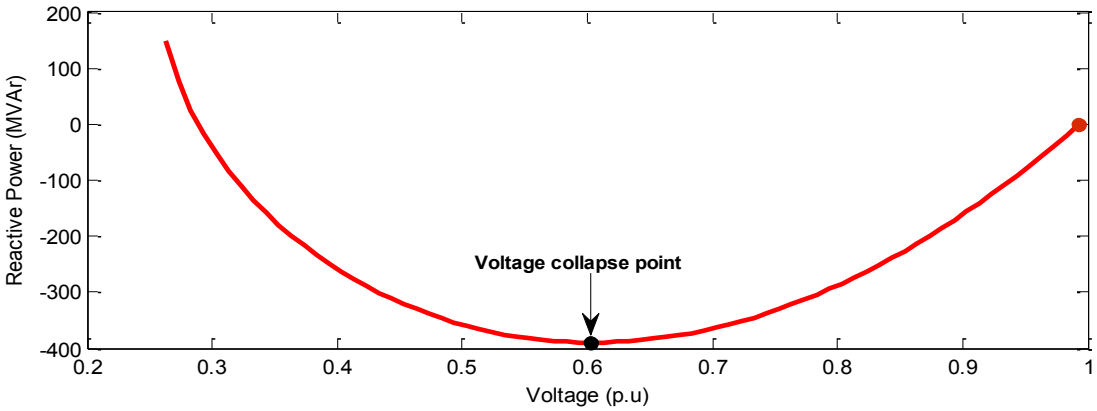

Figure 2.7: V-Q curve for the 2-bus system

The P-V and V-Q curves serve as the main techniques for voltage stability assessment in most utility (WECC, 2006). A system's maximum loadability is usually calculated from the nose point of the P-V or V-Q curves using the worst contingency. A 5% margin is defined for N-1 contingencies, while a 2.5% MW margin is defined for N-2 contingencies. Measurement-based V-Q curve was considered in (Huang *et al.,* 2007). Similar procedure to the load flow V-Q curve was followed, but based on online measurements. The measurement-based V-Q is non-parametric, and the segment of the V-Q curve around an operating point is measured online.

The Continuation Power Flow (CPF) method (Ajjarapu 2006; Ajjarapu and Christy, 1992) can be used to avoid the uncertainties associated with the conventional load flow calculation at the point of voltage collapse by tracing the path of a power system from an initial stable point to the critical point beyond which the system losses its equilibrium or stability. The CPF method uses a continuation method which is a path-following technique for solving a system of nonlinear equations. A predictor-corrector technique is used to trace the power flow solution paths. From a known operating point, a prediction is made towards a more stressed condition by increasing the load parameter λ to approximate the next point. In the corrector step, the solution of the

power system at the predicted parameters is obtained. This corresponds to the closest operating point. This process is repeated until a critical point is reached.

2.4.2.2 Modal Analysis

Other methods aside the curve analysis methods are sensitivity analysis- and modal analysis-based methods using the Jacobian matrix of the power system load flow. The sensitivity analysis method uses the relationship between the change in voltage and the change in reactive power at different buses using the reduced Jacobian matrix (Ajjarapu, 2006; Kundur, 1994). The relationship between these two variables is applied in the determination of the system's status and the mechanism of instability (Ajjarapu, 2006; Kundur, 1994).

Given a linearized steady-state system, the power flow equation is given by (Cutsem and Vounas, 1998; Kundur, 1994):

$$\begin{bmatrix} \mathbf{\Delta P} \\ \mathbf{\Delta Q} \end{bmatrix} = \begin{bmatrix} \mathbf{J_{P\theta}} & \mathbf{J_{PV}} \\ \mathbf{J_{Q\theta}} & \mathbf{J_{QV}} \end{bmatrix} \begin{bmatrix} \mathbf{\Delta\theta} \\ \mathbf{\Delta V} \end{bmatrix} \tag{2.8}$$

where $\mathbf{J_{P\theta}}$, $\mathbf{J_{PV}}$, $\mathbf{J_{Q\theta}}$, $\mathbf{J_{QV}}$ are the Jacobian matrices for the active and reactive power sensitivities with respect to the bus voltage angles and bus voltage magnitudes. $\mathbf{\Delta P}$ and $\mathbf{\Delta Q}$ are the changes in real and reactive powers respectively.

In order to focus the study on the reactive power in the system, and minimize the computational effort by reducing the dimensions of the Jacobian matrix $\mathbf{J}$, the real power $(\mathbf{\Delta P}=0)$ and angle component are eliminated.

If $\mathbf{\Delta P} = 0$, the reduced Jacobian resulting from this is given as (Kundur, 1994):

$$0 = \mathbf{J_{P\theta}}\mathbf{\Delta\theta} + \mathbf{J_{PV}}\mathbf{\Delta V} \tag{2.9}$$

From (2.8) and (2.9) above,

$$\mathbf{\Delta\theta} = -\mathbf{J_{P\theta}}^{-1}\mathbf{J_{PV}}\mathbf{\Delta V} \tag{2.10}$$

$$\mathbf{\Delta Q} = \mathbf{J_{Q\theta}}\mathbf{\Delta\theta} + \mathbf{J_{QV}}\mathbf{\Delta V} \tag{2.11}$$

Substituting for $\mathbf{\Delta\theta}$ in (2.11)

$$\mathbf{\Delta Q} = \mathbf{J_{Q\theta}}(-\mathbf{J_{P\theta}}^{-1}\mathbf{J_{PV}}\mathbf{\Delta V}) + \mathbf{J_{QV}}\mathbf{\Delta V} \tag{2.12}$$

$$\mathbf{\Delta Q} = \mathbf{\Delta V}\left(\mathbf{J_{QV}} - \mathbf{J_{Q\theta}}\mathbf{J_{P\theta}}^{-1}\mathbf{J_{PV}}\right) \tag{2.13}$$

The reduced Jacobian is then obtained as:

$$\mathbf{J_R} = \mathbf{J_{QV}} - \mathbf{J_{Q\theta}}\mathbf{J_{P\theta}}^{-1}\mathbf{J_{PV}} \tag{2.14}$$

From (2.14), the incremental bus voltage can be expressed as:

$$\mathbf{\Delta V} = \mathbf{J_R}^{-1}\mathbf{\Delta Q} \tag{2.15}$$

The modal analysis method gives the information regarding the mechanism of the instability. The mechanism of voltage stability/voltage instability can be identified by computing the eigenvalues and eigenvectors of the reduced Jacobian matrix (Kundur, 1994). Positive eigenvalues signify a voltage stable system, while otherwise represents a voltage unstable system. The eigenvalues of the reduced Jacobian matrix give a measure of the proximity to instability, while the eigenvectors are related to the mechanism of voltage stability.

Eigenvalue analysis of $\mathbf{J_R}$ results in the following presentation of the reduced Jacobian matrix (Kundur, 1994):

$$\mathbf{J_R} = \mathbf{\Phi \Lambda \Gamma} \tag{2.16}$$

where $\mathbf{\Phi}$ is the right eigenvector matrix of $\mathbf{J_R}$, $\mathbf{\Gamma}$ is the left eigenvector matrix of $\mathbf{J_R}$, $\mathbf{\Lambda}$ is the diagonal eigenvalue matrix of $\mathbf{J_R}$.

The right eigenvector gives the mode shape which defines the relative activity when a particular mode is excited. The left eigenvector weighs the contribution of this activity to that particular mode (Kundur, 1994).

Equation (2.16) can be rewritten as (Kundur, 1994):

$$\mathbf{J_R}^{-1} = \mathbf{\Phi \Lambda}^{-1} \mathbf{\Gamma} \tag{2.17}$$

Substituting Equation (2.17) in Equation (2.15) gives:

$$\mathbf{\Delta V} = \mathbf{\Phi \Lambda}^{-1} \mathbf{\Gamma \Delta Q} \tag{2.18}$$

After the left multiplication of Equation (2.18) by $\mathbf{\Gamma}$, and since the geometrical product between the right and left eigenvectors is equal to the identity matrix $\mathbf{I}$, Equation (2.18) can be rewritten as:

$$\mathbf{\Gamma \Delta V} = \mathbf{\Lambda}^{-1} \mathbf{\Gamma \Delta Q} \tag{2.19}$$

The modal variations $\nu = \mathbf{\Gamma \Delta V}$ can be referred to the modal reactive power variation $\mathbf{q} = \mathbf{\Gamma \Delta Q}$:

$$\mathcal{V} = \mathbf{\Lambda}^{-1} \mathbf{q} \tag{2.20}$$

where $\nu = \mathbf{\Gamma \Delta V}$ is the vector of the modal voltage variations and $\mathbf{q} = \mathbf{\Gamma \Delta Q}$ is the vector of the modal reactive power variations.

The magnitude of the eigenvalues $\mathbf{\Lambda}$ determines the degree of stability. For an ith mode, the smaller the magnitude of the positive eigenvalues, the closer the system is to instability. Based on the above equations, the modal voltage at the ith mode collapses when the ith mode eigenvalue equals zero. This is because at that point,

any change in the modal reactive power causes an infinite change in the modal voltage.

The relative Bus Participation Factor (BPF) of the bus k in the mode i is given as (Kundur, 1994):

$$P_{ki} = \Phi_{ki} * \Gamma_{ik} \tag{2.21}$$

where P_{ki} is the participation factor, Φ_{ki} is the kith element of the right eigenvector matrix of $\mathbf{J_R}$ for the bus k and the ith mode, Γ_{ik} is the ikth element of the left eigenvector matrix of $\mathbf{J_R}$ for the bus k and the ith mode. Large values of P_{ki} indicate the buses most prone to voltage collapse.

Similar to the BPF, the Branch Participation Factor (BrPF) is indicative of the branches in the system which consume the highest reactive power due to an increase in the reactive power loading in the system. This is used in the identification of the weak ties in the system, and how heavily loaded the branches are.

The BrPF is given as:

$$P_{lji} = \frac{\Delta Q_{lji}}{\Delta Q_{l\max i}} \tag{2.22}$$

P_{lji} is the BrPF, ΔQ_{lji} is the variation of the reactive power loss across branch lj, $\Delta Q_{lmax\,i}$ is the maximum value of ΔQ_{lji}.

The Generator Participation Factor (GPF) can be used in the assessment of the reactive power reserve on the generators in the system. The GPF gives an indication of the generators which supply the highest reactive power for a given mode as a response to the increase in the system's reactive power loading.

The GPF is given as:

$$P_{gki} = \frac{\Delta Q_{gki}}{\Delta Q_{g\max i}} \tag{2.23}$$

P_{gki} is the GPF, ΔQ_{gki} is the variation of the reactive power output at generator gk, and $\Delta Q_{gmax\,i}$ is the maximum value of $\Delta Q_{gk\,i}$.

2.4.2.3 Sensitivity Analysis

The matrix $\mathbf{J_R}$ in Equation (2.15) represents the relationship between the incremental changes in the bus voltage $(\Delta \mathbf{V})$ and the bus reactive power injection $(\Delta \mathbf{Q})$. The V-Q sensitivity at a particular bus corresponds to the slope of the V-Q curve at that particular operating point. When the sensitivities are positive, the system is stable. The sensitivity becomes infinite at the maximum loadability limit. A negative sensitivity is an indication of system instability. A small value of negative sensitivity signifies that the system is operating in a very unstable condition.

Singular value decomposition of the Jacobian matrix of load flow is a common approach in voltage stability analysis and assessment as reported in (Barquin *et al*., 1995; Lof *et al*., 1993). This is because the load flow Jacobian becomes singular (without solution) at the point of voltage collapse (Ajjarapu, 2006; Kundur, 1994).

Thus, the singular vectors obtained from the load flow Jacobian can be applied in the estimation of the power system's proximity to voltage collapse, and in the identification of the critical buses in the system. The proximity of the system to the voltage collapse point is given by the value of the smallest singular value. The right singular vectors of the Jacobian matrix indicate the sensitive voltage magnitudes and angles, while the left singular vectors indicate the most severe contingencies (Ajjarapu, 2006).

Sensitivities derived from the reactive power generation with respect to the real and reactive powers load requirement in the system was applied in the analysis of the voltage collapse problem in (Begovic and Phadke, 1992), saddle-node bifurcation was used in (Zambroni de Souza and Quintana, 1994; Canizares *et al*., 1992), while branch complex flow was applied in (Grijalva and Sauer, 2005).

2.4.2.4 Thevenin Equivalent Methods

The 2-bus system shown in Figure 2.8 can be related to a Thevenin equivalent system as shown in Figure 2.8. This is done by the representation of the voltage source and the rest of the system by their Thevenin equivalents as seen from the load bus.

If the load demand is $S = P + jQ$, the current flowing in the system is given by:

$$\frac{P + jQ}{\bar{V}} = \bar{I}^{*} = \left(\frac{\bar{E}_{th} - \bar{V}}{\bar{Z}_{th}} \right)^{*} \tag{2.24}$$

Equation (2.24) can be rewritten as:

$$(P + jQ)\,\overline{Z}_{th}^{*} = \overline{V}\left(\overline{E}_{th} - \overline{V}\right)^{*} \quad (2.25)$$

where P and Q are the real and reactive powers of the load demand, $\overline{V}$ is the voltage at the load bus, I is the current flowing to the load bus, $\overline{E}_{th}$ is the Thevenin voltage of the equivalent system, $\overline{Z}_{th}$ is the Thevenin equivalent impedance, and * denotes the complex conjugate.

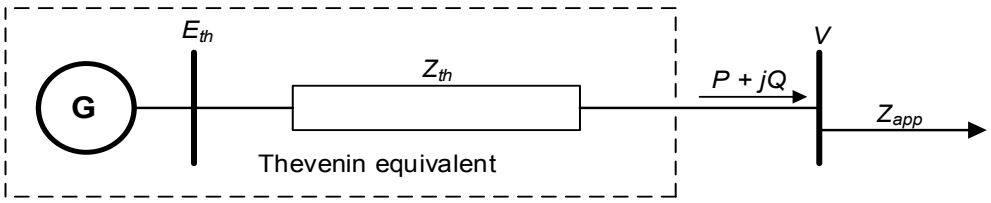

Figure 2.8: **A 2-bus system showing the Thevenin equivalent system as seen from a local bus**

The maximum loadability of a transmission system is obtained when the apparent load impedance is equal to the Thevenin impedance (Vu *et al*., 1999). Two solutions can be obtained from the solution of Equation (2.25). These are the $\overline{V}$ and the $\left(\overline{E}_{th} - \overline{V}\right)^{*}$ solutions respectively (Vu *et al*., 1999).

At the point of maximum loadability, the two solutions of Equation (2.25) will collide and become singular (Vu *et al*., 1999).
These solutions are:

$$\overline{V} = \left(\overline{E}_{th} - \overline{V}\right)^{*} \quad (2.26)$$

$$\overline{Z}_{app} \times \overline{I} = \left(\overline{Z}_{th} \times \overline{I}\right)^{*} \quad (2.27)$$

where $\overline{Z}_{app}$ is the apparent load impedance.

At the point of maximum system loadability corresponding to the voltage collapse point,

$$\left|\overline{Z}_{app}\right| = \left|\overline{Z}_{th}\right| \quad (2.28)$$

The distance between $\left|\overline{Z}_{app}\right|$ and $\left|\overline{Z}_{th}\right|$ can be used as the basis of the measure of the distance (proximity) of the power system to its voltage collapse point.

The Thevenin equivalent voltage is determined as:

$$\overline{E}_{th} = \overline{V} + \overline{Z}_{th}\overline{I}^{*} \quad (2.29)$$

For the four unknowns in Equation (2.29), $\overline{V}$ and $\overline{I}^*$ can be obtained as phasor measurements from a PMU, while $\overline{E}_{th}$ and $\overline{Z}_{th}$ would need to be estimated. The above derivations are also applicable to large interconnected power systems comprising of a study system and an external system (Aschmoneit & Verstege, 1979; Monticelli *et al*., 1979). The study system is made up of the internal system and the boundary buses which connect the internal system to the external system. The external system consists of interconnected control areas and parts of the internal control areas that are unobservable.

Therefore, the buses in a system can be divided into internal buses (I), boundary buses (B), and external buses (E) as shown in Figure 2.9.

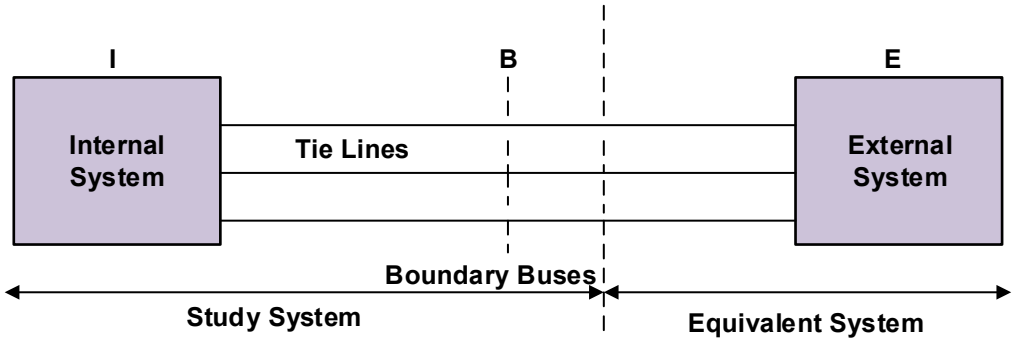

Figure 2.9: **Large interconnected power system (Monticelli *et al*., 1979)**

The injected currents into the interconnected system shown in Figure 2.9 can be represented as (Lof *et al*., 1993; Bose, 1984; Aschmoneit and Verstege, 1979):

$$\begin{bmatrix} \mathbf{i}_I \\ \mathbf{i}_B \\ \mathbf{i}_E \end{bmatrix} = \begin{bmatrix} \mathbf{Y}_{II} & \mathbf{Y}_{IB} & \mathbf{0}_{IE} \\ \mathbf{Y}_{BI} & \mathbf{Y}_{BB} & \mathbf{Y}_{BE} \\ \mathbf{0}_{EI} & \mathbf{Y}_{EB} & \mathbf{Y}_{EE} \end{bmatrix} \begin{bmatrix} \mathbf{v}_I \\ \mathbf{v}_B \\ \mathbf{v}_E \end{bmatrix} \tag{2.30}$$

where $\mathbf{i}_I, \mathbf{i}_B, \mathbf{i}_E$ are the injected currents into the internal system, boundary system, and the external system of the interconnected system respectively. $\mathbf{v}_I$, $\mathbf{v}_B$, $\mathbf{v}_E$ are the bus voltages in the internal system, boundary system, and the external system of the interconnected system.

The bus admittance matrix $\mathbf{Y}$ is given as (Lo *et al*., 1993; Monticelli *et al*., 1979):

$$\mathbf{Y} = \begin{bmatrix} \mathbf{Y}_{II} & \mathbf{Y}_{IB} & \mathbf{0}_{IE} \\ \mathbf{Y}_{BI} & \mathbf{Y}_{BB} & \mathbf{Y}_{BE} \\ \mathbf{0}_{EI} & \mathbf{Y}_{EB} & \mathbf{Y}_{EE} \end{bmatrix} \tag{2.31}$$

When the external system is equivalenced, the part of the admittance matrix $\mathbf{Y}_{th}$ that corresponds to the external system and the boundary buses is given as:

$$\mathbf{Y_{th}} = \begin{bmatrix} \mathbf{Y_{EE}} & \mathbf{Y_{EB}} \\ \mathbf{Y_{BE}} & \mathbf{Y_{BB}} \end{bmatrix} \tag{2.32}$$

Thus, the bus admittance matrix is given as:

$$\mathbf{Y_{th}} = [\mathbf{Y_{BB}}] - [\mathbf{Y_{BE}}]\,[\mathbf{Y_{EE}}]^{-1}\,[\mathbf{Y_{EB}}] \tag{2.33}$$

In the formulation of the equivalent system, prior information of the external system is not required. The details required are the topology of the external system and the state of the internal system. Thus, the external system data requirements are minimized. This helps to reduce the computation needed when applied in real-time applications.

When the above is related to the interconnected system in terms of load, tie, and generator buses, Equation (2.30) can be re-written for the injection currents into the load, tie, and generator buses ($\mathbf{i_L}$, $\mathbf{i_T}$, $\mathbf{i_G}$) as:

$$\begin{bmatrix} \mathbf{i_L} \\ \mathbf{i_T} \\ \mathbf{i_G} \end{bmatrix} = \begin{bmatrix} \mathbf{Y_{LL}} & \mathbf{Y_{LT}} & \mathbf{Y_{LG}} \\ \mathbf{Y_{TL}} & \mathbf{Y_{TT}} & \mathbf{Y_{TG}} \\ \mathbf{Y_{GL}} & \mathbf{Y_{GT}} & \mathbf{Y_{GG}} \end{bmatrix} \begin{bmatrix} \mathbf{v_L} \\ \mathbf{v_T} \\ \mathbf{v_G} \end{bmatrix} \tag{2.34}$$

L is the load bus, T is the tie bus, and G is the generator bus, $\mathbf{\upsilon_L}$, $\mathbf{\upsilon_T}$, $\mathbf{\upsilon_G}$ are the voltages at the load buses, tie buses, and the generator buses respectively.

The voltage at the load buses can be calculated by (Gong *et al*., 2006):

$$v_L = \mathbf{Z_{LL}}\,\mathbf{i_L} + \mathbf{Z_{LT}}\,\mathbf{i_T} + \mathbf{H_{LG}}\,\mathbf{v_G} \tag{2.35}$$

where

$$\mathbf{Z_{LL}} = \left(\mathbf{Y_{LL}} - \mathbf{Y_{LT}}\,\mathbf{Y_{TT}^{-1}}\,\mathbf{Y_{TL}}\right)^{-1} \tag{2.36}$$

$$\mathbf{Z_{LT}} = -\mathbf{Z_{LL}}\mathbf{Y_{LT}}\,\mathbf{Y_{TT}}^{-1} \tag{2.37}$$

$$\mathbf{H_{LG}} = \mathbf{Z_{LL}}\left(\mathbf{Y_{LT}}\,\mathbf{Y_{TT}^{-1}}\,\mathbf{Y_{TG}} - \mathbf{Y_{LG}}\right) \tag{2.38}$$

Impedance matrix is used because its computation does not require performing a series of iteration which could be a burden when working with a non-sparse matrix.
From Equation (2.35), since the injection currents to the tie buses equal zero, the i_T term is eliminated.

Thus, the voltage at the jth load bus is given as:

$$v_{Lj} = \sum_{i=1}^{N} Z_{LLji}\, i_{Li} + \sum_{k=1}^{M} H_{LGjk}\, \upsilon_{Gk}\,, \quad j=\overline{1, N_b} \tag{2.39}$$

N_b and M are the number of system buses and generator buses respectively.

If the injection currents are substituted with the complex powers flowing out of the buses, Equation (2.39) becomes:

$$v_{Lj} = Z_{LLjj}\left(\frac{-S_{Lj}}{v_{Lj}}\right)^{*} + \sum_{i=1,i\neq j}^{N} Z_{LLji}\left(\frac{-S_{Li}}{v_{Li}}\right)^{*} + \sum_{k=1}^{M} H_{LGjk}\, v_{Gk} \tag{2.40}$$

If $\upsilon_{thj} = \sum_{k=1}^{M} H_{LGjk}\,\upsilon_{Gk} + \sum_{i=1,i\neq j}^{N} Z_{LLji}\left(\frac{-S_{Li}}{v_{Li}}\right)^{*}$ and $Z_{thj} = Z_{LLjj}$

where υ_{thj} is the equivalent Thevenin voltage, Z_{thj} is the equivalent Thevenin impedance, S_{Li} is the complex power in the ith load bus.

Then, the complex load power at the jth bus is given by (Gong *et al*., 2006):

$$S_{Lj} = \left(\frac{v_{th} - v_{Lj}}{Z_{thj}}\right)^{*} v_{Lj} \tag{2.41}$$

From the foregoing, it can be seen that V_{th} decreases as the system loading increases. Also, Z_{th} is dependent on the topology of the system, the type of bus, and the characteristics of the line.

The methods discussed above in subsections 2.4.2.1-2.4.2.4 are commonly formulated into voltage stability assessment indices under the broad categorisation shown in Figure 2.10. Table 2.4 shows a comparative analysis of these methodologies.

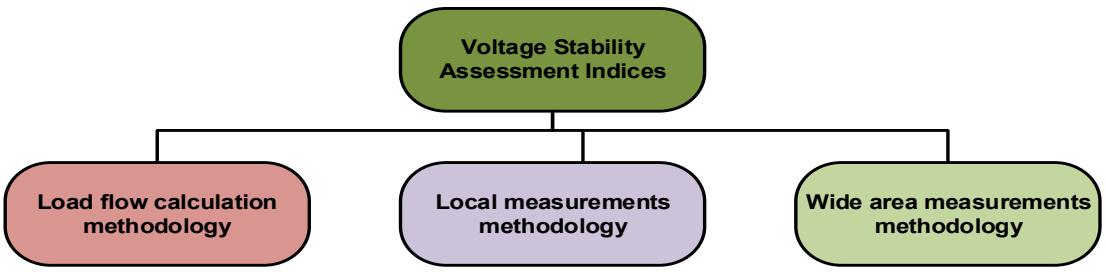

Figure 2.10: Categorisation of voltage stability assessment methodologies

Table 2.4: Voltage stability assessment methods

Methods	Theoretical Methods	Type of Measurements	Real-Time Implementation for Protection/Control
Load flow-based methodology	Curves analysis, modal analysis, sensitivity analysis	Off-line measurements	NA
Local measurements-based methodology	Sensitivity analysis, Thevenin method	Local RMS measurements	Local protection using conventional distributed protective relays.
Wide area-based methodology	Sensitivity analysis, Thevenin method, Computational Intelligence	Wide area measurements from SCADA or PMU-based systems	Wide area-based protection/control

A comprehensive literature review was conducted using the methodologies presented in Figure 2.10. It should be noted that in this review, a set of publications seen as representative of the various existing techniques and methods are used. Conference proceedings (except from renowned authors) were excluded in the review.

2.4.3 Review of the Load Flow Calculation-Based Methodologies

2.4.3.1 Review of Publications on Load Flow Calculation-Based Methodologies

Methods for voltage stability assessment using load flow calculations can be analysed using static analysis techniques. Techniques for static analysis provide insights into the nature of the voltage stability problem and identify the key contributing factors using a wide range of system conditions. Most electric utilities depend largely on static analysis carried out using conventional load flow programmes for their system planning and operation studies. The various techniques under the load flow calculation-based methodology is discussed under the following categories: (i) Curve-based methods; (ii) Modal analysis-based methods; and (iii) Sensitivity analysis.

Curve-Based Methods

The curve-based methods have been traditionally used by electric utilities for power system stability assessment (WECC, 2006; Taylor, 1994). The voltage stability of a power system was quantified in (Overbye *et al*., 1994) through the use of V-Q curves. The method was based on the use of the energy measured in a system as an indication of the system's voltage stability or instability. This was equated to the area enclosed by a V-Q curve (referred to as Q-V in the published article). A P-Q-V method was proposed by Lee *et al*. (2010). The P-Q-V curve was assumed to indicate the boundary of the maximum loadability point with respect to the real and reactive powers demand in the system. Similarly, the P-V and V-Q curves methods were applied by Zambroni de Souza *et al*. (2011) for voltage stability assessment and contingency screening applications respectively.

The application of the curve-based method is associated with repeated offline load flow studies. This prompted a comparative study on the V-Q based method and the dynamic simulation method by Chowdhury and Taylor (2000). Similarly, Huang *et al*. (2007) proposed a measurement-based V-Q curve method which can measure a part of the V-Q curve online.

The Continuation Power Flow (CPF) method (Ajjarapu 2006; Ajjarapu and Christy, 1992) was applied by Zambroni de Souza *et al*. (2011) to trace the V-Q curve used in

voltage stability analysis and contingency analysis. This is because the CPF method is not beset by the uncertainties associated with the conventional load flow calculation at the point of voltage collapse. A method to determine the stable part of the P-V curve was proposed in Pama and Radman (2009), and was applied in the estimation of the real power (MW) distance to voltage collapse.

Modal Analysis Methods

Schlueter *et al.* (1991) proposed a technique for the determination of the Voltage Control Areas (VCAs) in power systems and the calculation of the proximity to voltage collapse. Two indices were proposed and were based on the changes in the eigenvalues of the Jacobian sub-matrix (reactive power-voltage Jacobian) and the sensitivity matrix respectively. Morison *et al.* (1993) presented a comparison of the dynamic and static techniques for voltage stability analysis. The static technique was based on modal analysis, while the dynamic techniques made use of time-domain simulations. Also, the effect of load types, transformer ULTCs, and generator OXLs were investigated.

Modal analysis methods using the Jacobian matrix of the power system load flow calculation have been presented by some researchers. Gao *et al.* (1992) applied the modal analysis technique to a power system using a steady-state model. This involved the computation of the smallest eigenvalues and the eigenvectors of the reduced Jacobian matrix of the load flow, and the corresponding participation factors for the buses, branches, and generators in the system. The study network used was a 3700-bus test system.

Ajjarapu *et al.* (1994) used the Continuation Power Flow (CPF) technique for studying the proximity to steady-state voltage stability limits. Sequential quadratic programming was used in the optimization of the result obtained from the CPF. Also, sensitivity analysis was carried out using the tangent vector obtained from the CPF process. This sensitivity information was applied in the identification of the weak buses and the optimal locations for siting the reactive power compensation.

Barquinn *et al*. (1995) described a method for computing the minimum singular value of the load flow Jacobian corresponding to the maximum loadability limit of a power system. The proposed method used the information obtained from the voltage collapse area, and the relationship between system variables and parameters. Similarly, Hong *et al.* (1997) proposed a non-iterative technique for the estimation of the minimum singular value of the Jacobian for the load flow of a power system at a

particular operating condition. Ghiocel *et al.* (2014) presented an approach based on the reformulation of the load flow problem. Two techniques were proposed, together with the use of a phase angle-reactive power bus (AQ-bus).

Sensitivity-Based Methods

Sensitivity-based techniques using bifurcation and Singular Value Decomposition (SVD) abound in the literature. Kwatny *et al.* (1986) presented a static bifurcation technique for the analysis of voltage stability. The static bifurcations obtained from the load flow were analysed using Lyapunov-Schmidt reduction to obtain a reduced bifurcation equation which was then expanded using Taylor series. It was shown that the static bifurcation for voltage collapse exists and is associated with the divergence of the load flow solution. Ajjarapu and Lee (1992) used the Hopf bifurcation technique to study voltage stability in power systems. The premise behind this technique was that if the parameters of a power system are varied continuously, a critical point is reached whereby the system transitions from one state to another, and the new state may be different from the initial state.

The SVD information obtained from the load-flow calculations was used for voltage stability assessment in Lof *et al.* (1992). The process involves the computation of the SVD of the Jacobian matrix of the load flow, and the left and right singular vectors of the Jacobian matrix. The right sub-matrix of the Jacobian relates to the voltage and phase angles, while the left sub-matrix corresponds to the sensitivity directions for the real power and reactive power variations. Similarly, Hong *et al.* (1997) used the SVD obtained from the linearization of the load flow equations with the consideration of the effect of transformer ULTCs and the load characteristics at the load (PQ) bus. The SVD technique by Berizzi *et al.* (1998) was applied in the determination of the system's proximity to voltage collapse. The technique was implemented by using the maximum singular value obtained from the inverse of the load flow Jacobian.

Barquin *et al.* (1995) employed the smallest singular value obtained from the Lower-Upper (LU) factorization of the load flow Jacobian in the prediction of the system's proximity to voltage collapse. It further applied the relationship between the system variables and parameters to estimate the real power and reactive power margins to voltage collapse. Canizares *et al.* (1995) described a saddle-node bifurcation method which was applied to a power system with different load-types.

Equations showing the relationship of a system's loading margin with respect to the power system parameters were presented by Greene *et al.* (1997). The sensitivities

obtained can be used as an indication of the system's proximity to voltage collapse, and in the identification of the appropriate control actions to apply in order to prevent voltage collapse in the system. Huang *et al.* (1999) proposed a technique based on the smallest singular values of the load flow Jacobian combined with curve-fitting methods to estimate the maximum load factor at the point of the voltage collapse. Berizzi *et al.* (2000) suggested a technique based on the sensitivities obtained from the maximum singular values of the load flow Jacobian. The technique also provided a means of carrying out contingency ranking using the information obtained from the singular values.

Chen *et al.* (2003) proposed a technique using a combination of an index based on reactive power limits and a test function-based performance index in the prediction of the voltage collapse in a power system. Zambroni de Souza *et al.* (2005) presented a technique for the detection of the Hopf and saddle-node bifurcations using a saddle-node index based on a set of the dominant eigenvalues of the load flow Jacobian. A SVD method based on a Multi-Input Multi-Output (MIMO) transfer function was proposed by Cai and Erlich (2007). The effects of the input variables on the outputs were indicated by the elements of the input singular vectors. The singular vector of the output was then used to indicate the most critical buses in the network. The relationship between the active power flowing through the branches of a power system and the voltage collapse point was presented in Cao *et al*. (2015).

2.4.3.2 Discussion

A summarised comparative analysis of the load flow calculation method for voltage stability assessment is given in Table 2.5. Although, the P-V curve and V-Q curve techniques have found wide applications in the industry, the computation of the curves can be very complicated, tedious, and time-consuming due to the large number of generators, widespread applications of capacitor banks, uncertainty about the dynamic characteristics of system loads, and the variability of the power flow pattern. Also, the buses for the P-V and V-Q curves analysis must be carefully selected. In addition, a large number of curves would be required in order to obtain actionable information.

Aside the curves-plotting techniques, most of the other techniques in the literature are also based on static analysis using load flow calculation. This requires that a load flow solution (convergence) must be found. The inability of the power system load-flow calculation to converge is taken as an indication of the voltage instability.

Table 2.5: Literature review of the load flow calculation-based methodologies

S/N	Paper	Methodology	Proposed Index	Study Network(s)	Contribution(s)/ Implementation	Drawback(s)
1	Kwatny *et al*. (1986)	Static bifurcations from the load flow Jacobian were analysed using Lyapunov-Schmidt reduction.	The proposed index was based on static bifurcation using the load flow Jacobian.	3-bus test system.	Static bifurcation analysis was combined with symbolic computation.	Static bifurcation assumes that the point of voltage collapse coincides with the bifurcation point. Also, it is tedious to carry out bifurcation analysis for all the load buses in a large power system.
2	Schlueter *et al*. (1991)	Eigenvalue sensitivity of the load flow Jacobian was used.	Reactive power-voltage Jacobian and voltage sensitivity index.	30-bus New England test system.	Proposed a method for the determination of voltage control areas and indices based on the eigenvalues of the load flow Jacobian. Also, a relationship between the curves and the eigenvalues of the load flow Jacobian, and sensitivity matrices was introduced.	The proposed method for the identification of the VCAs would fail when there are changes in the system topology or operating conditions.
3	Ajjarapu and Lee (1992)	Sensitivity based using the continuation power flow calculation.	Hopf bifurcation theory.	33-bus system.	Calculation of Hopf bifurcation points. The prediction of voltage instability, proximity to voltage collapse, and identification of critical areas were considered.	Requires repeated load flow calculation to obtain the Hopf bifurcation. This is tedious and time consuming.
4	Chebbo *et al*. (1992)	Thevenin equivalent-based reactive power dispatch algorithm.	Impedance ratio used.	IEEE 30-bus test system.	Local measurements to compute $Z_{app,}$ Z_{th}, V_{bus}, and E_{th} required. Prediction of voltage instability, proximity to voltage collapse, and identification of the critical areas in the system.	It is assumed that the equivalent Thevenin V and Z are constant for 2 or more system states. However, during disturbances/contingencies, the system states are rapidly changing.

Table 2.5: Literature review of the load flow calculation-based methodologies cont'd

S/N	Paper	Methodology	Proposed Index	Study Network(s)	Contribution(s)/ Implementation	Drawback(s)
5	Gao *et al*. (1992)	Sensitivity-based using modal analysis.	Modal participation factors used.	3700-bus system.	Computation of the eigenvalues and the eigenvectors of the load flow Jacobian. These were applied in the prediction of voltage instability, proximity to voltage collapse, and identification of critical areas.	The load flow calculation diverges at the point of voltage collapse when the eigenvalues become negative. However, there is the possibility of load flow divergence even for positive eigenvalues.
6	Lof *et al*. (1992)	Singular Value Decomposition (SVD) of Jacobian matrix.	Singular value decomposition.	Ward-Hale 6-node system, AEP30- and 57-node systems, and 1033-node Swedish system.	Prediction of voltage instability, proximity to voltage collapse, and identification of critical areas from the minimum singular value of the load flow Jacobian.	System behaviour was analysed around the current operating point only.
7	Morison *et al*. (1993)	Comparison was made between static and dynamic techniques for voltage stability analysis.	Modal analysis and dynamic simulation.	10-bus multi-machine test system.	The results obtained using modal analyses were shown to be consistent with those using dynamic simulations. Also, the effect of load types, ULTC, and generator OXL were considered.	A comparison between the proposed modal participation factor and other methods was not made.
8	Ajjarapu *et al*. (1994)	Sensitivity analysis was used.	Continuation power flow.	IEEE 30-bus test system.	Predictor-corrector steps introduced and applied. Prediction of voltage instability, proximity to voltage collapse, and identification of critical areas.	Voltage magnitude only does not give a good indication of voltage collapse. Also, the use of load flow equations implies that only steady-state conditions are studied.
9	Barquin *et al*. (1995)	LU factorization of the load flow Jacobian to obtain the smallest singular value.	Singular value decomposition of the load flow Jacobian.	6 machine Cigre model, IEEE-118 bus test system.	A method for estimating the MW and MVAr margin in a power system is provided.	Computation of the singular value of the buses in large power system can be very tedious.

Table 2.5: Literature review of the load flow calculation-based methodologies cont'd

S/N	Paper	Methodology	Proposed Index	Study Network(s)	Contribution(s)/ Implementation	Drawback(s)
10	Canizares *et al*. (1995)	Saddle-node bifurcation of the eigenvalues obtained from the load flow Jacobian was used to indicate the voltage collapse point.	The voltage stability index was based on the saddle-node bifurcation of the eigenvalues of the load flow Jacobian.	115-bus SNI Ecuadorian system.	Investigated the application of saddle-node bifurcation technique in a power system with various load-types.	Bifurcations are detected by monitoring the eigenvalues of the operating point. The use of eigenvalues requires the computation of the load flow Jacobian at all these buses. This can be very tedious in large power systems.
11	Greene *et al*. 1997	Sensitivity index from linear and quadratic equations of the loading margin with respect to the system parameters or applied control action using the bifurcation theory.	Sensitivity analysis of the loading margin was used.	IEEE 118-bus test system.	The sensitivities obtained can be used as a proximity to voltage collapse index. Provides an estimate showing the relationship of the loading margin to the system parameters.	A loading parameter is used. Steps for the determination of the parameter value for the maximum loading margin was not specified.
12	Hong *et al*. (1997)	SVD of the Jacobian matrix of the load flow using an incremental condition estimation method.	Voltage stability index based on the singular value decomposition of the load flow Jacobian was used.	Taipower system.	Incremental condition estimation was applied to the SVD of the load flow Jacobian.	Computation of the singular value of the load flow Jacobian at all the buses in a large power system is very tedious.
13	Berizzi *et al*. (1998)	Sensitivity based using Jacobian matrix.	Singular value decomposition of the load flow Jacobian.	63-bus CIGRE network and Italian EHV network.	Prediction of voltage instability, proximity to voltage collapse, and the identification of the critical areas in the power system.	Computation of the singular value of the buses in large power system can be very tedious.
14	Huang *et al*. (1999)	Singular value decomposition of the load flow Jacobian combined with a curve-fitting method.	Singular value decomposition of the load flow Jacobian.	1490-bus ERCOT system.	Estimation of the maximum load factor and identification of the point of voltage collapse.	Requires the calculation of singular values of load flow Jacobian.
15	Berizzi *et al*. (2000)	Singular value decomposition of the load flow Jacobian is used in the ranking of various contingencies with respect to voltage collapse.	Contingency ranking using singular value decomposition of the load flow Jacobian.	1490-bus ERCOT system.	Second order information obtained from the maximum singular values is used for contingency ranking.	Computation of the singular value of the load flow Jacobian at all the buses in a large power system can be very tedious.

Table 2.5: Literature review of the load flow calculation-based methodologies cont'd

S/N	Paper	Methodology	Proposed Index	Study Network(s)	Contribution(s)/ Implementation	Drawback(s)
16	Chen *et al*. (2003)	The combination of reactive power limits and test function-based performance index.	Saddle-node bifurcation of the eigenvalues of the load flow Jacobian.	1490-bus ERCOT system.	An improvement is made over the existing Q-limit index, and does not require a corrector to tune the proposed index.	Repeated load flow calculations required.
17	Zambroni de Souza *et al*. (2005)	Monitoring of the real parts of the eigenvalues of the load flow Jacobian using an inverse power flow iteration algorithm.	A voltage stability index based on the critical eigenvalues of the load flow Jacobian was proposed.	1490-bus ERCOT system.	The detection of Hopf and saddle-node bifurcations.	Repeated load flow calculations required.
18	Cai and Erlich (2007)	Consideration of the active and reactive powers using Multi-Input Multi-Output (MIMO) transfer functions with analysis carried out using singular value decomposition.	Singular value decomposition of the load flow Jacobian matrix.	1490-bus ERCOT system.	The determination of the critical buses in the system.	The proposed technique is only suitable for static voltage stability analysis.
19	Ghiocel *et al*. (2014)	A power flow method based on the reactive power equation of the load flow using a newly proposed A-Q bus type.	An index for the calculation of the voltage stability margin and contingency analysis in power systems.	1490-bus ERCOT system.	A-Q bus-type proposed. The techniques do not experience numerical problems at the point of maximum loadability.	The proposed technique is suitable for steady-state voltage stability analysis, and not for dynamic analysis involving the interaction of various system components.
20	Cao *et al*. 2015	The branch active power was used in the identiication of the critical branches in the power system and the indication of the point of voltage collapse. Load flow equations were used.	The active power through the power system branches is related to the system's margin to voltage collapse.	IEEE 57-bus system and IEEE 118-bus system.	The branch active power was used for voltage stability analysis in terms of locating the critical branches and the point of voltage collapse.	The proposed method assumes that the point of maximum active power corresponds to the voltage collapse point.

However, it can be difficult to find a load flow solution near the voltage collapse point. This leads to uncertainly on whether the voltage collapse point was reached or otherwise. One of the disadvantages of the methods based on load-flow calculation is that a large set of simulations would have to be carried out. However, repeated load-flow calculations are time consuming, and might be inadequate due to the unreliable behaviour of most load flow algorithms when close to voltage collapse. Also, the accuracy of the simulation results depends mainly on the modelling of the various components in the power system.

Furthermore, techniques based on the calculation of load-flow are not suitable for online real-time applications. In addition, sensitivity-based techniques using the reduced Jacobian of the load flow might fail in situation where the active power is changing. This is because the active power is assumed to be negligible in the derivation of the reduced Jacobian.

2.4.4 Review of the Methodologies Based on Local Measurements

2.4.4.1 Review of Publications on Local Measurements-Based Methodologies

A review of the literature on techniques based on local measurements for voltage stability assessment showed that various methods based on optimisation techniques, derivation of bus and line indices, and load/generator reactive power consideration have been proposed. These are broadly classified and discussed under the following categories: (i) Sensitivity analysis; and (ii) Thevenin-based methods. A comparative analysis of a set of publications seen as representative of the various existing techniques is given in Table 2.6.

Sensitivity Analysis

Kessel and Glavitsch (1986) proposed an L index for predicting the onset of voltage instability and the proximity of the power system to voltage collapse. The L index was analytically derived from a set of power flow equations in which the union of a set of circles was used to form the feasible state space. The system's stability limit was indicated by the borderline curve of the area. The L index varies in the range of 0 at no load to 1 at the voltage collapse point. The bus with the largest L index is taken as the critical bus in the network.

Obadina and Berg (1988) presented a method in which an optimisation problem was formulated for maximizing the total MVA load. The optimisation problem was solved using sequential quadratic programming. A Stability Margin (SM) index was also proposed based on the MVA limit obtained at the critical state.

The proposed index by Tare and Bijwe (1998) was based on the angle between the gradient vectors of the real and reactive powers at the load buses. Also, an optimization problem was formulated to minimise the sum of the squares of the deviation in the voltage stability index at a set of weak buses. This served as a form of control action for maintaining the voltages at the load bus within limit.

Galiana (1984) suggested a technique based on the load flow feasibility region which comprised of a set of generalized bus injections with a load flow solution. The proximity of the bus injection values to the feasibility limit was used as an index to predict the onset of voltage collapse. A feasibility margin closer to 0 indicates a system stable state, while the system unstable state is indicated by a margin close to 1.

The Line Stability Index L_{mn} was proposed by Moghavvemi and Omar (1998). It utilized the concept of power flow in a single transmission line linking the sending end source and the load at the receiving end. Jasmon and Lee (1991) presented a technique for predicting the onset of voltage collapse by using power flow equations. This was done by using the power loss elements in the power flow equations to reduce the power system into a single-line network for which a system stability factor can be calculated. The system collapses when the stability factor has a value of 1.

Moghavvemi and Faruque (1999) presented a Voltage Collapse Proximity Index (VCPI) obtained by considering the complex power injected to a particular bus from another bus in the power system. The VCPI index is characterized by the bus voltages and the network admittance matrix. The VCPI can take any value between 0 and 1. The index equals 1 at the point of voltage collapse. The system global index $VCPI_{sys}$ is indicated by the highest value of VCPI obtained at any of the load buses. Similarly, the Fast Voltage Stability Index (FVSI) was proposed by Musirin and Rahman (2002) for predicting the voltage stability margin of a particular bus or line under various loading conditions. FVSI approaches 1 as the margin of the voltage stability decreases. The line with the highest FVSI was considered as the most sensitive line.

The Power Transfer Stability Index (PTSI) was described by Nizam *et al.* (2006) for voltage collapse prediction. It was obtained as the ratio between the load apparent power and the maximum loadability possible. The PTSI has a value of 1 at the point of voltage collapse point. A global index was also defined using the PTSI. This was taken as the maximum PTSI on any of the load buses in the system.

Vournas and Sakellaridis (2007), used a maximum loadability tracking technique where the voltage collapse point was heralded by the point in which the secondary voltage at the bus reaches a maximum along the system trajectory. Bedoya *et al.* (2008) proposed two techniques in the calculation of the minimum Voltage Stability Margin (mVSM) of a power system. An index based on load flow equations and the bus voltages and network admittance information was proposed by Balamourougan *et al.* (2004). The proposed index was referred to as the Voltage Collapse Prediction Index (VCPI), and it was computed at all the buses in the system. The system's proximity to voltage collapse was determined by the value of the index at all the buses. A VCPI closer to 0 signifies a stable condition, while a VCPI value closer to 1 indicates the onset of the voltage collapse. The method by Verbic and Gubina (2004) used the change in the apparent power flow in the line for the calculation of the voltage collapse margin. A voltage collapse occurs when the margin equals 0.

Thevenin-based Methods

A Thevenin method for voltage stability assessment was proposed by Chebbo *et al.* (1992). This was based on the maximum power transferred between two buses. Thevenin's equivalent circuit was used in the determination of the power and voltage values at the critical point by monitoring the point at which the Thevenin impedance equals the load bus impedance. The system is stable for as long as the impedance ratio is less than 1, and it loses its stability when the ratio exceeds 1.

Vu *et al.* (1999) proposed a Voltage Instability Predictor (VIP) technique where measurements collected at a load bus were used to calculate the Thevenin equivalent voltage E_{th} of the rest of the system as seen from that particular bus, as well as the Thevenin equivalent impedance Z_{th}. In particular, recursive least-square was used in the estimation of the parameters of the Thevenin equivalent whenever two or more measurement sets are available. The same technique was applied in Julian *et al.* (2000). However, further investigations related to the effectiveness of the VIP technique for dynamic conditions relating to generator dynamics and load characteristics were carried out. The technique was shown to predict the onset of voltage instability for scenarios in which conventional protective devices failed. Further improvement of the VIP technique was proposed by Warland and Holen (2001) and renamed VIP++. The technique was aimed at improving the observability and robustness of the VIP technique.

The maximum permissible loading of a power system was used in Hague (2002) in the prediction of the margin of the power system to voltage collapse. The required

parameters for the tracking of the Thevenin equivalents and for the estimation of the index were the bus voltages, real power demand, and the reactive power demand of the load respectively. The required variables can be obtained from load flow calculations or from online measurements. Milosevic and Begovic (2003) proposed a method based on the tracking of the Thevenin's equivalents by a Recursive Least Square (RLS) scheme using successive measurements.

A single-step calculation method was investigated by Smon *et al.* (2006) using Tellegen's theorem and adjoint networks. The technique also considered the effect of load increase in the system. Corsi and Taranto (2008) presented an adaptive algorithm in the estimation of the Thevenin equivalents of a power system. The Thevenin parameters were estimated over a short period of time. The procedure involved the identification of the Thevenin Electro-Motive Force (EMF) based on the observation that this EMF should decrease when the variations in the load impedance and the estimated Thevenin equivalent impedance are in the same direction. A five-step algorithm was afterwards proposed to identify the equivalent parameters.

Wang *et al*. (2009) proposed an index based on an equivalent system model. The input to the index was the voltage phasors of the local bus. It was capable of identifying the weak bus and the system's proximity to voltage collapse. Corsi *et al.* (2010) suggested a method whereby a voltage stability indicator was related to the margin of the reactive power generation in a region.

Tiwari *et al.* (2012) investigated an index developed from the ABCD parameters of a transmission system, and it took into account the direction of the active and reactive power flows. The proposed index was termed Line Collapse Proximity Index (LCPI). The system was stable when the LCPI was closer to 0, and became unstable as the value of the LCPI tended to 1. Tobon *et al.* (2014) used the impedance matching approach in the prediction of the point of voltage collapse. A RLS algorithm was used in solving the impedance matching equation. Lee (2015) proposed an equivalent nodal analysis method based on the reduction of the impedance matrix of a system into a 2-bus equivalent model. An equivalent nodal voltage sensitivity index was then applied to indicate the point of voltage collapse.

Table 2.6: Literature review of local measurements-based methodologies

S/N	Paper	Methodology	Proposed Index	Study Network(s)	Contribution(s)/ Implementation	Drawback(s)
1	Galiana (1984)	The proposed index was based on the computation of the load flow feasibility margin of bus injections of real and reactive powers.	Voltage Collapse Proximity Indicators (VCPI) using the concept of load flow feasibility region was proposed.	2-bus test system used.	Did not rely on load flow calculations. Thus, avoids the numerical problems associated with load flow methods.	Required prior knowledge of the network in order to define the VCPI threshold beyond which voltage collapse would occur.
2	Kessel and Glavitsch (1986)	Based on the load-flow calculation of the power system using the complex power, nodal voltage, and line admittance.	*L* index.	25-node system & IEEE 118-bus test system.	Prediction of voltage instability, proximity to voltage collapse, and identification of critical areas using the proposed index. Also, the proposed index is simple to calculate.	Did not explicitly consider the operating constraints of the system like the VAR limits from generators. Also, P & Q from other load buses were not taken into consideration.
3	Obadina and Berg (1988)	Sensitivity-based method for weak bus identification using the apparent power demand on the $_j$th load bus.	Stability Margin (SM) was proposed based on the optimization of the maximum loadability of the system.	American Electric Power (AEP) 14-bus system.	Prediction of voltage instability, proximity to voltage collapse, and identification of critical areas were considered. Also, system limitations were considered.	The proposed SM index is a static index, and its accuracy depends on the value of the per unit initial apparent power.
4	Jasmon and Lee (1991)	Power flow equations are used in the derivation of the voltage collapse index.	*L* index.	20-node test system.	The input parameters (real and reactive powers, voltage at the node) are easily obtainable from the measurements available in control centres. Thus, suitable for practical online application.	Power system dynamics were not considered.
5	Chebbo *et al*. (1992)	Thevenin equivalent method based on the ratio of the Thevenin equivalent impedance and the load impedance.	Voltage Collapse Proximity Index (VCPI) proposed for the indication of the margin to voltage collapse.	IEEE 30-bus test system.	Local measurements to compute Z_{app}, Z_{th}, V_{bus}, and E_{th} required. The Derivations for the prediction of voltage instability, proximity to voltage collapse, and identification of critical areas were given.	In order to obtain accurate estimate, it was assumed that the equivalent Thevenin voltage and impedance are constant for 2 or more consecutive system states.

Table 2.6: Literature review of local measurements-based methodologies cont'd

S/N	Paper	Methodology	Proposed Index	Study Network(s)	Contribution(s)/ Implementation	Drawback(s)
6	Moghavvemi and Omar (1998)	Maximum power transfer theory using Thevenin's equivalent for predicting the system's margin to voltage collapse. The receiving end reactive power, line reactance, sending end voltage, and phase angles.	Line Stability Index (L_{mn}).	IEEE 24-bus test system.	Prediction of voltage instability, proximity to voltage collapse, and identification of critical areas. It can be used as an alarm to detect the onset of voltage collapse.	The proposed method becomes sensitive when the loading is very close to the voltage collapse point.
7	Tare and Bijwe (1998)	Load flow Jacobian: Angle between real power and reactive power gradient vectors of load buses were used.	Cosϕ index.	6-bus and IEEE 30-bus test systems.	Voltage stability status and weak bus identification. Proposed for real-time voltage stability assessment.	Index was based on equivalent systems which are often over-simplified.
8	Vu *et al*. (1999)	Thevenin equivalent tracking for the estimation of the margin to voltage collapse using local bus voltages and load currents measurements.	Apparent and Thevenin impedances.	New England 39-bus test system used.	Local measurements of voltage & current based on the least-squares algorithm; Z_{app}, Z_{th}, V_{bus}, and E_{th} required. Simple, off-line simulations and training were not required. Implemented on hardware.	The update of the external network equivalent becomes difficult whenever successive measurements are identical.
9	Julian *et al*. (2000)	Thevenin equivalent based on local measurements of voltages and currents.	Voltage Instability Predictor (VIP) using the power margin to voltage collapse derived from the ratio between the Z_{app} and Z_{th}.	7000-bus AEP system.	Predicts the proximity to voltage collapse using the ratio between the Z_{app} and Z_{th}.	The VIP algorithm could mal-operate whenever the Thevenin equivalent is constantly changing.
10	Warland and Holen (2001)	Thevenin equivalent method derived from local bus measurements were used in the proposal of 2 VIP++ methods (VIP^{++1} & VIP^{++2}) using the loading information.	Voltage Instability Predictor ++ (VIP ++).	4-bus system.	The determination of the system's proximity to voltage collapse based on the system loading.	Considered only long term voltage instability. The criterion for the operation of the proposed relay was not considered.
11	Haque (2002)	Calculation of the Thevenin equivalent and system's maximum loadability.	Voltage Stability Margin with respect to admittance (VSMy), and apparent power (VSMs).	IEEE 14-bus and 30-bus test systems.	Local V, P, & Q used. Investigated the maximum permissible loading and the determination of the voltage stability margin.	The proposed VSMy index is sensitive to load at the Point of Collapse (PoC).

Table 2.6: Literature review of local measurements-based methodologies cont'd

S/N	Paper	Methodology	Proposed Index	Study Network(s)	Contribution(s)/ Implementation	Drawback(s)
12	Musirin and Abdul Rahaman (2002)	Derivation of a line index based on power flow equations. The measurements used are the line impedance, reactive power at the sending end, voltage at the sending end, and line reactance.	Fast Voltage Stability Index (FVSI).	IEEE 24-bus system.	Voltage collapse detection and contingency analysis using the proposed FVSI index.	The proposed index is non-linear especially towards the voltage collapse point.
13	Bao *et al*. (2003)	VAR reserves and PV curves of key generators are used as an indication of the voltage stability margin.	Correlation between VAR margin and system margin obtained from the reactive power.	1000-bus BC Hydro and 1800-bus Alberta systems.	Voltage stability monitoring using data fed from a SCADA system.	Required the examination of a lot of scenarios.
14	Milosevic and Begovic (2003)	Local monitoring based on the load characteristics for estimating the margin to voltage instability.	Two indices for voltage stability were prposed. Namely: Voltage Stability Load Bus Index (VSLBI) and the Reactive Power Reserve Index (RPRI).	2-bus equivalent, IEEE 39-bus test system.	Monitoring of voltage collapse, reactive power reserve, and emergency control. Considers mixed loads and generator reactive power reserves.	The Recursive Least Square algorithm used requires the determination of the optimal forgetting factor parameter. It would be difficult to track fast changes online if the wrong factor is used.
15	Balamourougan *et al*. (2004)	Power flow equations using voltage magnitude and voltage angles at the buses, and the admittance matrix of the system.	Voltage Collapse Prediction Index (VCPI) for the prediction of the onset of voltage collapse.	IEEE 14-bus, 30-bus, and 118-bus systems.	Voltage collapse prediction. Bus voltage, angle and admittance matrix used as inputs.	Required the network topology information and update whenever the topology changed.
16	Verbic and Gubina (2004)	Local measurements-based method for predicting voltage collapse using consecutive measurements of apparent power at the relay point.	S Difference Criterion (SDC).	IEEE 118-bus test system.	Voltage collapse prediction and critical bus identification. The index was proposed for implementation in a protection relay.	Required additional checks to determine if the transmission line was loaded below its natural loading. At the Point of Collapse (PoC), increase in the apparent power at the sending end of the line supply the losses.
17	Smon *et al*. (2006)	A voltage stability index was derived using the Tellegen's theorem in the calculation of equivalent Thevenin parameters. Local current and voltage measurements from PMUs were assumed to be available.	Impedance Stability Index (ISI).	2-bus system and 32-bus Belgian-French network.	Voltage stability index. Easy to implement in control centres or local relay. Tellegen's theorem and adjoint networks used.	The determination of the required load current difference between two operating points (ΔImin) threshold required a lot of tests.

Table 2.6: Literature review of local measurements-based methodologies cont'd

S/N	Paper	Methodology	Proposed Index	Study Network(s)	Contribution(s)/ Implementation	Drawback(s)
18	Vournas and Sakellaridis (2007)	The technique is based on the tracking of the point where there is a continuous decline in the Low Voltage (LV) side of the ULTC transformer.	An index based on the sensitivity of the ULTC secondary voltage with respect to the tap ratios.	3-bus system.	The proposed index uses readily available measurements from ULTC transformers for detecting the onset of voltage collapse.	The scalability of the proposed technique to large power systems was not carried out.
19	Corsi and Taranto (2008)	The technique is based on the computation of the Thevenin equivalent impedance and its comparison with the equivalent load impedance using assumed measurements from PMUs.	Voltage instability risk indicator.	2549-bus Italian EHV system.	A new algorithm for the adaptive computation of the equivalent Thevenin voltage and impedance was applied.	The proposed technique was not suitable for short-term voltage instability.
20	Bedoya *et al*. (2008)	The integration of the maximum loading point and load flow calculation.	minimum Voltage Stability Margin (mVSM).	IEEE 14-bus, 30-bus, 57 bus, 300-bus test systems & 1081-bus system.	A new method for voltage stability margin using the mVSM index and the load increase direction was proposed.	Used the left eigenvectors in its calculations. This is computationally intensive and requires several iterations.
21	Wang *et al*. (2009)	Local voltage phasor from assumed PMU measurements at the two ends of an equivalent system model is used in the identification of the weakest bus and the calculation of the voltage collapse point.	Equivalent Node Voltage Collapse Index (ENVCI).	IEEE 14, 30, 57, 118-bus test systems.	Voltage collapse indicator. Power flow calculations not required.	Used a simplified equivalent system model.
22	Corsi (2010)	Maximum power transfer using the calculation of the Thevenin equivalent voltage and the Thevenin equivalent impedance.	A proximity indicator (VSI_j) Index is proposed.	2549-bus Italian Power system.	Voltage stability prediction. Suitability of the proposed index for wide area protection and voltage regulation demonstrated.	Difficult to determine the value of the threshold used for the VSI_j (t) Index.

Table 2.6: Literature review of local measurements-based methodologies cont'd

S/N	Paper	Methodology	Proposed Index	Study Network(s)	Contribution(s)/ Implementation	Drawback(s)
23	Li *et al*. (2010)	Maximum loadability and Thevenin equivalent parameters from SCADA and local measurements were used in the calculation of the Thevenin equivalent impedance and the Thevenin equivalent voltage respectively.	Thevenin equivalent impedance and equivalent voltage are used together with a predictor-corrector algorithm.	IEEE 30-bus test system and Alberta 2016-bus system.	Local parameters of bus V & I used. Predictor-corrector concept proposed to improve the accuracy of the index. Determination of the maximum power transfer limits.	The estimation of the non-linear coupling voltage relating to the mutual impedance is complex.
24	Tiwari *et al*. (2012)	Line based evaluation using power flow based on the generalized ABCD parameters. P, Q, V, δ. Magnitude and directions of the receiving end P and Q are used for the assessment.	Line Collapse Proximity Index (LCPI).	IEEE 30 and 118-bus systems.	A methodology for voltage stability assessment and weak area identification was proposed.	Required the exact model of the transmission line.
25	Tobon *et al*. (2014)	Thevenin Local Impedance Matching (LIM) solved by direct and recursive least squares algorithm using voltage magnitudes only.	Voltage Margin Indicator (VMI).	IEEE 14-bus system.	Voltage collapse detection.	The update of external network equivalent becomes difficult whenever successive measurements are identical.
26	Lee (2015)	An equivalent nodal analysis based on the reduction of an impedance matrix of a power system into a 2-bus equivalent model as seen from a reference bus.	Equivalent nodal voltage sensitivity index.	IEEE 300-bus system.	A nodal approach in the derivation of the equivalent nodal voltage sensitivity index was proposed.	The practical real-time application of this method is difficult since the admittance matrix of the network will need to be updated for any change in topology or line contingencies.

2.4.4.2 Discussion

Most of the techniques based on local measurements use Thevenin equivalents which are usually estimated using over-simplified reduced power system networks. Another limitation of the Thévenin equivalent technique is that an assumption is made that the system's topology remains the same during two consecutive sets of measurements at the local load bus as done in (Julian *et al*., 2000; Moghavvemi and Faruque, 1999; Chebbo *et al*., 1992). However, the system's topology would likely not remain the same especially system disturbances.

Also, the RLS method used for the estimation of the Thevenin equivalents requires a large data window in order to suppress transient fluctuations, and would fail if successive measurements are identical (Tobon *et al*., 2014; Vu *et al*., 1999). Furthermore, the RLS method used in Milosevic and Begovic (2003) is limited by the tuning of the forgetting factor which is required for tracking fast changes in the Thevenin parameters (Genet and Maun, 2007). This coupled with the fact that the determination of the Thevenin equivalents in real-time is very difficult, makes the on-line implementation of these methods impractical. In addition, the above-mentioned Thevenin-based methods assumed the availability of PMU measurements and did not take into account the peculiarity of PMU measurements with respect to the reporting rates and performance classes available.

2.4.5 Review of the Methodologies Based on Wide Area Measurements

2.4.5.1 Wide Area Measurement Systems

Most electric power utilities around the world use Supervisory Control and Data Acquisition (SCADA) systems to provide data telemetry and telecontrol functions. SCADA systems are typically made up of sensors, meters, dataloggers, Remote Terminal Units (RTUs), Master Terminal Unit (MTU), Intelligent Electronic devices (IEDs), and Programmable Logic Controllers (PLCs). The RTUs collect field data from the sensors, meters, dataloggers, and IEDs, and transmits them to the MTU via a communication medium.

The MTU displays the acquired data on the Human-Machine Interface (HMI), and also issues remote control signals to the field devices. Some of the communication protocols used in SCADA systems include Profibus, Modbus, DNP 3.0, IEC 60870-5-101, and IEC 60870-5-104. However, SCADA systems are limited by their slow data sampling rate, slow reporting rate, and the measurements obtained from various locations are not time synchronized at the point of acquisition.

The advent of synchrophasors has brought about the use of synchronized measurements in Wide Area Measurement Systems (WAMSs), with the possibility of higher reporting rates of up to 240 frames per second (fps) for a 60Hz system and 200 fps for a 50 Hz system. WAMS based on synchrophasor measurements provide faster sampling and reporting rates, and the measurements from the various segments of the system are synchronized to a common time reference. A typical WAMS comprises of Phasor Measurement Units (PMUs) or Intelligent Electronic Devices (IEDs) with PMU functionality, Phasor Data Concentrators (PDCs), time synchronization source e.g. GPS satellite clock, data archiver/historian, and a communication network infrastructure.

A voltage or current signal *x(t)* has a behaviour defined by (IEEE C37.118.1):

$$x(t) = X_m(t)\cos\left(\omega t + \phi(t)\right) \tag{2.42}$$

The phasor representation *X(t)* of a signal *x(t)* is given below:

$$X(t) = \left(\frac{X_m(t)}{\sqrt{2}}\right)e^{j\phi(t)} \tag{2.43}$$

$$= \left(\frac{X_m(t)}{\sqrt{2}}\right)\left(\cos\phi(t) + j\sin\phi(t)\right) \tag{2.44}$$

$$= X_r(t) + jX_i(t) \tag{2.45}$$

where X_m is the peak magnitude of the filtered synchronized measurement, ϕ is the phase angle relative to a cosine function at the nominal system frequency ω, X_r and X_i are the real and the imaginary parts of the phasor measurement respectively.

From (2.42), a sinusoidal signal can be re-written as:

$$x(t) = X_m(t)\cos(2\pi f_0 t + \phi(t)) \tag{2.46}$$

The deviation from the nominal frequency $g(t)$ is given as:

$$g(t) = f(t) - f_0 \tag{2.47}$$

where f is the actual frequency, f_0 is the nominal angular system frequency.

The synchrophasor estimates over time are derived as follows (IEEE C37.118.1-2011; IEEE C37.118-2005):

$$x(t) = X_m(t)\cos\left(2\pi\int f(t)\,dt + \phi\right) \tag{2.48}$$

$$x(t) = X_m(t)\cos\left(2\pi\int\left(f_0 + g(t)\right)dt + \phi\right) \tag{2.49}$$

$$x(t) = X_m(t)\cos\left(2\pi f_0 t + 2\pi\int\left(g(t)\,dt + \phi\right)\right) \tag{2.50}$$

The phasor representation of equations (2.48)-(2.50) is:

$$X(t) = (X_m(t)/\sqrt{2})\, e^{j(2\pi \int g(t)dt + \phi)} \tag{2.51}$$

If $g(t) = \Delta f$ is equal to the deviation from the nominal system frequency and is constant, then

$$\int g(t)dt = \int \Delta f dt = \Delta f t \tag{2.52}$$

Thus, the synchrophasor measurement is given as:

$$X(t) = (X_m/\sqrt{2})\, e^{j(2\pi \Delta f t + \phi)} \tag{2.53}$$

The processing steps performed by a PMU are defined in the IEEE Std. C37.118.1™-2011 reference model as shown in Figure 2.11.

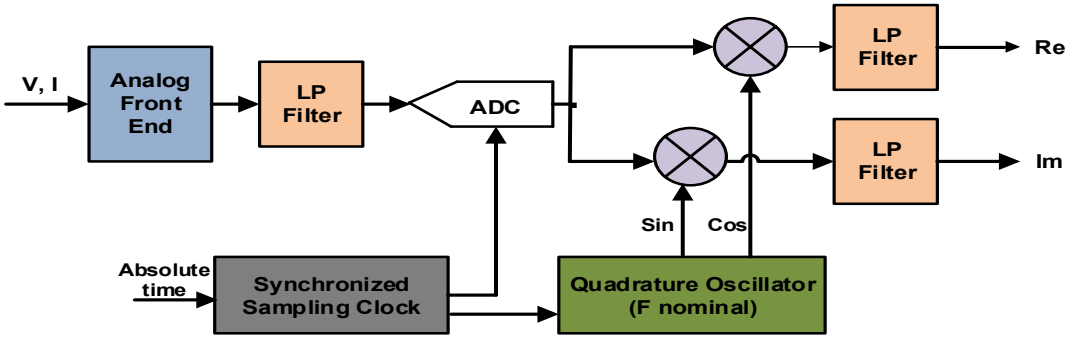

Figure 2.11: **Signal processing steps of the PMU reference model (IEEE Std. C37.118.1 TM -2011)**

In the reference model, a fixed frequency sampling synchronized to an absolute time base is used. This is followed by the complex multiplication of the sampled input with the nominal frequency carrier. Low-pass filters are then applied to the real and imaginary outputs of the complex demodulator. The outputs from the low-pass filters are the real and imaginary parts of the synchrophasor estimates respectively.

One of the concepts introduced in the IEEE Std. C37.118™-2005 is the performance compliance index known as the Total Vector Error (TVE). According to the standard, the TVE must be less than 1% under steady-state conditions. The TVE is defined as the measure of the difference between the theoretical synchrophasor measurement and the estimated measurement by the PMU for the same time instant.

This is given as (IEEE C37.118-2005):

$$TVE(n) = \sqrt{\frac{\left(\hat{X}_r(n) - X_r(n)\right)^2 + \left(\hat{X}_i(n) - X_i(n)\right)^2}{\left(X_r(n)\right)^2 + \left(X_i(n)\right)^2}} \tag{2.54}$$

where $\hat{X}_r(n)$ and $\hat{X}_i(n)$ are the estimates obtained from the PMU. $X_r(n)$ and $X_i(n)$ are the theoretical values of the input sinusoid at the time instant *(n)*.

Similarly, the concept of Frequency Error (FE) and Rate of Change of Frequency (ROCOF) Error (RFE) was introduced in the IEEE Std. C37.118.1-2011 to evaluate frequency and ROCOF measurements. FE is defined as the measure of the absolute of the error between the theoretical frequency and the measured frequency for a particular time instant. RFE on the other hand, is the measure of the absolute of the error between the theoretical ROCOF and the measured ROCOF for a particular time instant.

This is given as (IEEE C37.118.1-2011):

$$FE == \left| f_{true} - f_{measured} \right| = \left| \Delta f_{true} - \Delta f_{measured} \right| \tag{2.55}$$

$$RFE == \left| (df/dt)_{true} - (df/dt)_{measured} \right| \tag{2.56}$$

The maximum permissible TVE, FE, and RFE for steady-state and dynamic conditions can be found in Tables 3-8 of Sub-clause 5.5 of the C37.118.1-2011 standard (IEEE C37.118.1-2011), while the modification (amendments) of some of the performance requirements can be found in (IEEE C37.118.1a-2014).

2.4.5.2 Synchrophasor Standards

The first standard for synchrophasor measurements was developed after the success recorded with the first PMU prototype reported in (Phadke and Thorpe, 2008). The drafting of International standards for synchrophasors was as a result of the need to support the development of PMUs and their ancillary equipment.

Also important, was the need to establish a common platform for vendors to use in the design and manufacture of synchrophasor devices. Some relevant standards relating to synchrophasor measurements from PMUs and their various applications are provided in the proceeding subsections.

IEEE Std. 1344-1995

The first synchrophasor standard for power systems was the IEEE Std. 1344-1995 (IEEE, 1995). The standard was intended to introduce synchrophasors and define the basic concepts of synchrophasor measurements. It defined the synchronizing input, the computation of phasors from sampled analogue measurements, and the phasor measurements data outputs.

However, the IEEE Std. 1344-1995 did not specify the response time of the PMUs, accuracy requirements, and the reference model for computing the phasors. Also, the IEEE Std. 1344-1995 did not include the command frame for dialogues between the synchrophasor PDCs (Clients) and the PMUs (Servers). Only the data frame, header frame, and configuration frame were defined. The Second of Century (SOC) timing is calculated as the UTC time in seconds from the midnight of the 1st of January, 1900.

IEEE Std. C37.118-2005

The IEEE Std. 1344-1995 was reaffirmed in 2001 and replaced by the IEEE Std. C37.118-2005 (IEEE, 2005). The IEEE Std. C37.118-2005 provides additional clarification for phasor and synchronized phasor definitions.

Also, the standard introduced the calculation of Total Vector Error (TVE) to verify the compliance of phasor estimates with theoretical equivalents for the same time instants. Furthermore, compliance tests and data reporting rates that are submultiples of the nominal system frequency were defined. The message formats in the IEEE Std. C37.118 was updated from the IEEE Std. 1344-1995 to improve the exchange of information with other systems in higher hierarchies (regional PDCs). This includes the addition of the sync, frame size, and station identification fields to the data, configuration, header, and command message types respectively. The data frame also includes an additional field for analogue data (IEEE, 1995). The SOC timing is calculated as the UTC time in seconds from the midnight of the 1st of January, 1970.

IEEE Std. C37.118.1-2011/C37.118.2-2011

The current IEEE Std. C37.118.1™-2011 for synchrophasor measurements replaced the IEEE Std. C37.118.1™-2005 which was introduced in 2005. The IEEE Std. C37.118.1™-2011 is divided into two parts. These are: (i) IEEE C37.118.1™-2011 standard for synchrophasor measurements; and (ii) IEEE C37.118.2™-2011 standard for synchrophasor data communication.

The IEEE Std. C37.118.1-2011 is divided into 5 clauses and 6 annexes (IEEE Std. C37.118.1, 2011). While the IEEE Std. C37.118.2-2011 has 6 clauses and 6 annexes (IEEE Std. C37.118.2, 2011). The IEEE Std. C37.118.1-2011 has clauses that cover the scope and the needs of the standard, the definition of the measurements, the measurement requirements, the quantification of the measurement, the testing of the measurements, and the definition of the accuracy limits. The 6 annexes provide information on the bibliography, the time tagging, the algorithms used to confirm the performance requirements, time synchronization, TVE, and the measurement of generator internal voltages and power angles.

The IEEE Std. C37.118-2005 was modified in the IEEE Std. C37.118.1 to include new definitions for the phasors, frequency, and Rate of Change of Frequency (ROCOF), Frequency Error (FE), ROCOF Error (RFE), performance requirement for dynamic conditions, and the introduction of two performance classes (the M-Class and the P-Class). The P-Class was defined for applications that require fast response (e.g. protection applications), while the M-Class was defined for applications that require higher accuracy (e.g. metering applications). TVE requirements and the compliance tests are expanded in this standard by adding new temperature and dynamic performance tests respectively.

The IEEE Std. C37.118.2-2011 covers the scope of the standard, gives background information on synchrophasor measurements, synchrophasor measurement systems, communication protocol, and message formats. The annexes contain information on the bibliography, Cyclic Redundancy Check (CRC), communication bandwidth, message format, message mapping, and communication methods using Internet Protocol (IP).

Table 2.7: Comparison between the IEEE Std. C37.118-2011 and IEEE Std. C37.118-2005

S/N	C37.118-2011	C37.118-2005
1	Measurements and data transfer requirements are separated and defined in 2 standards. C37.118.1 - 2011 and C37.118.2-2011.	A single standard (C37.118-2005) is used to define both measurements and data transfer requirements.
2	C37.118.1 defines additional measurements comprising of the frequency and Rate Of Change Of Frequency (ROCOF) measurements respectively.	Frequency and ROCOF measurements not defined.
3	Compliance tests comprising of the Frequency error (FE), Rate of Frequency Error (RFE), and Total Vector Error (TVE) are defined.	Only TVE is defined.
4	Defines operation and measurement requirements under dynamic conditions.	Defines only for steady-state operation.
5	Two classes: P and M defined.	Level 0 and level 1 defined.
6	Additional configuration frame type (CFG-3) introduced.	Only 2 configuration frame types are defined (CFG-1 and CFG-2).
7	Provides the foundation for harmonization/compatibility with IEC 61850 standard.	Does not provide the foundation for harmonization of IEC 61850.

The IEEE Std. C37.118.2-2011 defines the synchrophasor data transfer requirements, clarifications, and modification regarding data transfer. The standard presents the structure of the message, the definition of the words used in the message, and the specification of the numbers of bytes per word. Also, the standard defines the time quality, and the organization of the data, configuration, header, and command frames respectively.

Modifications to the IEEE Std. C37.118.1-2011 were published in (IEEE Std. C37.118.1a-2014). This was done in order to correct inconsistencies, provide further

clarifications, and remove some of the limitations introduced by the IEEE Std. C37.118.1-2011. Table 2.7 gives a comparison of the IEEE Std. C37.118-2005 and the IEEE Std. C37.118.1-2011.

IEC 61850-90-5

The IEEE C37.118-2005 was primarily split into the IEEE C37.118.1-2011 and IEEE C37.118.2-2011 in order to be able to transport synchrophasor measurements using the IEC 61850 framework. The IEC 61850-90-5 is an International ElectroTechnical Commission (IEC) Technical Report (TR) released in 2012 for the transportation of synchrophasor information according to the IEEE Std. C37.118.

The IEC 61850 was considered for synchrophasor application because of its wide acceptance and the desire to have a communication method compliant to the principles of the IEC 61850 standard. Thus, plans were made to develop compatible methods within the IEC 61850 through the commissioning of Working Group (WG) 10 for the integration of synchrophasor transport over IEC 61850. This resulted to the IEC Technical Report (TR) 61850-90-5 (Falk, 2013; IEC 61850-90-5, 2012).

IEC 61850-90-5 specifies ways for exchanging synchrophasor measurements between the PMUs and the PDCs, and between control centre applications. The synchrophasor data are transported based on IEC 61850 principles. The IEC Technical Committee (TC) 57 WG10 chose the existing measurement logical node (MMXU). In addition to the use of an existing IEC 61850 logical node (MMXU), it was necessary to specify the performance class of the measurements as either Protection Class (P-Class) or Measurement Class (M-Class) as defined in IEEE C37.118.1. To accomplish this, the IEC 61850 Calculation Method (ClcMth) was extended to include P-Class and M-Class (Falk, 2013; IEC 61850-90-5, 2012). Also, the existing MMXU definition contained data objects that represented the voltage and current measurements, as well as frequency. However, IEC 61850 did not have provisions for ROCOF. Therefore, the IEC TR 61850-90-5 added the data object HzRte (Hertz Rate) to the MMXU logical node.

IEC 61850-90-5 specifies the use of routed GOOSE for routing event data, and routed Sampled Values (SVs) for routing periodic data. The IEC 61850-90-5 session protocol is capable of conveying groups of GOOSE or SV Application Protocol Data Units (APDUs) in a single Session Protocol Data Unit (SPDU). A means for the secure tunnelling of Ethernet-based IEC 61850 GOOSE and SV packets to facilitate the exchange between substations and control centres for the currently existing IEC

61850 GOOSE and SV messages is provided. Authentication procedures were also established to provide adequate communication security for synchrophasor data.

IEEE Std. C37.242-2013

The IEEE Std. C37.242-2013 is a guide for PMU synchronization, calibration, testing, and installation (IEEE C37.242, 2013). The guide provides techniques detailing the role of time synchronization, various time synchronization sources, time synchronization accuracy, and availability. Also, the common causes of timing errors, the vulnerability of satellite-based timing system to Radio-Frequency Interference (RFI)/disruption, performance testing and experimental tests for time synchronization sources were presented.

Also, IEEE Std. C37.242-2013 provides the procedures to be followed during PMU testing, calibration, quality conditions, and the accuracy class that must be fulfilled by the test/calibration equipment. This covers the functional factory acceptance testing, installation and commissioning tests, periodic maintenance, conformance testing, and interoperability testing with other PMUs and with PDCs.

Furthermore, the IEEE Std. C37.242-2013 gives guidance on the installation design, pre-installation procedures, selection and access to the power system instrument transformers, time source, and the communication infrastructure.

IEEE Std. C37.244-2013

The performance requirements of PDCs are covered in the IEEE Std. C37.244-2013. The IEEE Std. C37.244-2013 provides guidance on the functions and requirements of PDCs in terms of PDC latency, supported I/O streams, communication interface, transport protocol, time-alignment of PMU measurements, and error handling (IEEE C37.244, 2013). A description of the functional requirements of the PDC with respect to the concentration of synchrophasor data, data forwarding, data processing and reporting rate conversion, protocol conversion, data communication, and cyber security is provided.

Cyber security issues relating to availability/prevention of denial of service attacks, integrity and authenticity through the use of digital signatures/authentication codes, and confidentiality by using encryption/access control are discussed. Practical outlines for functionality testing of PDCs are provided in the standard. The tests covered include conformance testing, design testing, type testing, interoperability testing, commissioning testing, post-commissioning (field) testing, cyber security testing, and application-specific testing.

2.4.5.3 Review of Publications on Wide Area Measurements-Based Methodologies

A review of the literature on techniques using wide area measurements-based methodologies for voltage stability assessment showed that various methods comprising of sensitivity analysis, Thevenin-based methods, and other computational intelligence methods have been proposed. These methods and some related literature are presented below.

Sensitivity Analysis

The reactive power reserve across widely dispersed reactive power sources in a power system can be used as the basis for voltage stability assessment. It has been shown in (Ajjarapu, 2006; Van Cutsem and Vournas, 1998; Kundur, 1994; Taylor, 1994; Avramovic and Fink, 1992) that the depletion of the Reactive Power Reserves (RPRs) in a system directly impact the voltage stability margin.

Avramovic and Fink (1992) suggested a real-time reactive power security monitoring method using the available VAR margins of all the zones within a given power system. The zones in this context were defined as a group of one or more tightly coupled generator buses, together with the union of the sets of load buses that they provide reactive power support (voltage control) to. The idea behind the method was that voltage instability has a local origin, and it is directly related to the availability of reactive power sources in the system.

The reactive power reserves available on key generators, synchronous generators and Static VAR Compensators (SVCs) are sensitive indicators of the system stress. One of such monitoring schemes based on SCADA measurements using the key generators and Static VAR Compensators (SVC) is in operation at the Bonneville Power Administration (BPA) system (Taylor and Ramanathan, 1998). Another method using VAR reserve level on key generators was introduced in (Bao *et al.,* 2003).

The need to determine the effective reactive power reserves was emphasized in (Bao *et al.,* 2003; Taylor and Ramanathan, 1998) taking into account that reactive power sources must be close to the affected area to be effective. Also, it is necessary to find a relationship between the reactive power reserves in a system and voltage security. This issue was elaborated in (Leonardi and Ajjarapu, 2008), where various definitions for reactive power reserve were discussed. The work presented in (Leonardi and Ajjarapu, 2008) suggested the use of statistical multi-linear regression models to transform variations in reactive power reserves into direct information about the system's voltage stability margin.

Techniques analyzing the voltage stability of a power system using load Reactive Power Reserve (RPR) were presented in (Feng *et al.,* 2005; Song *et al.,* 2005; Schlueter, 1998). Schlueter (1998) defined a reactive reserve basin for each zone as the sum of the exhausted reactive reserves at the minimum of the V-Q curve. After a disturbance, the remaining percentage of the basin reactive reserve was used as a measure of the system's proximity to voltage instability. The reactive reserve based Contingency Constrained Optimal Power Flow (RCCOPF) presented in Song *et al.* (2005) was proposed to enhance the Voltage Stability Margin (VSM) of the power system. The technique was used to provide preventive control by using a decomposition method. Active power margin of the post-disturbance state was determined using the modified continuation power flow method.

The RPR method in Feng *et al.* (2005) managed the RPRs in critical areas based on the optimal power flow, and consequently improved the system's voltage stability based on this. A two-level Benders decomposition technique was used for the initial base case, and for a set of modified stressed (contingency) case studies. Reactive power reserves from both load and generation perspectives were discussed in (Ruiz and Sauer, 2006). Based on the observation that both reactive reserves are heavily dependent on the network topology, load demand, generation, and system control characteristics. Ruiz and Sauer (2006) emphasized why further work in the definition, computation, valuation and planning of RPRs is necessary. Analysis using multiport Thevenin equivalents was applied in the evaluation of a system comprising of several generators and loads.

An application based on wide area monitoring using synchrophasor measurements was implemented at the BPA (Martin, 2007). The application provided a means for transient stability detection, voltage support system using capacitors, and the use of phase angle and frequency for wide area protection and control. Three voltage stability indices based on synchrophasor measurements were investigated in Donolo *et al.* (2009). These include the Incremental Reactive Power Cost and Participation Factors (IRPC), the Incremental Load Cost (ILC), and the Power Transfer Margin (PTM). The indices provided the system's proximity to voltage collapse and the optimal load shedding scheme to implement.

Glavic and Van Cutsem (2009) presented a technique in which sensitivity analysis was performed on algebraic equations fitted onto sampled states. Synchrophasor measurements were used to identify the point when the real power at the buses passed through the maximum loadability point.

Gu and Wan (2010) proposed a linearized voltage stability index based on the determinant of the load state matrix. Measurement-based dynamic load-type comprising of an induction motor in parallel with a constant impedance model were used. The proposed technique assumed the availability of PMU measurements. The advantages of the proposed index include full linearity and less computation burden since there was no need for computing the network equivalents at each of the load buses.

Sodhi *et al.* (2012) proposed two criteria in the formulation of a Synchrophasor Based Voltage Instability Monitoring Index (SVIMI). The inputs used by the proposed index include the bus voltage and the voltage deviation at the system buses. A weighted sum of the two criteria was then applied in the derivation of the SVIMI. Leelaruji *et al.* (2015) presented a sensitivity-based technique derived from changes in the phasor voltages with respect to the real and reactive powers. RT-Lab was used in a hardware-in-the-loop simulation with a PMU. However, the article does not provide the relevant configuration settings and information pertaining to the PMU model used and the impact of communication delay on the technique presented.

Three generator-derived voltage stability assessment indices implemented in real-time were proposed in (Adewole and Tzoneva, 2015f; 2015c; 2014). These indices were derived from the reactive power at the generators, generator field currents, and the generator stator currents for a large interconnected system. Synchrophasor measurements from actual PMUs compliant to the IEEE C37.118 standard were used. Also, details regarding to the PMU configuration and synchrophasor communication were presented.

Thevenin-Based Method

Three voltage stability indices for the estimation of the system's margin to its maximum loadability limit were derived by Gong *et al.* (2006) using the real, reactive, and apparent powers in a system. The indices were initially derived for a two-bus equivalent system, and afterwards extended to cover multiport systems. Pordanjani *et al*. (2013) described a Channel Components Transform (CCT)-based method used in the decoupling of large interconnected systems into a multi-port Thevenin model. Liu and Chu (2014) proposed a modified single-port technique based on the reactive power of the equivalent system. The Thevenin equivalent impedance of the equivalent system was obtained using a mitigation factor derived from the extended Ward-type equivalent, and can be computed from two consecutive synchrophasor samples.

The method by Londono *et al*. (2014) used the concept of the Relative Electrical Distance (RED) between the nearest generator to the load bus was used in the calculation of the voltage drop across the Thevenin impedance. The Thevenin impedance matching method was used alongside a cubic spline extrapolation technique in the estimation of the voltage stability margin in a power system in Su and Liu (2015). Similarly, a model-based Thevenin method for the estimation of the post-contingency voltage stability status of the power system was proposed in Yuan and Li (2015).

Computational Intelligence Method

The use of Decision Trees (DTs) in the detection of the onset of voltage instability was considered in (Adewole and Tzoneva, 2014b; Khoshkhoo and Shahrtash, 2011; Diao *et al.* 2009; Khatib *et al.* 2004; Nuqui *et al.* 2001, Geurts and Wehenkel, 2000; Van Cutsem *et al.* 1993). DTs were used in voltage stability assessment in the detection of the onset of voltage instability and the proximity to voltage collapse using input attributes (predictors) obtained from direct measurements.

Beiraghi and Ranjbar (2013) described an approach based on a DT algorithm which classified the system status into ‘secure’ or ‘insecure’ states as the case may be. Bagging and adaptive boosting algorithms were used in growing the decision trees. Bahmanyar and Karami (2014) presented an Artificial Neural Networks (ANN) method for estimating the system’s margin to the maximum loadability point. The numbers of inputs required for training the ANN were reduced through the application of a Gram-Schmidt orthogonalization method.

Similarly, Hashemi and Aghamohammadi (2013) proposed an approach for predicting the system’s proximity to voltage collapse using Wavelet Transform (WT) and ANNs. The features used were extracted from the voltage profile using WT and Principal Component Analysis (PCA). Suganyadevi and Babulal (2014) suggested a Support Vector Machine (SVM) for estimating the system’s margin to its maximum loadability limit from a current operating point. The performance of the SVM was demonstrated for a normal loading condition and for different loading conditions.

2.4.5.4 Discussion

A summarised comparison of the various methods under wide area measurement-based voltage stability assessment is provided in Table 2.8. Asides a few publications (Adewole and Tzoneva, 2015f; 2015c; 2014b; Leelaruji *et al.* 2015; Donolo *et al*. 2009), the existing techniques in the literature based on voltage stability assessment using wide area measurements did not make use of actual synchrophasor measurements from PMUs.

Rather, time-domain measurements from power system simulation packages like MATLAB/Simulink, PSCAD, PSAT, SIMPOW, and DSA-Power Tools, were used. However, what distinguish synchrophasor measurements from other measurement-types are the estimation algorithm, filter types for the performance classes, reporting rates, data transfer, performance for steady-state and dynamic conditions, and compliance to international standards such as the IEEE C37.118/IEC 61850-90-5.

Practically, it would be difficult to implement wide area-based voltage stability assessment without measurements that are time-stamped at the point of acquisition. These synchronized time-stamp measurements are required in order to have an exact snapshot of a system at any given instant. Consequently, it will be difficult concentrating and correlating non time-stamped measurements for any meaningful analysis. Therefore, some of the existing methods in the literature might fail since they were not tested with actual synchrophasor measurements from PMUs.

In view of the foregoing, this thesis proposed a wide area measurement-based voltage stability assessment method using synchrophasor measurements from actual PMUs.

Table 2.8: Literature review of wide area measurements-based methodologies

S/N	Paper	Methodology	Proposed Index	Study Network(s)	Contribution(s)/ Implementation	Drawback(s)
1	Van Cutsem *et al*. (1993)	Two techniques for preventive and emergency voltage stability conditions were proposed using decision trees.	Decision Trees (DTs) were used for classifying the system's status into 'secure' and 'insecure' states.	Simulated French EHV system.	DT successfully applied in classifying the system's status using attributes from bus voltages, line flow, generated power, and reactive power reserves.	The proposed technique did not consider the use of DT for predicting the system's margin to voltage collapse.
2	Nuqui *et al*. (2001)	Bus angular differences obtained from synchrophasors are used in the prediction of the system status.	DTs were used for predicting the system's status with respect to voltage collapse.	360-bus AEP system.	The use of angular difference obtained from PMU measurements was successfully incorporated into a DT algorithm for classifying the system's status.	The proposed technique did not consider the use of DT for predicting the system's margin to voltage collapse.
3	Song *et al*. (2003)	The proposed method was based on load reactive power reserve monitoring.	Reactive Reserve-based Contingency Constrained Optimal Power Flow (RCCOPF) index.	IEEE 118-bus test system.	Voltage stability enhancement. Method uses a decomposition technique based on reactive reserve to mitigate the violations of the reactive reserve for severe contingencies.	The proposed technique assumed a constant weighing factor of 1000.0 for the generators and synchronous condensers. This implies that all these equipment were given the same priority rating irrespective of their output capability.
4	Khatib *et al*. (2004)	Transmission line reactive power flow and bus angular difference were used in the prediction of the system status.	DTs were used for predicting the system's status w.r.t. voltage collapse.	1097-bus system.	Transmission line reactive power flow and angular difference were successfully incorporated into a DT algorithm for classifying the system's status.	The proposed technique did not consider the use of DT for predicting the system's margin to voltage collapse. The bus voltage angles are assumed to be from PMUs.
5	Feng *et al*. (2005)	The proposed method was based on load reactive power reserve monitoring using Bender's decomposition.	Voltage stability index based on the optimal power flow in the system.	Reduced WECC system.	Voltage stability and reactive reserve management based on optimal power flow. The results presented showed that the method was capable of improving static and dynamic voltage stability.	The application of the proposed technique in a practical system would be tedious since several iterations would need to be carried out. There is also a possibility that the optimization problem could fail to converge.
6	Gong *et al*. (2006)	Equivalent Thevenin voltage and Thevenin impedance using synchrophasor measurements.	Voltage Stability Index (VSI) using P margin, Q margin, and S margin respectively.	10-bus & IEEE 30-bus test systems.	Voltage collapse prediction and critical bus identification. PMUs used.	Requires the calculation of the equivalent Thevenin voltage and impedance.

Table 2.8: Literature review of wide area measurements-based methodologies cont'd

S/N	Paper	Methodology	Proposed Index	Study Network(s)	Contribution(s)/ Implementation	Drawback(s)
7	Diao *et al*. (2009)	Synchrophasor-based method using DTs with voltage and current magnitudes, voltage phase angles, and branch reactive power inputs.	DT were used for predicting the system's status w.r.t voltage collapse.	American Electric Power (AEP) 2414-bus system.	Voltage security assessment. Proposed for online application.	The proposed technique did not consider the use of DT for predicting the system's margin to voltage collapse. Also, the assumed PMU measurements were conventional measurements from PSAT simulations; measurements from actual PMU were not used.
8	Genet and Maun (2007)	Bus voltage measurements were used in the computation of an index for voltage stability analysis.	Voltage Stability Index (VSI_k).	Belgian-French network.	Voltage stability monitoring.	Did not take into account all the generators in the system rather it used the closest generator to the load in the computation of the Thevenin voltage. The measurements were assumed to be from PMUs.
9	Glavic and Cutsem (2009)	Synchrophasor-based method using sensitivity analysis derived from the gradient of the reactive power and the inverse Jacobian.	Sensitivity-based using Jacobian information (SQ_{gqj}).	5-bus system.	Voltage instability detection. Classified PMU based VSI into: local measurements and observability-based. Long-term dynamics of load tap changer and field current limiter were considered.	Only long term voltage stability was considered. Short-term dynamics were assumed to be at equilibrium. The measurements were assumed to be from PMUs.
10	Donolo *et al*. (2009)	Synchrophasor-based method using derived indices.	Four indices were used. Namely: The reactive power margin, the incremental reactive power cost/participation factors, the incremental load cost, and the power transfer margin.	Natal power system network.	The voltage stability indicator was used in arming a SIPS for load shedding.	Description of the test platform used was not given.

Table 2.8: Literature review of wide area measurements-based methodologies cont'd

S/N	Paper	Methodology	Proposed Index	Study Network(s)	Contribution(s)/ Implementation	Drawback(s)
11	Gu and Wan (2010)	Wide area measurements from PMUs using the Determinant (Ai) of the Jacobian matrix.	Motor Voltage Stability Index (MVSI).	New England 39-bus test system.	Voltage stability index proposed. The dynamic model of induction motor was considered. Suitable for wide area control.	Required Jacobian matrix and the computation of the determinant of the matrix. The measurements were assumed to be from PMUs.
12	Leonardi and Ajjarapu (2011)	The method is based on generator reactive power reserve boosting and real-time voltage stability margin control.	Voltage Stability Margin (VSM).	IEEE 30-bus test system and 1648-bus system.	Multilinear Regression Models (MLRMs) used in the prediction of the system's margin to voltage collapse.	Feature selection is difficult with MLRM. Also, MLRMs are known to be sensitive to outliers and might give optimal estimate of the unknown parameter.
13	Sodhi *et al*. (2012)	Bus voltages from synchrophasors were used in the derivation of two voltage stability indices based on the deviation from the reference value and on the consecutive voltage deviation.	Two indices proposed. Voltage Deviation from its Reference (DFR) and the Consecutive Voltage Deviation (CVD).	New England 39-bus test system and Indian 246-bus system.	Voltage instability monitoring.	Only long term voltage stability was considered. The measurements were assumed to be from PMUs.
14	Beiraghi and Ranjbar (2013)	Synchrophasor-based method using DTs with voltage and current magnitudes, real and reactive powers, and the information of the faulted element.	DT was used for predicting the system's status w.r.t. voltage collapse.	IEEE 118-bus test system.	Voltage security assessment. Proposed for online application. Ensembles of DT were also used.	The proposed technique did not consider the use of DT for predicting the system's margin to voltage collapse. Also, simulated measurements were used, not actual PMUs.
15	Dasgupta *et al*. (2013)	Synchrophasor-based short-term voltage stability monitoring using Lyapunov exponents.	Stability criteria based on Lyapunov exponents.	IEEE 162-bus test system.	Synchrophasor-based Lyapunov exponents successfully applied for voltage stability monitoring.	Proposed technique was not validated using actual measurements from real PMUs. Also, proposed technique might fail when applied for long-term voltage stability conditions.
16	Hashemi and Aghamohammadi (2013)	Wavelet Transform (WT) and Artificial Neural Network (ANN).	Computational intelligence method using a Voltage Stability Analyzer Artificial Neural Network (VSANN) index.	New England 39-bus test system.	Online voltage stability assessment. Not affected by changes in topology.	Offline training of ANNs required

Table 2.8: Literature review of wide area measurements-based methodologies cont'd

S/N	Paper	Methodology	Proposed Index	Study Network(s)	Contribution(s)/ Implementation	Drawback(s)
17	Leelaruji *et al*. (2015)	Sensitivity based technique using changes in the phasor voltages w.r.t. real and reactive powers.	Sensitivity-based index.	Equivalent 5-bus system.	Lab-scale testbed implemented.	A 5-bus test system was used. Scalability of the proposed technique to large systems not demonstrated. Also, thresholds are required for the voltage instability indicator.
18	Liu and Chu (2014)	Measurements-based indicator using ward-type equivalents and reactive power response factor.	Synchrophasor Long Term Voltage Stability Indicator (SLVSI).	IEEE 13-bus and IEEE 37-bus radial test feeder systems.	Voltage stability assessment in the presence of renewable energy sources was considered.	Measurements used are not from actual PMUs.
19	Londono *et al.* (2014)	A Thevenin based method using the voltage measurements and the system's topology information was proposed for the estimation of the system's voltage stability margin. The concept of the relative electrical distance of the nearest generator to the load bus of interest was used in the computation of the proposed index.	Simplified Voltage Stability Index (SVSI).	IEEE 30-bus and IEEE 118-bus test systems.	The concept of the relative electrical distance of the nearest generator to the load bus of interest is used to calculate the voltage drop on the Thevenin impedance.	It is cumbersome to calculate the relative electrical distance to every load bus in the system. Also, approximations relating to the use of the Thevenin algorithm often lead to over-simplification. The availability of PMU measurements was assumed.
20	Su and Liu (2015)	A single-port Thevenin equivalent impedance matching method combined with cubic spline extrapolation was used in the estimation of the voltage stability margin.	The voltage stability margin is based on the Thevenin impedance and the load impedance.	IEEE 30-bus, IEEE 118-bus, and IEEE 300 bus test systems.	A Thevenin based method and extrapolation technique was used in the estimation of the voltage stability margin in a power system.	The availability of PMU measurements was assumed. Also, actual results from real-time implementation were not presented.
21	Yuan and Li (2015)	A voltage stability assessment method based on the system model is proposed for estimating the post-contingency status of the power system.	Sensitivity-based index.	IEEE 14-bus, IEEE 39-bus, and IEEE 118-bus test systems.	A model-based sensitivity method was applied in the estimation of the post-contingency status of the power system.	The availability of PMU measurements was assumed. The computation algorithm used is not suitable for real-time applications.

2.5 Chapter Summary

This Chapter has introduced the fundamental concept of power system stability with particular focus on voltage stability. The various causes of voltage instability were discussed with respect to the impact of system loading and system components. The classification of power system voltage stability according to the scale of the disturbance and the time reference were presented. Also, some of the voltage instability incidents that occurred in various parts of the world were discussed.

Voltage stability assessment techniques and stability indices were afterwards extensively reviewed. The various indices proposed in the literature were categorized into three main groups and subsequently discussed under these headings. P-V and V-Q curves are the most commonly used methods in utilities for system planning and operational studies related to voltage stability analysis. In recent times, many utilities are beginning to participate in research relating to the application of synchrophasor measurements from PMUs for wide area stability assessment, protection and control.

Chapter Three presents a review of the literature on wide area protection and control. This would be discussed under System Integrity Protection Schemes (SIPSs) incorporating transformer tap-changer control (ULTC-SIPS) and under-voltage load shedding (UVLS-SIPS) algorithms respectively.

CHAPTER THREE
SYSTEM INTEGRITY PROTECTION SCHEMES

3.1 Introduction

Protective relays are often inadequate for the task of protecting the system from system-wide abnormal conditions. This is because the configuration settings on protective relays are primarily for the local protection of a specific equipment based on predetermined static system conditions and configuration settings. However, the system conditions may change as a result of load variation, topology changes, and cascading contingencies. This implies that the configuration settings previously used in the protective relays would fall outside the maximum/minimum values used in their configuration. Thus, the protective relays may mis-operate when the overall system condition changes, and would be incapable of ensuring the security of the power system from system-wide disturbances.

Wide area protection and control schemes are required in the protection of the power system from system-wide disturbances. For a centralised protection/control scheme, this involves the use of measurements from geographically separated sections of the interconnected power system, and the transmission of these system-wide measurements to a control centre for system monitoring (situational awareness) and telecontrol (the issuance of the control signal) to the field actuating devices.

This Chapter presents an introduction to System Integrity Protection Schemes (SIPSs), the classification of SIPSs into various types, the functional elements of SIPSs, and the implementation of various SIPSs. Also, the Chapter gives a thorough review of the existing literature on transformer Under-Load Tap-Changer (ULTC) control and Under-Voltage Load Shedding (UVLS) schemes respectively. Furthermore, industrial use cases around the world are presented.

3.2 System Integrity Protection Schemes

Defence actions against power system instabilities can be generally classified under preventive and corrective actions respectively. Preventive actions are used in pre-contingency situations to increase the system security margin. Corrective actions on the contrary, are initiated in the post-contingency state in order to restore the system stability to its pre-contingency or an acceptable post-contingency margin. Corrective actions for system-wide disturbances are often implemented using System Integrity Protection Schemes (SIPSs) (Moors *et al*., 2000).

SIPSs belong to the class of automated remedial actions/Special Protection Schemes (SPSs) designed to detect certain predetermined system conditions (abnormal system conditions) that have a high probability of jeopardising the secure/reliable operation of the power system. Some sort of pre-planned remedial action deemed as appropriate for the preservation of the integrity of the power system are afterwards initiated to counteract the observed abnormal condition in a controlled manner (Madani *et al*., 2010; Savulescu, 2009; Anderson and LeReverend, 1996).

3.2.1 Classification of System Integrity Protection Schemes

SIPSs can be classified based into a number of groupings. These include (Madani *et al*., 2010; Savulescu, 2009; Horowitz *et al*., 2008; Moors *et al*., 2000):

- Classification according to the architecture: flat and hierarchical schemes.
- Classification according to the location of the controller: centralized and distributed schemes.
- Classification according to the input parameters used: event-based and response-based schemes.
- Classification according to the decision-making process: rule-based and algorithmic-based schemes.
- Classification according to the control design: closed-loop and open-loop schemes.

For the flat architecture SIPS, the measurement and decision-making is carried out at the same location. The hierarchical architecture SIPS involves the use of a multi-layer measurement and decision-making process whereby information is transmitted to multiple locations within the power system, local SIPS, and a regional/national SIPS. Figure 3.1 (Horowitz *et al*., 2008) further illustrates the flat and hierarchical SIPS classification.

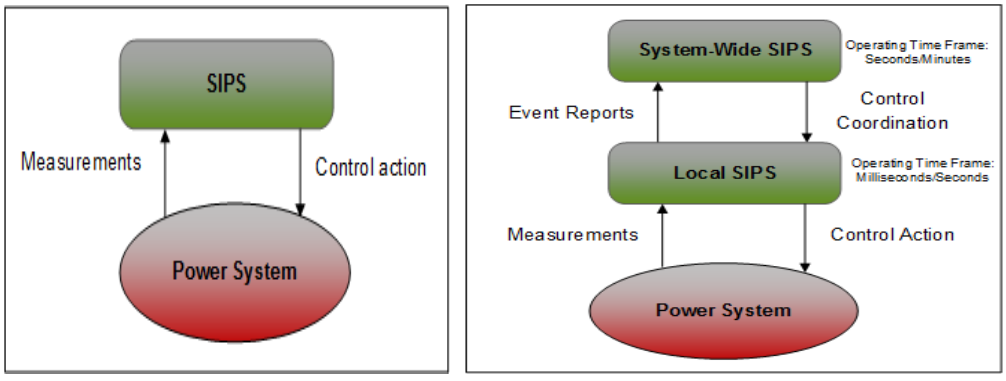

(a) **(b)**

Figure 3.1: System integrity protection scheme (a) Flat architecture; and (b) Hierarchical architecture (adapted from Horowitz *et al.,* 2008)

The centralized SIPS refers to the system protection schemes whereby information from remote field devices are transmitted to a central location via a communication infrastructure. The decision-making algorithm of the SIPS is implemented in a

controller at the central location, and the signal for the corrective action is issued from the control centre. For distributed SIPS, the measurement acquisition and decision/corrective actions are carried out by local controllers distributed across the power system. These distributed controllers may also operate independently without communicating with other similar controllers.

SIPSs can also be classified based on their input-type. For event-based SIPSs, outage events such as the status of major transmission lines, generators, transformers, and circuit breaker status can be monitored and used to initiate pre-planned remedial actions. For response-based SIPSs, measurements obtained from the system's response to a dynamic system condition/disturbance are used in the detection and implementation of the predetermined remedial actions.

Rule-based SIPSs make use of a set of *'if … then'* rules. These rules use predetermined thresholds obtained from offline system studies, while algorithmic-based SIPSs are implemented using the analysis of the system model.

For closed-loop SIPSs, the actions of the SIPS are based on the response of the system to previous control action. This implies that there is a feedback path from the power system (plant) to the SIPS (controller). The controller continuously monitors the system's responses and takes the appropriate successive remedial actions based on this. On the contrary, open-loop SIPSs do not have a feedback path from the power system to the controller. Generally, event-based SIPSs belong to the class of open-loop control system. While, response-based SIPSs are closed-loop systems.

3.2.2 Functional Elements of System Integrity Protection Schemes

The functional elements of SIPSs can be divided into three groups (Apostolov, 2014). These are:

- System monitoring element
- Protection element
- Execution element

The system monitoring element is used in the supervision and detection of the changes in the power system. These changes can be in the system loading condition, topology change, and generator dispatch. The protection element identifies system stability threats and arms the SIPS in order to mitigate such stability threats.

The execution element receives the output signal from the SIPS protection element, and performs the predetermined remedial action(s) to mitigate the instability. Figure 3.2 shows a typical block diagram of SIPS.

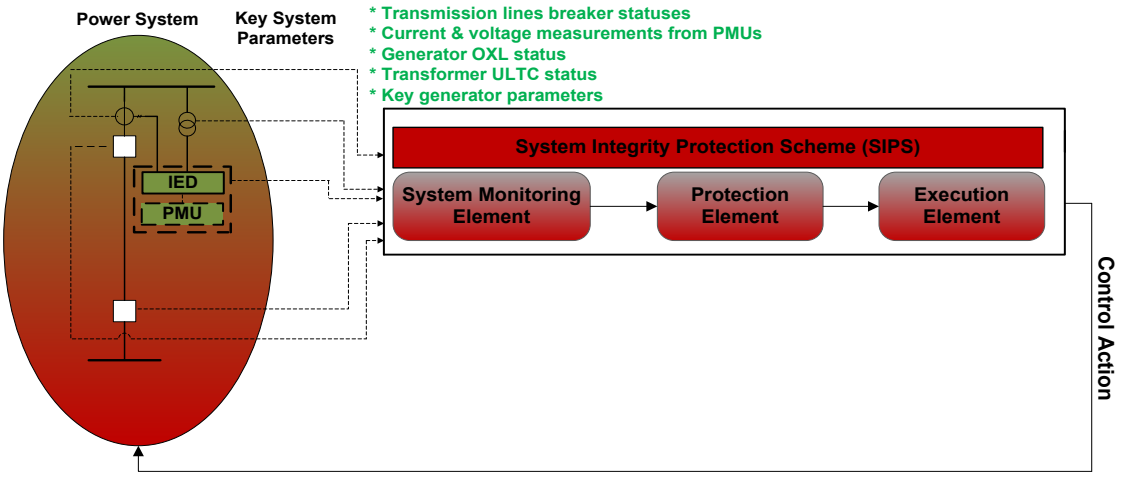

Figure 3.2: SIPS functional elements

3.2.3 Implementation of System Integrity Protection Schemes

SIPSs must satisfy the protective relaying conditions for sensitivity, dependability, security, and speed. Also, a well-designed SIPS must be selective, robust, and function correctly for expected steady-state and unforeseen dynamic system conditions. In addition, a well-designed SIPS must coordinate correctly with other protective actions, including other SIPSs, and conventional protective and control devices.

The particular type of SIPS implemented in a power system depends on the probable threats expected. SIPSs can be said to encompass a combination of protective relays, Intelligent Electronic Devices (IEDs), meters, control equipment, automation equipment, communication infrastructure, reactive power compensators, and Flexible Alternating Current Transmission System (FACTS) devices.

The various types of SIPSs for mitigating power system stability have been listed as (Madani *et al.,* 2010; Horowitz *et al.,* 2008; Begovic *et al.*, 2007):

- Generation rejection
- Tie-line runback
- Transmission transfer trip
- Under-frequency load shedding
- Under-voltage load shedding
- Adaptive load mitigation
- Out-of-step tripping
- Shunt capacitor switching
- Tap-changer control
- Static VAR Compensator (SVC) control
- Static Synchronous Compensator (STATCOM) control
- High-Voltage Direct Current (HVDC) controls
- Series capacitor bypass
- Turbine fast valving
- Automatic Generation Control (AGC) controls
- Gas turbine start-up

Other SIPSs capable of mitigating wide area disturbance can be found in (Horowitz *et al.,* 2008). Table 3.1 summarises the type of system disturbances for which some of the above-mentioned SIPSs can be effectively applied (Madani *et al.,* 2009; Horowitz *et al.,* 2008; Begovic *et al*., 2007).

Table 3.1: Mitigating actions for various power system instability problems

SIPS	Transient instability	Small-signal instability	Frequency instability	Voltage instability
Generation rejection	×	×	×	×
Remote load shedding	×	×		
HVDC controls	×	×	×	
Braking resistor	×	×		
Under-frequency load shedding			×	
Turbine fast valving	×	×	×	
Automatic shunt switching	×	×		×
Under-voltage load shedding				×
Tap-changer blocking			×	×
AGC controls		×		×
Gas turbine start-up			×	×

From Table 3.1, some of the SIPSs that can be implemented in the preservation of the system integrity with respect to voltage stability are generation rejection, automatic shunt capacitor switching, under-voltage load shedding, tap-changing controls, AGC controls, and gas turbine start-up.

Generally, the procedure followed in this review was to select, review, and analyze articles seen as representative of the various existing techniques and methods from reputable journals only. However, conference proceedings from renowned authors in this field were also included in the review.

3.3 Review of the Methods for Transformer Tap-Changer Control

3.3.1 Review of Publications

Similar to the procedure followed in Chapter Two, a literature survey was carried out using Elsevier's 'Engineering Village' database. The survey carried out spanned a period of 35 years (1980-2015).

When the search parameter was 'transformer tap-changer control in voltage stability', a total of 48 articles were reported. These articles comprise of conference proceedings, journal articles, and report reviews. When the search parameter was refined to 'transformer tap-changer blocking', only 11 articles were found. Out of which only 4 were journal articles.

The search parameter was further refined to 'transformer tap-changer control using synchrophasor measurements/phasor measurement units'. No result was obtained in this case. This is because no paper has been published on the use of synchrophasor measurements for transformer tap-changer controls.

Figure 3.3 shows the analysis per year for published research articles when the search parameter was 'transformer tap-changer control in voltage stability'. Although, the literature search was done for a time span of 1980-2015, no article was returned for 1980-1993. Table 3.2 shows the distribution according to document-type. From Table 3.2, it can be seen that only 25 out of 64 publications were actually journal articles.

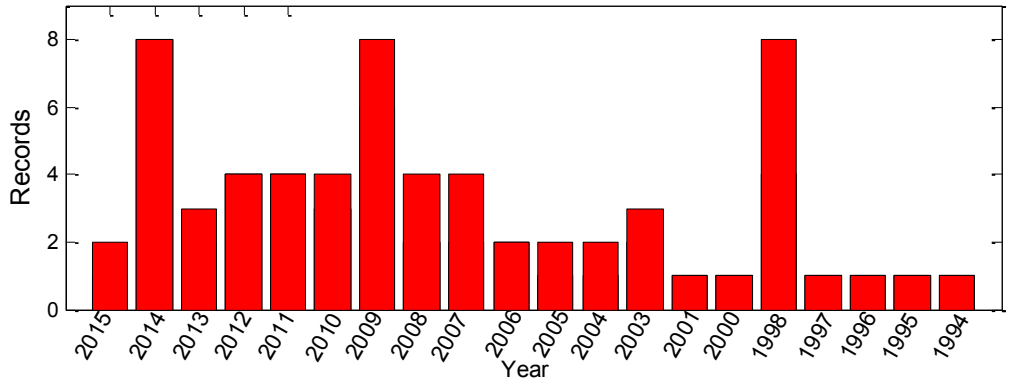

Figure 3.3: **Survey of published articles per year for 'transformer tap-changer control' from 1994-2015**

Table 3.2: **Survey of published articles according to document-type for 'on-load tap-changer control' from 1994-2015**

Type of Document	Number of Articles
Conference article	38
Journal article	25
Article in press	1

3.3.2 Literature Review of Methods for Transformer Tap-Changer Control

A transformer tap-changer is a selector mechanism for selecting variable number of turns in a transformer. The tap-changers are classified into two types. These include: (i) under-load (on-load) tap-changers; and (ii) off-load (de-energized) tap-changers. The tap action of under-load tap-changers is carried out while the transformer is online and connected to the live system. These are usually used in systems where the voltages are constantly changing and needs to be regulated. On the contrary, the off-load tap-changers are used to change the transformer taps offline with the transformer disconnected from the live system. They are mainly used in systems where the voltages rarely change.

The mechanism used in the control of a transformer tap-changer can be implemented using mechanical switches or solid-state electronics (Faiz and Siakolah, 2003). The mechanical-type tap-changer is prone to arcing, has slow reaction times, and high maintenance costs. These limitations are reduced through the use of solid-state tap-changers based on semiconductor devices.

The transformer ULTC begins to regulate the transformer Low Voltage (LV)-side U_2 as soon as if falls below its reference voltage U_{reg}.
where $U_{reg} = U_{set} \pm U_{deadband}$, U_{reg} is the LV set-point voltage with a tolerance, U_{set} is the set-point voltage. $U_{deadband}$ is the deadband voltage and it is given as a percentage of U_{set}.

When the transformer tap is raised, the number of turns on the High Voltage (HV)-side of the transformer (N_1) decreases, thereby increasing the transformation ratio $\frac{N_2}{N_1}$. This results to an increase in the LV-side voltage. N_2 is the number of turns on the secondary winding.

The literature relating to the general coordination and control of transformer ULTC is presented below.
Bassett (1993) presented a tap-changer controller based on Programmable Logic Controller (PLC) deployed at the Pennsylvania Power & Light (PP&L) Company. A circulating reactive power (MVArs) method was used. Gajic *et al*. (2010) described the utility experience gathered in the use of IEC 61850 GOOSE messages between the voltage regulators of the ULTCs of parallel transformers. Similar to the method in (Bassett, 1993), the circulating method for the control of parallel transformer ULTCs was applied.

Yarza and Cimadevilla (2014) considered both the master-follower method and the circulating current method for the parallel control of transformers. Sichwart *et al*. (2013) implemented a transformer ULTC controller using IEC 61850 GOOSE messages. Lab-scale set-up comprising of an assumed merging unit, control unit, and an actuator module were implemented using industrial-grade hardware. Analogue voltage inputs from an OMICRON test injection set were published as IEC 61850 analogue GOOSE messages by a SEL-2411 Programmable Automation Controller to the control unit (SEL-2414 Transformer Monitor). The ULTC control signal from the control unit to the actuator module was IEC 61850 GOOSE messages.

The application of transformer ULTC control in mitigating voltage instability has been considered in just a few publications. A review of these publications is given below.
Van Cutsem (1995) investigated how to control the transformer ULTC to mitigate voltage instability by blocking further taps of the transformer. This was used in combination with load shedding. The use of transformer tap reversal as emergency remedial action during voltage instability conditions was presented in (Vournas and Karystianos, 2004; Otomega *et al*., 2003). Tap reversal involves the lowering/moving of the tap position to a lower predefined level once a voltage threshold is reached. Otomega *et al*. (2003) further investigated the presence of multiple transformer ULTCs in a large power system. In this case, the transformer ULTCs are divided into clusters. Vournas *et al*. (2010) described a technique derived from tap reversal and LV side voltage set-point reduction.

Capitanescu *et al*. (2009) proposed a method for transformer blocking based on voltage thresholds. Results relating to this and its combination with load shedding were presented. The method by Bahadornejad and Nair (2014) used an additional input based on a derived tap-changer stability index to determine a set of control actions. Results were presented for control actions relating to ULTC blocking and the switching of a capacitor bank.

A centralised scheme for the coordinated control of transformer ULTCs in the prevention of voltage instability was proposed by Chang and Huang (1999). The method coordinated the tap changing action of the participating transformers by decoupling them and applying successive linearization. Zad *et al*. (2013) suggested a method for coordinating the transformer ULTCs with reactive power compensators for application in radial distribution systems. The Distributed Static Synchronous Compensator (D-STATCOM) was utilised in the provision of reactive power compensation at a radial distribution bus to provide voltage support since the ULTC transformer causes a voltage problem at the sending end of the long radial distribution system. Ohtsuki *et al*. (1991) investigated the impact of tap-changer reverse action caused by the increase in the transformation ratio of a transformer. Investigations relating to the tap-changer sensitivity with respect to voltage stability for various load types and operating conditions were presented in Liu *et al*. (2013); Vournas (2002); Choi and Kim (2001); and Yorino *et al*. (1997) respectively.

Although, ULTC blocking/unblocking would not restore the system's bus voltages to their pre-disturbance state, it can be used as a temporary remedial action to prevent further degradation of the system bus voltages (Capitanescu *et al*., 2009).

3.3.3 Discussion

A summarised comparison of the reviewed publications relating to transformer tap-changer control is presented in Table 3.3. The method by Gajic *et al*. (2010) was implemented at a utility for the control of the ULTCs of parallel transformers. However, the IEC 61850 GOOSE dataset used was vendor-specific and is not available in other IEC 61850-compliant IEDS produced by other vendors. While the method by Yarza and Cimadevilla (2014) was not implemented practically.

Although, a lab-scale implementation was carried out by Sichwart *et al*. (2013), process level measurements (IEC 61850-9-2 Sampled Values) from a Merging Unit (MU) were not used. Rather, the measurement inputs based on IEC 61850-8-1 analogue GOOSE message were used as inputs to the control unit instead of Sampled Values. Also, the IEC 61850 GOOSE message dataset(s) used in the implementation of this method is unclear as this information was not given. In Bahadornejad and Nair (2014), the simulation platform used was not stated. Also, the proposed method was not tested practically using industrial-grade hardware.

Some of the tap-changer control methods presented in the above review can further lead to the aggravation of the voltage instability problem being experienced in a system. This is because voltage thresholds were used as a trigger to their control algorithms. However, voltage magnitude is a poor indicator of the voltage instability experienced by a system. One alternative to the use of local measurement of bus voltages/thresholds is the application of system-wide measurements that reflect the prevailing wide area conditions.

A wide area synchrophasor-based machine-learning power system classifier for classifying the system state into ‘Stable’, ‘Alert’, and ‘Unstable’ is proposed in this thesis as a better alternative, rather than the use of voltage thresholds. Also, synchrophasor measurements have not been considered as an input to transformer ULTC controllers in the existing literature. This is considered and practically implemented in this thesis, together with the use of IEC 61850-8-1 GOOSE messages as the control signal from the ULTC controller to the transformer ULTC.

Table 3.3: Literature review of transformer tap-changer control

S/N	Paper	Objective(s) of the Paper	Methodology	Network Model Used	Type of Measurement	Implementation Platform	Contribution(s)/Drawback(s)
1	Ohtsuki *et al*. (1991)	Investigated the reverse action of tap-changers during voltage collapse.	Static and dynamic simulations involving the reverse action of transformer tap-changers for voltage collapse at the low voltage side of transformers. P-V curves were used in the analysis of the mechanism of tap-changer reverse action.	Simple model with induction motor.	Not specified.	Analysis carried out using P-V curves. Other details not given.	Presented results on the impact of voltage collapse at the Low Voltage (LV) and High Voltage (HV) sides of the transformer respectively. Drawback: The reverse action of the tap changers may lead to voltage collapse in heavily loaded systems.
2	Bassett (1993)	The adoption of Programmable Logic Controller (PLC) to control the tap-changer of the transformer.	The PLC control of a transformer tap-changer was adopted to replace the analogue transformer tap-changer controller that was in use at PP&L.	Pennsylvania Power & Light Company (PP&L).	Conventional current and voltage measurements from transformers were used.	SCADA PLC-to-tap-changer PLC communication in combination with software programmes.	The PLC tap controller uses a circulating MVArs to balance the transformers, rather than the use of circulating current. Drawback: The use of conventional measurements implies that copper cables hardwiring between the various inputs/outputs are used. This is expensive, requires multiple interconnections, and reduces flexibility/maintainability.
3	Van Cutsem (1995)	The application of tap-changer blocking in the mitigation of voltage instability.	Time domain simulation used in combination with sensitivity analysis.	Western region of the 410-bus Electricite De France (EDF) system.	Simulation platform used.	The implementation platform was reported to be in a fast voltage stability simulator.	Tap-changer blocking in combination with load shedding. Drawback: The sensitivity analysis used might be difficult to implement in practical real-time systems.
4	Yorino *et al*. (1997)	The investigations of the sensitivity of the voltage to the ULTC tap position.	A stability criterion based on the sensitivity of the voltage to the ULTC tap position was proposed.	Simple network model used.	Not specified.	Simulation platform used. Other details not given.	Applied a stability criterion in the investigations relating to ULTC tap position. Drawback: An equivalent power system model was used. The proposed method might be difficult to implement in large interconnected systems.
5	Chang and Huang (1999)	The design of a coordinated tap control for voltage stability enhancement.	The centralized tap-changer control is based on successive linearization aimed at the coordination of multiple tap adjustments of the participating transformers.	16-bus test system.	The availability of SCADA-based measurements was assumed.	Simulation platform used. Other details not given.	A centralized tap-changer control based on successive linearization combined with variable-structure control is proposed. Drawback: Requires load flow equation and the sensitivity matrix of the controlled voltage and the tap positions. This might be difficult to implement in real-time.
6	Choi and Kim (2001)	An online voltage regulation method for multiple distribution feeders.	The proposed method considered the diversity of unbalanced loads on multiple feeders. This was used in the determination of the optimal transformer tap position required to maintain the system within acceptable limits.	6-feeder distribution system.	Not specified.	Integer optimization is used in obtaining the optimal position of the ULTC tap.	An online voltage regulation method based on the load diversity and tap changing mechanism of the ULTC is proposed for multiple distribution feeders. Drawback: Optimization algorithms are iterative in nature. Thus, it is difficult to implement in real-time.

Table 3.3: Literature review of transformer tap-changer control

S/N	Paper	Objective(s) of the Paper	Methodology	Network Model Used	Type of Measurement	Implementation Platform	Contribution(s)/Drawback(s)
7	Vournas (2002)	The investigation of the impact of tap-changers on voltage stability.	The application of tap-changer blocking of a bulk power transformer ULTC was discussed.	6-bus test system.	Not specified.	Simulation platform used. Other details not given.	The paper discussed the use of transformer tap-changers in the prevention of emergency conditions and voltage stability. Rules for optimizing the transmission level tap-changers were presented. Drawback: The loadability sensitivities used are iterative and would be difficult to implement in real-time systems.
8	Otomega *et al*. (2003)	The application of a tap-changer reversal logic for mitigating voltage instability.	The application of a modified tap-changer control logic for preserving and regulating the transmission voltage to a given threshold.	1244-bus French RTE transmission system.	Not specified.	Simulation platform used. Other details not given.	The proposed modified tap-changer control logic was extended to clusters of transformer tap-changers. Drawback: The reverse action of the tap changers may lead to voltage collapse in heavily loaded systems.
9	Vournas and Karystianos (2004)	Discussion on the application of tap-reversing, optimization of the taps for high voltage transmission transformers.	The methodology used was based on the adjustment of the transmission voltage based on the active power flow. The optimal tap settings were determined through the solution of an optimization problem using the gradient projection method.	3-area system.	Not specified.	Simulation platform used. Other details not given.	A tap-changer reversal method for changing the regulated bus of the transmission side is reported in this paper. Transformer tap-changer blocking was combined with load shedding. Drawback: The reverse action of the tap changers may lead to voltage collapse in heavily loaded systems. Also, the solution to optimization problems is iterative in nature. Thus, not suitable for real-time practical application.
10	Capitanescu *et al*. (2009)	Transformer tap-changer control for voltage instability mitigation.	The proposed method investigated the blocking of the transformer tap at a current position or locked at a pre-determined tap.	French RTE transmission system.	Not specified.	Simulation platform used.	A combination of tap blocking and locking at pre-determined tap position was proposed. Drawback: The proposed method is based on voltage threshold. This may not be a good indicator of impending voltage instability in heavily compensated systems.
11	Gajic *et al*. (2010)	The control of parallel transformers fitted with on-load tap changers.	The circulating current principle was applied in the control of parallel transformers using IEC 61850 GOOSE messages.	110/20kV 20 MVA substation.	IEC 61850-8-1 analogue and binary GOOSE messages.	The transformer tap-changer controller was implemented in IEDs. The inputs to the IEDs were IEC 61850-8-1 GOOSE messages.	The proposed parallel tap-changer controller made use of IEC 61850 GOOSE messages for the communication of the signals required for the circulating current method. Drawback: The IEC 61850-8-1 datasets used are proprietary to the vendor of the IEDs used.

Table 3.3: Literature review of transformer tap-changer control cont'd

S/N	Paper	Objective(s) of the Paper	Methodology	Network Model Used	Type of Measurement	Implementation Platform	Contribution(s)/Drawback(s)
12	Vournas *et al*. (2010)	Transformer tap-changer reverse operation in the restoration of a system's voltage stability.	The proposed tap-changer controller is integrated with the algorithms for the alarm, range-limit monitoring, and set-point reduction.	52-bus Nordic-32 test system.	Locally available signal assumed.	The tap-changer control algorithm was proposed for deployment in a tap-changer controller of power transformers.	Three modules were presented. The first module was used in the identification of the onset of voltage instability. The second module was used for the tap reverse action of the tap-changer controller, while the third module is used in the restoration of controllability when the tap-changers are at their lower tap limits. Drawback: The reverse action of the tap changers may lead to voltage collapse in heavily loaded systems.
13	Yarza and Cimadevilla (2014)	The automatic voltage regular, master-follower, and the current circulating methods are implemented using IEC 61850 GOOSE messages.	A control system for the coordination of tap-changer controllers for parallel transformers.	Not specified.	IEC 61850-8-1 GOOSE messages.	IEC 61850-based platform was assumed. No practical implementation was presented.	Three tap-changer control methods were presented and the advantages of using the IEC 61850 GOOSE messages were highlighted. Drawback: The IEC 61850-8-1 GOOSE datasets used was not specified.
14	Liu *et al*. (2013)	An analytical method for transformer tap-changer control and strategies for preventing voltage collapse.	The influence of the mechanism of on-load tap changers on voltage stability using sensitivity information was presented. Different load models and tap-changer control strategies were discussed.	Not specified.	Not specified.	Simulation platform used. Other details not given.	The influence of transformer tap-changers on voltage stability using different load models. Drawback: No specific control strategy was presented to cover the various operating conditions/loads which a power system can be subjected to.
15	Sichwart *et al*. (2013)	An ULTC control method using IEC 61850.	The proposed method uses voltage measurements based on IEC 61850 analogue GOOSE messages. These serve as inputs to the control unit. An actuator module sends an actuating signal to the tap-changer controller motor on receipt of the command from the control unit.	A 500kV/169kV substation model was used.	IEC 61850 analogue and binary GOOSE messages	Lab-scale implementation comprising of IEC 61850-compliant IEDs and a PLC was used.	Actual industrial-grade hardware was used in the lab-scale implementation. Drawback: The ULTC control method was not specifically designed for power system stability applications.
16	Zad *et al*. (2013)	A method for the coordination of the transformer on-load tap changer and reactive power compensation using Distribution Static Synchronous Compensator (D-STATCOM).	The proposed method was based on the coordination of the transformer on-load tap changer and reactive power compensation in order to achieve a fast response voltage control method suitable for long radial distribution system without exceeding the limits of the D-STATCOM.	11kV radial distribution network was used.	Simulation-based environment.	NEPLAN simulation software used.	An approach based on the combination of a transformer tap-changer and a D-STATCOM for voltage control in radial distribution system was proposed. Drawback: The coordination of the transformer tap-changer and the D-STATCOM might be difficult to achieve in practical systems.

Table 3.3: Literature review of transformer tap-changer control cont'd

S/N	Paper	Objective(s) of the Paper	Methodology	Network Model Used	Type of Measurement	Implementation Platform	Contribution(s)/Drawback(s)
17	Bahadornejad and Nair (2014)	Transformer ULTC control strategy for monitoring the stability of the ULTC.	The Thevenin equivalent impedance of the supply was estimated using measurements from the transformer HV-side. This Thevenin impedance is then used in the calculation of the ULTC stability index.	BPA 10-bus system used.	Conventional measurements from current and voltage transformers.	An ULTC control scheme was discussed. However, details on the hardware-in-the-loop testing/integration with the simulated BPA test system were not given.	The presented ULTC method was proposed for integration in protection IEDs. Drawback: Thevenin equivalent parameters were used. This might be difficult to achieve in practical systems.

3.4. Review of Methods for Under-Voltage Load Shedding

Load shedding should only be considered when other less extreme alternatives have been exhausted. This is because it inconveniences the customers and results in a loss of revenue to the utilities. This section presents a review of publications on load shedding using conventional measurements, a review based on synchrophasor measurements, and a review of some industrial use cases.

3.4.1 Review of Publications

A literature survey was carried out using Elsevier's 'Engineering Village' database. The survey carried out spanned a period of 35 years (1980-2015). A total of 2838 articles were reported when the search parameters were 'power system load shedding'. These articles comprised of conference proceedings, journal articles, and report reviews. Out of which 1231 (43.4%) articles were journal publications.

Figure 3.4 shows the analysis per year for the published research articles when the search parameters were refined to 'power system under-voltage load shedding'. A total of 85 articles were reported. However, no article was returned for 1980-1984. Table 3.4 shows the distribution according to document-type. From Table 3.4, it can be seen that only 32 out of 85 publications were actually journal articles.

When the search parameters were refined to 'undervoltage load shedding using phasor measurement units', only 3 articles (conference articles) were obtained. This further emphasizes that this research area is still new, and relatively unexplored.

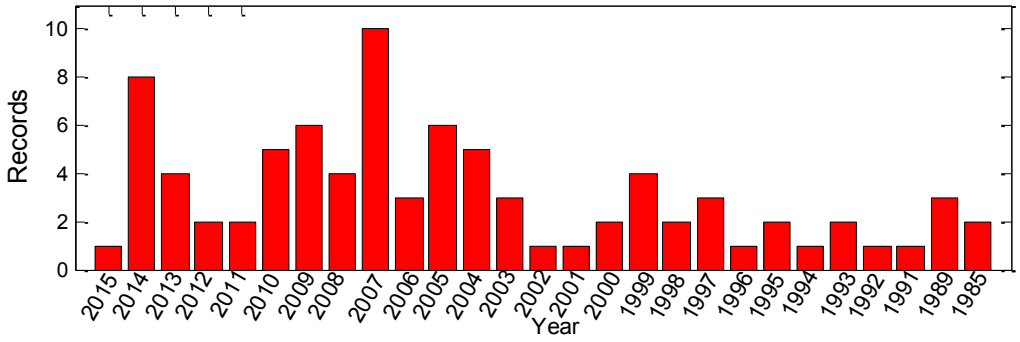

Figure 3.4: **Survey of published articles per year for 'undervoltage load shedding' from 1985-2015**

Table 3.4: **Survey of published articles according to document-type for 'power system undervoltage load shedding' from 1985-2015**

Type of Document	Number of Articles
Conference article	50
Journal article	32
Conference proceeding	2
Article in press	1

3.4.2 Literature Review of Methods for Under-Voltage Load Shedding Using Conventional Measurements

Methods for mitigating transient instability using load shedding have been proposed in some existing publications. The most representative publications can be found in (Hashiesh *et al*., 2012; Hsu *et al*., 2005; Wang *et al*., 2005). Similarly, the most representative publications on the application of under-frequency load shedding in mitigating frequency instability are given in (Abdelwahid *et al*., 2014; Yang *et al*., 2013; Dai *et al*., 2012; Hong and Wei, 2010; Seyedi and Sanaye-Pasand, 2009a; 2009b; Terzija, 2006; Delfino, *et al*., 2001; Anderson and Mirheydar, 1992).

Optimization techniques aimed at minimizing the amount of load to shed has been presented in some existing literature. The minimization of the load interruption cost have been considered using various techniques such as non-linear optimization (Wang *et al.,* 2011), heuristic algorithms such as genetic algorithm (Luan *et al.,* 2002; Moors *et al.,* 2000), combinatorial algorithm (Moors *et al.,* 2002; Van Cutsem *et al.,* 2002), Particle Swarm Optimization (PSO) (Amraee *et al.,* 2006), hybrid PSO with simulated annealing (Sadati *et al.,* 2009), linear programming and PSO (Hagh and Galvani, 2011), Newton-Raphson method (Ma and Yuan, 2011), and differential evolution (Arya *et al.,* 2012).

Some methods aside the above-mentioned optimization methods have also been considered in the past. Novosel and King (1994) applied an artificial neural network comprising of localised detectors for identifying overloaded transmission lines and predicting which load to shed and the amount to shed. Tuan *et al.* (1993) proposed two algorithms based on voltage change and load power sensitivities. Another algorithm based on the indicators of voltage instability risk and on the sensitivities of these indicators to the changes in the load to be shed was presented in (Tuan *et al*., 1994). These indicators were used in the selection of the location and in the determination of the amount of load to be shed.

An under-voltage load shedding strategy that maximizes the system reactive margin was proposed by (Berg, 1994). The methodology was based on nonlinear optimization formulation. Nanda and Crow (1995) developed a Lyapunov energy-based approach for under-voltage load shedding. These energy functions were used in generating a 3-dimentional plot, and the load shedding was based on the proximity of the system to the stability boundaries. Arnborg *et al.* (1997) proposed an analytical criterion for calculating the amount of the load to shed in order to prevent instability. The influence of load types in under-voltage load shedding was investigated in Arnborg *et al.* (1998). Dynamic loads and static loads influenced by transformer tap

changers were investigated to determine the influence of the load models on the amount of load to shed.

Tso *et al.* (1997) presented a load-shedding scheme for voltage instability mitigation using fuzzy reasoning. The load-shedding scheme determined the amount of load to shed and the location by identifying the fuzzy indicators for the control buses, and then correlating these indicators with the actual load shedding amounts through simulation studies conducted offline. Feng *et al.* (1998) used the invariant subspace parametric sensitivity method to achieve the least load shedding possible. An equilibrium tracing methodology was used in the calculation of the minimum amount of load to shed in order to restore the solvability of the system. The minimum load to shed was given by the difference in the loads at the pre-contingency state and the post-contingency state. Balanathan *et al.* (1998) presented an UVLS method in which the amount of load required to be curtailed was determined using the parameters of the dynamic load to calculate the real power mismatch between the steady-state real power loading and the instantaneous real power loading.

Bijwe *et al.* (1999) described an anticipatory load shedding scheme for loadability enhancement in which the load variation trends were used in predicting the amount of load to shed. An optimisation problem using a genetic algorithm was used by Moors *et al*. (2000) in the calculation of the minimum load to shed. Van Cutsem *et al.* (2002) proposed a combinatorial optimization method to optimize an objection function for the minimum load shedding possible for an unstable system scenario. Results were presented for the Hydro-Quebec system. This was an improvement of the previous work by Moors *et al.* (2001) on the comparison of three types of UVLS controllers, and the optimization (minimization) of the error between the total amount of load shed and the calculated amount of load to shed.

Lopes and Zambroni de Souza (2003) proposed a method based on power flow equations. It integrated the load shedding conditions into the load flow Jacobian. The buses to shed were determined using the bus with the lowest voltage level and the critical buses in the network were identified using the tangent vector method. Modal participation factor obtained from the load flow Jacobian was used by Affonso *et al*. (2004) in the identification of the load buses to shed during emergency conditions. Arya *et al.* (2005) suggested a method based on a voltage instability proximity detector obtained from the minimum eigenvalues of the load flow Jacobian. The amount of load to shed is calculated based on the proximity detector margin desired after the load shedding. A quadratic objective function was used in minimizing the

load to be shed. Amraee *et al.* (2007) also presented an algorithm based on static voltage stability and the sensitivities obtained at the point of maximum loadability. A mathematically method was used in solving the optimization problem, while 2 heuristic methods (PSO and GA) were used in the validation of the results obtained.

Otomega and Van Cutsem (2007) proposed a load shedding scheme against long-term voltage instability. The load shedding controllers are distributed and response-based using a set of rules and act in a closed-loop. Tsai and Wong (2008) used the maximum power transfer theorem in the calculation of an L index voltage stability indicator for identifying the optimal location for the placement of UVLS relays in a conventional UVLS scheme. P-Q curves were then used to determine the amount of load to shed and the time delay to use. Girgis and Mathure (2010) presented a load shedding scheme that combined the system frequency, voltage, rate of change of frequency and rate of change of voltage in the determination of the optimal amount of load to shed at suitable locations. Vournas *et al*. (2010) presented a comparison of a transformer tap-changer control scheme and a direct load shedding scheme based on fixed predetermined amount of load to shed. The location to shed is based on the bus where the Local Identification of Voltage Emergency (LIVES) alarm occurred.

Amraee *et al.* (2011) proposed an adaptive model predictive control scheme for UVLS. The proposed scheme was a distributed controller based on bus voltages and generator reactive power measurements. An optimization problem was then solved using sequential quadratic programming. Also, Otomega and Cutsem (2011) considered the use of a distributed UVLS controller for short- and long-term voltage instabilities in a power system with induction motor loads. Furthermore, Wang *et al*. (2011) used an optimization method in the calculation of the minimum amount of load to shed for an event-based UVLS. A multiport network model using modal participation factors were used in the identification of the loads to shed. In addition, the use of Differential Evolution (DE) in the minimization of the amount of load to shed was considered in Arya *et al*. (2012). The location to shed was determined using the eigenvalues of the load flow Jacobian.

Combinational load shedding schemes based on conventional measurements were proposed by Majidi *et al*. (2014); Ghaleh *et al*. (2011); Saffarian and Sanaye-Pasand (2011), in the simultaneous mitigation of frequency and voltage instabilities.
Table 3.5 gives a tabulated summary of some of the publications reviewed.

Table 3.5: Literature review of undervoltage load shedding using conventional measurements

S/N	Paper	Methodology	Network Model Used	Type of Trigger Used	Implementation /Simulation Platform	Contingencies Considered	Calc. of Amount to Shed/Nr. of Steps	Determination of Where to Shed	Time Delay Between Load Shedding Steps	Contribution(s)
1	Adibi and Thorne (1988)	The method is based on flow distributions and load decrement superposition for the mitigation of overloading.	Simulated 138kV Potomac Electric Power Company network.	Overload condition calculated using a percentage of the short-term emergency ratings.	Not specified.	Transformer/line contingencies.	Determined using flow distributions and load decrement superposition. 2 load shedding steps were used.	A load shedding list is used.	Extreme overload: 5 minutes delay. Moderate overload: 15 minutes delay.	Proposed a load shedding algorithm for an underground transmission system.
2	Anderson and Mirheydar (1992)	Changes in the system loading are obtained using the slope of the frequency deviation obtained after islanding for the mitigation of frequency instability.	Not specified.	Rate of change of frequency threshold.	Not specified.	Loss of generating unit and islanding.	System frequency response model. 5 steps-1st step: half of the static load shed. Others load shedding steps at 0.1 p.u. of system load.	Not specified.	Every 0.3 Hz increments. Generally specified at 6 cycles.	The first load shedding step is adaptive, while subsequent step(s) are based on predetermined amount and time delay.
3	Taylor (1992)	3 phase undervoltage relay used in a conventional scheme for the mitigation of voltage instability.	Equivalent system and the Puget Sound area network, USA.	Voltage threshold.	Not specified.	Line contingencies.	5% of total load.	Not specified.	3.5 s, 5.0 s, & 8.0 s respectively.	Decentralized UVLS was proposed and investigated.
4	Tuan *et al*. (1993) __ (1994)	Linear programming is used in the minimization of the amount of load to shed in order to attain acceptable voltage profile or acceptable voltage stability margin. In Tuan et al., (1994), the effect of generator field current limit was added.	New England test system and 206-bus French system.	Voltage threshold.	Not specified.	Not specified.	Linear programming. Load shedding of a maximum of 50% of initial load at each bus.	2 methods proposed: Sensitivities of change in voltage to load power, and voltage instability indicators.	Not specified.	Two sensitivity techniques were compared. (1) Technique based on the rate of change of voltage with load power; and (2) The sensitivity of the voltage stability indicators to the change in loads. This results to the system being restored to a secured state after load shedding.

Table 3.5: Literature review of undervoltage load shedding using conventional measurements cont'd

S/N	Paper	Methodology	Network Model Used	Type of Trigger Used	Implementation /Simulation Platform	Contingencies Considered	Calc. of Amount to Shed/Nr. of Steps	Determination of Where to Shed	Time Delay Between Load Shedding Steps	Contribution(s)
5	Berg and Sharaf (1994)	Non-linear programming was used to develop nose curves for indicating the system's margin to voltage collapse.	20-bus and 57-bus test systems.	Voltage threshold.	Not specified.	Loss of transmission lines.	1 p.u. load is shed at each load bus.	Q- and MVA-nose curves.	Not specified.	Proposed load shedding for maximizing the reactive power security of the system.
6	Novosel and King (1994)	ANN based using localized detectors with power system parameters as inputs for detecting overloaded lines and for the mitigation of the voltage instability.	IEEE 30-bus system.	ANN detectors.	Not specified.	Line overloading.	50% of initial load at selected load buses.	Contingency analysis.	Not specified.	Used ANN to predict where to shed and how much load to shed.
7	Nanda and Crow (1995)	Method is based on the sensitivities obtained from energy functions using the Lyapunov exponents for the mitigation of the voltage instability.	IEEE 30-bus and IEEE 57-bus test systems.	Proximity of the system state to the stability boundary.	Not specified.	Not specified.	Based on the comparison of the calculated energy sensitivity measure to an initial state sensitivity.	Based on the energy sensitivity measure at the load buses.	Not specified.	The amounts of load to shed are computed using the sensitivities of the energy to the real power and reactive power load.
8	Arnborg *et al*. (1997)	Analytical method comprising of soft and firm strategies for moving the current system trajectory towards acceptable system operating values in order to mitigate the voltage instability.	WSCC 9-bus test system.	No arming trigger specified.	Not specified.	Increased system loading.	Analytical method based on the system trajectory and the static load characteristics. The response of the load power to the voltage step was used in the calculation of the amount of load to shed.	Not specified.	Not specified.	Load characteristics used in the calculation of the amount of load to shed.
9	Ingelsson *et al*. (1997)	SCADA-based using bus voltages (V), generator reactive power (Q) & current limiter status.	Southern Sweden network.	Voltage threshold at 0.9125 p.u.	Proposed for SCADA-based systems. Hardware platform not used.	Not specified.	Not specified.	Load shedding at substations.	Area 1 time delay = 5 s at 365 kV pick-up Area 2 time delay = 2 s at 370 kV pick-up.	Long term voltage instability considered using wide area measurements from a SCADA.

Table 3.5: Literature review of undervoltage load shedding using conventional measurements cont'd

S/N	Paper	Methodology	Network Model Used	Type of Trigger Used	Implementation /Simulation Platform	Contingencies Considered	Calc. of Amount to Shed/Nr. of Steps	Determination of Where to Shed	Time Delay Between Load Shedding Steps	Contribution(s)
10	Tso *et al*. (1997)	Method is based on fuzzy reasoning for the mitigation of voltage instability.	Not specified.	Voltage threshold.	Not specified.	Increased loading and loss of transmission line.	Correlation of fuzzy indicators with pre-calculated amount of load to shed.	Fuzzy indicators.	Not specified.	Prediction of the amount of load to shed and location based on fuzzy reasoning.
11	Balanathan *et al*. (1998)	Method is based on derivations using real & reactive powers, and the bus voltages for the mitigation of voltage instability.	10-bus multi-machine equivalent system.	Not specified.	Not specified.	Line contingency.	Based on the parameters of the dynamic load model using a non-linear optimization method. Difference between the power at an initial state and the instantaneous power of the load at a given voltage.	Not specified.	Not specified.	Proposed the amount of load to shed during voltage instability by using the parameters of the dynamic load model obtained using a nonlinear least squares method.
12	Feng *et al*. (1998)	Method is based on the continuation method to determine the equilibrium point, before using parametric sensitivity to determine the amount of load to be shed for the mitigation of voltage instability.	39-bus New England system and 162-bus reduced Iowa system.	Not specified.	Not specified.	Generator/transmission contingency.	Load difference between the pre-contingency and the post-contingency boundary points.	Invariant Subspace Parametric Sensitivity (ISPS) used.	Not specified.	Method based on sensitivity analysis is used to determine the minimum amount of load to shed.
13	Bijwe *et al*. (1999)	Centralized scheme based on linear programming for the mitigation of voltage instability.	IEEE 30-bus and 91-bus systems.	Loadability margin used.	Not specified.	Load increase.	Linear programming used in the calculation of the amount of load to shed. 15% of the current load at each bus is sheddable.	Selected weak buses.	Not specified.	Proposed the use of loadability margin to anticipate the danger to the system & initiate load shedding before this occurs.

Table 3.5: Literature review of undervoltage load shedding using conventional measurements cont'd

S/N	Paper	Methodology	Network Model Used	Type of Trigger Used	Implementation /Simulation Platform	Contingencies Considered	Calc. of Amount to Shed/Nr. of Steps	Determination of Where to Shed	Time Delay Between Load Shedding Steps	Contribution(s)
14	Kolluri *et al*. (2000)	The method uses information from the SCADA system, load, bus voltages, and topology for the mitigation of voltage instability.	Western region of Entergy system in Texas, USA.	Transformer loading and bus voltages.	SCADA-based platform.	Transformer fault/line contingency.	Not specified.	Based on load priority.	2 s delay before shedding the 1st load block. 12 s delay before shedding the 2nd load block.	The proposed scheme was reported to be automatic and fast-acting.
15	Moors *et al*. (2000)	Genetic algorithm optimization was used to obtain the minimal load to shed. Rules are then used in the execution. The consideration was for the mitigation of voltage instability.	Hydro-Quebec System, Canada.	Voltage threshold.	Local and wide area measurements.	*N*-1, *N*-2, *N*-3 contingencies.	Branch and bound optimization method used.	Eigenvalue bus ranking.	Fixed delay, variable delay, and inverse-time delay considered.	The method proposed a closed-loop optimization method based on evolutionary computing.
16	Delfino, *et al*. (2001)	Conventional and adaptive schemes based on frequency and rate of change of frequency for the mitigation of frequency instability.	IEEE 24-bus system.	Frequency, Rate of Change of Frequency (ROCOF) thresholds.	Hardware platform not used.	Load increase.	Conventional scheme is based on 30% of the system load. Adaptive scheme is based on the system frequency response model using the swing equation.	All load buses.	0.2 s (10 cycles).	The method is adaptive and suitable for application in a deregulated environment.
17	Van Cutsem *et al*. (2002)	A combinatorial optimization method was used in minimizing the amount of load to shed. 3 load shedding controllers are investigated for the mitigation of voltage instability.	Hydro-Quebec System, Canada.	Voltage measurements.	Coordinated and uncoordinated controllers.	*N*-1, *N*-2, line contingencies.	Branch and bound optimization method used.	Bus ranking based on sensitivity analysis using eigenvector of load flow Jacobian.	Tuning and inverse-time characteristic used.	Investigated the control parameters to use for solving the optimization problem.

Table 3.5: Literature review of undervoltage load shedding using conventional measurements cont'd

S/N	Paper	Methodology	Network Model Used	Type of Trigger Used	Implementation /Simulation Platform	Contingencies Considered	Calc. of Amount to Shed/Nr. of Steps	Determination of Where to Shed	Time Delay Between Load Shedding Steps	Contribution(s)
18	Lopes and Zambroni de Souza (2003)	Based on the evaluation of the load flow Jacobian at the operating point obtained after a contingency. Load shedding is aimed at restoring the system to a stable operating point which satisfies the voltage constraints.	IEEE 57-bus and IEEE118-bus test systems.	Voltage threshold.	The simulation/implementation platform used was not specified.	Line contingency and increased system loading.	Load flow equations.	Two approaches used. i) Voltage measurements; ii) Critical buses.	Not specified.	Investigated the use of the tangent vector algorithm in the identification of the loads to shed (critical buses).
19	Affonso *et al*. (2004)	Modal analysis computed from the load flow Jacobian was used for the mitigation of voltage instability.	810-buses Brazilian Southeast system.	Eigenvector of Load Flow (LF) Jacobian	The simulation/implementation platform used was not specified.	Line contingencies.	Modal participation factor derived from the load flow Jacobian.	Modal participation factor.	Not specified.	Active and reactive power rescheduling was combined with load shedding.
20	Mechenbier *et al*. (2004)	Implementation of a high-speed and low-speed load shedding scheme for the mitigation of voltage instability.	Public Service Company of New Mexico transmission system.	Voltage threshold and transmission line logic used.	Distribution SCADA system.	Line contingency.	P-V curve analysis.	Not specified.	Not specified.	High-speed and low-speed load shedding schemes were implemented and deployed for a real power system.
21	Arya *et al*. (2005)	Quadratic objective function using the Hopfield neural network in the minimization of the amount of load to shed in the mitigation of voltage instability.	91-bus power system.	The minimum Eigenvalue of Load Flow (LF) Jacobian	The simulation/implementation platform used was not specified.	Increased loading.	Quadratic optimization method.	Sensitivity analysis.	Not specified.	A Voltage Stability Indicator (VSI) obtained from the Jacobian of the load flow was used with a Hopfield algorithm to achieve a desired stability margin based on the derived VSI.
22	Hsu *et al*. (2005)	ANN-based using total power generation, total load demand, and frequency decay for the mitigation of transient instability.	Taipower system.	Total power generated, total load demand, frequency decay rate.	Artificial Neural Network (ANN) controller. The simulation/implementation platform used was not specified.	Fault contingency.	Determined by the ANN controller. 15 stages were used.	Pre-determined loads.	Not specified.	The proposed method is adaptive and considers the real-time condition of the system.

Table 3.5: Literature review of undervoltage load shedding using conventional measurements cont'd

S/N	Paper	Methodology	Network Model Used	Type of Trigger Used	Implementation /Simulation Platform	Contingencies Considered	Calc. of Amount to Shed/Nr. of Steps	Determination of Where to Shed	Time Delay Between Load Shedding Steps	Contribution(s)
23	Terzija (2006)	The proposed method utilizes the Newton algorithm to estimate the frequency and ROCOF. The load to be shed is related to the magnitude of the disturbance estimated for the mitigation of frequency instability.	9-bus system and New England system	Rate of change of frequency threshold	The simulation/implementation platform used was not specified.	Additional load connection and generator contingency.	Based on the system frequency response model using the swing equation. 6 and 4 stages of UFLS investigated.	Based on the system frequency response model using the swing equation.	0.2 s, 0.5 s, and 1.0 s investigated.	Adaptive UFLS method proposed.
24	Amraee *et al*. (2007)	Heuristic method with PSO and GA. Conventional UVLS and centralized UVLS investigated.	IEEE 14-bus and IEEE 118-bus system	Loading margin and its sensitivities are computed using the continuation power flow method.	Hybrid PSO and GA method. The simulation/implementation platform used was not specified.	Increased loading and loss of transmission line.	Loading margin and its sensitivities are computed using the continuation power flow method. Heuristic method with PSO and GA.	Buses with high loading margin sensitivities are selected.	Not specified.	Load shedding algorithm utilized technical and economic criteria.
25	Otomega and Van Cutsem (2007)	Undervoltage load shedding for long-term voltage instability using distributed controllers based on the variations in the monitored bus voltage.	French RTE transmission system.	Voltage threshold.	Closed-loop centralized and distributed controllers.	Transmission line contingencies.	Based on the product of a constant and the average transmission voltage drop over time.	Pre-determined loads.	Based on the time evolution of the monitored transmission voltage.	A comparison of closed-loop centralized and distributed controllers for UVLS was presented.
26	Halpin *et al*. (2008)	An UVLS based on the rate of voltage recovery above a voltage threshold.	Southern Electric System, Georgia.	Voltage recovery slope threshold.	Distributed relays.	Multiple contingencies resulting in fault induced voltage recovery scenario.	Percentages of the area loads are to be shed in 4 stages.	Pre-determined distribution transformers.	Time delay per stage include 1.5 s, 1.7 s, 1.9 s, and 2.1 s.	A slope permissive undervoltage load shedding algorithm was proposed.

Table 3.5: Literature review of undervoltage load shedding using conventional measurements cont'd

S/N	Paper	Methodology	Network Model Used	Type of Trigger Used	Implementation /Simulation Platform	Contingencies Considered	Calc. of Amount to Shed/Nr. of Steps	Determination of Where to Shed	Time Delay Between Load Shedding Steps	Contribution(s)
27	Seyedi and Sanaye-Pasand (2009a)	Two methods proposed: (1) Response based method, and (2) Combination of event-based and response-based methods.	Simulated Khorasan power system	Voltage and frequency thresholds for the mitigation of frequency instability.	Control centre implementation.	Generator/transmission line/transformer contingencies.	System frequency response model using the swing equation. Threshold power is subtracted and the result is multiplied by 1.05.	V-Q curve analysis.	Time is adaptive, based on the rate of change of the frequency with time.	Centralized adaptive load shedding was proposed.
28	Tsai and Wong (2008)	Maximum power transfer is used in the placement of UVLS relays. P-Q curve is used in the determination of the amount of load to shed and the time delay between the load shedding stages.	New England 39-bus system and Taipower system.	Voltage threshold.	Distributed UVLS relays.	Load increase and transmission line fault.	Adaptive P-Q curve used.	The L indicator is used in the placement of the UVLS relays.	Adaptive P-Q curve used.	UVLS relay placement was carried out using an L indicator.
29	Hong and Wei (2010)	Optimization problem using genetic algorithm in the mitigation of frequency instability.	Not given.	Frequency threshold.	A distributed scheme comprising of underfrequency relays.	Generator and line contingencies.	The amount of load to shed was determined using genetic algorithm.	Pre-determined feeders.	0 s - 0.2 s.	Hierarchical method is used to minimize the amount of load to shed and the lowest swing frequency to be maximized.
30	Vournas *et al*. (2010)	The method is based on voltage instability detection, reverse tap actions, and secondary voltage reduction when the LTC reaches the lower tap limits.	52-bus Nordic32 network.	Voltage threshold.	Decentralized scheme integrated in a Load Tap Changer (LTC) controller.	Line contingency.	A percentage of the load at each bus was shed.	Pre-determined buses.	1 s.	Proposed method can be integrated in an ULTC transformer.
31	Amraee *et al*. (2011)	Adaptive multi-stage undervoltage load shedding based on Model Predictive Control (MPC). The MPC problem is solved using quadratic programming.	10-bus multi-machine system.	Generator reactive power and bus voltage thresholds.	Decentralized controllers using MPC.	Line contingencies.	Sequential quadratic programming.	Pre-determined load buses.	3 s - 10 s.	An adaptive multi-stage distributed controller scheme was proposed.

Table 3.5: Literature review of undervoltage load shedding using conventional measurements cont'd

S/N	Paper	Methodology	Network Model Used	Type of Trigger Used	Implementation /Simulation Platform	Contingencies Considered	Calc. of Amount to Shed/Nr. of Steps	Determination of Where to Shed	Time Delay Between Load Shedding Steps	Contribution(s)
32	Ghaleh *et al*. (2011)	Local measurements of frequency and voltage for the mitigation of frequency instability.	New England 39-bus system and simulated Khorasan network in Iran.	Frequency and voltage thresholds.	Distributed scheme. Hardware platform was not used.	Generator and line contingencies.	Pre-defined amount of load.	Based on a voltage decay calculation at the load buses.	100 ms.	The proposed combinational method does not require communication links between various measurement points.
33	Otomega and Cutsem (2011)	Logic-based wide area protection scheme for the mitigation of voltage instability.	55-bus Nordic32 network.	Generator field current and transmission line thresholds.	Decentralized controllers. Hardware platform was not used.	Short circuit faults and line contingency.	Based on the product of a constant and the average transmission voltage drop over time.	Pre-determined load buses.	0.3 s.	A coordinated and distributed scheme for mitigating short- and long-term voltage instability in systems with induction motor loads was proposed.
34	Saffarian and Sanaye-Pasand (2011)	Local measurements of voltage and frequency for the mitigation of frequency instability.	Simulated Khorasan power system, Iran.	Frequency threshold.	Distributed scheme using a combinatorial load shedding algorithm.	Generator and line contingencies.	Pre-defined amount of load.	Based on the rate of voltage decline.	50 ms.	An adaptive combinational load shedding was proposed.
35	Wang *et al*. (2011)	A multistage optimization method is used to relate the system operation reserve and the load to be shed for the mitigation of voltage instability.	IEEE 14-bus, 118-bus systems, and a 2038 bus real power system.	Event-based.	SCADA-based. Hardware platform not used.	Transmission line contingencies.	Optimization was applied to obtain the appropriate amount of demand curtailment needed.	Pre-determined locations.	Not specified.	A method for minimizing the total cost of demand response in order to achieve acceptable operation reserves.
36	Arya *et al*. (2012)	Differential evolution is used in the minimization of the amount of load to shed for the mitigation of voltage instability.	IEEE 6-bus and 14-bus test system.	Voltage stability proximity indicator used.	The simulation/implementation platform used was not specified.	Increased system loading.	Differential evolution used in the optimization of the amount of load to shed.	Based on sensitivity analysis.	Not specified.	Improvement over a previous method proposed in (Arya *et al*., 2005).
37	Dai *et al*. (2012)	The proposed method uses a prediction model based on the Extreme Learning Machine (ELS) for the mitigation of frequency instability.	New England 39-bus system.	Event-based.	Machine learning prediction model with database. No hardware platform used. Software platform (referred to as FASTEST) was used for the time domain simulation.	Generator contingencies.	Extreme learning machine-based prediction used.	A Transient Frequency Deviation Acceptability (TFDA) margin is used.	Not specified.	Load shedding method is event-based using extreme learning machine.

Table 3.5: Literature review of undervoltage load shedding using conventional measurements cont'd

S/N	Paper	Methodology	Network Model Used	Type of Trigger Used	Implementation /Simulation Platform	Contingencies Considered	Calc. of Amount to Shed/Nr. of Steps	Determination of Where to Shed	Time Delay Between Load Shedding Steps	Contribution(s)
38	Majidi *et al*. (2014)	An algorithm for intelligent load shedding based on critical line overloading is proposed for the mitigation of frequency instability.	New England 39-bus system.	Critical flow (transmission line real power) threshold and operation of zone-3 distance protection respectively.	No hardware platform was used. DIgSILENT PowerFactory software was used for simulations.	Increased system loading and 3 phase short circuit faults.	Designed to shed the loads at the buses by using the sensitivity analysis method.	Load flow-based sensitivity of the transmission lines to the load buses is used.	265 ms is used with 20 ms time delay between subsequent load shedding stages.	An algorithm for intelligent load shedding based on critical line overloading was proposed.

3.4.3 Literature Review of Methods for Under-Voltage Load Shedding Using Synchrophasor Measurements

Wang *et al*. (2005) proposed a synchrophasor-based load shedding and generator tripping schemes as countermeasures against transient instability. A transient stability index was used in the monitoring of the system and as a trigger to initiate these remedial actions. The equal-area criterion for a One-Machine-Infinite-Bus (OMIB) was used in the determination of the amount of remedial action required. However, the availability of PMUs was assumed in the study.

Nikolaidis *et al.* (2008) presented load shedding schemes for mitigating voltage instability using the sensitivities derived from the load margin and voltages. These sensitivities are used in the identification of the load shedding location and the amount of load to shed. Donolo *et al*. (2009) presented four synchrophasor-based voltage stability indices which were used for monitoring the power system, and in the determination of the optimal load shedding to implement in order to prevent voltage instability. However, the number of load shedding steps was fixed. Also, a fixed threshold was used as the trigger to the UVLS scheme.

Girgis and Mathure (2010) presented a load shedding algorithm for counteracting deficiencies in the system's real and reactive power margins after a disturbance. The system's ROCOF was used in the calculation of the generator-load mismatch, while the rate of change of voltage was used in the identification of the sensitive buses in the system. Corsi (2010) proposed an UVLS scheme based on a voltage stability index calculated using the Thevenin equivalents of the system and the local measurements from PMUs. The speed of the load shedding and the successive steps depended on the calculated voltage stability index.

An adaptive under-voltage load shedding scheme was suggested by Glavic and Van Cutsem (2010). The method is adaptive because the voltage thresholds used were determined from the power system measurements, rather than predetermined. Also, the amount of load to shed depended on the severity of the contingency. The UVLS scheme curtailed the loads until the measured voltage was greater than the Thevenin voltage threshold.

Seethalekshimi *et al*. (2011) presented a load shedding scheme to alleviate both frequency and voltage instabilities. The measurements for calculating the disturbance power and the voltage stability risk index used are assumed to come from PMUs. Tang *et al*. (2013) proposed a combined underfrequency and undervoltage load shedding algorithm for large disturbance contingencies.

The proposed algorithm used a power flow tracing method for the distribution of the real and reactive powers to shed at the load buses. The amount of load to shed was assumed to be equal to the real power imbalance in the power system. The real power imbalance was then calculated using the swing equation.

A summarised comparison of the various load shedding methods based on synchrophasor measurements is presented in Table 3.6.

3.4.4 Discussion

The use of optimization algorithms for calculating the minimum amount of load to shed (Arya *et al.,* 2012; Ma and Yuan, 2011; Hagh and Galvani, 2011; Sadati *et al.,* 2009; Amraee *et al.,* 2006; Luan *et al.,* 2002; Moors *et al.,* 2002; Van Cutsem *et al.,* 2002; Moors *et al.,* 2000) are usually computation intensive, iterative, and difficult to implement in real-time. The method by Feng *et al.* (1998) was based on the calculation of the load shedding amount obtained by using the difference in the loads at the pre-contingency and the post-contingency states. The methods presented by (Arnborg *et al*., 1998; Balanathan *et al.,* 1998) also calculated the amount of the load to shed using the load parameters. This implies that these methods are only suitable for increased loading scenarios and might fail for voltage instability as a result of transmission line/generator outages.

In Girgis and Mathure (2010), the operating conditions used were not stated. Also, the events leading to the voltage instability were not investigated. The knowledge-based methods given in (Tso *et al*., 1997; Novosel and King, 1994) might fail when deployed for system operating conditions or topologies different from the ones used in the generation of the dataset for training these methods.

Methods based on combinational load shedding aimed at mitigating frequency and voltage instabilities have been proposed in (Tang *et al*., 2013; Saffarian and Sanaye-Pasand, 2012; Ghaleh *et al*., 2011; Saffarian and Sanaye-Pasand, 2011; Seethalekshmi *et al*., 2011; Seyedi and Sanaye-Pasand, 2009a; 2009b). These studies assumed that the prevailing frequency instability condition was accompanied by voltage instability. However, a decline in the system voltages does not necessarily translate to voltage instability and could be a fault induced delayed voltage recovery condition. This is because power system voltages have been known to fluctuate with the angular oscillations associated with the loss of generators as reported in (Prasetijo *et al*., 1994), and do not necessarily imply voltage instability in the system.

Table 3.6: Literature review of undervoltage load shedding using synchrophasor measurements

S/N	Paper	Methodology	Network Model Used	Type of Trigger Used	Implementation /Simulation Platform	Contingencies Considered	Calc. of Amount to Shed/Nr. of Steps	Determination of Where to Shed	Time Delay Between Load Shedding Steps	Contribution(s)
1	Wang *et al*. (2005)	The method for determining the remedial actions is based on the equal-area criterion for estimating the One-Machine-Infinite-Bus (OMIB) for mitigating transient instability.	Simulated Taipower system.	Generator parameter and transmission line monitoring.	Control centre level. Hardware platform not used. The availability of synchrophasor measurements was assumed.	Tie-line fault contingency.	Equal area criterion.	Pre-determined loads.	Not specified.	System reduction to an OMIB system. Proposed scheme was tested on the simulated Taipower system.
2	Nikolaidis *et al*. (2008)	The location to shed is obtained using the sensitivities based on the loading margin and bus voltages. The amount of load to shed is minimized using L1 norm minimization technique.	Greek Hellenic interconnected system.	Voltage magnitude thresholds.	Centralized and distributed schemes were investigated. The availability of synchrophasor measurements was assumed.	Load increase, line and generator contingencies.	Calculated using L1 Norm minimization. Load shedding is done at the sensitive buses until the system margin exceeds the required margin.	Based on the sensitivities of the loadability margin, and the sensitivities calculated from the voltage and its relationship with the load parameters.	10 s used for the local decentralized UVLS scheme. 2 s for the centralized UVLS scheme.	An online voltage stability assessment tool is proposed as the arming signal to the UVLS scheme. Several UVLS designs using centralized and decentralized architecture were compared.
3	Donolo *et al*. (2009)	Voltage instability prediction and 3-step load shedding using synchrophasor measurements in the mitigation of voltage instability.	Simulated Natal region of the Eskom South African grid.	Q margin or Power Import Margin (PIM).	Centralized scheme using a synchrophasor-based testbed.	Transmission line contingency.	Based on pre-defined percentages of the area load.	Pre-defined loads.	Instantaneous load shedding without time delay.	Voltage instability indices proposed: QV margins, incremental reactive power cost, incremental load cost, and power transfer margin.
4	Girgis and Mathure (2010)	Rate of Change of Frequency (ROCOF) and system inertia is used in the calculation of the amount of load to shed. Rate of Change of Voltage (ROCOV) to the real power sensitivities are used in the determination of the sensitive buses where to shed load in the mitigation of frequency instability.	IEEE 30-bus system.	Voltage threshold.	Centralized scheme based on the assumed availability of synchrophasor measurements. Simulation was done in PSCAD only.	Generator contingency.	Based on the system frequency response model using the swing equation.	Based on the sensitivities obtained from the rate of change of voltage to the real power.	0.1 s between each load shedding step.	Proposes the combination of frequency, voltages, ROCOF, and ROCOV for optimal load shedding and location.

Table 3.6: Literature review of undervoltage load shedding using synchrophasor measurements cont'd

S/N	Paper	Methodology	Network Model Used	Type of Trigger Used	Implementation /Simulation Platform	Contingencies Considered	Calc. of Amount to Shed/Nr. of Steps	Determination of Where to Shed	Time Delay Between Load Shedding Steps	Contribution(s)
5	Corsi (2010)	PMU-based method using secondary and tertiary voltage regulation structures for the mitigation of voltage instability.	North Italy power system.	Voltage Stability Index (VSI).	Centralised scheme. The availability of synchrophasor measurements was assumed.	Load increase.	Based on pre-defined percentages of the area load.	Pre-defined loads.	Based on the VSI indication.	An algorithm for the computation of the equivalent Thevenin voltage and impedance used in the VSI was proposed.
6	Glavic and Van Cutsem (2010)	Based on wide area PMU measurements using pre-defined rules. The loads to shed are obtained using sensitivity derivations. The amount of load to shed is linked and calculated using the unrestored power.	52-bus Nordic32 network.	Voltage threshold.	Centralized scheme based on the assumed availability of synchrophasor measurements. Simulation was done in SIMULINK.	Line contingencies.	Based on the difference between the pre-contingency real power and the critical point real power.	Based on the sensitivities obtained from the bus voltages with respect to the load real power.	3 s.	Adaptive closed-loop method in which the threshold to use is determined from the system measurements.
7	Seethalekshmi *et al*. (2010)	PMU based load curtailment using optimal redispatch countermeasures for the mitigation of frequency instability.	New England 39-bus system.	Based on the voltage stability index VSRI threshold.	Centralized scheme. Synchrophasor measurements were assumed to be available. The simulation platform used was not given.	Generator contingency.	System frequency response model using the swing equation. Sequential quadratic programming used to obtain the minimum load shedding.	Based on 2 voltage stability indices – the VSRI and L-indices.	Various time delays experimented on.	Adaptive two-stage combinational load shedding scheme which considers the dynamic changes in the system voltages.
8	Seethalekshmi *et al*. (2011)	PMU based method calculates the load to shed using the disturbance power and the voltage stability margin in the mitigation of frequency instability.	New England 39-bus system and 246-bus Indian system.	Based on the voltage stability index VSRI threshold.	Centralized scheme. Synchrophasor measurements were assumed to be available. The simulation platform used was not given.	Generator contingency.	System frequency response model using the swing equation.	Based on the voltage stability index VSRI.	5 s time delay used.	Two-stage self-healing combinational load curtailment during critical contingencies.

Table 3.6: Literature review of undervoltage load shedding using synchrophasor measurements cont'd

S/N	Paper	Methodology	Network Model Used	Type of Trigger Used	Implementation /Simulation Platform	Contingencies Considered	Calc. of Amount to Shed/Nr. of Steps	Determination of Where to Shed	Time Delay Between Load Shedding Steps	Contribution(s)
9	Tang *et al*. (2013)	Centralized adaptive UFLS and UVLS for large disturbance contingencies. Reactive power load shedding was incorporated into the real power load shedding for the mitigation of frequency instability.	New England 39-bus system.	Eigenvalue of the load flow Jacobian, frequency, and ROCOF thresholds.	RTDS and the GTNET-PMU component within the RSCAD software were used. However, the computation was done offline by exporting the PMU measurements/plots obtained in RSCAD Runtime to MATLAB. Actual PMU hardware and C37.118 network streaming were not implemented.	Generator and line contingencies.	Calculation of the active power imbalance based on the system frequency response model using the swing equation.	Sensitivity analysis based on the power flow tracing method.	An investigation on several time delays was presented.	Proposed the use of power flow tracing in the determination of the optimal loads to shed.
10	Yang *et al*. (2013)	Centralized adaptive UFLS scheme using generator swing equation to calculate the real power mismatch. The load buses to curtail are identified using the voltage dip information at these buses for the mitigation of frequency instability.	New England 39-bus system.	Maximum frequency deviation.	Hardware platform not used. The availability of synchrophasor measurements was assumed.	Generator contingencies.	The calculation of the active power imbalance based on the system frequency response model using the swing equation.	Determined according to the initial active power load demand at the load buses.	0.2 s.	Provided a comparison of the proposed adaptive UFLS and conventional UFLS schemes.

Table 3.6: Literature review of undervoltage load shedding using synchrophasor measurements cont'd

S/N	Paper	Methodology	Network Model Used	Type of Trigger Used	Implementation /Simulation Platform	Contingencies Considered	Calc. of Amount to Shed/Nr. of Steps	Determination of Where to Shed	Time Delay Between Load Shedding Steps	Contribution(s)
11	Abdelwahid *et al*. (2014)	Centralized adaptive UFLS using the rate of frequency decline to calculate the amount of load to shed. The load buses to curtail are identified using the voltage dip information at these buses for the mitigation of frequency instability.	WECC 9-bus test system.	Based on a threshold obtained using the Centre of Inertia (COI) frequency.	OPAL-RT eMEGAsim OP5600 was used with actual PMU hardware connected.	Generator contingencies.	Calculation of the active power imbalance based on the system frequency response model using the swing equation.	The voltage dip information was used to compute the sensitivities for identifying the critical buses in the network.	Time delay for the proposed adaptive centralized UFLS scheme was not given. Time delay for the conventional decentralized UFLS scheme are given as 10, 20 30 cycles for 3 load shedding stages respectively.	UFLS using external PMUs in a hardware-in-the-loop simulation with OPAL-RT was implemented.

Also, (Tang *et al*., 2013; Saffarian and Sanaye-Pasand, 2012; Ghaleh *et al*., 2011; Saffarian and Sanaye-Pasand, 2011; Seethalekshmi *et al*., 2011; Seyedi and Sanaye-Pasand, 2009a; 2009b) did not consider the mechanism of voltage collapse involving transformer ULTCs, generator OXLs, and dynamic load characteristics in their studies.

Furthermore, the above-mentioned load shedding schemes for the combined mitigation of frequency and voltage instabilities were not tested on a classical voltage collapse condition. It would seem that the aim of these algorithms was to implement an UFLS scheme while preventing the system from degenerating into a low voltage condition. However, these do not serve as a remedial action for a purely voltage collapse problem involving the loss of critical transmission lines, the dynamics of tap-changer actions, generator OXL operation, and other mechanism of voltage instability.

Most of the existing synchrophasor-based methods in the literature (Tang *et al*., 2013; Seethalekshimi *et al*., 2011; Corsi, 2010; Girgis and Mathure, 2010; Glavic and Van Cutsem 2010; Seethalekshimi *et al*., 2010; Nikolaidis *et al.,* 2008; Wang *et al*., 2005) did not make use of actual synchrophasor measurements from real PMUs. Rather, the measurements used were assumed to be from PMUs.

However, it is necessary to understand that synchrophasors are distinct because of the type of filters used, the estimation algorithm, reporting rates, performance class, and the data communication across the Ethernet network. Also, it is important to investigate the impact of communication latency, jitter, congestion, and bandwidth on the synchrophasor-based load shedding scheme. The above were considered, and practically implemented in the various studies carried out in this thesis.

3.5 Industrial Use Cases

3.5.1 Review of Use Cases

Industrial use cases on under-voltage load shedding schemes implemented in electric power utilities are presented in this subsection.

Taylor (1992) presented an outline of a decentralised under-voltage load shedding scheme implemented by the US Pacific Northwest utilities for a winter season. UVLS protection relays were used at fixed load buses, the amount to shed was also fixed at 5%. The pick-up values were predetermined to be 0.9 p.u., 0.92 p.u. and 0.92 p.u. for steps 1-3 load shedding respectively. Similarly, the time delay used were fixed at 3.5 s, 5.0 s, and 8.0 s for steps 1-3 load shedding respectively.

Nirenberg and McInnis (1992) reported the development of a SCADA-based Fast Acting Load Shedding (FALS) scheme in Florida Light and Power Company in the US for counteracting the voltage collapse caused by multiple contingencies. The system conditions monitored were the bus voltages, line flows, or a massive deviation from a previous value. When triggered, 800 MW of load was shed with a time delay of 20 s.

Miller *et al*. (1993) presented a study carried out by five utilities in the Puget Sound area within the US. Decentralised UVLS relays with several load shedding steps were used with a pick-up voltage of 0.9 p.u. and time delay between 4 s to 13 s. Various under-voltage load shedding schemes implemented in the US utilities within the Western Electricity Coordinating Council (WECC) were reported in (WECC, 1999). These UVLS schemes were based on the shedding of pre-determined loads after a time delay. P-V curves and knowledge of the system were used in the determination of the amount of load to shed and the best location to shed.

A SCADA-based centralised load shedding scheme for mitigating voltage instability resulting from double contingencies was developed and used in the Entergy system in the US (Kolluri *et al*., 2000). The trigger for arming the UVLS scheme includes the system load level, bus voltages in three out of four load buses dropping to 0.92 p.u. or less, and the status of some selected generators. Three predetermined load blocks for three load shedding steps were chosen in the implementation of the UVLS scheme. The loads to shed for the three steps were 60 MW, 120 MW, and 150 MW respectively. The time delays used for the individual steps were 4 s, 12 s, and 20 s respectively.

Mechenbier *et al*. (2004) described an UVLS scheme designed for the Public Service Company of New Mexico (PNM) against short-term and long-term voltage collapse conditions respectively. The design resulted to the implementation of a fast and reliable scheme referred to as the Import Contingency Load Shedding Scheme (ICLSS). The delay and the unpredictability associated with this conventional UVLS scheme was shown to be minimal. The ICLSS was designed to trip radial lines during emergency conditions by opening the breaker(s) at one substation, while opening the breaker(s) at two substations for looped lines. This effectively disconnected the distribution stations until the voltage recovered above 0.95 p.u.

Trudel *et al*. (1999) presented the defence plan implemented at Hydro-Quebec in Canada against extreme emergencies. The defence plan included an UVLS scheme amongst three other protection schemes. The UVLS scheme was a distributed design

aimed at acting independently from the local 735 kV buses. A total of 2000 MW of load can be shed in multiple steps. An undervoltage load-shedding scheme implemented in BC Hydro, Canada was based on the measurements of under-voltage conditions in the system around Vancouver Island (Begovic *et al*., 1995). The UVLS scheme monitored the under-voltage in three areas of the system and issued a load shedding trip to the load blocks if two out of the three areas had under-voltage conditions, and if the reactive power outputs from four synchronous condensers in area 3 operated closer to their rated output. Block 1 was shed after 10 s, while blocks 2 and 3 loads were shed after 2 s and 4 s respectively.

Similarly, Ingelsson *et al*. (1997) described a SCADA-based wide area protection system for the Southern Sweden electric power network. The pick-up voltage for area 1 was 0.9125 p.u. with a time delay of 5 s. Area 2 had a pick-up voltage of 0.925 p.u. and a time delay of 2 s. The load shedding logic uses a combination of the information from the remote end voltages, generator current limiter, and the status of the system generators. Centralised and distributed UVLS schemes based on system events and responses were presented by Nikolaidis *et al*. (2008) for the Greek Hellenic Interconnected System (HIS). Two event-based schemes implemented in the Greek HIS were discussed. The first event-driven scheme was implemented in Attica. It was made up of ten commands for shedding specific load blocks in the northern interconnections. The second event-driven scheme was implemented in Peloponnese for tripping specific lines in the transmission system in order to protect the system against voltage collapse.

The UVLS scheme implemented at the Tokyo Electric Power Company (TEPCO) was described in Imai (2005). The scheme was implemented by deploying Monitoring and Judging (MJ) units at four 500 kV substations, and Load Shedding (LS) units at 275/154/66 kV substations. The decision-making logic used the statuses of three out of the four 500 kV substations. Load is shed continuously until the system recovered from the under-voltage condition. Shin *et al*. (2009) described an event-based UVLS scheme applied in the Korea Electric Power Corporation (KEPCO). The implemented UVLS scheme is a single-step load shedding scheme designed to shed 1000 MW of load after a 200 ms delay following a contingency involving one of the parallel 765 kV transmission lines, and the violation of the pre-set voltage threshold on a pilot bus.

3.5.2 Discussion

The most widely adopted under-voltage load shedding schemes in utilities around the world are based on the use of distributed undervoltage (ANSI 27) protection relays (Shin *et al*., 2009; Imai, 2005; Trudel *et al*., 1999; WECC, 1999; Begovic *et al*., 1995; Miller *et al*., 1993; Taylor, 1992).

However, these schemes are usually based on the threshold derived from the local bus voltage magnitude. Also, a fixed pre-determined amount of load is shed at the bus at a pre-determined time irrespective of the level of the disturbance in the system. Furthermore, the load shedding locations are fixed. This implies that some healthy buses will be shed by the local protective relay, while some unhealthy buses will be left untouched. This could lead to an over-voltage condition in some buses while some other buses will experience a severe under-voltage condition. Centralised schemes based on a central decision-making controller were presented in (Nikolaidis *et al*., 2008; Kolluri *et al*., 2000; Ingelsson *et al*., 1997; Nirenberg and McInnis, 1992). However, these schemes were based on SCADA measurements with slow polling rates.

From the foregoing, it can be inferred that these UVLS schemes might fail for short-term voltage instability conditions accompanied by a fast voltage decay. These fast system dynamics can be reliably captured using high speed synchrophasor measurements from PMUs. Also, these time-synchronized measurements (synchrophasors) can be published to centralised controllers where decisions can be made based on the real-time observability of the system.

3.6 Chapter Summary

This Chapter has presented an introduction to SIPSs, and a comprehensive review of the literature covering the control of transformer tap-changers and under-voltage load shedding methods and schemes. The various methods available in the existing literature were compared and contrasted. The reviewed transformer tap-changer control methods considered in the literature are related to the control and coordination of tap-changers for multiple transformers in parallel. Also, tap-changer control methods for counteracting voltage instability were considered. This includes tap-changer blocking, tap-reversal, and voltage set-point changing.

From the review carried out, it was observed that synchrophasor measurements have not been applied in tap-changer control methods for mitigating voltage instability. Therefore, this thesis considers the implementation of a tap changer

blocking/unblocking algorithm using IEEE C37.118 synchrophasor measurements and IEC 61850 GOOSE messages as control signals.

The review of undervoltage load shedding methods based on conventional and adaptive schemes using distributed under-voltage relays, SCADA-based measurements and synchrophasor measurements were conducted. Most of these methods were generally based on the use of the P-V curve method, analytical methods using the System Frequency Reference (SFR) model, and the real power mismatch methods. The drawbacks of these methods include the following:
(i) The SFR model will fail for voltage instability conditions where the change in frequency is negligible; and
(ii) Under certain conditions, the synchronous generators in the power system are controlled by governors with a fixed mechanical torque set-point, and the real power generated will not vary. Thus, the methods based on the relationship between the load real power and the generated real power are inadequate for such conditions.

Also, the use of conventional SCADA measurements implies that measurements from various parts of the power system will be incorrectly concentrated and analysed. This is because SCADA measurements are not time-synchronised at the point of acquisition and are polled only every 2-10 s. This means that the correlation of measurements from different sections of the system is difficult. Also, certain system dynamics might not be detected in time.

Some of the existing methods in the academic literature made use of optimization techniques which are usually iterative in nature. This makes their application in practical systems cumbersome. The use of synchrophasor measurements and a proposed reactive power mismatch method will address the drawbacks mentioned above, and would facilitate the design of an adaptive UVLS scheme that can be applied during short-term and long-term disturbances respectively.

Chapter Four presents the proposed synchrophasor-based voltage stability assessment method and its various algorithms. Three types of generator-derived indices were proposed. The proposed indices were further extended for wide area application comprising of various voltage control areas. This included the derivation of an adaptive weighted factor for calculating the contribution of the individual generators to the reactive power support of their respective voltage control areas.

CHAPTER FOUR

METHODOLOGY FOR THE DESIGN OF WIDE AREA VOLTAGE STABILITY ASSESSMENT SYSTEM

4.1 Introduction

State Estimation (SE) using Supervisory Control and Data Acquisition (SCADA) measurement is commonly used by electric power utilities for providing information on the state of the power system. The concept of SE is well documented in (Monticelli, 1999; Schweppe and Rom, 1970).

The operating state of a power system can be estimated by using the network model and the voltage magnitudes at the system buses. If the bus admittance matrix Y and the bus voltage phasors V are known, the branch current I can be calculated from a given matrix equation of the form:

$$\mathbf{I} = \mathbf{YV} \tag{4.1}$$

SCADA systems use system variables which include voltage magnitudes, real and reactive power, and system topology information polled from field devices like meters, transducers, relays, and Intelligent Electronic Devices (IEDs) for the estimation of the system's state. A scan of these devices could take 2 to 10 s (Thomas and McDonalds, 2015). Figure 4.1 shows a typical SCADA architecture. Measurements acquired from the field devices are transmitted via the communication links (channel) to the SCADA-level using Remote Terminal Units (RTUs)/IEDs.

For a SCADA-based system, the measurements from the substation instrument transformers are converted to the appropriate signal level using transducers. The analogue signals are afterwards converted to digital signals by the analogue input module of the RTU for onward transmission to the master station in the control centre. With emerging technologies based on the IEC 61850 standard, the measurements from the instrument transformers can be published as IEC 61850 analogue GOOSE or sampled value messages on the Ethernet communication infrastructure without the need for transducers. At the master station, a collection of peripherals and Inputs/Outputs (I/Os) are used by the operators to monitor the system's state and execute the appropriate control actions. The Human-Machine Interface (HMI) is used as the interface to display the interaction between the master station and the SCADA operators.

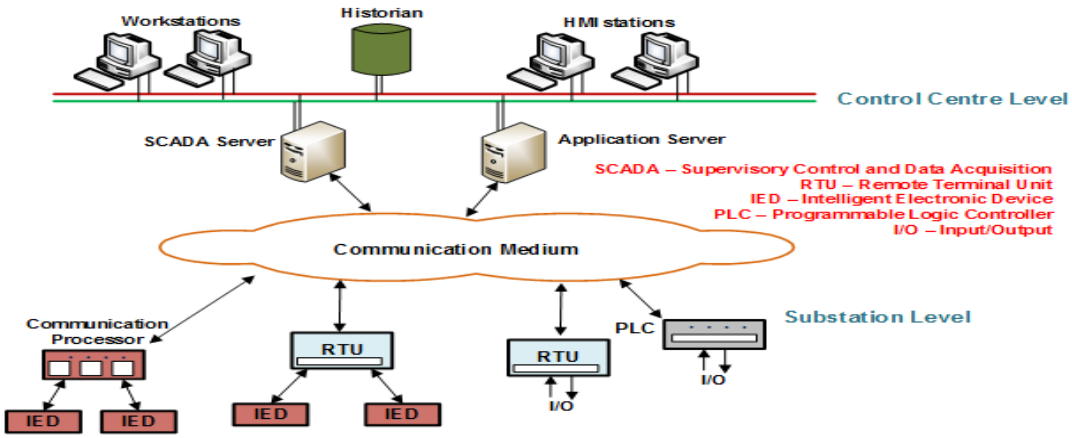

Figure 4.1: A typical SCADA architecture

In recent times, the concept of wide area measurement and applications using synchrophasor measurements has been widely discussed. Very good results have been reported in the literature on academic research and pilot schemes relating to this.

Some of the major synchrophasor-based applications include:

- Monitoring and real-time situational awareness.
- Improving power system state estimation.
- Adaptive protection and real-time control.
- Power system restoration.
- Real-time congestion management.
- Benchmarking, validation and fine-tuning of system models.
- Overload monitoring and dynamic rating.
- Postmortem disturbance analysis.

A comparison of SCADA-based measurements and synchrophasor measurements is presented in Table 4.1. From Table 4.1, it can be seen that SCADA systems are limited by their slow data sampling rate, slow data communication rates, unsynchronised measurements, and time-consuming state estimation.

In order to prevent voltage instability/voltage collapse in a timely manner, it is necessary to implement real-time stability assessment indices for monitoring the grid security through improved situation awareness and wide area monitoring. As the system tends towards its emergency state, appropriate countermeasures can be implemented to halt this progression and restore the system to its normal acceptable state. Wide Area Monitoring, Protection and Control (WAMPAC) systems are implemented using system-wide measurements from dispersed Phasor Measurement Units (PMUs) time-synchronized to a reference time source such as the Global Positioning System (GPS). The synchrophasor measurements obtained from various parts of the system are streamed (transmitted) to the control centre where monitoring and control algorithms are applied.

Table 4.1: Comparison of PMU-based systems and SCADA-based systems

S/N	PMU-Based Measurements	SCADA-Based Measurements
1	Measurements are synchronized and referenced to a common time base usually the GPS.	Measurements are asynchronous and not acquired simultaneously.
2	Time synchronization is done at the measurement stage.	Time synchronization is done on arrival at the Energy Management System (EMS).
3	Data acquisition can be done with reporting rates of up to four times the nominal system frequency/second (240fps or 200fps).	Relatively slow. Scanning of devices done periodically (1 observation every 4 seconds) and takes 2-10 seconds.
4	Adequate for transient disturbances.	The low data rate of SCADA-based system could be too slow to capture transient disturbances.
5	Requires fewer measurements to provide the system state and does not require iterative state estimation. Angle measurements are obtained directly, no need for calculations.	Requires more system variable for SE. Measurements required are voltage magnitudes, real and reactive power, and system topology to calculate phase angles.
6	Having direct measurement of angle eliminates the errors due to the inaccuracies in network parameters.	The calculation of angles depends on system reactance which depends on system topology. Thus, SCADA-based SE is prone to inaccuracies.
7	Suitable for capturing dynamic changes.	Fails when the system state is changing quickly especially during dynamic conditions.
8	Suitable for wide area monitoring, protection and control as a result of the time-stamped phasor measurements.	Only suitable for local monitoring and control.
9	Capable of oscillation detection.	Not suitable for oscillation detection.
10	Perfect for steady-state, dynamic, & transient conditions.	Steady-state only.

This Chapter proposes methods and algorithms for the design and implementation of a real-time wide area voltage stability assessment system using actual synchrophasor measurements from PMUs. The methods and algorithms are designed for a large interconnected multi-area power system.

This can be summarized as comprising of the following as shown in Figure 4.2:

- Complete system observability through the determination of the minimum number of PMUs and their optimal placement using a Binary Integer Programming (BIL) algorithm, the consideration of Zero Injection Buses (ZIBs), and the critical bus information obtained from the Modal Participation Factors (MPFs) derived from the eigenvalues of the load flow Jacobian.
- The partitioning of a large interconnected power system into multiple coherent areas with similar voltage collapse problem and clusters of reactive power sources providing reactive power support to the load buses.
- Real-Time Voltage Stability Assessment (RVSA) indices derived from the synchronous machines in the power system are newly proposed in this thesis. The RVSA indices are computed from the reactive power margin, field current margin, and stator current margin. Synchrophasor measurements from actual PMUs are used as inputs to the obtained derivations.

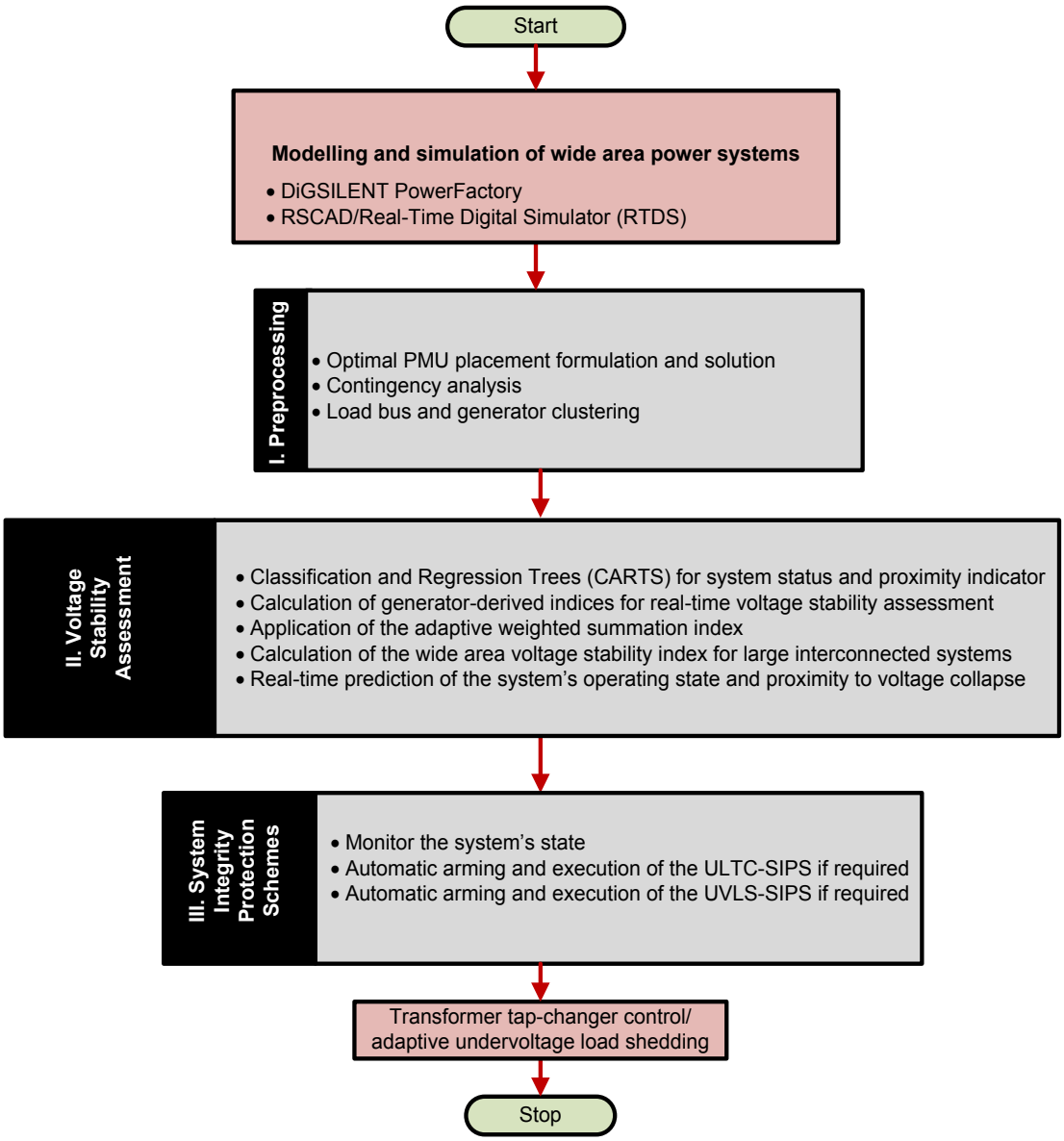

Figure 4.2: **Breakdown structure of the proposed methods and algorithms**

4.2 Optimal PMU Placement for Voltage Stability Assessment

Synchrophasor measurements from Phasor Measurement Units (PMUs) are increasingly being applied in Wide Area Monitoring, Protection, and Control (WAMPAC) schemes. Consequently, it is important to optimally determine the location of these PMUs in order to reduce the cost of PMU integration and the amount of PMU data that would be processed or analysed.

The Optimal PMU Placement (OPP) algorithm proposed in this thesis provides formulations and methods of solution for the OPP problem with respect to voltage stability assessment by considering the impact of ZIBs, critical/weak buses, and PMU redundancy for single device outage.

The connectivity matrix for the Binary Integer Programming (BIL) method was extended, and observability constraints were introduced on the basis of the analyses of the network topology, Modal Participation Factors (MPFs) from the load flow Jacobian, and the introduction of redundancy for N-1 PMU outage in the observability of the critical buses in the system.

The OPP problem formulations and solutions are presented in (Adewole and Tzoneva, 2015e; 2014a). The MATLAB code for the OPP implementation is given in Appendix B.

4.3 Measurement-Based Load Bus and Generator Clustering for Voltage Stability Assessment

The proposed synchronous generator-derived RVSA index provides system-wide situation awareness using the information obtained from the widely dispersed synchronous generators in the power system. This implies that, the use of the power system's admittance matrix to achieve complete system observability and wide area monitoring is no longer required. Consequently, the total number of PMUs required in the system is substantially reduced.

Indices derived from the Reactive Power Reserves (RPRs) at the generators have been shown to be effective for voltage stability assessment in (Adewole and Tzoneva, 2015c; 2014f; 2014b; Liu and Chu, 2014; Leonardi and Ajjarapu, 2013; Mousavi *et al*., 2013; Choi *et al*., 2011; Capitanescu and Van Cutsem, 2001; Schlueter, 1998). Thus, the availability of an adequate level of RPR is an indication that the system is stable and operating within acceptable system limits.

In order to effectively monitor the voltage stability of a power system, it is necessary to determine the set of synchronous generator(s) providing reactive power support/voltage control at the load buses for various system operating conditions. A set of generators providing voltage control for a set of load buses or area belongs to a coherent group, and serves as the Reactive Power Reserve Basin (RPRB) for those load buses (Schlueter, 1998). This provides a less complex, but practical way of determining the state of the power system and its margin to voltage instability.

4.3.1 Previous Work

The traditional application of coherency grouping in power system is in the development of reduced order models for the decomposition of large interconnected systems into smaller equivalent systems (Kim *et al*., 2004; Chow *et al*., 1995; Zaborszky *et al*., 1982; Podmore, 1978). The use of reduced equivalent models allows power system analysis to be less complex, with less computational effort especially when a large number of scenarios need to be studied. Generator coherency analysis was used in (Wei *et al*., 2014; Ariff and Pal, 2013; Agrawal and Thukaram, 2013; Juarez *et al*., 2011; Xue and Pavella, 1993; Nath *et al*., 1985) for transient stability studies.

Other applications of coherency grouping include oscillation detection (Jonsson *et al*., 2004), vulnerability assessment (Kamwa *et al*., 2009), and fault event location (Mei *et al*., 2008). Coherency methods for reduced order models, oscillation detection, vulnerability assessment, and transient stability studies would fail when applied in voltage stability assessment because the operating conditions and sequence of events leading to power system oscillation or transient instability are different for voltage instability. Also, the system variables used in transient stability studies, oscillation detection, and vulnerability assessment are mainly generator speed, generator rotor angles, or other generator swing-related variables.

Exploratory investigations carried out in this thesis have shown that these variables are poor indicators of a purely voltage instability event. Also, for voltage stability assessment, it is only at the voltage collapse point that generators tend to accelerate and swing against each other. However, control actions are usually unpredictable when implemented in the unstable region of the power system. Thus, the system must be monitored continuously and control actions must be timely initiated at the system 'Alert' state before the system becomes unstable.

An algorithm for clustering the generators in the system into RPR basins by using the Jacobian of the reactive power and voltage was described in (Schlueter, 1998). The partitioning method by (Nuhanovic *et al*., 1998) was based on voltage variation at each load bus with respect to real power and reactive power variations at the other load buses. The real and reactive powers at the load buses of interest were related to the voltage level by computing the reduced Jacobian of the load flow.

The generator coherency method proposed by (Nath *et al*., 1985) for transient stability study was modified by (Zambroni de Souza and Quintana, 1994) for voltage stability studies. In (Nuhanovic *et al*., 1998) the reduced Jacobian matrix and modal

analysis of the system load flow was used. A method based on sensitivities derived from the reactive power flowing in a line with respect to the reactive power injection at a load bus was suggested in (Aumuller and Saha, 2003), while Rameshkhah *et al*. 2010 made use of modal-analysis and the shuffled frog-leaping algorithm.

Some of the limitations of these existing methods include: (i) the computation of the reduced Jacobian is required for each load bus in the system; (ii) the use of modal analysis requires multiple load flow studies for each operating point. This is rather time consuming for a large system; and (iii) an assumption made by Rameshkhah *et al*. 2010) was that the clustering can be done just once. However, a single event can lead to a sequence of cascading events resulting in voltage instability. This combination of cascading disturbances would likely result to the formation of a group of clusters different from the original one.

In practical systems, online wide area protection and control schemes would require fast real-time coherency analysis to be carried out. This is easily achieved by using a measurement-based method. Measurement-based methods have been proposed for coherency grouping in transient stability studies (Wei *et al*., 2014; Ariff and Pal, 2013), dynamic vulnerability assessment (Kamwa *et al*., 2009), event location after a disturbance (Mei *et al*., 2008). However, PMU-related hardware was not used in (Wei *et al*., 2014; Ariff and Pal, 2013; Kamwa *et al*., 2009; Mei *et al*., 2008). Rather, assumptions were made that the simulation measurements from MATLAB/Simulink, SIMPOW®, DSA-PowerTools, PSAT, and other power system simulation tools are equivalent to the synchrophasor measurements from PMUs.

A novel measurement-based approach in the identification of the coherent groups in load buses and synchronous generators for voltage stability assessment application in large interconnected power systems is presented and investigated in this subsection. The proposed measurement-based approach uses synchrophasor voltage and voltage deviation for load bus clustering, and generator reactive power and its derivatives for generator clustering respectively. A hybrid Calinski-Harabasz criterion and *k*-means clustering algorithm is applied in the determination of the cluster groups in the power system with respect to voltage stability and its assessment.

4.3.2 Proposed Measurement-Based Coherency Algorithm

A measurement-based coherency algorithm using the Calinski-Harabasz criterion and *k*-means algorithm is proposed for clustering the load buses and the generators in the system into Voltage Control Areas (VCAs) and Reactive Power Reserve Basins (RPRBs) respectively.

Clustering is an unsupervised knowledge-based learning algorithm which is used to discover the pattern within a set of objects. Thus, similar objects are grouped into the same cluster, with objects belonging to the same cluster sharing similar properties with one another. Objects belonging to different clusters share less similarity together.

Clustering algorithms can be broadly classified into two types (MATLAB Statistic Toolbox, 2014; Hardle and Simar, 2007; Johnson and Wichern, 2007):

- Hierarchical algorithms; and
- Partitioning algorithms.

The *k*-means algorithm is a type of clustering algorithm (partitioning type), and it groups the objects into pre-selected k mutually exclusive clusters by searching for partitions in which objects within each partition are closer to each other, and far from objects in the other partitions. The centroid for the respective clusters is the point that has the minimum summation distance from all objects in that cluster. An iterative algorithm is used to minimize the sum of the distances to the cluster centroid by exchanging objects between the clusters until the minimum sum is obtained. The Euclidean distance is the length of the line segment between two points A and B.

The Euclidean distance is given as (MATLAB Statistic Toolbox, 2014):

$$\| A - B \| = \sqrt{(A_1 - B_1)^2 + (A_2 - B_2)^2 + \ldots + (A_n - B_n)^2} \tag{4.2}$$

The *k*-means algorithm was applied in this thesis because it is non-hierarchical, non-overlapping, has faster convergence, it is memory-efficient, good for large amount of data, and the results obtained from it are easy to interpret (MATLAB Statistic Toolbox, 2014).

The steps involved in the implementation of the *k*-means algorithm are given below:

Step 1: Choose the number of clusters k to partition the objects in the data into.

Step 2: Read the input synchrophasor measurements.

Step 3: Obtain the centroids of the cluster.

Step 4: Calculate the distance between the objects in the data and the cluster centroids.

Step 5: Allocate the objects to the closest cluster.

Step 6: Repeat Steps 3-5 until the stopping criteria are satisfied.

The stopping criteria are:

- The number of iterations;
- No changes in the vectors of the centroid over an iteration threshold; and
- No changes in the cluster membership.

Although, the number of clusters k needs to be known before the *k*-means algorithm can be applied, the Calinski-Harabasz Criterion (CHC) can be used in the optimal determination of the number of clusters to use.

The CHC is given as (Calinski and Harabasz, 1974):

$$V(k) = \max_k CHC(k) = \frac{SS_{Bk}}{SS_{Wk}} \times \frac{(N_o - k)}{(k-1)}, \quad k = \overline{1, N_g} \tag{4.3}$$

where SS_{Bk} is the overall variance between the clusters, SS_{Wk} is the overall variance within the cluster, N_g is the maximum number of clusters considered, and N_o is the number of observations.

$$SS_{Bk} = \sum_{k=1}^{N_g} n_k \left\| m_k - m \right\|^2 \tag{4.4}$$

$$SS_{Wk} = \sum_{k=1}^{Ng} \sum_{x \in C_k} \left\| x - mk \right\|^2 \tag{4.5}$$

where m_k is the centroid of the kth cluster, m is the mean of the data, n_k is the number of points in the kth cluster, x is the data point, C_k is the kth cluster, $\left\| m_k - m \right\|$ and $\left\| x - m_k \right\|$ are the Euclidean distances between the two vectors respectively.

The optimal number of clusters is obtained by maximizing CHC_k with respect to the number of clusters k. This is because the best partitioning is obtained with the largest CHC_k possible by using a large value of SS_B and a small value of SS_W respectively.

A hybrid algorithm combining the Calinski-Harabasz criterion and the *k*-means algorithm is proposed in this thesis for the synchronous generators and load bus clustering carried out with respect to voltage stability assessment. The flowchart for the proposed hybrid *k*-means clustering algorithm is summarized in Figure 4.3.
where V_k is a vector of the $CHC(k)$ values for $k = \overline{1, N_g}$.

An exploratory investigation was carried out to determine the best variables to use as inputs to the proposed hybrid clustering algorithm. The results obtained were evaluated using the CHC values and the silhouette coefficient respectively.

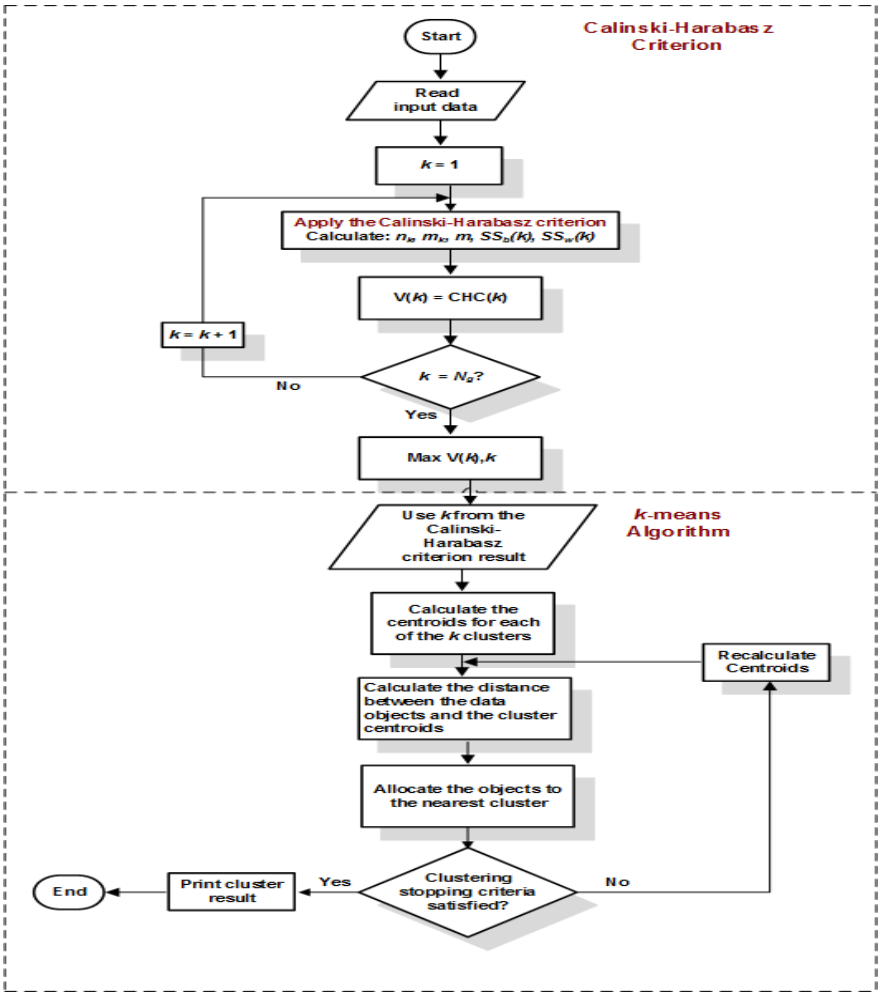

Figure 4.3: **Proposed algorithm using a hybrid CHC and k-means clustering**

The silhouette coefficient gives an indication of how well-defined the cluster is and the proximity of points in one cluster to points in the neighbouring clusters. The coefficient is made up of the mean distance (a) between an object and all other points in the same cluster, and the mean distance (b) between an object and all other points in the next neighbouring cluster(s). A well partitioned cluster groups should have positive silhouette coefficients.

The silhouette coefficient (s) is given as (MATLAB Statistic Toolbox, 2014):

$$s = \frac{b-a}{\max(a,b)}, \quad -1 \le s \le 1 \tag{4.6}$$

The result of the Calinski-Harabasz algorithm gives the optimal number of clusters which must be used as the input to the *k*-means algorithm for clustering the load buses and the reactive power sources in the system into VCAs and RPRBs respectively. The MATLAB code for the clustering algorithm is given in Appendix C, while the Graphical User Interface (GUI) developed is given in Appendix J.

4.4 Voltage Stability Assessment Indices Based on Synchrophasor Measurements

The measurement-based clustering algorithm proposed in Section 4.3 is first applied to a large interconnected power system to partition the power system into coherent areas comprising of load buses with similar voltage collapse problem, and reactive power sources providing voltage control to the respective individual voltage control areas.

The generator-derived Voltage Stability Assessment (VSA) indices for large interconnected power systems are then applied to the various voltage control areas and their respective reactive power reserve basin for real-time prediction of the system's operating state and margin to voltage collapse.

Comparative analyses are carried out between the existing index based on generator reactive power reserve, and the newly proposed indices based on generator field current and generator stator current respectively. Voltage instability could be caused by small disturbances such as incremental changes in load conditions and the effects of discrete and continuous controls. While large disturbance voltage instability is due to the loss of transmission line(s), loss of generation, and system faults. An in-depth review of the various methods for VSA was previously presented in Chapter Two.

The proposed VSA method in this thesis is based on actual PMU measurements, and can be easily applied in practical power systems for real-time VSA. It should be noted that since the VSA algorithm is measurements-based, no iteration is needed in its computation.

4.4.1 Effective Generator Reactive Power Reserve (EGRPR) Index

Synchronous generators have been reported to be the most dynamic source of reactive power supply in power systems, and are primarily responsible for voltage control in power systems (Van Cutsem and Vournas, 2008; Avramovik and Fink, 1992). They are typically made up of armature (stator) windings, field winding, and damper windings. These windings are magnetically coupled to one another with their inductances varying with time periodically.

The field windings produce a magnetic field from the direct current flowing through it. This induces an alternating voltage in the armature windings of the generator. The magnetic coupling between these windings, and the flux linkage in each winding is a function of the rotor position (Andersson and Fouad, 2003; Fitzgerald *et al*., 2003). Figure 4.4 shows the schematic diagram of a typical synchronous machine with the various windings and orientation.

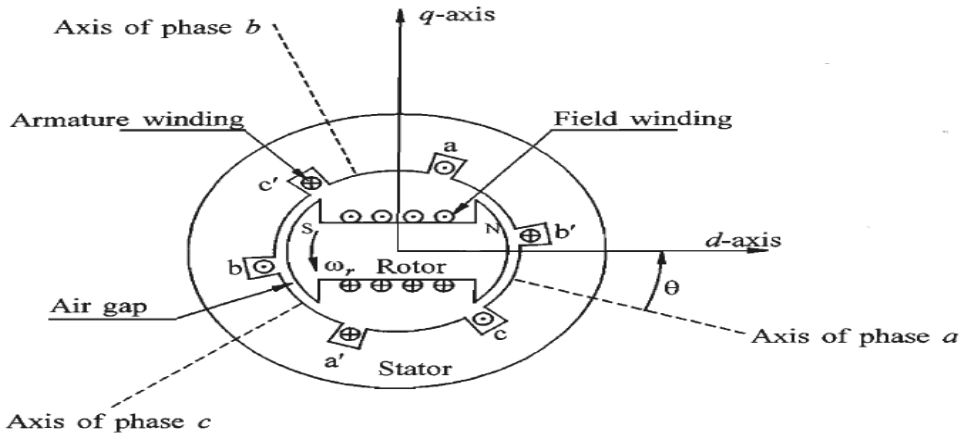

Figure 4.4: **Schematic diagram of a synchronous machine (Kundur, 1994)**

Power system stability is greatly influenced by the available RPR in the system. Heavily stressed power systems without adequate reactive power support are more prone to voltage collapse. The concept of VCAs and RPRBs was presented in (Schlueter, 1998; Avramovic and Fink, 1992). This was based on the partitioning of the load buses in the power system into coherent VCAs with similar voltage collapse problem. A set of synchronous machines providing reactive power support and protecting a particular VCA from voltage collapse was referred to as the RPRB for that VCA. Thus, a measure of the reactive power support available in each RPRB can be used as an indication of the system's voltage stability margin.

The Technical Generator Reactive Power Reserve (TGRPR) is the difference between the generator's maximum reactive power (obtained from the generator capability curve) and the generator's reactive power at the current operating point. Although, the TGRPR is easier to understand and is readily available from the generator manufacturer datasheet (generator capability curve), the TGRPR may be misleading in situations where the TGRPR is positive yet voltage collapse occurs. This is because not all the reactive power specified in the manufacturer's capability curve is available for voltage control at the voltage collapse point.

Also, the capability curve does not take into cognizance the power system operating condition and the dynamic interaction with other generators within the power system. A more suitable reserve is the Effective Generator Reactive Power Reserve (EGRPR) (Mousavi *et al.*, 2013; Leonardi and Ajjarapu, 2008; Ruiz and Sauer, 2006; Capitanescu and Van Cutsem, 2001). The EGRPR is the difference between the generator's maximum reactive power at the voltage collapse point and the generator reactive power at the current operating point. These definitions are further illustrated in Figure 4.5.

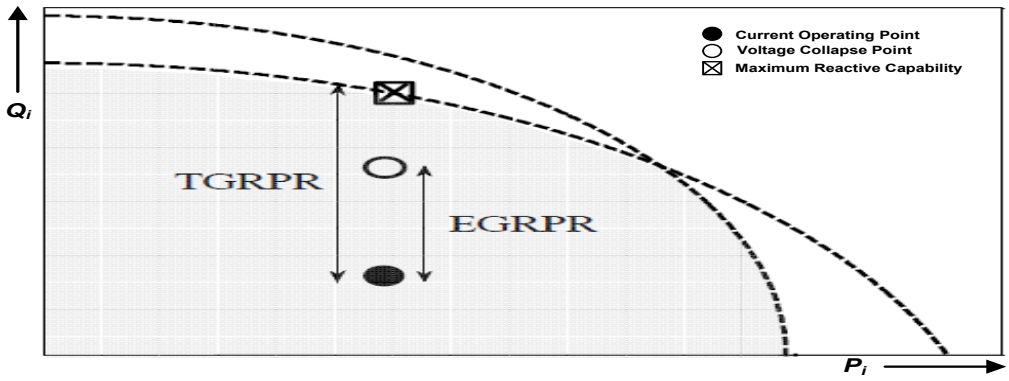

Figure 4.5: **Generator capability curve for TGRPR and EGRPR (Mousavi *et al.*, 2013)**

The complex power per phase generated by a synchronous generator is given as (Kundur, 1994):

$$S_g = P_g + jQ_g = V_g I_a^* \tag{4.7}$$

The internal voltage of a synchronous generator is:

$$E_{af} = V_g + R_a I_a + jX_s I_a \tag{4.8}$$

where P_g and Q_g are the generator real and reactive powers per phase respectively. E_{af} and V_g are the internal and terminal generator phase voltages, I_a is the stator phase current, X_s is the synchronous reactance per phase, and R_a is the armature resistance per phase.

Since R_a is negligible for the synchronous generators (Fitzgerald *et al.*, 2003), then:

$$E_{af} = V_g + jX_s I_a \tag{4.9}$$

From Equation (4.8), I_a can be obtained and substituted in Equation (4.7). If synchrophasor measurements of the generator internal and terminal voltage magnitudes ($|E_{af}|$, $|V_g|$) and stator current magnitudes ($|I_a|$) are used, this gives:

$$P_g + jQ_g = |V_g| \left(\frac{|E_{af}| - |V_g|}{jX_s} \right) \tag{4.10}$$

If $E_{af} \approx I_{fdmax}$ (Walker, 1953), then $P_g = P_{gmax}$, $Q_g = Q_{gmax}$, where P_{gmax} and Q_{gmax} are the maximum real and reactive powers of the synchronous generator, and I_{fdmax} is the maximum field current. I_{fdmax} can be obtained as analogue measurements from PMUs. The derivation for the considered generator is given below:

$$P_{g\max}^2 + \left(Q_{g\max} + \frac{|V_g|^2}{X_s} \right)^2 = \left(\frac{|V_g| I_{fd\max}}{X_s} \right)^2 \tag{4.11}$$

$$\left(Q_{g\max} + \frac{|V_g|^2}{X_s} \right)^2 = \left(\frac{|V_g| I_{fd\max}}{X_s} \right)^2 - P_{g\max}^2 \tag{4.12}$$

$$\left(Q_{g\max} + \frac{|V_g|^2}{X_s} \right) = \sqrt{\left(\frac{|V_g| I_{fd\max}}{X_S} \right)^2 - P_{g\max}^2} \tag{4.13}$$

The maximum reactive power that the synchronous generator can produce while considering the generator field current is given as:

$$Q_{g\max} = -\frac{|V_g|^2}{X_s} + \sqrt{\frac{|V_g|^2 I_{fd\max}^2}{X_s^2} - P_{g\max}^2} \tag{4.14}$$

On the basis of Equation (4.14), the EGRPR is given mathematically as:

$$EGRPR = Q_{g\max}^c - Q_{gk} \tag{4.15}$$

where $Q_{g\max}^c$ is the maximum synchronous generator reactive power at the point of voltage collapse (usually less than the manufacturer defined reactive power capability rating Q_{gmax}), Q_{gk} is the reactive power of the synchronous generator at the current operating time k.

From the foregoing, a Real-Time Voltage Stability Assessment (RVSA) index based on the reactive power reserve (EGRPR) is defined as:

$$RVSA_{Q,ik} = \left(\frac{Q_{g\max i}^c - Q_{gki}}{Q_{g\max i}^c} \right) \times 100\ \% \quad , \quad k = 0, 1, 2, \ldots \tag{4.16}$$

where k is the discrete time for the operation of the RVSA index.

Equation (4.16) can be rewritten as:

$$RVSA_{Q,ik} = \left(1 - \frac{Q_{gki}}{Q_{g\max i}^c} \right) \times 100\ \% \ , \quad k = 0, 1, 2, \ldots \tag{4.17}$$

where $Q_{g\max i}^c$ is the maximum reactive power of the ith generator at the voltage collapse point, Q_{gki} is the reactive power of the ith generator at the kth operating point. It should be noted that the reactive power is computed in this thesis using phasors and analogue measurements obtained from the PMUs located in the power system.

4.4.2 Proposed Effective Generator Field Current Reserve (EGFCR) Index

Existing indices based on the maximum reactive power margin available at a synchronous generator uses Equation (4.15) in their computation, and four variables are thereby needed. This requires more computation time, computational resources, more measurement sensors, and project/maintenance costs. Therefore, a simple, easy to implement index with fewer variables readily obtained from the synchrophasor measurements is necessary.

The formulation of a generator-based index is done on the basis of the consideration of the voltage collapse point as the limit of the synchronous generator using $EGRPR$ = 0, as $Q_{g\max}^{c} = Q_{gk}$, $P_{g\max}^{c} = P_{gk}$ at this point based on Equations (4.14)-(4.15), then:

$$-\frac{|V_g|^2}{X_s}+\sqrt{\frac{|V_g|^2 I_{fd\max}^{c2}}{X_s^2} - P_{g\max}^2} = -\frac{|V_g|^2}{X_s}+\sqrt{\frac{|V_g|^2 I_{fdk}^{2}}{X_s^2} - P_{gk}^2} \quad (4.18)$$

where $I_{fd\max}^{c}$ is the generator maximum field current at the point of collapse, I_{fdk} is the field current of the generator at the kth operating time.

Therefore,

$$I_{fd\max}^{c} = I_{fdk}\ ,\ k = 0, 1, 2, \ldots \quad (4.19)$$

$$\frac{I_{fdk}}{I_{fd\max}^{c}} = 1 \quad (4.20)$$

The relationship between $Q_{\max}^{c}$ and $I_{fd\max}^{c}$ forms the basis of the synchronous generator-derived VSA index based on the generator field current limit. This is termed in this thesis as the Effective Generator Field Current Reserve (EGFCR), and it is defined as the difference between the maximum generator field current at the voltage collapse point and the generator field current at the current operating point.

The EGFCR can be defined with respect to the generator field current margin I_{fdm} as given below:

$$EGFCR = I_{fdm,k} = I_{fd\max}^{c} - I_{fdk} \quad (4.21)$$

where I_{fdm} is the effective generator field current reserve from the current operating point to the voltage collapse point at the kth operating time.

Thus, the RVSA index using the ith synchronous generator is:

$$RVSA_{Ifdk} = \left(\frac{I_{fdmik}}{I_{fd\max i}^{c}}\right) \times 100\ \% \quad (4.22)$$

From Equation (4.21), this can be written as:

$$RVSA_{Ifd,ik} = \left(1 - \frac{I_{fdki}}{I_{fd\max i}^{c}}\right) \times 100\ \% \quad (4.23)$$

where I_{fdmik} is the effective generator field current margin on the ith synchronous generator at the kth operating time, $I_{fd\max i}^{c}$ is the maximum field current of the ith generator, I_{fdki} is the field current of the ith generator at the kth operating point, and it is published as analogue synchrophasor measurements using PMUs.

The same formulation would apply to synchronous generators with brushless excitation. Synchronous generators with brushless exciters are a type of synchronous machines whose field current is supplied electromagnetically by induction to the rotor. The Alternating Current (AC) in the field winding is afterwards rectified at the rotor. Although, there is no direct measurement of the DC field current, other possibilities can be explored to obtain this. Two methods are proposed by (Kjaer *et al*., 2005; IEEE Task Force on Excitation Limiters, 1995) using the exciter rotor current and the exciter rotor voltages respectively.

4.4.3 Proposed Effective Generator Stator Current Reserve (EGSCR) Index

A generator-derived VSA index using stator current is newly proposed in this thesis. From Equation (4.7), the reactive power obtainable from a generator based on the consideration of the generator stator current is given as:

$$Q_{ga} = \sqrt{\left|\mathrm{V_g}\right|^2 \left|\mathrm{I_a}\right|^2 - P_{ga}^2} \tag{4.24}$$

where P_{ga}, and Q_{ga} are the generator real and reactive powers, $|I_a|$ is the generator stator current phasor magnitude.

The maximum reactive power Q_{gamax} is given as:

$$Q_{ga\max} = \sqrt{\left|\mathrm{V_g}\right|^2 \left|\mathrm{I_{amax}}\right|^2 - P_{ga\max}^2} \tag{4.25}$$

where P_{gamax} and Q_{gamax} are the maximum real and reactive powers, $\left|\mathrm{I^c_{amax}}\right|$ is the maximum generator stator current phasor magnitude.

The formulation is done on the basis of the consideration of the voltage collapse point as the limit of the synchronous generator using $EGRPR = 0$, as $Q^c_{ga\max} = Q_{gak}$, $P^c_{ga\max} = P_{gak}$, then:

$$\sqrt{\left|\mathrm{V_g}\right|^2 \left|\mathrm{I^c_{amax}}\right|^2 - P_{ga\max}^2} = \sqrt{\left|\mathrm{V_g}\right|^2 \left|\mathrm{I_{ak}}\right|^2 - P_{gak}^2} \tag{4.26}$$

where $\left|\mathrm{I_{ak}}\right|$ and P_{gak} are the generator stator current phasor magnitude and the real power output at the kth operating time respectively.

From (4.51),

$$\left|\mathrm{I^c_{amax}}\right| = \left|\mathrm{I_{ak}}\right| \tag{4.27}$$

$$\frac{\left|\mathrm{I_{ak}}\right|}{\left|\mathrm{I^c_{amax}}\right|} = 1 \tag{4.28}$$

Therefore, the relationship between $Q^c_{ga\max}$ and $\left|\mathrm{I^c_{amax}}\right|$ forms the basis of the synchronous generator-derived RVSA index based on the generator stator current

limit. This is termed in this thesis as the Effective Generator Stator Current Reserve (EGSCR) and it is defined as the difference between the maximum generator stator current at the voltage collapse point and the generator stator current at the current operating point.

Thus, the EGSCR can be defined with respect to the generator stator current margin I_{am} as given below:

$$EGSCR_k = I_{am} = \left|\mathrm{I}^{\mathrm{c}}_{\mathrm{amax}}\right| - \left|\mathrm{I}_{\mathrm{ak}}\right| , \; k = 0, 1, 2, ... \tag{4.29}$$

where I_{am} is the effective generator stator current reserve from the current operating point to the voltage collapse point.

From the foregoing, the relationship between the synchronous generator maximum reactive power $Q^{c}_{ga\max}$ at the voltage collapse point and the maximum generator stator current phasor magnitude $\left|\mathrm{I}^{\mathrm{c}}_{\mathrm{amax}}\right|$ at the voltage collapse point is established.

Thus, the proposed RVSA index for the ith generator based on its armature current is proposed as:

$$RVSA_{lak} = \left(\frac{\left|\mathrm{I}_{\mathrm{amik}}\right|}{\left|\mathrm{I}^{\mathrm{c}}_{\mathrm{amaxi}}\right|}\right) \times 100\ \% , \qquad k = 0, 1, 2, ... \tag{4.30}$$

Equation (4.29) can be written as:

$$RVSA_{la,ik} = \left(1 - \frac{\left|\mathrm{I}_{\mathrm{aki}}\right|}{\left|\mathrm{I}^{\mathrm{c}}_{\mathrm{amaxi}}\right|}\right) \times 100\ \% , \qquad k = 0, 1, 2, ... \tag{4.31}$$

where $\left|\mathrm{I}_{\mathrm{amik}}\right|$ is the effective generator stator current margin on the ith synchronous generator at the kth operating time, $\left|\mathrm{I}^{\mathrm{c}}_{\mathrm{amaxi}}\right|$ is the maximum stator current phasor magnitude of the ith generator, $\left|\mathrm{I}_{\mathrm{aki}}\right|$ is the stator current phasor magnitude of the ith generator at the kth operating time.

Practically, the generator stator currents can be taken from the Current Transformers (CTs) mounted at the generator terminals. The outputs from these generator terminal CTs can be used as the current inputs to the PMUs located at the generators.

4.4.4 Indices for Large Interconnected Multi-Area Systems

The RVSA indices presented above can be related to a wide area index for multi-area power systems with N areas and number of generators in each area N_r. This is proposed in the following Equations (4.32)-(4.34) for the indices based on the generator RPR, field current and stator current margins respectively:

$$RVSA_{Q,sysk} = \min_{r=1,N}\left\{RVSA_{Q,rk}\right\} = \min_{r=1,N}\left\{\left(1 - \frac{Q_{grk}}{Q^{c}_{g\max r}}\right) \times 100\ \%\right\} \tag{4.32}$$

$$RVSA_{Ifd,sysk} = \min_{r=1,N}\left\{RVSA_{Ifd,rk}\right\} = \min_{r=1,N}\left\{\left(1 - \frac{I_{fdrk}}{I^{c}_{Ifd\max r}}\right) \times 100\ \%\right\} \tag{4.33}$$

$$RVSA_{Ia,sysk} = \min_{r=1,N}\left\{RVSA_{Ia,rk}\right\} = \min_{r=1,N}\left\{\left(1 - \frac{\left|\mathbf{I}_{ark}\right|}{\left|\mathbf{I}^{c}_{\mathrm{lamax r}}\right|}\right) \times 100\ \%\right\} \tag{4.34}$$

where $RVSA_{Q,rk}$, $RVSA_{Ifd,rk}$, $RVSA_{Ia,rk}$ are obtained for every separate area following the same rule, described by Equations (4.32)-(4.34).

The necessary time-synchronized measurements for these algorithms defined in Equations (4.32)-(4.34) for widely dispersed generating units in a large interconnected power system are obtained using synchrophasor measurements.

For $RVSA_{Q,sysk}$, voltage and current phasor magnitudes at the individual generating units are required. While for the $RVSA_{Ifd,sysk}$ and $RVSA_{Ia,sysk}$ given by Equations (4.32)-(4.34), only the current phasor magnitudes are needed. Thus, less measurement sensors, less communication bandwidth, less computation, and less data archiving facilities are required. Therefore, the EGFCR and EGSCR algorithms are cost-effective, and are easily implemented for practical real-time VSA.

4.4.5 Adaptive Weighted-Summation Approach

For large interconnected power systems with multiple coherent generators, the use of the available reactive power reserve, field current reserve, or stator current reserve on these individual generators might give misleading results in that the contribution of the individual generators to a VCA comprising of coherent load buses could be under-/over-stated depending on the prevailing system condition.

An adaptive weighted-summation approach is proposed in this thesis for the respective VCAs in the interconnected power system. The weights are adaptively updated based on the online computation of the available margin on the generators in the respective RPRB at the current operating point. Thus, this weighting approach

reflects the true dynamics of the current operating point and the prevailing system condition.

The adaptive weighted-summation index for a RPRB for the rth area with a group of n_r generators is proposed as:

$$vca\,RVSA_{rk} = \sum_{i=1}^{n_r} w_{ik}\,RVSA_{ik}, \quad i = \overline{1,n_r} \quad r = \overline{1,N} \quad k = 0,1,2,\ldots \tag{4.35}$$

where w_i are the individual generator weights, $RVSA_i$ are the computed generator-derived indices, i is the ith generator within a RPRB, $vcaRVSA$ is the weighted summation of the $RVSA$ in the RPRB. n_r is the total number of generators in the rth RPRB, N is the total number of RPRBs.

Equation (4.35) above can be applied to any of the proposed generator-derived RVSA indices. For the RPR-based RVSA index, this is proposed as:

$$vca\,RVSA_{Q,rk} = \sum_{i=1}^{N_r} w_{ik}\,RVSA_{Qik}, \quad i = \overline{1,N_r} \quad r = \overline{1,N} \quad k = 0,1,2,\ldots \tag{4.36}$$

w_{ik} is the individual generator weight, $RVSA_{Q,rk}$ is the computed $RVSA_{Qik}$ index using the RPR.

The weight on the ith generator is proposed to be calculated on the basis of the real-time measurements from the PMUs as:

$$w_{ik} = \frac{Q^c_{g\max i} - Q_{gki}}{\sum_{i=1}^{N_r}\left(Q^c_{g\max i} - Q_{gki}\right)}, \qquad \sum_{i=1}^{N_r} w_{ik} = 1, \quad i = \overline{1,N_r}, \quad k = 0,1,2,\ldots \tag{4.37}$$

where $Q^c_{g\max i}$ is the maximum reactive power of the ith generator at the voltage collapse point, Q_{gki} is the reactive power of the ith generator at the kth operating point. Synchrophasor measurements are used in the calculation of the weights in real-time in order to adapt the weights to the prevailing system condition.

The above derivations also apply to the RVSA indices based on the generator field current and stator current reserves respectively.

For the EGFCR index, this is proposed as:

$$vca\,RVSA_{Ifd,rk} = \sum_{i=1}^{N_r} w_{ik}\,RVSA_{Ifd,ik}, \quad i = \overline{1,N_r}, \; r = \overline{1,N}, \; i = \overline{1,N_r}, \; k = 0,1,2,\ldots \tag{4.38}$$

w_{ik} is the individual generator weight, $RVSA_{Ifd,rk}$ is the computed $RVSA_{Ifdik}$ index using generator field current.

The weight on the ith generator is proposed as:

$$w_{ik} = \frac{I^{c}_{fd\,\max i} - I_{fdki}}{\sum_{i=1}^{n_r}\left(I^{c}_{fd\,\max i} - I_{fdki}\right)}, \quad \sum_{i=1}^{N_r} w_i = 1, \quad i = \overline{1, N_r}, \; k = 0,1,2,\ldots \tag{4.39}$$

where $I^{c}_{fd\,\max i}$ is the maximum field current of the ith generator at the voltage collapse point, I_{fdki} is the field current of the ith generator at the kth operating point.

Similarly, for the EGSCR, this is given as:

$$vca\,RVSA_{Ia,rk} = \sum_{i=1}^{n_r} w_i\, RVSA_{Ia,i}, \quad i = \overline{1, n_r}, \; r = \overline{1, N} \tag{4.40}$$

w_i is the individual generator weight, $RVSA_{Ia,r}$ is the computed $RVSA_{Iai}$ index using the generator stator current, i is the ith generator within a RPRB.

The weight on the ith generator is given as:

$$w_i = \frac{\left|I^{c}_{a\max i}\right| - \left|I_{aki}\right|}{\sum_{i=1}^{n_r}\left|I^{c}_{a\max i}\right| - \left|I_{aki}\right|}, \quad \sum_{i=1}^{n_r} w_i = 1, \quad i = \overline{1, n_r} \tag{4.41}$$

where $\left|\mathrm{I}^{\mathrm{c}}_{\mathrm{amaxi}}\right|$ is the maximum stator current phasor magnitude of the ith generator at the voltage collapse point, $\left|\mathrm{I}_{\mathrm{aki}}\right|$ is the stator current phasor magnitude of the ith generator at the kth operating point.

The weighted wide area $vcaRVSA$ index is calculated using Equations (4.32)-(4.34). It should be noted that as long as these indices are positive, the system is stable. The system losses its stability and voltage collapse occurs as soon as any of the indices at any of the RPRB becomes exhausted and turns negative. The use of an adaptive weighted summation gives priority to the synchronous generators with large availability of reactive power reserve in each RPRB at any given operating point. Thus, a higher weight and relative importance is given to the synchronous generator with a larger RPR.

Compared to the use of pre-determined weights, the adaptive weighted-summation approach gives a truer situational awareness of the state of the system, unlike pre-determined weights where unnecessary high weightage (priority) is given to a generator even when little RPR is available at a particular operating point and system condition.

The proposed adaptive weighted summation algorithm for real-time voltage stability assessment was implemented and deployed in a PLC using a real-time lab-scale testbed. The RVSA indices are used in the prediction of the operating state of the

power system's state ('Stable', 'Alert', 'Unstable') and the system's margin to voltage collapse in an online mode in real-time using synchrophasor measurements from PMUs. Further details on the DT-classifiers for predicting the system operating state are given in Section 4.5.

4.5 Synchrophasor-Based Voltage Stability Assessment Using Classification and Regression Trees (CART)

Machine learning-based algorithms were used in the implementation of a real-time classification model (classifier) for the prediction of the operating state of the power system, and in the implementation of a regression model (regressor) for predicting the system's proximity (margin) to voltage instability. Wide area synchrophasor measurements obtained from PMUs using various scenarios involving the short-term and long-term voltage stability dynamics of transformer ULTCs, generator OXLs, load increase, and credible generator/line contingencies were used in the generation of the knowledge base for training the Classification and Regression Trees (CARTs).

The trained CARTs were afterwards deployed online in the SEL-3378 Synchrophasor Vector Processor (SVP) which functions as a substation PDC and as a PLC. Further details on the real-time hardware implementation are presented in Chapter 5. Figure 4.6 shows the functional block diagram of the proposed CARTs algorithms.

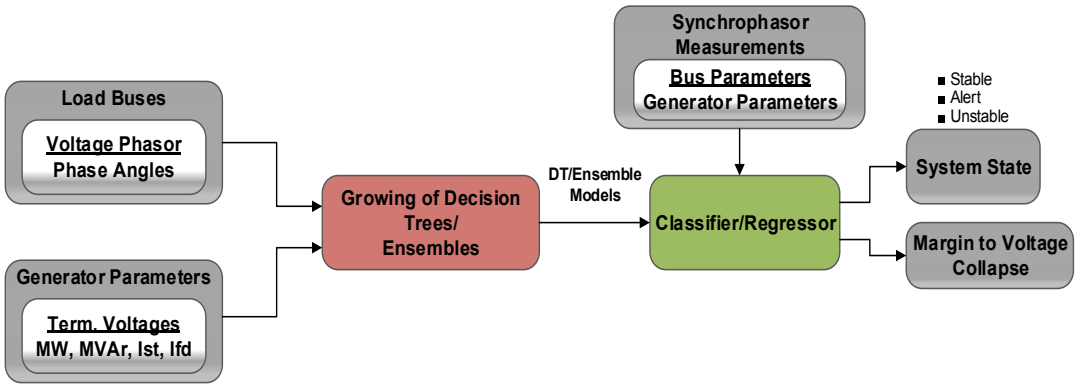

Figure 4.6: Functional diagram of the proposed CARTs algorithms

4.5.1 Machine Learning-Based Algorithm

Machine learning is the process of knowledge discovery from data especially for systems with complex governing functions. The properties learnt from the training dataset during the training process are then used for prediction using a new independent dataset (Witten *et al*., 2011).

Machine learning can be broadly categorized into supervised and unsupervised learnings. Supervised learning involves the training of associated input-output pairs in

an attempt to generalise a function that relates the input attributes to the output(s). Examples of supervised learning methods include Artificial Neural Networks (ANNs), linear and nonlinear regressions, Decision Trees (DTs), ensemble methods, Support Vector Machines (SVM), and the Naive Bayes method (Witten *et al*., 2011). In unsupervised learning, training is done with inputs only, with the output unknown. Examples of unsupervised learning methods include certain types of ANNs, k-means model, Gaussian model, hierarchical model, fuzzy c-means, and the hidden Markov models (Witten *et al*., 2011).

4.5.2 Decision Trees (DTs)

The real-time voltage stability assessment algorithm proposed in this thesis uses supervised DTs incorporating CARTs in the classification of the power system status and its margin to voltage collapse. The DT-classifier has a discrete output and it is used for the classification of the state of the power system into 'Stable', 'Alert', or 'Unstable'. While the DT-Regression Tree (RT) has a continuous output and it is used for the prediction of the value of the system's margin to voltage collapse.

Decision Trees (DTs) were introduced in (Breiman *et al*., 1984) and were first used for a power system problem involving transient stability assessment by (Wehenkel *et al*., 1989). DTs are tree-structured classifiers/predictors which use Learning Sets (LS) to obtain the relationship between the independent input attributes and the dependent outcome(s). The relationship obtained from the LS is afterwards applied to accurately predict the dependent outcome(s) based on new values of the input attributes. DTs consist of a root node, internal/decision nodes, and the terminal/leaf nodes. They are generally fast, efficient, easy to interpret, able to perform under uncertainties, and are capable of extracting complex nonlinear relationship between the input attributes and outcomes. These make them particularly suitable for online applications.

Tree splitting is the division of a given LS into subsets where a particular class is dominant in each subset, such that the resulting subsets are purer than the parent set. Thereby, resulting in a decrease in the impurity at the subset level. This is known as the 'goodness of split' criterion (Breiman *et al*., 1984). The splitting criterion used in this thesis is the Gini's Diversity Index (GDI). The GDI is a measure of the inequality among the values of a probability distribution in the tree's node (node impurity).

For a given impurity function ϕ comprising of $(p(c_1),(p(c_2),...,(p(c_i),...(p(c_k))$ class probabilities with $p(c_i) \geq 0$, the impurity $I(t)$ for a node t of the DT is given as (Breiman *et al*., 1984):

$$I(t) = \phi(p(c_1|t),\ p(c_2|t),\ ...,(p(c_i),\ ...,\ p(c_k|t)\ ,\quad i = \overline{1,k} \tag{4.42}$$

where c_i refers to the object class, $p(c_i)$ is the prior probability associated with the ith class c_i, $p(c_i|t)$ is the conditional probability associating a given object with class c_i with the node t, $i = \overline{1,k}$, and k is the number of classes considered.

The decrease in impurity $\Delta I(s,t)$ for a given split for a node t of the DT is given by:

$$\Delta I(s,t) = I(t) - (p(c_1|t),\ p(c_2|t),\ ...,(p(c_i),\ ...,\ p(c_k|t) \tag{4.43}$$

The Gini Diversity Index (GDI) adopted by (Breiman *et al*., 1984) is given below:

$$\phi(p(c_1|t), p(c_2|t),..., p(c_k|t)) = \sum_{i=1}^{k} \sum_{j=1,\ j\neq i}^{k} p(c_i|t)\, p(c_j|t)$$

$$= 1 - \sum_{i=1}^{k} (p(c_i|t))^2 \tag{4.44}$$

A node with just one class (pure node) with all the cases belonging to the same class has a Gini index of 0 (zero impurity or misclassification error). For a regression predictor, a tree may split halfway between any two adjacent unique values of the regression outcome (Breiman *et al*., 1984).

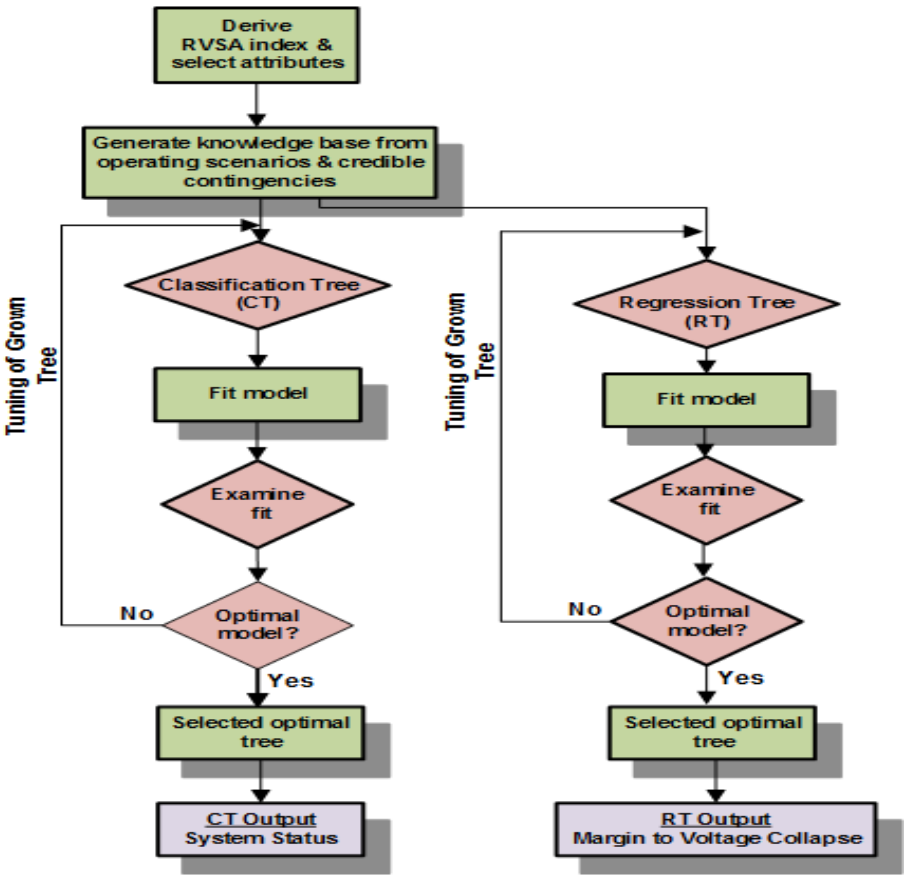

Figure 4.7: Flowchart detailing the process for growing the decision trees

Figure 4.7 shows a flowchart of the proposed procedure used in the growing of the CARTs. The growing of the trees involves the fitting of the attributes in the LS into prediction models. Each of the internal nodes tests the learning set attributes until a class/prediction is given at the terminal nodes. Afterwards, the fit of the grown tree is evaluated. If the optimal tree is obtained, then the process is stopped.

The splitting of the nodes during the tree growing process is stopped when: (i) the node becomes pure; (ii) there are fewer minimum parent (MinParent) observations in the branch node; and (iii) further split would result in children with fewer minimum leaf (MinLeaf) observations per tree leaf. Further information on the splitting process can be found in (MATLAB Statistic Toolbox guide, 2014). MATLAB 7.12.0 (2011a) and MATLAB Statistics Toolbox were used in the implementation of the DT-classifier and RT algorithms respectively. The MATLAB codes for the implementation of the CART algorithms are given in Appendix D1.

4.5.3 Ensembles of Decision Trees

Predictors obtained from CARTs can be further improved by using Ensembles of Decision Trees (EDTs). Ensembles are a collection of weakly grown decision-making predictors which are aggregated to form a single high quality predictor based on the voting decisions of these individual predictors. Examples of ensemble methods used for the classification task in this thesis are the Bootstrap Aggregation (Bagging) method in Breiman (1996), and the Adaptive Boosting (AdaBoost) method proposed in Freund and Schapire (1997). For the regression task, the Bagging and the Least Square Boosting (LSBoost) methods were used.

The Bagging ensemble method is grown by generating bootstrap replicas of the original dataset and training decision trees on each of these generated replicas (Breiman *et al*., (1996). The bootstrap replicas can be obtained from a random selection of observations. Ensemble learning using the Bagging method is implemented by growing a large number of weak learners (trees) from resampled version of the initial dataset. Bootstrap replicas are generated from the dataset and the decision trees are grown using these replicas. During this process, the decision trees can randomly select the input attributes to use for the tree-splitting.

For the Boosting algorithms, a sequential procedure in the training of the learners is followed and the weighted classification error is calculated for each of the learners (Freund and Schapire, 1997). The weights of the observations misclassified by a learner are increased, while the weights of the correctly classified observations are reduced at every boosting step. The updated weights are then used in training the

next learner. This is referred to as boosting by weighting. Alternatively, the original dataset can be resampled to obtain a new dataset by using a probability proportional to their weights. This is known as boosting by sampling. The prediction from the ensemble obtained from the boosting technique is given by the weighted summation of the results from the ensembles.

The Bagging ensemble is implemented as the TreeBagger method in MATLAB. It is known to grow deep trees which are usually memory-intensive and time consuming (MATLAB Statistic Toolbox guide, 2014). This results in slow predictions. Conversely, Boosting grows shallow trees which use less memory and less time. However, Boosting might need more numbers of weak ensemble learners than Bagged trees (MATLAB Statistic Toolbox guide, 2014). The MATLAB codes for the implementation of the EDTs are given in Appendices D2-D3.

4.6 Chapter Summary

This Chapter presented the algorithms proposed in this thesis for real-time voltage stability assessment based on synchrophasor measurements from PMUs. The theoretical derivations of the voltage stability assessment techniques are presented for the three algorithms that make up the proposed methodology. Also, a measurement-based hybrid clustering algorithm with focus on voltage stability assessment was presented.

The hybrid algorithm based on the Calinksi-Harabasz criterion and *k*-means algorithm was proposed for the clustering of the load buses with similar voltage collapse problem, and the clustering of generators in the power system providing reactive power support to the respective clusters of load buses. Voltage stability assessment indices derived from generators were presented for application in large interconnected power systems. The generator parameters considered were generator reactive power, field current, and stator current respectively.

Chapter Five describes the 'proof-of-concept' Wide Area Monitoring, Protection and Control (WAMPAC) testbed used in the generation of the dataset for the growing of the DT-classifiers and regressors, and for the real-time implementation, testing and validation of the proposed algorithms and methods of solution.

CHAPTER FIVE

DESIGN AND IMPLEMENTATION OF A LAB-SCALE TESTBED FOR WIDE AREA VOLTAGE STABILITY ASSESSMENT, PROTECTION/CONTROL

5.1 Introduction

The algorithms and methods for voltage stability assessment, wide area protection and control proposed in this thesis are tested and validated using a newly designed 'proof-of-concept' Wide Area Monitoring, Protection and Control (WAMPAC) testbed.

The testing and validation were carried out using benchmark test systems modelled using the RSCAD software in a Hardware-in-the-Loop (HITL) simulation with industrial-grade devices typically used in electric power utilities. Synchrophasor measurements from external hardware PMUs and from software PMUs (RTDS-GTNET PMU card) synchronized to the Global Positioning System (GPS) common time reference were streamed to the first level PDCs (substation PDCs), and from the substation PDCs to the control centre PDCs (Super-PDC). The setup for the HITL simulation is illustrated in Figure 5.1. The equipment utilised in the implementation of the WAMPAC testbed are further described in the proceeding subsections. The code written for the RTDS® batchmode simulations is given in Appendix E.

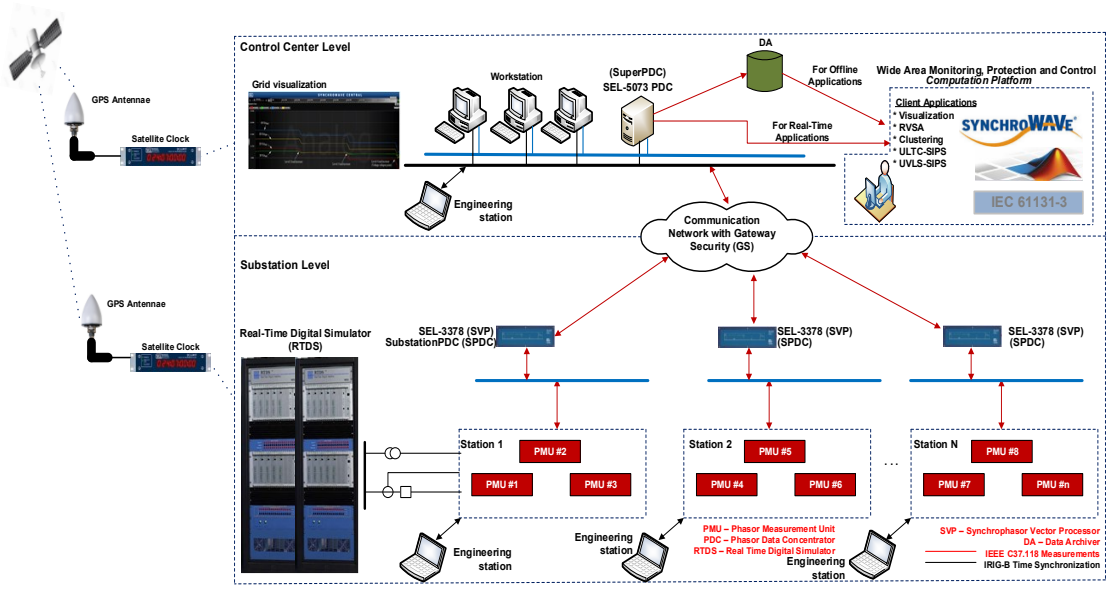

Figure 5.1: Wide Area Monitoring, Protection, and Control (WAMPAC) architecture

5.2 Description of the Equipment Used

A laboratory-scale testbed was developed for this thesis at the Centre for Substation Automation and Energy Management Systems (CSAEMS) located at the Cape Peninsula University of Technology for the real-time implementation and verification of the proposed methods and algorithms. The testbed consists of the Real-Time Digital Simulator (RTDS®) indicated by [1] in Table 5.1 and Figure 5.2, analogue output amplifiers [2], GTNET-PMU cards [3], GPS satellite clock [4], industrial communication network switches [6], Phasor Data Concentrators (PDCs) [7], Phasor Measurement Units (PMUs) [8, 9, 10], Intelligent Electronic Devices (IEDs) [5, 11], and IEC 61850-9-2 Merging Unit (MU) [12], as given in Table 5.1 and Figure 5.2 respectively. Table 5.1 presents the various equipment in the WAMPAC testbed implemented, and the respective software tools used in their setup configuration. . Figure 5.2 shows a picture of the industrial-grade equipment utilised in the lab-scale WAMPAC scheme.

Table 5.1: Hardware and software tools used in the WAMPAC testbed implemented

S/N	Equipment/Software	Configuration Software
1	Real-Time Digital Simulator® (RTDS)	RSCAD V4.004
2	Omicron CMS 156 Amplifier	N/A
3	GTNET-PMU Card	Telnet
4	SEL-2407 Satellite Clock	HyperTerminal
5	Schneider Electric MiCOM P546 Sampled Values IED	MiCOM S1 Studio V3.5.1
6	RuggedCom RSG 2288 Network Switch	Terminal emulators (HyperTerminal/Putty/Telnet)
7	SEL-3378 SVP	SVP Configurator V2.372
8	Alstom MiCOM P847 PMU/IED	MiCOM S1 Studio V3.5.1
9	SEL-421 (with IEC 61850 GOOSE Configuration)	AcSELerator QuickSet (and AcSELerator Architect V1.1.145.0)
10	SEL-451 (with IEC 61850 GOOSE Configuration)	AcSELerator QuickSet (and AcSELerator Architect V1.1.145.0)
11	Alstom MiCOM P446	MiCOM S1 Agile V1.2.0
12	Alstom MU Agile	MiCOM S1 Agile V1.2.0
13	Alstom MiCOM P645	MiCOM S1 Agile V1.2.0
14	SEL-2488 Satellite Synchronized Network Clock	Web-based configuration
15	Moxa PT-7728-PTP Network Switch	Terminal emulators (HyperTerminal/Putty/Telnet)
16	MATLAB	MATLAB R2014a, GUI Toolbox, Optimization Toolbox, NN Toolbox, Statistic Toolbox
17	DIgSILENT	PowerFactory V14.1.7
18	Grid Protection Alliance Software for PDC	openPDC V1.5.143.0
19	Grid Protection Alliance Software for PDC testing	PMU Connection Tester V4.3.7

The RTDS® simulator was used in running the simulation of the test systems modelled using the RSCAD software. The simulation outputs from the runtime

environment of the RTDS® simulator are exported to external equipment via the RTDS® Giga Transceiver Analogue Output (GTAO) card.

Figure 5.2: **Implemented 'Proof-of-concept' WAMPAC testbed**

The export of simulation quantities from the RTDS® is made possible through a GTAO analogue output component within the RSCAD draft model. An OMICRON CMS 156 Amplifier is connected to the GTAO card in order to amplify the ±10 V signal level at the GTAO card to the actual CT and VT values as obtained within the RSCAD simulation. CT output of 1 A and VT output of 110 V were used respectively. The output from the OMICRON CMS 156 amplifier then served as the input to the analogue input module of the IEDs/PMUs and MUs.

The PMUs receive the analogue inputs, perform the signal processing and phasor estimations, and then publish the IEEE C37.118 synchrophasor messages to the Ethernet network as configured. Similarly, the GTNET-PMU card publishes the synchrophasor messages received from the GTNET component modelled within the RSCAD model onto the Ethernet network

5.2.1 Real-Time Digital Simulator

The Real-Time Digital Simulator® (RTDS) is a power system simulator for solving electromagnetic transient simulation using a 50 μs time-step. It utilizes advanced parallel processing techniques in order to achieve the computation speeds required to maintain continuous real-time operation (RTDS manual, 2014).

The RTDS® processor cards, Input/Output (IO) cards, and power supply are mounted in racks within a cubicle.

Typical applications of the RTDS® simulator include (RTDS hardware manual, 2014):

- High speed power system simulations.
- Hardware-in-the-loop (HIL) testing of protection relays.
- Closed-loop testing of power system controllers.
- Power system stability studies.
- Smart grid and distributed generation studies.
- Power Hardware-in-the-Loop (PHIL) testing of renewable energy devices, electric vehicles, motors, and loads.
- Simulation of communication protocols for substation automation using IEC 61850, IEC 60870-5-104, and IEEE C37.118 standards respectively.

Some of the available cards in the RTDS® racks at the Centre for Substation Automation and Energy Management Systems (CSAEMS) include:

- Gigabit Processor Card (GPC) cards.
- PB5 processor cards.
- Gigabit Transceiver Work Station Interface (GTWIF) card.
- Gigabit Transceiver Network Interface Card (GTNET) cards running the PMU, Generic Substation Events (GSE), Sampled Values (SV), DNP 3.0, and TCP/UDP socket protocols.
- Gigabit Transceiver Analogue Output Card (GTAO).
- Gigabit Transceiver Analogue Input Card (GTAI).
- Gigabit Transceiver Synchronization (GTSYNC) card.
- Gigabit Transceiver Front Panel Interface (GTFPI) card.
- Digital I/O panel.
- HV Patch Panel.

The processor cards (PB5 and GPC cards) are used in solving mathematically the equations representing the components modelled in the RSCAD software and the network solution of the modelled power system. The communication interface between the RTDS® simulator racks and the RSCAD workstation is via an Ethernet Local Area Network (LAN) linking the GTWIF card and the workstation running the RSCAD software. The GTNET card provides a real-time Ethernet communication link to/from the RTDS® based on various communication network protocols. The GTAO/GTAI cards serves as the interface between the analogue signals to/from the RTDS® to external devices. Time synchronization is provided by the GTSYNC card. This ensures that the RTDS® simulator time-step for PMU and SV applications is

locked to an external accurate time reference such as the GPS. The synchronization source to the GTSYNC card can be the unmodulated IRIG-B, 1 Pulse Per Second (1 PPS), and IEEE 1588 Precision Time Protocol (PTP). The GTFPI card is the interface between the processor cards (PB5 and GPC), the digital I/O panel, and the HV interface panel. More information on the above-mentioned hardware modules can be found in (RTDS hardware manual, 2014).

In order to run simulations using the RTDS® simulator, the RSCAD software suite serves as the user's interface to the RTDS® hardware. The power system circuit, runtime environment, and simulation results are modelled and controlled through the RSCAD software. Since the simulation is in real-time, system parameters like online plotting, controls, and metering can be viewed and manipulated during the simulation.

The RSCAD software has three main software modules. These are: (i) the Draft; (ii) the Transmission Line (T-Line); and (iii) the Runtime software modules respectively. The Draft software module is used for the assemblage and configuration of the power system and control components to form a complete electrical circuit. While the T-Line module is used in the modelling of the transmission lines within the power system model. The Runtime module controls the operation of the hardware. Through the Runtime module, the simulation can be started/stopped, disturbance can be initiated, and results can be plotted/displayed in real-time.

5.2.2 Signal Amplification

For HITL simulations with external devices like protective IEDs/PMUs, it is required that the exact simulated values from the instrument transformers (CT and VT) be interfaced to the protective IEDs/PMUs via the onboard analogue input module of the IEDs/PMUs. Actual values from the RTDS® simulation are exported to the GTAO card via a GTAO (*rtds_risc_ctl_GTAOOUT*) component modelled within the RSCAD draft. The GTAO card is then wired to the CMS 156 OMICRON Amplifier, and from the CMS 156 Amplifier to the onboard analogue input module of the IEDs/PMUs.

The voltage and current channels of the GTAO component and the CMS 156 OMICRON Amplifier need to be configured respectively to give an overall gain of unity. The current-to-voltage amplifier gain for the CMS 156 OMICRON Amplifier is set by default to 5. The scaling gain for the current channel of the GTAO component is given by:

$$Gain_A = GTAO_{GainA} \times Amplifier_{GainA} = 1 \quad (5.1)$$

$$Gain_A = \frac{5}{S_i}\left(\frac{Volts}{Amps}\right) \times 5\left(\frac{Amps}{Volts}\right) = 1 \quad (5.2)$$

where s_i is the scaling factor for the current channels.

This gives a scaling factor of 25 for the current channel since the current-to-voltage gain of the amplifier is 5.

Similarly, the voltage-to-voltage amplifier channels can be calculated as given above for the voltage-to-current amplifier channel. Since the voltage-to-voltage amplifier gain for the CMS 156 OMICRON Amplifier is set to 50. The GTAO gain for the voltage channel is given as:

$$Gain_V = GTAO_{GainV} \times Amplifier_{GainV} = 1 \quad (5.3)$$

$$Gain_V = \frac{5}{S_v}\left(\frac{Volts}{Volt}\right) \times 50\left(\frac{Volts}{Volt}\right) = 1 \quad (5.4)$$

where s_v is the scaling factor for the current channels.

Thus, the scaling factor for the voltage channel is 250. Figure 5.3 shows the GTAO component within the RSCAD software and the configuration settings used.

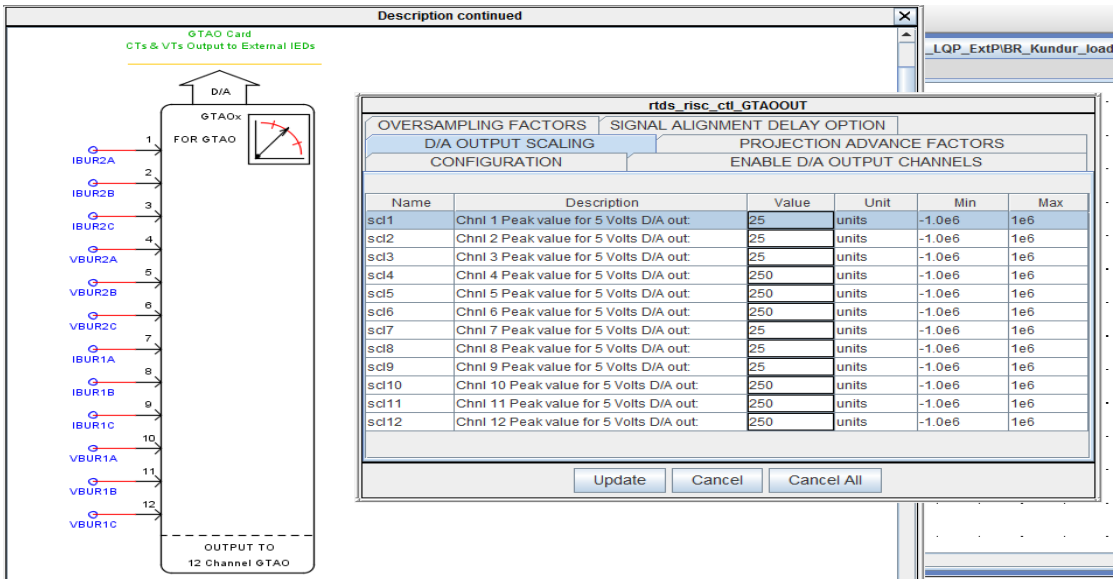

Figure 5.3: RSCAD-GTAO component and scaling parameters

5.2.3 Satellite Synchronized Clocks

Time synchronization input to the RTDS-GTSYNC card, PMUs, IEDs, SEL-3378 SVP, and network switches was obtained from a SEL-2407 satellite clock and a SEL-2488 satellite synchronized network clock using coaxial (RG-58) cables terminated on both ends with BNC connectors. The SEL-2407 has 1 modulated IRIG-B output, 6 demodulated IRIG-B outputs, and a GPS antennae input. The time synchronization to

the MU and Alstom MiCOM P847 is 1 PPS, and it is obtained from the RTDS-GTSYNC 1 PPS fiber output ports.

The SEL-2407 satellite clock provides a very accurate time of ±100 ns when the clock is locked onto four GPS satellites, after which the clock must continuously track three GPS satellites in order to stay locked and give accurate timing (SEL-2407 Manual, 2014). This is indicated by a green satellite lock LED. When the clock is in its holdover mode, a green LED signifies a time quality lesser than 1 µs, while yellow and red LEDs give a time quality of ±100 µs and time quality greater than ±100 µs respectively. Figure 5.4a shows a snapshot capture from the SEL-2407 satellite clock.

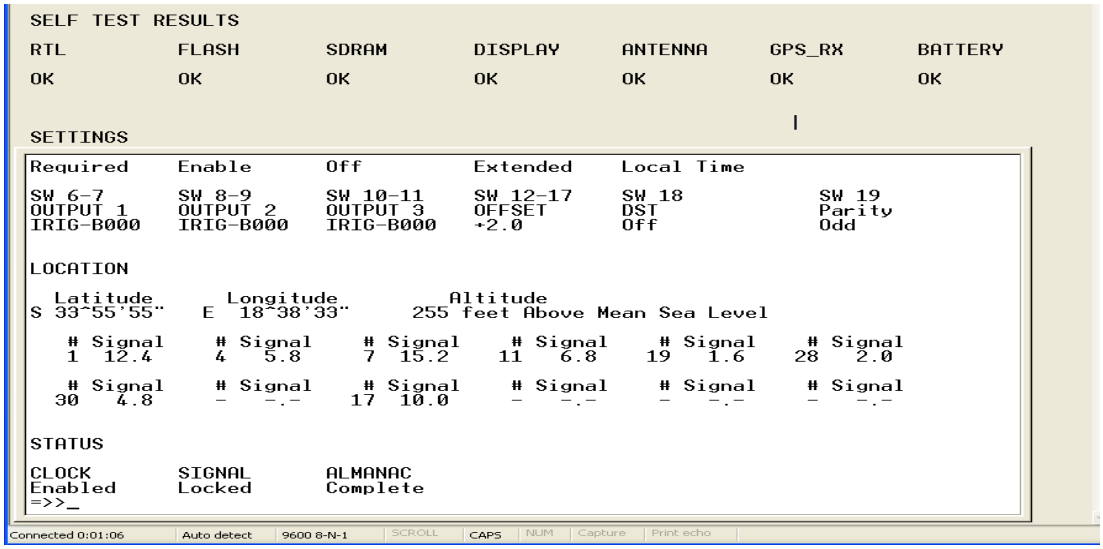

(a)

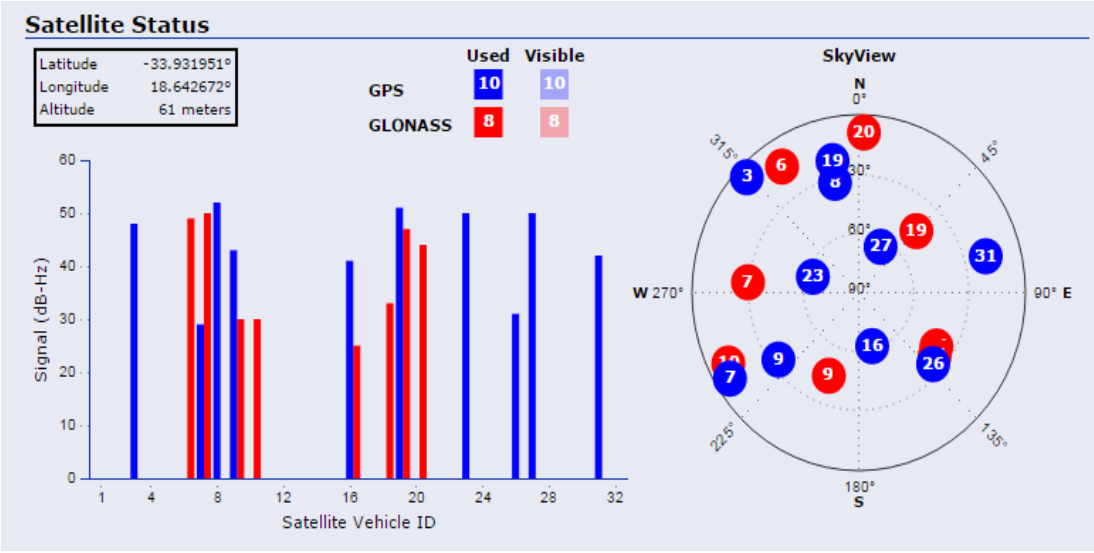

(b)

Figure 5.4: Signal statistic obtained for **(a)** the SEL-2407 satellite clock; **(b)** the SEL-2488 satellite clock

The # in (*# signal*) signifies the GPS satellite number (0–32), while the signal value *dd.d* corresponds to the GPS signal power received in linear Antenna Measurement Units (AMU).

The SEL-2488 satellite synchronized network clock provides precise time with various formats ranging from IRIG-B, Network Time Protocol (NTP), and Precision Time Protocol (PTP). It has 8 BNC connector time outputs (configurable to IRIG-B, PPS, or kPPS), 1 DB-9 port (configurable to IRIG-B, PPS, or kPPS), four Ethernet ports (IEEE 1588 format), and a GPS antennae input (SEL-2488 Manual, 2015).

Figure 5.4b shows a snapshot of the satellite signal statistic acquired by the SEL-2488 satellite synchronized network clock. From Figure 5.4b, the available GPS and GLONASS satellites, their signal strengths, azimuth and elevation information can be seen. Additional IRIG-B time synchronization can be obtained using the IRIG-B outputs from the SEL-3378 SVP, Ruggedcom network switches' TTL/AM ports, and the GYSYNC card IRIG-B/1 PPS/IEEE 1588 output ports respectively.

5.2.4 Phasor Measurement Units

Phasor Measurement Units (PMUs) are devices capable of publishing phasor quantities synchronized to a common time reference such as the GPS. Three PMU types were used in the WAMPAC lab-scale testbed implemented in this thesis.
These include:

- RTDS® (GTNET-PMU)
- Schweitzer Engineering Laboratories (SEL-421 and SEL-451 Intelligent Electronic Devices (IEDs))
- MiCOM Alstom (P847)

The RTDS-GTNET card loaded with the IEEE C37.118.1-2011 PMU protocol works in conjunction with the RSCAD Draft component (*rtds_GTNET_PMU_v4/rtds_GTNET_PMU_v5*) to stream synchrophasor measurements onto the Ethernet network. With the *rtds_GTNET_PMU_v4* component, eight PMU datastreams can be configured using one GTNET component with each PMU operating independently. Two PMU algorithms comprising of the IEEE C37.118.1-2011 Annex C reference signal processing model for M-class (measurement) and P-class (protection) are selectable. The *rtds_GTNET_PMU_v5* component is capable of streaming 24 datastreams. However, only P-class positive sequence synchrophasor measurements of voltages and currents are possible. A reporting rate of up to 240/200fps is available with the RTDS GTNET PMU.
The configuration of the respective PMU within the PMU component mainly comprises of the station name, hardware ID code, output port, reporting rate, phasor

format, the phasors/analogues/digital quantities, and the PMU performance class. Figure 5.5 shows the RSCAD-GTNET PMU component and some of the configuration parameters used.

The SEL-421, SEL-451, and MiCOM P847 are multi-functional IEDs with PMU functionality. The PMU configuration of Schweitzer Engineering Laboratories (SEL) IEDs was done using the Acselerator QuickSet software, while that of the MiCOM P847 IED was done using the MiCOM S1 Studio software. The current and voltage signals from the CTs and VTs are fed into the IEDs/PMUs via the onboard analogue input module comprising of current and voltage transformers respectively. The PMUs typically sample the signals at 48 samples per cycle (MiCOM P847 manual, 2011).

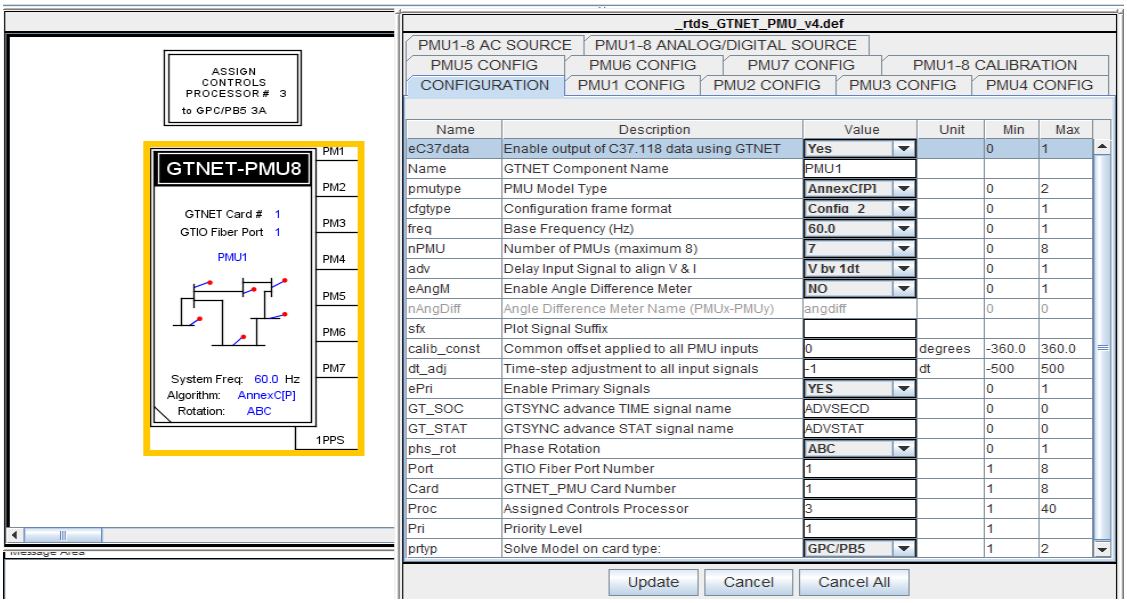

Name	Description	Value	Unit	Min	Max
eC37data	Enable output of C37.118 data using GTNET	Yes		0	1
Name	GTNET Component Name	PMU1			
pmutype	PMU Model Type	AnnexC[P]		0	2
cfgtype	Configuration frame format	Config 2		0	1
freq	Base Frequency (Hz)	60.0		0	1
nPMU	Number of PMUs (maximum 8)	7		0	8
adv	Delay Input Signal to align V & I	V by 1dt		0	1
eAngM	Enable Angle Difference Meter	NO		0	1
nAngDiff	Angle Difference Meter Name (PMUx-PMUy)	angdiff		0	0
sfx	Plot Signal Suffix				
calib_const	Common offset applied to all PMU inputs	0	degrees	-360.0	360.0
dt_adj	Time-step adjustment to all input signals	-1	dt	-500	500
ePri	Enable Primary Signals	YES		0	1
GT_SOC	GTSYNC advance TIME signal name	ADVSECD		0	0
GT_STAT	GTSYNC advance STAT signal name	ADVSTAT		0	0
phs_rot	Phase Rotation	ABC		0	1
Port	GTIO Fiber Port Number	1		1	8
Card	GTNET_PMU Card Number	1		1	8
Proc	Assigned Controls Processor	3		1	40
Pri	Priority Level	1		1	
prtyp	Solve Model on card type:	GPC/PB5		1	2

Figure 5.5: RSCAD-GTNET PMU component and configuration parameters

The analogue quantities are digitalized and the synchrophasor estimates are calculated. These estimates can be presented in either the polar format made up of the magnitude and angle, or in the rectangular format made up of the real and imaginary parts respectively. The time synchronization required by the SEL IEDs/PMUs is the demodulated IRIG-B time synchronization format, while the MiCOM P847 requires both the 1PPS and the IRIG-B time synchronization format. The 1PPS time signal is used by the MiCOM P847 for the phasor calculation, while the IRIG-B time synchronization is used for the synchrophasor data framing (MiCOM P847 manual, 2011).

Generally, the synchrophasor measurements available from the PMUs include the three phase voltages and currents, positive sequence, negative sequence, and zero sequence voltages and currents. Also included in the PMU measurements are the

system frequency and Rate of Change of Frequency (ROCOF) respectively. A reporting rate of up to 50/60 fps is possible with the SEL-451, SEL-421, and MiCOM P847 PMUs. The main PMU configuration settings include the selection of the current and voltage input channels, hardware (device) ID code, port number, message format, reporting rate, phasor format, and phasor representation. It should be noted that the phasor format to use is dependent on the user preference/application, and the PDC configuration. Figures 5.6-5.9 show some of the PMU configurations required in the setup of the SEL-451 and MiCOM P847 respectively.

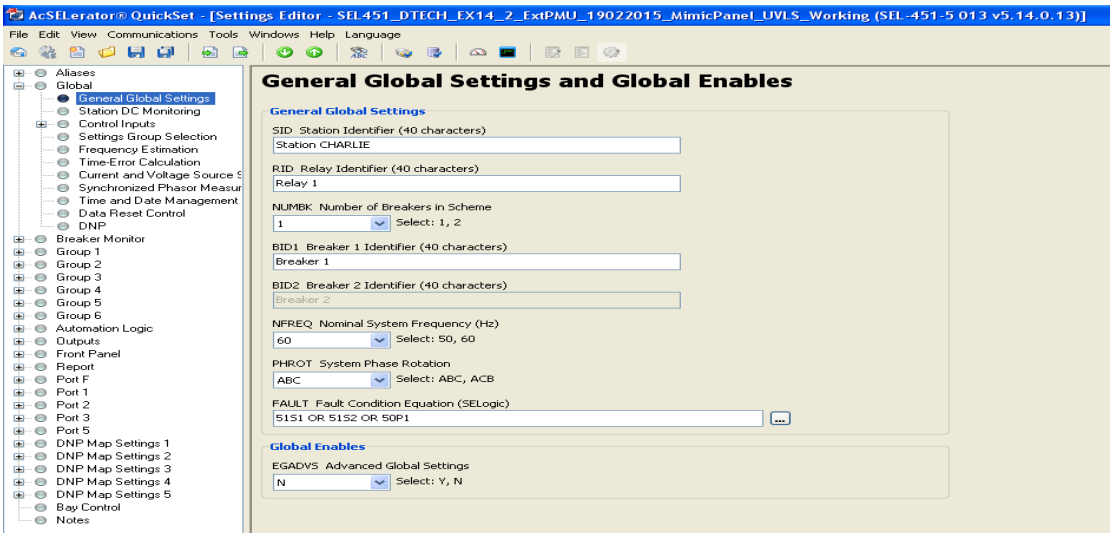

Figure 5.6: SEL-451 configuration (global settings)

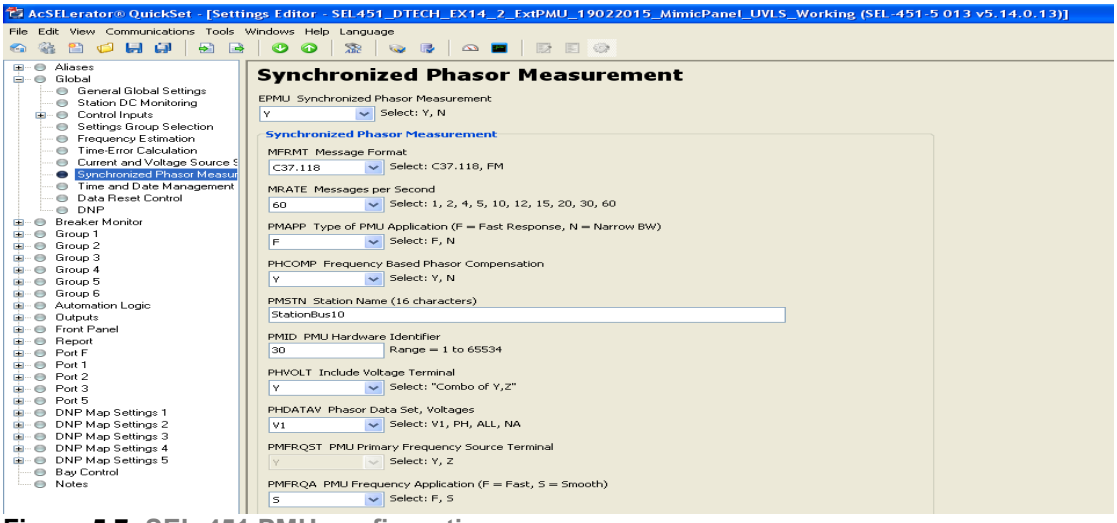

Figure 5.7: SEL-451 PMU configuration

The same procedure used in the configuration of the PMU functionality of the SEL-451 IED was followed for the SEL-421 IED. Further information on the configuration of the IEDs can be found in (SEL-451 manual, 2015; SEL-421 manual, 2013; MiCOM P847 manual, 2011) respectively.

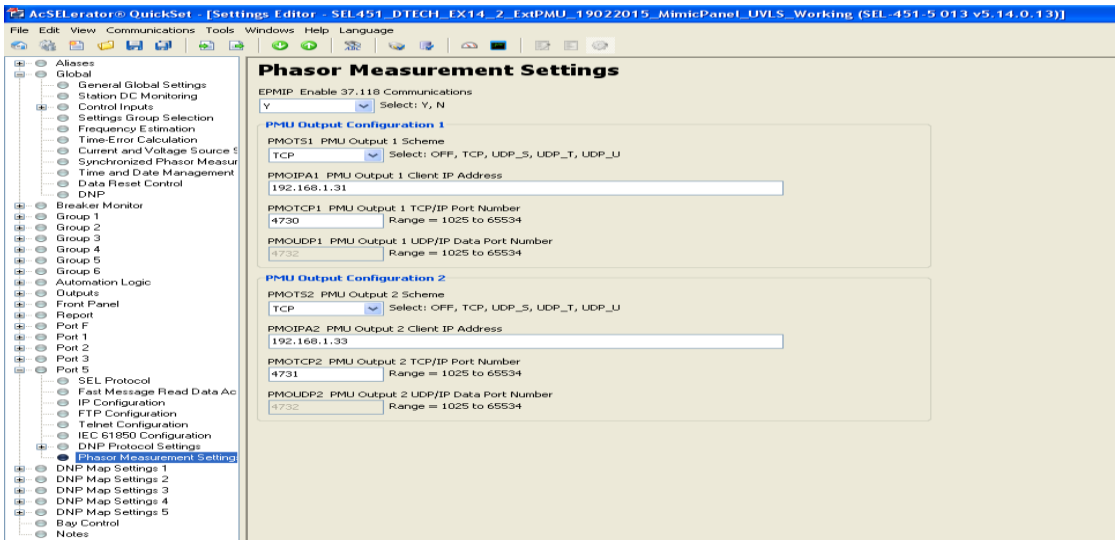

Figure 5.8: SEL-451 PMU communication configuration

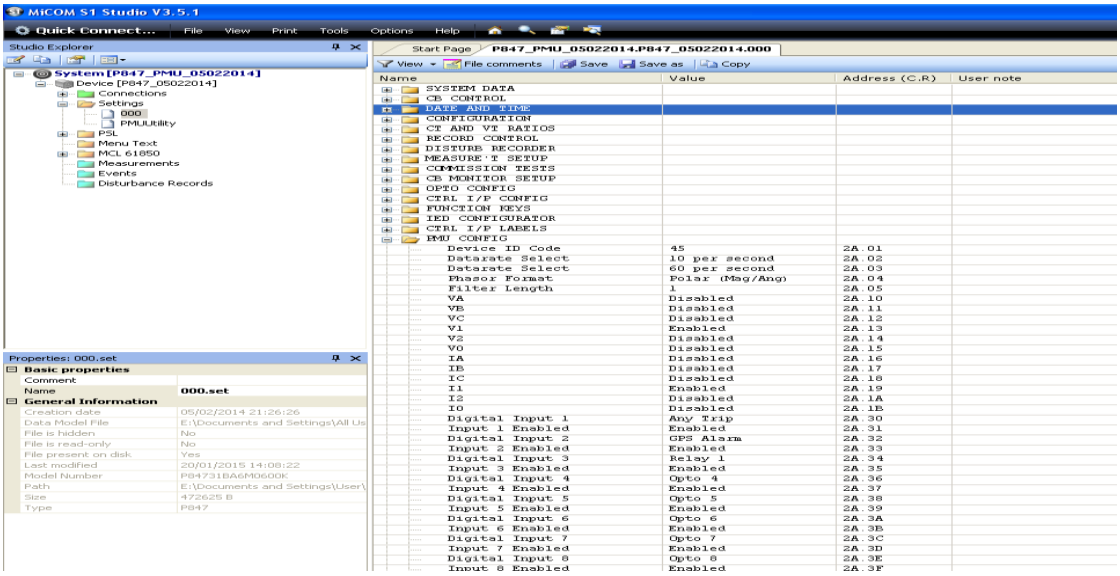

Figure 5.9: MiCOM P847 PMU configuration

5.2.5 Phasor Data Concentrator

Phasor Data Concentrators (PDCs) collect and time-align the synchrophasor measurements received from various synchrophasor-based devices (PMUs/PDCs). The time-alignment is done on the basis of the time-tags of the concentrated measurements referenced to the GPS.

The PDCs used in this research are the:

- SEL-3378 Synchrophasor Vector Processor (SVP) from Schweitzer Engineering Laboratories.
- SEL-5073 PDC software from Schweitzer Engineering Laboratories.
- openPDC Software from Grid Protection Alliance (GPA)

The SEL-3378 SVP was used as a substation PDC because it provided the necessary ruggedness required for the substation environment, while the SEL-5073 PDC and openPDC software were used as superPDCs at the control centre level of the implemented WAMPAC testbed. This is because software PDCs can be used to

concentrate more PMUs compared to hardware PDCs. The SEL-5073 is capable of collecting and time-aligning measurements from 20 PMUs, and can be extended to 500 PMUs.

The software used in the configuration of the SEL-5073 PDC is the SEL PDC Assistant. The configuration for the inputs, outputs, calculation, and archiving functionalities are made using the PDC Assistant software. An important feature of the SEL PDC Assistant is the real time display, which shows the status of the PMUs and the time-aligned measurements. The SEL-5073 has an optional archiving functionality which can be configured as a historian and retrieved when required for post-mortem analysis (SEL-5073 Manual, 2015).

The archiving function can also be configured for automatic archiving triggered based on system events. Automatic archiving was implemented using the Archive Collection Service (ACS) in the data acquisition of the synchrophasor measurement inputs to the Calinski-Harabasz/k-means clustering algorithm proposed in this thesis. The triggered PDC recording can have a maximum of 90 minutes of pre-trigger duration, and a maximum of 90 minutes of post-trigger duration respectively. If continuous PDC recording is desired rather than the triggered recording, the duration can be for days, depending on the size of the PDC archiving storage facility. Figure 5.10 shows a snapshot of the SEL-5073 PDC.

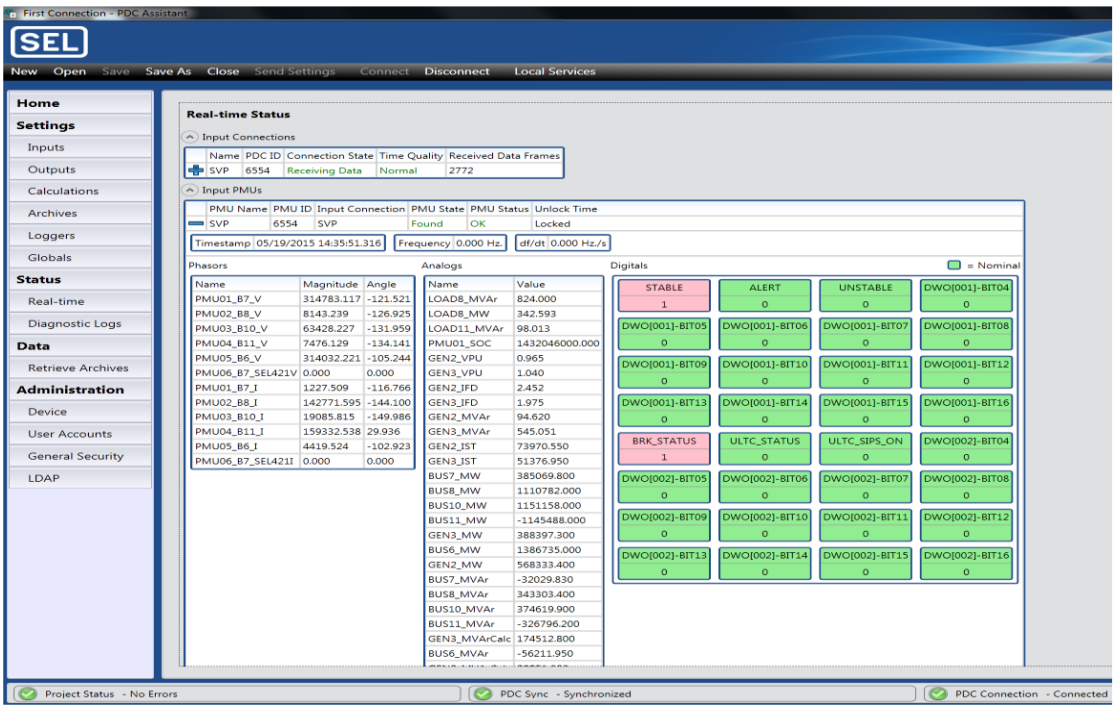

Figure 5.10: **Real-time tab of the SEL-5073 PDC for the 10-bus multi-machine equivalent system**

The use of the SEL-3378 SVP as a PDC is discussed in detail in the proceeding subsection. The openPDC software was configured using the openPDC Manager. The configuration of the PDC inputs, outputs, and historian can be done using the openPDC Manager. The SEL-5078 SynchroWAVE Central software was also used as a visualization tool alongside the SEL-5073 PDC.

5.2.6 SEL-3378 Synchrophasor Vector Processor

The SEL-3378 SVP is a computer rated device for utility applications operating with specialized I/O and processing capabilities. It is designed to preserve µs timing, and perform vector and matrix mathematics at high speed with great computational efficiency. Also, the SEL-3378 SVP platform is made up of a 1.1 GHz processor, 512 kB of RAM, and 1 GB Flash memory. It is capable of connecting to 20 PMUs (Servers) and 7 Clients at a maximum reporting rate of 60 fps.

Furthermore, the SEL-3378 SVP can publish a maximum of 640 phasors, 320 analogue measurements, and 80 digital words of user-configurable IEEE C37.118 synchrophasor measurements (SEL-3378 manual, 2014). It can serve as a soft-core Programmable Logic Controller (PLC) based on the IEC 61131-3 standard.
Figure 5.11 shows a layout depicting the role of the SEL-3378 SVP in one of the experimentations carried out using the WAMPAC testbed.

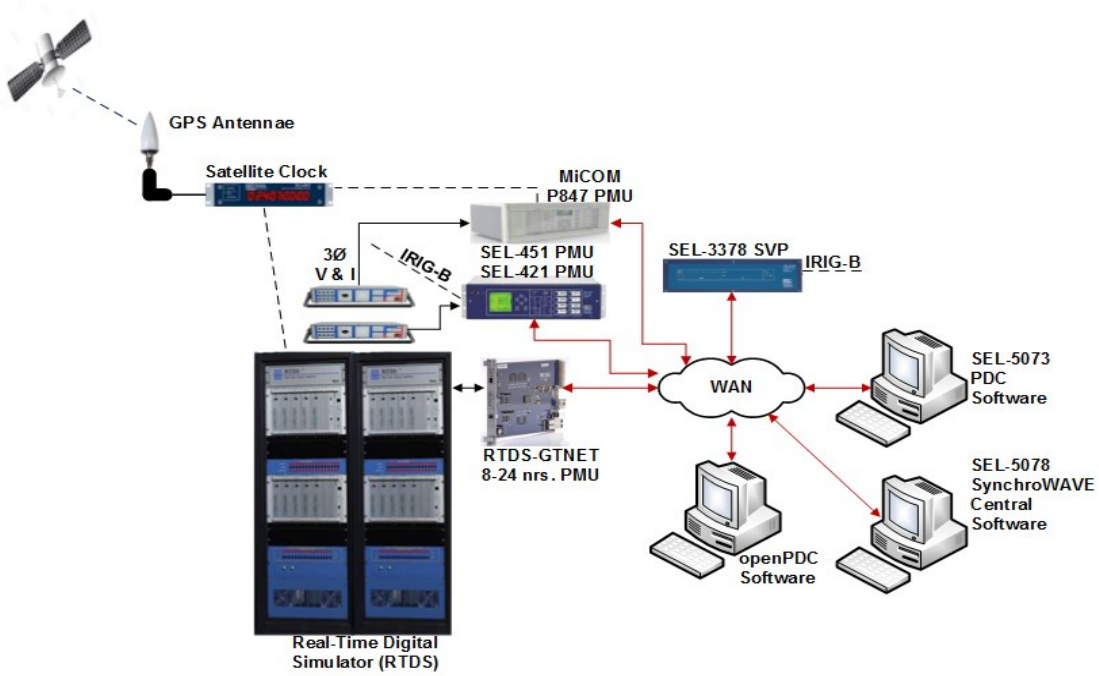

Figure 5.11: Layout showing the SEL-3378 SVP connection to other devices in the WAMPAC testbed implemented

The SEL-3378 SVP was used as a PDC to concentrate the substation PMU measurements according to their time-stamps, and also as a PLC for carrying out mathematical/logical computation for the voltage stability assessment, wide area protection and control algorithms.

5.2.7 IEC 61850-9-2LE Merging Unit

The IEC 61850-9-2LE Merging Unit (MU) was used in Chapter Eight to publish Sampled Values (SV) measurements onto a shared communication network on the process level of the substation (process bus). This together with IEC 61850-8-1 GOOSE messages and a wide area emulator were used in the investigations relating to the evaluation of the impact of adverse communication network conditions on the transmission of synchrophasor messages through the communication network infrastructure developed for the WAMPAC testbed.

The SVs are published from the RTDS® GTNET-SV Card and 2 nos. Alstom Agile Analogue Merging Units (AMUs). The RTDS® GTNET-SV card takes its input from a GTNET-SV component (*rtds_ctl_GTNET_SV9-2_V5*) modelled within the RSCAD Draft module. The RTDS GTNET-SV card is capable of publishing 2 Application Service Data Unit (ADSU) of SVs comprising of four currents and four voltage channels at a sample rate of 80 samples/cycle or 1 ASDU at 256 samples/cycle. The RTDS GTNET-SV card can subscribe to 1 ASDU for sample rates of 80 samples/cycle or 256 samples per cycle.

The analogue inputs to the Alstom AMUs are from the CMS 156 OMICRON Amplifiers connected to the GTAO outputs of the RTDS. AMUs carry out the sampling of the analogue inputs, Analogue-to-Digital Conversion (ADC), and the calculation of the magnitude and phase angle of the measured quantities. The SVs (1 ASDU) from each respective AMU is afterwards multicasted to the IEDs through the Ethernet communication network.

5.2.8 IEC 61850-9-2LE Intelligent Electronic Devices

The Intelligent Electronic Devices (IEDs) used in the implemented WAMPAC testbed can be divided into two categories. The first IED category includes the IEDs with PMU functionality, while the second category is made up of IEDs without PMU functionality.

The first category consists of the SEL-421, SEL-451, and Alstom MiCOM P847 IEDs. These IEDs were configured to publish IEEE C37.118 synchrophasor measurements. Also, the protection elements of these IEDs were configured to provide overcurrent

(ANSI 50/51) protection to trip the appropriate breakers during fault/overload conditions. Furthermore, the SEL-451 and SEL-421 were configured for undervoltage (27) protection for the investigations in Chapter Seven relating to the application of the proposed UVLS-SIPS algorithm.

The IEDs in the second category were used for the investigations in Chapter Eight relating to the performance analysis of the communication network of the WAMPAC testbed under adverse network conditions emulated using a Wide Area Network (WAN) emulator, and Ethernet traffic made up of IEC 61850-8-1 GOOSE messages and IEC 61850-9-2LE Sampled Values. This category of IEDs includes 2 nos. Alstom MiCOM P547, 1 no. Alstom MiCOM P446, and 1 no. Alstom MiCOM P645 IEDs. The verification tests of PMU measurements and PDC services are given in Appendix I.

5.3 Software Programming: Programmable Logic Controller

The SEL-3378 SVP has a real-time computational engine that can be used as a PLC in the execution of user-defined programmes in the implementation of automated monitoring, protection and control schemes. A PLC is a microprocessor-based controller with a programmable memory and functionality capable of logic, sequencing, and mathematical computation required in order to control a process.

Typically, a PLC is made up of a power supply unit, Central Processing Unit (CPU), memory unit, Inputs/Outputs (I/Os), and the programming interface. The CPU is made up of the Arithmetic and Logic Unit (ALU), registers for storing the programme execution, and the Control Unit (CU) for controlling the timing of the programming operations.

The functionality of the SEL-3378 SVP is illustrated in Figure 5.12. The Time Alignment Client Server (TCS) subscribes to the synchrophasor measurements from the external IEEE C37.118 Servers (PMUs), concentrates, time-aligns, and makes the measurements available to the SEL-3378 SVP Run-Time System (RTS) via an internal IEEE C37.118 Client as shown in Figure 5.12. Similarly, the local PMU shown in Figure 5.12 is a virtual IEEE C37.118 Client internal to the SEL-3378 SVP, and it is used in publishing the output datastream of the SEL-3378 SVP to external IEEE C37.118 Clients (e.g. SEL-5073 PDC/openPDC).

Monitoring, protection and control tasks can be programmed into the SEL-3378 SVP based on the synchrophasor measurements from the external IEEE C37.118 Servers. It is also capable of publishing the concentrated measurements and the computed

monitoring and control outputs to external IEEE C37.118 Clients via the Internal IEEE C37.118 Server.

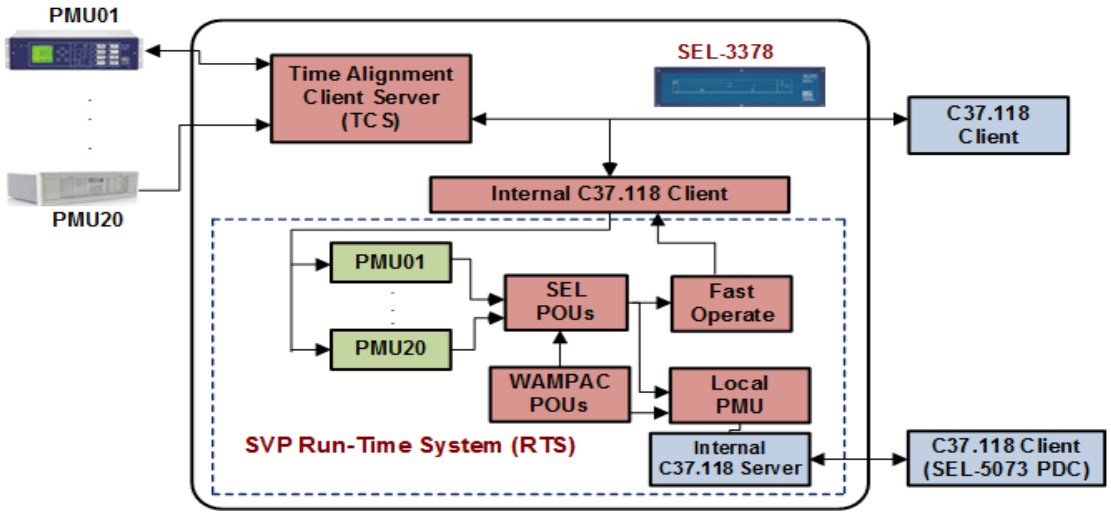

Figure 5.12: SEL-3378 SVP internal blocks and functionality

5.3.1 PLC Programming

The SEL-3378 SVP was used as a central processing unit for computing the Programme Organisation Units (POUs) required for the real-time implementation of the proposed algorithms and methods of solution for the voltage stability assessment and wide area protection/control formulations. The SVP Configurator is used in the configuration of the SEL-3378 SVP.

The POUs for the various proposed algorithms were written using the IEC 61131-3 programming language for PLCs and are given in Appendix F. The IEC 61131-3 standard defines ladder Diagrams (LAD), Structured Text (ST), Instruction List (IL), Sequential Function Charts (SFC), and Function Block Diagram (FBD) for PLC programming. In addition to the IEC 61131-3 programming languages, the SEL-3378 SVP also uses the Continuous Function Chart (CFC) programming language. The ST and FBD programming languages were used in this thesis. The procedure for creating a new project involves nine steps as shown in Figure 5.13.

The steps start with the creation of a new project, followed by the selection of the target RTS. In this case, the RTS to use is the *SEL-3378 RTS V.2.4 For Linux Helens V.1.0*. Afterwards, a new POU is added. The type of POU and the programming language to use has to be specified. The task configuration settings are made at this stage. The task settings involve the specification of the type of task, priority, interval of operation, and the programme call linkage to the respective POU. The creation of a

new project is concluded by saving and building the project, logging and downloading the code into the SEL-3378 SVP RTS, and finally running the code.

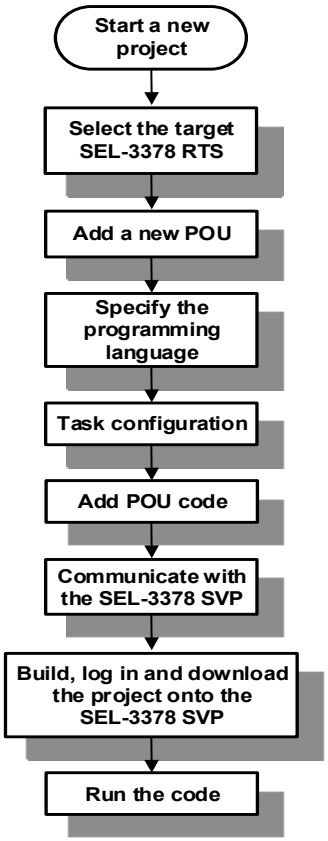

Figure 5.13: Programming of the PLC (SEL-3378 SVP)

5.3.2 Task Configuration

The runtime properties of the POUs are configured using the task configuration settings. This was done through the declaration of the priority and processing time for the execution of the respective POUs.

Three processing task groups were defined. These include:

- Configuration tasks
- High speed tasks
- Control tasks

A breakdown of the task configuration process is as shown in Table 5.2. The intervals defined in the fourth column of Table 5.2 gives the programme scan interval. That is, the operating cycle within which the processor reads the measurements, executes the proposed algorithms, and sends out the corresponding outputs. From Table 5.2, it can be seen that the *Configuration_Task* was assigned a low priority (30) and set to execute every 2 s. The *HighSpeed_Tasks* was set to execute every 4 ms and was assigned the highest priority (0) because it is meant to run highly critical tasks such as the collection of synchrophasor measurements and time-alignment.

The *Control_Tasks* was configured with a priority of 2 and the POUs under it were set to run every cycle at 16 ms. Figure 5.14 shows a snapshot detailing the various POUs designed, the task configuration, and the task attributes used.

Table 5.2: PLC task configuration

Task Configuration	POUs	Priority	Type	Interval
Configuration Tasks	TCS, Diagnostics	30	Cyclic	T#2s0ms
HighSpeed Tasks	PMCU_Assign, LocalPMCU, Vpu_PWRcalc	0	Cyclic	T#4ms
Control Tasks	CARTC, CARTR, SIPS_ULTC, SIPS_UVLS, wSUM_VCA	2	Cyclic	T#16ms

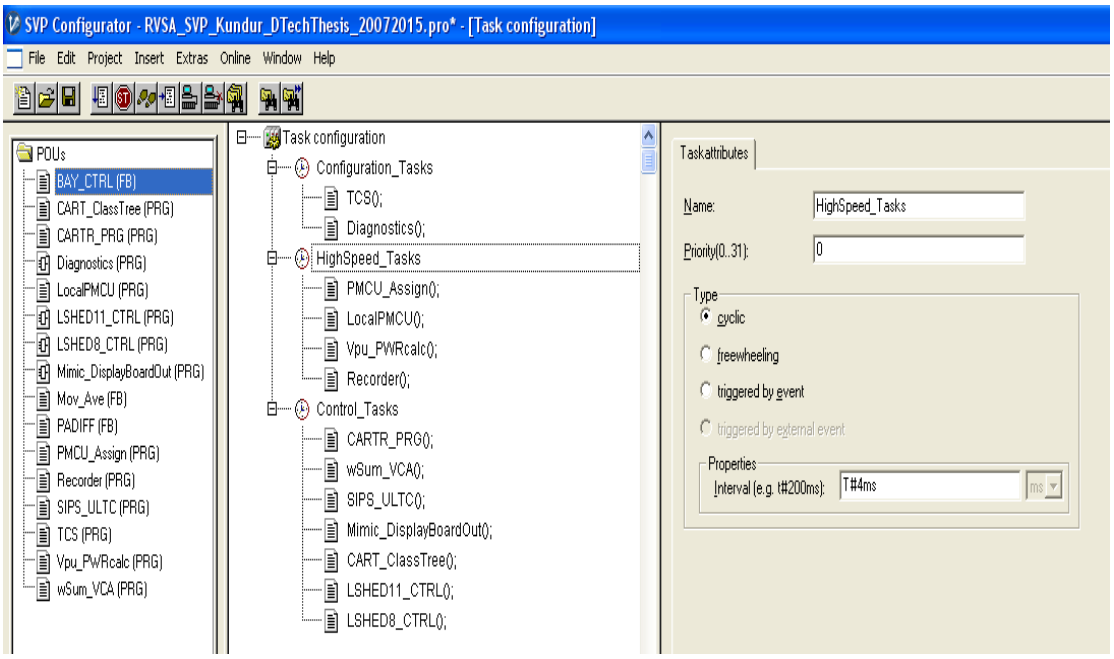

Figure 5.14: Task configuration snapshot of the SEL-3378 SVP POUs

5.3.3 Programme Organisation Unit Design

The real-time implementation of the proposed algorithms was carried out using IEC 61131-3 POUs. The tasks to be carried out by the SEL-3378 SVP include the subscription of the IEEE C37.118 synchrophasor measurements streamed by the external PMU devices (IEEE C37.118 Servers), the calculation of the moving averages of the phasors for filtering out transients and noise, the calculation of the power flow, voltage stability assessment algorithm, implementation of the Decision Tree (DT) classifier and predictor, and the SIPS algorithms for transformer tap changer blocking/unblocking (ULTC-SIPS) and undervoltage load shedding (UVLS-SIPS).

The voltage stability assessment algorithm uses phasors from PMUs as input to the DT-classifier proposed in Chapter Four. The real-time system's state and the margin

to voltage collapse is computed and displayed on the designed Human-Machine Interface (HMI). During stressed system operating conditions, the CART POU predicts the transition of the system from the 'Stable' to the 'Alert' state. When the pickup timer times out, the ULTC-SIPS POU issues an arming signal to initiate the ULTC-SIPS algorithm for transformer tap-changer control proposed in Chapter Seven. The tap-changer blocking/unblocking signals are issued from the SIPS_ULTC POU. The remote bit set is sent via a Fast Operate (FO) messaging to the SEL-451 IED (acting as a substation field actuating I/O device). The SEL-451 IED subscribes to the FO message and publishes an IEC 61850 GOOSE message to block/unblock the transformer ULTC model in the RSCAD software.

If the voltage instability does not improve and the output of the CART POU transitions from the system 'Alert' state tending towards the 'Unstable' state, an UVLS-SIPS POU is used as the last line of defence and loads are shed in order to restore the system to an acceptable operating state (Chapter Seven).

The POUs can be a programme, a function script, or a function block, and it consists of three elements. These elements are:

- POU name and type.
- Declaration part for the declaration of the variables used within the POU.
- POU body for the PLC instructions using the IEC 61131-3 programming language.

The POUs designed and utilised in the implementation of the proposed WAMPAC 'proof-of-concept' testbed are as highlighted in Figure 5.15 and include:

- Time Alignment Client Server (TCS) POU
- Phasor Measurement and Control Unit (PMCU_Assign) POU
- Local PMCU POU
- Phase angle difference (PADIFF) POU
- wSUM_VCA POU
- SIPS-ULTC POU
- BAY_CTRL (FB)
- CART_CT POU
- CART_RT POU
- Mimic_DisplayBoardOut (SEL Fast Operate) POU
- Diagnostics

The integrity of the various algorithms implemented in the SEL-3378 SVP is maintained by using enable bits logic based on the status (online/offline) of the PMUs to activate the algorithms. If the measurements from a PMU are lost due to communication failure or loss of time synchronization, the execution of the POUs using that particular PMU measurements will be rightly blocked.

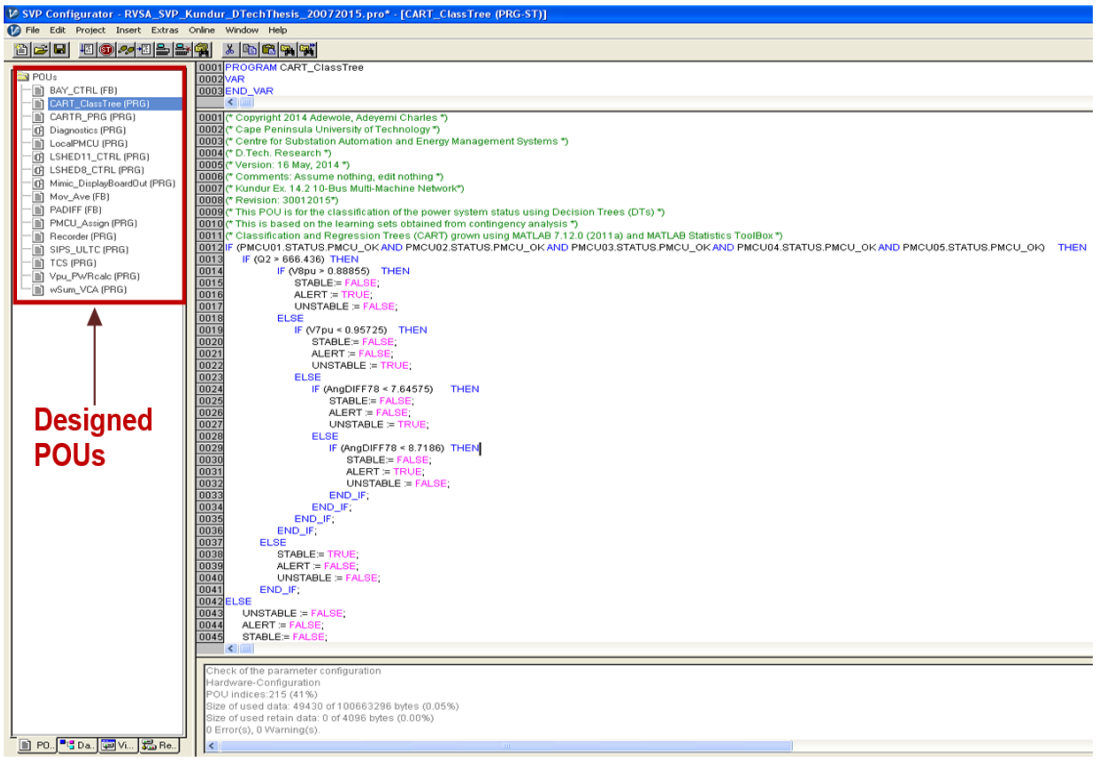

Figure 5.15: POUs for the proposed WAMPAC algorithms

A description of the various POUs is given below:

- The TCS (PRG) POU: receives and time-aligns the synchrophasor measurements from external IEEE C37.118 Servers. Also, it provides an interface for the transmission of the control signals.
- The PMCU_Assign (PRG) POU: serves as the interface for accessing the synchrophasor measurement for use in the other POUs.
- The LocalPMCU (PRG): is used for streaming synchrophasor measurements and user-programmed POUs to the external PDCs on a higher hierarchical level.
- The PADIFF (FB) POU: is the phase angle difference POU and it is used in the calculation of the angle difference between two phasor angles.
- wSUM_VCA POU: this POU is used in the calculation of the proposed weighted summation wide area RVSA index.
- SIPS-ULTC POU: implements the proposed transformer ULTC blocking/unblocking SIPS algorithm.
- BAY_CTRL (FB): A Function Block (FB) designed as a bay controller for the proposed load shedding was named *BAY-CTRL*. In the design of the FB, the calculated amount of load to shed was distributed across 5 feeders per bus depending on the magnitude of the disturbance and the power mismatch was calculated. Instances of the *BAY_CTRL* FB were then called by the bay controllers for each voltage control area.

- CART_CT POU: implements the trained DT-classifier in the SEL-3378 SVP. The trained classifier is used in the classification of the system's operating state.
- CART_RT POU: is used in the implementation the trained DT predictor in the SEL-3378 SVP. The trained DT predictor is used in the prediction of the system's percentage margin to voltage collapse.
- Recording POU: is used for the contingency analyses carried out for the monitoring and recording of the voltage phasors and system measurements for various operating conditions at the acceptable steady state condition and at the point of voltage collapse.
- Mimic_DisplayBoardOut POU: uses the SEL Fast Operate (FO) message to transmit remote bit signals to the substation I/O device (SEL-451 IED).
- The Diagnostics POU: gives the information relating to the SEL-3378 SVP system's status, alarm contact status, time synchronization, temperature, and CPU usage.

5.4 Chapter Summary

This Chapter presented the details of the lab-scale implementation of the Wide Area Monitoring, Protection and Control (WAMPAC) 'proof-of-concept' testbed for the proposed real-time voltage stability assessment algorithm, generator/load bus clustering, system integrity protection schemes using transformer blocking/unblocking (ULTC-SIPS), and undervoltage load shedding (UVLS-SIPS).

A description of the various equipment utilized in the real-time implementation of the algorithms and methods of solution, their configuration, and various settings are presented. Details of the design of the POUs for the programmable logic controller are given. Several POUs were designed and programmed using the IEC 61131-3 structured text and function block programming languages respectively.

Chapter Six presents the results obtained for the proposed measurement-based clustering algorithm and the real-time voltage stability assessment indices. The growing of decision trees and ensembles of decision trees for the classification of the system's operating state and the prediction of the system's margin to voltage instability is reported.

CHAPTER SIX
RESULTS FOR THE WIDE AREA VOLTAGE STABILITY ASSESSMENT METHOD

6.1 Introduction

The results obtained through the application of the proposed methods and algorithms in Chapter Four using the WAMPAC testbed presented in Chapter Five are given in this Chapter.

These include the results for the clustering of the generators and load buses, and the proposed voltage stability assessment indices. The proposed machine learning-based classification and prediction for real-time voltage stability assessment are presented and discussed.

Also, the procedure for the generation of the dataset for the training and testing of the decision trees is given herein. Furthermore, the results for the training and testing of the decision trees and ensembles of decision trees are elucidated.

6.2 Measurement-Based Clustering for Voltage Stability Assessment

The results for the measurement-based power system clustering proposed in Chapter Four for the identification of the buses with similar voltage collapse problem and synchronous generators providing reactive power support to these load buses are presented in this section. The focus was with respect to voltage stability assessment in large interconnected power systems. Results are presented for the New England 39-bus benchmark test system (Pai, 1989) shown in Figure 6.1.

The generators are connected to buses 30-39, and are equipped with the IEEE Type-1 excitation systems and governors. The transformer between buses 11 and 12 is modified to include an Under-Load Tap Changer (ULTC). Also, generator G3 is modified to include an Over-Excitation Limiter (OXL). The parameters for the transformer ULTC and OXL are given in Appendix A.

The measurement-based clustering method is implemented using synchrophasor measurements obtained from the control centre PDC configured for triggered archiving defined using a system event (e.g. line and generator contingency). After the load and generator partitioning stages, a jth Voltage Control Area (VCA) is allocated to its corresponding Reactive Power Reserve Basin (RPRB) based on the

calculated electrical distance between them. The electrical distance can be calculated as the distance between the terminal of the generators in the RPRB and the load buses within a VCA. The RPRB and VCA with the minimum distance are paired using the formulation in:

$$D_{rp} = \min\left(D_{rp}\right) \quad r = \overline{1, n_{rj}},\ p = \overline{1, N_{bj}} \tag{6.1}$$

where the electrical distance given in (Blumsack *et al*., 2009) is $[D] = \left|[Y_{bus}]^{-1}\right|$, D_{rp} is the electrical distance between the rth synchronous machine within a RPRB and the pth load bus in the jth VCA, n_{rj} is the number of generators in the RPRB, N_{bj} is the number of the load buses in the jth VCA.

6.2.1 Simulations Scenarios for the Measurement-Based Clustering Algorithm

The simulation scenarios considered include the application of the measurement-based clustering algorithm during increased loading conditions, transmission line and generator contingencies, the impact of the transformer ULTC, and the generator OXL operation. Four (4) case studies relating to the application of the proposed synchrophasor measurements-based load and generator clustering algorithm were investigated.

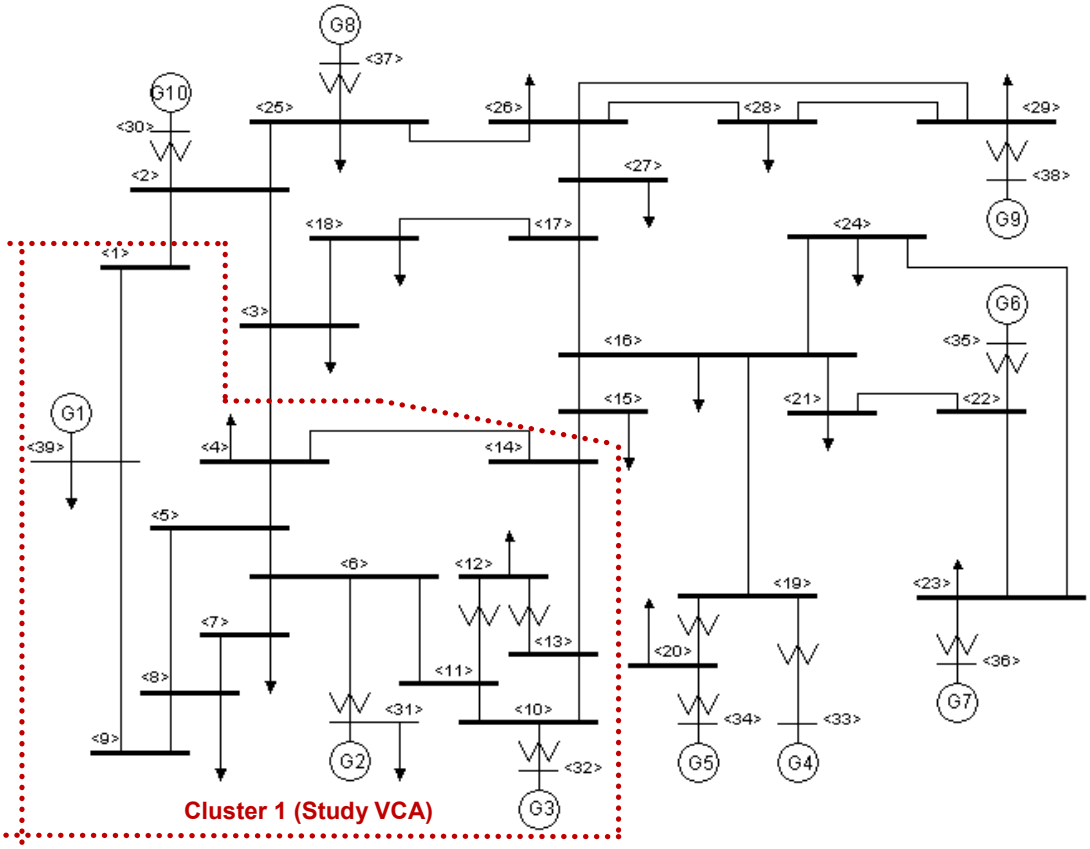

Figure 6.1: New England 39-bus test system (Pai, 1989)

These cases are:

- Load bus clustering;
- Generator clustering;
- Clustering of the generators with OXL action; and
- Effects of various PMU reporting rates on the generator clustering.

In order to drive the system to its 'Alert' state and determine the corresponding generators in the Reactive Power Reserve Basins (RPRBs), an increased loading condition involving increments in the real power (ΔP) and reactive power (ΔQ) at a constant power factor was carried out at all the load buses in the VCA of interest. This was done with the real and reactive powers of the loads in the other clusters in the system unchanged.

It should be noted that for the case studies considered in this Chapter, 10% load increase at the load buses of interest was carried out every 60 s. 180 s measurement window (obtained from PDC triggered recording) corresponding to the third consecutive load increase was used in order to account for voltage deviations up to the third level of the load increase. This is equivalent to the measurements for a stressed system in the 'Alert' state for the study network used. The number of measurements equals (*60 fps x 180 s)* synchrophasor measurement points. Table 6.1 gives a summary of the PMU locations and their type of measurements.

Table 6.1: Measurement acquisition by PMUs

PMU Locations	Phasor Measurements	Analogue Measurements	PMU DigitalStatus
Critical load buses	Positive sequence of voltage and current	Real power, Reactive power	Line breaker status
Generator buses	Positive sequence of voltage and current	Real power, Reactive power, generator field current, generator rotor speed	Generator status

6.2.2 Case Study 1: Load Bus Clustering

Figure 6.2 shows the RSCAD-runtime bus voltages for the steady-state and for system loading conditions respectively. At the steady-state condition, the load buses -4, -7, -8, -12, and -20 already have voltages below 1.0 p.u. However, the voltage p.u. at these buses was still within the acceptable limit for the steady-state conditions i.e ±5% of nominal values.

Stressing the system by increasing the loading at the buses mentioned above, is capable of causing the voltage at these load buses to drop below the acceptable level with the system going into its 'Alert' state and consequently resulting in a voltage collapse.

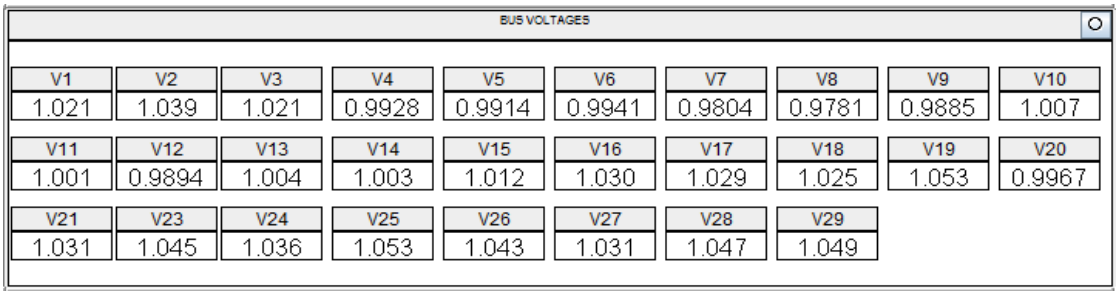

(a)

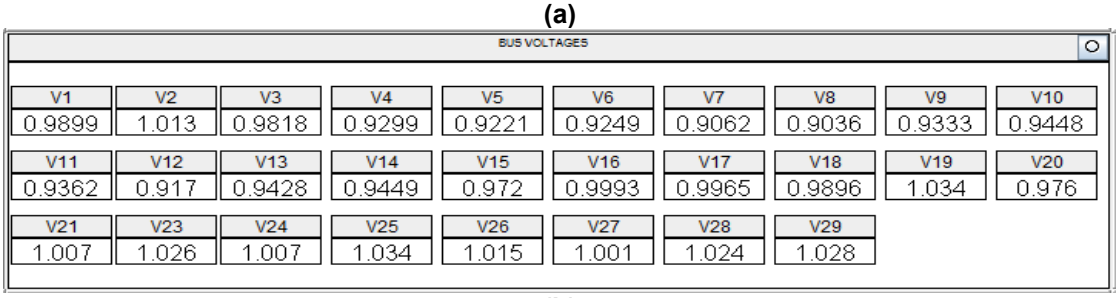

(b)

Figure 6.2: RSCAD-runtime measurement palette for Vp.u. **(a)** At the steady-state condition; **(b)** Under system loading conditions

The hybrid Calinski-Harabasz criterion and *k*-means clustering algorithm was applied to the synchrophasor measurements of the bus voltages obtained from an increased system loading condition. Figure 6.3 shows the plot of the Calinski-Harabasz criterion for the various clusters k.

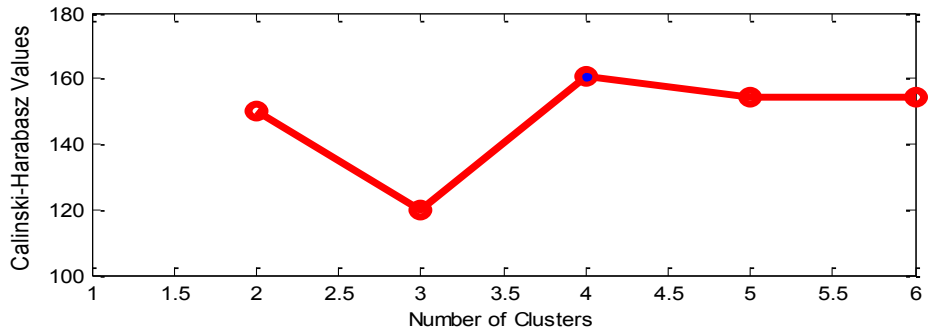

Figure 6.3: Plot of Calinski-Harabasz index for the synchrophasor measurements at the load buses

Table 6.2: Cluster groups for the load buses

Cluster Number	Cluster Buses	Load Buses in the Cluster
Cluster 1	**{4, 5, 6, 7, 8, 9, 10, 11, 12, 13, 14}**	**{4, 7, 8, 12}**
Cluster 2	{1, 3, 18}	{3, 18}
Cluster 3	{2, 15, 16, 17, 20, 21, 24, 26, 27}	{15, 16, 20, 21, 24, 26, 27}
Cluster 4	{19, 23, 25, 28, 29}	{23, 25, 28, 29}

The optimal number of k for this scenario is obtained as 4 clusters. The result of the application of the clustering algorithm gives the various clusters and the buses in each respective cluster. Table 6.2 gives the buses in each cluster. Cluster 1 (in bold) in Table 6.2 was selected for further studies related to the identification of the

generators in each cluster. Cluster 1 was chosen for further analysis because it was the most critical VCA in the study network and it is capable of driving the rest of the system into voltage instability. The study area in the study network is indicated in Figure 6.1 with dotted lines.

6.2.3 Case Study 2: Generator Clustering

Case Study 2 was carried out in order to investigate the best variables for the generator coherency in the study network, and to identify the RPRB providing voltage control/reactive power support at the VCA identified in Case Study 1. A study was carried out using simultaneous load increase at the load buses in Cluster 1 of Table 6.2 {load buses -4, -7, -8, and -12}. Figures 6.4-6.5 show the terminal voltages and the field currents I_{fd} for generators G1-G4.

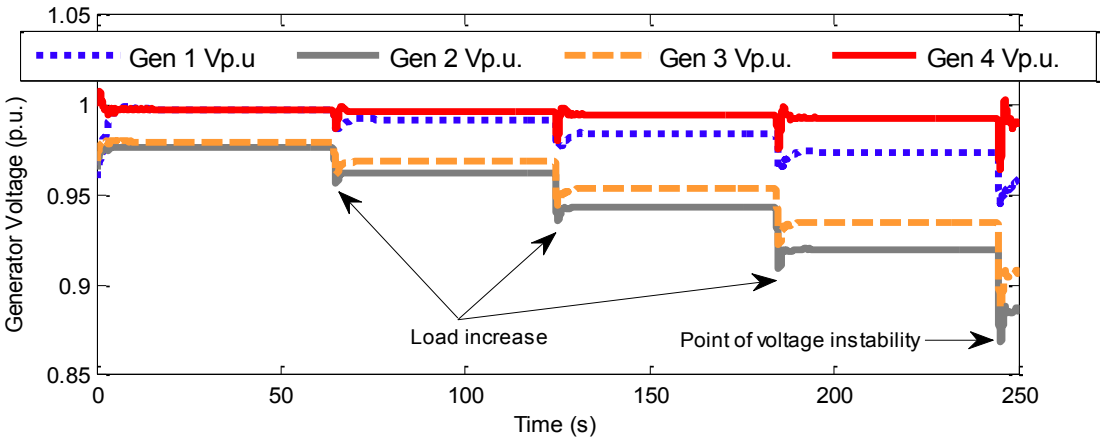

Figure 6.4: Terminal voltages for generators G1-G4

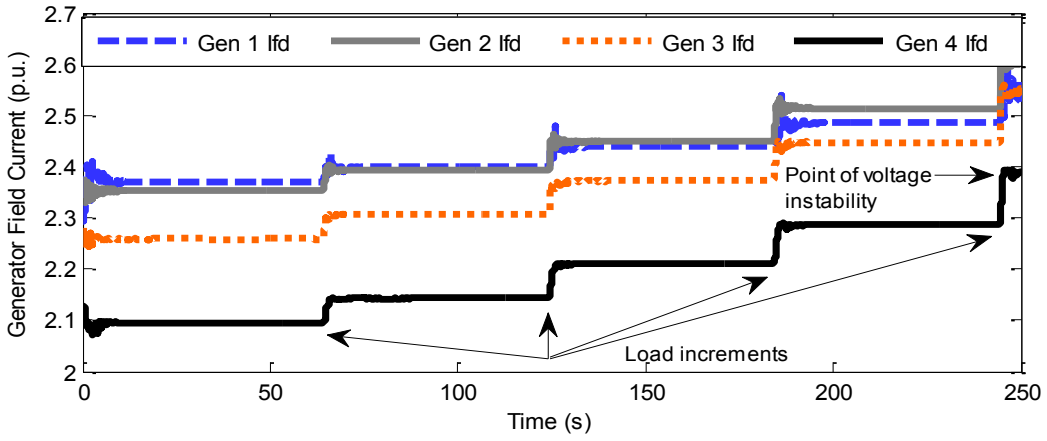

Figure 6.5: Field currents for generators G1-G4

Although, generator G4 does not belong to the RPRB in Cluster 1, it was the most responsive of the generators external to Cluster 1. Therefore, the terminal voltage for generator G4 was added in these figures to show that the response of the generators in other clusters can be ignored since these external generators do no exhaust their reactive power reserves. From Figures 6.4-6.5, it can be seen that the most stressed generators are generators G2 and G3 as shown by the drop in their terminal voltages and the increase in their field currents respectively.

Seven generator/generator-derived variables were investigated to determine the best variable for the generator clustering algorithm with respect to the voltage stability assessment.

These include:

- Generator reactive power $(MVAr)$;
- Generator field current (I_{fd});
- Generator stator current $(|I_a|)$;
- Generator terminal voltage $(|V_g|)$;
- Generator rotor speed (rad/sec);
- Real-Time Voltage Stability Assessment Index using generator field current reserve $(RVSA_{Ifd})$;
- Real-Time Voltage Stability Assessment Index using generator reactive power reserve $(RVSA_Q)$ proposed in (Choi *et al*., 2011; Dong *et al*., 2005; Bao *et al*., 2003; Capitanescu and Van Cutsem, 2001).

Figure 6.6 shows the plots of the Calinski-Harabasz index for the above-mentioned variables. From Figure 6.6, it can be seen that the highest Calinski-Harabasz value is from the $RVSA_{Ifd}$ index obtained from the generator field current. The final decision on the best variable to use was based on the number of clusters and the silhouette coefficients obtained as detailed in Chapter Four. Figure 6.7 shows the silhouette plot for the $RVSA_{Ifd}$ variable.

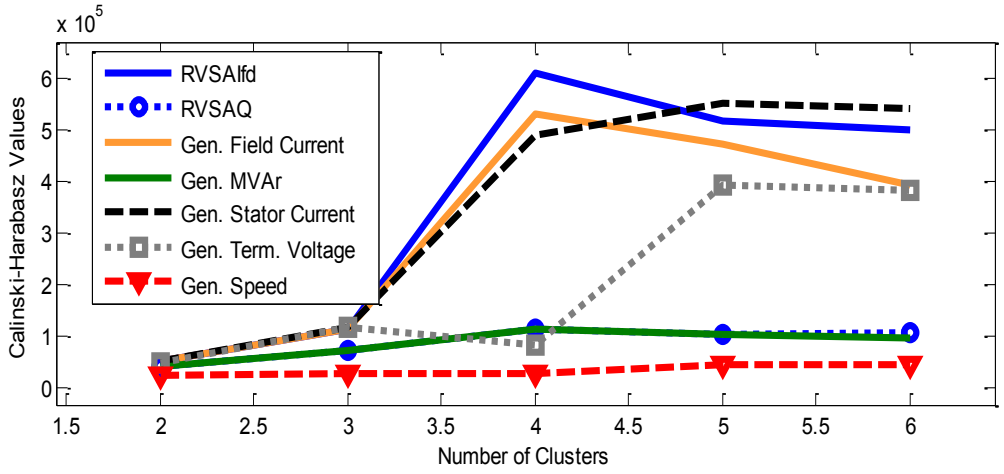

Figure 6.6: Plot of Calinksi-Harabasz index for various generator variables

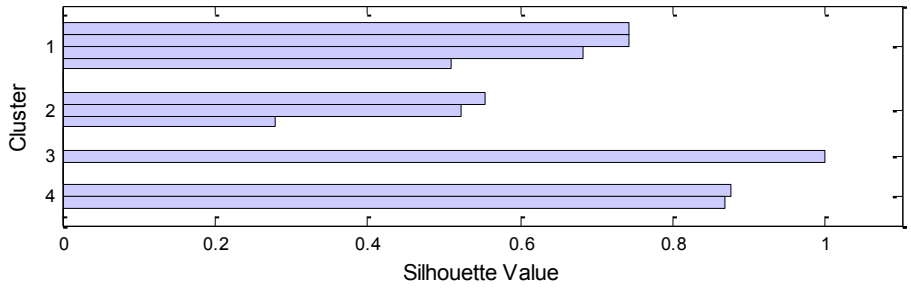

Figure 6.7: Silhouette plot obtained using $RVSA_{Ifd}$ variable

Compared with Figure 6.8 obtained using generator reactive power variables, it can be seen that all the generators in the clusters have positive silhouette values in Figure 6.7, while Figure 6.8 has a generator with a negative silhouette coefficient in Cluster 4.

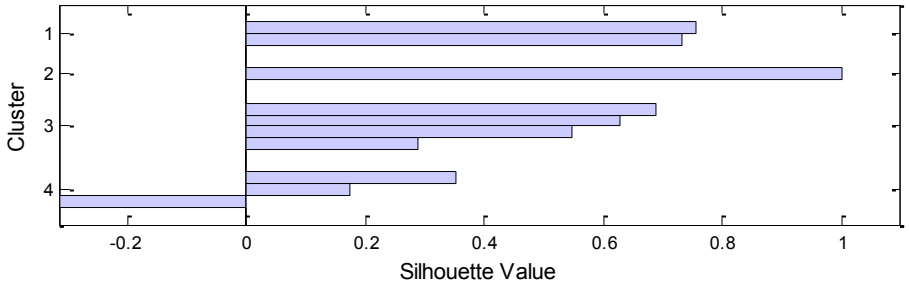

Figure 6.8: **Silhouette plot obtained using $MVAr$ variable**

Table 6.3 shows the generators in each cluster for an increased loading scenario at the load buses given in Cluster 1 of Table 6.2. From Table 6.3, it can be seen that the generators in the study network have been clustered into 4 or 5 coherency groups depending on the variable used. In bold text is the selected cluster group for the case being investigated based on the values of the Calinski-Harabasz criterion, the number of clusters, and the silhouette coefficients obtained.

Table 6.3: **Cluster groups for the system generators for various variable types**

Variable Type	Number of Generator Clusters	Generator Cluster Members
Generator Reactive Power (MVAr)	4	{1, 3}; {4, 5, 7}; {8, 9}; {2, 6, 10}
Generator Field Current (I_{fd})	4	{1, 2, 3}; {4, 6, 7, 8, 9}; {5}; {10}
Generator Stator Current (I_a)	5	{2, 3, 4}; {5, 8}; {1}; {10}; {7}
Generator Terminal Voltage (V_g)	5	{2, 3}; {4, 5}; {8, 10}; (1}; {7}
Generator Rotor Speed (Rad./sec.)	5	{4, 5, 6, 7, 9}; {8, 9}; {1}; {2}; {3}
$RVSA_{Ifd}$	4	**{1, 2, 3}; {4, 7, 8, 10}; {6, 9}; {5}**
$RVSA_Q$	4	{1, 2, 3, 6}; { 4, 5, 10}; {8, 9}; {7}

6.2.4 Case Study 3: Clustering of the Generators with OXL Action

In Case Study 3, the transformer between two buses (buses-11 and -12) was modified to include an ULTC. Also, an OXL was incorporated into generator G3. This was done in order to investigate the impact of the ULTC and OXL actions on the clustering algorithm. Figure 6.9 shows the generator field currents for the system loading scenario (in Case Study 2) and the operation of the OXL at generator G3. It can be seen that there was an increase in the field current of generator G2 as a result of the ramping down of the field current of generator G3 by the OXL.

This is because generator G2 which belonged to the same RPRB as generator G3, picked up and supplied the additional reactive power which generator G3 was unable to supply due to the operation of its OXL. The clustering result for this Case Study is ({1, 2}; {3, 6, 9}; {4, 7, 8, 10}; {5}). Compared to the result obtained in Table 6.3, generator G3 was reassigned to the cluster group {6, 9}. Figure 6.10 shows the plot of the silhouette coefficients for Case Study 3 with the OXL action.

The above scenario shows that coherency clustering in VCAs and RPRBs for voltage stability assessment should be done online, and should consider the effects of system dynamics like transformer ULTC and generator OXL actions. Also, the once-off approach proposed in (Rameshkhah *et al*., 2010) might fail in this case.

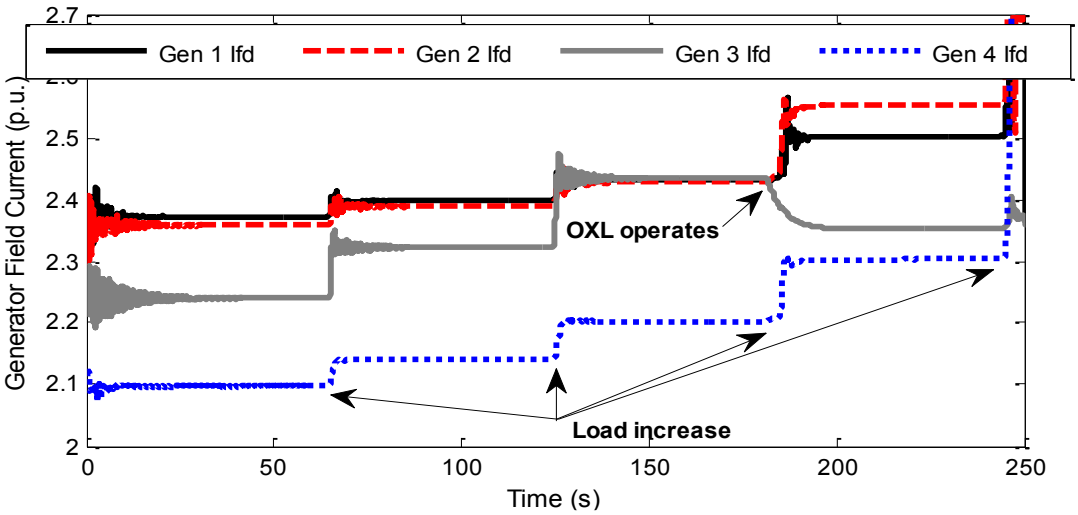

Figure 6.9: Field currents for generators G1-G4

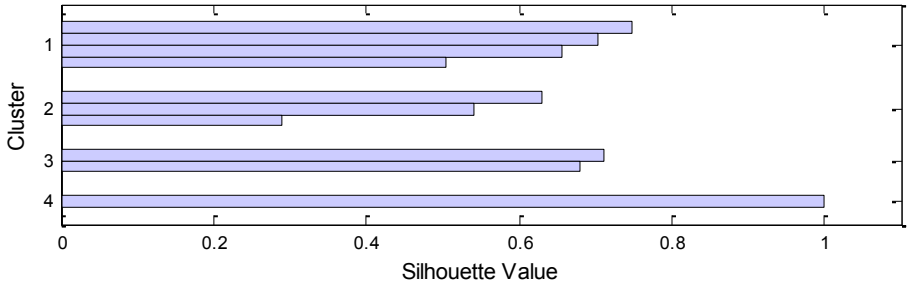

Figure 6.10: Silhouette plot obtained for Case Study 3 using the $RVSA_{Ifd}$ variable

6.2.5 Case Study 4: Effects of PMU Reporting Rates

The effect of the various PMU reporting rates on generator clustering was investigated for the increased loading scenario at the load buses in Cluster 1 of Table 6.2. The Calinski-Harabasz and silhouette values for each reporting rate were computed. Figure 6.11 shows the plots for the Calinski-Harabasz values for various PMU reporting rates. From Figure 6.11, it can be seen that the highest Calinski-Harabasz values were obtained for the 60 fps reporting rate.

Reporting rates higher than 60 fps could not be used because the substation PDC (SEL-3378 SVP) has a maximum reporting rate of 60 fps, even though higher reporting rates were possible with the PMUs and the regional PDC (SEL-5073). Table 6.4 shows the various generator clusters obtained for various PMU reporting rates using the $RVSA_{Ifd}$ index.

Table 6.4: Cluster groups for various PMU reporting rates

Reporting Rate	Number of Clusters	Generator Cluster
60fps	4	**{1, 2, 3}; {4, 7, 8, 10}; {6, 9}; {5}**
30fps	4	{1, 2, 5}; {4, 7, 8, 10}; {6, 9}; { 3}
20fps	4	{1, 2, 3, 5}; {4, 7, 8, 10}; {6,} {9}
15fps	4	{1, 2, 3, 5}; {4, 8, 10}; {6, 9}; {7}
12fps	4	{1, 2, 5}; {4, 7, 8, 10}; {6, 9}; {4}
10fps	5	{1, 2, 3}; {4, 8, 10}; {6, 9}; {5}; {7}
5fps	5	{1, 2, 5}; {4, 8, 10}; {6, 9}; {3}; {7}
1fps	5	{1, 2, 3}; {4, 7, 8}; 0{6, 9}; {5}; {10}

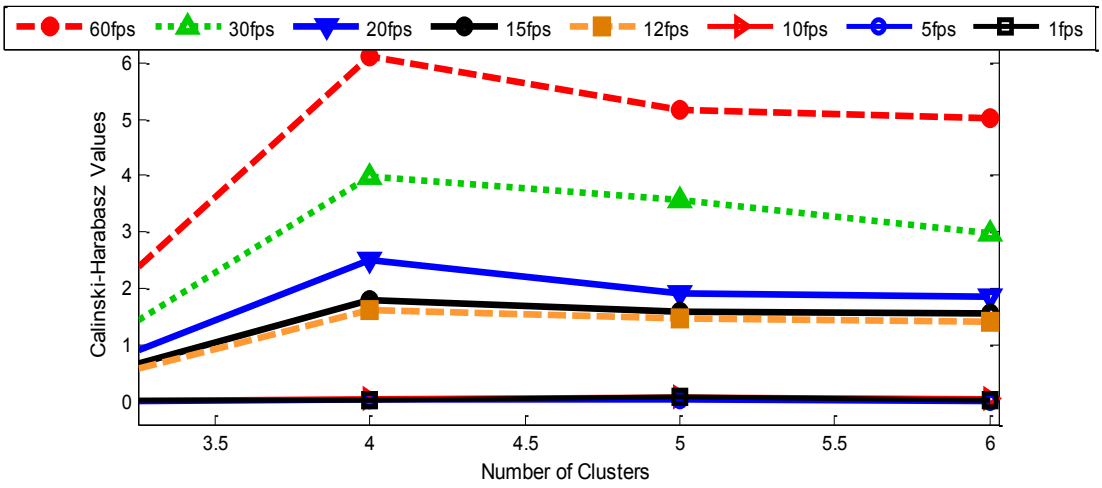

Figure 6.11: Plot of Calinksi-Harabasz index for various PMU reporting rates

6.2.6 Discussion on Measurement-Based Clustering Algorithm

This section presented the results obtained for the proposed online measurement-based clustering approach for application in voltage stability assessment. In contrast to the conventional model-based methods, the proposed approach is based on system variables directly obtained from synchrophasor measurements. Thus, suitable for online real-time application.

The simulation scenarios considered include increased loading conditions, the effects of transformer ULTC and generator OXL. It was shown that the determination of the generator clusters is not static, but rather a dynamic task that should be done in real-time as the system conditions changes. Also, the effects of PMU reporting rates were

investigated, and it was shown that the use of 60 fps gave the best results for the reporting rates considered.

From the results, it can be seen that the proposed coherency clustering approach can be applied in the monitoring of large interconnected power systems in real-time since voltage stability indices can easily be derived for the monitoring of each of the respective clusters (VCAs).

6.3 Static Voltage Analyses

DIgSILENT PowerFactory software is utilised for static analyses comprising of P-V and V-Q curves which are the most commonly used voltage stability analysis techniques in the industry. This was carried out in order to validate the VCAs obtained using the online measurement-based clustering approach proposed in Section 4.3. Also, static voltage analysis was used in the selection of the most critical area in the network. The selected critical area was afterwards made the focus of the detailed dynamic simulation studies carried out using the RTDS®. Furthermore, the static voltage analysis methods were applied in the investigation of the maximum point of loadability and the required reactive margin to prevent voltage collapse.

The area that showed the largest deviation in bus voltages/the lowest loadability during the steady-state operating conditions (base case) and when subjected to contingencies will be selected as the most critical area.

6.3.1 P-V Curve Simulations

The P-V curve was used to investigate the loadability of the load buses with respect to the maximum load permissible before voltage collapse.

The steps used in the calculation of the P-V curve are:

- Select the candidate load bus or load buses for which the P-V curve is to be calculated.
- Starting from the base case, increase the real power (P) MW of the load at the candidate bus by 0.2 p.u. from the base value.
- Run load flow program, note the voltage (V) at the candidate bus.
- Increase the load MW until the load flow calculation fails to converge.
- Plot (P) against (V) to obtain the P-V curve for that particular candidate bus.

The procedure used involved a systematic increase in the real power loading at a load bus or area from the current operating point at a constant power factor. Load flow calculation was carried out after each increment in loading, until the maximum loadability point was reached. At this point, the load flow diverges, and no solution was obtained.

The upper part of the P-V curve is the stable region, while the lower part indicates the unstable region. The nose point of the P-V curve corresponds to the saddle-node bifurcation point (the voltage collapse point). Figure 6.12 shows the P-V curve for the load increase carried out at load buses -4, -7, and -8. The load buses belonging to the stressed VCA include buses -4, -7, -8, and -12 as verified by their bus voltages dropping below 0.85 p.u. It can be seen from Figure 6.12 that buses -15, -19, -24, -25, and -29 belonged to a different VCA. This is because their bus voltages were unaffected and remained within the acceptable values.

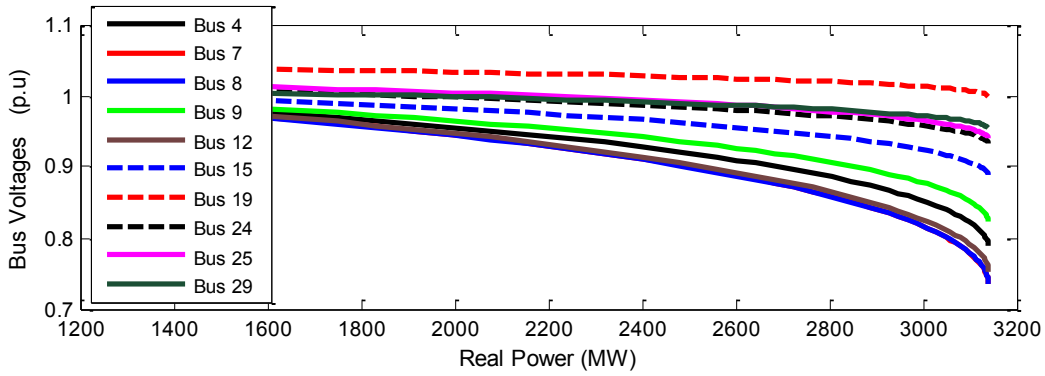

Figure 6.12: **P-V curves for the New England 39-bus test system with the generator limits off (system loading at buses -4, -7 and -8)**

On the basis of this, buses -7, -8, -12, -15, -20, -28, -29 were selected as the monitoring buses. Simulations carried out showed that the New England 39-bus test system is secure for line contingencies since the voltage profile at the buses remained within the acceptable ±5% of the nominal bus voltage values. It was observed that N-2 generator contingencies, or a combination of both N-1 generator contingency and increased system loading were required in order to drive the system to its voltage collapse point. Figure 6.13 shows the P-V curves for the generator contingencies considered. From the figure, it can be seen that the bus loadability is reduced for these contingencies, and the loss of generator G1 was the most severe N-1 contingency in the test system.

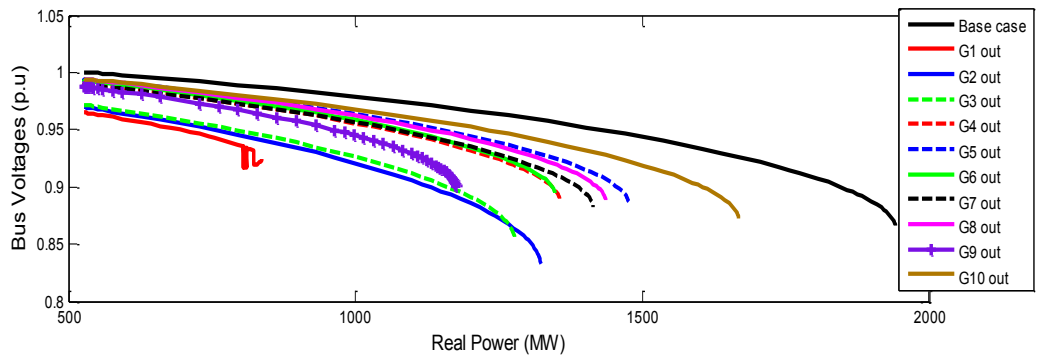

Figure 6.13: **P-V curves for the New England 39-bus test system with the generator limits off (generator contingencies)**

While the loss of generators G2 and G3 is ranked as the second and the third most severe N-1 contingencies respectively. A plot of the N-1 generator contingencies and N-2 contingencies is given in Figure 6.14. It was observed that the worst N-2 contingency was the loss of generators G2 and G3.

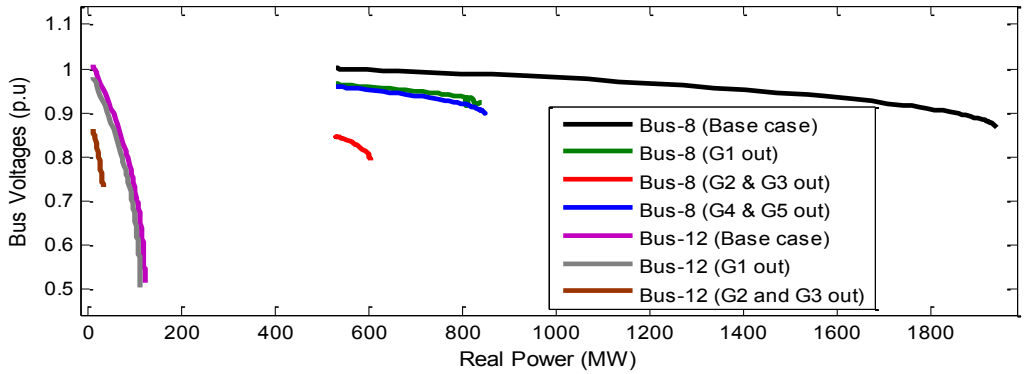

Figure 6.14: **P-V curves for the New England 39-bus test system with the generator limits off (effects of severe generator contingencies)**

6.3.2 V-Q Curve Simulations

The V-Q curve was used in the calculation of the reactive power margin required on each load bus in the system. This signified the reactive power compensation that must be available on the load bus in order to have adequate voltage control. Typically, the V-Q curve is calculated by connecting a fictitious synchronous condenser to a candidate load bus.

The steps for the calculation of the V-Q curve include the following:

- Select the candidate load bus or load buses for which the V-Q curve is to be calculated.
- Change the candidate bus/buses to a fictitious PV bus/buses by connecting a fictitious synchronous condenser with zero real power.
- Using a range of voltages (V), run the load flow calculation.
- Record the reactive power output (Q) of the synchronous condenser.
- Reschedule the candidate bus voltages until the load flow calculation fails to converge.
- Plot the incremental values of (V) at the candidate bus against the calculated (Q) from the synchronous condenser to obtain the V-Q curve for that candidate bus.

The reactive power of the generators was recorded for various values of bus voltages. The right part of the V-Q curve is the stable region, while the left part is the unstable region. The available margin before voltage collapse is from the current operating point to the bottom (nose point) of the V-Q curve. Figures 6.15-6.18 show the V-Q curves calculated for the New England 39-bus test system for the base case, N-1 and N-2 generator contingencies respectively. These V-Q curves illustrate the variation in the bus voltages at the load buses with respect to the required reactive power support.

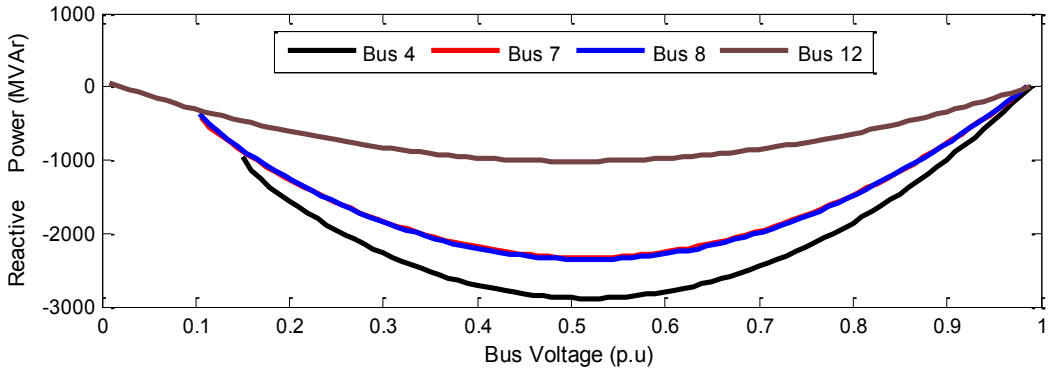

Figure 6.15: V-Q curves for New England 39-bus test system with the generator limits off (system loading at buses-4 and -8)

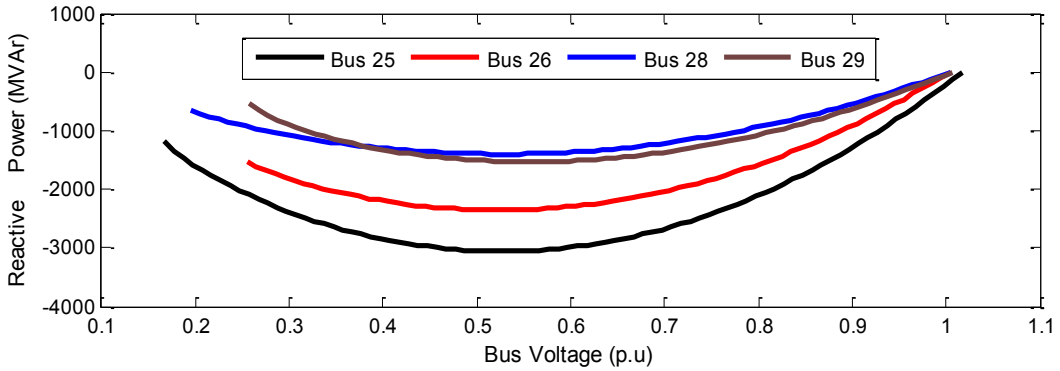

Figure 6.16: V-Q curves for New England 39-bus test system with the generator limits off (system loading at bus-25)

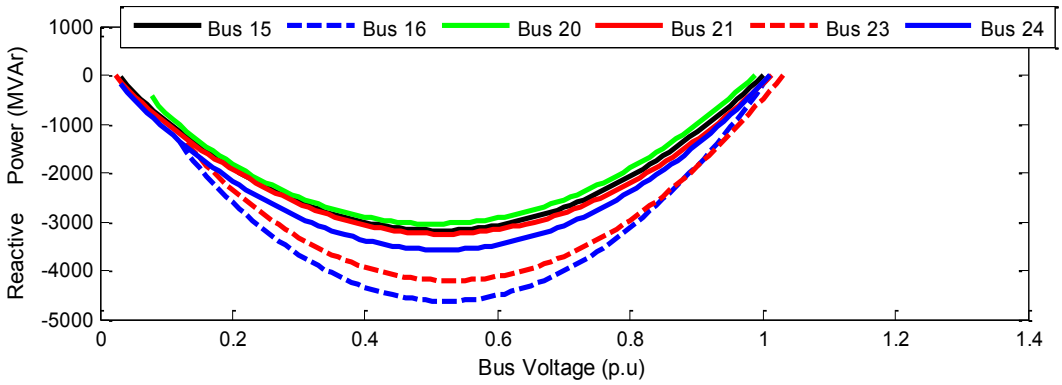

Figure 6.17: V-Q curves for New England 39-bus test system with the generator limits off (system loading at bus-15)

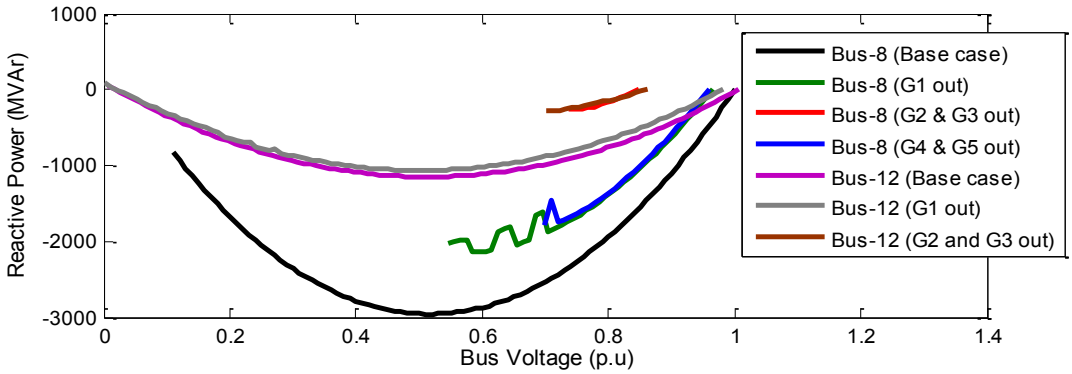

Figure 6.18: V-Q curves for 39-bus New England test system with the generator limits off (effects of severe generator contingencies)

6.3.3 Discussion on Static Analyses

Curve analyses (P-V and V-Q curves) were used in the determination of the loadability of the load buses and the estimation of the required reactive power margin at the load buses in the New England 39-bus test system.

Exploratory investigations carried out showed that buses-4, -7, -8, -12 experienced similar voltage instability as shown in Figure 6.12. It was observed that the New England 39-bus test system remained stable for line contingencies. Generator contingencies and increased system loading was thus necessary in order to drive the system to voltage collapse. The severe contingencies and the percentage of increased system loading capable of driving the system to its voltage collapse point were identified using the P-V and V-Q curves respectively.

Dynamic simulation provides the means of capturing the Electro-Magnetic Transient (EMT) response of power systems. This is because the power system components used are accurately modelled using algebraic and differential equations. Thus, dynamic simulations allow for power system dynamic conditions such as voltage stability to be accurately investigated in detail. EMT time-domain simulations using the RTDS® were used in the simulation of unscheduled outages of generation, transmission, and distribution components respectively. Subsequent sections in this Chapter would elaborate more on the dynamic simulation studies carried out.

6.4 Generation of Knowledge Base

A knowledge base encompassing several operating conditions and scenarios was used in building a database of datasets for training (growing) the Classification and Regression Trees (CARTs) and Ensembles of Decision Trees (EDTs). The elements in the database were obtained from the PDCs during real-time simulations. Two knowledge bases for the two test systems investigated were built and are discussed in the proceeding subsections. The test systems considered are the 10-bus multi-machine equivalent test system, and the New England 39-bus test system.

A 10-bus multi-machine test system (Kundur, 1994) was modelled in RSCAD software to study the Operating Conditions (OCs) relating to voltage stability dynamics as a result of load increase, loss of transmission lines, operation of generator OXL, and the effect of the transformer ULTC supplying the load at bus-11. The transformer ULTC used had a time delay of 30 s for the first tap operation and 5 s interval for the subsequent taps. Also, it had a tap range of $\pm$ 16 steps, 0.625% step size, and $\pm$ 1 % dead band.

Similarly, in order to study the impact of generator dynamics on the proposed algorithms, generator G3 was modelled with an OXL. The OXL was implemented with integrator and gain control components available in RSCAD software. Further information on the study network parameters can be found in (Kundur, 1994). Also, the load at bus-8 was modelled as a constant power load, while the real and reactive components of the load at bus-11 were made up of a combination of 50% constant impedance and 50% constant current components.

Various operating scenarios and credible line contingencies (N-1, N-2 contingencies) likely to result in voltage collapse were used in the generation of the input attribute-outcome knowledge base required for the training and testing of the DT-classifier and RT-predictor respectively. The scenarios considered are given in Table 6.5. Symmetrical and unsymmetrical fault types were not considered so as not to initiate other types of power system instability.

Table 6.5: System operating scenarios and contingencies for the 10-bus multi-machine test system (Test system-1)

S/N	Load Level	Scenario	ULTC	OXL
1	Load level 1	Loss of a transmission line between buses 6 and 7	x	x
2	Load level 2	Loss of a transmission line between buses 6 and 7	✓	✓
3	Load level 3	Loss of a transmission line between buses 6 and 7	x	x
4	Load level 1	Loss of 2 transmission lines between buses 6 and 7	✓	✓
5	Load level 2	Loss of 2 transmission lines between buses 6 and 7	✓	✓
6	Load level 3	Loss of 2 transmission lines between buses 6 and 7	✓	✓
7	Load level 1	5% load increase every 60 s	✓	✓
8	Load level 2	5% load increase every 60 s	✓	✓
9	Load level 3	5% load increase every 60 s	✓	✓
10	Load level 1	5% load increase every 60 s + loss of a transmission line between buses 6 and 7	✓	✓
11	Load level 2	5% load increase every 60 s + loss of a transmission line between buses 6 and 7	✓	✓
12	Load level 3	5% load increase every 60 s + loss of a transmission line between buses 6 and 7	✓	✓

The learning set used in the growing of the classification and regression trees is from synchrophasor measurements obtained from the real-time digital simulations using the WAMPAC 'proof-of-concept' testbed implemented in this thesis. A total of 504 observations made up of transmission line contingencies, increased system loading, transformer ULTC actions, and generator OXL operations are obtained using the scenarios given in Table 6.5.

Similar procedure to the 10-bus multi-machine test system was followed for the New England 39-bus test system. This was modelled in RSCAD software to study several

OCs and contingencies that could lead to voltage instability using load increase, transmission line contingencies, generator contingencies, operation of generator OXL, and the effect of the transformer ULTC. The loads in the cluster of interest were modelled as constant power loads using the dynamic load component in RSCAD software, while the other loads were modelled using RL components in RSCAD software. The scenarios considered are given in Table 6.6.

Table 6.6: System operating scenarios and contingencies for the 39-bus New England Test System (Test system 2)

S/N	Scenario	ULTC	OXL
1	Loss of a transmission line (line 3-4, line 4-5, line 14-15, line 15-16)	x	x
2	Loss of combinations of transmission lines (line 3-4, line 4-5, line 14-15, line 15-16)	x	x
3	5% load increase every 60 s at the load buses 4, 7, 8, 12	x	x
4	5% load increase every 60 s at the load buses 4, 7, 8, 12	✓	✓
5	5% load increase every 60 s + loss of a transmission line (line 3-4, line 4-5, line 14-15, line 15-16)	x	x
6	5% load increase every 60 s + loss of a transmission line (line 3-4, line 4-5, line 14-15, line 15-16)	✓	✓
7	*N*-1 loss of generators (G2-G9)	x	x
8	*N*-2 loss of generators (G2-G9)	x	x
9	*N*-1 loss of generators (G2-G9)	✓	✓
10	*N*-2 loss of generators (G2-G9)	✓	✓

Similar procedure to the 10-bus multi-machine test system, the learning sets for the classification and regression trees were from synchrophasor measurements obtained using the WAMPAC testbed. The learning sets in the knowledge base are given in Table 6.7.

Table 6.7: Instances of Operating Conditions (OCs) included in the knowledge-base

Test System	Class Distribution			Total OCs for the Classification Task	Total OCs for the Regression Task
	Stable	Alert	Unstable		
Test system 1	181 (35.91%)	97 (19.25%)	226 (44.84%)	504	504
Test system 2	501 (25.85%)	345 (17.80%)	1092 (56.35%)	1938	1938

6.5 Synchrophasor-Based Voltage Stability Assessment Classifier

The knowledge base comprising of several operating scenarios carried out in section 6.4 is used in this section in the training of a voltage stability assessment classifier for classifying the system operating state into ‘Stable’, ‘Alert’, or ‘Unstable’. In the training of a classifier, input attributes and the corresponding outcome (output) are required. Feature selection is a technique used in order to reduce the amount of data to be processed by the machine-learning algorithm. In this case, input attributes from the

dataset that are not important to the decision-making process of the DT-classifier are automatically discarded.

The input attributes in the dataset are made up of phasors, analogue values, and digital bits from synchrophasor measurements of bus voltages, transmission line currents, generator terminal voltages/stator currents, generator real/reactive powers, real/reactive power flows, and line breaker status. A feature selection technique based on the Bootstrap Aggregation (Bagging) implemented using the MATLAB TreeBagger method was used in this thesis to identify the important input attributes to use in the training of a high performance classifier. The out-of-bag error obtained using the Treebagger method was used in the calculation of the importance of each of the attributes in the dataset.

Classifiers are afterwards grown with the input attributes obtained above. Three different methods were used in the training of the classifiers. These are the decision tree method, Boosting ensemble (AdaBoostM2) method, and the Bagging (TreeBagger) method respectively. The performance of the classifiers is then compared.

6.5.1 Decision Tree-Based Classifier for Test System-1

An exploratory experimental process was followed to determine the best attributes for the voltage stability assessment system operating state classifier. The total dataset generated was randomly partitioned into two parts. 70% of the dataset was used as the Learning Set (LS) for training the classifier. The other 30% was used as the Test Set (TS) for testing the grown classifier.

The terminal nodes of the DT-classifier give the system's status with respect to voltage stability. The discrete output/response of the DT-classifier is 'Stable', 'Alert', and 'Unstable'. Using the observations from extensive RSCAD real-time simulations, the system's operating states were classified into:

Stable: $if\ \left\{\left(RVSA_{Ifd} \geq \eta_{Alt}\right)\ AND\left(Load\ 1\ \ V\ p.u. \geq 0.9\ \ AND\, Load\ 2\ \ V\ p.u. \geq 0.9\right)\right\}$ (6.2)

Alert: $if\ \left\{\left(RVSA_{Ifd} \leq \eta_{Alt}\right)\ AND\left(Load\ 1\ \ V\ p.u. \geq 0.9\ \ AND\, Load\ 2\ \ V\ p.u. \leq 0.9\right)\right\}$ (6.3)

Unstable: $if\ NOT\ (Stable\ OR\ Alert)$ (6.4)

where η_{Alt} is the threshold for the generator-derived field current-based real-time voltage stability assessment index $\left(RVSA_{Ifd}\right)$ and it was chosen as 32% for this test system based on the observations obtained from simulations. Loads 1 and 2 are located at buses-8 and -11 respectively.

The input attribute-outcome pairs used for the training of the DT-classifier include 22 input-attributes comprising of the generator variables (real power, reactive power, terminal voltage, field current, and stator current), voltage magnitudes at the critical buses, voltage phase angles, and phase angle differences. The outcome includes the system operating state (Stable, Alert, or Unstable). The MATLAB function used in training the DT-classifier is the *ClassificationTree.fit*.

The growing of the DT-classifier involves the following steps:

- Input the training dataset.
- Create a $n \times d$ matrix of predictors with n observations and d input attributes (predictors).
- Create a vector of response outcome $\mathbf{Y}$.
- Partition the training dataset into LS and TS.
- Grow the tree by considering all the possible splits on every input attribute-outcome pairs.
- Select the split with the best value of the Gini Diversity Index (GDI) optimisation criterion.
- Impose the node split.
- Conduct performance analysis of the grown tree using the confusion matrix, resubstitution error, and the cross-validation error.
- Prune if necessary.

It should be noted that at each node of the tree, the value of the input attributes given is checked. The choice of the particular input attribute to be used in the decision process is based on the splitting criterion. The attribute with the smallest GDI is selected for the corresponding node.

In order to grow a robust tree that is simple and with good predictive performance, a balance in terms of the leafiness/tree-depth needs to be achieved. This can be done by selecting the appropriate tree-depth. An investigation was carried out experimentally to determine the optimal leaf size to be used based on the cross-validated error obtained.

The resubstitution (resub.) error is the computed error when the grown DT-classifier is tested using the same training dataset that was used in growing it. While the cross-validation (cross-val) error is the error obtained when the DT-classifier grown using the *k*-fold cross-validation method is tested using the 'holdout' fold as the test dataset during the growing/cross-validation process.

More information on the determination of the optimal tree-depth for decision trees can be found in (MATLAB Statistic Toolbox guide, 2014). Figure 6.19 shows the optimal leaf size to be about 36 observations per leaf (terminal node). For the optimal leaf

size of 36 observations per leaf, the predictive attributes obtained are *#13* (generator G2 MVAr) and *#20* (bus-8 voltage phasor) respectively.

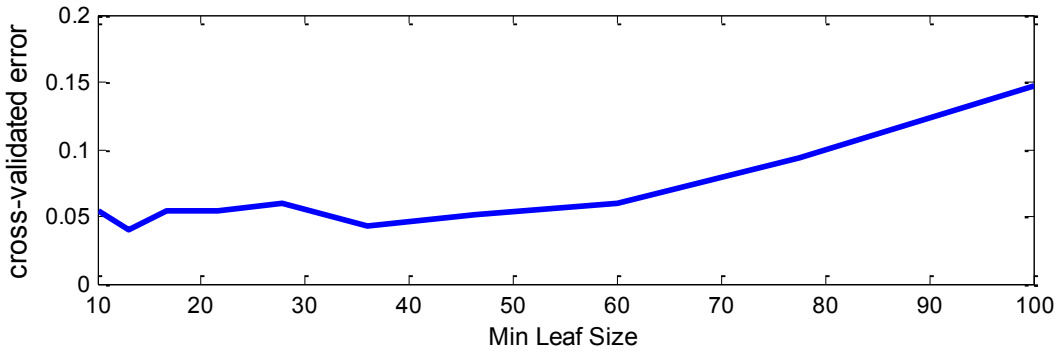

Figure 6.19: Investigations on the optimal tree depth

The confusion matrix given in Figure 6.20 shows that the classifier has a predictive accuracy greater than 95% for the 'Stable' and 'Unstable' states, for both the training and test datasets respectively. While the 'Alert' state was wrongly classified as the 'Stable' or 'Unstable' states in some cases.

The output represents the outcome corresponding to the respective input attributes, while the target represents the predicted outcome obtained using the trained DT. In the output and target classes shown in Figure 6.20, class 1 represents the 'Stable' state, class 2 is the 'Alert' state, while class 3 is the 'Unstable' state respectively.

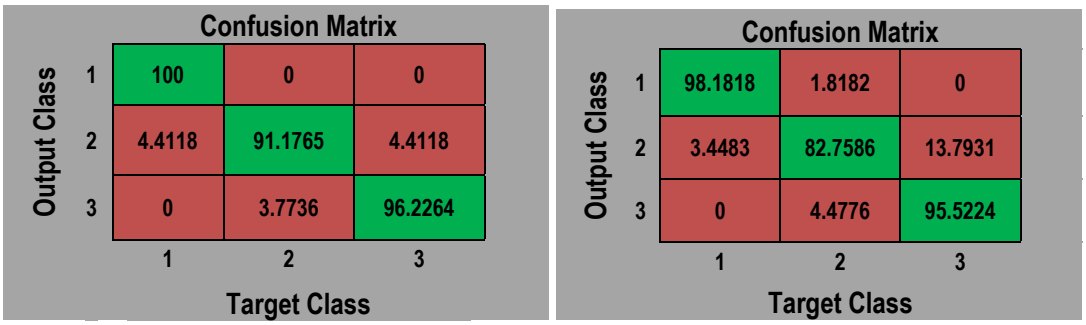

Figure 6.20: Confusion matrices when the observations per leaf = 36 for **(a)** training dataset; **(b)** test dataset

6.5.2 Decision Tree-Based Classifier for Test System-2

The same procedure used in subsection 6.5.1 for Test System-1 was followed in the design of the decision tree-based classifier for Test System-2. The total dataset generated was randomly partitioned into two parts. 70% of the dataset was used as the LS and 30% as the TS. Using the observations from extensive real-time

simulations, the system's operating states were classified using the real-time voltage stability margin and the voltage p.u. at the critical buses into:

$$\text{Stable: } if\ \left\{\left(RVSA_{Ifd} \geq \eta_{Alt}\right) AND\left(Load\ bus_{crit}\ V\ p.u. \geq 0.9\right)\right\} \quad (6.5)$$

$$\text{Alert: } if\ \left\{\left(RVSA_{Ifd} \leq \eta_{Alt}\right) AND\left(Load\ bus_{crit}\ V\ p.u. \geq 0.9\right)\right\} \quad (6.6)$$

$$\text{Unstable: } if\ NOT\ (Stable\ OR\ Alert) \quad (6.7)$$

where η_{Alt} is the threshold for the generator-derived field current-based real-time voltage stability assessment index $\left(RVSA_{Ifd}\right)$ and it was chosen as 25% for this test system based on observations obtained from the simulations.

The input attribute-outcome pairs used for the training of the DT-classifier include 44 input-attributes comprising of the generator variables (real power, reactive power, terminal voltage, field current, and stator current), voltage magnitudes at the critical buses, voltage phase angles, and phase angle differences. The outcome is the system state ('Stable', 'Alert', or 'Unstable').

The MATLAB function used in training the DT-classifier is the *ClassificationTree.fit*. The optimal leaf size to use was obtained to be about 28 observations per leaf. The predictive attributes obtained for the tree grown using the optimal leaf size are ***#12*** (generator G2 I_{fd}), ***#39*** (bus-5 voltage phasor), ***#40*** (bus-13 voltage phasor), ***#42*** (bus-15 voltage phasor) respectively.

The confusion matrices obtained for the training and test datasets are as shown in Figure 6.21. The confusion matrices given in Figure 6.21a show that the classifier has a predictive accuracy greater than 90% for the 'Stable' and 'Unstable' states, for the training dataset, and an accuracy greater than 90% for the 'Stable' and 'Alert' states for the test dataset.

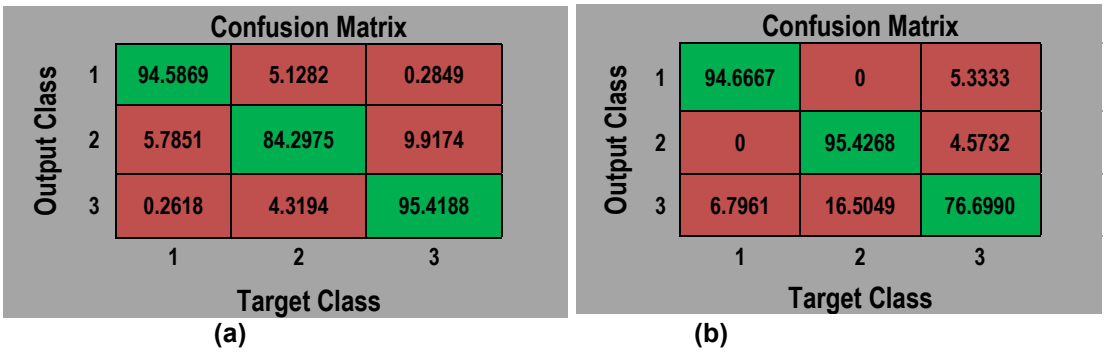

Figure 6.21: Confusion matrices when the observations per leaf = 28 for **(a)** training dataset; **(b)** test dataset

6.5.3 Ensembles-Based Classifiers for Test System-1

Ensemble of Decision Trees (EDTs) methods based on the Bagging (TreeBagger) and Boosting (AdaBoostM2) methods were used in growing the learners for classifying the system's operating state.

The procedure followed in creating the ensembles are as follows:

- Input the training dataset.
- Create a $n \times d$ matrix of predictors with n observations and d input attributes (predictors).
- Create a vector of response outcomes $\mathbf{Y}$.
- Select the ensemble method to use.
- Choose the number of ensemble members.
- Grow weak learners.
- Create the ensemble of the weak learners.

The classification task involves multiple classes ('Stable', 'Alert', and 'Unstable'). The weak learners are grown using decision trees. However, before creating the ensembles, an exploratory experimentation was carried out to estimate the optimal leaf size, the number of trees, and the selection of the most important features (input attribute predictors). A data-driven approach was used in the determination of the parameters for these models.

Figure 6.22 shows the plots for the trees grown using various leaf sizes of 1, 5, 10, 20, 50, and 100. The plot with the lowest Mean Squared error (MSE) of the training outputs and the obtained targets gives the optimal leaf size. This equals 1 in this case. Therefore, 1 was used as the leaf size for growing the decision trees in the ensembles.

The importance of the features in the dataset can be estimated by carrying out permutations for each feature across the observations in the dataset, and the value of the MSE after the permutation. This is obtained by using the increase in the average MSE from the trees for each variable. The most important variable has the highest value from this computation. Figure 6.23 shows the result obtained for the 10-bus multi-machine test system.

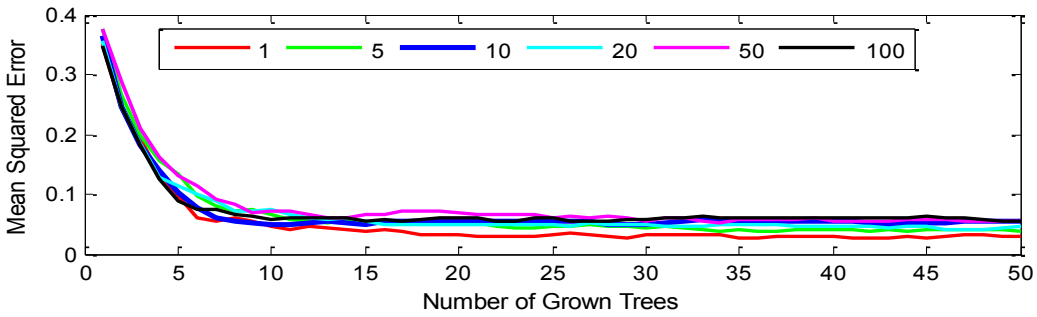

Figure 6.22: **The determination of the optimal leaf size for the classification task**

From Figure 6.23, if a 50% cut-off is used, the most important features include the feature ***#5*** (angle difference between buses -7 and -8), feature ***#12*** (generator G3 field current), feature ***#13*** (generator G2 reactive power), feature ***#15*** (generator G2 stator current), feature ***#19*** (bus-7 voltage phasor), feature ***#20*** (bus-8 voltage phasor), feature ***#21*** (bus-10 voltage phasor), feature ***#22*** (bus-11 voltage phasor).

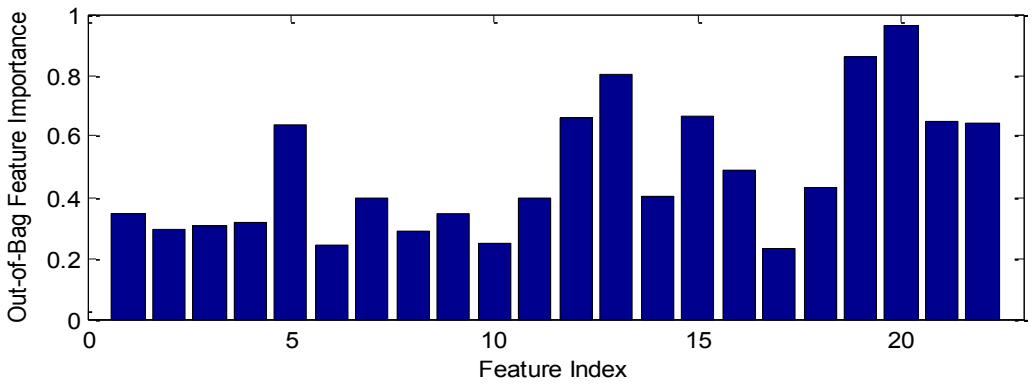

Figure 6.23: **Out of Bag (OOB) feature importance using the TreeBagger method**

Figure 6.24 shows the plot obtained for ensembles grown with different number of feature attributes. The plot in red was obtained using the full set of the feature attributes, while the plot in blue was obtained using the features selected by the TreeBagger method.

Results showed that growing an ensemble of 50 trees gave the same accuracy obtained using 100 trees. A MSE of 0.02183 was obtained when the full set of feature attributes was used, while a MSE of 0.03175 was obtained with the reduced feature attributes from the TreeBagger method (shown in Figure 6.23) was used. Similarly, Figure 6.25 shows the visualization of the various classes within the dataset. The classification errors for the TreeBagger method obtained for the independent holdout testing, cross-validation, and out-of-bag performance analyses are shown in Figure 6.26.

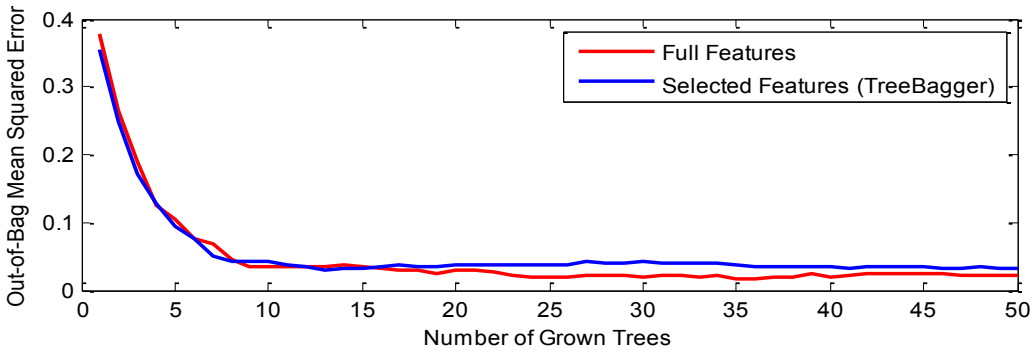

Figure 6.24: Plot showing the MSE for the full and selected features (using the TreeBagger method)

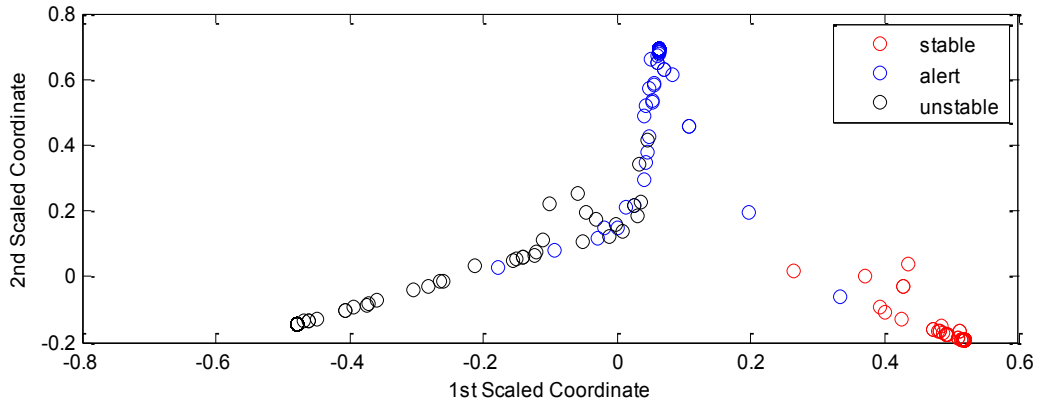

Figure 6.25: Visualization of the classes in the generated dataset

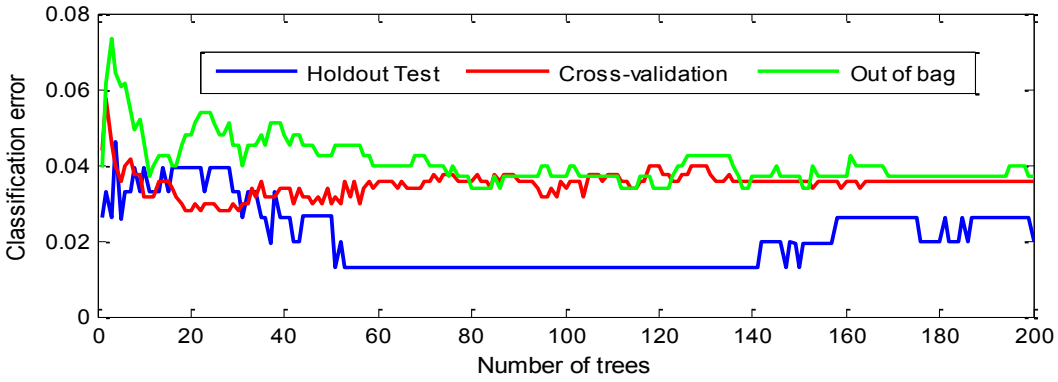

Figure 6.26: Plots showing the results for independent holdout testing, cross-validation testing, and OOB testing for 200 trees trained using the TreeBagger method

The confusion matrices obtained for the TreeBagger for the training and test sets are given in Figure 6.27 below. The confusion matrices show that the classifier has a predictive accuracy greater than 95% for all the system operating states possible for both the training and test datasets.

The AdaBoostM2 Boosting method suitable for multi-class classification was used. 70% of the dataset served as the TS for fitting (growing) the classifier, while 30% was used as an independent holdout dataset for testing the quality of the grown classifier.

The number of weak learners grown was 200. Figure 6.28 shows a plot of the classification error against the number of weak learners grown.

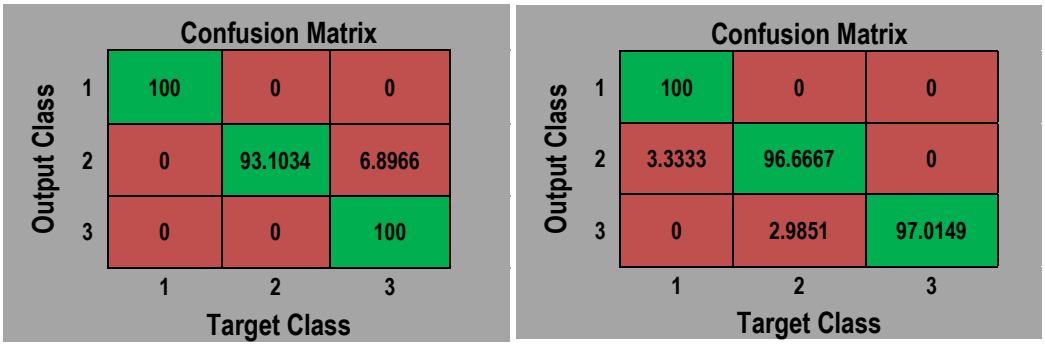

Figure 6.27: Confusion Matrices (TreeBagger method) for **(a)** training dataset; **(b)** test dataset

The lowest classification error of about 0.28% was obtained for about 135 trees during the growing of the EDT, while a classification error of 3.3% was obtained when the EDT was tested using the test dataset. This implies an accuracy rate of 96.7%.

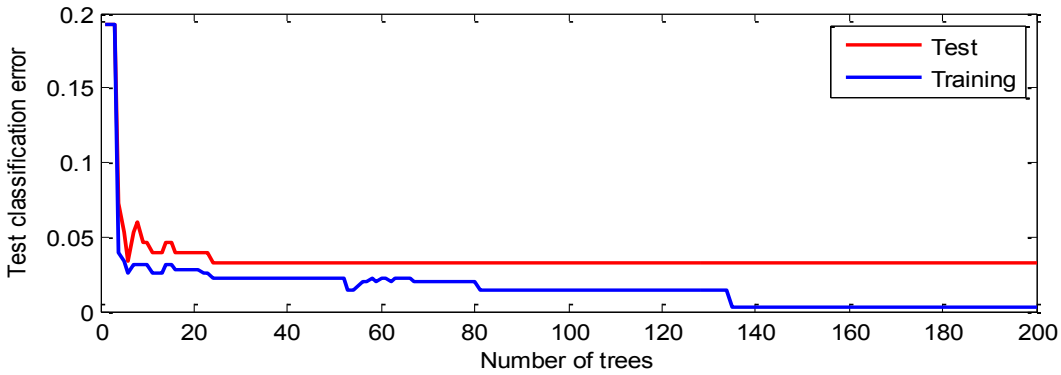

Figure 6.28: Test classification error obtained using AdaBoostM2 ensembles for the independent hold out sample

Figure 6.29 gives the confusion matrices for the respective classes as a percentage of the true class. The confusion matrices obtained using the AdaBoost Boosting method gave a predictive accuracy greater than 95% for all the system operating states for both the training and test datasets. Figure 6.30 shows plots of the classification error against the number of weak learners grown using the TreeBagger and AdaBoostM2 Boosting methods respectively.

The cross-validation carried out indicates that the minimum classification error obtained for the AdaBoostM2 method was about 3.3%, for about 94 trees when the ensemble is tested using the test dataset. The cross-validation classification error obtained for the TreeBagger method was about 2.9% for 20 trees.

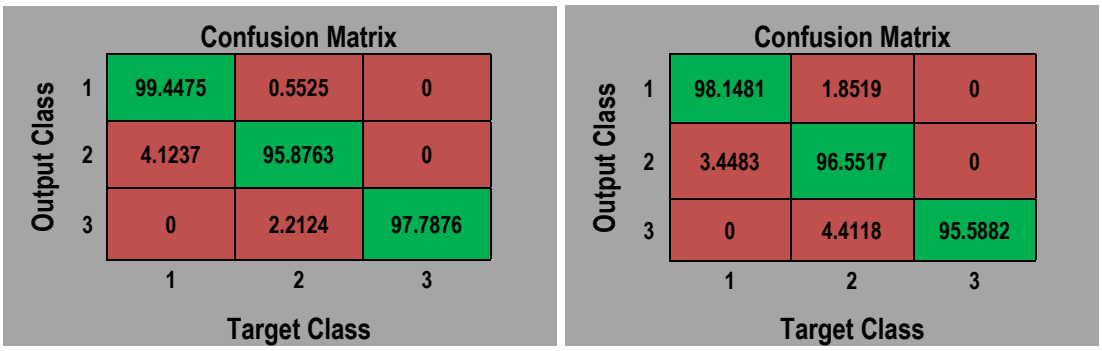

(a) (b)

Figure 6.29: Confusion Matrices (AdaBoost method) for **(a)** training dataset; **(b)** test dataset

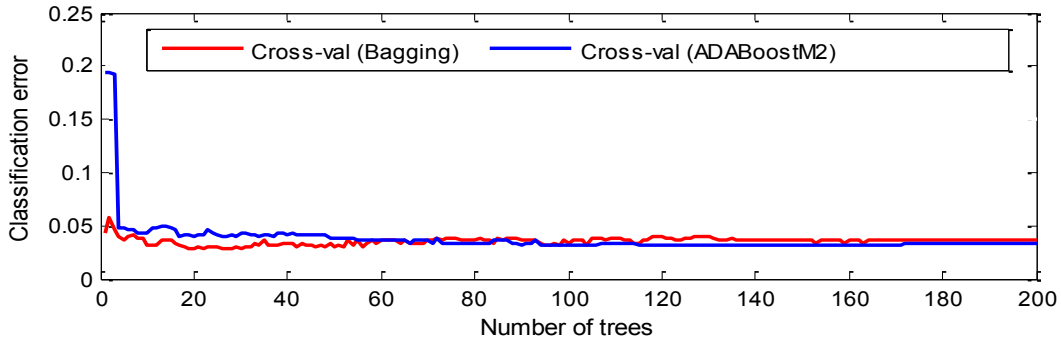

Figure 6.30: Classification error obtained using cross-validation technique for the TreeBagger method and the ADABoostM2-based ensembles

6.5.4 Ensembles-Based Classifier for Test System-2

An exploratory experimentation was carried out to estimate the optimal leaf size, the number of trees, and the selection of the most important feature attributes. Figure 6.31 shows the plots for the trees grown using various leaf sizes of 1, 5, 10, 20, 50, and 100. The plot with the lowest Mean Squared error (MSE) is the optimal leaf size, and was obtained as 5 in this case.

The importance of the features in the dataset can be estimated by carrying out permutations for each feature across the observations in the dataset, and the value of the MSE after the permutation. The result obtained when the feature selection technique is applied is as shown in Figure 6.32.

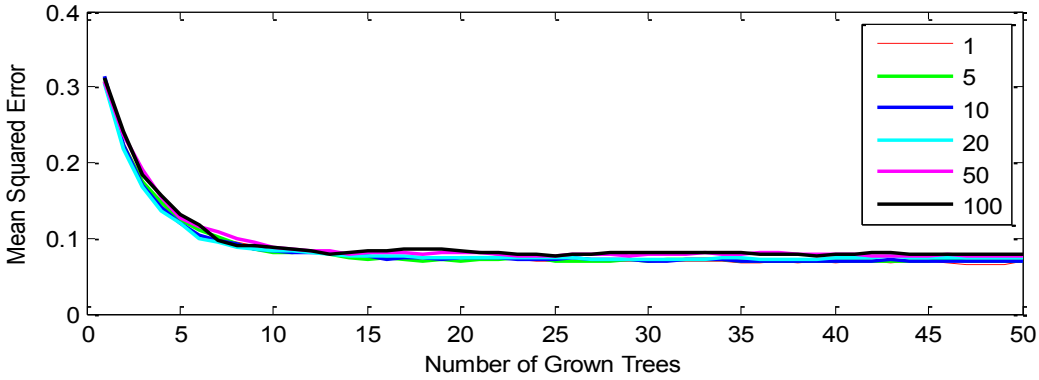

Figure 6.31: Optimal leaf size for classification task

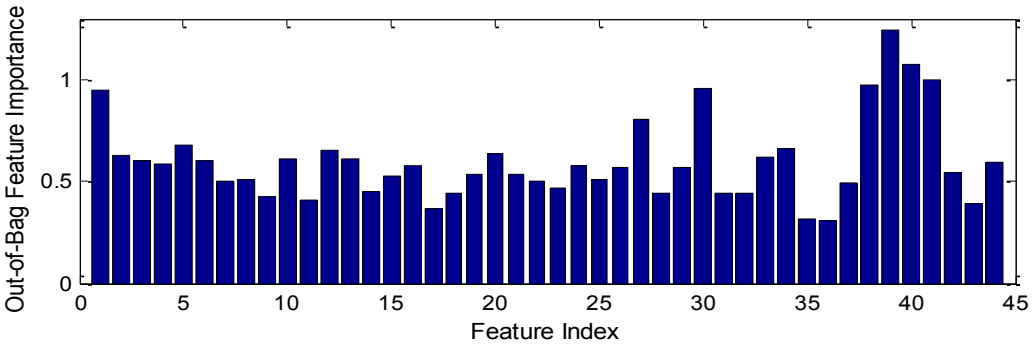

Figure 6.32: OOB-based feature importance using the TreeBagger method

From Figure 6.32, if a 60% cut-off is used, the most important features include the reactive power of the generators G1, G2, G3, G5, G6, G10, the generator field current I_{fd2}, I_{fd3}, I_{fd10}, the generator stator current I_{a8}, terminal voltages of generator G2, G5, G7, bus-4 voltage p.u., bus-5 voltage pu., bus-13 voltage p.u., bus-14 voltage p.u. Figure 6.33 shows a comparison of the TreeBagger ensemble grown using the full set of attributes and attributes selected above respectively. The utilization of the full features resulted in a MSE of 0.06398 when the number of trees grown is 50, while the obtained MSE was 0.0743 for the same number of trees for the reduced features.

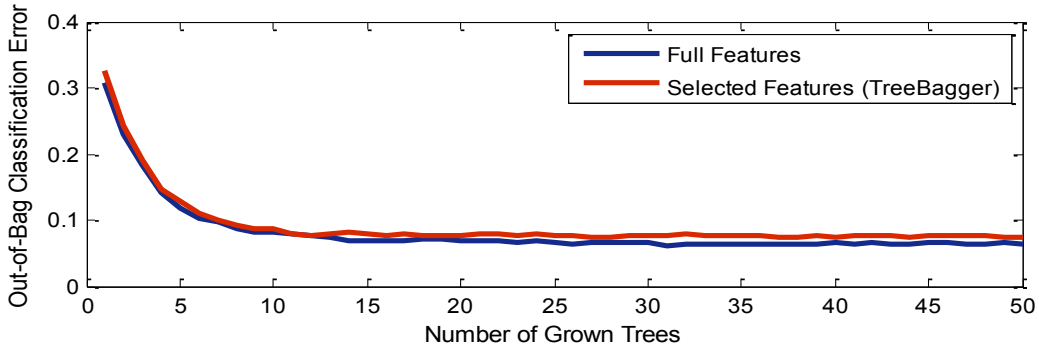

Figure 6.33: Plot showing the MSE obtained using the full attributes and the selected attributes obtained from the application of the TreeBagger method

Similarly, Figure 6.34 shows the visualization of the various output classes within the dataset. Figure 6.35 gives the classification errors obtained for the independent holdout, cross-validation, and out-of-bag performance analysis respectively for 200 trees trained by the TreeBagger method.

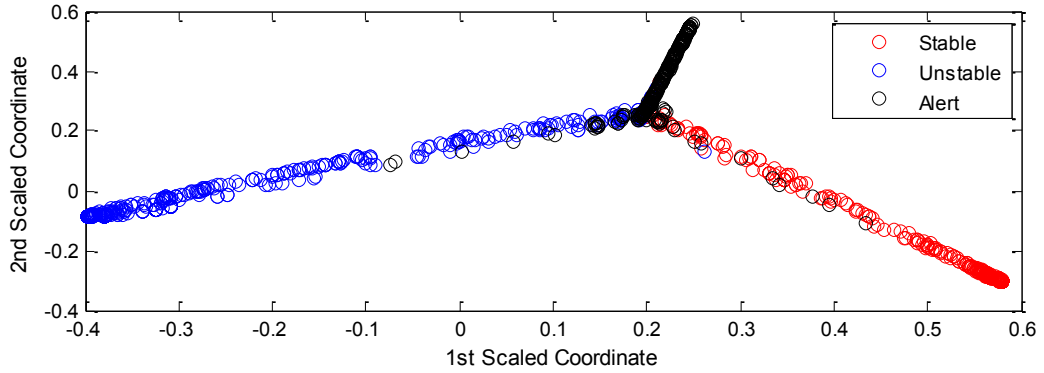

Figure 6.34: Visualization of the classes in the dataset

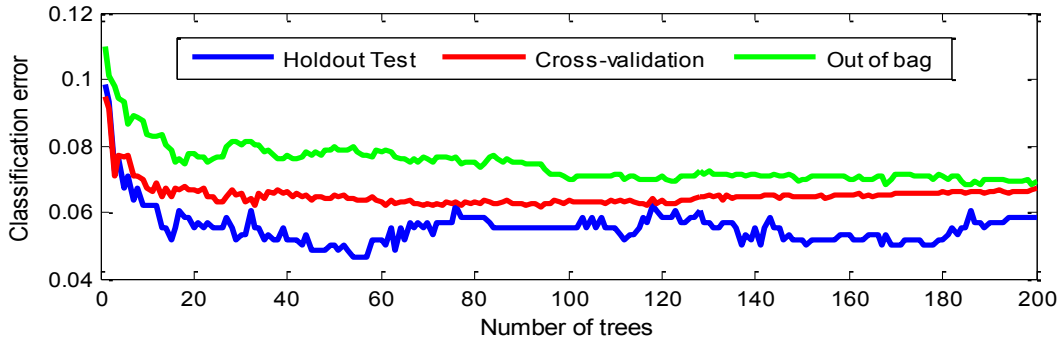

Figure 6.35: Plots showing the classification error results for independent holdout testing, cross-validation testing, and OOB testing for 200 trees trained using TreeBagger method

The confusion matrices obtaining for the TreeBagger method for the training and test set are given below. The confusion matrices given in Figure 6.36 show that the classifier has a predictive accuracy greater than 95% for all the system states possible for both the training and test datasets respectively.

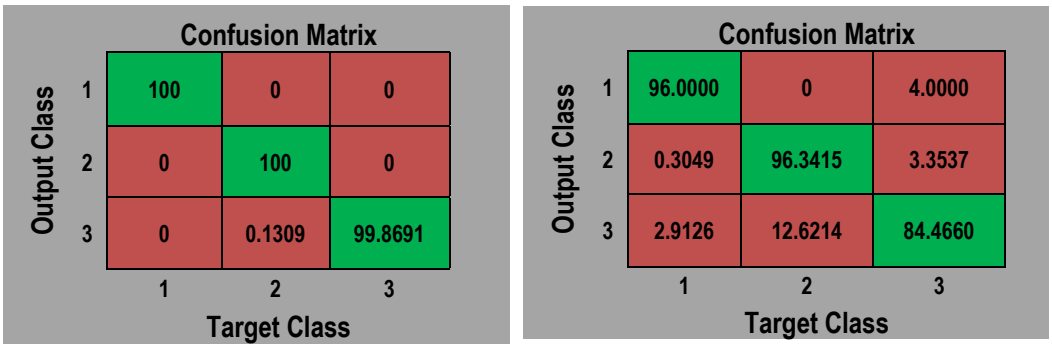

(a) (b)

Figure 6.36: Confusion Matrices (TreeBagger method) for (a) training; (b) testing

The Boosting method for a multi-class classification was used. 70% of the dataset was used in fitting (growing) the classifier, while 30% was used as an independent holdout dataset for testing the quality of the grown classifier. The number of weak learners grown was 200. Figure 6.37 shows a plot of the classification error against the number of weak learners grown. Figure 6.38 gives the confusion matrices for the respective classes as a percentage of the true class.

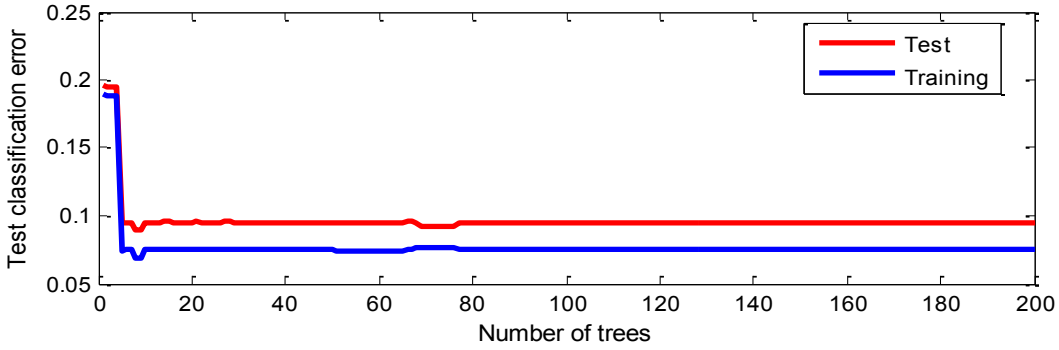

Figure 6.37: Classification error obtained using AdaBoostM2 ensembles for the independent hold out sample

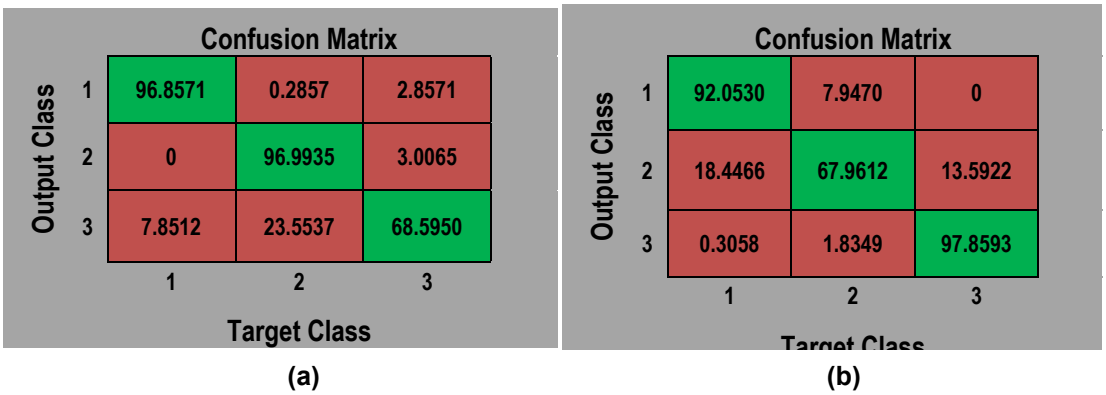

Figure 6.38: Confusion Matrices (AdaBoost method) for **(a)** training; **(b)** testing

Figure 6.39 shows plots of the classification error against the number of weak learners grown using the TreeBagger and AdaBoostM2 Boosting methods respectively. The cross-validation carried out shows that the minimum classification error obtained for AdaBoostM2 Boosting method was about 3.3%, obtained for about 94 trees when the ensemble is tested with the holdout test dataset. The cross-validation classification error obtained for the TreeBagger method was about 2.9% for about 20 trees.

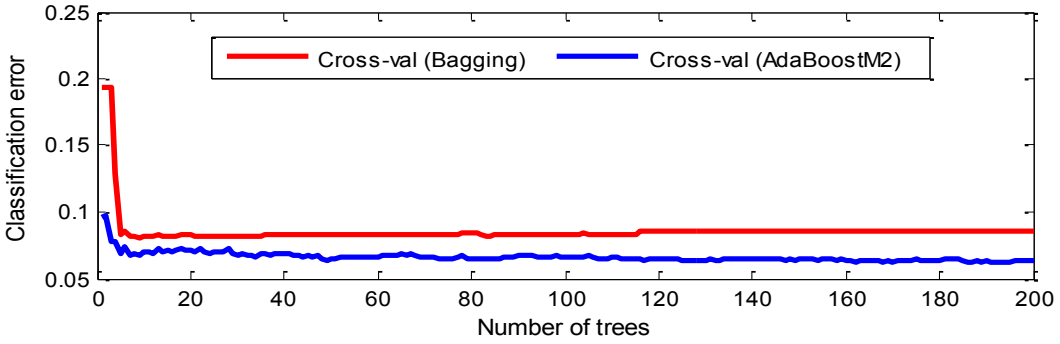

Figure 6.39: Classification error obtained using cross-validation technique for the TreeBagger method and AdaBoostM2 ensembles

6.5.5 Analyses of the Required Computational Resources

The computational resources required by the three methods used in growing the DT-classifier and the ensembles (Boosting and Bagging) are analysed and presented. The three analyses carried out include:

- Computation time
- Memory usage
- CPU usage

Figure 6.40 shows the plots for the memory and CPU usages for the TreeBagger ensemble method. Tables 6.8-6.9 summarize the computational resources used for the training and testing phases of the DT-classifier, the Treebagger, and the AdaBoostM2 ensemble methods respectively.

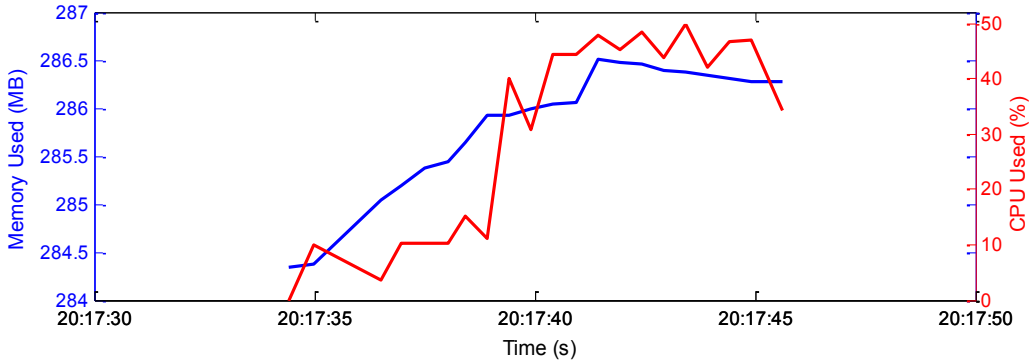

Figure 6.40: Memory utilization and CPU Usage for the TreeBagger method for Test System-1

Table 6.8: Memory, computational speed (CPU), and computational time for training classifiers

Decision Tree Method	Training Time (s)	Mean Memory Usage (MB)	Mean CPU Usage (%)	Max Memory Usage (MB)	Max CPU Usage (%)
DT-classifier	0.42	246.18	8.78	246.83	10.52
TreeBagger	11.88	285.85	39.31	286.51	49.92
AdaBoostM2	9.81	259.89	34.29	260.20	51.58

Table 6.9: Memory, computational speed (CPU), and computational time for testing classifiers using the holdout test dataset

Decision Tree Method	Prediction Time (s)	Mean Memory Usage (MB)	Mean CPU Usage (%)	Max Memory Usage (MB)	Max CPU Usage (%)
DT-classifier	0.40	283.71	6.96	283.80	13.93
TreeBagger	3.37	258.40	29.67	258.63	51.65
AdaBoostM2	3.04	262.32	34.86	262.43	45.42

For the New England 39-bus test system, Tables 6.10-6.11 summarize the computational resources used for the training and testing phases of the DT-classifier, TreeBagger, and AdaBoostM2 ensemble methods respectively. Figure 6.41 shows the plots for the memory and CPU usages for the TreeBagger ensemble method.

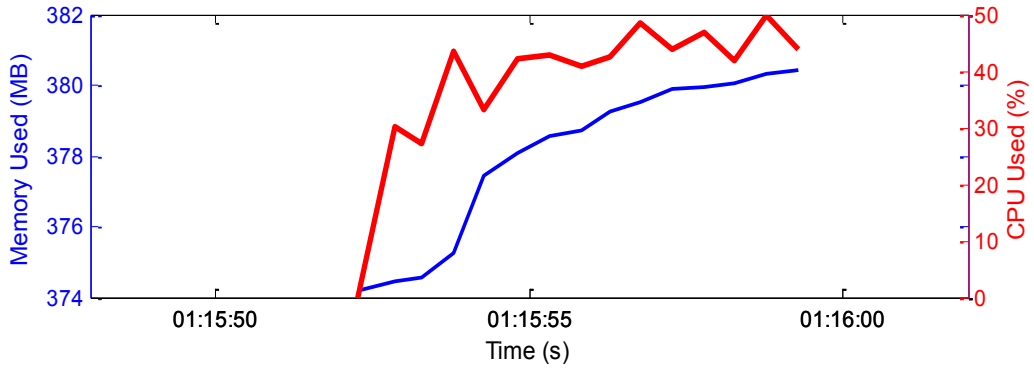

Figure 6.41: Memory utilization and CPU Usage for the TreeBagger method for Test System-2

Table 6.10: Memory, computational speed (CPU), computational time for training classifiers

Decision Tree	Training Time (s)	Mean Memory Usage (MB)	Mean CPU Usage (%)	Max Memory Usage (MB)	Max CPU Usage (%)
DT-classifier	2.05	382.03	22.27	383.97	40.71
TreeBagger	7.79	378.04	38.46	380.42	49.71
AdaBoostM2	8.63	391.17	35.54	391.49	51.99

Table 6.11: Memory, computational speed (CPU), computational time for testing classifiers using the holdout test dataset

Decision Tree	Prediction Time (s)	Mean Memory Usage (MB)	Mean CPU Usage (%)	Max Memory Usage (MB)	Max CPU Usage (%)
DT-classifier	0.85	368.30	0.00	368.30	0.00
TreeBagger	1.66	384.02	26.29	384.21	41.33
AdaBoostM2	1.28	392.42	20.44	392.48	40.89

6.5.6 Discussion

Machine learning-based classification tree (DT-classifier) and ensembles of decision trees were applied to classify the system operating state into 'Stable', 'Alert', or 'Unstable'. The performance of the DT-classifiers was compared to that obtained using the TreeBagger and the ADABosstM2 ensembles methods respectively.

It was observed that the number of levels in the grown tree increased as the number of observations per leaf decreased. Also, the predictive accuracy of the grown tree improved as the number of observations decreased. However, leafy trees grown with fewer observations per leaf tend to overfit to the training dataset and are usually give poor results when tested with new datasets. The performance of the classifiers was evaluated using the confusion matrices, resubstitution errors, and cross-validation errors respectively. The classifier grown with the TreeBagger ensemble method was seen to give the best performance results, followed by that obtained from the ADABoostM2 ensemble method.

The computational resources required by the three methods used in growing the DT-classifier and ensembles are analysed with respect to computation time, memory usage, and CPU usage. From the results obtained, it was observed that the DT-classifier used the least amount of resources. Also, the training and response times of the DT-classifier were also the lowest. Although, the TreeBagger and the AdaBoostM2 ensemble methods gave better predictive performance compared to the grown DT-classifiers, the former are complex, difficult to interpret and implement in real-time applications such as voltage stability assessment. This is because these ensembles are grown using multiple DT-classifiers (weak learners). The interpretation and integration of such weak learners are tedious and cumbersome. Generally, all the trees grown using the three methods (DT-classifier, TreeBagger, and ADABoostM2 methods) gave acceptable performance.

6.6 Classifiers' Robustness to Missing Synchrophasor Measurements

6.6.1 Test System-1

Since synchrophasor measurements are time-series measurements, there is the probability that some synchrophasor measurements might arrive later than the maximum waiting time configured on the PDC. Typically, the PDC fills the missing data with zeroes. An investigation was carried out on the robustness of the various machine learning methods to missing synchrophasor measurements. Figures 6.42-6.43 show the plots of the classification errors obtained using the TreeBagger and AdaBoostM2 methods for 10% to 50% missing PMU measurements during the training of the classifiers.

From Figures 6.42-6.43, it can be seen that the predictive accuracy of the trained ensembles depreciates as the percentage missing measurements increases. Results obtained also showed that the ensembles grown using the TreeBagger method were more robust to missing measurements than the ensembles grown using the AdaBoostM2 method.

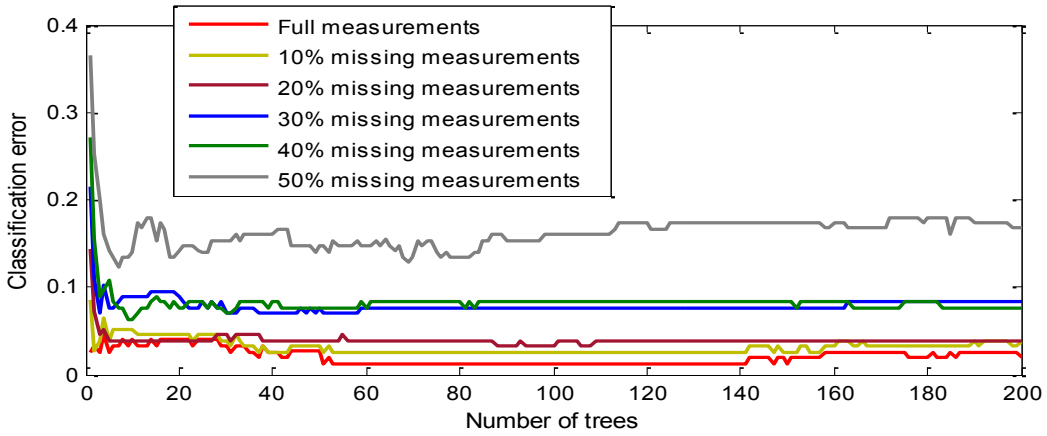

Figure 6.42: Classification error for the TreeBagger method (without surrogate splits) with missing PMU measurements

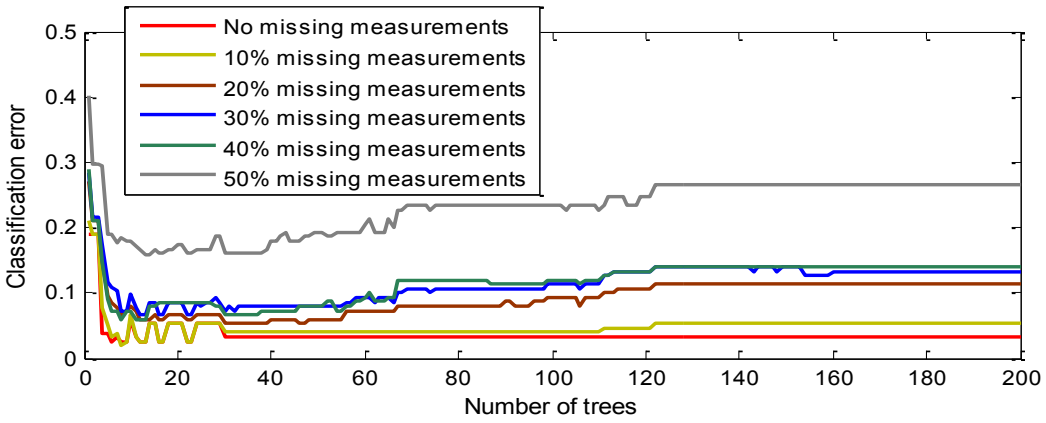

Figure 6.43: Classification error for the AdaBoost method (without surrogate splits) with missing PMU measurements

Ensembles that are immune to missing measurements can be grown using the surrogate splits technique. This approach selects alternatives to the optimal split at a particular node of a decision tree. The optimal split is usually determined by using the split (impurity) criterion during the growing of the decision tree. The surrogate split uses a correlated predictor variable and the split criterion that best mimics the split of the training data hitherto obtained by the optimal split. The surrogates feature attributes are ranked according to their predictive measure of association in descending order. The first surrogate is used when the optimal split feature attribute for a particular node is missing in the measurements.

If both the optimal split and surrogate splits feature attributes are missing, the second surrogate splits feature attribute obtained based on the predictive measure of association ranking is used. The classification errors obtained in Figures 6.44-6.45 are quite low compared to that obtained in Figures 5.42-6.43. This shows that the EDTs grown using the surrogate splits are more robust to missing measurements.

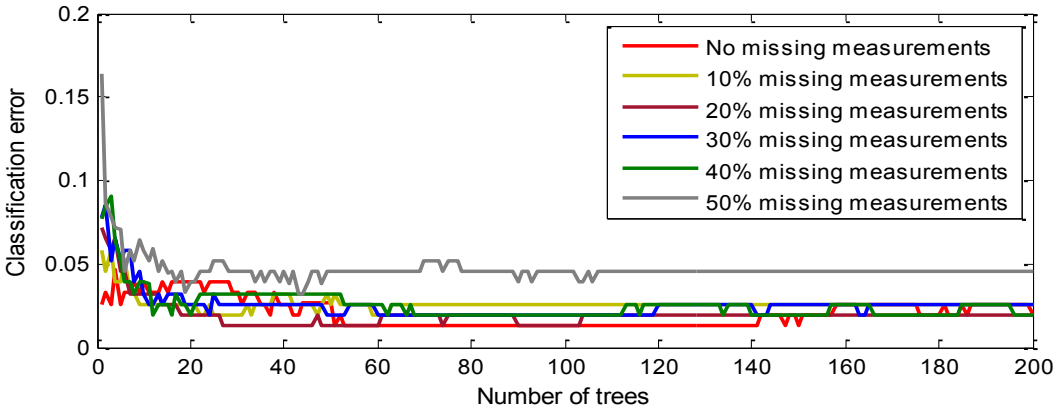

Figure 6.44: **Classification error for the TreeBagger method (with surrogate splits) with missing PMU measurements**

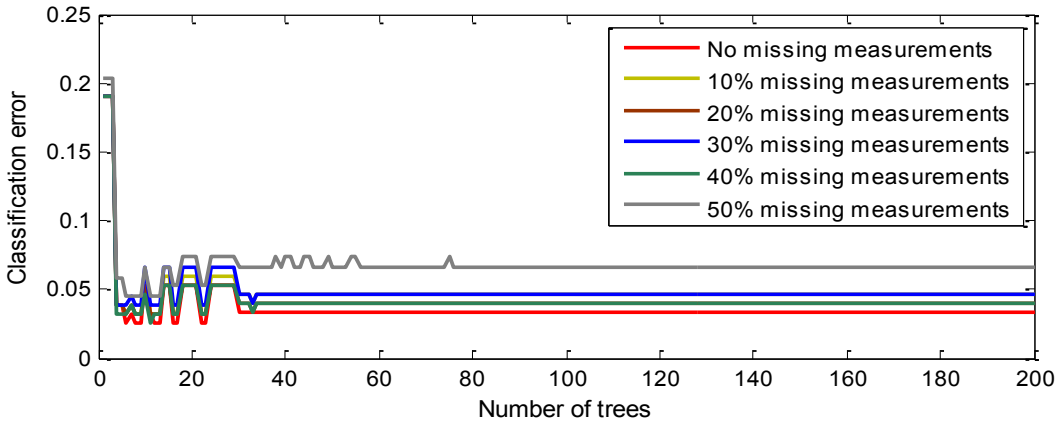

Figure 6.45: **Classification error for the AdaBoost method (with surrogate splits) with missing PMU measurements**

Figures 6.44-6.45 show that using the surrogate splits with the TreeBagger method and the AdaBoostM2 methods produced ensembles that were more robust to missing measurements compared to what was obtained without the surrogate splits (Figures 6.42-6.43). However, the TreeBagger method produced the best results in terms of the robustness to the missing measurements when surrogate splits were used.

The confusion matrices obtained for 10% and 20% missing synchrophasor measurements for the default DT classifier, TreeBagger ensembles, and AdaBoostM2 Boosting ensembles are given in Figures 6.46-6.48 respectively.

In a typical power system, the misclassification of an 'Unstable' state as 'Stable' would have severe and devastating consequences than the misclassification of a

'Stable' state as 'Alert' or 'Unstable'. Therefore, the failure to identify an 'Unstable' state was used as the performance criterion in the validation of the classifiers' robustness to missing synchrophasor measurements.

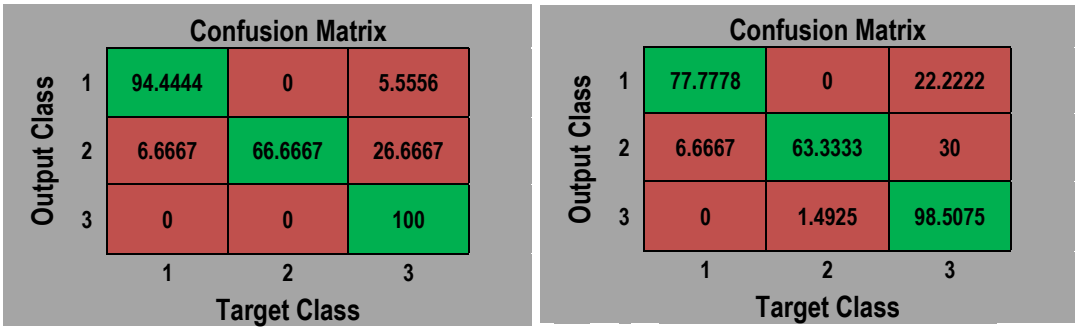

Figure 6.46: Confusion matrices for the training of the DT-classifier for **(a)** 10% missing measurements; **(b)** 20% missing measurements

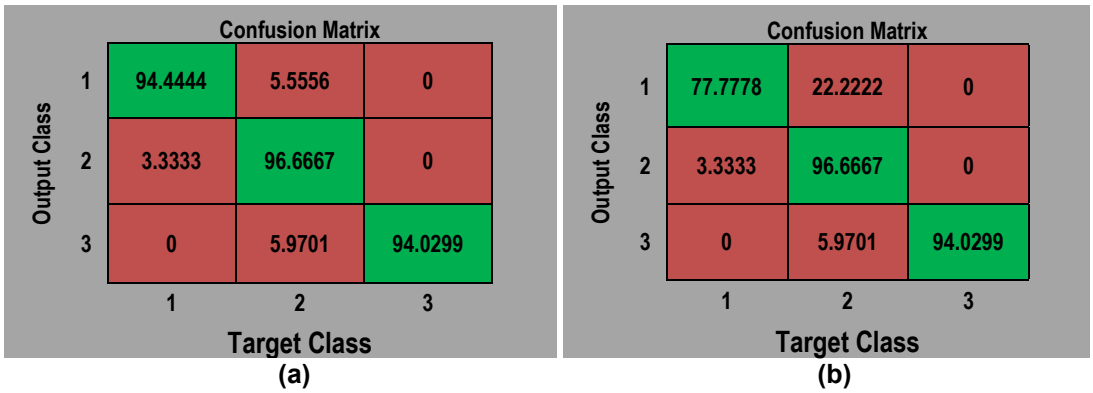

Figure 6.47: Confusion matrix for the training of the AdaBoost Boosting classifier for **(a)** 10% missing measurements; **(b)** 20% missing measurements

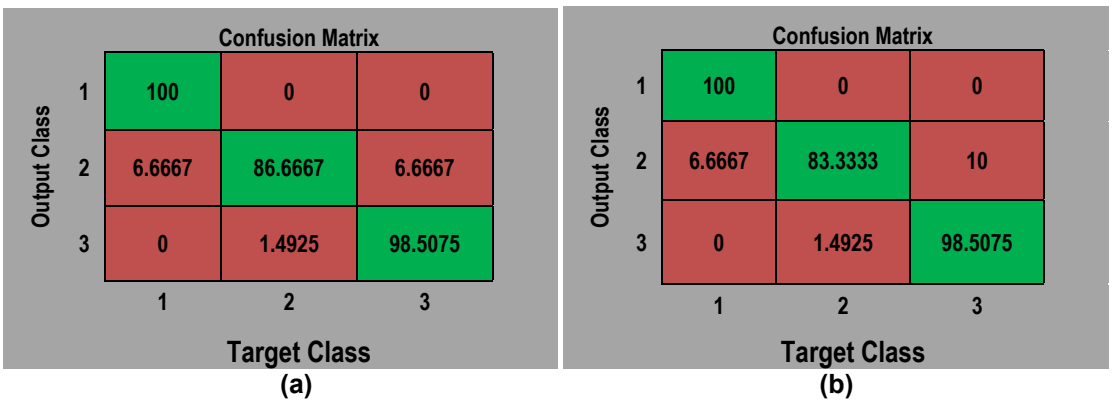

Figure 6.48: Confusion matrix for the training of the TreeBagger classifier for (a) 10% missing measurements; (b) 20% missing measurements

From Figures 6.46-6.48 it can be seen that all the classifiers grown demonstrated acceptable robustness to missing measurements. This is because the prediction of the 'Unstable' state did not depreciate as a result of missing measurements. The TreeBagger classifier gave the best performance for all the system states ('Stable',

'Alert', and 'Unstable) when tested with the independent dataset with missing measurements.

6.6.2 Test System-2

Similar investigations to that carried out for Test System-1 in subsection 6.6.1 were carried out for Test System-2 to investigate the robustness of the various training and testing methods to missing synchrophasor measurements. Figures 6.49-6.50 show the plots obtained using the TreeBagger and AdaBoost methods for 10% to 50% missing measurements respectively.

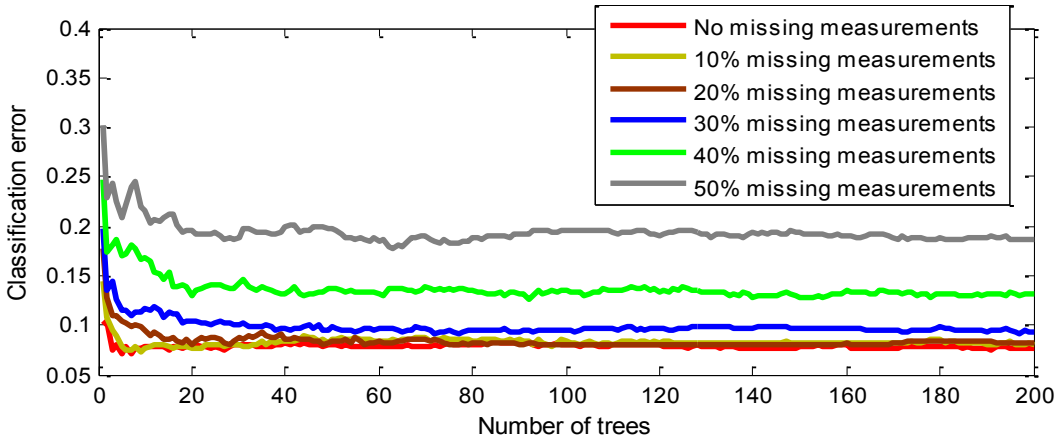

Figure 6.49: **Classification error for the TreeBagger (without surrogate splits) with missing PMU measurements**

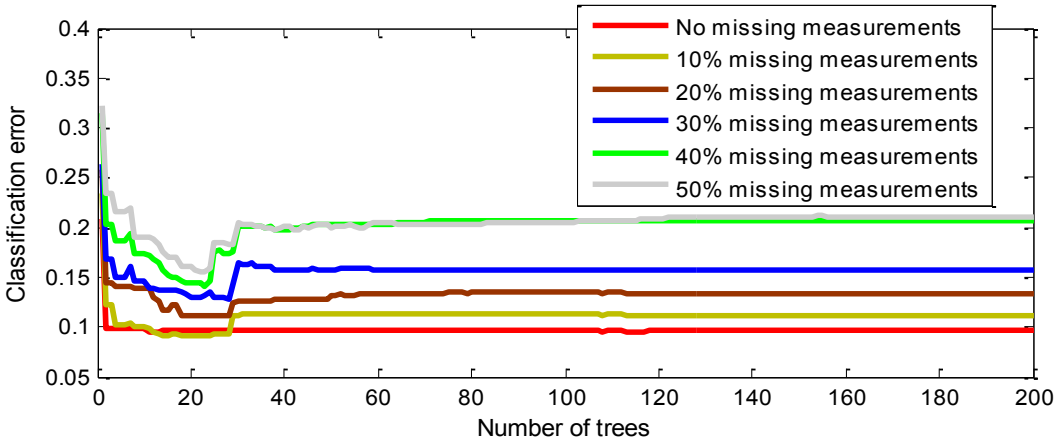

Figure 6.50: **Classification error for the AdaBoost (without surrogate splits) with missing PMU measurements**

From Figures 6.49-6.50, it can be seen that the predictive accuracy of the trained ensembles depreciates as the percentage missing measurements increases. The EDTs grown using the Boosting (ADABoostM2) method had the worst performance compared to the EDT grown using the TreeBagger method.

Figures 6.51-6.52 show that using the surrogate splits technique with the TreeBagger method and the AdaBoostM2 methods produced ensembles that were more robust to missing measurements compared to what was obtained without surrogate splits (Figures 6.49-6.50). However, the TreeBagger method produced the best results in terms of robustness to missing measurements with/without surrogate splits.

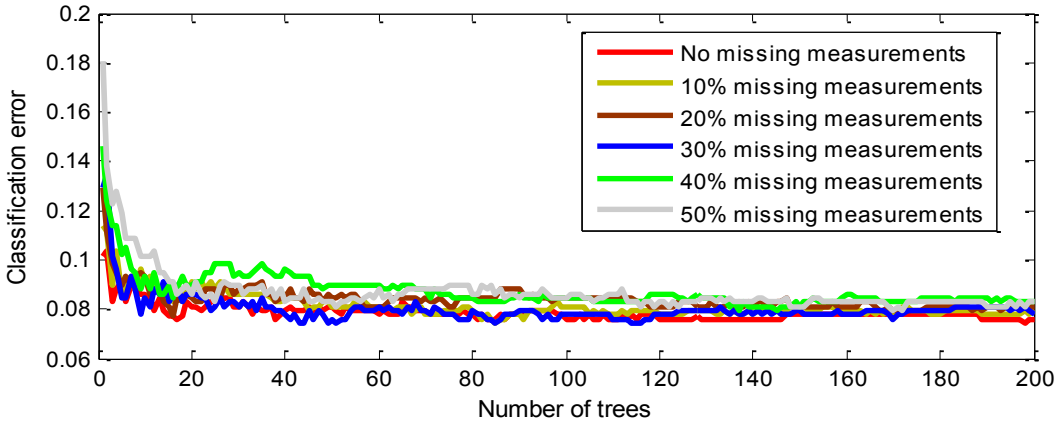

Figure 6.51: **Classification error for the TreeBagger (with surrogate splits) with missing PMU measurements**

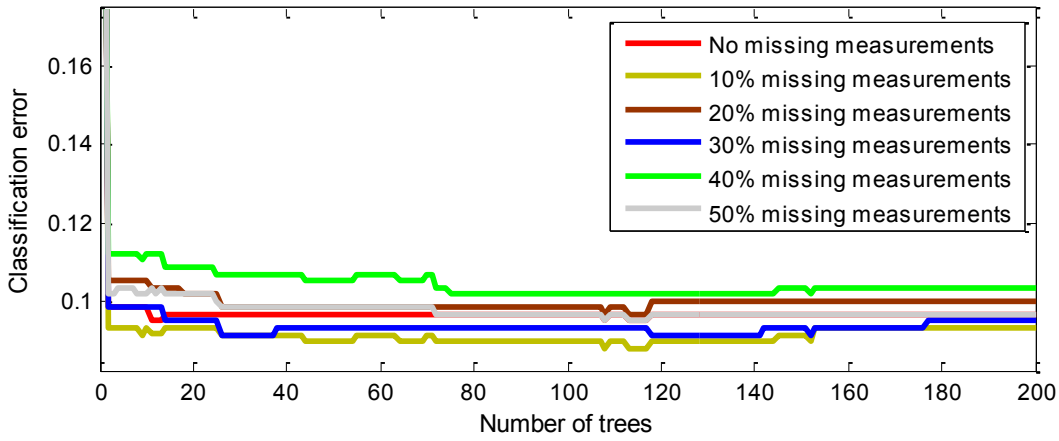

Figure 6.52: **AdaBoost (with surrogate splits) with missing PMU measurements**

The confusion matrices obtained for 10% and 20% missing synchrophasor measurements for the default DT, TreeBagger-based ensembles, and AdaBoostM2-based ensembles are given in Figures 6.53-6.55 respectively.

From the results obtained for Test System-1 and Test System-2, it can be seen that all the classifiers grown demonstrated acceptable robustness to missing measurements. This is because the prediction of the 'Unstable' state did not depreciate as a result of missing measurement. The TreeBagger classifier gave the best performance for all the system states ('Stable', 'Alert', and 'Unstable) when tested with the independent dataset with missing measurements. The results for the investigations on the impact of missing synchrophasor measurements and the use of

the surrogate splits technique for the regression predictors of the system's margin to voltage collapse are not presented here for lack of space. These results are documented in (Adewole and Tzoneva, 2016b).

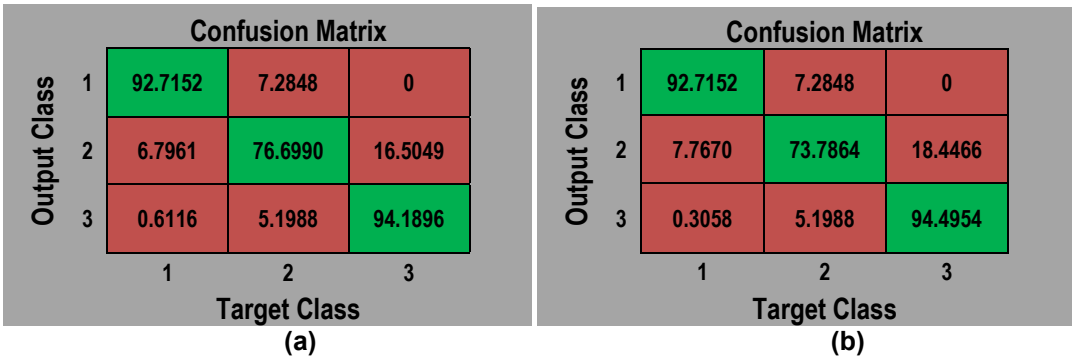

Figure 6.53: Confusion matrix for the training of the DT-classifier with surrogate split for **(a)** 10% missing measurements; **(b)** 20% missing measurements

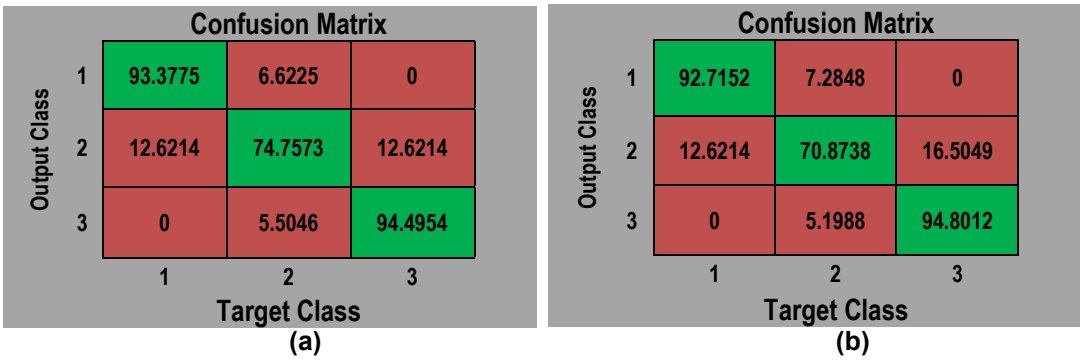

Figure 6.54: Confusion matrix for the training of the AdaBoost Boosting classifier with surrogate split for **(a)** 10% missing measurements; **(b)** 20% missing measurements

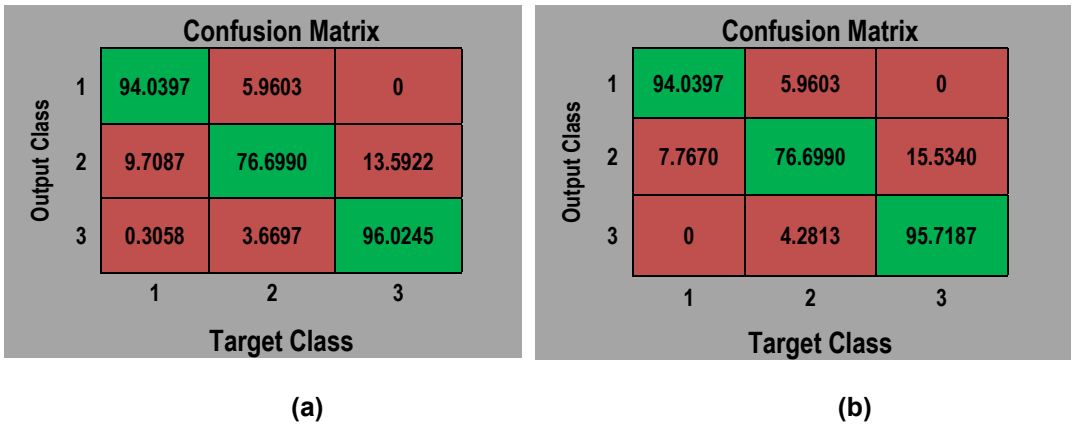

Figure 6.55: Confusion matrix for the training of the TreeBagger classifier with surrogate splits for **(a)** 10% missing measurements; **(b)** 20% missing measurements

6.7 Chapter Summary

This Chapter presented the results for the measurement-based power system clustering for the identification of system's load buses with similar voltage collapse problem and the cluster of synchronous generators providing voltage support to these load buses.

Machine learning-based classification tree and ensembles of trees were applied for voltage stability assessment. The ensembles of decision trees were grown using the TreeBagger and Boosting methods respectively. A feature selection method using the TreeBagger method was applied in the identification of the most important input attributes based on the out-of-bag error. The performance requirement with respect to computation speed, memory and CPU resources was also presented. The impact of missing PMU measurements on the algorithm, and the mitigation of this by using the surrogate splits technique was carried out.

Chapter Seven presents the results obtained for the real-time testing and validation of the voltage stability assessment and wide area protection/control algorithms and methods. Two response-based centralised System Integrity Protection Scheme (SIPSs) algorithms based on transformer under-load tap changer control (ULTC-SIPS) and undervoltage load shedding (UVLS-SIPS) are considered. The algorithms are designed to be adaptive to the prevailing level of disturbance in the system using synchrophasor measurements from actual PMUs. Also, the control signals used in the implementation of the ULTC-SIPS and UVLS-SIPS algorithms are based on IEC 61850-8-1 GOOSE messages.

CHAPTER SEVEN

REAL-TIME VOLTAGE STABILITY ASSESSMENT AND WIDE AREA PROTECTION/CONTROL

7.1 Introduction

The real-time voltage stability assessment and wide area protection/control algorithms and methods proposed in the preceding chapters of this thesis were implemented using the developed 'proof-of-concept' lab-scale WAMPAC testbed for real-time testing and validation. The RVSA index presented in Chapter Four was applied as one of the feature attributes to the Decision Tree (DT) and Ensembles of DT-classifiers (EDTs) grown in Chapter Five. The DT-classifier then predicts the system operating state, while the DT-regressor predicts the system's margin to voltage collapse. The DT-classifier also serves as one of the inputs to the system monitoring element of the System Integrity Protection Schemes (SIPSs) proposed in this Chapter as countermeasures to mitigate the voltage instability problem.

Two synchrophasor-based SIPSs using transformer Under Load Tap Changer control (ULTC-SIPS) and Under Voltage Load Shedding (UVLS-SIPS) are presented in this Chapter. The ULTC-SIPS algorithm was designed to act first in an attempt to halt the system's descent into voltage collapse by preventing further transformer ULTC taps. If the ULTC-SIPS is unsuccessful, the UVLS-SIPS will be armed to initiate undervoltage load shedding. The formulation of how much load to shed and the distribution of the amount of load to shed are presented for an interconnected power system. Also, a least squares fitting algorithm is proposed for the online calculation of the amount of load to shed in real-time. The results for the real-time testing of the proposed voltage stability assessment and SIPS algorithms are presented and discussed hereafter.

7.2 Test System Modelling

Two test systems were modelled using the RSCAD software and are used for the real-time implementation of the methods and algorithms proposed in this thesis. The test systems include:

(a) 10-bus multi-machine equivalent test system; and

(b) New England 39-bus test system.

7.2.1 Description of Test System-1

The 10-bus multi-machine equivalent system made up of three generators supplying aggregated loads of about 6655 MW at load level-1 is denoted as Test System-1. The load area is located at the east end and it is heavily compensated by three shunt capacitor banks supplying reactive power. Generators G1 and G2 inject 5717 MW across five 200 km, 500 kV transmission lines. Figure 7.1 shows the 10-bus multi-machine study network with the location of the PMUs used (Kundur, 1994).

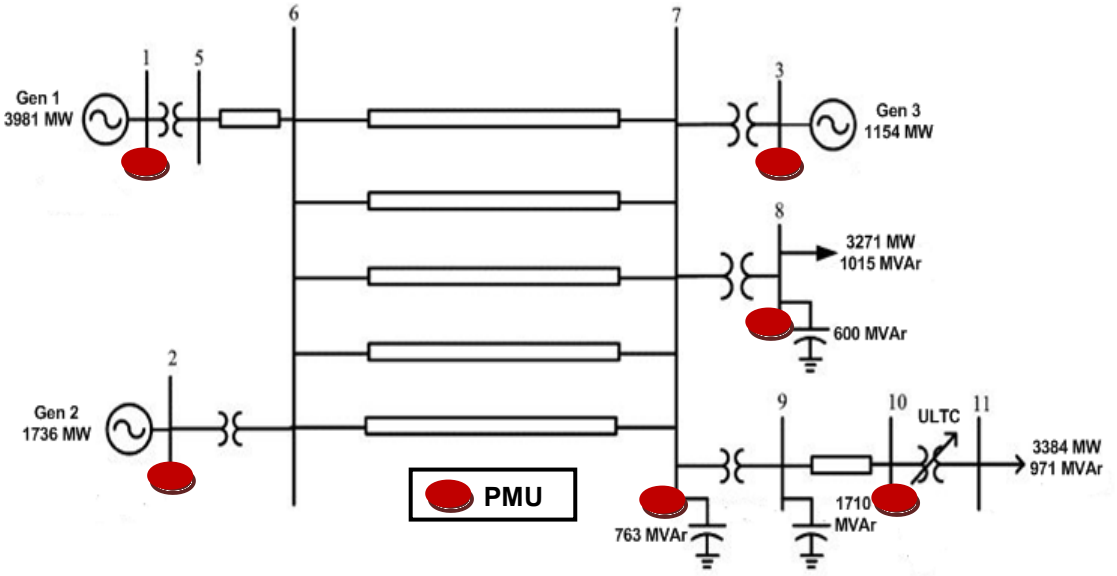

Figure 7.1: **10-bus multi-machine equivalent system showing the PMU locations**

A tap changer is used with the RSCAD 3-phase two-winding transformer component (*lf_rtds_sharc_sld_TRF3P2W*) located at bus-10. A transformer ULTC controller was built in the RSCAD software using the control components available in the RSCAD library. The transformer ULTC has a tap range of ± 16 steps, $5/8\,\%$ step size, and a $\pm 1\%$ dead band. It has a time delay of 30 s for the first tap operation and 5 s for subsequent taps. The initial tap position for load-level 2 is at position 16. The loads at buses-8 and -11 were defined in (Kundur, 1994) as constant power loads at bus-8, and 50% constant impedance and 50% constant current load at bus-11 respectively. The RSCAD Draft and the Runtime modules are shown in Appendix H.

7.2.2 Description of Test System-2

Test System-2 is the New England 39-bus benchmark model. It is made up of 10 synchronous generators, 39 buses, 12 transformers, 34 transmission lines, and 19 loads. The total system load is given as 6150 MW, while the total generated power is 6192 MW.

The synchronous generators are equipped with IEEE Type-1 excitation systems and governors. Figure 7.2 shows the single line diagram of the New England 39-bus test system. The parameters for the test system are given in (Pal, 1979).

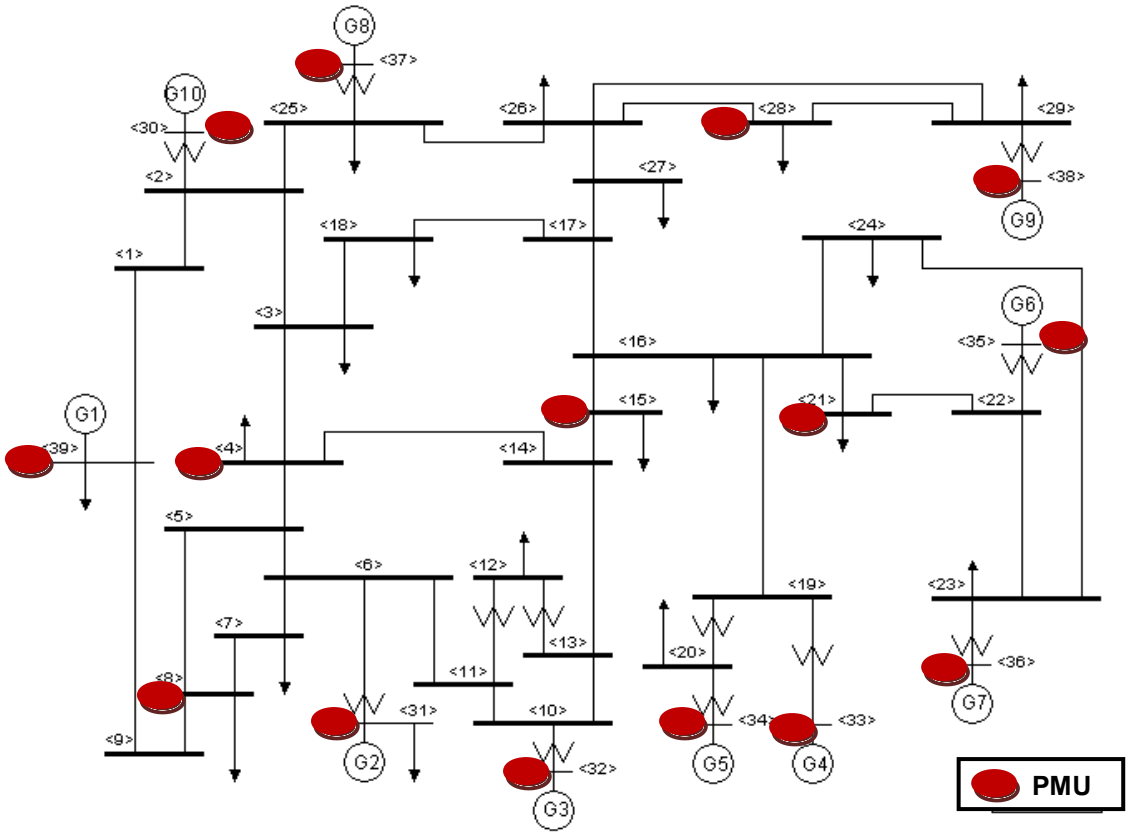

Figure 7.2: **New England 39-bus test system showing the PMU locations**

7.3 Real-Time Voltage Stability Assessment

7.3.1 Real-Time Voltage Stability Assessment for Test System-1

An exploratory experimentation using various load models was carried out to investigate the impact of various load types on voltage stability and its assessment in power systems.

The following two operating scenarios were considered:

- Line contingency, generator G3 OXL operation, and transformer ULTC action at bus-11.
- Line contingency, increased loading condition at bus-8, generator G3 OXL operation, and transformer ULTC action.

Polynomial load models comprising of 50% Constant Impedance and 50% Constant Current (Constant ZI) are used as the load composition at bus-11, while the load at bus-8 was modelled as a constant power load using a dynamic load component. After the initial voltage drop as a result of the line contingency, the transformer ULTC will tap after 30 s in an attempt to restore the bus voltage to its reference value.

Figure 7.3 shows the plots of the synchrophasor voltages (in p.u.) at buses-8 and -11 archived at the control centre PDC. As shown in Figure 7.3, the ULTC tap action resulted in an increase in the system's reactive power demand. This was supplied by the generators until the OXL at G3 reached its limit. Consequently, the distribution, sub-transmission, and transmission voltages began to drop. Further tap actions did not result in the restoration of the bus voltages (red plot) for the constant ZI load.

The above simulation was repeated for a 100% Constant Impedance (Constant Z) load at bus-11. From Figure 7.3 (blue plot), it can be seen that after the initial drop in bus voltages due to the transmission line outage, the bus voltages remained constant for the duration of the simulation. The above scenario was repeated for a 100% Constant Current (Constant I) load at bus-11 (black plot).

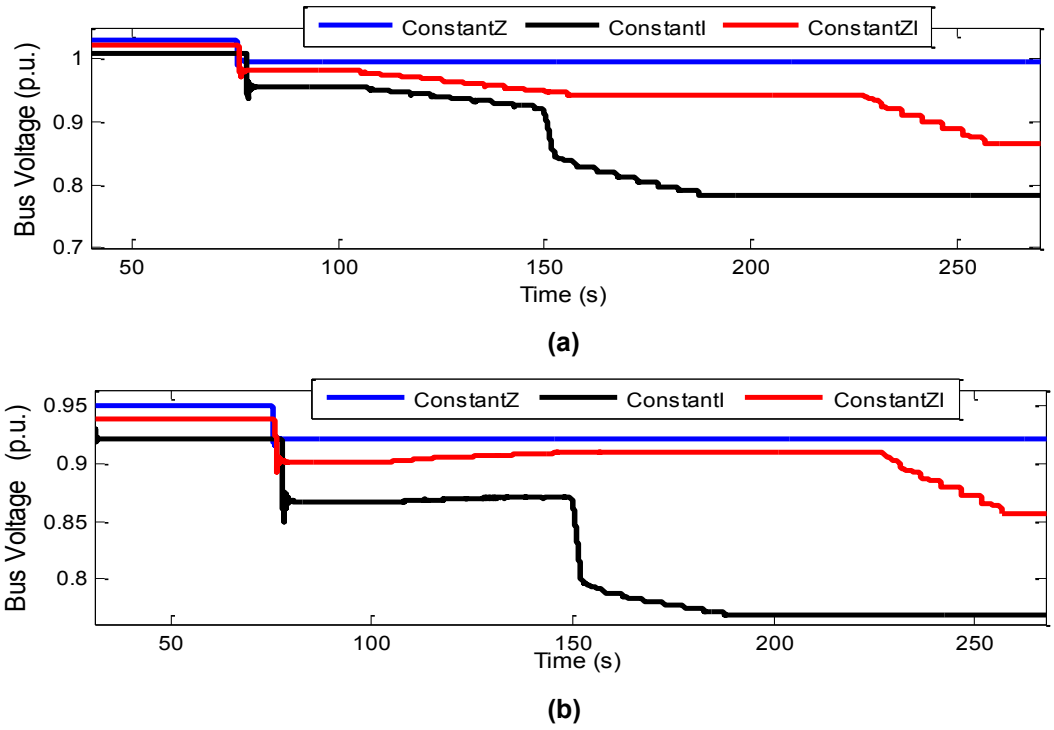

Figure 7.3: Load characteristics for line contingency scenario (a) Bus-8 voltage; and (b) Bus-11 voltage

The transformer ULTC was able to increase the voltage at bus-11 until the OXL at G3 operated. Afterwards, there was a steep drop in bus voltages and further ULTC tap caused the bus voltages to drop even more as shown in Figure 7.3 (black plot). It was observed that the Constant Z load model had a flat response (Figure 7.3) after the line contingency, and did not respond to the transformer tap changer actions unlike the Constant I and Constant ZI load models respectively. The Constant I load model had the lowest voltages. From Figure 7.3, it can be seen that for the Constant I load, the bus voltage dropped to about 0.87 p.u. after the line contingency. In systems with induction motor loads, this would have resulted to the stalling of the induction motors.

When motors stall, they draw up to 6 times their rated current as they attempt to restart (Taylor, 1994).

For the second operating scenario considered, a 5% load increase was carried out every 60 s at bus-8 using Equations (7.1)-(7.2). The load at bus-8 was modelled as a Constant Power (Constant PQ) industrial load using the dynamic load model in RSCAD Draft. The impact of this load increase and the effects of the transformer ULTC action and the OXL of generator G3 on the load at bus-11 are studied.

The load increase carried out in Test Systems 1 and 2 is given by:

$$P_L = P_{L0}^0 (1 + \lambda) \tag{7.1}$$

$$Q_L = Q_{L0}^0 (1 + \lambda) \tag{7.2}$$

where P_L and Q_L are the real and reactive powers of the load at the current operating time. P_{L0}^0 and Q_{L0}^0 are the initial real and reactive power demands, λ is the varying parameter representing the load factor.

The dynamic load component (*rtds_udc_DYLOAD*) was used in conjunction with the scheduler component (*rtds_sharc_ctl_SCHED*) to achieve the dynamic load increments in real time. It can be seen from Figure 7.4 that a voltage collapse condition occurred with all the load models considered.

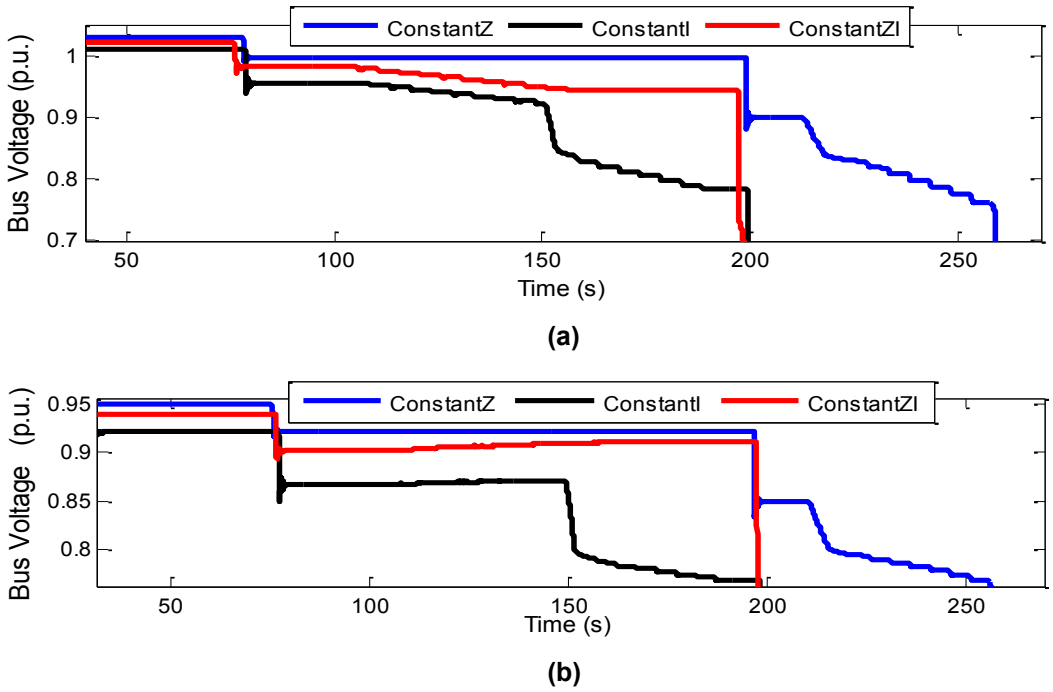

Figure 7.4: **Load characteristics for increased loading scenario (a) Bus-8 voltage; and (b) Bus-11 voltage**

The Constant I load model resulted to the fastest voltage collapse immediately after the OXL operation. The Constant ZI load model survived the OXL operation and tap action, but voltage collapse occurred abruptly later compared to the other two scenarios when Constant Z and Constant I load models were used. The Constant Z load gave an optimistic voltage profile. This can be misleading especially in smart grids where the load demand and the load characteristics could change at different times of the day based on the tariff and other demand response considerations.

The operating scenario given above in Figure 7.3 was repeated with the load at bus-11 replaced by an exponential load model which was used in combination with a polynomial load model. The coefficients of np and nq of the exponential load model obtained from (Taylor, 1994) add to the load model the effects of air conditioners, fans, and pump loads typically obtainable at the customer end during hot summer conditions. The load parameters at bus-11 are given in Table 7.1.

Table 7.1: **Exponential and polynomial load parameters for bus-11**

Load Component	Percentage of the Bus Load (%)	Coefficients	
		np	*nq*
Exponential load	20	0.5	2.5
Exponential load	20	0.08	1.6
Polynomial load	60	50% Constant Z and 50% Constant I	

From the results (Figure 7.5), it can be seen that lower bus voltages were obtained at the transmission and distribution networks compared to that obtained for the operating condition as presented in the first scenario in Figure 7.3. This third scenario depicts the impact of high reactive power demand on the voltage stability of a power system.

The increased reactive power demand resulted to very low system-wide voltages as shown in Figure 7.5 compared to the results obtained in the previous scenarios respectively. An attempt was made to replace the load at bus-8 with an induction motor load using the motor parameters given in Kundur (1994). However, this caused a voltage collapse condition immediately. This could be because this particular test system initializes from a very low voltage condition due to start-up transients during the real-time simulation. The presence of an induction motor characterized by a heavy start-up demand probably resulted in the stalling of the motor, and consequently the voltage collapse that was observed.

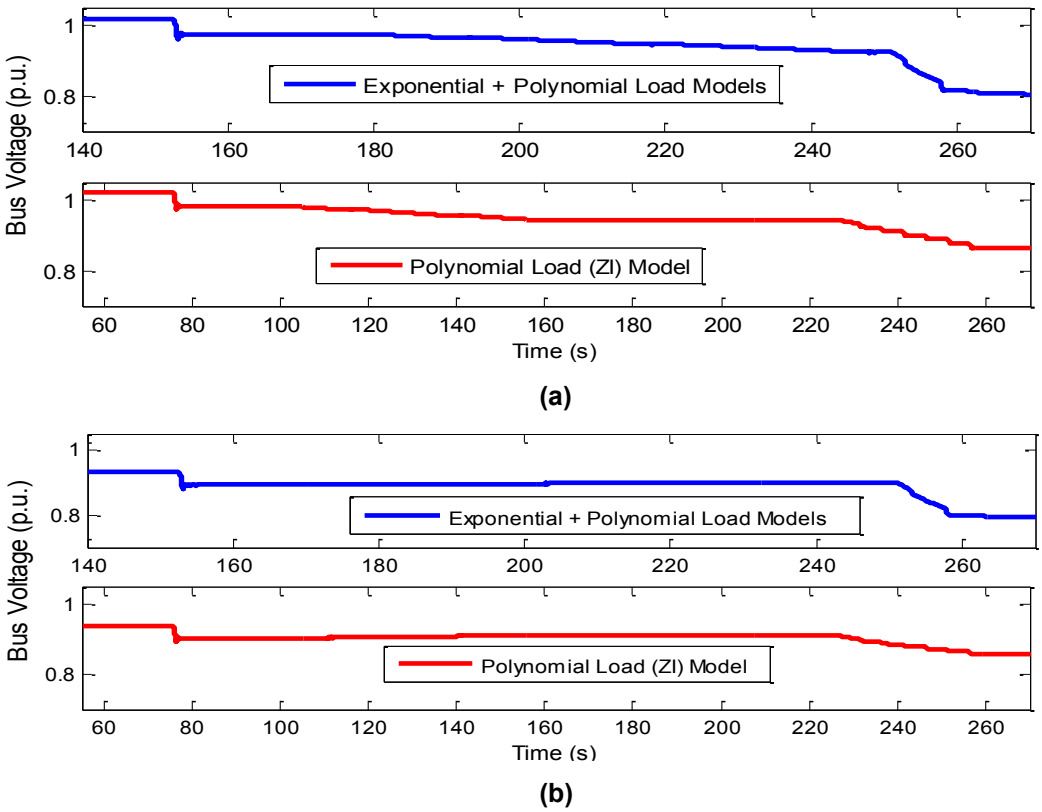

Figure 7.5: Load characteristics for line contingency with exponential and polynomial load combinations (a) Bus-8 voltage; and (b) Bus-11 voltage

During the contingency study, the system parameters are memorised at the steady state operating condition and at the point of voltage instability. The system parameters at the point of voltage collapse were applied in Equation (4.35) in the computation of the wide area RVSA indices based on the worst contingency obtained for the various contingency grouping.

Figure 7.6 shows a classical voltage instability scenario in which a transmission line contingency involving the loss of one of the transmission lines between buses-6 and -7 caused the system bus voltages to drop. This resulted in the tap action of the transformer ULTC at bus-10. Further ULTC taps consequently caused an increase in the reactive power demand thereby resulting in an increase in the field current produced at generator G3 beyond its field current limit. Figure 7.7 shows the real-time plots of the proposed RVSA indices obtained for two case studies comprising of transmission line contingency and increased system loading respectively.

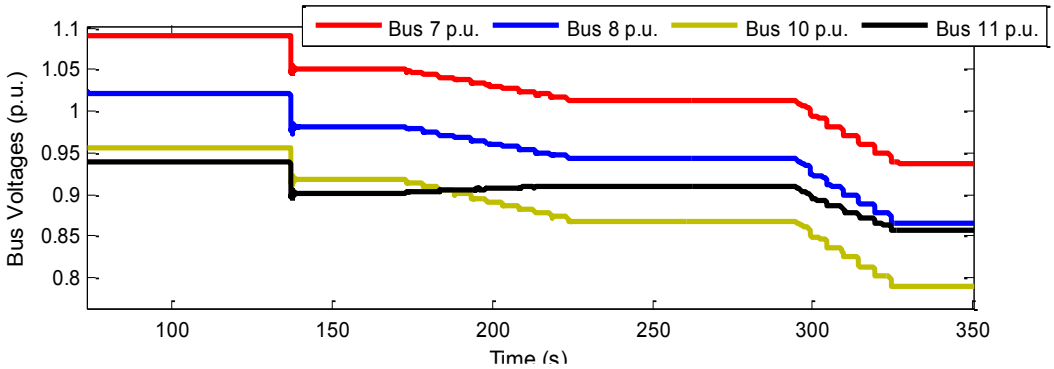

(a)

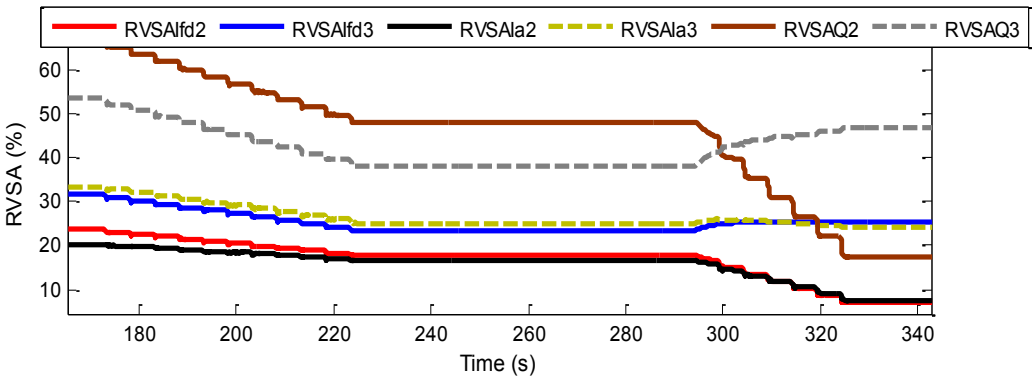

(b)

Figure 7.6: Classical voltage instability showing the impact of loss of transmission line, transformer ULTC taps, and generator G3 OXL operation (a) Plots of bus voltages; (b) Voltage stability indices

From Figure 7.8, it can be seen that the indices derived from the generator field and stator currents responded to the system disturbances at the same instant with the index derived from the generator reactive power. Since generator reactive power have already been applied in some existing indices for voltage stability monitoring and assessment, this served as an indication of the possibility of using the generator field and stator currents as indices for voltage stability assessment.

The impact of load characteristics on voltage stability assessment indices was investigated for the Line Stability Index (LQP) in (Mohamed and Jasmon, 1989), the Fast Voltage Stability Index (FVSI) in (Musirin and Rahman, 2002), and the proposed RVSA index. Figure 7.8 shows the results of the voltage stability assessment indices computed using the LQP index, the FVSI index, and the proposed RVSA index for the operating scenarios in subsection 7.2.1 for various load models (Constant Z, Constant I, and Constant ZI loads respectively). During the steady state operating condition, the LQP and FVSI indices are meant to have values close to 0, and should be equal to or greater than unity at the voltage collapse point. From Figure 7.8a, it was observed that the LQP and FVSI indices were affected by the type of load models used and their characteristics. Further details on the LQP and FVSI indices are given on page 211.

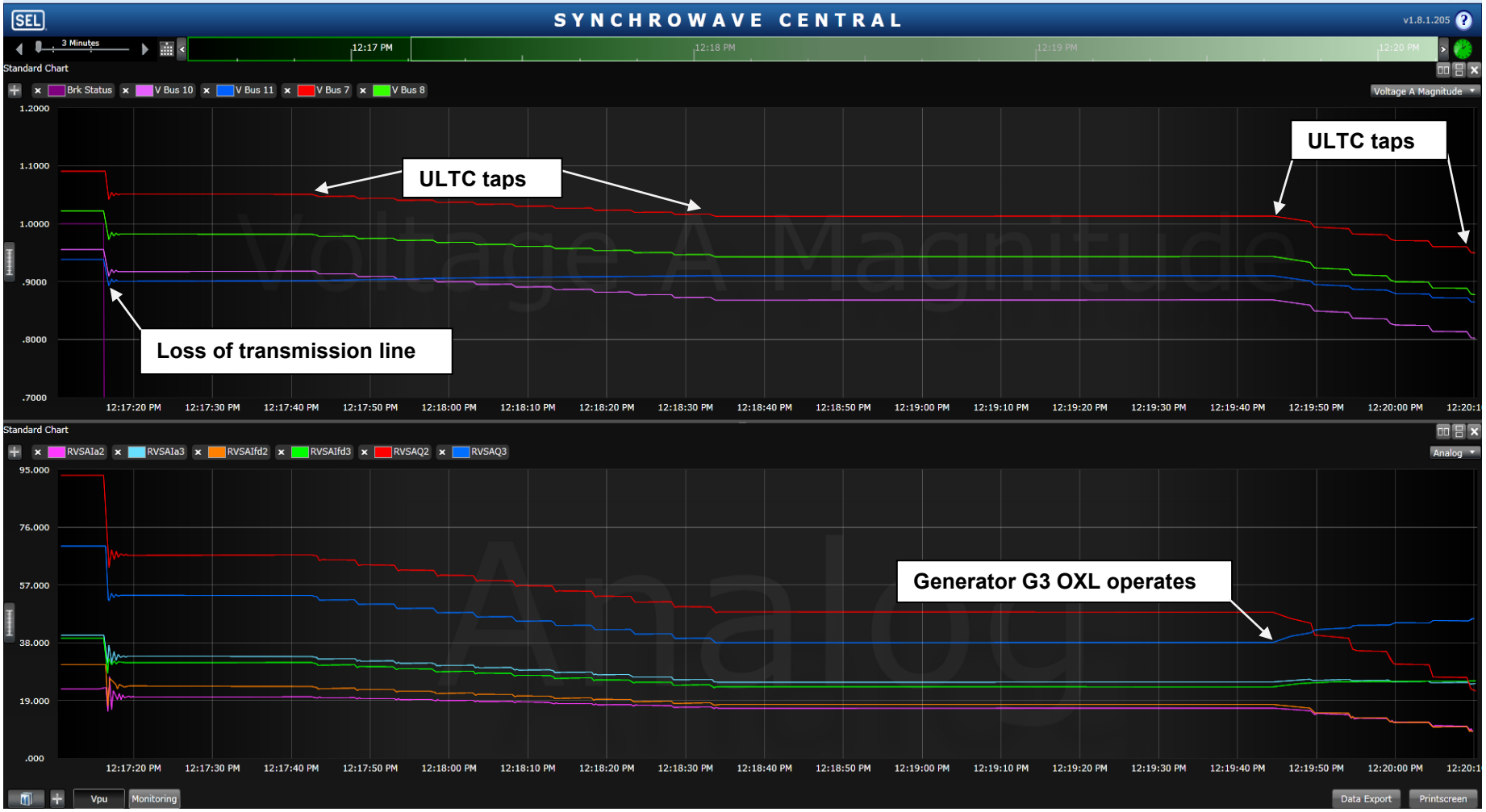
SEL
SYNCHROWAVE CENTRAL
v1.8.1.205
3 Minutes
12:17 PM
12:18 PM
12:19 PM
12:20 PM
Standard Chart
Brk Status
V Bus 10
V Bus 11
V Bus 7
V Bus 8
Voltage A Magnitude
1.2000
1.1000
1.0000
.9000
.8000
.7000
ULTC taps
ULTC taps
Loss of transmission line
Voltage A Magnitude
12:17:20 PM
12:17:30 PM
12:17:40 PM
12:17:50 PM
12:18:00 PM
12:18:10 PM
12:18:20 PM
12:18:30 PM
12:18:40 PM
12:18:50 PM
12:19:00 PM
12:19:10 PM
12:19:20 PM
12:19:30 PM
12:19:40 PM
12:19:50 PM
12:20:00 PM
Standard Chart
RVSAIa2
RVSAIa3
RVSAIfd2
RVSAIfd3
RVSAQ2
RVSAQ3
Analog
95.000
76.000
57.000
38.000
19.000
.000
Generator G3 OXL operates
Analog
12:17:20 PM
12:17:30 PM
12:17:40 PM
12:17:50 PM
12:18:00 PM
12:18:10 PM
12:18:20 PM
12:18:30 PM
12:18:40 PM
12:18:50 PM
12:19:00 PM
12:19:10 PM
12:19:20 PM
12:19:30 PM
12:19:40 PM
12:19:50 PM
12:20:00 PM
Vpu
Monitoring
Data Export
Printscreen

(a)

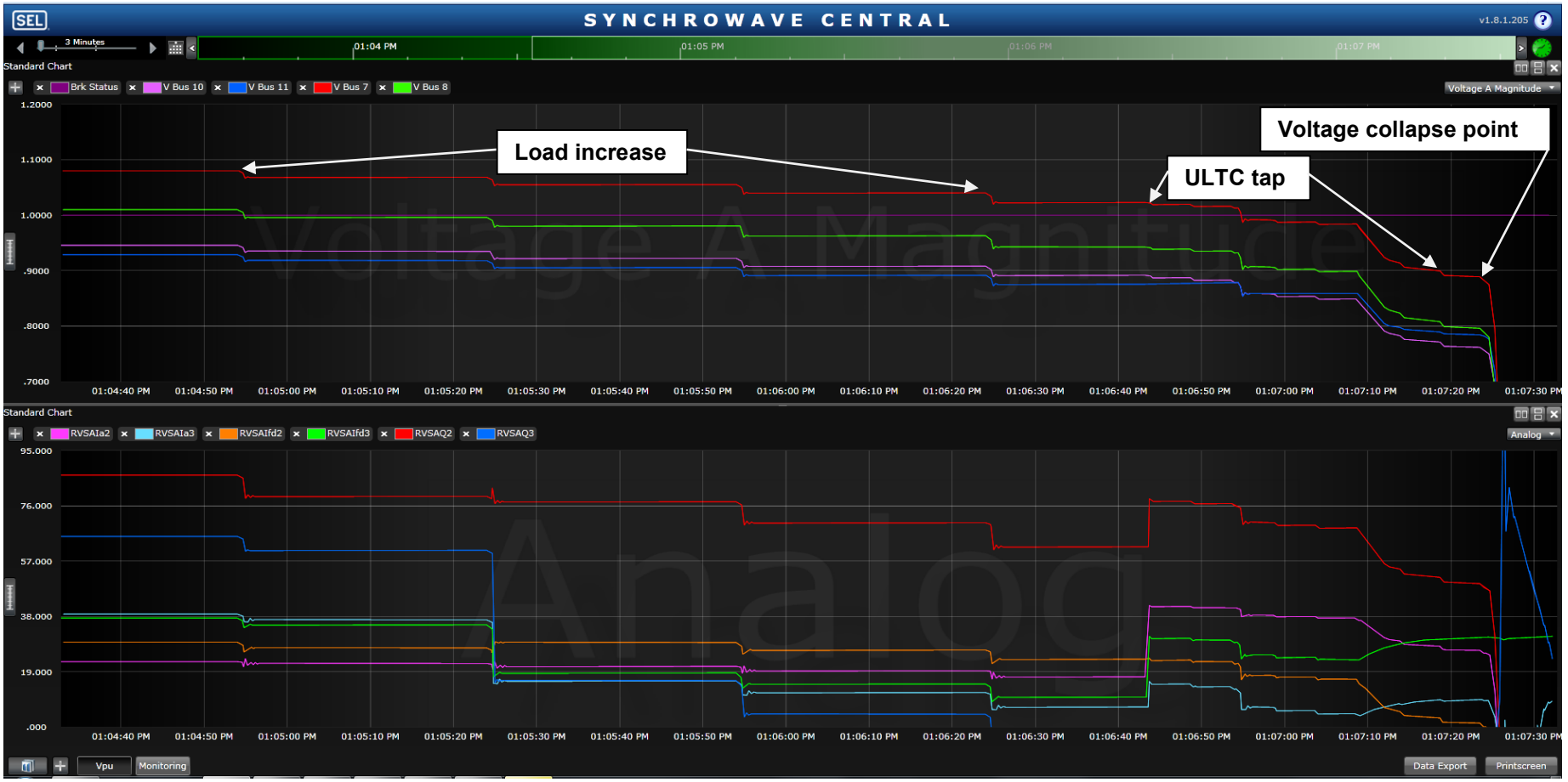

(b)

Figure 7.7: Real-time plots of voltage stability assessment for **(a)** Loss of transmission line; and **(b)** Increased loading condition at bus-8, transformer ULTC taps, and generator G3 OXL operation

The result for the Constant I load model showed that the values of the LQP and FVSI indices were greater than 1 even though voltage collapse did not occur for this particular scenario. Similar results were obtained for the Constant ZI load model. Figure 7.8b shows the results obtained for the LQP and FVSI indices for the operating scenario involving load increase at bus-8. The LQP and FVSI indices gave the wrong indications for the Constant I load model. For the RVSA index, the system operating condition and the disturbance in the system were correctly indicated for all the load models considered as shown in Figures 7.8c-7.8d.

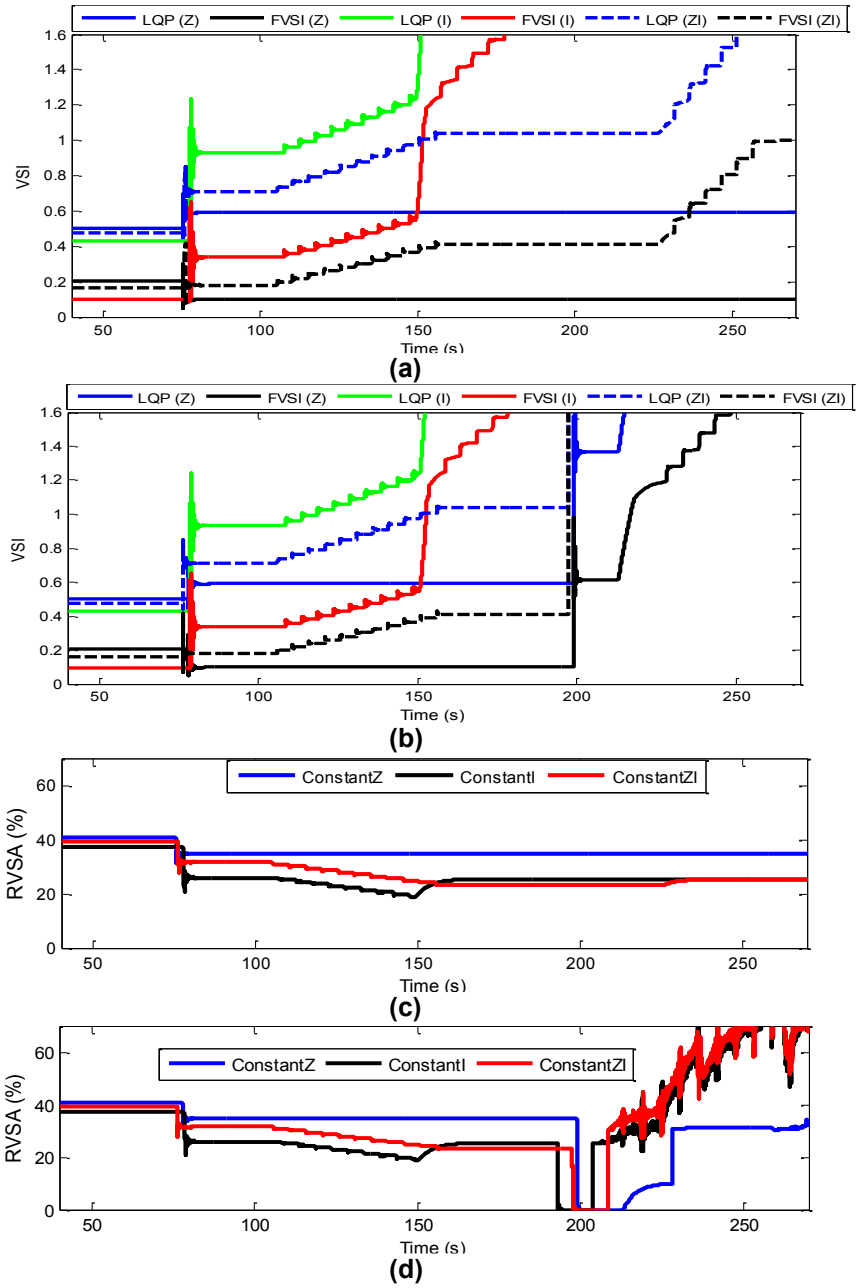

Figure 7.8: Load model characteristics for (a) FVSI and LQP indices for line outage; (b) FVSI and LQP indices for increased loading; (c) RVSA index for line outage; (d) RVSA index for increased loading;

The reason why the RVSA index performed better than the LQP and FVSI indices could be because the former is based on generator-derived index which gives system-wide situation awareness, while the latter is computed at the local buses. This indicates that the LQP and FVSI indices are affected by system topology and the parameters at the local bus.

7.3.2 Real-Time Voltage Stability Assessment for Test System-2

In order to verify the scalability of the proposed real-time voltage stability assessment indices, a large interconnected power system using Test System-2 (the New England 39-bus test system) was modelled in the RSCAD software. However, some modifications had to be made in order to carry out an effective study of the voltage collapse problem.

The modifications include the following:

- the addition of OXLs at generators G2 and G3.
- the use of dynamic load models at buses-4, -7, -8, and -12 respectively.

The results obtained in the validation of the proposed wide area-based RVSA indices are presented below.

Case Study 1

From the preliminary studies carried out, it was observed that Test System-2 was able to withstand N-2 transmission line contingencies and N-1 generator contingencies (except for generator G1 outage representing an equivalent interconnected system). One way by which Test-System-2 was stressed to the voltage collapse point was through the simulation of an increased system loading condition. The loads at buses-4, -7, -8, -12 were increased until the system collapsed at the sixth load increase as shown in Figure 7.9. All the RVSA indices indicated the stress in the system. However, the index obtained from the reactive power reserve on the synchronous generators had a steep transition from an acceptable level to the collapse point.

Case Study 2

The above scenario in Case Study 1 was repeated with an OXL enabled at generator G3. The system collapsed at the fourth load increase compared with the previous scenario in Case Study 1 that collapsed at the sixth load increase. This demonstrates the impact of generator protective limiters on voltage stability and the ability of the generators to provide voltage control in the power system. From Figure 7.10, it was observed that the OXL at generator G3 operated just after the third load increase at buses-4, -7, -8, 12.

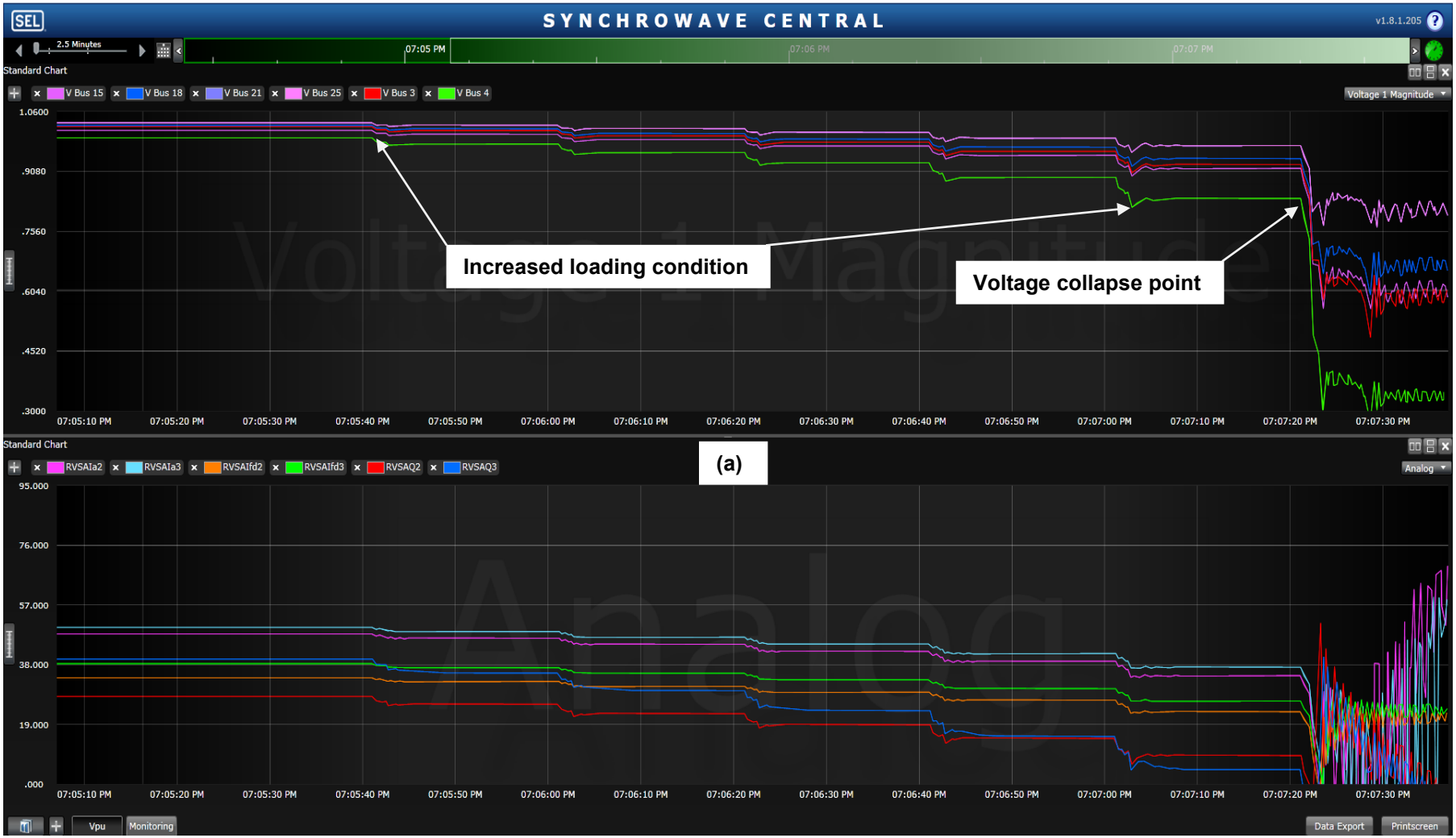

(b)

Figure 7.9: Real-time plots for Case Study 1 for **(a)** Plots of bus voltages; **(b)** RVSA indices for generators G2 and G3

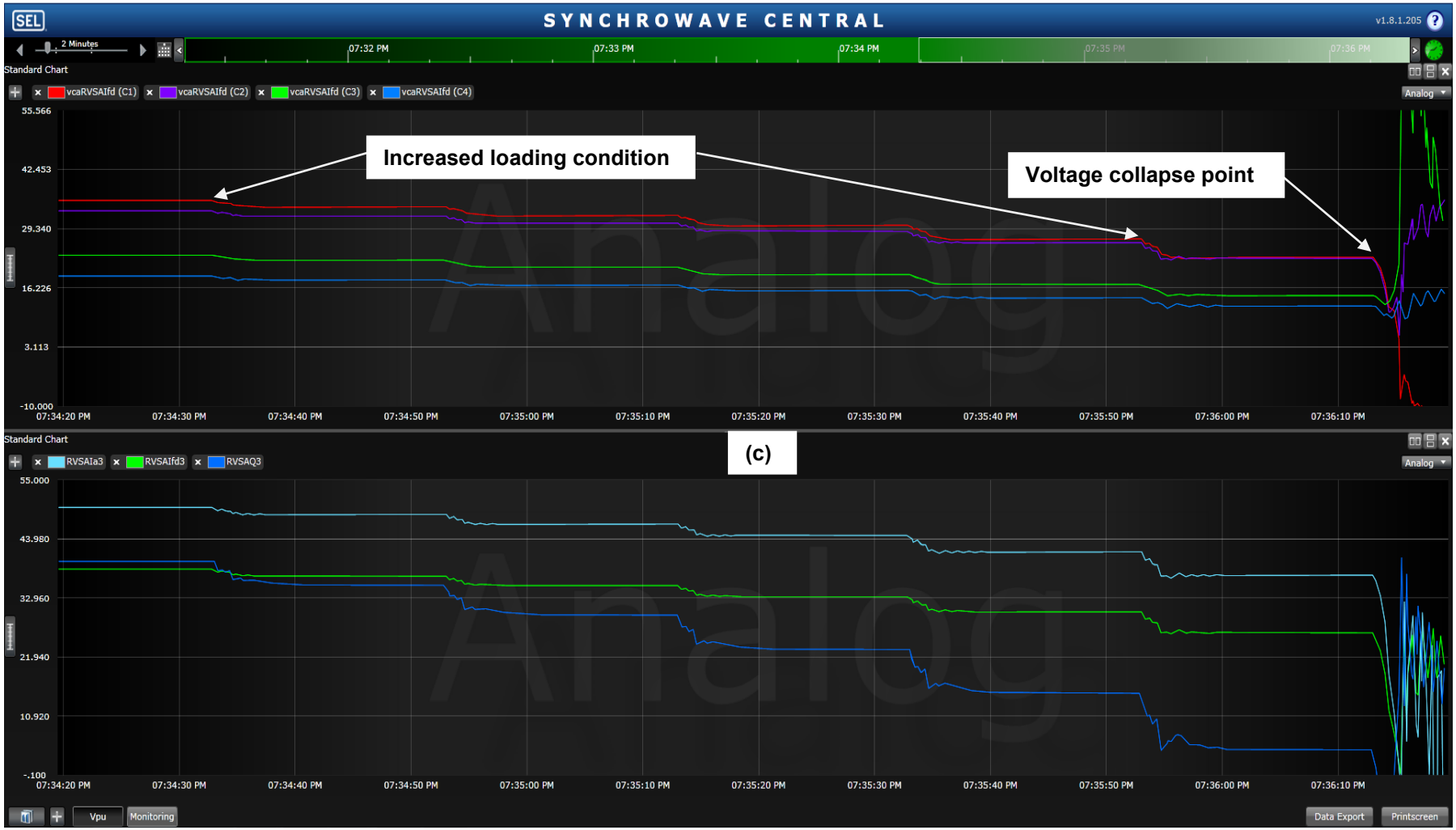

Figure 7.9: Real-time plots for Case Study 1 for **(c)** vcaRVSA indices for the VCA 1-4; **(d)** RVSA indices derived from generator G3

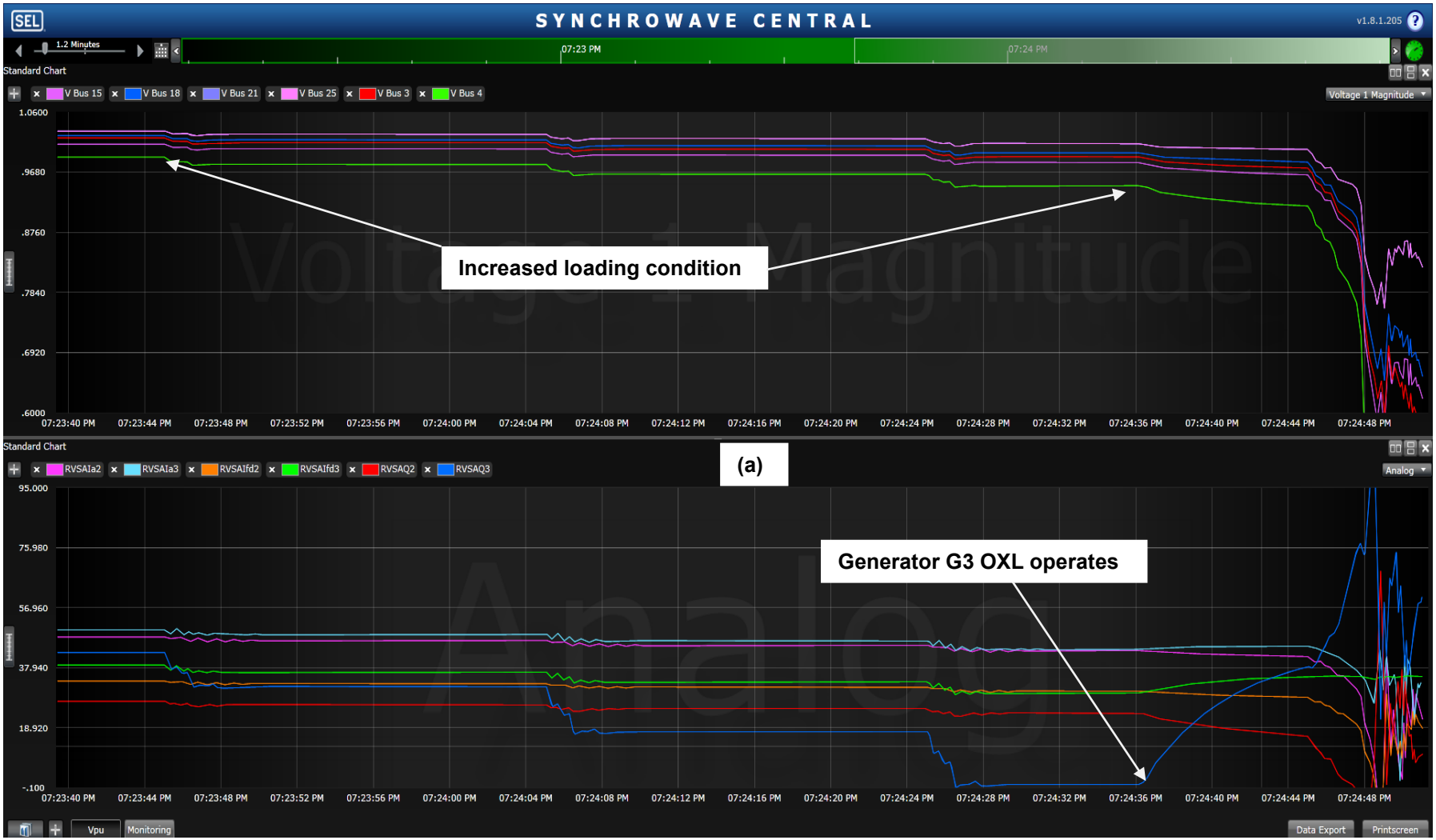

(b)

Figure 7.10: Real-time plots for Case Study 2 for **(a)** Plots of bus voltages; **(b)** RVSA indices for generators G2 and G3

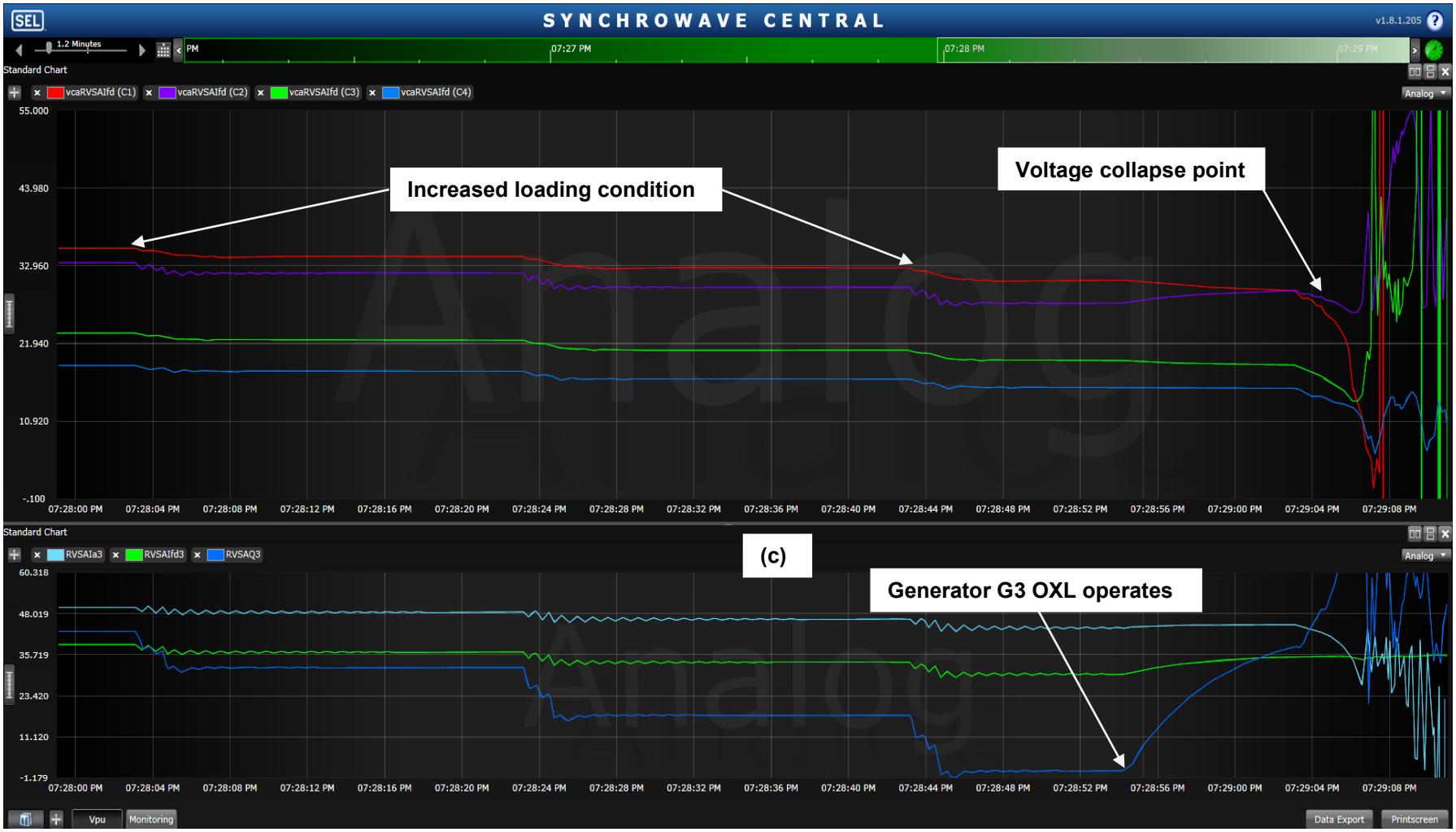

(d)

Figure 7.10: Real-time plots for Case Study 2 for **(c)** vcaRVSA indices for the VCA 1 to 4; **(d)** RVSA indices for generator G3

The implication of this is that generator G3 terminal ceased to be a PV bus and became a PQ bus. This resulted in the failure of the RVSA indices derived from the reactive power reserve and field current reserve. From Figure 7.10, it can be seen that the RVSA indices based on the reactive power reserve and field current began to increase despite the impending voltage collapse. This would give a false sense of system security that might impact the timely operation of the control action of the system's SIPS. However, the RVSA index based on the stator current from the synchronous generators gave a true indication of the system state.

Case Study 3

A scenario comprising of line (Line 15-16) and generator (G6) contingencies, and increased system loading was considered in Case Study 3. The results obtained for some of these contingencies using the proposed RVSA indices and their comparison with the existing indices proposed in (Musirin and Rahman, 2002; Mohamed and Jasmon, 1989) are given in Table 7.2. Figure 7.11 shows the real-time plot obtained.

The Line Stability Factor (LQP) is a transmission line loadability indicator which directly relates to how much real and reactive powers a transmission line can sustain before reaching its design limits.

The LQP index given by (Mohamed and Jasmon, 1989) can be expressed using synchrophasor measurements as:

$$LQP = 4\left(\frac{X}{|\mathrm{V_i}|^2}\right)\left(\frac{X}{|\mathrm{V_i}|^2}P_i^2 + Q_j\right) \tag{7.3}$$

where X is the line reactance, $|\mathrm{V_i}|$ is the voltage phasor magnitude from a PMU at the sending end, P_i is the real power at the sending end, Q_j is the reactive power at the receiving end.

The value of the LQP index for any of the transmission lines closest to unity indicates that the transmission line is at its voltage instability point which may lead to system-wide collapse.

The Fast Voltage Stability Index (FVSI) is a voltage stability index that can either be referred to a load bus or to a transmission line. It relates to how much real and reactive powers a bus or a transmission line can be loaded with before reaching its design limits.

Mathematically, the FVSI proposed in (Musirin and Rahman, 2002) can be given as:

$$FVSI_{ij} = \frac{4Z^2Q_j}{|\mathrm{V_i}|^2 X} \tag{7.4}$$

where Z is the line impedance, Q_j is the reactive power at the receiving end, $|\mathrm{V_i}|$ is the voltage phasor magnitude from a PMU at the sending end, X is the line reactance.

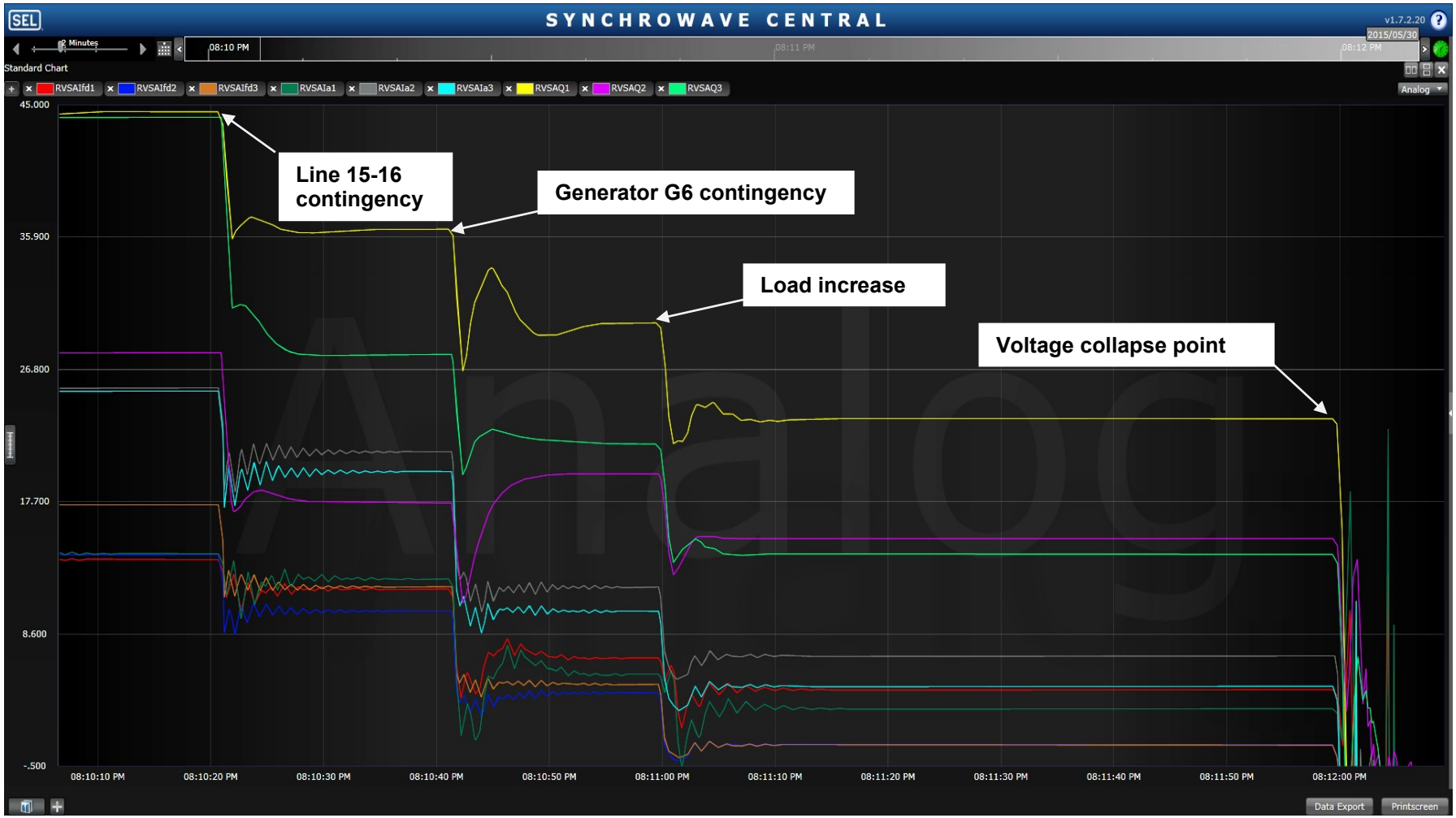

Figure 7.11: Real-time plots for Case Study 3 consisting of line and generator contingencies, and increased system loading condition

The value of the FVSI index of any of the buses/transmission lines closest to unity indicates that the transmission line is at its voltage instability point and may lead to system-wide collapse.

Table 7.2: Voltage stability indices for various transmission line and generator contingencies

Contingency	$FVSI_{3-4}$ (Line 3-4)	LQP_{3-4} (Line 3-4)	$RVSA_{Q,2}$ (%)	$RVSA_{Q,3}$ (%)	$RVSA_{Ifd,2}$ (%)	$RVSA_{Ifd,3}$ (%)	$RVSA_{Ia,2}$ (%)	$RVSA_{Ia,3}$ (%)
Loss of Line 3-4	0.137	0.178	26.57	41.49	13.11	16.13	24,25	23.77
Loss of Line 14-15	0.154	0.195	27.27	40.51	12.82	15.65	24.08	23.43
Loss of Line 15-16	0.232	0.267	31.63	45.40	11.52	14.08	20.82	19.98
Loss of Generator 6	0.173	0.247	25.58	32.81	8.06	10.16	16.23	15.86
Loss of Generator 7	0.170	0.252	23.36	36.44	7.69	10.55	17.06	16.51
Loss of Generator 8	0.173	0.247	25.58	32.81	8.06	10.16	16.23	15.86
Loss of Generator 9	0.183	0.275	12.99	28.49	6.72	9.47	14.19	13.48

Case Study 4

The adaptive weighted-summation approach proposed in Chapter Four was compared with the key generator RVSA approach used in (Adewole and Tzoneva, 2015f; 2014b; Bao *et al*., 2003; Avramovic and Fink, 1992). For an increased loading condition in the VCA of interest (load buses-4, -7, -8, -12), generator G2 was the most responsive generator for the stressed VCA with respect to the reactive power support provided.

If the key generator principle is applied, this would be indicated by $RVSA_{Ifd2}$ for the index based on field current of the synchronous generators, or by $RVSA_{Ia2}$ if the index based on the stator currents of the synchronous generators is used. The adaptive-weighted summation index for the study VCA is given as $vcaRVSA_{Ifd2}$ for the index derived from the field current of the synchronous generators, and it is the weighed summation of the available margins on generators G1, G2, and G3 from the considered VCA at the current operating point. Figure 7.12 shows a plot of the adaptive weighted-summation index ($vcaRVSA_{Ifd2}$) of the generators for the study VCA (VCA-2) and the plot of generator G2 $RVSA_{Ifd2}$ and $RVSA_{Ia2}$ indices respectively.

From the plot, it can be seen that the $vcaRVSA_{Ifd2}$ and $RVSA_{Ifd2}$ were close during the steady state condition. After the first load increase, $RVSA_{Ifd2}$ dropped while the $vcaRVSA_{Ifd2}$ for the VCA was slightly higher as a result of the higher margins available on generators G1 and G3 respectively.

In the situation whereby the OXL of the key generator (G2) operates, the index given by the generator G2 ceases to be true and no longer reflects the stressed state of the system as shown in Figure 7.12.

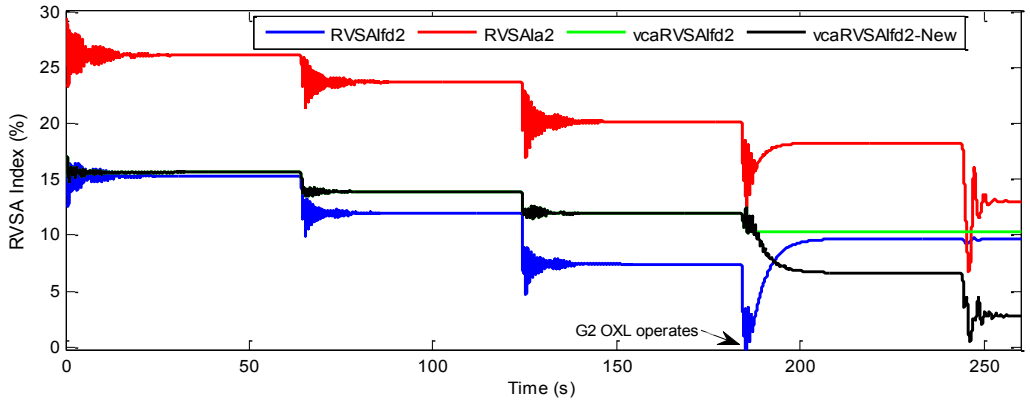

Figure 7.12: **Case Study 4 - RVSA indices showing the comparison of the *vcaRVSA* and the key generator principles**

With the adaptive weighted-summation approach, once a generator is limited by its OXL, it becomes a PQ bus and a new $vcaRVSA$ index is computed using only the generators within their continuous field current rating. Figure 7.12 shows that the newly computed RVSA index based on the weighted summation $(vcaRVSA_{IfdNew})$ continues to drop thereby reflecting the true state of the system as it moved towards voltage instability.

The adaptive weighted summation is particularly suitable for situations where a generator OXL acts to limit the field current in the generator field winding. Typically, in a case whereby the OXL of a key generator (G2) acts, other generators in the RPRB would have to pick up the reactive power previously supplied by generator G2. In Figure 7.12, it was observed that the proposed weighted $vcaRVSA$ index was not affected by such system dynamics. Thus, the weighted summation index is robust to system changes, is consistent, and gives a much more accurate reflection of the state of the power system for various operating conditions at any particular operating point.

7.3.3 Discussion

Generally, the responses obtained from the various indices are indicative of their respective ability to respond to the various system contingencies. The best system indicators for monitoring the prevailing system condition were obtained using the field and stator currents respectively. For instance, at the point of voltage collapse, the indices based on the reactive power margin (EQRPR) had a steep descent to zero from about 24%. Also, the LQP and FVSI indices had steep changes.

These indices were less than 0.4 and shot up suddenly at the voltage collapse point. The LQP and FVSI indices just like the index based on the EGRPR would give a false situation awareness or security, and would result in the late operation of the remedial action of any implemented SIPS.

The advantages of the newly proposed index based on the stator currents and field currents of the synchronous generators include the use of fewer variables, less measurement sensors are required, reduced project costs, ease of maintenance, less computation, and suitability for real-time application. Also, the new indices were shown to be robust to scenarios where the generator OXL operated and limited the generator field current.

The proceeding section presents two voltage collapse countermeasures comprising of the transformer under-load tap changer blocking and unblocking (ULTC-SIPS) algorithm and the under-voltage load shedding (UVLS-SIPS) algorithm.

7.4 System Integrity Protection Scheme: Transformer Tap-Changer Control Design

The first System Integrity Protection Scheme (SIPS) investigated and implemented in this thesis is based on the control of transformer Under-Load Tap-Changers (ULTCs) using computations based on wide area synchrophasor measurements, and control signals transmitted using the IEC 61850-8-1 Generic Object Oriented Substation Event (GOOSE) messages.

As the system deteriorates and tends towards instability, a blocking signal is sent to the transformer ULTC in order to prevent further taps of the transformer ULTC. Conversely, when the system recovers, an unblocking signal is sent to the transformer ULTC.

7.4.1 Background

The IEEE Power System Relaying Committee (PSRC) Working Group C4 Report of October 2010 on ‘Global Industry Experiences with System Integrity Protection Schemes’ (Madani *et al*., 2010) identified a couple of remedial actions for mitigating power system instability. Some of the corrective actions that can be applied in mitigating voltage collapse in particular include shunt capacitor switching (Nikolaidis and Vournas, 2008; Van Cutsem and Vournas, 2007), load shedding (Taylor, 1992;), and tap-changer control (Sichwart *et al*., 2013; Capitanescu *et al*., 2009; Otomega *et al*., 2007).

A system can be driven to voltage collapse through the action of transformer ULTCs, operation of generator OXLs), and the recovery characteristics of dynamic loads at low voltages (Kundur, 1994; Taylor, 1994). In order to prevent further degradation of the system voltages, transformer ULTC control is a countermeasure that can be used to prevent further tappings of the transformer. Tap-changer control using voltage thresholds was proposed in (Sichwart *et al*., 2013; Capitanescu *et al*., 2009; Otomega *et al*., 2003).

However, these methods (Sichwart *et al*., 2013; Capitanescu *et al*., 2009; Otomega *et al*., 2003) used voltage threshold as their control parameter. This results in control actions being initiated prematurely without giving the system adequate time for recovery. Unlike existing transformer tap-changer control algorithms based on voltage thresholds as triggers to the remedial action, the proposed ULTC-SIPS algorithm uses the system operating state obtained from the DT-classifier and wide area synchrophasor measurements as inputs. The synchrophasor measurements are used in conjunction with IEC 61850-8-1 GOOSE messages to provide the control action to the transformer tap-changer.

7.4.2 Proposed ULTC-SIPS Algorithm and Method

The SIPS functional elements mentioned in Chapter Three are implemented in the proposed SIPS algorithm. Figure 7.13 shows the structure of the proposed ULTC-SIPS algorithm. The system monitoring element of the SIPS is used in the supervision and detection of the changes in the power system. This thesis proposes the use of the combination of the system operating state (obtained from a Decision Tree-DT-classifier), generator OXL status, and load bus voltage deviation, rather than voltage thresholds only as used in the existing publications.

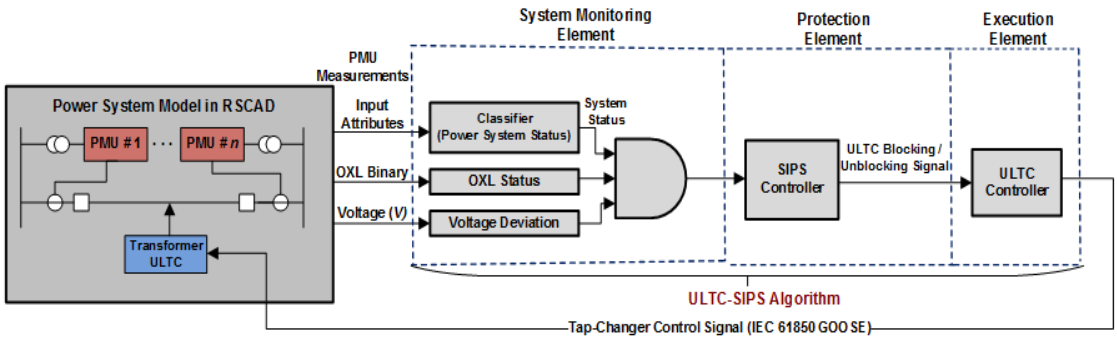

Figure 7.13: **Structure and functional elements of the proposed ULTC-SIPS algorithm**

The system status is obtained from the voltage stability assessment DT-classifier as 'Stable', 'Alert', or 'Unstable'. The use of the system status information makes the proposed algorithm robust, as it is able to respond to various system dynamics as the

power system condition changes. The status of the OXL of the key generator obtained from PMU analogue measurements is the second parameter tracked by the system monitoring element. The last parameter is the voltage deviation of the bus connected to the ULTC transformer, and it is computed using the positive sequence voltage phasor from PMUs. The activation of generator OXLs in a power system can be used as an early warning system to indicate the unavailability of reactive power supply in a Voltage Control Area (VCA).

The protection element of the SIPS is applied in the arming of the SIPS when system stability threats are identified. The output from the system monitoring element and a predetermined pick-up time delay are used by the ULTC-SIPS protection element. Figure 7.14 shows the logic proposed for the algorithm of the SIPS controller ULTC-SIPS algorithm.

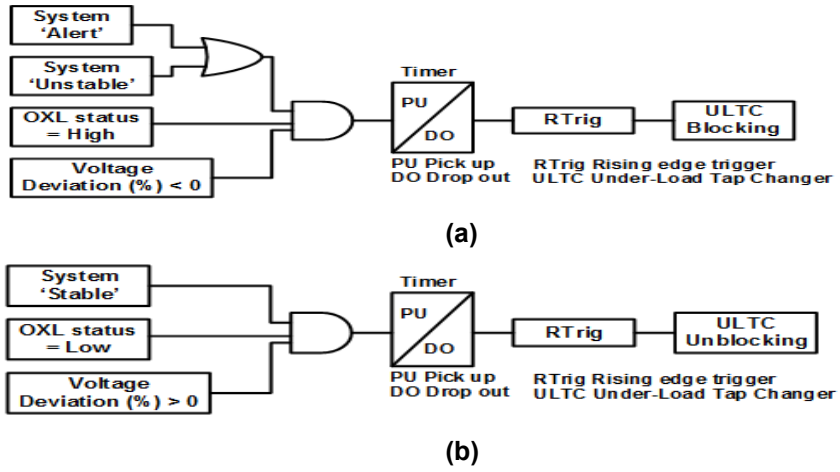

Figure 7.14: ULTC-SIPS algorithm for (a) ULTC blocking signal; and (b) ULTC unblocking signal

The algorithm in Figure 7.14a is used for blocking the transformer ULTC taps during stressed conditions, while the algorithm in Figure 7.14b is for unblocking the transformer ULTC after the system recovers. PU and DO in the Timer clock shown in Figure 7.14 represent the pickup and dropout times of the system monitoring element respectively.

The execution element receives the output signal from the protection element and performs the required remedial action. In this regard, the remedial action is the blocking of further taps of the transformer ULTC. The system monitoring element continues to track the system parameters, and an unblocking signal is sent to the transformer ULTC to unlock it when the system recovers. Figure 7.15 gives the offline and online processes involved in the design and implementation of the proposed

ULTC-SIPS algorithm. The offline design process is based on the method for growing an optimal DT-classifier model described in Chapter Four.

The grown DT-classifier and regressor are integrated in the Programmable Logic Controller (PLC) of the real-time 'proof-of-concept' testbed for online real-time classification of the operating state of the power system and the prediction of the system's margin to voltage collapse. In the real-time mode, synchrophasor measurements from PMUs installed in the power system served as the feature attributes (inputs) to the DT-classifier for real time prediction. The output of the DT-classifier is then used as one of the inputs to the system monitoring element of the ULTC-SIPS algorithm.

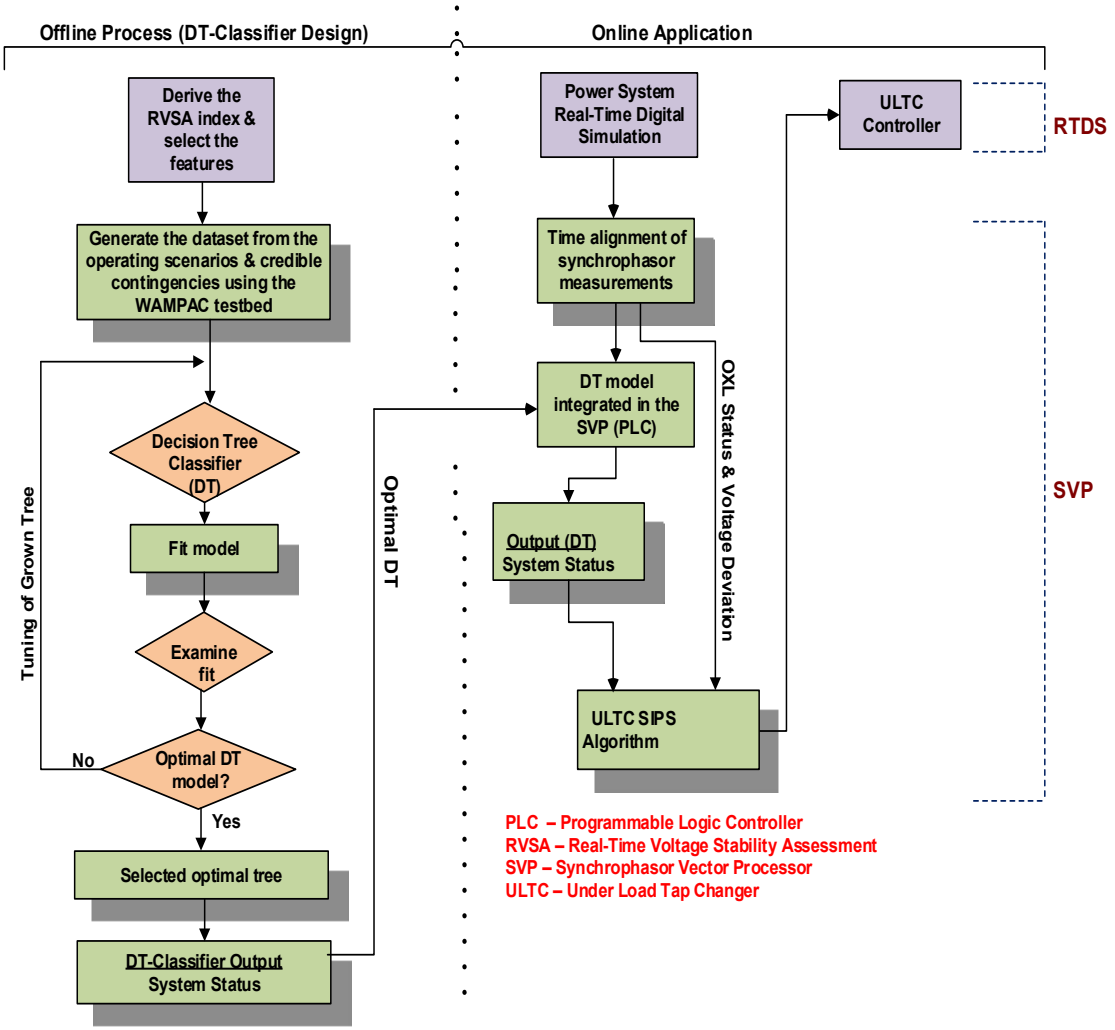

Figure 7.15: Flow chart for the implementation of the ULTC-SIPS algorithm

7.4.3 Simulations for Testing the ULTC-SIPS Algorithm

Figure 7.16 shows the plot of a voltage collapse scenario using the 10-bus multi-machine equivalent test system without the proposed ULTC-SIPS algorithm.

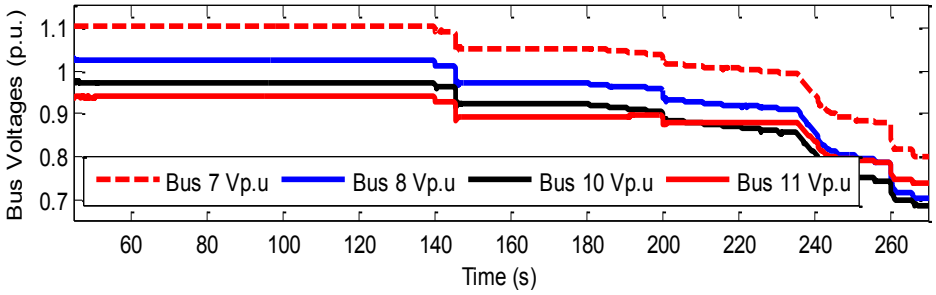

Figure 7.16: **Voltage plots for buses-7, -8, -10, and -11 of the 10-bus multi-machine equivalent test system**

In this scenario, an operating condition involving an increased loading condition at bus-8, loss of one of the transmission lines between buses-6 and -7, ULTC tap-action, and generator G3 OXL operation were considered. From Figure 7.16, it can be seen that voltage instability occurred with the voltage at bus-10 equal to 0.6663 p.u., while the voltage at bus-11 was 0.7220 p.u. Further increase in load would have resulted in a voltage collapse condition.

In order to implement the proposed ULTC-SIPS algorithm, a comparison was carried out using various trigger inputs to the SIPS protection element in the ULTC-SIPS algorithm. Table 7.3 gives the various trigger-types considered.

Table 7.3: **Investigation on various ULTC-SIPS trigger-types**

Trigger No.	Trigger-Type
1	Voltage threshold only
2	OXL status only
3	System status only
4	Voltage threshold and OXL status
5	System status, voltage threshold, and OXL status

The real-time implementation layout of the proposed ULTC-SIPS algorithm is given in Figure 7.17. The various components of the system monitoring element comprising of the real-time voltage stability assessment index, system status, OXL status of the key generator, and the voltage deviation calculation were implemented in the SEL-3378 SVP together with the system protection element using the IEC 61131-3 Structured Text (ST) programming.

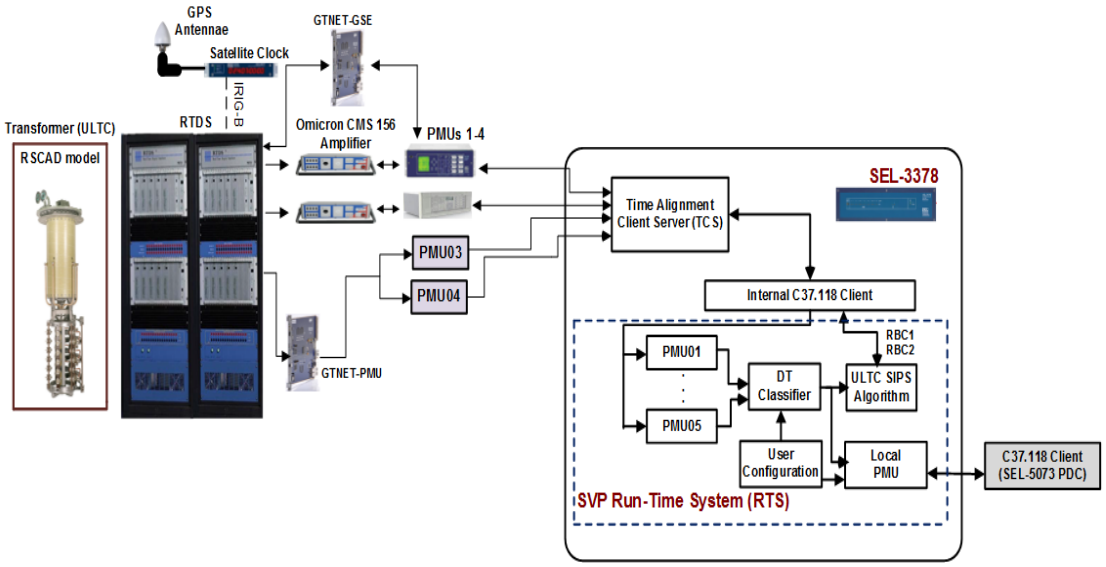

Figure 7.17: Functional implementation layout of the ULTC-SIPS algorithm

The Fast Operate (FO) command is published from the SEL-3378 SVP port to the telnet port of the SEL-451 IED/PMU which functions as the substation I/O (actuator module) and to the transformer ULTC controller which is the execution element of the ULTC-SIPS algorithm modelled in RSCAD software. It should be noted that the FO command received from the SEL-3378 SVP by the SEL-451 IED is published as an IEC 61850 GOOSE message to the RSCAD transformer ULTC controller using the GTNET card of the RTDS®. The green highlight shown in Figure 7.18 indicates the IEC 61850 GOOSE message input to the transformer ULTC controller for the 10-bus multi-machine equivalent test system.

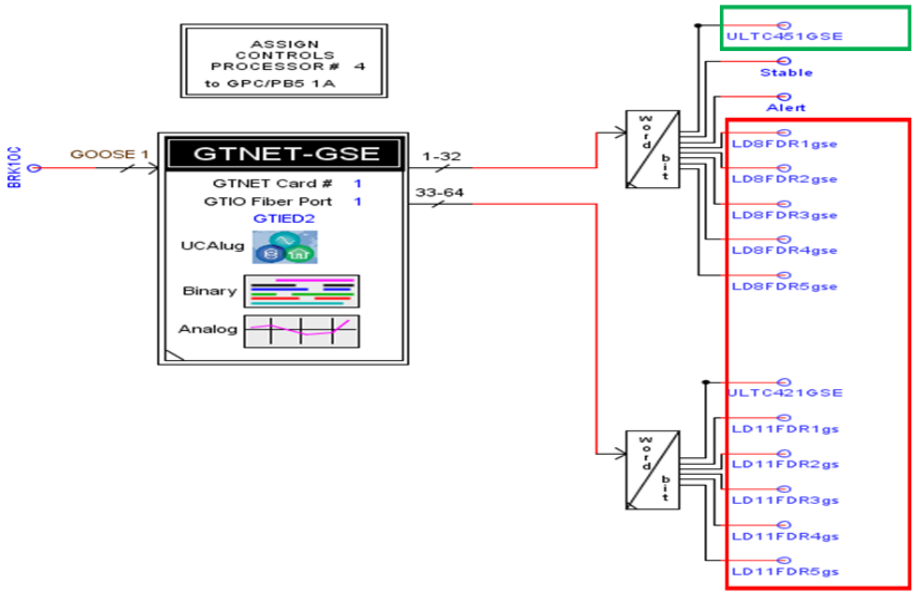

Figure 7.18: Input/output configuration of the RTDS-GTNET IEC 61850 GSE component

Figure 7.19 shows the plot of trigger-type 1 which is commonly used, and trigger-type-5 which is proposed in this thesis. The voltage threshold used in trigger type-1

was 0.95 p.u. ULTC-SIPS trip time is calculated from the start of the increased loading condition to when the protection element of the ULTC-SIPS (trigger) was armed.

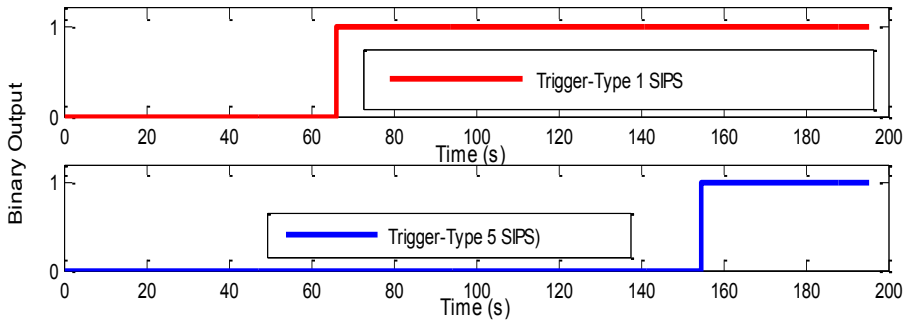

Figure 7.19: **Plots of trigger-type 1 and trigger-type 5 for the proposed ULTC-SIPS algorithm**

Table 7.4 presents the average ULTC-SIPS trip time for all the SIPS trigger-types considered. From Table 7.4, it can be seen that the fastest trip time was obtained using trigger-type 1. However, it was observed from Table 7.5 that the voltage levels were still high at the time of the operation of the ULTC-SIPS trigger-type 1. Thus, trigger-type 1 based on voltage threshold was shown to operate prematurely without giving the system adequate time to recover. Good ULTC-SIPS operate time with an acceptable voltage level was obtained using trigger-type 3 (in bold) which was based on the system status only.

Table 7.4: **Average ULTC-SIPS trip time for various trigger types**

Trigger No.	Trigger-Type	Time (s)
1	Voltage threshold only	66.15
2	OXL status only	156.10
3	System status only	120.60
4	Voltage threshold and OXL status	156.00
5	System status, voltage threshold, and OXL status	156.20

Table 7.5: **Bus voltages for various trigger-types for the case studies with and without ULTC-SIPS algorithm**

	With SIPS				Without SIPS	
Trigger No.	Bus 7 (p.u.)	Bus 8 (p.u.)	Bus 10 (p.u.)	Bus 11 (p.u.)	Bus 10 (p.u.)	Bus 11 (p.u.)
1	1.0116	0.925	0.8863	0.8541	0.6663	0.7222
2	0.8679	0.774	0.7458	0.7726		
3	**0.9963**	**0.9092**	**0.8671**	**0.8564**		
4	0.8679	0.774	0.7458	0.7726		
5	**0.8679**	**0.774**	**0.7458**	**0.7726**		

However, trigger-type 5 (in bold) was selected since it incorporates all the various trigger-types with an acceptable voltage level, includes an input based on the status of the OXL of the key generator in the system, and demonstrated dependability for all

the simulation cases considered. Also, the operate time for trigger-type 5 was acceptable since it acted faster than what is obtainable with undervoltage load-shedding relays which typical operate in 250 ms (Wester *et al*., 2014).

Figures 7.20-7.21 show a case study when the proposed ULTC-SIPS algorithm using trigger-type 5 is active. The ULTC-SIPS algorithm operated and blocked further taps of the transformer ULTC before the onset of the voltage collapse. Voltage collapse was avoided with the voltage at bus-10 settling at 0.7458 p.u., while the voltage at bus-11 settled at 0.7726 p.u.

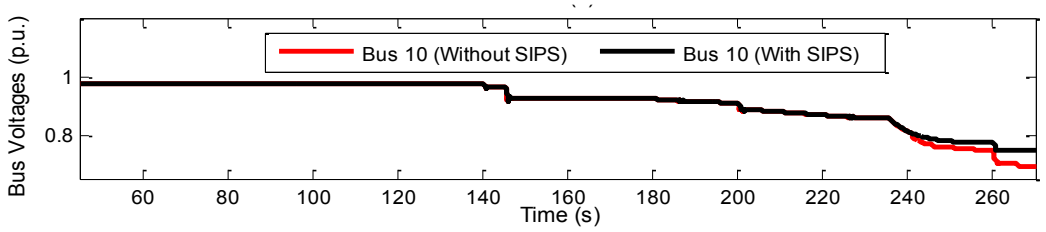

Figure 7.20: **Voltage plots for bus-10 with and without the proposed ULTC-SIPS**

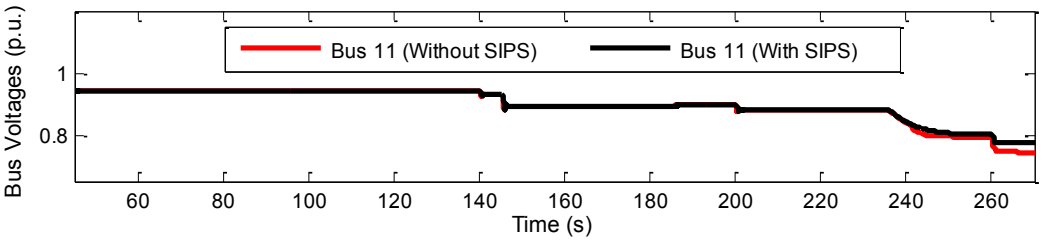

Figure 7.21: **Voltage plots for bus-11 with and without the proposed ULTC-SIPS**

From the foregoing, it can be seen that the system can be prevented from reaching the voltage collapse point if the transformer ULTC tap action is blocked at the right time before the system becomes unstable. The proposed ULTC-SIPS algorithm was also shown to be appropriate for providing temporary relief in the prevention of further degradation of the system voltages.

7.5 System Integrity Protection Scheme: Adaptive Under-Voltage Load Shedding Design

7.5.1 Introduction

The second SIPS designed and implemented in this thesis is the Under-Voltage Load Shedding (UVLS) scheme. Generally, load shedding should only be used as a last resort remedial action after other less drastic actions may have been exhausted. This is because it is an extreme action, and it could result in dissatisfied customers, ligations by the aggrieved customers, and a drop in the utility revenue. Therefore, UVLS schemes should serve as the last line of defence to prevent a voltage instability

condition from culminating into voltage collapse or system-wide blackout. In view of this, it is assumed in this thesis that shunt compensation switching, shunt reactor disconnection, FACTS devices, and synchronous condensers have been tried in order to mitigate the voltage instability prior to the arming of the proposed UVLS-SIPS algorithm.

Since SIPSs are system specific, it is important to design the UVLS-SIPS algorithm using system studies to identify the characteristics of the power system to be protected through the consideration of the system generation, loading, topology, probable contingencies, and extreme contingencies respectively. This is required in order to design an efficient countermeasure capable of alleviating the system stress during emergencies.

Three aspects relating to the design of an effective UVLS-SIPS method and algorithm are considered as follows:

- The amount of load to shed;
- The location where to shed load; and
- When to shed the load(s).

It is important that load shedding is carried out promptly at the appropriate time, in the right location, and with the right amount. This in effect, has been shown to reduce the total amount of load that must be shed in order to restore the system to an acceptable operating condition (Capitanescu *et al*., 2009). Thus, the above-mentioned design parameters are used as a guide in the design of the proposed UVLS-SIPS algorithm.

The improvement over the existing UVLS schemes in the literature is in the use of wide area synchrophasor measurements as the protection element (trigger) to arm the UVLS-SIPS algorithm, rather than the use of measurements at the local bus. One of such wide area-based inputs is the status of the system operating state obtained from the DT-classifier described in Chapter Six. This was used rather than voltage thresholds as found in (Glavic and Van Cutsem, 2010; Vournas *et al*., 2010; Moors *et al*., 2000; Ingelsson *et al*., 1997; Berg and Sharif, 1994; Tuan *et al*., 1993; Taylor, 1992).

The proposed SIPS algorithm is a response-based centralised SIPS, and the amount of load to shed is adaptive (not pre-determined). Rather, it is calculated online based on the level of the prevailing disturbance. Also, the load buses to shed are not fixed. The load buses are chosen based on the effect of the disturbance on the voltage

profile at the load buses in the system and also according to the voltage stability index at the respective Voltage Control Areas (VCAs).

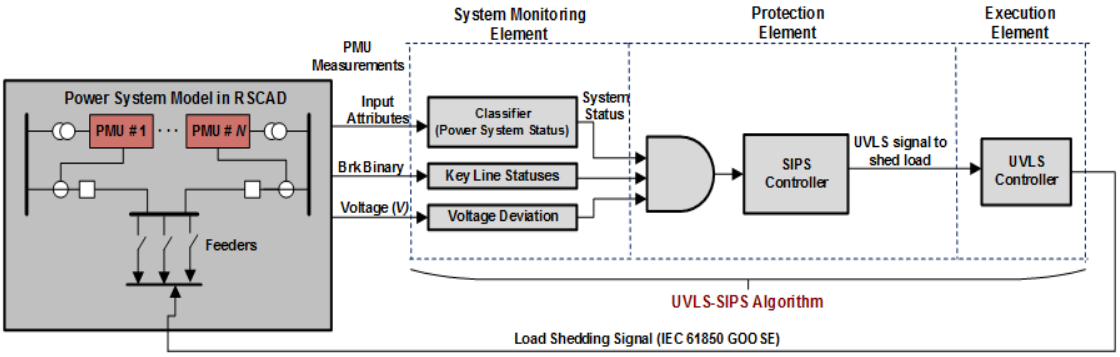

Figure 7.22: **Functional block diagram of the proposed UVLS-SIPS algorithm**

Figure 7.22 illustrates the functional block diagram of the UVLS-SIPS algorithm of the proposed method. The system monitoring element of the UVLS-SIPS algorithm performs the monitoring of the power system using the system status (obtained from the output of the DT-classifier), the phasor voltage magnitude deviation, and the breaker statuses of key transmission corridors or generators.

The protection element calculates the amount of system load to shed, the distribution of these loads across the VCAs and the determination of the load buses to shed within the VCAs based on the voltage profile at the load buses. The execution element performs the load shedding actions by opening the appropriate load breakers with the IEC 61850 GOOSE messages.

The design considerations for the proposed UVLS-SIPS method and algorithms include:

- Adaptivity of the load shedding algorithm to changing system operating conditions and disturbance level.
- Real-time calculation of the amount of load to shed at the various VCAs/load buses.
- Adaptive number of load shedding steps.
- Determination of the pick-up time before load shedding and the time delay between the load shedding steps.
- The time delay between load shedding steps should also allow adequate time for system response e.g. for generator field current to drop below OXL set-point limit, and for bus voltages to recover above the transformer ULTC voltage threshold.
- Ease of practical implementation in power systems.

7.5.2 Amount of Load to Shed in the Interconnected System

7.5.2.1 Derivation of the Amount to Shed

Many interesting methods (Glavic and Van Cutsem, 2010; Nikolaidis and Vournas, 2008; Otomega *et al*., 2007; Moors *et al*., 2001; Balanathan *et al*., 1998; Arnborg and Andersson, 1997; Tuan *et al*., 1994) have been proposed in the determination of the appropriate amount of load to shed in order to restore a voltage unstable system to an acceptable state with system parameters operating within the acceptable limits with no equipment overload.

Shedding fewer loads than required will obviously not be effective in mitigating the voltage instability. It may actually exacerbate the voltage instability and lead to system-wide voltage collapse/blackout. Conversely, shedding too much load might cause the system to transition from an under-voltage condition to an over-voltage condition. Generally, the determination of the amount of load to shed in most of the existing UVLS methods is based on the difference between the post- and pre-disturbance real power demand (Glavic and Van Cutsem, 2010; Balanathan *et al*., 1998; Feng *et al*., 1998; Arnborg *et al*., 1997).

This can be related to the P-V curve analysis method which is commonly applied in the industry. Figure 7.23 shows the P-V curve for a critical load bus (bus-8) in the New England 39-bus test system. If the system's current operating state is given as *Point A* for a base case (black plot), the system is secure, voltage stable, and far from the voltage collapse point indicated by the nose point (*Point B)*. For a generator contingency (G1 outage) indicated by the green plot, it can be seen that the system is operating at the nose point (*Point D*), and the system is insecure, voltage unstable, and some loads would need to be shed. The maximum loadability limit for a N-1 contingency is obtained as 5% from the nose point of the P-V curve using the criterion in (WECC, 2006). This is given as *Point C* on the green plot.

If the system recovery goal is to restore the system to a point where the system is secure and voltage stable, the minimum amount of load P_{shed} that needs to be shed is given as:

$$P_{shed} = P_A - P_C \tag{7.5}$$

where P_A and P_C are the real power loading at *Point A* and *Point C* respectively.

However, the above process would need to be carried out for a large number of load buses in the system and for various contingencies/system operating conditions. From

the foregoing, it can be seen that new methods that are suitable for online real-time application with less computation overhead are required.

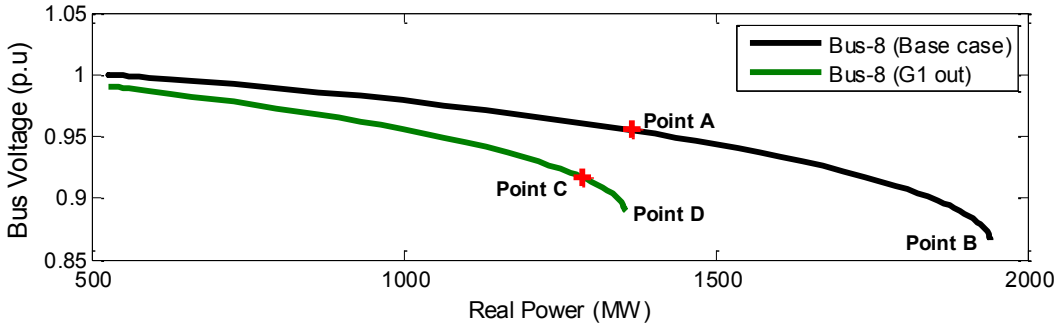

Figure 7.23: P-V curves for the New England 39-bus test system

A generator-based method is proposed in this thesis. For a practical network such as the WECC interconnected system reported in (CEC report, 2013), a 1:4 ratio of 3307 generators to 14324 high- and medium-voltage transmission lines was noted. This implies that less sensors/PMUs and computation is required for the proposed generator-based method. Also, the proposed method is measurement-based using real-time measurements from PMUs, while the P-V curve method is an offline process. The offline methods will give wrong results for system conditions different from the ones used in the offline design process.

This thesis proposes an adaptive UVLS method in which the calculation of the amount of load to shed is based on the computation of the reactive power imbalance in the network. The combinational methods by (Saffarian and Sanaye-Pasand, 2012; Ghaleh *et al*., 2011; Saffarian and Sanaye-Pasand, 2011) did not specify how the amount of load to shed was obtained. However, the use of the real power (MW) imbalance calculated using the System Frequency Response (SFR) model as used in (Tang *et al*., 2013; Seethalekshmi *et al*., 2011; Seyedi and Sanaye-Pasand, 2009a; 2009b) would fail for a purely voltage instability condition where the rate of change of frequency as a result of the disturbance is negligible.

The limitation of the SFR model for voltage stability-related algorithms was proven during the exploratory investigations carried out in this thesis using the 10-bus multi-machine equivalent system. Figures 7.24-7.26 show the real-time plots of the system frequency, ROCOF, real and reactive powers obtained for generators G2 and G3 respectively during a typical voltage instability scenario involving a line contingency, increased loading at Bus-8, and the dynamics of transformer ULTC action and generator OXL operation.

Similar results were obtained for the individual investigations relating to line contingency, increased loading, and the dynamics of transformer ULTC action and generator OXL operation respectively. From Figures 7.24-7.26, it can be seen that the system parameters and the generator parameters relating to the real power output were not affected by the system disturbance.

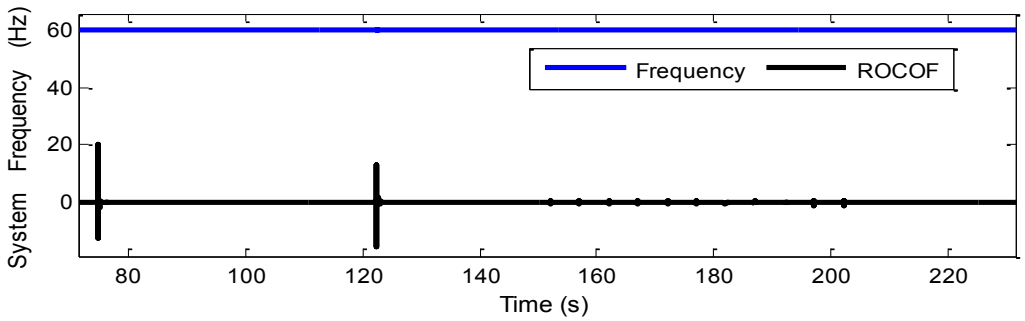

Figure 7.24: Plots of system frequency and ROCOF for an operating condition involving increased loading and line contingency

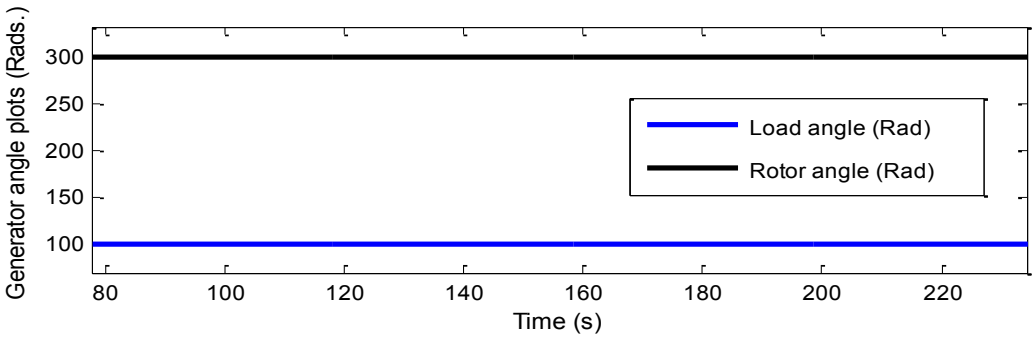

Figure 7.25: Plots of generator rotor and load angles for an operating condition involving increased loading and line contingency

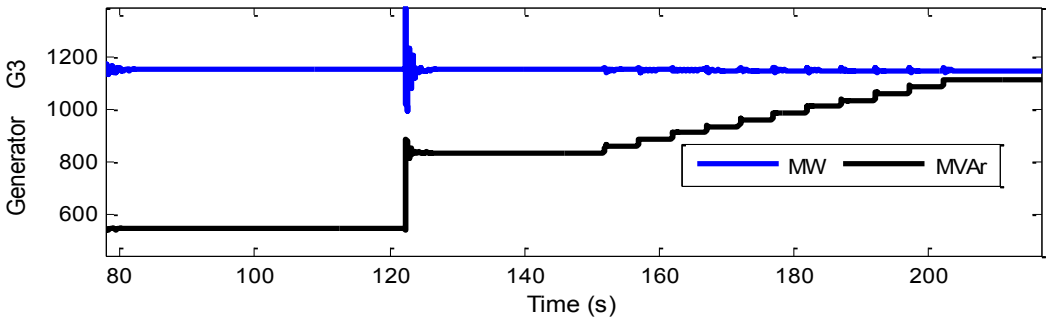

Figure 7.26: Plots of generator real and reactive powers for an operating condition involving increased loading and line contingency

This is because the real power generated by a synchronous machine will remain constant when it is controlled by a governor with a fixed mechanical torque set-point (Gong and Pinheiro, 2010). In view of the above, a reactive power (MVAr) deficit method is proposed in this thesis to calculate the appropriate amount of load to shed

in order to restore the system to an acceptable system operating margin. The proposed method is described below.

The reactive power mismatch of an ith synchronous generator at the kth operating time can be derived as:

$$\Delta Q_{gik} = Q_{gik} - Q_{gi0}, \quad i = \overline{1, N_g}, \quad k = 0, 1, 2, \ldots \tag{7.6}$$

where ΔQ_{gik} is the MVAr mismatch of the ith synchronous generator at the kth operating time, Q_{gi0} is the synchronous generator MVAr output at an initial steady-state condition, Q_{gik} is the synchronous generator MVAr output at the kth operating time.

The total MVAr deficit ΔQ_{gTk} from the entire synchronous generators in the system at the kth operating time can be approximated using:

$$\Delta Q_{gTk} = \sum_{i=1}^{N_g} \Delta Q_{gi} = \sum_{i=1}^{N_g} \left(Q_{gik} - Q_{gi0} \right), \quad k = 0, 1, 2, \ldots \tag{7.7}$$

where

$$Q_{gik} = -\frac{\left|\mathrm{V_{gik}}\right|^2}{X_{si}} \pm \sqrt{\frac{\left|\mathrm{V_{gik}}\right|^2 I_{fdik}^2}{X_{si}^2} - P_{gik}^2}, \quad k = 0, 1, 2, \ldots \tag{7.8}$$

$$Q_{gi0} = -\frac{\left|\mathrm{V_{gi0}}\right|^2}{X_{si}} \pm \sqrt{\frac{\left|\mathrm{V_{gi0}}\right|^2 I_{fdi0}^2}{X_{si}^2} - P_{gi0}^2} \tag{7.9}$$

ΔQ_{gTk} is the total MVAr deficit at the kth operating time, N_g is the number of generators in the system, Q_{gik} is the reactive power of the ith generator at the current operating point k, $|\mathrm{V_{gik}}|$ is the terminal voltage phasor magnitude of the ith generator at the current operating point k, X_{si} is the synchronous reactance of the ith generator, I_{fdik} and P_{gik} are the field current and the real power of the ith generator at the kth operating time respectively. I_{fdi0}, P_{gi0}, and Q_{gi0} are the field current, real power, and reactive power output of the ith generator at the initial operating point respectively.

For a system condition in which the reactive power demand is met by the reactive power sources in the system, the relationship between the change in the reactive power output ΔQ_{gTk} and the change in the reactive power demand ΔQ_{Lk} can be related as:

$$\beta_K \cdot \sum_{i=1}^{N_g} \Delta Q_{ik} - \sum_{l=1}^{N_l} \Delta Q_{Llk} = 0, \quad k = 0, 1, 2, \ldots \tag{7.10}$$

where β_K is a load factor relating ΔQ_{Tk} to ΔQ_L, N_l are the load buses where loads can be shed.

From the above, in order to restore the system to the initial operating condition or to an acceptable system operating point after a disturbance, the amount of load to shed at the operating time k can be given as:

$$Q_{shed,k} = \sum_{l=1}^{N_l} \Delta Q_{Llk} \ , \ k = 0,1,2,... \tag{7.11}$$

By substituting Equation (7.7) and (7.11) in Equation (7.10), Equation (7.12) is given as:

$$\beta_K \cdot \sum_{i=1}^{N_g} \Delta Q_{gik} - \sum_{l=1}^{N_l} \Delta Q_{Llk} = 0 \tag{7.12}$$

Therefore:

$$Q_{shed,k} = \beta_K \cdot \sum_{i=1}^{N_g} \Delta Q_{gik} \ , \ k = 0,1,2,... \tag{7.13}$$

$Q_{shed,k}$ are related to Q_{gTk} empirically using simulation results. The amount of the real power (MW) load to shed corresponding to the reactive power load shed is given as:

$$P_{shed,k} = \sum_{i=1}^{N} \tan^{-1}\left(\cos\left(power\ factor_{ik}\right)\right) \times \Delta Q_{gik}, \quad k = 0, 1, 2, \ldots \tag{7.14}$$

7.5.2.2 Amount of Load to Shed Per VCA

The total amount of load to shed as given by Equation (7.13) has to be further distributed amongst the VCAs in the power system. This thesis proposes an adaptive load distribution methodology based on the weighted summation RVSA index computed for each of the VCAs in the interconnected power system.

The vcaRVSA index for the jth VCA is computed as a sum of the corresponding RVSA indices of the area, and is given by Equation (4.35).

Therefore, the amount of loads to be shed in the jth VCA of a large interconnected power system with n numbers of VCAs is proposed as:

$$\Delta Q_{shed,VCA_{jk}} = \left(\frac{100 - vcaRVSA_{jk}}{100n - \left(\sum_{j=1}^{n} vcaRVSA_{jk} \right)} \right) \times Q_{shed,k}, \qquad j = \overline{1,n}, \ \ k = 0, 1, 2, \ldots \tag{7.15}$$

It should be noted that the computations in the first multiplier in Equation (7.15) are carried out using synchrophasors measurements obtained from PMUs. Thus, it can be seen that the amount of load to be shed can be calculated online in real-time using these synchrophasor measurements. Also, the proposed method is suitable for uncertainties since system losses, load type uncertainties, and the increase in the reactive demand is already accounted for in the $\beta_K \cdot \sum_{i=1}^{N_g} \Delta Q_{gik}$ term in Equation (7.15) above.

From the foregoing, it can be seen that fewer calculations are required for the generator-based adaptive under-voltage load shedding method proposed in this thesis for the amount of load to be shed. Also, the amount of load to shed can be calculated online in real-time using synchrophasor measurements from the PMUs. Furthermore, the proposed method can be applied for diverse system operating condition other than for increased system loading. In addition, it is suitable for uncertainties since system losses, load type uncertainties, and the increase in the reactive demand is already accounted for in the $\beta_K \cdot \sum_{i=1}^{N_g} \Delta Q_{ik}$ term.

7.5.3 Tuning of the Load Factor

The load factor in Equation (7.13) is calculated empirically using real-time simulations. The steps for this are proposed as given below:

i. For the base case at steady state system conditions, calculate β_K using Equation (7.13).
ii. Develop a series of load increase starting from the base case.
iii. Perform voltage stability assessment using Equation (4.35).
iv. For each unstable case in step (ii), empirically shed a percentage of the total reactive demand.
v. If voltage recovers and the post-load shedding system margin is acceptable, then calculate β_K using Equation (7.13).
vi. If the system does not recover after the reactive demand shedding, increase the percentage of the amount of the reactive demand to shed and repeat steps (iv)-(v) respectively.
vii. For contingencies and other system operating conditions, repeat steps (ii) to (vi) and calculate β_K.
viii. Develop a curve fitting model using the least squares fitting algorithm for the real-time prediction of the load factor β_K required in the calculation of the amount of reactive demand to shed.

A curve fitting model using the least squares fitting algorithm is proposed for the real-time prediction of the amount of load to shed based on the change in the reactive power mismatch in the power system. Typically, the least squares fitting method (Rawlings *et al*., 1998) provides an estimate of the model coefficients relating the predictor $\left(\sum_{i=1}^{N_g} \Delta Q_{ik} \right)$ in this case to the response $(Q_{shed,k})$ for various operating scenarios.

For a polynomial curve fitting application, the fitted output is given as (MATLAB Curve Fitting Toolbox, 2014; Rawlings *et al*., 1998):

$$y = \sum_{oc}^{d+1} p_{oc}\left(x^{d+1-oc}\right), \quad oc = \overline{1,(d+1)} \tag{7.16}$$

where y is the fit (output), d is the degree of the polynomial, $d+1$ is the order of the polynomial, P_{oc} is the oc^{th} polynomial of x, x is the predictor.

Equation (7.16) can be rewritten to relate the predictor $\left(\sum_{i=1}^{N}\Delta Q_{gik}\right)$ to the output $\hat{Q}_{shed}$ as given in (7.17):

$$\hat{Q}_{shed,k} = \sum_{oc}^{d+1} p_{oc}\left(\sum_{i=1}^{N} Q_{ik}^{d+1-oc}\right), \quad oc = \overline{1,(d+1)} \tag{7.17}$$

where $\hat{Q}_{shed}$ is the predicted fit of the amount of load to be shed.

The model coefficients of the least-squares fitting algorithm are calculated using the minimization of the sum of the squares of the residual error r_d as given in Equations (7.18)-(7.19):

$$\min_{P_{oc}} S = \sum_{d}^{np} r_d^2, \quad d = \overline{1,np} \tag{7.18}$$

$$\min_{P_{oc}} S = \sum_{d}^{np}\left(Q_{shed,d} - \hat{Q}_{shed,d}\right)^2, \quad d = \overline{1,np} \tag{7.19}$$

where np is the number of data points, r_p is the residual (error) of the dth data point, S is the sum of squares error, K_p is the actual output, while $\hat{K}_p$ is the fitted output.

The result of an exploratory investigation carried out using the New England 39-bus test system is shown in Figure 7.27. The models used in fitting the reactive power produced to the amount of reactive power loads to shed include the quadratic polynomial (poly2), cubic polynomial (poly3), quartile polynomial (poly4), fifth-degree (poly5) polynomial and exponential (exp1) models respectively.
From Figure 7.27, it can be seen that the best models were obtained using the quadratic polynomial and the exponential models respectively.

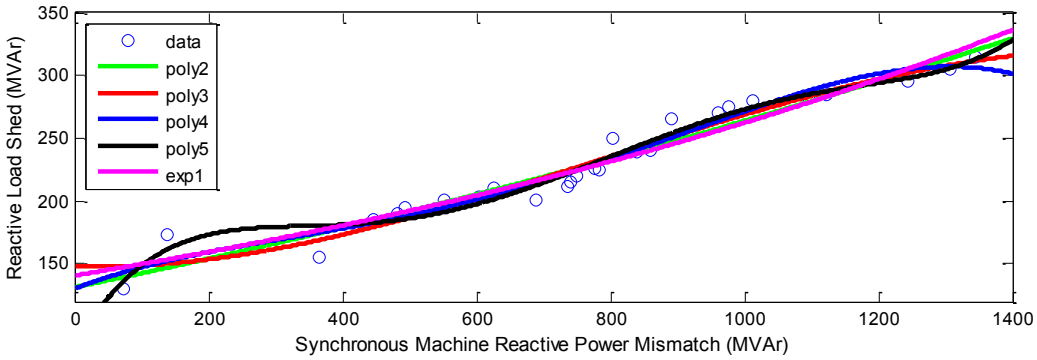

Figure 7.27: Least squares fitting using polynomial and exponential models

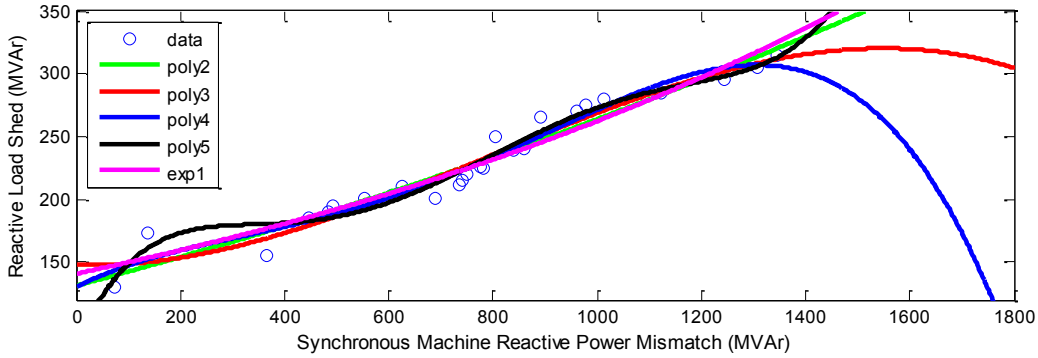

Figure 7.28: Prediction of new points using the polynomial and exponential models

The best models were selected using the prediction intervals, Sum of Squares Error (SSE) and the adjusted R-square statistics. Figure 7.28 shows the result obtained when the fitted curves were tested with new data. Figures 7.29-7.30 show the prediction intervals obtained using the quadratic polynomial model and the exponential model respectively. The MATLAB code for the curve fitting algorithm is given in Appendix G.

The fit equation for the quadratic polynomial obtained for the New England 39-bus test system is:

$$y = -2.288\times10^{-5}x^2 + 0.1096x + 131.4 \tag{7.20}$$

For the various points $k = 0, 1, 2, \ldots$, $x_k = \sum_{i=1}^{N}\Delta Q_{ik}$, $y_k = Q_{shed,k}$.

Therefore, the total amount of load to shed in the interconnected system in real-time is given by:

$$Q_{shed,k} = -2.288\times10^{-5}\left(\sum_{i=1}^{N}\Delta Q_{gik}\right)^2 + 0.1096\left(\sum_{i=1}^{N}\Delta Q_{gik}\right) + 131.4 \tag{7.21}$$

Equation (7.21) is used together with Equation (7.15) in order to determine the amount of load to be shed in the jth VCA at the kth operating point.

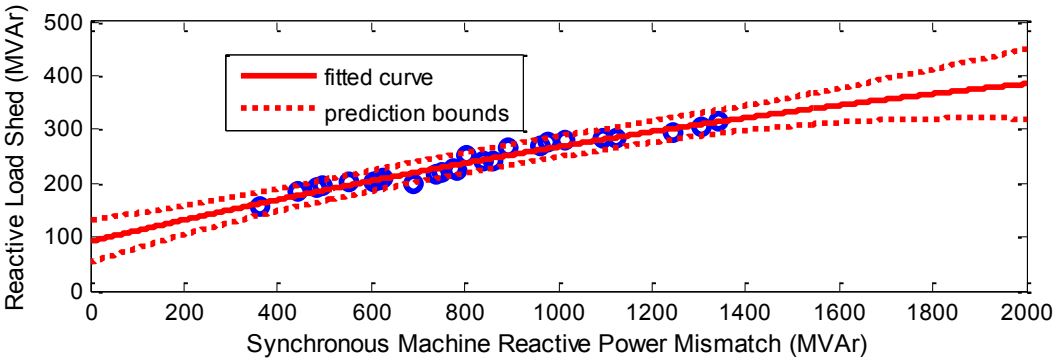

Figure 7.29: Prediction intervals for the quadratic polynomial model

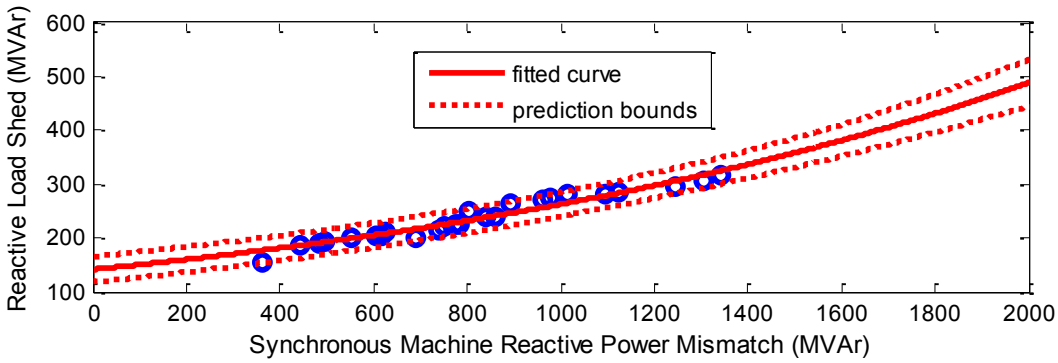

Figure 7.30: Prediction intervals for the exponential model

7.5.4 Where to Shed

Although, Nikolaidis *et al*. (2008) and Concordia *et al*. (1995) proposed the shedding of loads according to the local areas within a power system, this thesis extends this by proposing a methodology based on the reactive power deficit and a method for an adaptive multi-bus load curtailment at non-priority load buses within a VCA.

In each respective VCA, the load buses to shed are ranked in descending order based on their respective voltage dip information. This is because if loads are shed at the wrong places, this action might not bring about any improvement in the system margin or voltage profile as shown in (Affonso *et al*., 2004). The load buses with the highest voltage deviation/dip are selected and the amount of load to shed in that VCA is distributed at the selected load buses based on the computed value of their voltage deviation. It was assumed that 20% of the load at each feeder is a priority load.

Similar to what is obtainable in practical power systems, it was assumed that certain feeders are dedicated to priority loads which must not be curtailed. For example, the auxiliary supply to the Koeberg nuclear power station in South Africa is considered as the most important load in the entire power system, and therefore, not available for load shedding (RSA System Operation Code, 2010).

The $\Delta Q_{shed,VCAik}$ for the jth VCA is distributed among the non-priority load buses according to their voltage deviation value. The amount of load to shed ($\Delta Q_{shed,jBp}$) at the pth load bus within the jth *VCA* is proposed as:

$$\Delta Q_{shed,jBp} = w_{j\Delta VBp} \times \Delta Q_{shed,VCAjk} \tag{7.22}$$

where

$$w_{j\Delta VBpk} = \frac{\left|\Delta V_{jBpk}\right|}{\sum_{p}^{Nb_j}\left|\Delta V_{jBpk}\right|} = \frac{\left|V_{jp0}\right| - \left|V_{jpk}\right|}{\sum_{p}^{Nb_j}\left(\left|V_{jp0}\right| - \left|V_{jpk}\right|\right)} \tag{7.23}$$

where N_{bj} is the number of load buses in the jth *VCA*, $W_{j\Delta V_{Bpk}}$ is the weighted voltage deviation at the pth bus at the operating time k, $\left|\Delta V_{jBpk}\right|$ is the voltage phasor magnitude deviation at the pth bus at the operating time k, $|V_{jp0}|$ is the reference voltage at an initial steady-state condition, $|V_{jpk}|$ is the pth load bus voltage phasor magnitude at the kth operating time for the jth VCA.

It should be noted that unlike methods in (Tang *et al*., 2013; Seethalekshmi *et al*., 2011) where different formulations are required for large and small disturbances respectively, the proposed method in this thesis uses the same formulation for both large and small disturbances since Equation (7.15) eliminates all forms of uncertainties in the estimation of the reactive power deficit.

Also, from the above formulations, a non-priority load bus with a high voltage deviation value will have a large part of its load curtailed in the VCA. This implies that the VCA closest to the source of the disturbance would experience a larger portion of the load curtailment and the load bus closest to the disturbance would also experience a large part of the load curtailment compared to the other load buses in the VCA. In the event of a loss of generation in a local area, the proposed load shedding distribution prevents a heavy increase in transmission power flow that may occur as remote generators in other areas attempt to supply the loads within the vicinity of the disturbance.

Furthermore, the proposed method provides a procedure for distributing the amount of load to curtail amongst the VCAs in the system rather than concentrating the amount of load to be shed in just the local area where the disturbance is located. This distribution of load amongst the VCAs allows for system stability to be maintained. In addition, the distribution of loads to be curtailed across the VCAs helps prevent the formation of islands in the system, prevents line overloading (Concordia *et al*., 1995), and prevents overshedding at the local bus (Arnborg *et al*., 1997).

7.5.5 When to Shed

The decision on when to shed load(s) is based on a control logic comprising of the output of a DT-classifier supervised by the status of the ULTC-SIPS algorithm, the RVSA index, and the statuses of some key generators/transmission lines in the system. The use of voltage information only would result to loads being shed prematurely (Otomega and Van Cutsem, 2007). It is important not to shed the load too early. Adequate time should be allowed before load shedding in order to ascertain that the system is unquestionably tending towards collapse.

However, the shedding of loads must be timely. If not, more loads would need to be curtailed in order to restore the system to an acceptable operating state (Moors and Van Cutsem, 1999; Van Cutsem and Vournas 1998). A time delay of 3-10 s has been proposed for conventional UVLS schemes (WECC, 1999; Taylor, 1992). Multiple load shedding steps could be used in order to prevent the over-shedding of loads. The number of load shedding steps can range from 3-6 steps as used in (WECC, 1999).

The proposed UVLS-SIPS algorithm is a closed-loop process and would operate several times depending on the severity of the disturbance and the system response obtained. The first stage of the proposed UVLS-SIPS method is an instantaneous operation which occurs immediately the UVLS-SIPS execution element is armed. For the subsequent UVLS stages, intentional time delays are introduced. These time delays should be tuned to allow for sufficient time such that the system generators/controls are able to respond to the shed load, and also allow the transformer tap-changers to readjust their tap positions.

7.5.6 Proposed UVLS-SIPS Algorithm

The proposed UVLS-SIP algorithm is a wide area centralized response-based scheme supervised by events from key system parameters. Synchrophasor measurements from PMUs are used as the inputs to the system monitoring element of the proposed UVLS-SIPS algorithm, and they reflect the prevailing system condition including the system's response to a disturbance.

The trigger-type used is made up of the system status obtained from a DT-classifier, breaker statuses from the key transmission line corridors, and OXL status of the key generator in each VCA. This was done in order to ensure that the UVLS-SIPS algorithm does not operate for severe faults which are not related to the system's voltage stability.

The acceptable steady state operating point is taken as the operating point where all the system bus voltages are above 0.95 p.u., and none of the generators has reached their reactive power limit. It is assumed that maximum load that can be scheduled for load shedding in an emergency state at a non-priority load bus is 80%. This is in accordance with standard practice as reported in (Tuan *et al*., 1994).

The advantages of the proposed adaptive UVLS-SIPS algorithm are summarized below:

- A centralised response-based scheme using real-time measurements from actual IEEE C37.118 synchrophasor compliant devices is proposed.
- It computes the approximate amount of load required to be shed in real-time using the least squares fitting algorithm.
- An adaptive weighted distribution of the amount of load to shed amongst the VCAs is proposed.
- The proposed UVLS-SIPS algorithm adapts to the prevailing system conditions in the computation of the amount of load to shed.

The operation of the UVLS-SIPS algorithm is summarized in the flowchart given in Figure 7.31. The first stage of the UVLS-SIPS action is at the most critical VCA in the power system. Typically, this corresponds to the VCA closest to the source of the disturbance. This implies that this VCA would experience a larger portion of the load curtailment compared to the other VCAs. At the point of operation of the protection element of the UVLS-SIP, the total amount of load to shed $(Q_{shed,k})$ and its distribution across the VCAs $(\Delta Q_{shed,VCAjk} \quad j=\overline{1,n})$ in the system is memorized (latched). The memorized parameters are obtained from the array buffer of the PLC in which the moving averages computed for every 60 fps are stored. The measurements in the buffer are latched using a logic comprising of the system operating state, and the statuses of key generators/transmission lines.

For the subsequent load shedding stages, an on-delay timer is used to determine when the next load shedding stage is initiated across the remaining VCAs. The proposed UVLS-SIPS algorithm is a closed-loop process and would operate according to the severity of the disturbance and the system response. Therefore, intentional time delays need to be introduced for the subsequent load shedding stages.

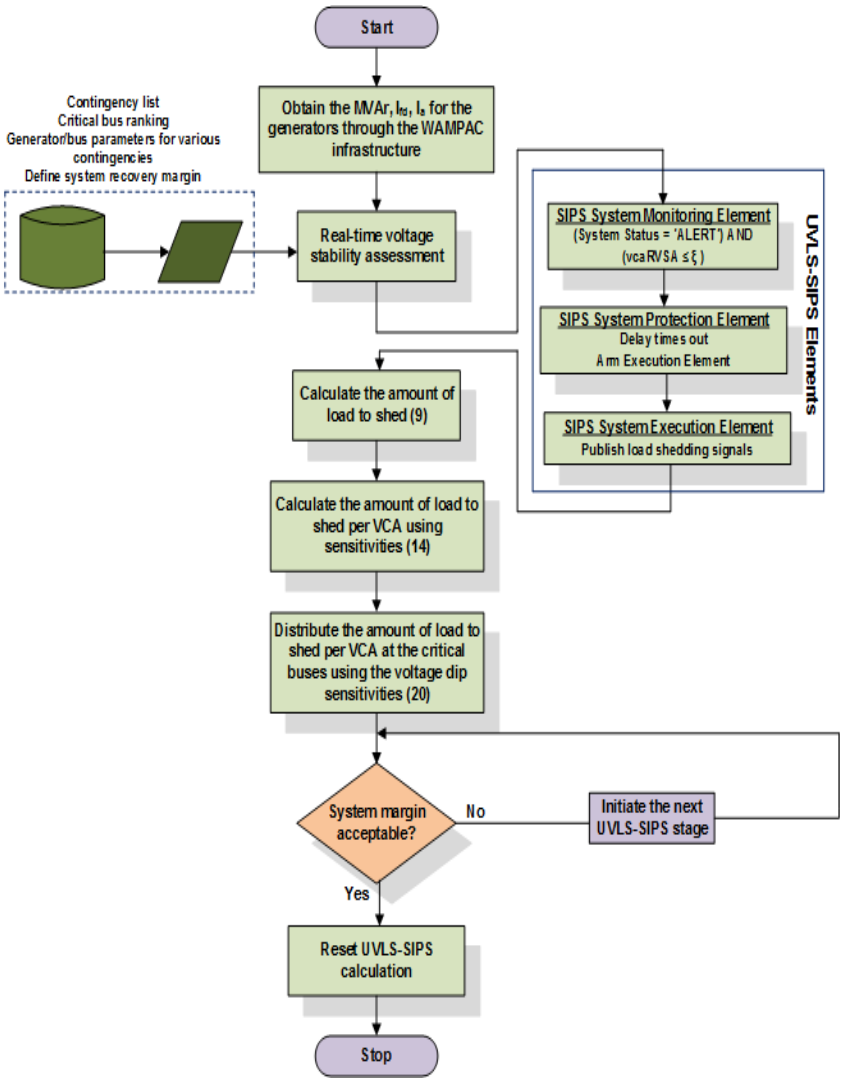

Figure 7.31: Flowchart of the proposed UVLS-SIPS algorithm

7.5.6.1 UVLS-SIPS Algorithm for Test System-1

The proposed adaptive UVLS-SIPS algorithm is first developed using the 10-bus multi-machine equivalent network (Test System-1) prior to scalability testing using the New England 39-bus test system. The mechanism of the voltage instability/voltage collapse was brought about using transmission line contingencies, transformer ULTC tap action, reactive power output limitation at the generator located at the local end, dynamic load model with exponential composition, and increased system loading condition.

It was observed that for constant impedance and constant current loads, the drop in voltage also resulted in a drop in the load demand. Therefore, using the methods proposed in (Glavic and Van Cutsem, 2010; Balanathan *et al.*, 1998; Feng *et al.*, 1998; Arnborg *et al.*, 1997) based on the difference between the post- and pre-disturbance real power demand would fail for undervoltage load shedding because of the characteristics of the various loads in the system.

In the proposed UVLS-SIPS method and algorithm, the reactive power mismatch caused by the disturbance is calculated using Equation (7.13). Also, the calculation of the voltage deviation at the critical buses is done using Equation (7.22). The system monitoring element of the implemented UVLS-SIPS method uses PMU measurements from the synchronous machines, load buses, and the status of the power system. The system's operating status ('Stable', 'Alert', or 'Unstable') is predicted using a real-time DT-classifier. When the logic of the system monitoring element is 'True' *{(System operating state = 'Alert') AND (vcaRVSA ≤ ξ)}*, the protection element is activated. The execution element of the UVLS-SIPS is armed by the output signal from the UVLS-SIPS protection element after the pickup time elapses. The threshold (*ξ*) of the *vcaRVSA* index and time delay were obtained from studies carried out to be 10% and 3 s respectively.

The load buses in the RSCAD draft model were divided into outgoing feeders as obtainable in typical power systems where the loads are supplied by the distribution feeders connected to substation transformers. These loads are segmented from the feeders using RSCAD Circuit Breakers (CBs) models *(if_rtds_sharc_sld_BREAKER)*. Since there are only two load buses in the Test System-1, it is assumed that the two loads at bus-8 and bus-11 are within the same voltage control area because they have similar response to the system dynamics.

The SEL-3378 SVP was configured to publish onto the Ethernet network a Fast Operate (FO) Remote Bit (RB) 'set' output corresponding to each of the outgoing load feeders. External IEDs (SEL-421 and SEL-451 IEDs) served as substation switchyard I/Os by subscribing to the RB 'set' signal(s) issued by the SEL-3378 SVP, and then publish the IEC 61850 GOOSE messages to open the corresponding CB models in the RSCAD software. The SEL-3378 SVP was configured to publish a RB 'clear' output to clear the load shedding binary (high) signal during the system restoration phase.

In order to publish or subscribe to the IEC 61850 GOOSE messages, a GTNET component is used within the RSCAD model to carry out the definition and formatting of the IEC 61850 GOOSE messages. The IEC 61850 GOOSE messages were then subscribed to or published onto the network via a RTDS-GTNET card loaded with the GSE protocol. The red highlight in Figure 7.18 shows the RSCAD setup used in the IEC 61850 implementation of the load shedding.

The RTDS GTNET-GSE card subscribes to the IEC 61850 GOOSE messages from the PMUs (which served as the switchyard I/O for the conversion of the FO signals to IEC 61850 GOOSE messages). The RTDS GTNET-GSE card was also configured to publish the status of the CBs for the load buses after the load shedding.

Seven case studies comprising of transmission line outage, increased loading, and possible scenarios of unavailability of UVLS control signals were investigated.

Case Study 1

The first case study carried out was a voltage collapse scenario without under voltage load shedding by the UVLS-SIPS algorithm. The loss of one of the transmission lines between buses-6 and -7 was simulated. This resulted to a large drop in the sub-transmission and distribution buses, and the operation of the transformer ULTC at bus-11. A 5% increase in the system loading condition every 60 s from the defined base case (load level-2) coupled with the tap action of the transformer ULTC every 5 s, and the operation of the OXL at generator G3 resulted to a voltage collapse condition.

Figure 7.32 shows the voltage profiles at the distribution network buses during the steady state condition and at the point of voltage collapse respectively. Figure 7.33 shows the real-time plots of the bus voltages and generator field currents. The system parameters before and after the contingency are given in Tables 7.6-7.7.

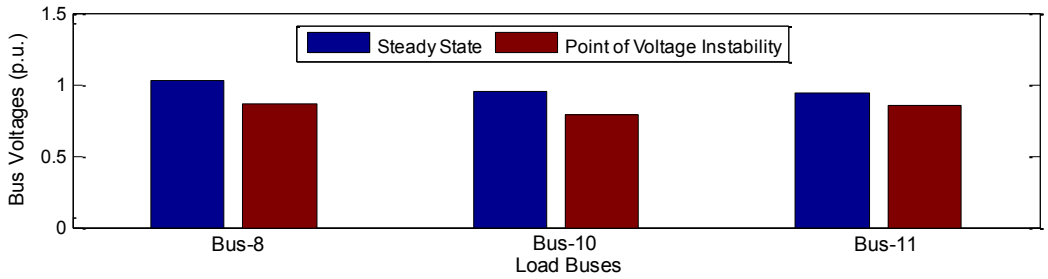

Figure 7.32: **Voltage profile for selected buses during the steady state condition and at the point of voltage instability for Case Study 1**

Table 7.6: **Generator parameters for Case Study 1**

Measurement instant	G2 Ifd (p.u.)	G3 Ifd (p.u.)	G2 (MVAr)	G3 (MVAr)	G2 Ia (A)	G3 Ia (A)
Steady-state	2.4446	1.9951	98.0434	544.616	73707.2	51426.1
Nose Point	3.0200	2.6506	1123.21	957.894	88537.2	65449.2

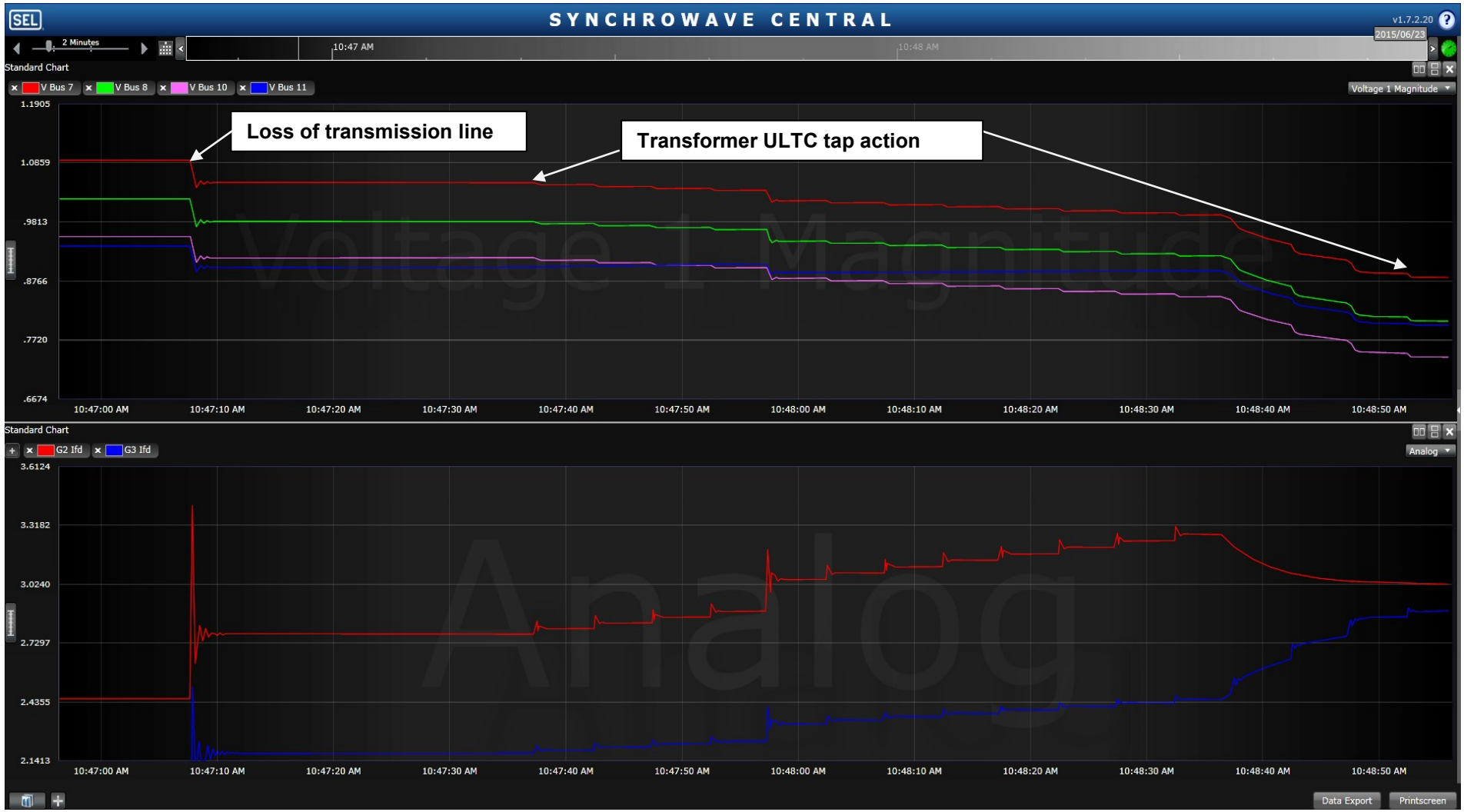

Figure 7.33: Real-time plots of the key system parameters for Case Study 1

Table 7.7: Stability indices for generators G2 and G3 in Case Study 1

Measurement instant	RVSAIfd2 (%)	RVSAIfd3 (%)	RVSAIa2 (%)	RVSAIa3 (%)	RVSAQ2 (%)	RVSAQ3 (%)
Steady-state	30.916	39.4241	23.0533	40.3893	93.202	69.7071
Nose Point	7.1274	25.432	7.5716	24.1344	17.4721	46.8427

Case Study 2

The second case study carried out is the simulation scenario described in Case Study 1 with the addition of the UVLS-SIPS algorithm. The amount of load (Q_{shed}) to be shed at buses-8 and -11 was obtained in real-time using Equation (7.15). The amount of load shed is 90.12 MVAr and 89.80 MVAr at buses-8 and 11 respectively. The corresponding real power was also shed alongside the reactive power. The results obtained for the bus voltages and the wide area RVSA indices are shown in Figure 7.34.

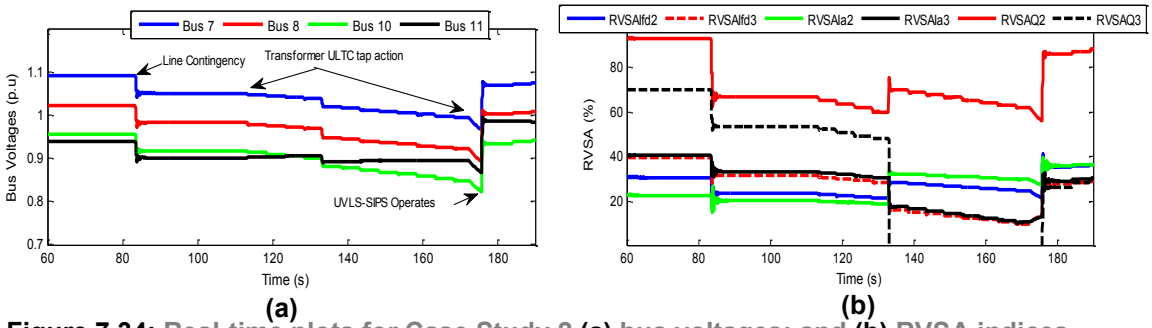

Figure 7.34: Real-time plots for Case Study 2 **(a)** bus voltages; and **(b)** RVSA indices

The system parameters at the point of operation of the UVLS-SIPS algorithm and after the UVLS-SIPS operation can be seen in Figure 7.34. The voltage profiles at the distribution network buses during the steady state condition, before UVLS-SIPS operation, and after UVLS-SIPS operation are shown in Figure 7.35.

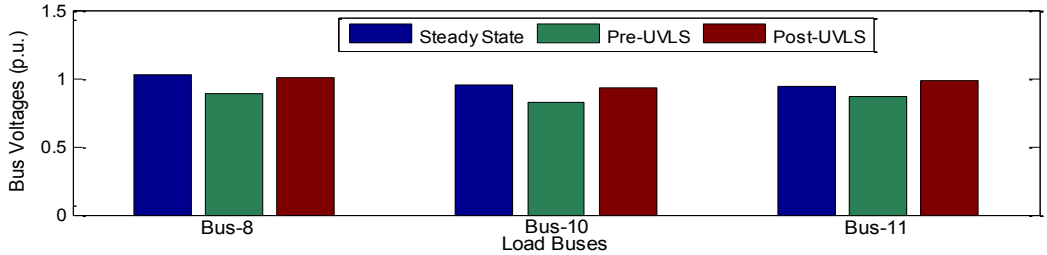

Figure 7.35: Voltage profile for selected buses during steady state condition, before UVLS-SIPS operation, and after UVLS-SIPS operation for Case Study 2

Case Study 3

This case study investigated a partial load shedding scenario for Case Study 2. The UVLS-SIPS signal to bus-11 was made to fail by disconnecting the Ethernet connection to the switchyard I/O (SEL-451) for bus-11, and only the amount calculated to be shed at bus-8 (90.12 MVAr) was carried out. Figure 7.36 shows the real-time plots obtained during the real-time simulation of the case study.

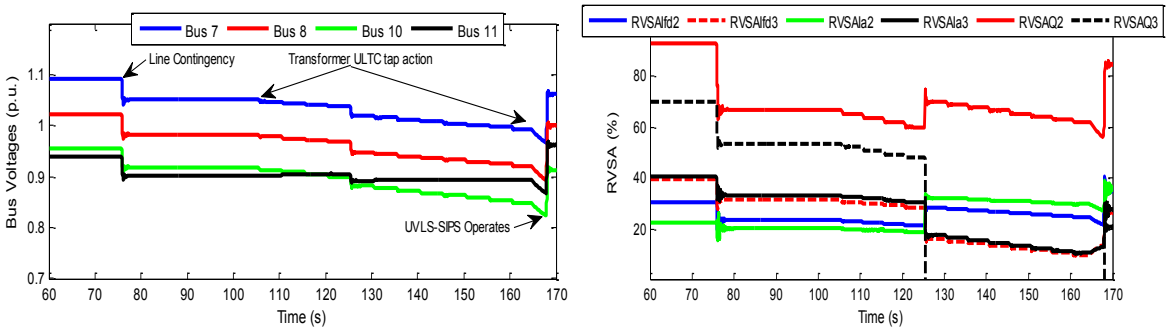

(a) **(b)**

Figure 7.36: **Real-time plots for Case Study 3 (a) bus voltages; and (b) RVSA indices**

Results show that even with just a single load shedding action at bus-8, the system recovered to an acceptable level of ±10% of the nominal bus voltage at all the system buses. However, further load increase would certainly push the system to its voltage collapse state. Thus, partial load shedding does not give system security. Figure 7.37 shows the voltage profiles at the distribution network buses during the steady state condition, before UVLS-SIPS operation, and after UVLS-SIPS operation respectively.

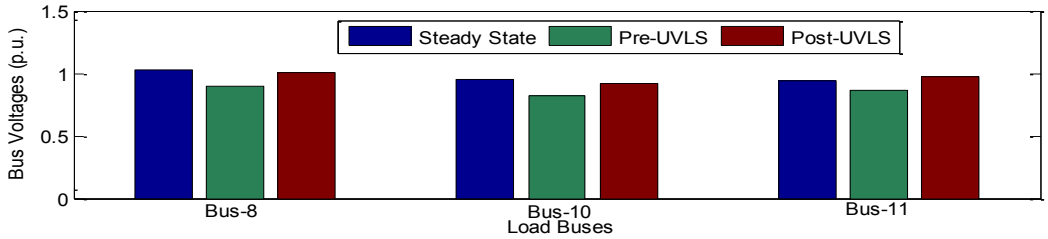

Figure 7.37: **Voltage profile for selected buses during steady state condition, before UVLS-SIPS operation, and after UVLS-SIPS operation for Case Study 3**

Case Study 4

Case Study 4 investigated a similar scenario to Case Study 3. A partial load shedding scenario whereby the UVLS-SIPS signal to bus-8 failed and only the amount calculated to be shed at bus-11 (89.80 MVAr) was carried out. Figure 7.38 shows the plots obtained during the real-time simulation of the case study.

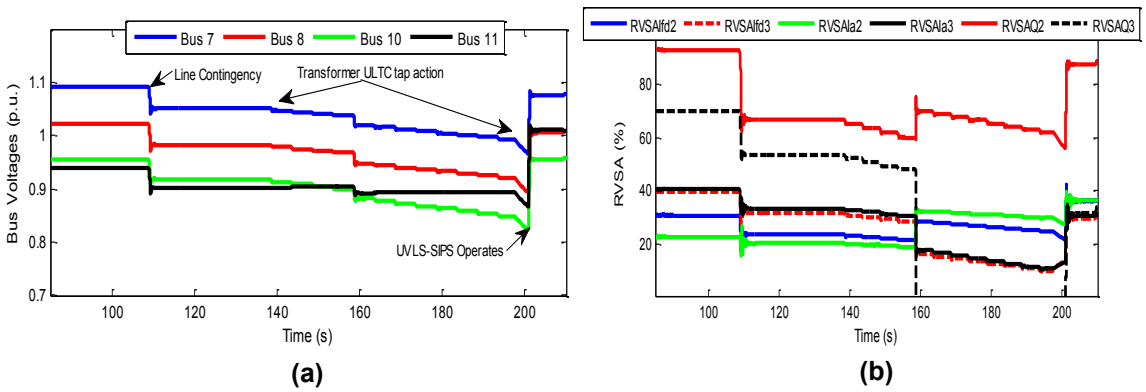

Figure 7.38: Real-time plots for Case Study 4 **(a)** bus voltages; and **(b)** RVSA indices

The results obtained showed an acceptable system recovery. Further load increase would push the system to its voltage collapse state because adequate system security is not obtained with partial load shedding. The voltage profiles at the distribution network buses during the steady state condition, before UVLS-SIPS operation, and after UVLS-SIPS operation are shown in Figure 7.39.

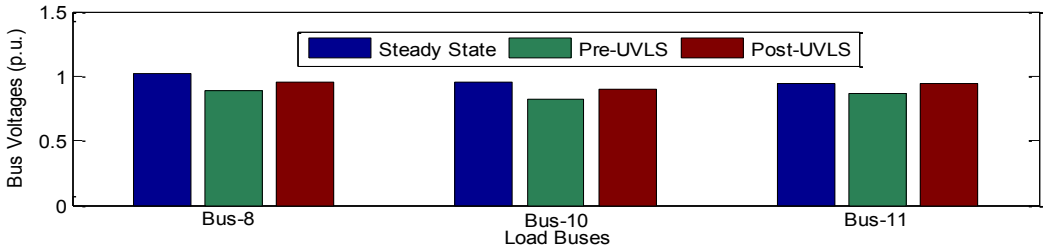

Figure 7.39: Voltage profile for selected buses during steady state condition, before UVLS-SIPS operation, and after UVLS-SIPS operation for Case Study 4

Case Study 5

Case Study 5 presents a scenario whereby only 50% (45.06 MVAr) of the amount calculated for load shedding at bus-8 was carried out, while no load was shed at bus-11. From Figure 7.40, it can be seen that the system did not recover totally from the voltage instability.

Further contingencies would certainly result to a system collapse. The voltage profiles at the distribution network buses during the steady state condition, before UVLS-SIPS operation, and after UVLS-SIPS operation are shown in Figure 7.41.

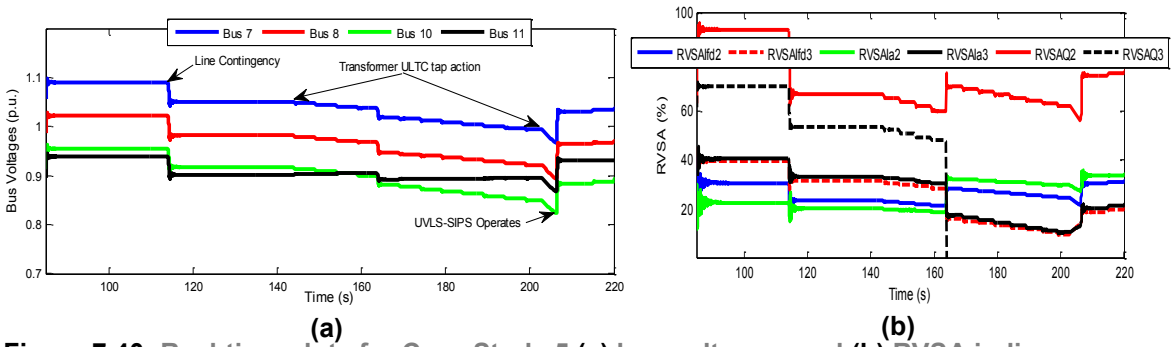

(a) (b)

Figure 7.40: Real-time plots for Case Study 5 **(a)** bus voltages; and **(b)** RVSA indices

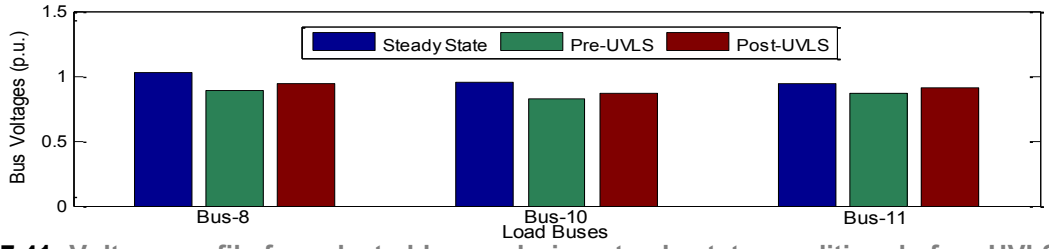

Figure 7.41: Voltage profile for selected buses during steady state condition, before UVLS-SIPS operation, and after UVLS-SIPS operation for Case Study 5

Case Study 6

Similar to Case Study 5, an operating scenario whereby only 50% (44.90 MVAr) of the amount calculated for load shedding at bus-11 was carried out with none shed at bus-8 was investigated in Case Study 6. Figure 7.42 shows the real-time plots obtained for this case study.

The system did not recover totally and further contingencies would result to a system collapse. Figure 7.43 shows the voltage profiles at the distribution network buses during the steady state condition, before UVLS-SIPS operation, and after UVLS-SIPS operation respectively.

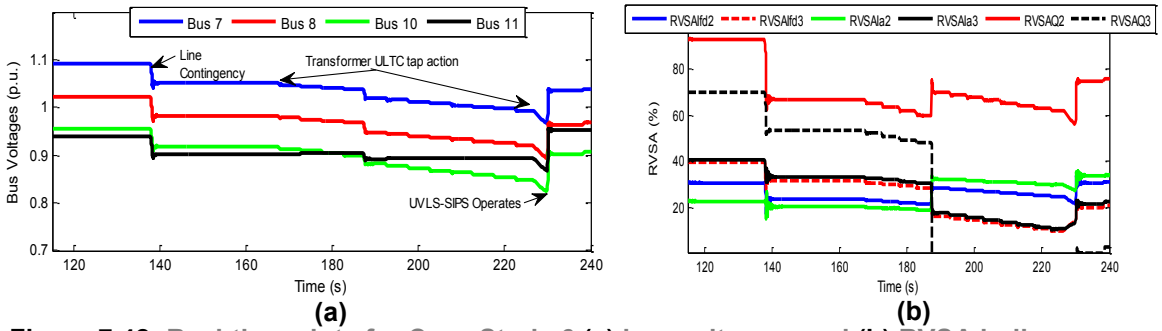

(a) (b)

Figure 7.42: Real-time plots for Case Study 6 **(a)** bus voltages; and **(b)** RVSA indices

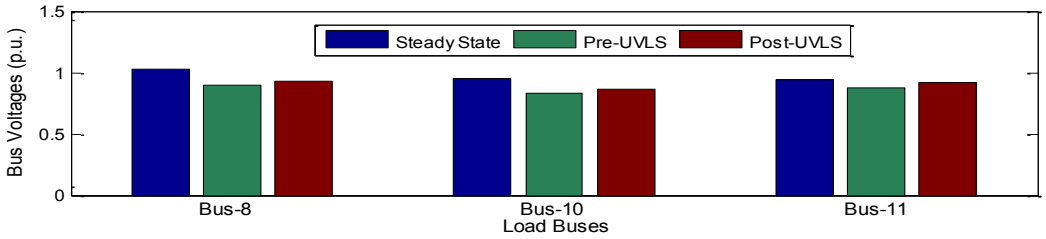

Figure 7.43: **Voltage profile for selected buses during steady state condition, before UVLS-SIPS operation, and after UVLS-SIPS operation for Case Study 6**

Case Study 7

Case Study 7 used the simulation scenario described in Case Study 1 for comparison of the proposed UVLS-SIPS algorithm with the conventional undervoltage (27) load shedding protective relay scheme. Undervoltage relays are placed at buses-8 and -10 (HV-side of the ULTC transformer) respectively, and their pickup voltage is set to 0.95% of their nominal values. The amount of load to shed was fixed at 5% of the total system load. This corresponds to 51.5 MVAr at bus-8 and 49.25 MVAr at bus-11.

The real-time plots obtained are given in Figure 7.44. From Figure 7.44, it was observed that the convention undervoltage protective relaying resulted in more loads being shed compared to the proposed UVLS-SIPS algorithm. Also, even though the voltage magnitude at bus-8 was still within technically acceptable range, the undervoltage protective relay operated because the pickup voltage was reached.

Figure 7.45 shows the voltage profiles at the distribution network buses during the steady state condition, before relay operation, and after relay operation respectively. From Figure 7.45, an over-voltage condition occured at bus-11 as a result of the operation of the undervoltage relay at bus-10.

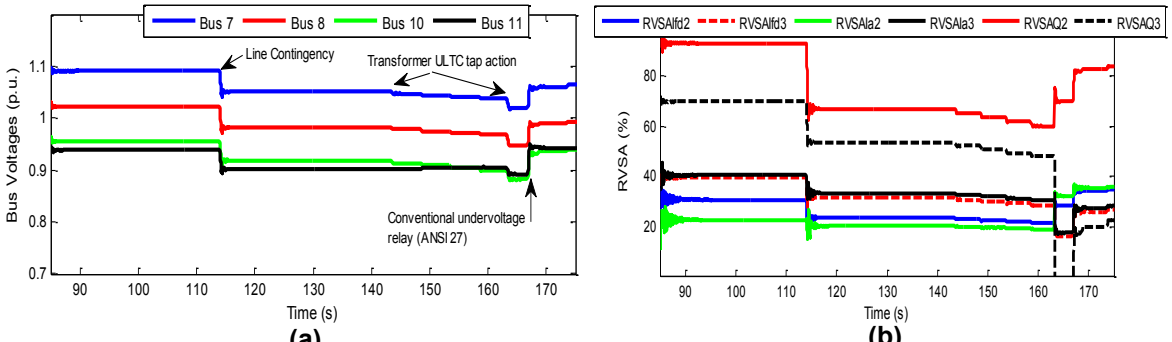

Figure 7.44: **Real-time plots for Case Study 7 (a) bus voltages; and (b) RVSA indices**

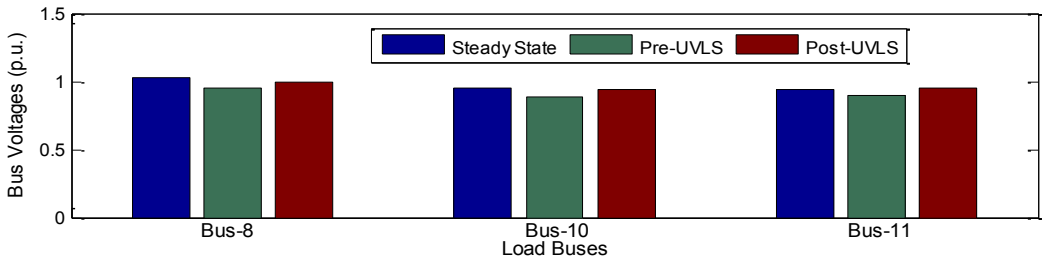

Figure 7.45: Voltage profile for selected buses during steady state condition, before UVLS-SIPS operation, and after UVLS-SIPS operation for Case Study 7

7.5.6.2 Discussion for Test System-1

The results obtained for Case Study 1 showed a voltage collapse scenario caused by the combination of the loss of transmission line(s), increased loading condition, transformer ULTC taps, and the operation of the generator protection limiters (over-excitation field current limiters).

From Case Study 2, it was observed that about 9.1% of the total system loading of 1986 MVAr was shed. This effectively restored the system to a secure operating condition where further load increase or contingency did not immediately result in the system becoming stressed. The load shedding mitigated the voltage collapse recorded in Case Study 1. For Case Study 3 where the calculated amount of load to shed was only carried out partially at bus-8, the system recovered, but the system was susceptible to instability if there was a further occurrence of any contingency/increase in the load demand.

In the case of a partial load shedding at bus-11 as shown in Case Study 4, the system failed to recover. Low bus voltages and RVSA indices were obtained compared to Case Studies 2 and 3 respectively. In Case Studies 5 and 6, the impact of partial load shedding was presented. The amount of load shed was equivalent to 25% of the total amount required to be shed. This action did not result in a secure operating condition.

Case Study 7 presented the results obtained using conventional undervoltage (27) protective relays with a fixed amount of load to shed. The conventional undervoltage relay operated earlier compared to the proposed UVLS-SIPS algorithm since a fixed voltage threshold was used in the former. Acceptable operating conditions were obtained. However, an over-voltage condition occured at bus-11 as a result of the operation of the undervoltage relay at bus-10.

Also, for certain scenarios such as the loss of 2 transmission lines, the conventional undervoltage protective relay will respond too early by shedding 5% of the load at bus-11, while bus-8 still had a voltage magnitude above its pickup point. This would result to partial load shedding and could further aggravate the instability. Table 7.8 presents a comparison of the voltage at bus-8 obtained for Case Studies 1-7 before and after load shedding. From Table 7.8, it can be seen that the ULTC-SIPS action successfully restored the voltage at load bus-8 to ± 10% of its nominal steady state values for Case Studies 2, 3, and 7.

Table 7.8: Comparative analysis of the voltage at bus-8 for all case studies

Case Study	Steady State Voltage (A)	Voltage Before UVLS-SIPS Operation (B)	Voltage Before UVLS-SIPS Operation (C)	Percentage Deviation (%) (C-A)
1	1.022	No load shed	No load shed	No load shed
2	1.022	0.8933	1.0025	1.9080
3	1.022	0.8938	1.0064	1.5264
4	1.022	0.8933	0.9512	6.9275
5	1.022	0.8932	0.9396	8.0626
6	1.022	0.8975	0.9313	8.8747
7	1.022	0.9502	0.9899	3.1409

The proposed UVLS-SIPS algorithm was shown to be adaptive and responsive to the level of the prevailing disturbance in the power system without using voltage thresholds, and did not result in an overvoltage condition at bus-11 compared to what was obtained in Case Study 7.

7.5.6.3 UVLS-SIPS Algorithm for Test System-2

The New England test system was partitioned using the proposed measurement-based clustering algorithm with each VCA having their respective reactive power sources providing voltage control at the respective load buses. Only the critical loads within the VCAs are considered for load shedding. The justification for this is obtained from practical use cases where the lightly loaded feeders/buses are usually dedicated to priority loads.

In most cases, it is often difficult for these lightly loaded priority buses to become critical. Therefore, the candidate location to shed within a VCA should be the heavily loaded/critical buses. The red highlight in Figure 7.46 shows the RSCAD IEC 61850 variable names used in subscribing to the load shedding signals emanating from the PLC (SEL-3378 SVP). The UVLS-SIPS elements used are similar to that implemented for Test System-1. The threshold (ξ) of the *vcaRVSA* index and time delay were obtained

from exhaustive simulations as 10% and 3 s respectively. Details of the results obtained for each case study investigated are given below:

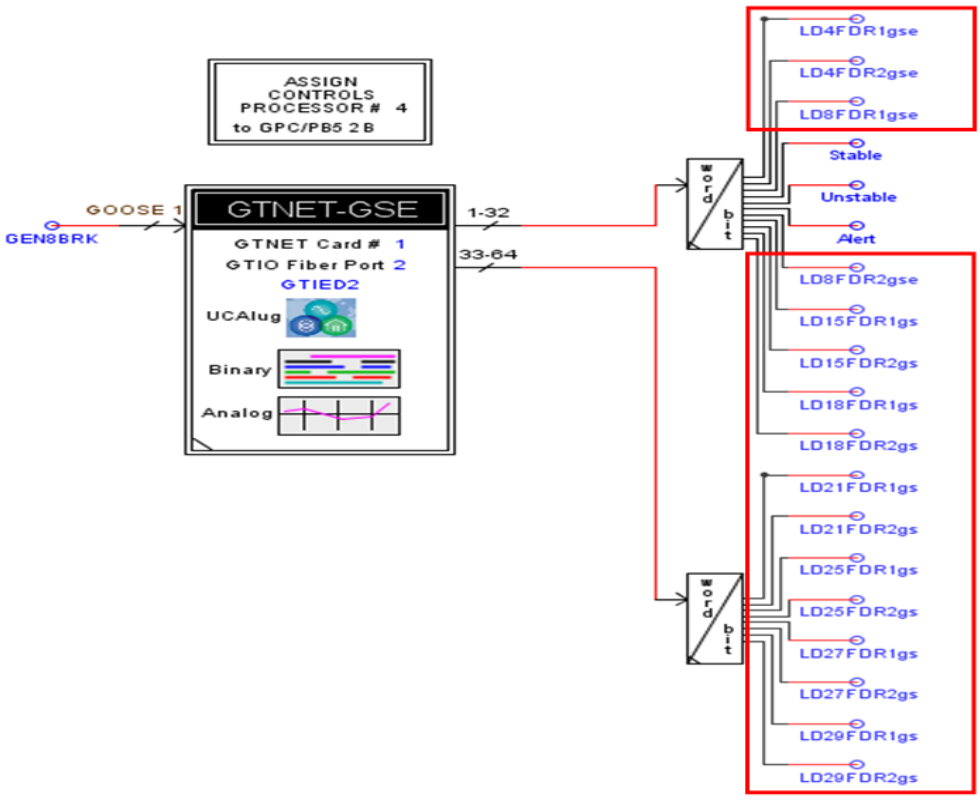

Figure 7.46: **Input/output configuration of the RTDS-GTNET IEC 61850 GSE component**

Case Study 1

The first case study carried out was a small disturbance voltage collapse scenario without the operation of the proposed UVLS-SIPS algorithm. This was brought about by an increased loading condition at load buses-4, -7, -8, and -12 in the most critical coherent area (VCA-2). If no countermeasures are initiated, the system collapsed just after the fourth load increase.

Figures 7.47-7.48 show the plots of the synchrophasor voltage magnitude at some load buses, and the RVSA indices of the system. Figure 7.48b shows a comparative plot of the voltage profile at some of the key load buses before and at the point of voltage collapse.

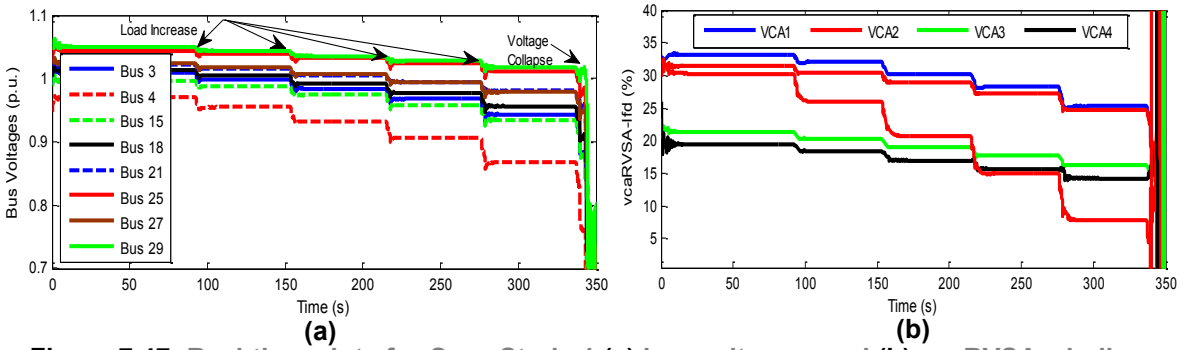

(a) (b)

Figure 7.47: Real-time plots for Case Study 1 **(a)** bus voltages; and **(b)** $vcaRVSA_{Ifd}$ indices

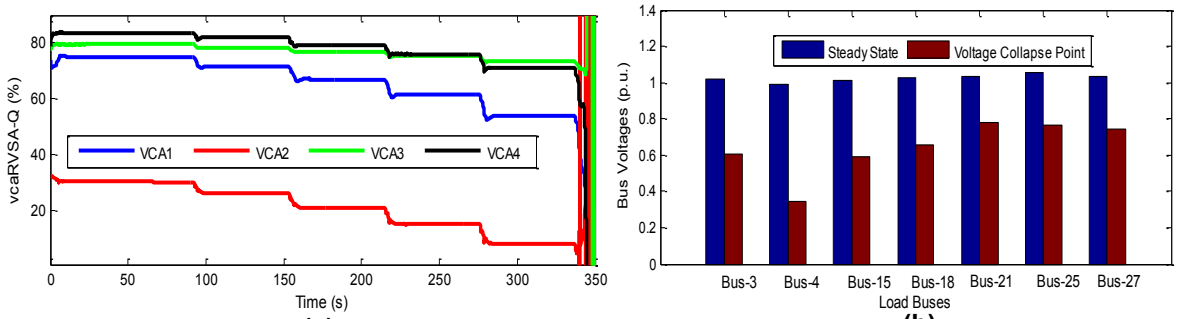

(a) (b)

Figure 7.48: Real-time plots for Case Study 1 **(a)** $vcaRVSA_Q$ indices; and **(b)** voltage profile for selected buses

Case Study 2

The second case study carried is the simulation of the small disturbance voltage stability scenario described in Case Study 1 with the addition of the proposed UVLS-SIPS algorithm. As the system became stressed and moved towards voltage instability, the signal to arm the UVLS-SIPS algorithm was automatically issued by the system monitoring element to the protection element of the UVLS-SIPS.

The amount of load to be shed (Q_{shed}) was calculated by the POUs running in the PLC (SEL-3378 SVP) using Equation (7.13). Only a single stage UVLS-SIPS action was required and 89.78 MVAr of load was shed in the most stressed VCA (VCA-2). Figures 7.49-7.50 show the real-time plots obtained for Case Study 2. The remedial action was successful. Therefore, no further loads were shed in the other VCAs. A comparative plot of the voltage profile at the load buses during the steady state condition, before the UVLS-SIPS operation, and after the UVLS-SIPS operation is shown in Figure 7.50b.

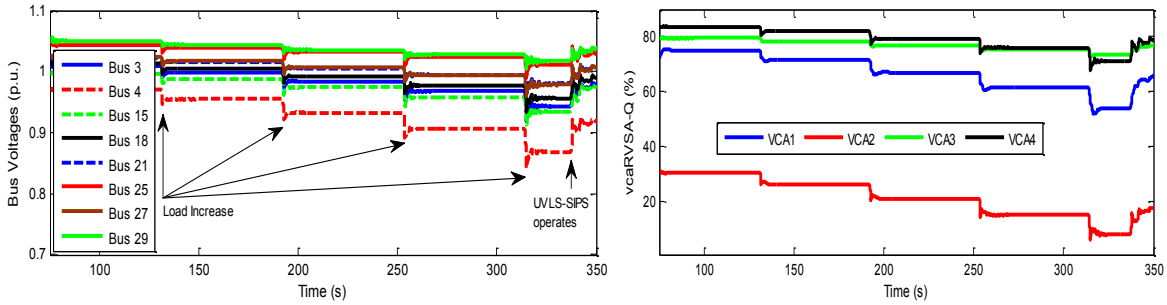

Figure 7.49: Real-time plots for Case Study 2 (a) bus voltages; and (b) $vcaRVSA_{lfd}$ indices

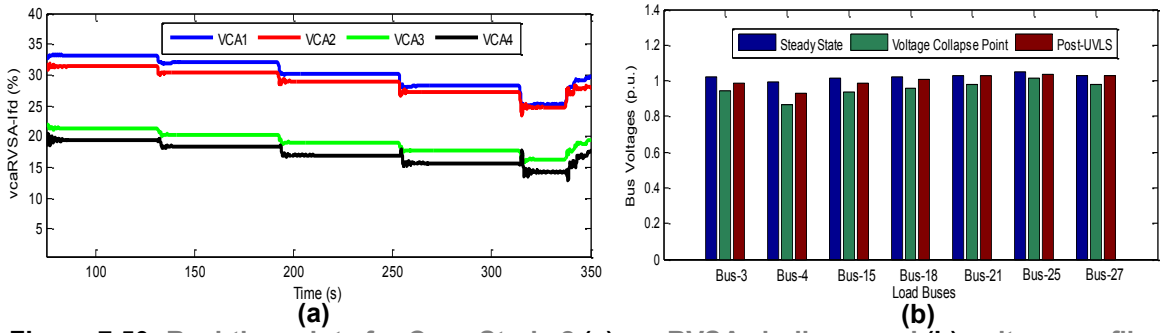

Figure 7.50: Real-time plots for Case Study 2 **(a)** $vcaRVSA_Q$ indices; and **(b)** voltage profile for selected buses

Case Study 3

This case study simulates a heavy loading condition where all the load buses in the system are loaded simultaneously by 5% every 60 s. The two initial UVLS-SIPS stages initiated did not lead to full system recovery. Thus, three stages of the UVLS were required at three of the VCAs before the system recovered to an acceptable voltage and RVSA index as shown in Figure 7.51-7.52.

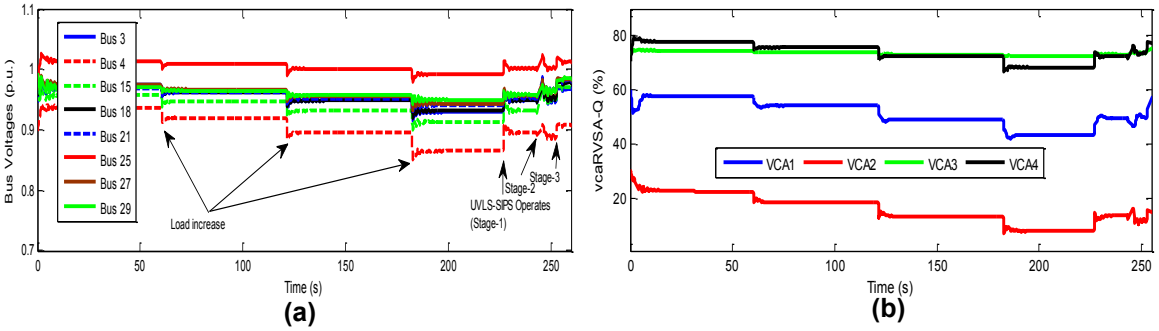

Figure 7.51: Real-time plots for Case Study 3 **(a)** bus voltages; and **(b)** $vcaRVSA_{lfd}$ indices

The total load shed was 256.88 MVAr at VCA-2, VCA-3, and VCA-1 consecutively. The voltage profile at the load buses during the steady state condition, before the UVLS-SIPS operation, and after the UVLS-SIPS operation is shown in Figure 7.52b.

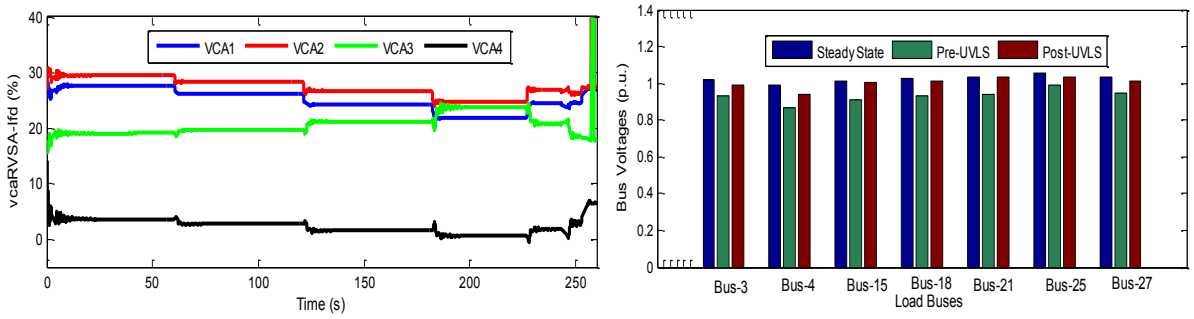

(a) (b)

Figure 7.52: Real-time plots for Case Study 3 **(a)** $vcaRVSA_Q$ indices; and **(b)** voltage profile for selected buses

Case Study 4

A N-2 line contingencies (line 5-6, line 14-15) was simulated alongside an increased loading condition at buses-4, -7, -8, -12 in VCA-2. The UVLS-SIPS was automatically triggered and the calculated amount of load to shed was curtailed. Two stages of UVLS-SIPS action were consecutively carried out at VCA-2 and VCA-3 respectively. The results obtained are shown in Figures 7.53-7.54.

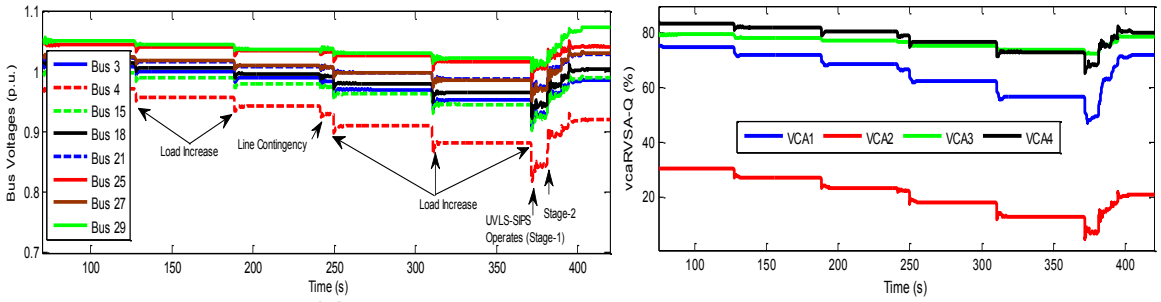

(a) (b)

Figure 7.53: Real-time plots for Case Study 4 **(a)** bus voltages; and **(b)** $vcaRVSA_Q$ indices

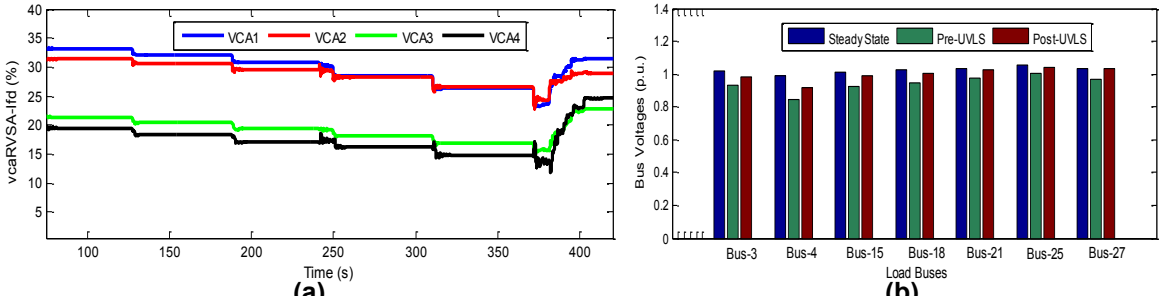

(a) (b)

Figure 7.54: Real-time plots for Case Study 4 **(a)** $vcaRVSA_{lfd}$ indices; and **(b)** voltage profile for selected buses

From Figure 7.53, it can be seen that after the first UVLS-SIPS action (Stage-1), the voltage magnitude at bus-4 and the RVSA index did not recover and were below the

acceptable values defined as ±5% of the nominal values. Thus, an additional UVLS-SIPS stage (Stage-2) was automatically initiated. A total of 141.92 MVAr of load was shed. The voltage profiles at the distribution network buses during the steady state condition, before the UVLS-SIPS operation, and after the UVLS-SIPS operation are shown in Figure 7.54b.

Case Study 5

The effect of the limitation of the reactive power produced by the synchronous generators through the operation of their Over-Excitation limiters (OXLs) has been highlighted in preceding Chapters. Case Study 5 investigates the impact of the OXLs of the synchronous generators on the proposed UVLS-SIPS algorithm. The operating scenario in Case Study 1 was used. Figure 7.55a shows the result obtained without the action of the UVLS-SIPS algorithm. The system collapsed just after the second load increase. Figure 7.55b and Figure 7.56 shows the results obtained when the UVLS-SIPS algorithm was initiated to mitigate the voltage collapse.

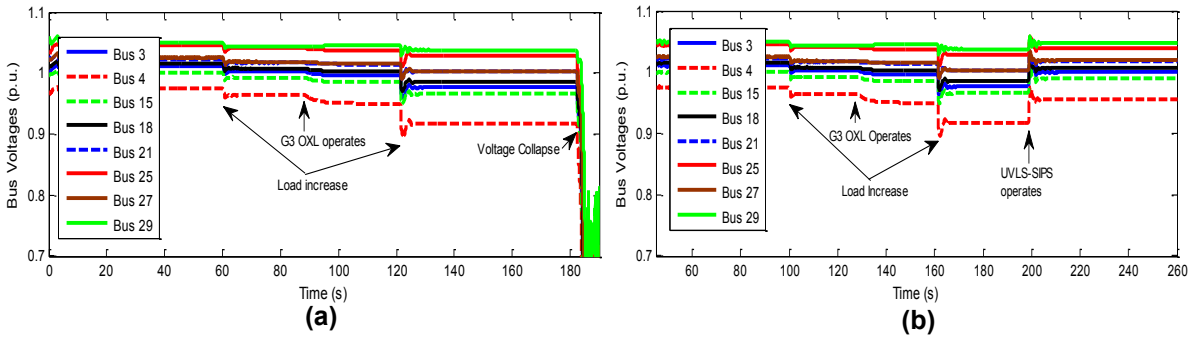

Figure 7.55: Real-time bus voltage plots for Case Study 5 **(a)** without UVLS-SIPS; and **(b)** with UVLS-SIPS

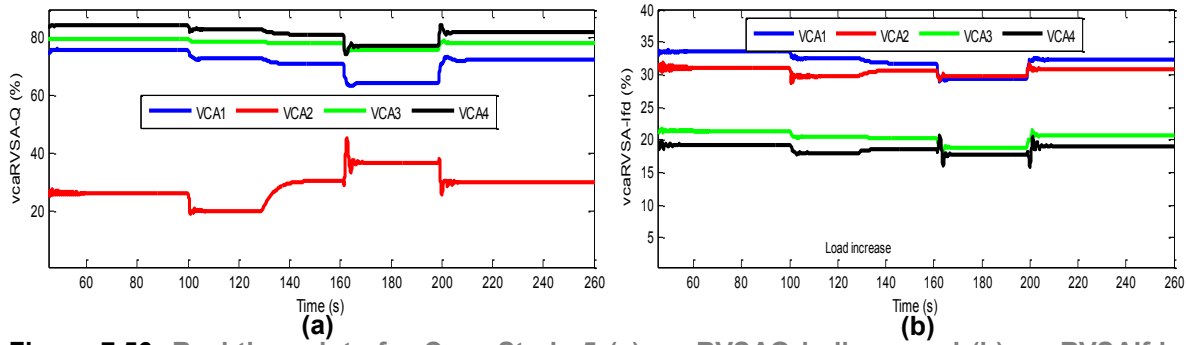

Figure 7.56: Real-time plots for Case Study 5 (a) vcaRVSAQ indices; and (b) vcaRVSAIfd indices

It can be seen that the voltage collapse occurred faster compared to that of Case Study 1. This is as a result of the operation of the OXL at generator G3. From the results obtained, it can be seen that the system collapsed while the bus voltages were well

above the 0.9 p.u. margin. As a result of this, the UVLS-SIPS algorithm would have to be initiated fast before the system condition transitions into an unstable state.

One way of adapting the proposed UVLS-SIPS algorithm for fast voltage collapse scenario like the one presented in this case study is to include the statuses of the synchronous generator OXLs as one of the triggers for arming the proposed UVLS-SIPS algorithm. A single stage UVLS-SIPS action with a total of 71.0 MVAr was shed in VCA-2. The voltage profiles at the distribution network buses during the steady state condition, before the UVLS-SIPS operation, and after the UVLS-SIPS operation are shown in Figure 7.57.

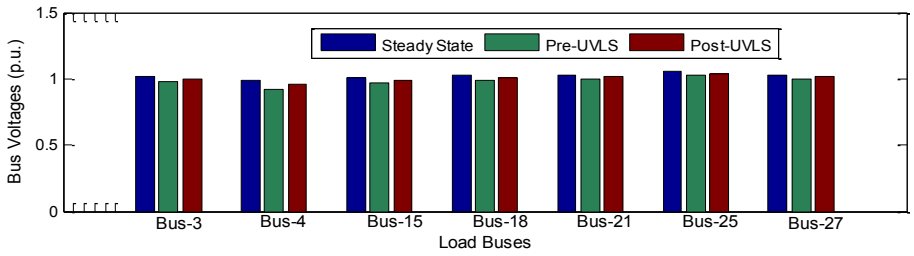

Figure 7.57: **Voltage profile for selected buses for Case Study 5**

Case Study 6

Case Study 6 investigates a N-2 generator contingency whereby an outage of generator G7 was followed by the outage of generator G6 after 30 s. This brought about an increase in the field current (reactive power generated) of the other generators in the same RPRB-3 with generators G6 and G7) as shown in Figure 7.58.

An increase in the field current (Figure 7.58b) of the generators in the neighbouring RPRB-2 for VCA-2 was also observed. Without the proposed UVLS-SIPS, the voltage collapse occurred as a result of the action of the generator OXL protection at generator G3 which limited the field current of the generator to the acceptable limit. The ramping down of the field current at generator G3 by its OXL triggers the loss of voltage control, and the system collapse occurred as a result of the inability of the generators in the system to provide the required reactive power support. The operation of the UVLS-SIPS method successfully led to an acceptable level as shown in the voltage profile and RVSA index plots given in Figures 5.59-5.60. The total load shed was 211.42 MVAr at VCAs-3 and -2 respectively.

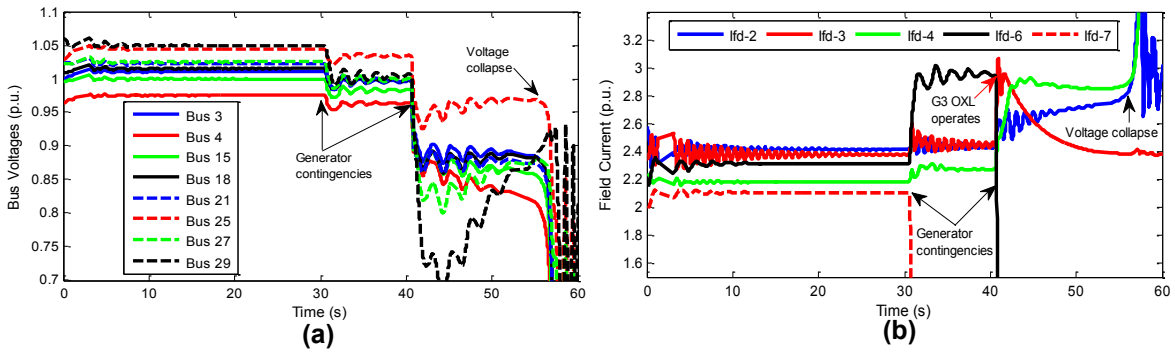

Figure 7.58: Real-time plots for Case Study 6 **(a)** Bus voltages; and **(b)** generator field currents with UVLS-SIPS

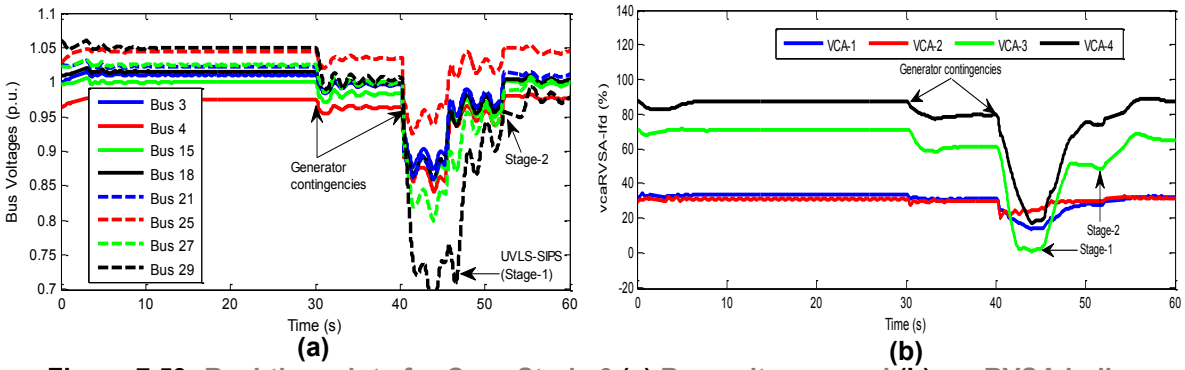

Figure 7.59: Real-time plots for Case Study 6 **(a)** Bus voltages; and **(b)** vcaRVSA indices derived from the reactive power reserve on the synchronous generators

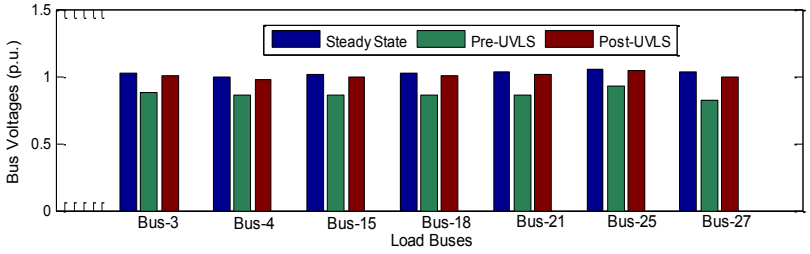

Figure 7.60: Voltage profile for selected buses for Case Study 6

Case Study 7

The conventional UVLS scheme was compared to the proposed UVLS-SIPS algorithm. In the conventional UVLS scheme, undervoltage (27) protective relays are installed at the critical load buses in the network. The pick-up voltage settings, time delay settings, and the amount of load to shed are fixed. The loads to be shed by these relays are also fixed to the load feeders to which they are connected to, and cannot be selected adaptively.

Analysis was carried out on the load buses using P-V curves. The buses are ranked according to their voltages and reactive power margin. The load buses with the lowest voltages are selected as the critical buses and are used as the monitoring buses for the

conventional UVLS protective relays. The requirement was that adequate amount of load is shed in order to ensure that the bus voltages and system margin recover after a disturbance. In this regard, various amounts of loads were shed at different buses. Different combinations of load curtailment and amount of load to shed based on the results of the P-V and V-Q analyses were also studied.

The undervoltage elements of the protective relay at the load buses operate (trips) whenever the bus voltage falls below the predetermined threshold for more than the pre-determined time delay. The threshold to use can be determined using the values obtained from the P-V curve analysis. The recommendation in (WECC, 1999) was used. Based on this, the voltage corresponding to 5% margin from the nose point of the P-V curve for the worst N-2 contingency was obtained. A time delay between 3-10 s was recommended in (WECC, 1999; Taylor, 1992). Experimentation was carried out to select the optimal time delay within this range. Also, the number of load shedding steps (3-5 steps) recommended in (WECC, 1999; Taylor, 1992) was adopted. The voltage pick-up was recommended as 8-15% of the lowest steady-state voltage magnitude (Taylor, 1992).

Case Study 7 uses the same operating scenario considered in Case Study 1. The UVLS-SIPS was replaced with the conventional undervoltage (27) protective relays. It is required that the protective relays are placed at pre-selected critical buses (buses-4, 7, 8, 12, 15, 20) and configured with a pickup setting of 0.95% of their nominal values for stage 1 load shedding. The undervoltage protective relays shed a fixed amount of loads at the pre-specified buses at a fixed voltage threshold. Since the bus voltages at buses-4 and 8 are the first to reach their pickup values, two external protective relays (SEL-421 and SEL-451) were configured for this case study and were placed at buses-4 and -8 respectively. Due to the constraints in external low voltage amplifiers, additional threshold-based protective relay function blocks were implemented in the PLC (SEL-3378 SVP) to shed the load at buses-7, 12, 15, 20 respectively.

From the results shown in Figures 7.61-7.62, it can be seen that the protective relay at bus-8 will be the first to operate. This resulted in the UVLS relay issuing a trip signal to the circuit breaker located at bus-8. The voltage profiles at the distribution network buses during the steady state condition, before relay operation, and after relay operation are shown in Figure 7.62b. A total of 315.2 MVAr of load was shed.

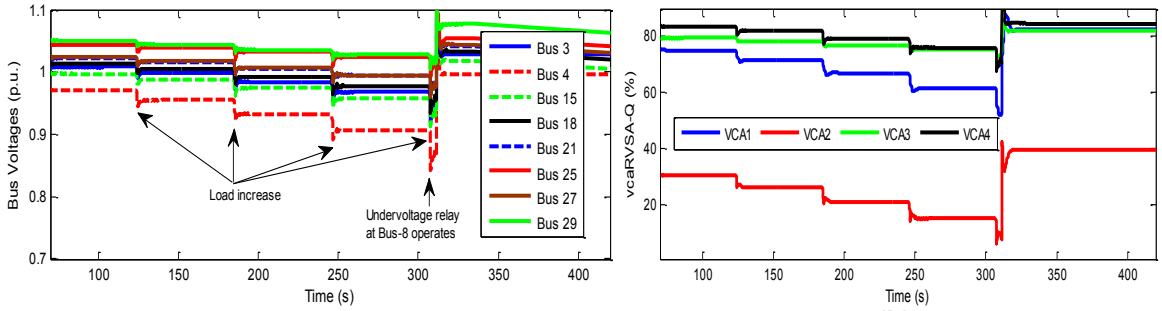

(a) **(b)**

Figure 7.61: Real-time plots for Case Study 7 **(a)** bus voltages; and **(b)** $vcaRVSA_Q$ indices

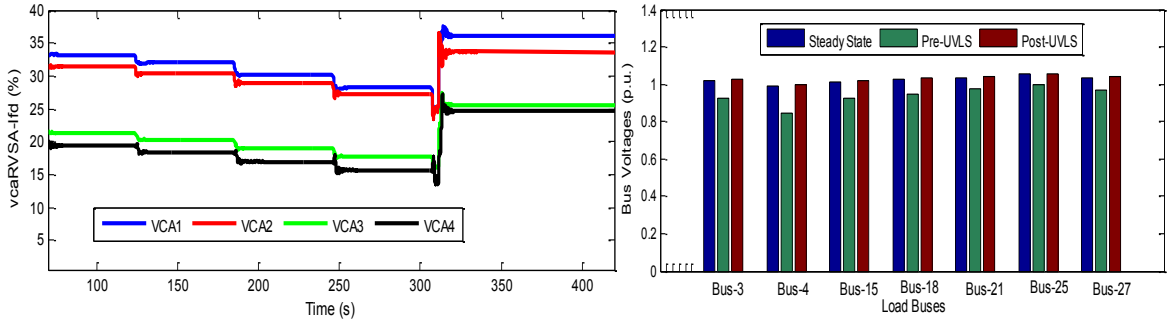

(a) **(b)**

Figure 7.62: Real-time plots for Case Study 7 **(a)** $vcaRVSA_{Ifd}$ indices; and **(b)** voltage profile for selected buses

7.5.6.4 Discussion for Test System-2

The case studies investigated validate the proposed UVLS-SIPS methodology, and it was shown to give better results compared to that obtained using the existing distributed undervoltage protective relaying. Table 7.9 presents a comparison of the bus voltages obtained for Case Studies 1-7 before and after load shedding. From Table 7.9, it can be seen that the UVLS-SIPS action successfully restored the voltage at load bus-4 to less than ± 10% of its nominal steady state values.

Table 7.9: Comparative analysis of the voltage at bus-4 for all case studies

Case Study	Steady State Voltage (A)	Voltage Before UVLS-SIPS Operation (B)	Voltage Before UVLS-SIPS Operation (C)	Percentage Deviation (%) (C-A)
1	0.9928	No load shed	No load shed	No load shed
2	0.9928	0.8680	0.9302	6.3054
3	0.9928	0.8650	0.9366	5.6608
4	0.9928	0.8455	0.9194	7.3932
5	0.9928	0.9170	0.9556	3.7469
6	0.9928	0.8566	0.9770	-1.5915
7	0.9928	0.9430	0.9955	-0.2719

For Case Study 7, the protective relays operated based on fixed thresholds and shed a fixed percentage of the total load at the load bus. It was observed that the undervoltage

relay at bus-8 operated early even when the voltages at the other buses were still within acceptable limits. Since a fixed percentage of the load at bus-8 was shed, this resulted in an over-voltage condition in the system. This resulted in 22.7% over-shedding and a system-wide over-voltage condition as shown in Figure 7.62b.

7.6 Chapter Summary

Real-time hardware-in-the-loop simulations were carried out with the developed WAMPAC 'proof-of-concept' testbed for testing the proposed methods and algorithms developed in this thesis. Results are presented for the real-time voltage assessment algorithm, the ULTC-SIPS algorithm, and the UVLS-SIPS algorithm respectively. The application of the proposed synchrophasor-based transformer ULTC-SIPS control in preventing further deterioration of the system voltages by blocking further tap actions of the transformer ULTC was demonstrated. A new trigger-type based on the combination of the system operating state, ULTC transformer voltage, the status of the generator OXL of the key generator, and IEC 61850 GOOSE messages is proposed for arming the ULTC-SIPS protection element in this thesis.

Also, a centralized response-based UVLS-SIPS algorithm was proposed in this Chapter. The design methodology used for the proposed UVLS-SIPS algorithm was discussed. A procedure for the identification of the loads to shed per VCA in the system was presented. Also, a least squares calculation method based on synchrophasor measurements was proposed for the calculation of the amount of load to shed in the system. The amount of load to shed per VCA was calculated adaptively using the RVSA weight per VCA. The load buses to shed in each VCA are adaptively selected based on the voltage deviation computed in each VCA.

Chapter Eight presents an investigation on the structure of the synchrophasor measurements from actual PMU devices, and their comparison with the specification given in the IEEE C37.118 standard. Also, the impact of pervasive (adverse) wide area communication network conditions on the synchrophasor measurements published by the substation PMUs to the PDCs at the control centre is investigated. The pervasive conditions considered are latency, jitter, packet losses and random noise.

CHAPTER EIGHT

PERFORMANCE EVALUATION OF IEEE STD. C37.118-BASED COMMUNICATION NETWORK IN THE DEVELOPED WAMPAC TESTBED

8.1 Introduction

The importance of the communication networks used in the implementation of the protection, automation, and control schemes in power systems cannot be over-emphasized. This Chapter presents the communication transport layer protocols for the streaming of the IEEE C37.118 synchrophasor measurements. Also, details on the communication network for the developed WAMPAC testbed are discussed.

In order to build an effective communication network, a comprehensive evaluation of the bandwidth requirement for various communication transport protocols was carried out. Also, an investigation of the synchrophasor message structure from PMUs from various Original Equipment Manufacturers (OEMs) was conducted. Furthermore, the impact of communication degradation caused by pervasive (adverse) communication network conditions due to the network latency, jitter, packet loss, and random noise on the developed WAMPAC testbed was investigated using a Wide Area Network (WAN) emulator in a software-in-the-loop simulation with the developed WAMPAC testbed.

8.2 Communication Protocol

The transmission of synchrophasor measurements from PMUs to PDCs can be done via serial communication protocols and by using Ethernet-based communication protocols. The serial communication protocol is via RS232 serial communication, while the Ethernet communication protocols can be the User Datagram Protocol (UDP) or Transmission Control Protocol (TCP) respectively. The UDP is a connectionless protocol whereby the source broadcasts the data to the destination Internet Protocol (IP) address without handshaking and predetermining the transmission channel. Also, the source does not verify if the data was received at the destination or not. As a result of this, the UDP provides low overhead in the delivery of the data. However, an error-free data transmission is not guaranteed.

The TCP protocol is a connection-oriented, full-duplex protocol whereby a handshaking process takes place between the source and the destination nodes, and the data is only transported upon the determination and acknowledgement of an end-to-end connection

between the source and the destination. If some packets are not received, a request to re-transmit is sent by the destination. Typically, the TCP guarantees an error-free data transmission through checksum and packet re-ordering.

In comparison, the UDP protocol has 8 bytes of overhead in the application layer encapsulation header, while the TCP protocol has an overhead of 20 bytes. Although, the TCP protocol is more secure, the added security introduces latency which makes the UDP protocol faster.

Four types of messages are defined in the IEEE Std. C37.118. These include data, configuration, header, and command messages (IEEE Std. C37.118-2005). The data, configuration, and header messages are transmitted from a data source (PMU/PDC) to the data sink (PDC). While the command messages are sent from the data sink and received by the data source. It should be noted that the PDC often serves as an IEEE C37.118 Client. However, it can act as an IEEE C37.118 Server when it outputs the concentrated time-aligned measurements hitherto received from the PMUs, to other PDCs existing on a higher hierarchy.

The data frame contains the synchrophasor measurements computed by the PMU or PDC. It includes an identification header, message length, message source ID, status information, and the data itself. The data includes the phasors, frequency, ROCOF, analogue, and digital data types. The data from each PMU is organized as a block of data as shown in Figure 8.1 (IEEE Std. C37.118-2005).

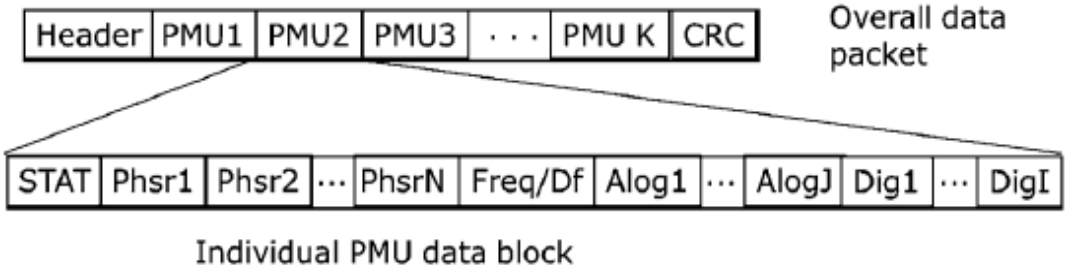

Figure 8.1: **PMU data packet organization (IEEE C37.118-2005)**

The *Config2* (CFG-2) configuration frame gives the measurements currently being reported in the data frame by the data source. CFG-2 is a fixed length frame with 19 fields excluding the data rate and the Cyclic Redundancy Check (CRC). It is denoted by bits 4-6 (011) of the frame synchronization word (SYNC), with fields 8-19 defining the

measurements from the PMU(s).

The *Config3* (CFG-3) is an optional configuration frame, and it is used to give the measurements currently being reported in the data frame by the data source. CFG-3 is an extensible variable length frame with 27 fields excluding the data rate and the CRC. It is denoted by bits 4-6 (101) of the frame synchronization word (SYNC), with fields 9-27 defining the measurements from the PMU(s).

The header frame is a human-readable frame in ASCII format sent from the data source to the data destination (PDC). It is user configured, and contains the information relating to the PMU, type of algorithm, data sources, type of signal processing, and scaling.

The command frame is sent from the data sink (PDC) to the data source (PMU/PDC) to start or stop the transmission of data, or to request for the configuration data prior to the transmission of the data.

8.2.1 Communication Network

The backbone of the lab-scale communication network implemented in this thesis is made up of Ruggedcom RSG2288 communication network switches and Moxa PT-8828 communication network switches.

These network switches belong to a class of Gigabit Ethernet managed switches, industrially hardened to provide reliable service in substation environments with the possibility of 10/100/1000BaseTX copper or 100FX/1000BaseX fibre connections. Some of the features of the switches are IEEE 1588 version 2 Precision Time Protocol (PTP), IEEE 802.1q Virtual Local Area Network (VLAN), link aggregation for bundling several Ethernet ports into a link with a higher bandwidth, and Simple Network Management Protocol (SNMP).

Generally, two types of system architecture can be used in synchrophasor-based applications. These are: the central concentration and the local concentration architectures respectively (SEL, 2009). In the central concentration architecture, all the individual PMUs in all the substations send their synchrophasor measurements to the control centre. While in the local concentration architecture, the PMUs within a substation

send their synchrophasor measurements to a substation PDC. The substation PDC then sends a single output to the control centre (SEL, 2009) .

The advantages of the local concentration architecture include a reduction in the required bandwidth for synchrophasor communication from the substation to the control centre, and an improved system security since a secured connection using an encryption method can easily be provided to the outgoing data at a common point (SEL, 2009).

For the 'proof-of-concept' testbed implemented, a combination of the local and central concentration methods was used. This implies that the synchrophasor measurements from the substation PMUs (RTDS GTNET-PMU and external PMUs) were streamed to the local substation PDC (SEL-3378 SVP) and from the substation PDC to the central SuperPDC (SEL-5073) located at the control centre. The transport protocol used for the intra-substation synchrophasor streaming was the TCP protocol. While the UDP protocol was used for the synchrophasor streaming from the substation PDC to the control centre SuperPDC. The UDP protocol used is known as the UDP Send-only (UDP_S) protocol. The UDP_S is suitable for such an application because it is more secure since it only sends the synchrophasor data without listening to incoming commands (SEL 5073 Manual, 2013).

The TCP protocol was used for intra-substation communication because it is a connection-oriented protocol, and it is suitable for the substation environment where the number of PMU measurements (and overhead) is lesser than what is obtainable at the control centre where a large number of measurements from several PMUs are concentrated.

The justification for the use of the UDP protocol in this thesis for the substation to the control centre data transmission is because of the need to reduce the overhead/bandwidth required. A higher communication bandwidth would be required if the TCP protocol was used because of the extra overhead encapsulating the application layer data. Also, the TCP protocol introduces latency in the measurements because of the delivery and flow control mechanism implemented in it. This latency would be more pronounced when used for substation to control centre communication. In order to prevent the loss of data which may occur with the UDP transmission because of the lack of data retransmission mechanism, a higher synchrophasor reporting rate is used.

Such that, even if there are data losses, these losses would have little or no impact on the developed WAMPAC algorithms.

Another possibility for synchrophasor data transfer is the use of the communication mechanism defined in the IEC 61850-90-5 Technical Report (TR) on synchrophasor communication. This involves the transmission of synchrophasor measurements using the IEC 61850 data modelling, configuration, and infrastructure. Typically, the UDP protocol with multicast addressing is used. This can be implemented using the Routed GOOSE (R-GOOSE) or Routed Sampled Values (R-SV) (IEC 61850-90-5, 2012). The communication medium to use can be optical fibre, power line carrier, leased line, satellite, microwave link, radio link, or IP-based network.

8.2.2 PMU Bandwidth Planning

The bandwidth requirements for a synchrophasor-based communication network depend mainly on the number of PMUs, phasor format, PMU reporting rate, transmitted data, and the transport protocol used. For the New England 39-bus test system, a total of 18 PMUs with a reporting rate of 60 fps were used. The synchrophasor measurements published by each PMU include the positive sequence voltage and current, system frequency, ROCOF, 2-4 analogue measurements, and a 16-bit binary word. Table 8.1 shows the typical data frame size calculated for each PMU used.

Table 8.1: Data frame calculation per PMU

No	Field	Size (Bytes)
1	SYNC	2
2	FRAMESIZE	2
3	IDCODE	2
4	SOC	4
5	FRACSEC	4
6	STAT	2
7	PHASORS Positive sequence voltage and current (floating-point format)	8 x PHNMR* 8 x 2 = 16
8	FREQ (floating-point format)	4
9	DFREQ (floating-point format)	4
10	ANALOG (floating-point format)	4 x ANNMR** 4 x 4 =16
11	DIGITAL	2 x DGNMR*** 2 x 1 = 2
	Repeat 6-11	For the number of PMUs in the data frame
12+	CHK	2
	Total	**60**

** Number of phasors ** number of analogue values *** number of digital status word*

The TCP/IP overhead per frame is given by:

$$TCP/IP\,overhead = TCP\,overhead + IP\ overhead + MAC\,overhead \quad (8.1)$$

$$TCP/IP\,overhead = (24 + 20 + 18)\,bytes = 62\,bytes$$

The total PMU frame length for data transmission using TCP protocol is given as:

$$TCP\ frame\ length = PMU\ data\ frame + TCP/IP\ overhead \quad (8.2)$$

From Table 8.1 the data frame per PMU was calculated as 60 bytes.

Therefore,

$$TCP\ frame\ length = (60+62)bytes = 122\ bytes$$

The bandwidth required per PMU based on the calculated framesize above is given as:

$$Bandwidth = Framesize(bits) \times PMU\ reporting\,rate \quad (8.3)$$

$$Bandwidth = 122 \times 8 \times 60\,bps$$

$$Bandwidth = 58.56\ kbps$$

A network analyser was used to test the basic communication infrastructure used in the WAMPAC testbed implemented in this thesis. The result obtained for the RTDS® communication network is presented in Table 8.2.

Table 8.2: Test results for the RTDS segment of the implemented WAMPAC communication infrastructure

No.	Parameters	Result
1	Latency	0.1683 ms
2	Loss of packet	0.0000%
3	Jitter	0.1781
4	Available bandwidth	51.3418 Mbps

From row 4 of Table 8.2, it can be seen that the lowest available bandwidth for the streaming of the synchrophasor measurements was over 50 Mbps obtained for the RTDS segment of the communication network. A 1 Gbps network is available using the RuggedCom communication switch. It should be noted that 10/100Mbps twisted copper cable was used.

For a worst case scenario (50 Mbps network), the maximum theoretical number of PMUs that can be used is given by:

$$Number\ of\ PMUs = \frac{Available\ \ bandwidth}{Required\ bandwidth\ per\ PMU} \quad (8.4)$$

$$Number\ of\ PMUs = \frac{50\,Mbps}{58.56\,kbps}$$

Therefore, a total of 853 PMUs can be accommodated using the 50 Mbps communication infrastructure. Only 18 PMUs were used in this thesis, and the required bandwidth was about 1.054 Mbps network. Thus, the 18 PMUs used can be adequately supported. The bandwidth required can further be reduced by using the fixed 16-bit (integer) format for the phasors, analogues, frequency, and ROCOF measurements respectively.

For the PDC to control centre communication, UDP protocol was used. If the synchrophasor measurements from the 18 PMUs used are published, the required bandwidth is given as:

$$UDP\ frame\ length = PMU\ data\ frame + UDP/IP\ overhead \tag{8.5}$$

$$\begin{aligned} UDP/IP\,overhead &= Source\,Port + Destination\ port + \\ &\quad + UDP\,length + UDP\,checksum + IP\,overhead \end{aligned} \tag{8.6}$$

$$UDP/IP\,overhead = (2+2+2+2+20)\,bytes = 28\,bytes$$

From Table 8.2, the data frame per PMU was calculated as 60 bytes. Therefore, the frame length using the UDP protocol is:

$$UDP\ frame\ length = (60+28)\,bytes = 88\,bytes$$

The bandwidth based on the calculated framesize above is given as:

$$Bandwidth = 88 \times 8 \times 60\,bps$$

s

$$Bandwidth = 42.24\,kbps$$

8.3 Synchrophasor Message Protocol Conformance Testing

8.3.1 Testbed Setup

A lab-scale conformance investigation comprising of the RTDS®, PMUs, PDCs, GPS satellite clock, industrial communication network switches, and network protocol analyzer software was used for the investigations relating to the verification of the synchrophasor message structure.

The conformance verification tests and analyses are carried out in order to verify the conformance of the message framework and formats obtained from the PMUs from the

various vendors, with the specifications defined in the IEEE C37.118 synchrophasor standard. The setup used for the investigation is as shown in Figure 8.2.

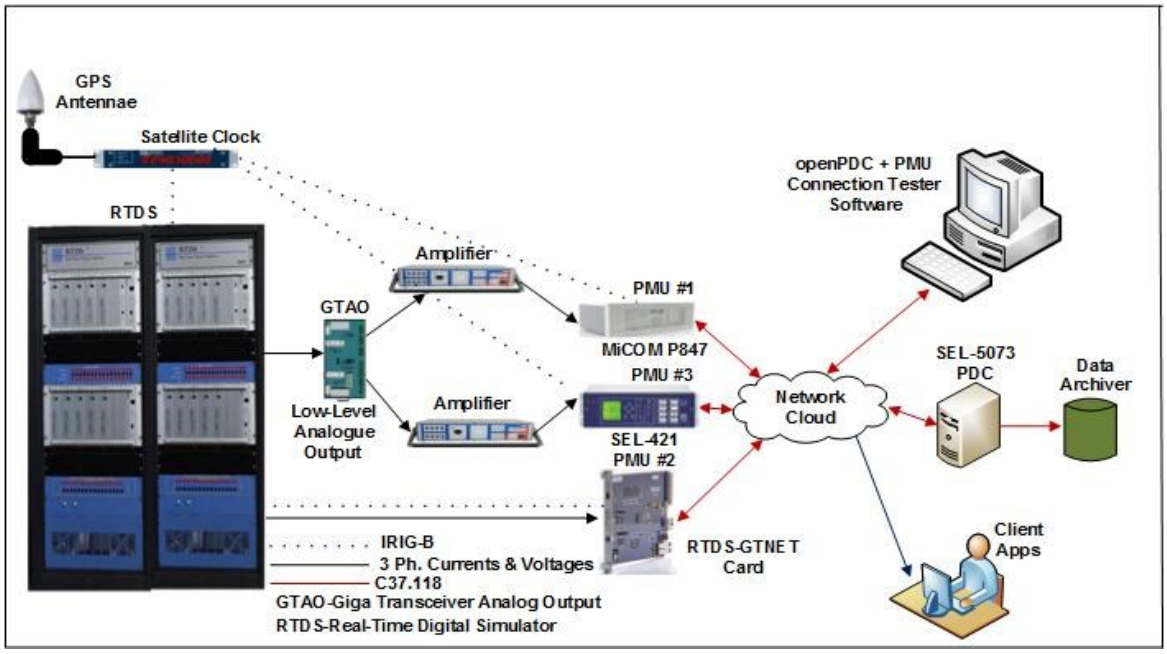

Figure 8.2: **Structure of the lab-scale conformance testing platform**

The 10-bus multi-machine equivalent system (Test System 1) was modelled using the RSCAD software. Measurement variables from the real-time simulation were exported via signal amplifiers (OMICRON CMS-156 amplifier) as analogue inputs to the external devices (IEDs/PMUs).

Three types of PMUs were used. These are MiCOM P847 IED, RTDS GTNET-PMU, and the SEL-421 IED. These PMUs are denoted as PMUs 1-3 respectively. The three PMUs were placed at a High Voltage (HV) transmission bus (bus-7) of the test system as shown in Figure 8.3.

The PMUs were all connected to the same instrument transformers (VT and CT) at bus-7 in order to ensure that they receive the same primary quantities. The measurements of interest were published as IEEE C37.118 synchrophasor measurements by the PMUs onto the communication network.

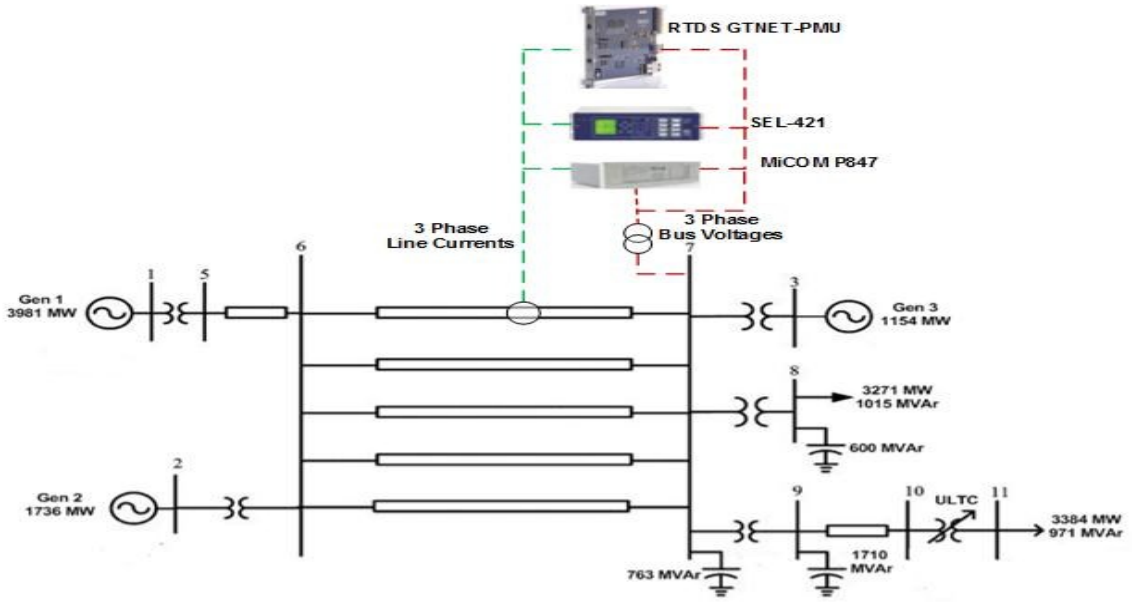

Figure 8.3: PMU comformance test setup

It should be noted that PMU-1 and PMU-3 both comply with the IEEE Std. C37.118-2005, while PMU-2 complies with the IEEE Std. C37.118.2-2011. The time synchronization source was a demodulated IRIG-B time signal from a SEL-2407/SEL-2488 satellite clock to all the PMUs. However, the MiCOM P847 IED also required a 1 Pulse Per Second (1 PPS) signal in order to publish its synchrophasor measurements.

The PDCs used for this test are the SEL-5073 PDC and the openPDC software respectively. The PDCs perform the task of data concentration and time-alignment of the synchrophasor measurements coming from the PMUs. Figure 8.4 depicts the layout for the investigations carried out. The PMUs (MiCOM P847 IED, SEL-421, RTDS-GTNET PMU) streaming the synchrophasor measurements are referred to as Servers 1-3 and are assigned the IP addresses 192.168.1.45, 192.168.1.203, and 192.168.1.206 respectively.

In order to capture the synchrophasor message frames using Wireshark network protocol analyzer software, an IEEE C37.118 Client must subscribe to the data published by the PMUs. The Wireshark network protocol sniffs raw binary data off the network. To do this, the network interface is put in the promiscuous mode whereby the network interface can listen to all the traffic on the network. The extracted information is then analysed. Wireshark network protocol analyzer software includes a libPcap/WinPcap driver used in the switching of the network interface into the promiscuous mode (Sanders, 2011).

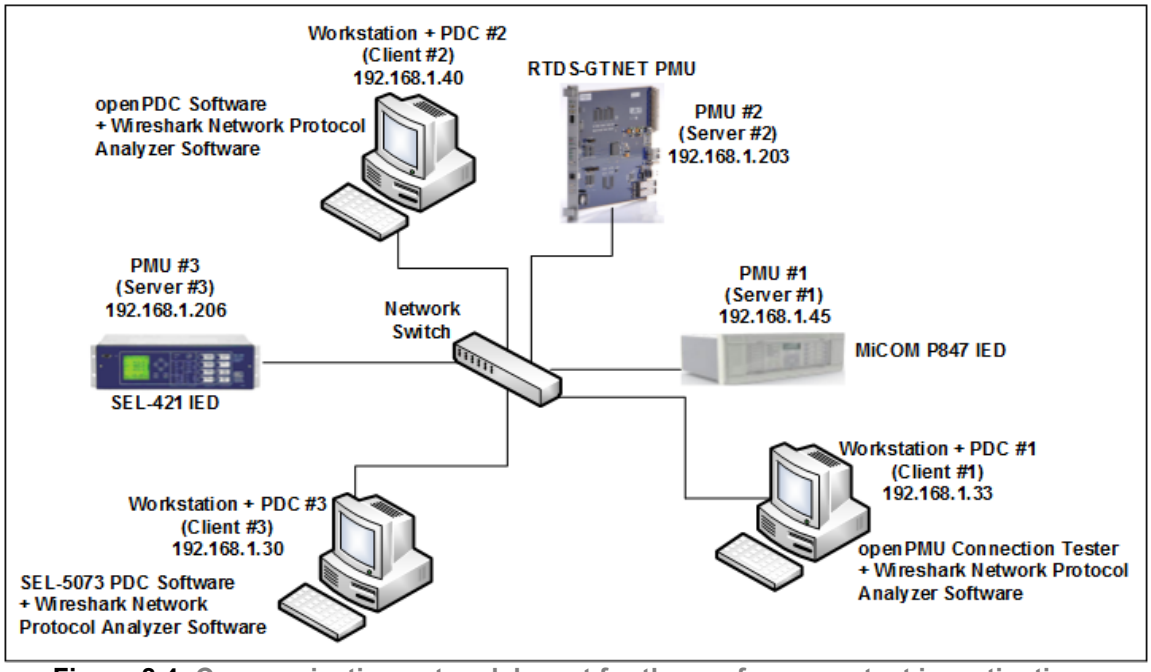

Figure 8.4: Communication network layout for the conformance test investigations

The SEL-5073 PDC, openPDC, and PMU Connection tester software were used for this purpose as illustrated in Figure 8.4, and are referred to as Clients 1-3 with IP addresses 192.168.1.33, 192.168.1.40 and 192.168.1.30 respectively. Wireshark network protocol analyzer software running on each of the workstations connected to the communication network was then used in sniffing the relevant packets (synchrophasor frames) off the network.

8.3.2 Verification of the IEEE C37.118 Synchrophasor Message Structure

Investigation of the Synchrophasor Message Structure

The verification of the IEEE C37.118 synchrophasor message structure as given in the IEEE C37.118 standard was carried out using the three PMUs mentioned above. Figure 8.5 shows the packets from PMU-1 (source) and PDC-1 (destination) obtained using the Wireshark network protocol analyser.

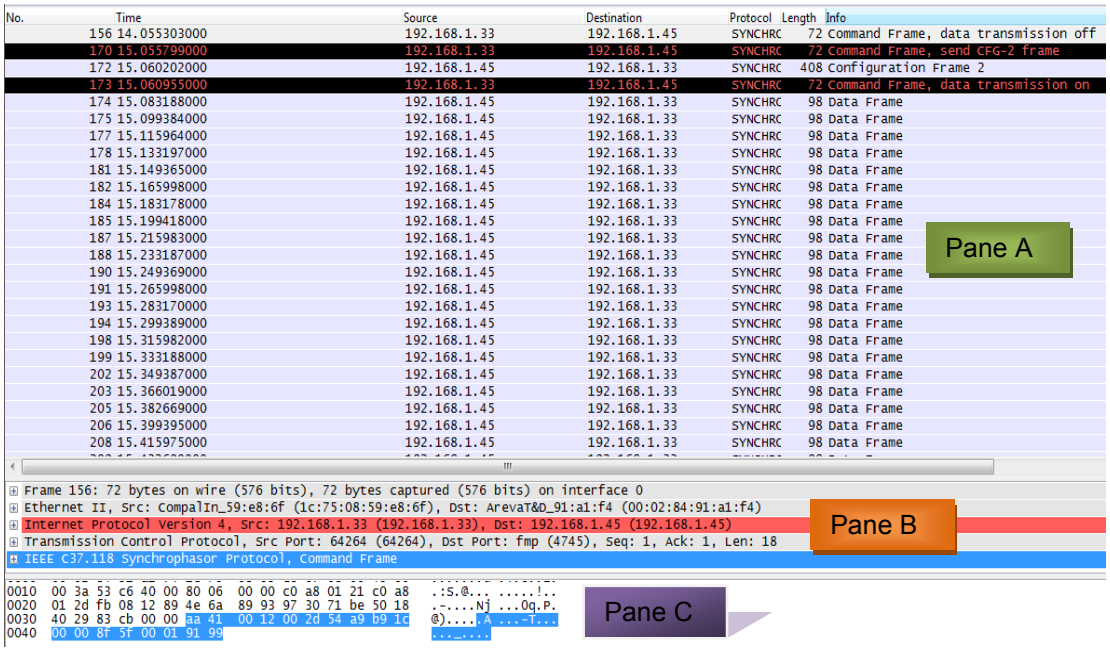

Figure 8.5: Synchrophasor messages for PMU-1 and PDC-1 captured using the Wireshark protocol analyzer

Wireshark network protocol analyser was used to sniff the network, capture network packets in real-time, and display them in a human-readable format. Figure 8.5 has been partitioned into three panes (Panes A-C) for better analysis. Pane A presents a list of all the packets captured at the Ethernet interface in real-time. It has six columns showing the time of capture, the source, destination, type of protocol, frame length, and the message type.

Column 1 gives the time of capture of the packet. The IP address of the source device is given in column 2, while column 3 presents the IP address of the destination device. The type of protocol was rightly given as SYNCHRC in column 4, signifying the synchrophasor protocol. The frame length gives the size of the information contained in the message type as shown in column 5.

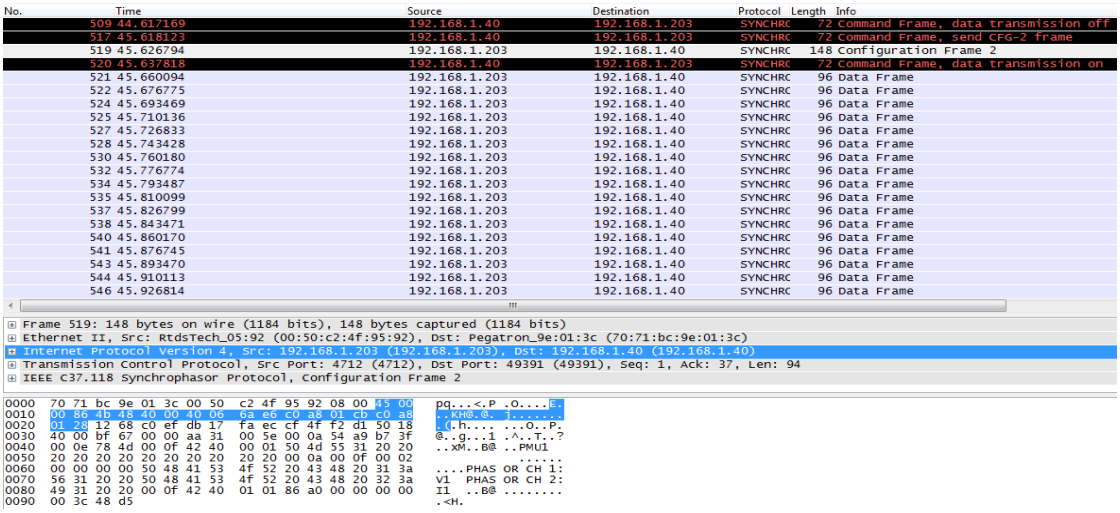

Figure 8.6: Synchrophasor messages for PMU-2 and PDC-2 captured using the Wireshark protocol analyzer

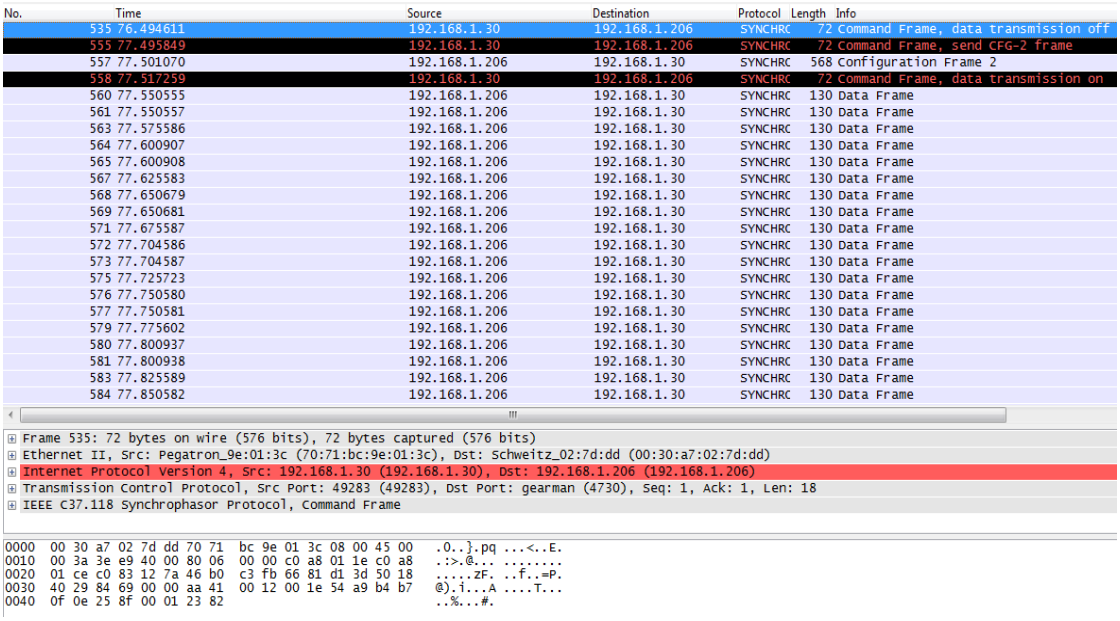

Figure 8.7: Synchrophasor messages for PMU-3 and PDC-3 captured using the Wireshark protocol analyzer

Column 6 of Pane A shows the information relating to the sequence of interaction between the PDC (data concentrator) and the PMU (data source). It can be seen that the PDC initiates a query (Command frame) requesting for the CFG-2 Configuration message from the PMU. The PMU responds to the Command frame query by issuing its CFG-2 configuration, and shortly afterwards, commences the data transmission of synchrophasor measurements to the PDC.

Pane B of Figure 8.5 gives a layered classification of the selected packet in Pane A. The hexadecimal values corresponding to the messages in the captured packet are given in Pane C of Figure 8.5. The above applies to the captured packets for PMUs 2-3 as shown

in Figures 8.6-8.7 respectively.

Based on the synchrophasor messages captured in Figures 8.5-8.7, the connection (communication) between the IEEE C37.118 Client (PDC) and an IEEE C37.118 Server (PMU/PDC) can be summarized as given in Figure 8.8.

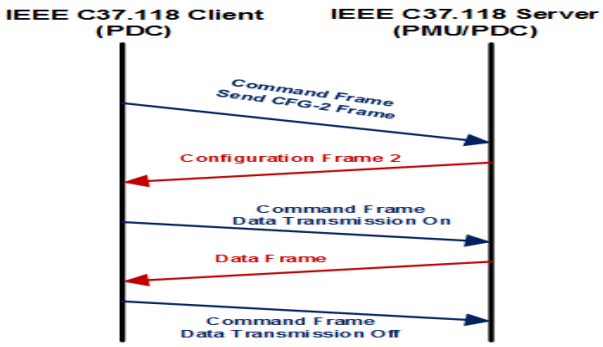

Figure 8.8: IEEE C37.118 Synchrophasor Client-Server communication

Synchrophasor Message Types

Conformance testing is performed for the following synchrophasor message types: i) command frame; configuration frame; data frame; and the command frame for 'data transmission on'.

The fields for the command frame in the synchrophasor message are specified in Table 14 of the IEEE Std. C37.118.2-2011 as presented in Table 8.3. In order to verify the compliance with the IEEE Std. C37.118, a comparison between the fields in Table 8.3 and the command frame from an actual PDC was carried out. The command frame issued by each PDC to their respective PMU was captured using Wireshark network protocol analyzer as shown in Figures 8.9-8.11.

Table 8.3: Command frame organization (excerpts from Table 14 of the IEEE Std. C37.118.2-2011)

No.	Field	Size (bytes)
1	SYNC	2
2	FRAMESIZE	2
3	IDCODE	2
4	SOC	4
5	FRACSEC	4
6	CMD	2
7	EXTFRAME	0-65518
8	CHK	2

From Figures 8.9-8.11, the message fields contained in the command frame from the IEEE C37.118 Clients to the IEEE C37.118 Servers were shown to provide details on the synchronization word, framesize, ID code, Second of Century (SOC), Fraction of Second (FRACSEC), command (CMD) to the PMU, and the checksum (CHK).

The same message fields as specified in the IEEE Std. C37.118 were obtained for the command frame from PDC-2 to PMU-2, and PDC-3 to PMU-3 respectively. From the captured packets in Figures 8.9-8.11, compliance with the IEEE Std. C37.118 was verified in terms of the field contained in the message frame, and also the size of the field.

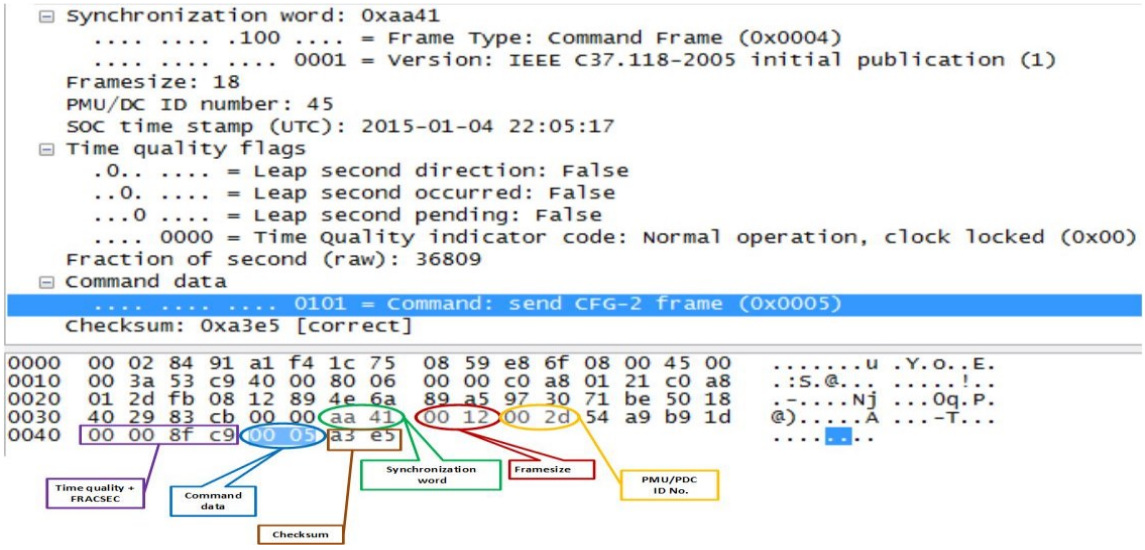

Figure 8.9: Wireshark capture of a command frame from PDC-1 to PMU-1

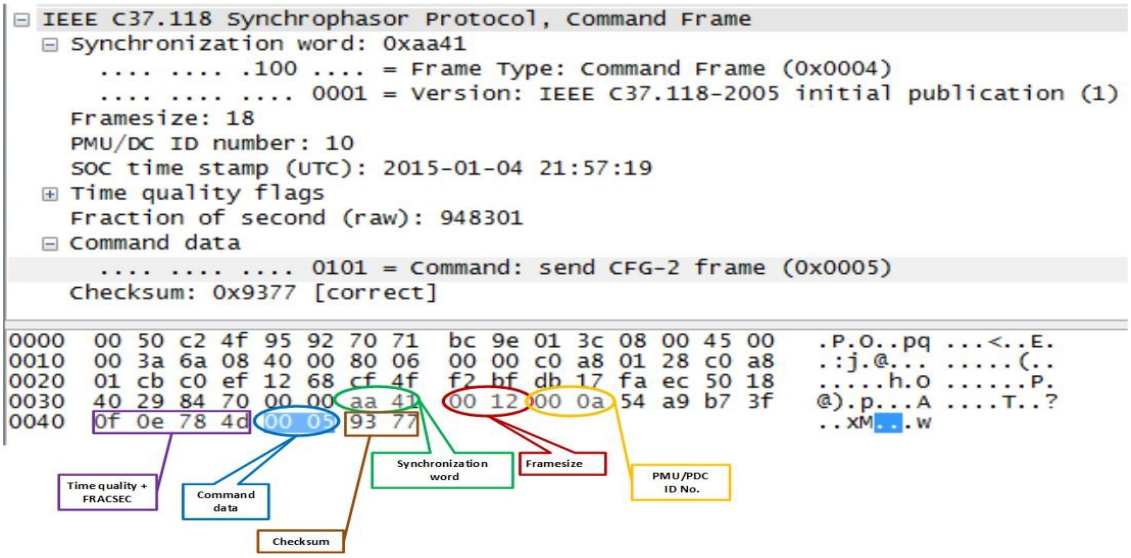

Figure 8.10: Wireshark capture of a command frame from PDC-2 to PMU-2

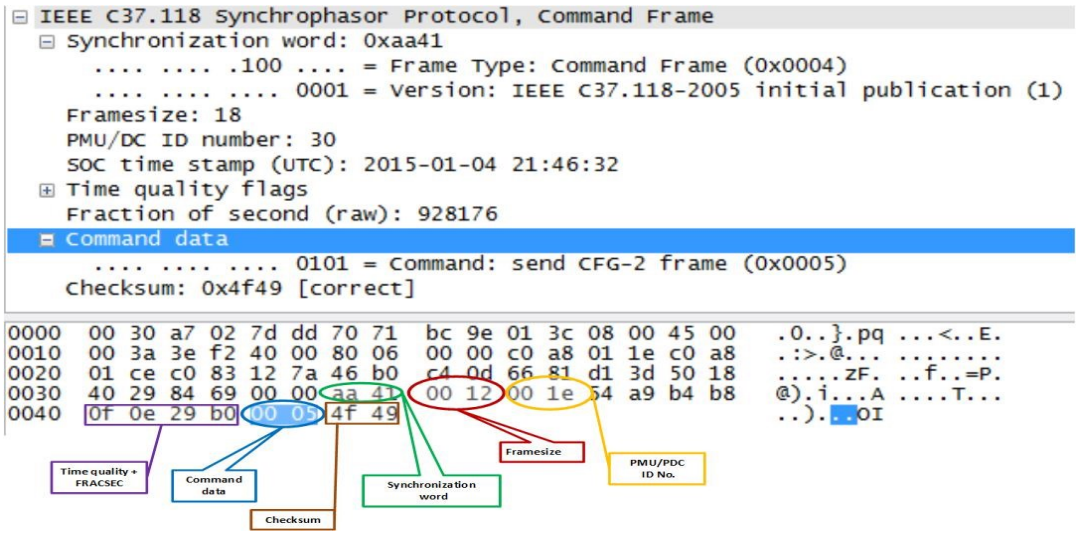

Figure 8.11: Wireshark capture of a command frame from PDC-3 to PMU-3

The information relating to the frame synchronization word (sync), the message frame size, device ID code, SOC, FRACSEC, the command being sent, and the checksum can be seen in the Wireshark capture.The configuration frame is a binary dataset containing the required parameters for processing the synchrophasor data stream. The fields in the configuration frame are specified in Table 8 of the IEEE Std. C37.118.2-2011 as shown in Table 8.4. It contains the information relating to the SYNC word, framesize, ID code, SOC, FRACSEC.

Table 8.4: Configuration frame organization (Table 8 of the IEEE Std. C37.118.2-2011)

No	Field	Size (Bytes)	Description
1	SYNC	2	Synchronization word. Proceeded by the frame-type and version.
2	FRAMESIZE	2	Number of bytes in the frame.
3	IDCODE	2	User assigned PMU source ID number (1-65534).
4	SOC	4	Second of Century time count from 01-01-1970
5	FRACSEC	4	Fraction of Second and time quality
6	TIME_BASE	4	FRACSEC time stamp resolution.
7	NUM_BASE	2	The number of PMUs in the data frame.
8	STN	16	Station name.
9	IDCODE	2	PMU data source ID number
10	FORMAT	2	Data frame format.

Table 8.4: Configuration frame organization (Table 8 of the IEEE Std. C37.118.2-2011) con't

No	Field	Size (Bytes)	Description
11	PHNMR	2	Number of phasors.
12	ANNMR	2	Number of analogue values.
13	DGNMR	2	Number of digital status words.
14	CHNAM	16 x (PHNMR + ANNMR + 16 x DGNMR)	Phasor and channel names for each phasors, analog and digital channel.
15	PHUNIT	4 x PHNMR	Conversion factor for the phasor channels.
16	ANUNIT	4 x ANNMR	Conversion factor for the analog channels.
17	DIGUNIT	4 x DGNMR	Mask word for the digital status word.
18	FNOM	2	Nominal frequency.
19	CFGCNT	2	Configuration change count.
20 +	DATA_RATE	2	Reporting rate of the data.
21+	CHK	2	CRC-CCITT

In addition to these, the configuration frame contains information relating to the data format (integer or floating point), phasor names, conversion factors for the phasors, configuration change count, reporting rate, and the checksum. The configuration frames published by PMUs-2 and -3 were captured using the Wireshark network protocol analyzer as shown in Figures 8.12-8.13.

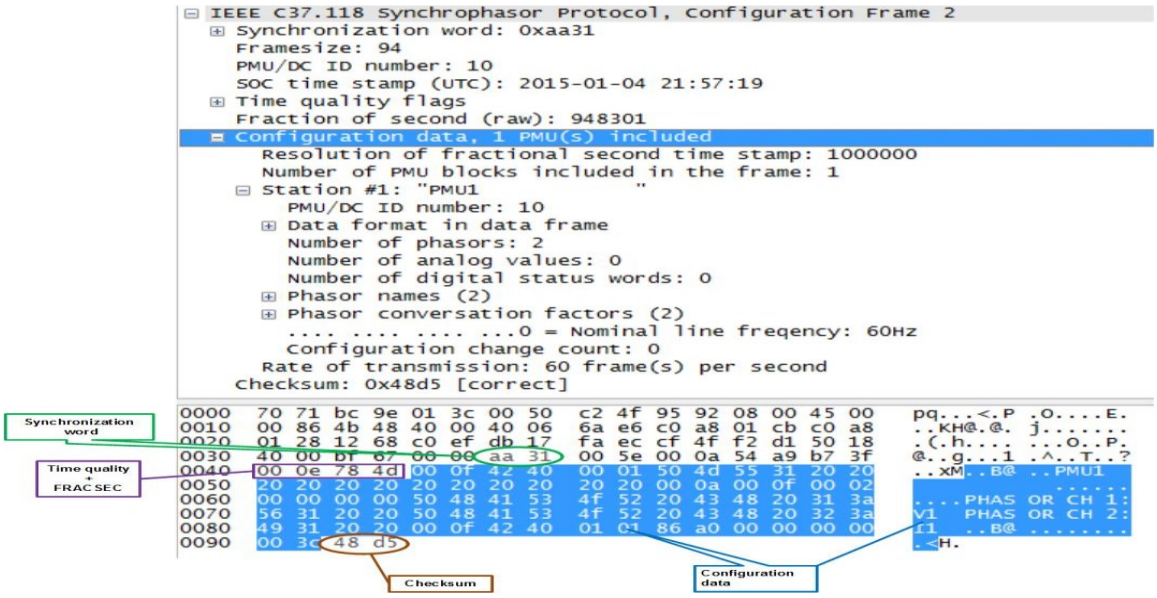

Figure 8.12: Organization of the captured configuration frame from PMU-2

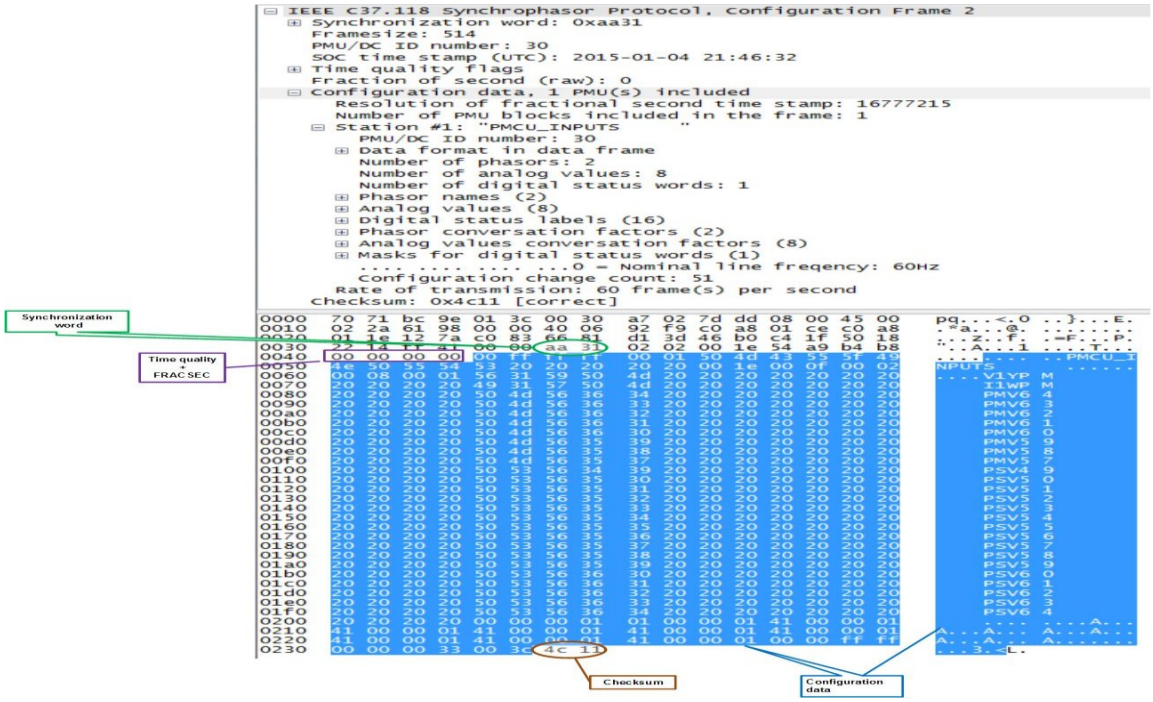

Figure 8.13: Organization of the captured configuration frame from PMU-3

The specified fields indicated in the configuration frame sent by the PMU/PDC were confirmed as correct in the data frame. As shown in Table 8.5, the fields in the data frame organization consist of the synchronization word, framesize, ID code, SOC, FRACSEC, STAT, Phasors, Frequency, ROCOF, analogues, digitals, and checksum. The data frame packet captured using the network protocol analyzer is shown in Figure 8.14. Figure 8.15 shows the capture for the 'data transmission on' command frame from PDC-2 to PMU-2.

Table 8.5: Data frame organization (excerpts-Table 5 of the IEEE Std. C37.118.2-2011)

No	Field	Size (Bytes)
1	SYNC	2
2	FRAMESIZE	2
3	IDCODE	2
4	SOC	4
5	FRACSEC	4
6	STAT	2
7	PHASORS	8 x (PHNMR)
8	FREQ	4
9	DFREQ	4
10	ANALOG	4 x ANNMR or 4 x ANNMR
11	DIGITAL	2 x DGNMR
	Repeat 6-11	
12+	CHK	2

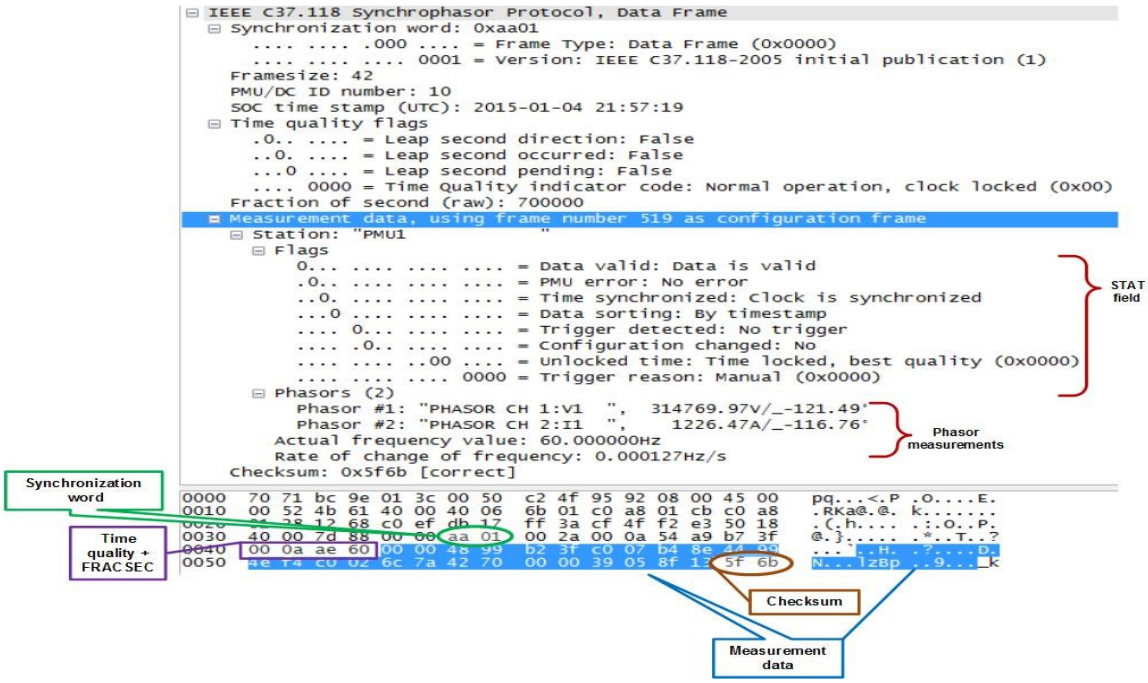

Figure 8.14: Data frame organization from the captured data frame (PMU-2)

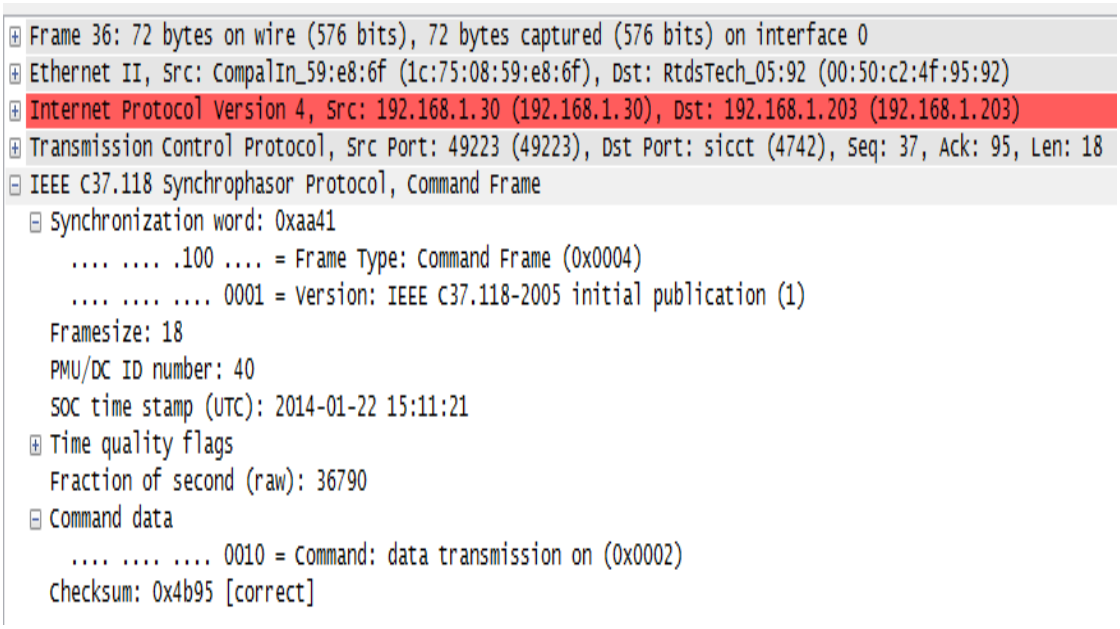

Figure 8.15: Packet analysis for the 'data transmission on' command frame from PDC-2 to PMU-2

8.3.3 Discussion

The fields in the captured network packet for the command frames (send CFG-2 frame) shown in Figures 8.9-8.11 are further analysed. The fields and the word size were in agreement as given in Figures 8.9-8.11, except for the EXTFRAME field which is field 7 of Table 14 in the IEEE Std C37.118.2-2011. The EXTFRAME field was missing in the

captured command frame for PMUs 1-3. This might not have been implemented by the OEMs because the EXTFRAME field is optional.

Also, it was observed that in field 5 of Table 14 of the IEEE Std C37.118.2-2011, the size of the FRACSEC and time quality were bunched together as 4 bytes. Analysis done on the Wireshark capture of the command frames from PMUs 1-3 shows the FRACSEC to be 3 bytes, while the time quality was 1 byte.

The SYNC word was analysed and obtained as hex AA41 signifying the frame type and version number. The Send CFG-2 frame command was correctly given as 0000 0000 0000 0101 as shown in Figures 8.9-8.11. Also, the time quality indicator was noted as 0x00 (locked state) signifying a good time synchronization.

The checksum had a hex value of 0x5f6b and was given as ‘correct’. This implies that the data was received without any error. The command frame had a total of 18 bytes corresponding to the summation of the above-mentioned messages in compliance with the specification in Table 14 of the IEEE Std C37.118.2-2011.

Another command frame is the ‘data transmission on’ command. This was also issued by the PDC (data concentrator) to the PMU (data source). The only difference between this and the ‘Send CFG-2’ command was that the command word bits was 0000 0000 0000 0010, rather than 0000 0000 0000 0101 which is the ‘Send CFG-2’ command. This is as shown in Figure 8.15.

Analysis of the fields obtained from the captured packet for the configuration frame is shown in Figures 8.12-8.13. From Figures 8.12-8.13, the SYNC word was obtained as hex AA31. This corresponds to CFG-2. All the PMUs report the FRACSEC and time quality separately, and their sizes are obtained in the captured packet as 3 bytes and 1 byte respectively.
Peculiar to the configuration frame is the message content relating to the station name, data format in the data frame, number of phasors, number of analogue values, number of digital status words, phasor names, and phasor conversion factors. The packet size for PMU-2 for this particular configuration frame was 94 bytes, while PMU-3 has a framesize of 514 bytes because of its additional analogue measurements and digital word. The total size of the configuration frame was determined by the number of phasors, number of

analogues, and the digital word being reported. The respective fields and their sizes were verified to be in accordance with the IEEE Std. C37.118 as shown in Figures 8.12-8.13.

The data frame for PMU-2 was analysed as shown in Figure 8.14. From the figure, the SYNC word was obtained as hex AA01. This corresponds to the version 1 IEEE Std C37.118-2005 frame. The FRACSEC and time quality in field 5 are separated and their sizes were obtained in the captured packet as 3 bytes and 1 byte respectively. Field 6 of Table 5 in the IEEE Std C37.118.2-2011 was specified as 'STAT'. However, this was named as 'Flags' in PMUs 1-3.

For the 'Flags' field, bits 15-14 have a value of 00 (good measurement data without errors), and bit 13 equals 0. This signifies PMU synchronization to a UTC traceable time source. Bit 12 is 0 for data sorting using time stamp rather than the order of arrival, and bits 08-06 are 00, signifying a PMU time quality of 00 synchronized and locked with the best quality time. The size of the data frame was 42 bytes. This included the size of the SYNC word, framesize, ID code, SOC, time quality, FRACSEC, the measurement values of the phasors, frequency, ROCOF, analogues, and digitals.

From the foregoing, it can be seen that the PMUs tested complied with the IEEE C37.118 standard. The information obtained from this conformance investigation is useful in the development of control centre applications for troubleshooting and diagnosis using the synchrophasor Ethernet frames captured in real-time. Also, this can serve as the foundation in the development of cyber security applications for detecting synchrophasor message spoofing or 'synchrophasor poisoning'.

8.4 Performance Analysis under Pervasive Network Conditions

8.4.1 Introduction

The performance of centralized WAMPAC applications is strongly dependent on the communication network infrastructure for transmitting the data between the field devices and the control centre, and the communication of the control signal from the control centre to the field actuating devices. Therefore, application-specific testing should be carried out as recommended in the IEEE Std. C37.244-2013 (IEEE Std. C37.244-2013, 2013).

In (Zhang *et al*., 2015; Naduvathuparambi *et al*., 2002; Taylor *et al*., 2000), attempts were made to measure the communication delays in wide area control applications. However,

no attention has been given to the impact of pervasive (adverse) wide area communication network conditions that could affect the performance of protection/control schemes in smart grids. For any wide area measurement, protection, and control application, the maximum allowable network latency, jitter, packet losses, and noise/attenuation need to be quantified. These adverse communication network conditions can occur as a result of the communication route length between the clients and the servers, the presence of repeaters, electromagnetic interference, ambient temperature, constraints in the available bandwidth per channel, and the type of communication infrastructure deployed. These adverse network conditions are further discussed in the proceeding subsections.

8.4.1.1 Latency

Latency or delay is the time taken by a network packet to travel from one host to another. Jitter is associated with latency and it is the variation recorded in each consecutive delay. Latency is usually caused by insufficient bandwidth or path congestion. Five types of delays are present in wide area protection/control systems. These are: (i) measurement delay (t_{meas}), (ii) measurement uplink delay (t_{up}); (iii) computation delay (t_{comp}), (iv) control action downlink delay (t_{down}); and (v) control action delay (t_{con}). The total delay possible in a WAMPAC system is given by (Zhang *et al*., 2015; Cowley, 2007):

$$T_{delay} = t_{meas} + t_{up} + t_{comp} + t_{down} + t_{con} \tag{8.7}$$

The measurement delay is introduced during the measurement acquisition stage by the CTs and the VTs respectively. The uplink delay is caused by the serialization of data packets, data framing, signal propagation delay, and the queuing delays from the substation PMUs to the PDC.

The computation delay results from the time required in the concentration of PMU measurements at the control centre, the execution of the WAMPAC applications, and the issuance of the control signals to the actuating devices. The time between when the control signals were issued to when they were received by the field actuating devices is referred to as the control downlink delay. The delay due to the time taken for the field actuating devices to receive the control signals and implement the required remedial actions is referred to as the controller action delay.

8.4.1.2 Packet Loss

Data packet losses may degrade the performance of power systems wide area applications. It may occur as a result of congestion, routing instability, and signal loss in the communication network. For instance, in PMU applications where the required bandwidth is not appropriately sized, congestion may occur as a result of the inability of the communication network to support the large amount of PMU measurements being streamed onto the communicatiom network.

8.4.1.3 Network Corruption

Network corruption can be introduced in the network packets as a result of data transmission errors, noise in the communication channel, and signal attenuation. This degrades the throughput of the communication network and causes packet losses and congestion.

In practical systems, this can be as a result of the electrical noise in the substation, noisy communication channel, interference, signal attenuation, and network congestion.

8.4.2 Communication Network Modelling

A co-simulation platform combining System-In-The-Loop (SITL) and Hardware-In-the-Loop (HIL) emulations made up of real substation devices publishing synchrophasor measurements transmitted through a simulated Wide Area Network (WAN) using the Wide Area Network emulator (WANem) tool was carried out.

As shown in Figure 8.16, the SITL emulation was carried out using a Linux-based WAN emulator acting as a Gateway Server and as a transparent proxy server. This was used in the routing of the synchrophasor measurements being streamed onto the communication network by the HIL devices.

The WANem software is a Linux-based emulation tool developed using a bootable Linux distribution (live CD) known as Knoppix. The architecture of the WANem software is divided into three layers as illustrated in Figure 8.17 (Kalita and Nambiar, 2011). These are the Linux kernel, the shell, and the web interface respectively.

The Linux kernel consists of a Hierarchical Token Bucket (HTB) module for queuing discipline, a netfilter module for network packet handling (filtering), a conntrack module for the TCP/IP connection tracking, and the Netem module which provides the functionality for emulating wide area networks using the Linux operating system.

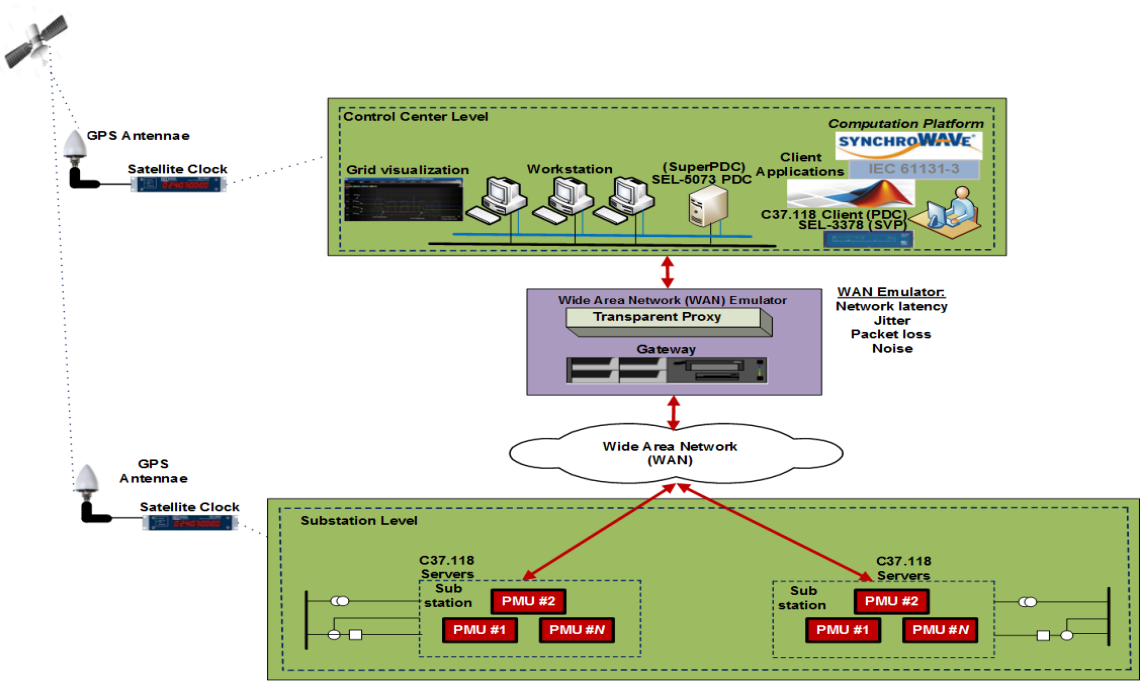

Figure 8.16: Routing synchrophasor measurements through the Linux-based WAN emulator

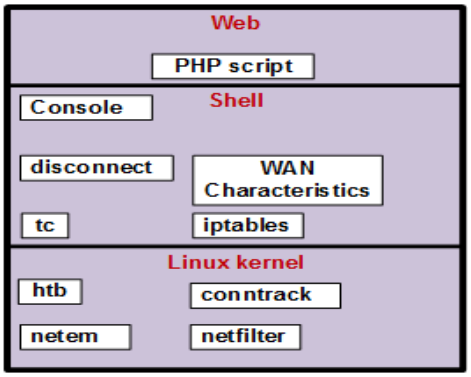

Figure 8.17: WANem software architecture (adapted from Kalita and Nambiar, 2011)

The WAN emulator shell consists of a command line tool (tc), a disconnect module for emulating the network disconnection characteristics, and an iptable module respectively. The iptable is used in the configuration of the operating system for the network connection. The console is used in the management of the application using the command line interface. The WAN characterizer was utilized in the measurement of the characteristics of the network such as the available bandwidth, latency, jitter, and packet loss. The last layer is the Web layer which serves as the configuration interface for the WAN emulator. This layer consists of PHP scripts and Apache HTTP Server respectively.

Data packets from actual PMUs/substation PDCs are transmitted via the WAN emulator, and are fed through the rule sets defined in the WAN emulator to emulate actual wide area network conditions, before being transmitted to the network for subscription by other network devices like the SEL-3378 SVP or superPDCs located in the control centre.

The WAN emulator can emulate a variety of network characteristics including latency, packet loss, jitter, duplicate delivery, packet reordering, corruption, bandwidth limitation, and disconnection. In the implementation of the WAN emulation, the WAN emulator was placed between the IEEE C37.118 Clients (control centre PDCs) and the IEEE C37.118 Servers (substation PMUs).
The WAN emulator was configured as a transparent proxy server acting as a gateway for the bi-directional traffic between the IEEE C37.118 Clients and the IEEE C37.118 Servers.

The required configuration for the kernel involved in the transparent proxy server using the Linux-based WAN emulator is as follows:

- Enable Network Address Translation (NAT) on the ethernet interface (eth0) used for the WAN emulator using the 'ifconfig' command.
- Set up the routing rules for the Linux system using the 'iptables' command.
- Use the IP address of the transparent Proxy Server (WAN emulator) as the Server address in the Clients' configuration settings.

The ifconfig command is used in the assignment of the Ethernet interface *eth0* to the WAN emulator, thereby making the interface accessible to the network layer of the Linux kernel.
The iptable command adds a route to the routing table of the kernel such that the packets from the IEEE C37.118 Servers and emanating from the *eth0* are routed through the Gateway Server (WAN emulator).

The investigations relating to WAN emulation and the results obtained are presented in the proceeding subsection.

8.4.3 Real-Time Communication Network Performance Analysis under Pervasive Conditions

Real-time protection and control have critical time requirements, and the timely and accurate processing of measurements by the PDCs is fundamental to the operation of the various WAMPAC applications at control centres. The two delays that account for the PDC latency are the PDC wait time and the PDC processing time respectively.

The PDC wait time is the absolute length of time the PDC is configured to wait for the synchrophasor measurements relating to a specific time-stamp before processing the acquired synchrophasor measurements from the PMUs.
The PDC processing time is the length of time between the receipt of the last synchrophasor measurements and the publishing of a data frame for that specific time-stamp.

The impact of pervasive network conditions on the performance of the proposed synchrophasor-based WAMPAC algorithms is investigated in this subsection.
The pervasive network conditions considered include latency, jitter, packet loss, random noise and their combinations.

The testbed used for this investigation is made up of 8 PMUs from the RTDS GTNET-PMU, the SEL-5073 PDC and the SEL-3378 SVP. The SEL-5073 PDC subscribes to the synchrophasor measurements from the RTDS GTNET-PMU and publishes these measurements via the emulated virtual WAN (using the WAN emulator) to the SEL-3378 SVP for the execution of the WAMPAC applications.

The WAN emulator served as the network gateway through which all communication from the PMUs, the SEL-5073 PDC, and the SEL-3378 SVP route their network packets. The synchrophasor measurements archived at the SEL-5073 are further analyzed. Figure 8.18 illustrates the implementation of the test setup. The solid arrow head indicates the normal communication path of the synchrophasor measurements to the control centre, while the broken arrow head shows the communication path for the emulated WAN.

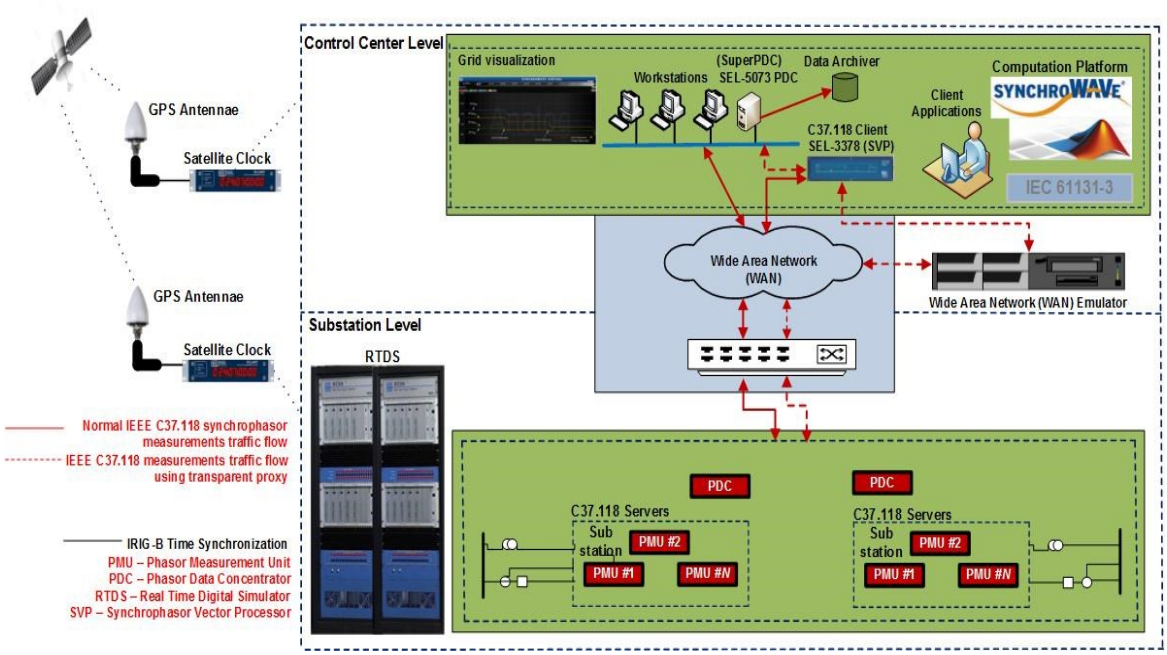

Figure 8.18: **Wide Area Network (WAN) emulation using transparent proxy**

A network analyzer was used in testing the various segments of the implemented lab-scale communication network. The lowest communication bandwidth of about 50 Mbps was obtained between the RTDS® and the rest of the testbed as shown in Table 8.2.

A data payload of 2 positive sequence voltage and current phasors, 4 analogue measurements, and 1 binary word will have a data frame of 60 bytes. If the TCP protocol is used with a 60 fps reporting rate, a 50 Mbps network will efficiently support 853 PMUs using Equation 8.4.

WAN characteristics involving latency, jitter, packet loss, and random noise were carried out in real-time to investigate how the proposed WAMPAC algorithms would perform under real WAN conditions. These are defined by using rule sets applied to the packets routed through the WAN emulator. Table 8.6 shows the parameters of the WAN conditions used.

Table 8.6: Parameters for the emulation of the WAN pervasive conditions

S/N	Network condition	Parameters
1	Latency	(100:50:1000) ms
2	Jitter	10% of latency
3	Packet loss	0.1% - 10.0 %
4	Noise	0.1% - 10.0 %

8.4.3.1 Case Study 1

The first case study involves a N-1 line contingency on the 10-bus multi-machine test system. This was investigated for the emulated network conditions given in Table 8.7. Figure 8.19 shows the plot of the synchrophasor voltage at Bus-8 obtained without any network latency, and for the emulated network latency of 250 ms to 750 ms with a jitter of 10% of the network latency.

Figure 8.20 shows the results obtained for a latency greater than 750 ms. From Figure 8.20, it can be seen that the network latency greater than 800 ms had adverse effects on the synchrophasor messages. This is demonstrated by the loss in the synchrophasor measurements as indicated by the vertical lines highlighted in the figure.

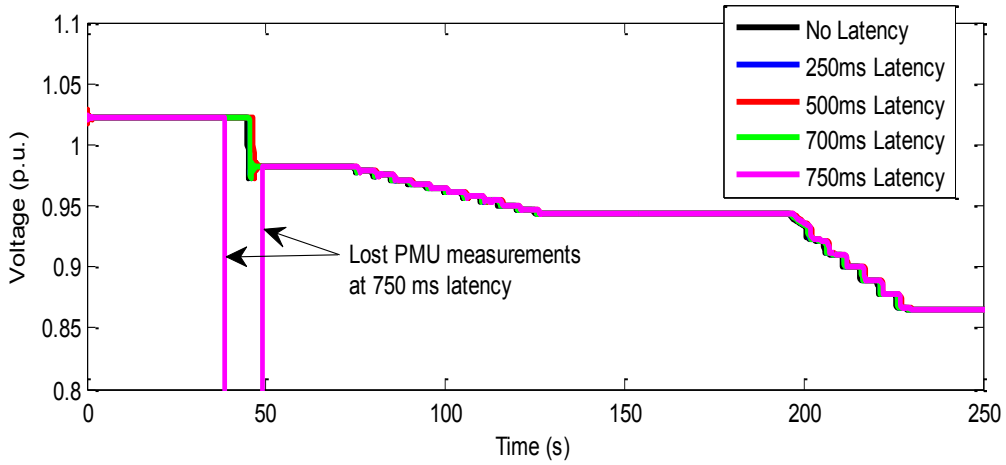

Figure 8.19: WAN emulation of network latency of 0-750 ms

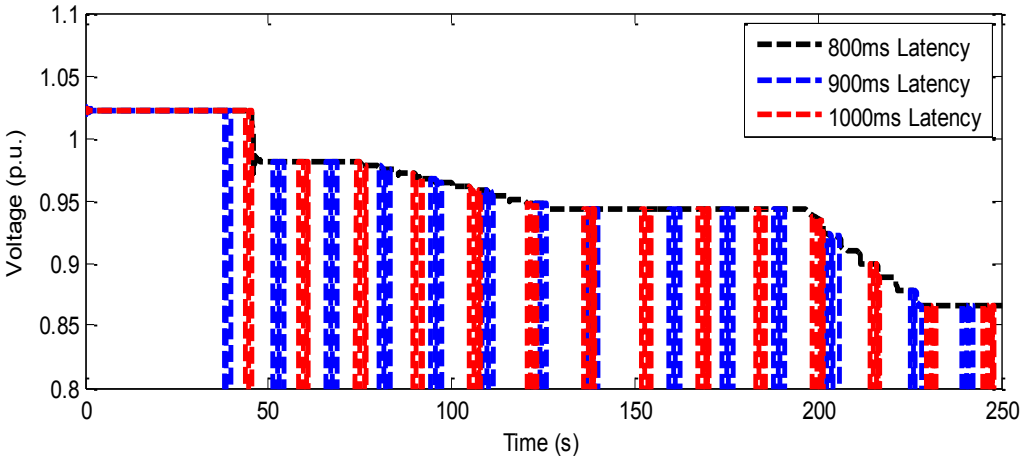

Figure 8.20: WAN emulation of network latency of 800-1000 ms

8.4.3.2 Case Study 2

Case Study 2 investigates the impact of packet losses using a N-1 line contingency. From the results obtained as shown in Figure 8.21, it was observed that packet losses up to 2.5% might be acceptable. Above a packet loss of 2.5%, the loss in the data packets had a greater impact as indicated by the increase in the number of measurement losses.

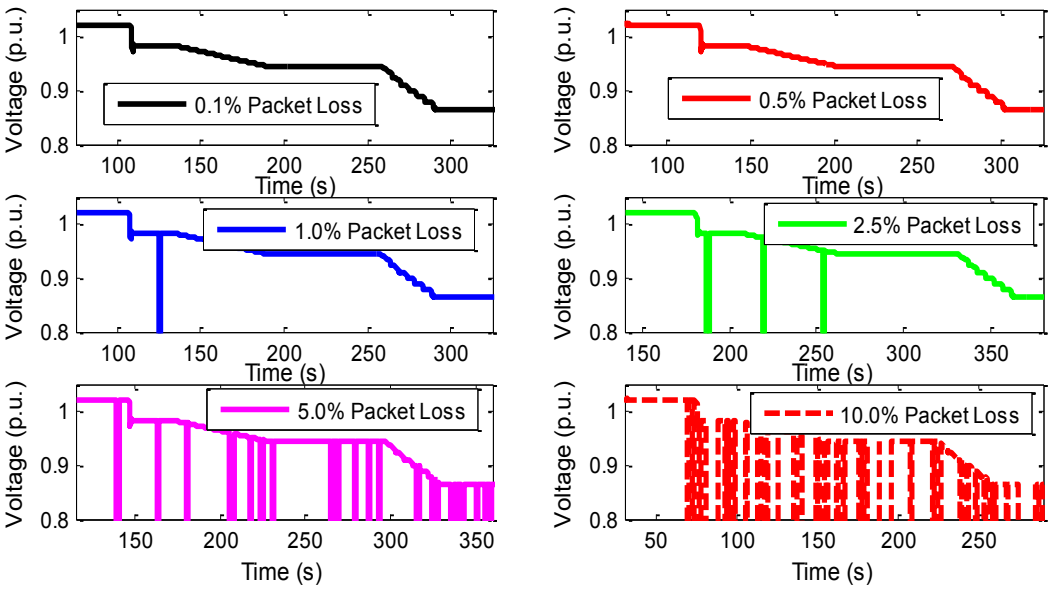

Figure 8.21: WAN emulation of packet losses

8.4.3.3 Case Study 3

Case Study 3 presents an investigation of the impact of the corruption resulting from noise and signal attenuation. From Figure 8.22, it can be seen that corruption up to 1.0% is acceptable and did not have an adverse effect on the integrity of the synchrophasor measurements.

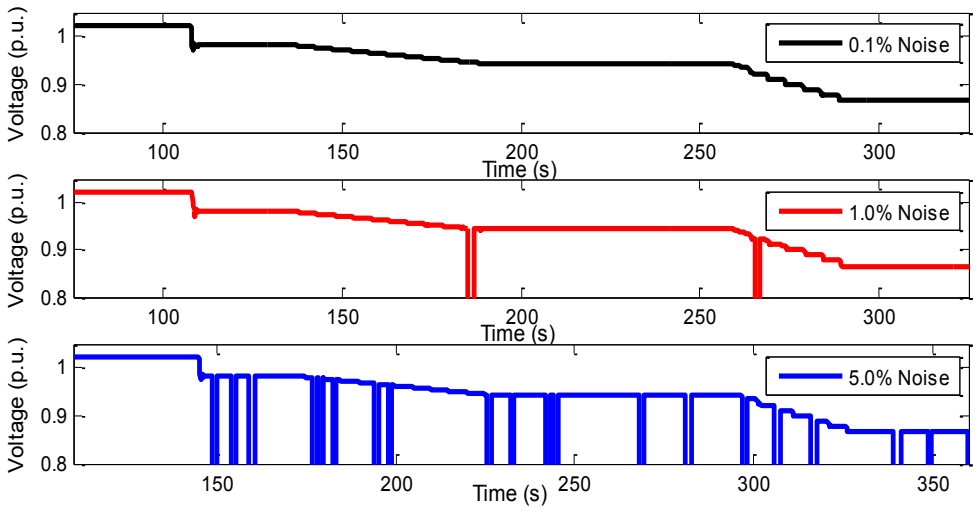

Figure 8.22: WAN emulation of network noise

8.4.3.4 Case Study 4

WAN conditions consisting of network latency, packet losses, and random noise were emulated in Case Study 4. From Figure 8.23-8.25, it can be seen that for a latency of 500 ms, the synchrophasor measurements could only tolerate a packet loss of about 0.1%. Beyond a packet loss of 0.1% and a latency of 500 ms, the lost packets increased and the network was severely degraded.

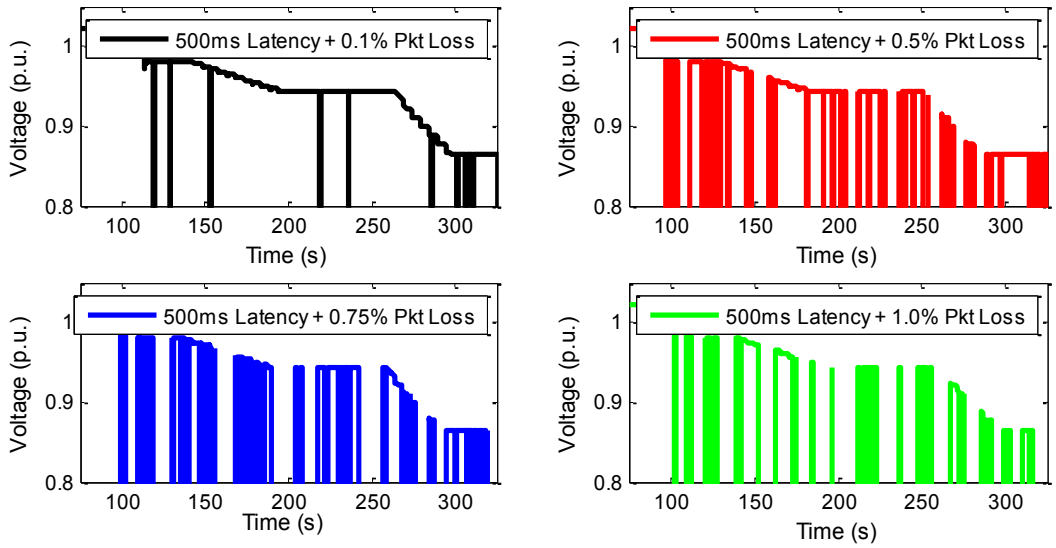

Figure 8.23: WAN emulation of combined network latency, jitter and packet losses

The implication of this is that the communication network implemented could only support a latency of 500 ms with ±10% jitter, 0.1% packet loss, and 1.0% random noise respectively. Beyond these network parameters, the network degraded to an unacceptable level.

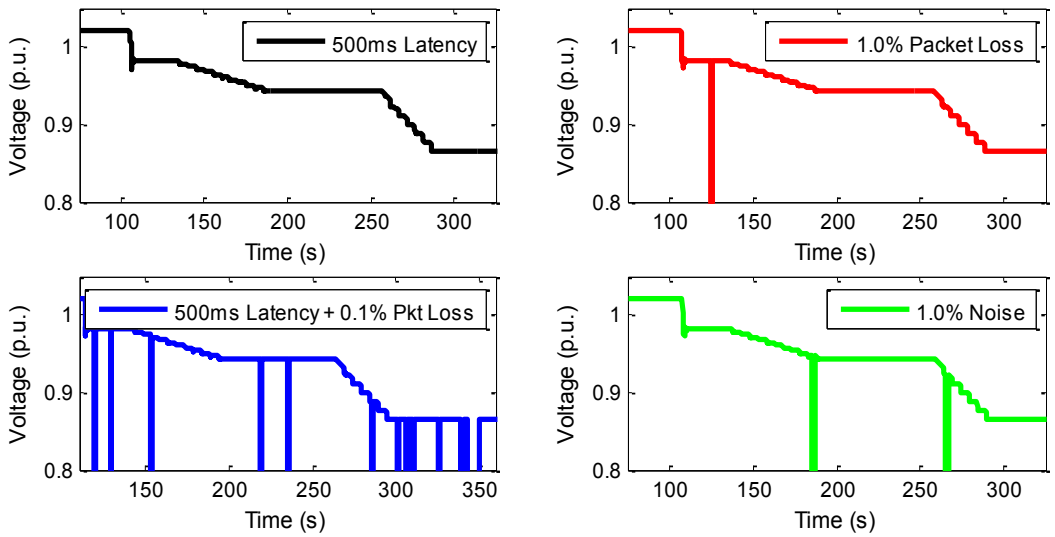

Figure 8.24: Wide Area Network (WAN) emulation for various pervasive network conditions for Bus-8 synchrophasor voltage magnitude

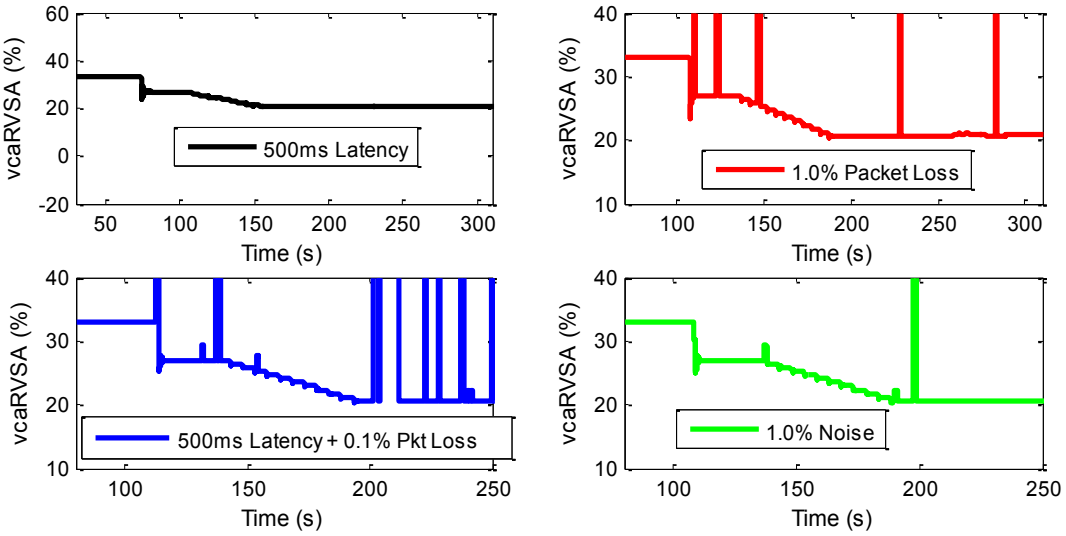

Figure 8.25: WAN emulation for various pervasive network conditions for the proposed generator-derived voltage stability assessment indices

8.4.3.5 Case Study 5

The impact of a network condition comprising of latency, jitter, packet loss, and noise on wide area protection/control signals was investigated with a N-2 line contingency that required emergency control using the proposed undervoltage load shedding SIPS (UVLS-SIPS) method.

Figure 8.26 shows the bus voltages without any pervasive WAN condition and without any emergency control. Figure 8.27 shows the plots of the binary control signal when the pervasive conditions are simulated. It can be seen from the results that the UVLS-SIPS control signal was lost as a result of the emulated pervasive network condition. The UVLS-SIPS control signal required to prevent the system from voltage collapse was not received. This resulted in a voltage collapse as shown in Figure 8.28.

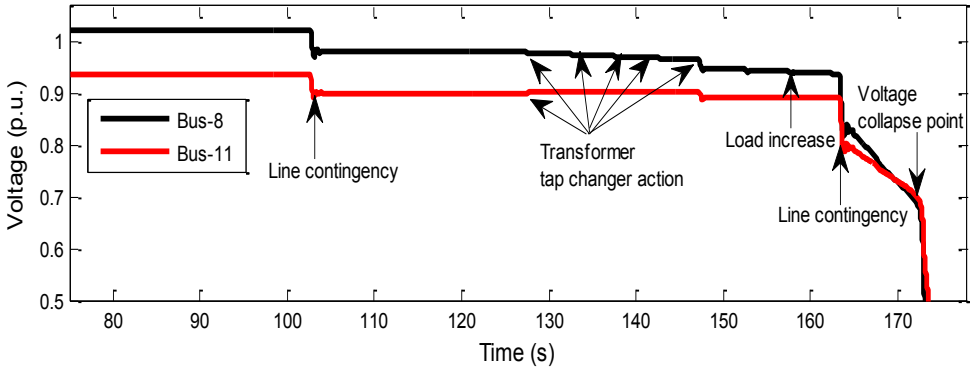

Figure 8.26: Phasor measurements of buses-8 and -11 (without latency)

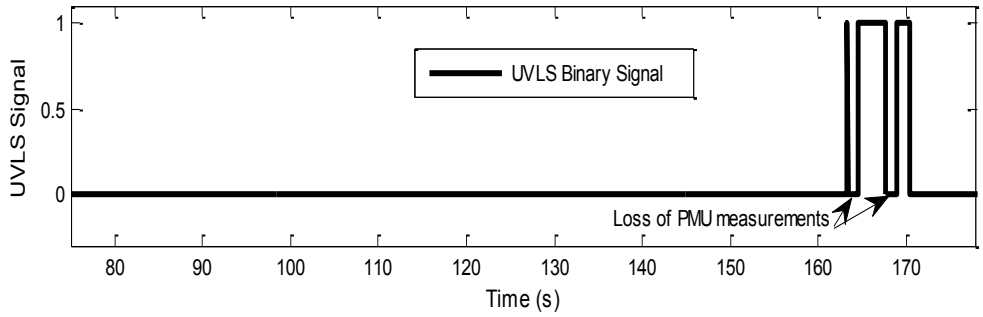

Figure 8.27: Binary signal for Case Study-5 (UVLS-SIPS fails)

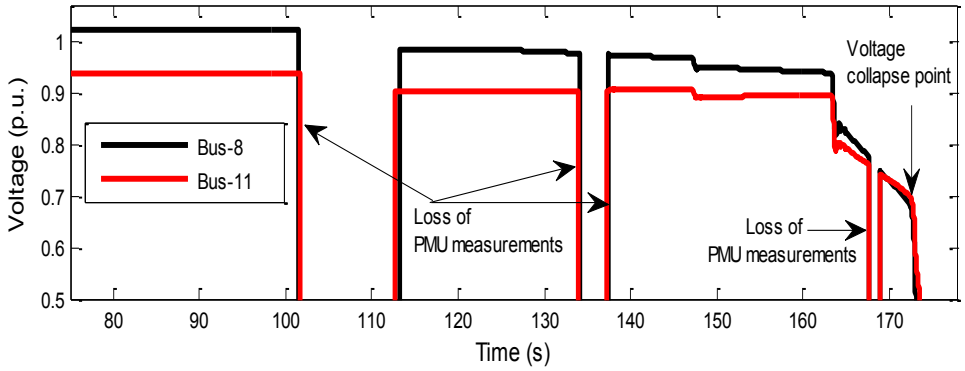

Figure 8.28: **Phasor measurements of buses-8 and -11 (UVLS-SIPS fails)**

The N-2 line contingency and increased system loading scenario was repeated using the maximum allowable network condition obtained from the studies carried out in case Studies 1-4. The UVLS-SIPS control signal was unaffected by network conditions with a latency of 500 ms, 0.1% packet loss, and 1.0% noise as shown in Figure 8.29. Figure 8.30 shows the synchrophasor measurements for buses-8 and 11 respectively. From Figure 8.30, it can be seen that the UVLS-SIPS control signal required for the undervoltage load shedding scheme was received, and voltage collapse was averted.

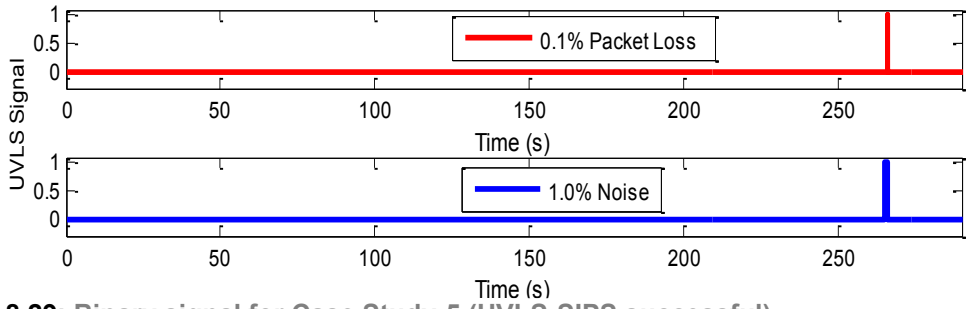

Figure 8.29: **Binary signal for Case Study-5 (UVLS-SIPS successful)**

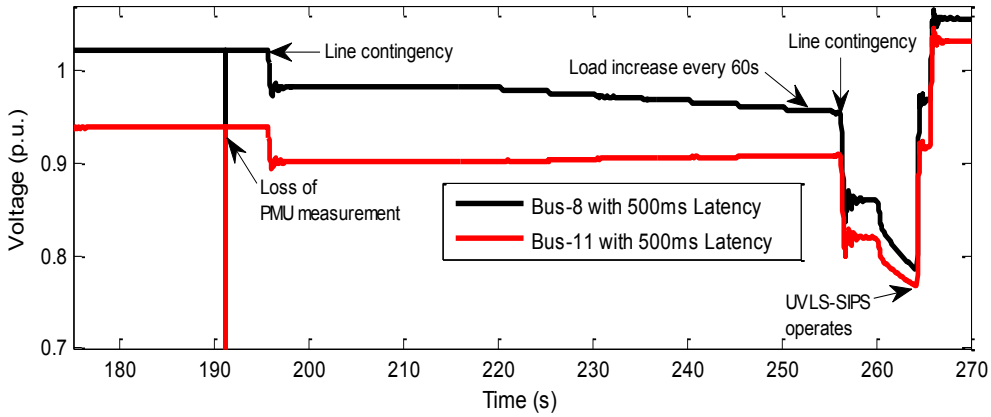

Figure 8.30: **Phasor measurements of buses-8 and -11 for Case Study-5 (UVLS-SIPS successful)**

8.4.4 Discussion

From the results obtained for the latency investigations in Case Study 1, it was observed that a delay greater than 800 ms would severely degrade the network throughput of the synchrophasor data packets. However, a latency of 800 ms represents a worst case network scenario since the typical latency obtainable in most utility communication network is about 200 ms (Thomas and McDonald, 2015). Thus, a latency of 800 ms would only occur in rare exceptional cases. Similar results were obtained for the investigations on packet losses in Case Study 2. In general, packet losses less than 2.5% were shown to be acceptable. With increased packet loses, the communication network degraded badly.

The impact of corruption due to noise and signal degradation was demonstrated in Case Study 3, while in Case Study 4, a combination of pervasive network conditions showed a reduction in the throughput of the network. As shown in Figure 8.23, only a latency of 500 ms could be tolerated simultaneously with packet losses of 0.1% and network noise of 1% for the communication network implemented in this thesis. The impact of these adverse network conditions could affect the control signals designed for mitigating power system stability as shown in Case Study-5. This would result in a failure of the wide area control/protection scheme meant to prevent collapse and system-wide blackouts.

In practical systems, the mis-operation of the control/protection scheme as a result of a signal loss can be mitigated by using the binary bit of the status of the PMUs (for example, *PMCU.OK := True*) to supervise the operation of the SIPS method. Also, channel redundancy can be used for important measurements and control signals by transmitting them using a redundant channel.

For instance, even though there was a loss in signal for the bus voltages at bus-8 and bus-11 as shown in Figure 8.26, the digital channel carrying the UVLS-SIPS control signal might not be affected. Furthermore, using higher PMU reporting rates can be applied as a countermeasure for minimizing the impact of adverse communication network conditions. A concept similar to the Parallel Redundancy Protocol (PRP) and High-availability Seamless Redundancy (HSR) protocol used in IEC 61850-based applications can also be adopted.

In addition, IP multicasting can be used in transmitting the PMU measurements to multiple PDCs simultaneously. Optionally, multiple PMUs can be used to publish important measurements and control signals. This can easily be implemented in an IEC 61850-compliant substation where all measurements are easily accessible at the process bus using an Ethernet communication network. The current and voltage measurements can then be used as the inputs to multi-channel PMUs to publish multiple synchrophasor streams. This provides redundancy, such that the noise affecting a PMU connected to a certain communication channel would probably not affect another PMU connected to a different communication channel.

The reliability of the communication network used in wide area protection/control scheme is very important. It is necessary to ensure that the communication system is available and can reliably transmit the necessary information from the substation devices to the control centre and vice versa. Migration from the existing WAN infrastructure based on power line carrier or leased lines to internet-based network should be implemented since support for some of these existing communication media (e.g. leased lines) are gradually being phased out by their service providers.

The above investigations for pervasive network conditions using the WAN emulator can be carried out for a shared communication network typically implemented in substations. Aside synchrophasor measurements, the substation process level and station level could contain IEC 61850-8-1 GOOSE messages and IEC 61850-9-2LE Sampled Values (SV) messages which are increasingly being used for process level communication, intra-substation communication, substation-to-substation communication, substation-to-control centre communication, and control centre-to-control centre communication respectively.

Preliminary studies carried out with 2 nos. merging units, a RTDS GTNET-SV card, and 4 nos. IEDs publishing a combination of IEC 61850-9-2LE SVs and IEC 61850-8-1 GOOSE messages onto a communication network shared with the synchrophasor measurements did not show any degradation in the synchrophasor measurements acquired by the control centre PDC (data archiver).

8.5 Chapter Summary

This Chapter presented the details of the investigations related to the communication network infrastructure implemented for the lab-scale testbed developed in this thesis. The communication transport protocols that are used in the streaming of the IEEE C37.118 synchrophasor measurements were discussed.

A comprehensive evaluation of the bandwidth requirement for various communication protocols was presented. Also, an investigation of the synchrophasor message structure from various PMU OEMs was carried out. Furthermore, the impact of the communication network degradation as a result of network latency, jitter, packet loss, and random noise was investigated using a Wide Area Network (WAN) emulator in a software-in-the-loop simulation with the developed WAMPAC testbed.

Chapter Nine presents a summary of the thesis, the deliverables therein, and the areas of application of the developed algorithms/methods of solution. Also, recommendations for future work and the publication outputs related to this thesis are presented.

CHAPTER NINE
CONCLUSION AND RECOMMENDATIONS

9.1 Introduction

This thesis has proposed algorithms and methods for real-time voltage stability assessment and wide area protection/control using synchrophasor measurements from PMUs. In order to successfully analyse the voltage stability of a power system, it is necessary to investigate the system's proximity to voltage collapse and the mechanism of the voltage instability/collapse. The mechanism of voltage instability involves the examination of how and why voltage instability occurs, the key factor of the voltage instability, the voltage critical/weak areas, and the effective countermeasures that can be applied to mitigate the voltage instability.

The research addressed in this thesis can be further sub-divided into two major objectives:

- Real-time voltage stability assessment.
- Centralised wide area protection/control using System Integrity Protection Schemes (SIPSs).

The first objective of this thesis is the development of algorithms and methods for wide area Real-Time Voltage Stability Assessment (RVSA). This comprises of a new measurement-based clustering method for partitioning the load buses/the synchronous generators in the system into coherent areas, and the analysis of the voltage stability of the power system using the derived RVSA indices. Three synchrophasor-based RVSA indices derived from the Reactive Power Reserve (RPR), Field Current Reserve (FCR), and Stator Current Reserve (SCR) of synchronous generators were proposed in this thesis.

The second objective of the thesis is the development of algorithms and methods that are most effective for counteracting the impending voltage instability/voltage collapse. In this regard, two SIPSs using transformer Under Load Tap Changer (ULTC) control (ULTC-SIPS) and Under-Voltage Load Shedding (UVLS-SIPS) were proposed and developed.

In order to achieve this in real-time, synchrophasor measurements from PMUs are used as inputs to all the algorithms and methods proposed in this thesis. Compared to the

conventional SCADA measurements (1 measurement every 2-10s) typically used in utilities around the world, synchrophasor measurements are capable of high speed reporting rate of up to 200 measurements every second (200 fps for 50 Hz nominal system frequency or 240 fps for 60 Hz nominal system frequency). The particular advantage of synchrophasor-based systems is that measurements from widely dispersed PMUs can be applied in accelerated schemes for real-time situational awareness and wide area protection/control.

A 'proof-of-concept' Wide Area Monitoring, Protection and Control (WAMPAC) testbed was designed, implemented and deployed at the Centre for Substation Automation and Energy Management Systems (CSAEMS) for the investigations relating to this thesis. Industrial grade equipment comprising of the RTDS®, PMUs, PDCs, PLC, IEDs, satellite clocks, and communication network switches were used.

Transmission line contingencies (N-1, N-2), generator contingencies, impact of generator OXL, and transformer ULTC actions were investigated using two test systems (the 10-bus multi-machine test system and the New England 39-bus test system) modelled in RSCAD and DIgSILENT PowerFactory software, and hardware-in-the-loop simulations were carried out for various operating scenarios.

9.2 Thesis Deliverables

The deliverables of this research are based on the aim and objectives hitherto highlighted in Chapter One. The various aspects of the deliverables are further elucidated in the subsections below.

9.2.1 Literature Review

Extensive literature review covering a span of 35 years (1980-2015) was carried out on voltage stability assessment and system integrity protection schemes. The review on voltage stability assessment methods were categorised and discussed under the following: (i) methodologies based on load flow calculations; (ii) methodologies based on local measurements; and (iii) methodologies based on wide area measurements. Also, the literature review on system integrity protection schemes was discussed under (i) transformer tap-changer control; and (ii) method for under-voltage load shedding. These reviews are presented in Chapters Two and Three respectively.

9.2.2 Optimal PMU Placement (OPP) Problem

New formulations and modification of the methods of solution of the OPP problem for minimising the number of PMUs required and their optimal location with respect to voltage stability assessment in power systems is proposed. For lack of space, references are made to the technical articles emanating from this as presented in (Adewole and Tzoneva, 2015e; 2014a). The proposed OPP formulations incorporate the impact of the critical/voltage weak buses and the buses with zero injection on the full observability of the system. Also, the problem formulation for measurement redundancy for a single PMU outage was proposed and investigated. The related MATLAB code developed for this is presented in Appendix B.

9.2.3 Measurement-Based Clustering Algorithm for Voltage Stability Assessment

A measurement-based approach in the identification of coherent groups in load buses and synchronous generators for voltage stability assessment application was developed. The newly proposed method is a hybrid combination of the Calinski-Harabasz algorithm and the *k*-means algorithm, and was developed in MATLAB. The Calinski-Harabasz algorithm was used in the determination of the optimal number of clusters, while the *k*-means algorithm was used in the partitioning of the load buses and the synchronous generators in the system. The derivations relating to these are presented in Chapter Four, and in one publication (Adewole and Tzoneva, 2015a). The related MATLAB code developed for this is presented in Appendix C.

9.2.4 Real-Time Voltage Stability Assessment Method

Voltage stability assessment was carried out using newly derived synchrophasor-based Real-Time Voltage Stability Assessment (RVSA) indices obtained from the RPR, FPR, and SCR of synchronous generators. These indices effectively provided the percentage margin of the system from its current operating point to the voltage collapse point for both small disturbance voltage instability and large disturbance voltage instability resulting from various system conditions such as increased system loading, line/generator contingencies, operation of transformer Under-Load Tap Changers (ULTCs), and generator Over Excitation Limiters (OXLs).

The RVSA indices were also applied in the design of a real-time machine learning classifier and regressor for the online prediction of the operating state of the power system and the system's margin to voltage collapse. The developed DT-classifier is used in the classification of the operating state of the system into 'Stable', 'Alert', or 'Unstable'

state depending on the prevailing operating condition of the power system as captured by the synchrophasor measurements.

The proposed RVSA indices were extended for application in large interconnected systems using the key generator approach, and were further extended for large interconnected multi-area power systems by proposing a weighted-summation approach. The derivations relating to all these are presented in Chapter Four, and in five publications (Adewole and Tzoneva, 2016d; 2015f; 2015c; 2015b; 2014b) respectively. The related software codes are developed using the IEC 61131-3 Structured Text (ST) programming language and are presented in Appendices D1-D6.

9.2.5 Transformer Tap-Changer Control (ULTC-SIPS) Method

In order to halt the transition of a voltage instability condition in the power into a voltage collapse or cascading blackouts, a system integrity protection scheme using transformer tap-changer control (ULTC-SIPS) for blocking and unblocking the key transformer ULTCs in the system was proposed. The ULTC-SIPS algorithm was designed for real-time online application using synchrophasor measurements from PMUs and accelerated control actions using IEC 61850 GOOSE messages.

The design of the ULTC-SIPS algorithm is presented in Chapter Seven. Also, this is documented in two publications (Adewole *et al*., 2015d; 2014c). The related software codes developed for this are written using the IEC 61131-3 ST programming language and are presented in Appendix D7.

9.2.6 Under-Voltage Load Shedding (UVLS-SIPS) Method

An Under-Voltage Load Shedding SIPS (UVLS-SIPS) algorithm was designed in this thesis as the second line of defence if the ULTC-SIPS fails to halt the system's transition into a voltage instability condition. This resulted in the formulation and design of a non-threshold adaptive UVLS-SIPS method and algorithm based on the reactive power mismatch at the reactive power sources in the smart grid.

Since the System Frequency Response (SFR) model method is highly dependent on the rate of change of frequency and the commonly used real power mismatch method cannot be applied in power system controlled by synchronous generator governors with fixed mechanical torque set-point, a method based on the reactive power mismatch was proposed in this thesis.

The reactive power mismatch is used in the prediction of the amount of load to shed in real-time using the Least Squares (LS) algorithm. Also, the UVLS-SIPS method and algorithm are formulated and designed for large interconnected smart grids using synchrophasor measurements from PMUs and not SCADA measurements.

Furthermore, the distribution of the amount of load to shed among the Voltage Control Areas (VCAs) in an interconnected smart grid is based on the computed adaptive weighted summation Real-Time Voltage Stability Assessment (RVSA) index. In addition, the candidate load buses for load shedding within each respective VCA were selected based on the level of the prevailing disturbance in the system using the voltage dip information at the load buses. Comparisons were made with the conventional distributed undervoltage (27) protective relays. The design, implementation, and results obtained are presented in Chapter Seven and in (Adewole *et al*., 2016a). The IEC 61131-3 ST codes are given in Appendix D8.

9.2.7 Real-Time Lab-Scale WAMPAC Testbed

The algorithms and methods proposed in this thesis are tested and validated in real-time using the lab-scale hardware-in-the-loop WAMPAC testbed designed and implemented in Chapter Five. This was carried out using industrial-grade equipment comprising of the RTDS®, analogue output amplifiers, GPS satellite clock, RTDS-GTNET-PMU, PMUs, PDCs, SEL-3378 SVP, and substation communication network switches.

Two power system benchmark networks were modelled in RSCAD software and used with the RTDS® for real-time HIL batchmode simulations. The software code written for the batchmode simulations are given in Appendix I. The software codes written to execute the various algorithms and methods are integrated in the SEL-3378 SVP using the IEC 61131-3 programming language as given in Appendices B1-B8. Also, the developed WAMPAC testbed was used in the experimentation relating to the analysis of the IEEE C37.118 synchrophasor message framework.

Furthermore, the impact of the degradation of the communication network infrastructure from pervasive network conditions due to network latency, jitter, packet loss, and random noise on the developed WAMPAC testbed was investigated using a Wide Area Network (WAN) emulator in a software-in-the-loop simulation with the WAMPAC testbed.

The implementation and results obtained are presented in Chapter Eight and in (Adewole *et al*., 2016c).

9.3 Software Development

The software codes for the implementation of the real-time voltage stability assessment and wide area protection/control algorithms and methods proposed in this thesis are presented in Table 8.1. The codes covered the MATLAB subroutines, the IEC 61131-3 ST POUs, and the programming code for the RTDS® batchmode simulations.

Table 9.1: Software developed

S/N	Function name	Application	Appendix
1	OPP_binint_prog.m	OPP method	Appendix B
2	kmeans_coherency.m	Measurement based clustering of load and generator buses	Appendix C
3	CART_CT.m	Growing of DT for the classification task	Appendix D1
4	CART_CT_Bag.m	Growing of EDT for the classification task using the Bagging technique	Appendix D2
5	CART_CT_ADABoostM.m	Growing of EDT for the classification task using the Boosting technique	Appendix D3
6	RTDS Batchmode simulation	Automated script for real-time simulations using the RTDS	Appendix E
7	Time Alignment Client Server (TCS) POU	Concentrates and time-aligns the synchrophasor measurements from the PMU	Appendix F1
8	Mov_Avg POU	Used in the calculation of the moving averages of the PMU measurements concentrated by the PDC	Appendix F2
9	Local PMCU POU	Used for configuring the PLC as a C37.118 server	Appendix F3
10	Phase angle difference (PADIFF) POU	Phase angle difference calculation	Appendix F4
11	wSUM_VCA POU	Calculation of the weighted summation wide area RVSA index	Appendix F5
12	CART_CT POU	Implements the DT-classifier in the PLC for real-time application	Appendix F6
13	SIPS-ULTC POU	Implements the transformer ULTC-SIPS algorithm	Appendix F7
14	BAY_CTRL (FB)	POU for the implementation of the UVLS-SIPS algorithm	Appendix F8
15	UVLS_Curve_Fitting.m	Least squares algorithm for undervoltage load shedding	Appendix G

9.4 Application of the Developed Algorithms and Methods of Solution

The synchrophasor-based algorithms and methods of solution proposed in this thesis for voltage stability assessment and wide area protection/control can be used for both academic and industrial applications relating to power systems. These various applications are presented below.

9.4.1 Industrial Application

The developed algorithms and methods of solution can be effectively applied in electric power utilities and can be used in the development of new devices by Original Equipment Manufacturers (OEMs) for application in smart grids. Some of these applications include:

- Power system planning and analysis in utilities.
- Power system operations.
- Power system monitoring, protection and control at the control centre.
- The ideas and approaches presented can be used for research and development at utility companies, and in the development of devices for smart grid applications by OEMs.
- The outcome of the thesis can also be used in the training and retraining of engineers, control centre dispatchers, and technicians.
- The proposed algorithms and methods can be applied practically with little modification in utilities for real-time situational awareness of the power system, and the rapid mitigation of an impending voltage collapse through the application of the proposed system integrity protection schemes comprising of transformer tap-changer control (ULTC-SIPS) and under-voltage load shedding (UVLS-SIPS).

9.4.2 Academic Application

The developed algorithms and methods of solution can be used for teaching, training, and research at universities as described below:

- The developed benchmark models of the 10-bus multi-machine test system and the New England 39-bus test system incorporating recent technologies such as the IEEE C37.118 synchrophasor measurements and IEC 61850 GOOSE messages can be used in the teaching and training of Students in preparation for future employment in electric power utilities.
- The developed WAMPAC testbed can be further used for future research work by Post Graduate Students.
- The concepts and dynamics in power system stability and control can be better taught to Students practically through the use of the developed real-time WAMPAC testbed.

9.5 Future Work

Some of the algorithms and methods proposed in this thesis can be further extended as summarised below:

- Summer loads are made up of air conditioning loads typically modelled using induction motor loads. Similarly, winter loads are mainly heating loads controlled by thermostats. The impact of these load types on the proposed RVSA indices with respect to voltage stability can be further investigated through the development of composite load models comprising of induction motor model, ZIP load model, and exponential load model using the CBuilder module in RSCAD.
- Investigations on strategies to coordinate the UVLS-SIPS with reactive power sources would be highly beneficial. This can be taken further by considering the reactive power support possible in power systems integrated with wind farms comprising of Doubly-Fed Induction Generators (DFIG) and Permanent Magnet Wind Generators (PMWGs).
- The proposed UVLS-SIPS algorithm is presented as a practical method which can be applied in utilities for undervoltage load shedding. The optimal amount of load to shed can be further investigated by using optimization methods. However, the use of optimization algorithms usually requires several iterations. Thus, it would be difficult to have an UVLS-SIPS algorithm running in real-time mode except if high-speed parallel computation is utilised.
- This thesis can be further extended by considering the restoration of loads after load shedding. This would involve preferably a central restoration process whereby the dispatcher after being satisfied that the system is operating within acceptable limits with all the faults/contingencies cleared, can now begin the load restoration sequence. The load to be restored must be adequately distributed across the system just as the load shedding process was distributed. In this regard, the load restoration process for large interconnected multi-area power systems would need to consider when to restore, where to restore, the time delay, how much to restore, and the distribution of the loads to restore.
- In Chapter Eight, an investigation on the impact of network latency and packet loss on synchrophasor measurements from PMUs was carried out. This can further be extended to cover methods for mitigating network latency, noise, and interpolation methods for missing synchrophasor measurements in WAMPAC schemes. Also, the security of synchrophasor measurements with respect to confidentiality, integrity, and availability should be investigated. Furthermore, the

possible impact of the delays that can be caused by cyber security authentication and encryption on synchrophasor-based wide area schemes can be investigated. In addition, IEC 61850 Parallel Redundancy Protocol (PRP) and High-availability Seamless (HSR) Protocol can be adapted for use in synchrophasor applications. This would require a study of the impact of these protocols on synchrophasor data communication, communication bandwidth, and data archiving.

9.6 Publications Related to the Thesis

Publications in reputable journals and peer-reviewed conferences that have directly stemmed from this thesis are presented in this section.

9.6.1 Journal Publications

1. Adewole, A.C., Tzoneva, R., Apostolov, A. 2016a. Adaptive Under-Voltage Load Shedding Scheme for Large Interconnected Smart Grids Based on Wide Area Synchrophasor Measurements. *IET Generation, Transmission, & Distribution,* vol. 10, iss. 8, pp. 1957-1968 (ISI Thompson and Scopus indexed).
2. Adewole, A.C., Tzoneva, R. 2016b. Wide Area Real-Time Voltage Stability Assessment using Surrogate-Splits from Synchrophasor Measurements. *Electric Power Systems Research (EPSR),* pp. 1-24 (*Under review*) (ISI Thompson and Scopus indexed).
3. Adewole, A.C., Tzoneva, R. 2015a. Synchrophasor-Based Online Coherency Identification in Voltage Stability Assessment. *Advances in Electrical and Computer Engineering (AECE)*, vol. 15, no. 4, pp. 33-42 (ISI Thompson and Scopus indexed).
4. Adewole, A.C., Tzoneva, R. 2015b. Using generator-derived indices to assess wide area voltage stability. *Energize Magazine, October 2015*, pp. 21-26.
5. Adewole, A.C., Tzoneva, R. 2015c. Extended Synchrophasor-Based Online Voltage Stability Assessment Using Synchronous Generator-Derived Indices. *International Transactions on Electrical Energy Systems*, pp. 1-23 (*accepted, in print*) (ISI Thompson and Scopus indexed).
6. Adewole, A.C., Tzoneva, R., Apostolov, A. 2015d. Real-Time Under-Load Tap-Changer Control Based on Synchrophasor Measurements. *Revue Roumaine Des Sciences Techniques Serie Electrotechnique et Energetique*, pp. 1-10 (*accepted, in print*) (ISI Thompson and Scopus indexed).

7. Adewole, A.C., Tzoneva, R. 2015e. Extended Optimal PMU Placement Problem for Voltage Stability Assessment. *WSEAS Transactions on Power Systems*, pp. 1-13 (a*ccepted for publication*) (Scopus indexed).
8. Adewole, A.C., Tzoneva, R. 2014a. Optimal PMU Placement for Voltage Stability Assessment in Power System Networks. *International Review of Electrical Engineering (IREE)*, vol. 9, no.4, pp. 811-820 (Scopus indexed).
9. Adewole, A.C., Tzoneva, R. 2014b. Real-Time Deployment of a Novel Synchrophasor-Based Voltage Stability Assessment Algorithm. *International Review of Electrical Engineering (IREE)*, vol. 9, no.5, pp. 1021-1033 (Scopus indexed).

9.6.2 Conference Publications

10. Adewole, A.C., Tzoneva, R., Apostolov, A. 2016c. Analysis of the Impact of Pervasive Wide Area Communication Network Conditions on the Disturbance Recordings from Phasor Measurement Units (PMUs). *19th Annual Georgia Tech Fault and Disturbance Analysis Conference, 18-19 April, 2016*, Atlanta, Georgia, USA, pp. 1-8.
11. Adewole, A.C., Tzoneva, R. 2016d. Impact of Customer Load Characteristics on Voltage Stability Assessment in Smart Grids using Synchrophasor Measurements. *Domestic Use of Energy Conference (DUE) Conference 2016*, *29-31, March 2016*, Cape Town, South Africa, pp. 91-97.
12. Adewole, A.C., Tzoneva, R. 2016e. Real-Time Simulations Using a Synchrophasor-Based Wide Area Monitoring, Protection, and Control (WAMPAC) Testbed. *RTDS 2016 Southern Africa User's Group Meeting, 25th January, 2016, Johannesburg, South Africa*.
13. Adewole, A.C., Tzoneva, R. 2015f. Wide Area Voltage Stability Assessment Based on Generator-Derived Indices Using Phasor Measurement Units. *Industrial and Commercial Use of Electricity (ICUE) Conference 2015*, 17-19 August 2015, Cape Town, South Africa, pp. 291-298.
14. Adewole, A.C., Tzoneva, R. 2015g. Emerging Technologies for Wide Area Monitoring, Protection and Control for Electric Power Utilities in Africa. *Presentation at African Utility Week, 12-14 May 2015*, Cape Town, South Africa.
15. Adewole, A.C., Tzoneva, R., Apostolov, A. 2014c. *System Integrity Protection Scheme Based on Under-Load Tap Changer Blocking Using Synchrophasor Measurements and IEC 61850 GOOSE Messages*. *PAC World Americas*

Conference 2014, 23–25 September 2014, Raleigh, North Carolina, USA, pp. 1-20.

9.7 Conclusion

This thesis proposed algorithms and methods for voltage stability assessment using synchrophasor measurements from actual IEEE C37.118 compliant PMUs. Three synchronous generator-derived RVSA indices were investigated and tested using two benchmark test systems modelled in the RSCAD software. Results were presented for various operating conditions to validate the proposed RVSA indices. The RVSA index derived from the reactive power of the synchronous machines was shown to give steep response which can be misleading. The RVSA index obtained from the stator current of the synchronous machines was shown to give good results indicative of the true situation of system operating state. The RVSA index from the field current of the synchronous machines also gave acceptable indication when used with the proposed adaptive weighted summation vcaRVSA index.

Two countermeasures to mitigate voltage instability and blackouts that can be caused by voltage collapse in the power system were proposed. The first SIPS method (ULTC-SIPS) is based on transformer tap-changer control, while the last resort method (UVLS-SIPS) is based on undervoltage load shedding. The measurements to the SIPSs are IEEE C37.118 synchrophasor measurements, while the control signals are via high speed IEC 61850-8-1 GOOSE messages.

The deliverables of this thesis were successfully achieved as highlighted above. The various fields where the proposed algorithms and methods can be applied have been described. Also, the possible directions by which the research in this thesis can be further extended were discussed. Finally, a list of the publications emanating from this thesis was presented.

REFERENCES

[1] Abdelwahid, S., Babiker, A., Eltom, A., Kobet, G. 2014. Hardware Implementation of an Adaptive Centralized Underfrequency Load Shedding Scheme. *IEEE Transactions on Power Delivery,* vol. 29, no. 6, pp. 2664-2673.

[2] Adewole, A.C., Tzoneva, R. 2014a. Optimal PMU Placement for Voltage Stability Assessment in Power System Networks. *International Review of Electrical Engineering (IREE)*, vol. 9, no.4, pp. 811-820.

[3] Adewole, A.C., Tzoneva, R. 2014b. Real-Time Deployment of a Novel Synchrophasor-Based Voltage Stability Assessment Algorithm. *International Review of Electrical Engineering (IREE)*, vol. 9, no.5, pp. 1021-1033.

[4] Adewole, A.C., Tzoneva, R., Apostolov, A. 2014c. System Integrity Protection Scheme Based on Under-Load Tap Changer Blocking Using Synchrophasor Measurements and IEC 61850 GOOSE Messages. *PAC World Americas Conference 2014, 23–25 September 2014*, Raleigh, North Carolina, USA, pp. 1-20.

[5] Adewole, A.C., Tzoneva, R. 2015a. Synchrophasor-Based Online Coherency Identification in Voltage Stability Assessment. *Advances in Electrical and Computer Engineering (AECE)*, vol. 15, no. 4, pp. 33-42.

[6] Adewole, A.C., Tzoneva, R. 2015b. Using generator-derived indices to assess wide area voltage stability. *Energize Magazine, October 2015*, pp. 21-26.

[7] Adewole, A.C., Tzoneva, R. 2015c. Extended Synchrophasor-Based Online Voltage Stability Assessment Using Synchronous Generator-Derived Indices. *International Transactions on Electrical Energy Systems*, pp. 1-23.

[8] Adewole, A.C., Tzoneva, R., Apostolov, A. 2015d. Real-Time Under-Load Tap-Changer Control Based on Synchrophasor Measurements. *Revue Roumaine Des Sciences Techniques Serie Electrotechnique et Energetique*, pp. 1-10.

[9] Adewole, A.C., Tzoneva, R. 2015e. Extended Optimal PMU Placement Problem for Voltage Stability Assessment. *WSEAS Transactions on Power Systems*, pp. 1-13.

[10] Adewole, A.C., Tzoneva, R. 2015f. Wide Area Voltage Stability Assessment Based on Generator-Derived Indices Using Phasor Measurement Units. *Industrial and Commercial Use of Electricity (ICUE) Conference 2015*, 17-19 August 2015, Cape Town, South Africa, pp. 291-298.

[11] Adewole, A.C., Tzoneva, R., Apostolov, A. 2016a. Adaptive Under-Voltage Load Shedding Scheme for Large Interconnected Smart Grids Based on Wide Area Synchrophasor Measurements. *IET Generation, Transmission, & Distribution,* pp. 1-12.

[12] Adewole, A.C., Tzoneva, R. 2016b. Wide Area Synchrophasor-Based Voltage Stability Assessment Using Surrogate-Splits Decision Trees. *Journal of Electrical Engineering (JEE),* pp. 1-8.

[13] Adewole, A.C., Tzoneva, R., Apostolov, A. 2016c. Analysis of the Impact of Pervasive Wide Area Communication Network Conditions on the Disturbance Recordings from Phasor Measurement Units (PMUs). *19th Annual Georgia Tech Fault Disturbance and Analysis Conference, 18-19 April, 2016*, Georgia, USA.

[14] Adewole, A.C., Tzoneva, R. 2016d. Impact of Customer Load Characteristics on Voltage Stability Assessment in Smart Grids using Synchrophasor Measurements. *Domestic Use of Energy Conference (DUE) 29-31, March 2016, Cape Town, South Africa, pp. 91-97.*

[15] Adibi, M.M., Thorne, D.K. 1988. Local Load Shedding. *IEEE Transactions on Power Systems,* vol. 3, no. 3, pp. 1220-1226.

[16] Affonso, C.M., da Silva, L.C.P., Lima, F.G.M., Soares, S. 2004. MW and MVAr Management on Supply and Demand Side for Meeting Voltage Stability Margin Criteria. *IEEE Transactions on Power System,* vol. 19, pp. 1538-1545.

[17] Agrawal, R., Thukaram, D. 2013. Support Vector Clustering-Based Direct Coherency Identification of Generators in a Multi-Machine Power System. *IET Generation, Transmission & Distribution,* vol. 7, no. 12, pp. 1357-1366.

[18] Ajjarapu, V., Christy, C. 1992. The Continuation Power Flow: A Tool for Steady State Voltage Stability Analysis. *IEEE Transactions on Power Systems*, vol. 7, no. 1, pp. 416-423.
[19] Ajjarapu, V., Lee, B. 1992. Bifurcation Theory and Its Application to Nonlinear Dynamical Phenomena in an Electrical Power System. *IEEE Transactions on Power Systems,* vol 7, pp. 424-431.
[20] Ajjarapu, V., Lau, P.L., Battula, S. 1994. An optimal reactive power planning strategy against voltage collapse. *IEEE Transactions on Power Systems,* vol. 9, pp. 906-917.
[21] Ajjarapu, 2006. Computational Techniques for Voltage Stability Assessment and Control. New York: Springer.
[22] Amraee, T., Ranjbar, A.M., Mozaferi, B., Sadati, N. 2006. An enhanced under-voltage load-shedding scheme to provide voltage stability. *Electric Power Systems Research*, vol. 77, pp. 1038-1046.
[23] Amraee, T., Ranjbar, A.M., Mozafari, B., Sadati, N. 2007. An enhanced under-voltage load-shedding scheme to provide voltage stability. *Electric Power Systems Research*, vol. 77, pp. 1038-1046.
[24] Amraee, T., Ranjbar, A.M., Feuillet, R. 2011. Adaptive under-voltage load shedding scheme using model predictive control. *Electric Power Systems Research*, vol. 81, pp. 1507-1513.
[25] Anderson, P.M., Mirheydar, M. 1992. An Adaptive Method for Setting UnderFrequency Load Shedding Relays. *IEEE Transactions on Power Systems,* vol. 7, no. 2, pp. 647-653.
[26] Andersson, P.M., Fouad, A.A. 2003. Power System Control and Stability 2 ed. John Wiley & Sons.
[27] Anderson, P.M., LeReverend, B.K. 1996. Industry experience with special protection schemes. *IEEE Transactions on Power System,* vol. 11, no. 3, pp. 1166-1179.
[28] Apostolov, A. 2014. System Integrity Protection Schemes: Functional Testing. *PAC World Magazine*, *March, 2014,* vol. 27, pp. 47-51.
[29] Arefi, A., Hagfiham, M.R., Fathi, S.H. 2011. Observability analysis of electric networks considering branch impedance. *Electrical Power and Energy Systems*, vol. 33, pp. 954-960.
[30] Ariff, M.A.M., Pal, B.C. 2013.Coherency Identification in Interconnected Power System-An Independent Component Analysis Approach. *IEEE Transactions on Power Systems,* vol. 28, no. 2, pp. 1747-1755.
[31] Arnborg, S., Andersson, G., Hill, D.J., Hiskens, I.A. 1997. On undervoltage load shedding in power systems. *Electrical Power & Energy System*, vol. 19, no. 2, pp. 141-149.
[32] Arnborg, S., Andersson, G., Hill, D.J., Hiskens, I.A. 1998. On Influence of Load Modelling for Undervoltage Load Shedding Studies. *IEEE Transactions on Power System*s, vol. 13, no. 2, pp. 395-400.
[33] Arya, L.D., Pande, V.S., Kothari, D.P. 2005. A technique for load-shedding based on voltage stability consideration. *Electrical Power and Energy Systems,* vol. 27*,* pp. 506-517.
[34] Arya, L.D., Singh, P., Titare, L.S. 2012. Differential evolution applied for anticipatory load shedding with voltage stability considerations. *Electric Power Systems Research*, vol. 42, pp. 644-652.
[35] Aschmoneit, F.C., Verstege, J.F. 1979. An External System Equivalent for On-Line Steady-State Generator Outage Simulation. *IEEE Transactions on Power Apparatus and Systems,* vol. pas-98, no. 3, pp. 770-779.
[36] Aumuller, C.A., Saha, T.K. 2003. Determination of Power System Coherent Bus Groups by Novel Sensitivity-Based Method for Voltage Stability Assessment. *IEEE Transactions on Power Systems, vol. 18, no. 3,* pp. 1157-1164.
[37] Avramovik, B., Fink, L.K. 1992. Real-Time Reactive Security Monitoring. *IEEE Transactions on Power Systems,* vol. 7, no. 1, pp. 432-437.

[38] Bahadornejad, M., Nair, NK.C. 2014. Intelligent Control of On-Load Tap Changing Transformer. *IEEE Transactions on Smart Grid,* vol. 5, no. 5, pp. 2255-2263.
[39] Bahmanyar, A.R., Karami, A. 2014. Power System Voltage Stability Monitoring using Artificial Neural Networks with a Reduced Set of Inputs, *Electric Power and Energy Systems,* vol. 58, pp. 246-256.
[40] Balamourougan, V., Sidhu, T.S., Sachdev, M.S. 2004. Technique for online prediction of voltage collapse. *IEEE Proceedings in Generation, Transmission and Distribution*. vol. 151, no. 4, pp. 453-460.
[41] Balanathan, R., Pahalawaththa, N.C., Annakkage, U.D. 1998. A Strategy for Undervoltage Load Shedding in Power Systems. in *Proceedings International Conference on Power System Technology*, POWERCON Beijing, China, 18-21 August, 1998, vol. 2, pp. 1494-1498.
[42] Bao, L., Huang, Z., Xu, W. 2003. Online Voltage Stability Monitoring Using VAR Reserves. *IEEE Transactions on Power Systems*, vol. 18, pp. 1461-1469.
[43] Barquin, J., Gomez, T., Pagola, F.L. 1995. Estimating the Loading Limit Margin Taking into Account Voltage Collapse Areas. *IEEE Transactions on Power Systems*, vol. 10, no. 4, pp. 1952-1962.
[44] Bassett, D.L. 1993. Control of Tap Change Under Load Transformers Through the Use of Programmable Logic Controllers. *IEEE Transactions on Power Delivery*, vol. 8, no. 4, pp. 1759-1765.
[45] Bedoya, D., Bedrinana, M.F., Castro, C.A., da Silva, L.C.P. 2008. Power system critical areas by using sensitivities and participation factors for online applications. *IEEE/PES* Transmission and Distribution Conference, 2008, pp. 1-6.
[46] Begovic, M.M., Phadke, A.G. 1992. Control of Voltage Stability using Sensitivity Analysis. *IEEE Transactions on Power Systems,* vol. 7, no. 1, pp. 114-123.
[47] Begovic, M., Fulton, D., Gonzalez, M.R., *et al*., 1995. Summary of System Protection and Voltage Stability. *IEEE Transactions on Power Delivery,* vol. 10, no. 2, pp. 631-638.
[48] Begovic, M., Madani, V., Novosel, D. 2007. System Integrity Protection Schemes (SIPS). *2007 iREP Symposium-Bulk Power System Dynamics and Control-VII, Revitalizing Operational Reliability August 19-24, 2007, Charleston, USA,* pp.1-6.
[49] Beiraghi, M., Ranjbar, A.M. 2013. Online Voltage Security Assessment Based on Wide – Area Measurements. *IEEE Transactions on Power Delivery,* vol. 28, no. 2, pp. 989-997
[50] Berg G.J., Sharaf T.A. 1994. System loadability and load shed. *Electric Power System Research,* vol. 28, pp. 217-225.
[51] Berizzi, A., Finazzi, P., Dosi, D., Marannino, P., Corsi, S. 1998. First and Second Order Methods for Voltage Collapse Assessment and Security Enhancement. *IEEE Transactions on Power Systems,* vol. 13, no. 2, pp. 543-551.
[52] Berizzi, A., Zeng, Y.G., Marannino, P., Vaccarini, A., Scarpellini, P.A. 2002. A Second Order Method for Contingency Severity Assessment with respect to Voltage Collapse. *IEEE Transactions on Power Systems, vol. 15, no. 1*, pp. 81-87.
[53] Bijwe, P.R., Tare, R.S., Kelapure, S.M. 1999. Anticipatory load shedding scheme for loadability enhancement. *IEE Proceedings on Generation, Transmission, & Distribution*, vol. 146, no.5, pp. 483-490.
[54] Blumsack, S., Hines, P., Patel, M., Barrows, C., Sanchez, E.C. 2009. Defining Power Network Zones from Measures of Electrical Distances. *in Proceeding IEEE PES General Meeting*, Jul. 26-30, pp. 1-8.
[55] Bose, A. 1984. Modelling of External Networks for On-Line Security Analysis. *IEEE Transactions on Power and Apparatus and Systems,* vol. PAS-103, no. 8, pp. 2117-2125.
[56] Breiman, L. 1996. Bagging predictors. *Machine Learning*, vol. 24, no. 2, pp. 123-140.
[57] Breiman, L., Friedman, J., Olshen, R.A., Stone, C.J. 1984. *Classification and Regression Trees*, Belmont Wadsworth.

[58] Cai, L.J., Erlich, I. 2007. Power System Static Voltage Stability Analysis Considering all Active and Reactive Power Controls-Singular Value Approach. *2007 IEEE Power Tech Lausanne*, pp. 367-373.
[59] California Energy Commission: Energy Research and Development-Final Project Report on Extreme Events, 2013.
Available: http://www.energy.ca.gov/2013publications/CEC-500-2013-031/CEC-500-2013-031.pdf.
[60] Calinski, T., Harabasz, J. 1974. A dendrite method for cluster analysis. *Communications in Statistics*, vol. 3, no. 1, pp. 1-27.
[61] Canizares, C.A., Alvarado, F.L., DeMarco, C.L., Dobson, I., Long, W.F. 1992. Point of Collapse Methods Applied to AC/DC Power Systems. *IEEE Trans. Power Systems,* vol. 7, no. 2, pp. 673-683.
[62] Canizares, C.A. 1995. On Bifurcations, Voltage Collapse and Load Modelling. *IEEE Trans. Power Systems,* vol. 10, no. 1, pp. 512-518.
[63] Capitanescu, F., Van Cutsem, T. 2001. Evaluation of reactive power reserves with respect to contingencies. *In Proceedings Bulk Power System Dynamics and Control V, Onomichi, Japan,* pp. 377-386.
[64] F. Capitanescu, B. Otomega, H. Lefebvre, V. Sermanson, T. Van Cutsem, Decentralized tap changer blocking and load shedding against voltage instability: Prospective tests on the RTE system, *International Journal Electrical Power & Energy Systems*, vol. 31, pp. 570-576, 2009.
[65] Cepeda, J.C., Ramirez, D., Colome, D.G. 2014. Real-time adaptive load shedding based on probabilistic overload. *Proceedings IEEE PES Latin America Transmission and Distribution Conference and Exposition*, *10-13 September 2014*, pp. 1-6.
[66] Chakrabarti, S., Kyriakides, E. 2008. Optimal Placement of Phasor Measurement Units for Power System Observability. *IEEE Transaction on Power Systems*, vol. 23, no. 3, pp. 1433-1440.
[67] Chang, C.S., Huang, J.S. 1999. Centralized Control of Transformer Tap Changing for Voltage Stability Enhancement. *Electric Machines & Power Systems*, vol. 27, no.10, pp. 1041-1054.
[68] Chebbo, A.M., Irving, M.R., Sterling, M.J.H. 1992. Voltage Collapse Proximity Indicator: Behaviour and Implications. *IEE Proceedings,* vol. 139, no. 3, pp. 241-252.
[69] Chen, K., Hussein, A., Bradley, M.E., Wan, H. 2003. A Performance-Index Guided Continuation Method for Fast Computation of Saddle-Node Bifurcation in Power Systems, *IEEE Transactions on Power Systems,* vol. 18, no.2, pp. 753-760.
[70] Choi, J.H., Kim, J.C. 2001. The Online Voltage Control of ULTC Transformer for Distribution Voltage Regulation. *Electrical Power and Energy Systems,* vol. 23, pp. 91-98.
[71] Choi, Y.H., Seo, S., Kang, S., Lee, B. 2011. Justification of Effective Reactive Power Reserves With Respect to a Particular Bus Using Linear Sensitivity. *IEEE Transactions on Power Systems.* vol. 26, no. 4, pp. 2118-2124.
[72] Chow, J.H., Galarza, R., Accari, P., Price, W.W. 1995. Inertial and Slow Coherency Aggregation Algorithms for Power System Dynamic Model Reduction. *IEEE Transactions on Power Systems,* vol. 10, no. 2, pp. 680-685.
[73] Chowdhury, H., Taylor, C.W. 2000. Voltage stability analysis: V–Q power flow simulation versus dynamic simulation. *IEEE Transactions on Power Systems,* vol. 15, no.4, pp. 1354–1359.
[74] Concordia, C., Fink, L.H., Poullikkas, G. 1995. Load shedding on an isolated system. *IEEE Transactions on Power System,* vol. 10, no. 3, pp. 1467-1472.
[75] Corsi, S. 2010. Wide Area Voltage Protection. *IET Generation, Transmission, & Distribution,* vol. 4, no. 10, pp. 1164-1179.

[76] Corsi, S., Taranto, G.N. 2008. A real-time voltage instability identification algorithm based on local phasor measurements. *IEEE Transactions on Power Systems,* vol. 23, no. 3, pp. 1271–1279.
[77] Cowley, J. 2007. Communication and Networking: An Introduction. London: Springer-Verlag.
[78] Dai, Y., Xu, Y., Dong, Z.Y., Wong, K.P., Zhuang, L. 2012. Real-time Prediction of Event-Driven Load Shedding for Frequency Stability Enhancement of Power Systems. *IET Generation, Transmission & Distribution,* vol. 6, no. 9, pp. 914-921.
[79] Dasgupta, S., Paramasivam, M., Vaidya, U., Ajjarapu, V. 2013. Real-Time Monitoring of Short-Term Voltage Stability Using PMU Data. *IEEE Transactions on Power Systems*, vol. 28, no. 4, pp. 3702-3711.
[80] Delfino, B., Massucco, A., Morini, A., Scalera, P., Silvestro, F. 2001. Implementation and Comparison of Different Under-Frequency Load Shedding Schemes. pp. 307-312.
[81] de Leon, D., Taylor, C.W. 2002. Understanding and Solving Short-Term Voltage StabilityProblems. *IEEE Power Engineering Society Summer Meeting,* vol. 2, pp. 745-752.
[82] Diao, R., Sun, K., Vittal, V., O'Keefe, R.J., Richardson, M.R., Bhatt, N., Stradford, D., Sarawgi, S.K. 2009. Decision Tree-Based Online Voltage Security Assessment Using PMU Measurements. *IEEE Transactions on Power Systems*, vol. 24, no. 2, pp. 832-839.
[83] Dong, F., Chowdhury, B.H., Crow, M.L., Acar, L. 2005. Improving voltage stability by reactive power reserve management. *IEEE Transactions on Power Systems,* vol. 20, no. 1, pp. 338-344.
[84] Donolo, M., Venkatasubramanian, M., Guzman, A., de Villiers, F. 2009. Monitoring and Mitigating the Voltage Collapse Problem in the Natal Network. pp. 1-5.
[85] Falk, H., Adamiak, M., Baigent, D., Madani, V. 2013. An Overview of the New IEC 61850 Synchrophasor Publish-Subscribe Profile. *66th Annual Conference for Protective Relay Engineers,* pp. 309-321.
[86] Faiz, J., Siakolah, B. 2003. New Solid-State Onload Tap-Changers Topology for Distribution Transformers. *IEEE Transactions on Power Delivery*, vol. 18, no. 1, pp. 136-141.
[87] Feng, Z., Ajjarapu, V., Maratukulum, D.J. 1998. A Practical Minimum Load Shedding Strategy to Mitigate Voltage Collapse. *IEEE Transactions on Power Systems*, vol. 13, no. 4, pp. 1285-1291.
[88] Feng, D., Chowdhury, B.H., Crow, M.L., Acar, L. 2005. Improving voltage stability by reactive power reserve management. *IEEE Transactions on Power System*, vol. 20, no. 1, pp. 338-345.
[89] Fink, L.H., Carlsen, K. 1978. Operating Under Stress and Strain. *IEEE Spectrum, March 1978,* pp. 48-53.
[90] Fitzgerald, A.E., Kingsley, C., Umans, S. 2003. Electric Machinery, McGraw-Hill.
[91] Freund, Y., Schapire, R.E. 1997. A decision-theoretic generalization of on-line learning and an application to boosting. *Journal of Computer and System Sciences,* vol. 55, no. 1. pp. 119–139.
[92] Gajic, Z., Aganovic, A, Benovic, J., Leci, G., Gazzari, S. Using IEC 61850 analogue GOOSE messages for OLTC control of parallel transformer. 10th *IET International Conference on Developments in Power System Protection (DPSP 2010). Managing the Change*, January 2010, pp. 43-47.
[93] Galiana, F.D. 1984. Load Flow Feasibility and the Voltage Collapse Problem. *Proceedings of 23rd Conference on Decision and Control, Las Vegas NY,* pp. 485-487.
[94] Gao, B., Morison, G.K., Kundur, P. 1992. Voltage stability evaluation using modal analysis. *IEEE Transactions on Power Systems*, vol. 7, pp. 1529-1542.
[95] Genet, B., Maun, J.C. 2007. Voltage stability monitoring using wide-area measurement systems. *IEEE Power Tech, Lausanne*, July 2007, pp. 1712-1717.
[96] Geurts, P., Wehenkel, L. 2000. Temporal machine learning for switching control.

Proceedings of 4th European Conference of Principles and Practice of Knowledge Discovery in Databases (PKDD), Lyon, France, pp. 401-408.
[97] Ghaleh, A.P., Sanaye-Pasand, M., Saffarian, A. 2011. Power System Stability Enhancement Using a New Combinational Load-Shedding Algorithm. *IET Generation, Transmission, & Distribution,* vol. 5, no. 5, pp. 551-560.
[98] Ghiocel, S.G., Chow, J.H. 2014. A Power Flow Method Using a New Bus Type for Computing Steady-State Voltage Margins. *IEEE Transactions on Power Systems,* vol. 29, no. 2, pp. 958-965.
[99] Girgis, A.A., Mathure, S. 2010. Application of Active Power Sensitivity to Frequency and Voltage Variations on Load Shedding. *Electric Power Systems Research,* vol. 80, pp. 306-310.
[100] Glavic, M., Van Cutsem, T. 2009. Wide-Area Detection of Voltage Instability From Synchronized Phasor Measurements. Part II: Simulation Results. *IEEE Transactions on Power Systems*, *vol. 24*, *no. 3*, pp. 1417-1425.
[101] Glavic, M., Van Cutsem, T. 2010. Adaptive Wide-Area Closed-Loop Undervoltage Load Shedding Using Synchronized Measurements. *IEEE Power and Energy Society General Meeting,* pp. 1-8.
[102] Gong, B., Pinheiro, A. 2010. Online Voltage Collapse Prevention Through Optimal Load Shedding and Dynamic Generation Control. *2010 Asia-Pacific Power and Energy Engineering Conference (APPEEC),* pp. 1-6.
[103] Gong, Y., Schulz, N, Guzman, A. 2006. Synchrophasor-Based Real-Time Voltage Stability Index. *IEEE PES Power Systems Conference and Exposition, pp. 1029-1036.*
[104] Greene, S., Dobson, I., Alvarado, F.L. 1999. Contingency ranking for voltage collapse via sensitivities from a single nose curve, *IEEE Transactions on Power Systems,* vol. 14, no. 1, pp. 232-240.
[105] Grijalva, S., Sauer, P.W. 2005. Static Collapse and Topological Cuts. *Proceedings of the 38th Hawaii International Conference on System Science,* pp. 1-7.
[106] Gu, W., Wan, Q. 2010. Linearized Voltage Stability Index for Wide-Area Voltage Monitoring and Control. *Electric Power and Energy Systems,* vol. 32, pp. 333-336.
[107] Hagh, M.T., Galvani, S. 2011. Minimization of load shedding by sequential use of linear programming and particle swarm optimization. *Turk j Elec Eng & Comp Sci.,* vol. 19, no. 4, pp. 551-563.
[108] Hague, M.H. 2002. On-Line Monitoring of Maximum Permissible Loading of a Power System within Voltage Stability Limits. *IEE Proceedings Generation, Transmission, Distribution,* vol. 150, no. 1, pp. 107-112.
[109] Halpin, S.M., Harley, K.A., Jones, R.A., Taylor, L.Y. 2008. Slope-Permissive Under-Voltage Load Shed Relay for Delayed Voltage Recovery Mitigation. *IEEE Transactions on Power Systems,* vol. 23, no. 3, pp. 1211-1216.
[110] Hardle, W., Simar, L. 2007. Applied Multivariate Statistical Analysis. New York: Springer.
[111] Hashemi, S., Aghamohammadi, M.R. 2013. Wavelet Based Feature Extraction of Voltage Profile for Online Voltage Stability Assessment using RBF Neural Network. *Electrical Power and Energy Systems,* vol. 49, pp. 86-94.
[112] Hashiesh, F., Mostafa, H.E., Mansour, M.M., Khatib, A.R., Helal, I. 2008. Wide Area Transient Stability Prediction Using on-Line Artificial Neural Networks. *IEEE Canada Electric Power Conference* (EPEC 2008), 6-7 Oct. 2008, pp. 1-7.
[113] Hong, Y.H., Pan, C.T., Lin, W.W. 1997. Fast Calculation of a Voltage Stability Index of Power Systems. *IEEE Transactions on Power Systems,* vol. 12, no. 4, pp. 1555-1560.
[114] Hong, Y.Y., Wei, S.F. 2010. Multiobjective Underfrequency Load Shedding in an Autonomous System Using Hierarchical Genetic Algorithms. *IEEE Transactions on Power Systems,* vol. 25, no. 3, pp. 1355-1362.
[115] Horowitz, S., Novosel, D., Madani, V., Adamiak, M. 2008. System-Wide protection: Wide-Area Measurements for Improved Power System Protection. *IEEE Power & Energy Magazine, September/October 2008,* pp. 34-42.

[116] Hsu, C.T., Kang, M.S., Chen, C.S. 2005. Design of Adaptive Load Shedding by Artificial Neural Networks. *IEE Proceedings on Generation, Transmission, Distribution,* vol. 152, no. 3, pp. 415-421.
[117] Huang, G., Zhu, T. 1999. A New Method to Find the Voltage Collapse Point. *IEEE Power Engineering Society Summer Meeting,* vol. 2, pp. 1324-1329.
[118] Huang, Z., Bao, L., Xu, W. 2007. A Method to Measure QV Curves and its Applications in Power Systems. *Electrical Power and Energy Systems,* vol. 29, pp. 147-154.
[119] IEC 61850-90-5:2012. Communication networks and systems for power utility automation-Part 90-5: Use of IEC 61850 to transmit synchrophasor information according to IEEE C37.118.
[120] IEEE Power Systems Test Case Archive. Available at: http://www.ee.washington.edu/research/pstca/ [Accessed 13 January 2014].
[121] IEEE Standard 1344™-1995, IEEE Standard for Synchrophasors for Power Systems.
[122] IEEE Standard C37.118™-2005, IEEE Standard for Synchrophasors for Power Systems, 2005.
[123] IEEE Standard C37.118.1™-2011, IEEE Standard for Synchrophasor Measurements for Power Systems, 2011.
[124] IEEE Standard C37.118.2™-2011, IEEE Standard for Synchrophasor Data Transfer for Power Systems, 2011.
[125] IEEE Standard for Synchrophasor Measurements for Power Systems—Amendment 1: C37.118.1a-2014 Modification of Selected Performance Requirements.
[126] IEEE Guide for Synchronization, Calibration, Testing, and Installation of Phasor Measurement Units (PMUs) for Power System Protection and Control: IEEE C37.242-2013.
[127] IEEE Guide for Phasor Concentrator Requirements for Power System Protection, Control, and Monitoring: IEEE C37.244-2013.
[128] IEEE Task Force On Excitation Limiters, Recommended Models For Overexcitation Limiting Devices. *IEEE Transaction on Energy Conversion* 1995; vol. 10, no. 4, pp. 706–713.
[129] Imai, S. 2005. Undervoltage Load Shedding Improving Security as Reasonable Measure for Extreme Contingencies. *IEEE Power Engineering Society General Meeting,* vol. 2, pp. 1754-1759.
[130] Ingelsson, B., Lindstrom, P.O., Karlsson, D., Runvik, G., Sjodin, J.O. 1997. Wide-Area Protection against Voltage Collapse. *IEEE Computer Applications in Power, October 1997,* pp. 30-35.
[131] Jasmon, G.B., Lee, Callistus, L.H., Lee, C. 1991. Prediction of Voltage Collapse in Power Systems. *International Conference on Control,* vol. 1, pp.32-36.
[132] Johnson, R.A., Wichern, D.W. 2007. Applied multivariate statistical analysis. New Jersey: Pearson Prentice-Hall.
[133] Jonsson, M., Begovic, M., Daalder, J. 2004. A New Method Suitable for Real-Time Generator Coherency Determination. *IEEE Transactions on Power Systems,* vol. 19, no. 3, pp. 1473-1482.
[134] Juarez, C., Messina, A.R., Castellanos, R., Espinosa-Perez, G. 2011. Characterization of Multimachine System Behavior Using a Hierarchical Trajectory Cluster Analysis. *IEEE Transactions on Power Systems,* vol. 26, no. 3, pp. 972-981.
[135] Julian, D.E., Schulz, R.P., Vu, K.T., Quaintance, W.H., Bhatt, N.B., Novosel, D.2000. Quantifying Proximity to Voltage Collapse Using the Voltage Instability Predictor (VIP). *IEEE Power Engineering Society Summer Meeting,* vol. 2, pp. 931-936.
[136] Kalita, H.K., Nambiar, M. 2011. Designing WANem: A Wide Area Network Emulator Tool. *The Third International Conference on Communication Systems and Networks (COMSNETS'11), Bangalore 04-08 Jan*, pp. 1-4.
[137] Kjaer, P.C., Kjellqvist, T., Delaloye, C. 2005. Estimation of Field Current in Vector Controlled Synchronous machine Variable-Speed Employing Brushless Asynchronous

Exciters. *IEEE Transactions on Industry Applications.* vol. 41, no. 3, pp. 834-840.
[138] Kamwa, I., Samantaray, S.R., Joos, G. 2009. Development of rule-based classifiers for rapid stability assessment of wide-area post-disturbance records. *IEEE Transactions on Power Systems*, vol. 24, pp. 258-270.
[139] Kessel, P., Glavitsch, H. 1986. Estimating the voltage stability of a power system. *IEEE Transactions on Power Delivery*. vol. 1, no. 3*,* pp. 346-354.
[140] Khatib, A.R., Nuqui, R.F., Ingram, M.R., Phadke, A.G. 2004. Real-time Estimation of Security from Voltage Collapse Using Synchronized Phasor Measurements. *IEEE Power Engineering Society General Meeting, vol. 1,* pp. 582-588.
[141] Kim, H., Jang, G., Song, K. 2004. Dynamic Reduction of the Large-Scale Power Systems Using Relation Factor. *IEEE Transactions on Power Systems,* vol. 19, no. 3, pp. 1696-1699.
[142] Kolluri, S., Tinnium, K., Stephens, M. 2000. Design and Operating Experience with Fast Acting Load Shedding Scheme in the Entergy System to Prevent Voltage Collapse", *IEEE PES Winter Meeting,* vol. 2, pp. 1489-1494.
[143] Khoshkhoo, H., Shahrtash, S.M. 2011. On-Line Dynamic Voltage Instability Prediction Based on Decision Tree Supported by a Wide-Area Measurement System. *IET Generation, Transmission & Distribution,* vol. 6, no. 11, pp. 1143-1152.
[144] Kosterev, D.M., Taylor, C.W., Mittelstadt, W.A. 1999. Model Validation for the August 10, 1996 WSCC System Outage. *IEEE Trans. on Power System,* vol. 14, no. 3, pp. 967-979.
[145] Krumpholz, G.R., Clements, K.A., Davis, P.W. 1980. Power System Observability: a Practical Algorithm using Network Topology. *IEEE Transactions on Power Apparatus and Systems,* vol. 99, no. 4, pp. 1534-1542.
[146] Kundur, P. 1994. Power System Stability and Control, McGraw-Hill.
[147] Kundur, P., Paserba, J., Ajjarapu, V. et al. 2004. Definition and Classification of Power System Stability. *IEEE Transactions on Power Systems*, vol. 19, no. 2, pp. 1387-1401.
[148] Kwatny, H.G., Pasrija, A.K., Bahar, L.Y. 1986. Static bifurcations in electric power networks: Loss of steady-state stability and voltage collapse. *IEEE Transactions on Circuits and Systems*, vol. 33, no.10, pp. 981-991.
[149] Larrson, S., Danell, A. 2006. The Black-out in Southern Sweden and Eastern Denmark, September 23, 2003. *IEEE PES Power Systems Conference and Exposition,* pp. 309-313.
[150] Lee, C.Y., Tsai, S.H., Wu, Y.K. 2010. A New Approach to the Assessment of Steady-State Voltage Stability Margins. *Electric Power and Energy Systems,* vol. 32, pp. 1091-1098.
[151] Lee, D.H.A. 2015. Voltage Stability Assessment Using Equivalent Nodal Analysis. *IEEE Transactions on Power Systems,* vol. PP, no. 99, pp. 1-10.
[152] Leelaruji, R., Vanfretti, L., Uhlen, K., Gjerde, J.O. 2015. Computing Sensitivities from Synchrophasor Data for Voltage Stability Monitoring and Visualization. *International Transactions on Electrical Energy Systems,* vol. 25, no. 6, pp. 933-947.
[153] Leonardi, B., Ajjarapu, V. 2008. Investigation of Various Generator Reactive Power Reserve (GRPR) Definitions for Online Voltage Stability/Security Assessment, *Proceedings of 2008 IEEE PES General Meeting, Tampa, USA,* pp. 1-7.
[154] Leonardi, B., Ajjarapu, V. 2011. Development of Multilinear Regression Models for Online Voltage Stability Margin Estimation, *IEEE Transactions on Power Systems,* vol. 26, no. 1, pp. 374-383.
[155] Leonardi B, Ajjarapu V. 2013. An Approach for Real Time Voltage Stability Margin Control via Reactive Power Reserve Sensitivities. *IEEE Transactions on Power Systems,* vol. 28, pp. 615-625.
[156] Liu, J.H., Chu, C.C. 2014. Wide-Area Measurement-Based Voltage Stability Indicators by Modified Coupled Single-Port Models. *IEEE Transactions on Power Systems,* vol. 29, no. 2, pp. 756-764.

[157] Li, W., Chen, T., Xu, W. 2010. On Impedance Matching and Maximum Power Transfer. *Electric Power Systems Research,* vol. 80, pp. 1082-1088.
[158] Liu, X., Niu, X., Zhu, Y. 2013. Influence of Regulation of OLTC Transformation Ratio on Voltage Stability. *Fourth International Conference on Digital Manufacturing & Automation,* pp. 696-699.
[159] Lof, P.A., Smed, T., Andersson, G., Hill, D.J. 1992. Fast Calculation of a Voltage Stability Index. *IEEE Transactions on Power Systems,* vol. 7, pp. 54-64.
[160] Lof, P.A., Andersson, G., Hill, D.J. 1993. Voltage stability indices for stressed power systems. *IEEE Transactions on Power Systems*, vol. 8, no. 1, pp. 326–335.
[161] Londono, S., Rodriguez, L.F., Olivar, G. 2014. A Simplified Voltage Stability Index (SVSI). *Electrical Power and Energy Systems,* vol. 63, pp. 806-813.
[162] Lopes, B.I.L., Zambroni de Souza, A.C. 2003. An Approach for Under Voltage Load Shedding. *IEEE Bologna PowerTech Conference, June 23-26, Bologna, Italy,* pp. 1-5.
[163] Luan, W.P., Irving, M.R., Daniel, J.S. 2002. Genetic Algorithm for Supply Restoration and Optimal Load Shedding in Power System Distribution Networks. *IEE Proceedings - Generation, Transmission and Distribution*, vol. 149, no. 2, pp. 145-151.
[164] Ma, P., Yuan, B.Q. 2011. A practical corrective control strategy to mitigate voltage collapse. *in Proceedings 4th* International Conference *Electric Utility Deregulation and Restructuring and Power Technologies (DRPT),* pp.1039-1043.
[165] Madani, V., Novosel, D., Horowitz, S., Adamiak, M., Amantegui, J., Karlsson, D., Imai, S., Apostolov, A. 2010. IEEE PSRC Report on Global Industry Experiences With System Integrity Protection Schemes (SIPS), *IEEE Transactions on Power Delivery,* vol. 25, no. 4, pp. 2143-2155.
[166] Majidi, M., Aghamohammadi, M.R., Manbachi, M. 2014. New design of intelligent load shedding algorithm based on critical line overloads to reduce network cascading failure rates. *Turk j Elec Eng & Comp Sci.,* vol. 22, pp. 1395-1409.
[167] Martin, K. 2007. Synchrophasors for WAMS. *PAC World Magazine, autumn 2007,* pp. 20-25.
[168] MATLAB Curve Fitting Toolbox: User's Guide, 2014. *The MathWorks Inc., Natick, Massachusetts*.
[169] MATLAB Statistic Toolbox: User's Guide, 2014. *The MathWorks Inc., Natick, Massachusetts.*
[170] MATLAB Optimization Toolbox: User's Guide 2013b. *User's Guide. The MathWorks Inc., Natick, Massachusetts*.
[171] Mei, K., Rovnyak, S., Ong, C.M. 2008. Clustering-Based Dynamic Event Location Using Wide-Area Phasor Measurements. *IEEE Transactions on Power Systems*, *vol. 23, no.2*, pp. 673–679.
[172] MiCOM P847 Technical Manual. 2011. Alstom Phasor Measurement Unit.
[173] Mili, L., Baldwin, T., Adapa, R. Phasor Measurement Placement for Voltage Stability Analysis of Power Systems. *Proceeding of the 29th Conference on Decision and Control*, 1990, Hawaii, pp. 3033-3038.
[174] Miller, N.W., D'Aquila, R., Jimma, K.M., Sheehan, Comegys, G.L. 1993. Voltage Stability of the Puget Sound System Under Abnormally Cold Weather Conditions. *IEEE Transactions on Power Systems*, *vol. 8, no.4*, 2003, pp. 1133-1139.
[175] Milosevic, M., Begovic, M, Voltage-stability protection and control using a wide-area network of phasor measurements. *IEEE Transactions on Power Systems*, *vol.18, no.1*, pp. 121–127.
[176] Midwest ISO (MISO) Synchrophasor Deployment Project. 2010. Synchrophasor Integration into Planning and Operational Reliability Process, version 1.
[177] Moghavvemi, M., Omar, F.M. 1998. Technique for Contingency Monitoring and Voltage Collapse Prediction. *IEE Proceedings Generation, Transmission & Distribution,* vol. 145, no. 6, pp. 634-640.
[178] Moghavvemi M, Faruque O. 1998. Real-time contingency evaluation and ranking

technique. *IEE Proceedings on Generation, Transmission, Distribution, vol.* 145, no. 5, pp. 517-524.
[179] Mohamed, S.Y.A., Jasmon, G.B. 1989. A Static Voltage Collapse Indicator Using Line Stability Factors. *Journal of Industrial Technology*, vol. 7, pp. 73–85.
[180] Monticelli, A. 1999. Electric Power System State Estimation. *Proceedings of the IEEE,* vol. 88, no. 2, pp 262-282.
[181] Monticelli, A., Deckmann, S., Garcia, A., Stott, B. 1979. Real-Time External Equivalents for Static Security Analysis. *IEEE Transactions on Power Apparatus and Systems*, *vol. Pas-18, no.2*, pp. 498-508.
[182] Moors, C., Lefebvre, D., Van Cutsem, T. 2000. Design of load shedding schemes against voltage instability. *Proceedings. IEEE Power Engineering Society Winter Meeting*, vol. 2, pp. 1495-1500.
[183] Moors, C., Lefebvre, D., Van Cutsem, T. 2001. Load Shedding Controllers against Voltage Instability: A Comparison of Designs. *IEEE Porto Power Tech Conference, 10-13 September,* pp. 1-6.
[184] Moors, C., Lefebvre, D., Van Cutsem, T. 2002. Design of load shedding schemes against voltage instability using combinatorial optimization. *IEEE Power Engineering Society Winter Meeting*, *27-31, Jan.,* vol. 2, pp. 848-853.
[185] Morison, G.K., Gao., B., Kundur, P. 1993. Voltage Stability Analysis Using Static and Dynamic Approaches. *IEEE Transactions on Power Systems,* vol., 8, no. 3, pp.1159-1171.
[186] Mousavi, O.A., Bozorg, M., Chekaoui, R. 2013. Preventive Reactive Power Management for Improving Voltage Stability. *Electric Power System Research,* vol. 96, pp. 36-46.
[187] Musirin, I, Rahman, T.K.A. 2002. On-line voltage stability based contingency ranking using fast voltage stability index (FVSI). *In Proceedings of IEEE/PES Transmission and Distribution Conference and Exhibition*, vol. 2, pp.1118–1123.
[188] Nanda, A., Crow, M.L. 1995. An energy based approach to undervoltage load shedding'. *Electric Power Systems Research*, vol. 32, pp. 11-18.
[189] Nath, R., Lamba, S.S., Prakasa Rao, K.S.P.1985. Coherency Based System Decomposition into Study and external Areas Using Weak Coupling. *IEEE Transactions on Power Apparatus and Systems*, *vol.Pas-104, no.6*, pp. 1443-1449.
[190] Naduvathuparambi, B., Valenti, M.C. Feliachi, A. 2002. Communication delays in wide area measurement systems. *Proceedings of 34th Southeastern Symposium on System Theory, USA,* pp. 118-122.
[191] NERC report on the August 14, 2003 blackout in the United States and Canada: causes and recommendations. 2004. U.S.–Canada Power System Outage Task Force.
[192] Nikolaidis, V.C., Vournas, C.D. 2008. Design Strategies for Load Shedding Schemes Against Voltage Collapse in the Hellenic System. *IEEE Transactions on Power Systems*, vol. 23, no. 2, pp. 582-591.
[193] Nirenberg, S.A., McInnis, D.A., Sparks, K.D. 1992. Fast acting load shedding. *IEEE Transactions on Power Systems,* vol. 7, no. 2, pp. 873-877.
[194] Nizam, M., Mohamed, A, Hussein, A. 2006. Dynamic Voltage Collapse Prediction in Power Systems Using Power Transfer Stability Index. *First International Power and Energy Conference PECon 2006, 29-29 Nov., Malaysia,* pp. 246-250.
[195] Novosel, D., King, R.L. 1994. Using artificial neural networks for load shedding to alleviate overloaded lines. *IEEE Transactions on Power Delivery*, vol. 9, no.1, pp. 425-433.
[196] Nuqui, R.F., Phadke, A.G., Schulz, R.P., Richard, P., Bhatt, N. 2001. Fast On-Line Voltage Security Monitoring Using Synchronized Phasor Measurements and Decision Trees. *IEEE Power Engineering Society Winter Meeting*, vol. 3, pp. 1347-1352.
[197] Nuqui, R.F., Phadke, A.G. 2005. Phasor measurement unit placement techniques for complete and incomplete observability. *IEEE Transactions on Power Delivery*, vol. 20, no. 4, pp. 2381-2388.

[198] Nuhanovic, A., Glavic, M., Prljaca, N. 1998. Validation of a Clustering Algorithm for Voltage Stability Analysis on the Bosnian Electric Power System. *IEE Proceedings on Generation, Transmission, and Distribution,* vol. 145, no. 1, pp. 21-26.
[199] Obadina, O.O., Berg, G.J. 1988. Determination of Voltage Stability Limit in Multimachine Power Systems. *IEEE Transactions on Power Systems,* vol. 3, no. 4, pp. 1545-1553.
[200] Ohno, T., Imai, S. 2006. The 1987 Tokyo Blackout. *IEEE PES Power Systems Conference and Exposition, PSCE '06,* pp. 314-318.
[201] Ohtsuki, H., Yokoyama, A., Sekine, Y. 1991. Reverse Action of On-Load tap Changer in Association with Voltage Collapse. *IEEE Transactions on Power Systems,* vol. 6, no. 1, pp. 300-306.
[202] Otomega, B., Sermansin, V., Van Cutsem, T. 2003. Reverse-Logic Control of Load Tap Changers in Emergency Voltage Conditions. *IEEE Bologna PowerTech Conference, June 23-26, Bologna, Italy*, pp. 1-7.
[203] Otomega, B., Van Cutsem, T. 2007. Undervoltage load shedding using distributed controllers. *IEEE Transactions on Power Systems*, vol. 22, no. 4, pp. 1989-1907.
[204] Otomega, B., Van Cutsem, T. 2011. A Load Shedding Scheme Against both Short- and Long-term Voltage Instabilities in the Presence of Induction Motors. *IEEE Trondheim Power Tech,* pp. 1-7.
[205] Overbye, T.J., Dobson, I., DeMarco, I. 1994. Q-V Curve Interpretations of Energy Measures for Voltage Security. *IEEE Transactions on Power Systems,* vol. 9, no. 1, pp. 331-340.
[206] Pai, M.A. 1989. *Energy Function Analysis for Power System Stability,* Boston: Kluwer Academic Publishers, pp. 223-227.
[207] Pama, A., Radman, G. 2009. A New Approach for Estimating Voltage Collapse Point Based on Quadratic Approximation of PV-Curves. *Electric Power Systems Research,* vol. 79, pp. 653-659.
[208] Phadke, A.G., Thorpe, J.S. 2008. Synchronized Phasor Measurements and Their Applications, Springer.
[209] Podmore, R. 1978. Identification of Coherent Generators for Dynamic Equivalents. *IEEE Transactions on Power Apparatus and Systems*, *vol. Pas-97, no.4*, pp. 1344-1354.
[210] Pordanjani, I.R., Wang, Y., Xu, W. 2013. Identification of Critical Components for Voltage Stability Assessment using Channel Components Transform. *IEEE Transactions on Smart Grid,* vol. 4, no. 2, pp. 1122-1132.
[211] Prasetijo, D., Lachs, W.R., Sutanto, D. 1994. A New Load Shedding Scheme for Limiting Underfrequency. *IEEE Transactions on Power System,* vol, 26, no. 3, pp. 1371-1378.
[212] Rameshkhah, F., Abedi, M., Hosseinian, S.H. 2010. Comparison and Combination of Shuffled Frog-Leaping Algorithm and K-Means for Clustering of VCAs in Power System. *International Review of Electrical Engineering (IREE),* vol. 5, no. 1, pp. 194-204.
[213] Report on the Indian blackout. 2012. Accessed: www.cercind.gov.in/2012/orders/Final_Report_Grid_Disturbance.pdf
[214] RTDS hardware manual, 2014. RTDS Technologies Inc.
[215] RTDS manual, 2014. RTDS Technologies Inc.
[216] Ruiz, P.A., Sauer, P.W. 2006. Reactive Power Reserve Issues. *In Proceedings 2006 North American Power Symposium*, *Carbondale,* pp. 539-545.
[217] Sadati, N., Amraee, T., Ranjbar, A.M. 2009. A global particle swarm based-simulated annealing optimization technique for undervoltageload shedding problem. *Applied Soft Computing,* vol. 9, pp. 652–657.
[218] Saffarian, A., Sanaye-Pasand, M. 2011. Enhancement of power system stability using adaptive combinational load shedding methods. *IEEE Transactions on Power System,* vol. 26, no. 3, pp. 1010-1020.
[219] Sanders, C. 2011. Practical Packet Analysis. Canada: No Starch Press, Inc.
[220] Savulescu, S.C. 2009. Real-Time Stability Assessment in Modern Power System Control Centers. Wiley-IEEE.

[221] Southern California Edison Smart Grid Strategy & Roadmap, SCE. 2010.
[222] Schlueter, R.A., Hu, I., Chang, M.W., Lo, J.C., Costi, A. 1991. Methods for Determining Proximity to Voltage Collapse, *IEEE Transactions on Power Systems,* vol. 6, no. 1, pp. 285-292.
[223] Schlueter, R.A. 1998. A Voltage Stability Security Assessment Method. *IEEE Transactions on Power Systems,* vol. 13, pp. 1423-1438.
[224] Schweppe, F.C., Rom, D.B. 1970. Power System Static-State Estimation, Part II: Approximate Model. *IEEE Transactions on Power Apparatus and Systems,* vol. PAS-89, no. 1, pp. 125-130.
[225] Seethalekshmi, K., Singh, S.N., Srivastava, S.C. 2010. Adaptive Scheme for Minimal Load Shedding Utilizing Synchrophasor Measurements to Ensure Frequency and Voltage Stability. *Electric Power Components and Systems,* vol, 38, pp. 1211-1227.
[226] Seethalekshmi, K., Singh, S.N., Srivastava, S.C. 2011. A Synchrophasor-Assisted Frequency and Voltage Stability Based Load Shedding Scheme for Self-Healing of Power System. *IEEE Transactions on Smart Grid*, 2011, 2, (20), pp. 221-230.
[227] SEL Report. 2009. The Synchrophasor Report on Synchrophasors and Communication Bandwidth. 2009. Schweitzer Engineering Laboratories.
[228] SEL-5073 SynchroWAVe Phasor Data Concentrator Instruction Manual. 2015. Schweitzer Engineering Laboratories.
[229] SEL-2407 Satellite-Synchronized Clock Instruction Manual. 2015. Schweitzer Engineering Laboratories.
[230] SEL-2488 Satellite-Synchronized Network Clock Instruction Manual. 2015. Schweitzer Engineering Laboratories.
[231] SEL-421-4, -5 Relay Protection, Automation, and Control System Instruction Manual. 2013. Schweitzer Engineering Laboratories.
[232] SEL-451-5 Relay Protection, Automation, and Control System Instruction Manual. 2015. Schweitzer Engineering Laboratories.
[233] SEL-3378 Synchrophasor Vector Processor Instruction Manual. 2014. Schweitzer Engineering Laboratories.
[234] Seyedi, H., Sanaye-Pasand, M. 2009a. New Centralised Adaptive Load-Shedding Algorithms to Mitigate Power System Blackouts. *IET Generation, Transmission & Distribution,* vol. 3, no. 1, pp. 99-114.
[235] Seyedi, H., Sanaye-Pasand, M. 2009b. Design of New Load Shedding Special Protection Schemes for a Double Area Power System. *American Journal of Applied Sciences,* vol. 6, no. 2, pp. 317-327.
[236] Shin, J., Nam, S., Lee, J., Choy, Y., Kim, T., Song, H. 2009. Application of Multi-step Undervoltage Load Shedding Schemes to the KEPCO System. *Journal of Electrical Engineering & technology,* vol. 4, no. 4, pp. 476-484.
[237] Sichwart, N., Eltom, A., Kobet, G. 2013. Transformer Load Tap Changer control using IEC 61850 GOOSE messaging. *IEEE Power and Energy Society General Meeting*, pp. 1-5.
[238] Smon, I., Verbic, G., Gubina, F. 2006. Local Voltage-Stability Index Using Tellegen's Theorem. *IEEE Transactions on Power Systems,* vol. 21, no. 3, pp. 1267-1275.
[239] Sodhi, J., Srivastava, S.C., Singh, S.N. 2012. A Simple Scheme for Wide Area Detection of Impending Voltage Instability. *IEEE Transactions on Smart Grid,* vol. 18, no. 4, pp. 1538-1546.
[240] Song, H., Lee, B., Kwon, S.H., Ajjarapu, V. 2003. Reactive Reserve-Based Contingency Constrained Optimal Power Flow (RCCOPF) for Enhancement of Voltage Stability Margins. *IEEE Transactions on Power Systems,* vol. 21, no. 3, pp. 1267-1275.
[241] H. Song, B. Lee, Y.H. Moon, "Reactive Optimal Power Flow incorporating margin enhancement constraints with non linear interior point method," *IEE Proceedings on Generation Transmission and Distribution*, vol. 152, n. 6, 2005, pp. 961-968.

[242] Su, H.Y., Liu, C.W. 2015. Estimating the Voltage Stability Margin Using PMU Measurements. *IEEE Transactions on Power Systems,* vol. PP, no. 99, pp. 1-9.
[243] Suganyadevi, M.V., Babulal, C.K. 2014. Fast Assessment of Voltage Stability Margin of a Power System. *J. Electrical Systems,* vol. 10-3, pp. 305-316.
[244] South African Grid Code. 2010. The System Operation Code version 8.0.
[245] Tang, J., Liu, J., Ponci, F., Monti, A. 2013. Adaptive load shedding based on combined frequency and voltage stability assessment using synchrophasor measurements. *IEEE Transactions on Power System*, vol. 28, no. 2, pp. 2035-2047.
[246] Tare, R.S., Bijwe, P.R. 1998. A new index for voltage stability monitoring and enhancement. *Electrical Power and Energy Systems*, vol. 20, no. 5, pp. 345-351.
[247] Taylor, C.W. 1992. Concepts of Undervoltage Load Shedding for Voltage Stability. *IEEE Transactions on Power Delivery*, vol. 7, no. 2, pp. 480-488.
[248] Taylor, C.W. 1994. Power System Voltage Stability, McGraw-Hill.
[249] Taylor, C.W., Erickson, D.C. 1997. Recording and Analyzing the July 2 Cascading Outage. *IEEE Computer Applications in Power*, vol. 10, no. 1, pp. 26–30.
[250] Taylor, C.W., Ramanathan, R. 1998. BPA reactive power monitoring and control following August 10, 1998 power failure. *In proceedings, VI Symposium Specialists Elect. Oper. Expansion Planning, Salvador, Brazil*.
[251] Taylor, C.W., Venkatasubramanian, V., Chen, Y. 2000. Wide Area Stability and Voltage Control. *In Proc. 7th Symposium Specialists in Electric Operational and Expansion Planning,* pp. 1-9.
[252] Terzija, V.V. 2006. Adaptive Underfrequency Load Shedding Based on the Magnitude of the Disturbance Estimation. *IEEE Transactions on Power System*, vol. 21, no. 3, pp. 1260-1266.
[253] Thomas, M.S., McDonalds, J.D. 2015. Power System SCADA and Smart Grids. Boca Raton: CRC Press.
[254] Tiwari, R., Niazi, K.R., Gupta, V. 2012. Line Collapse Proximity Index for prediction of Voltage Collapse in Power Systems. *Electrical Power and Energy Systems,* vol. 41, pp. 105-111.
[255] Tobon, J.E., Gutierrez, R.E.C., Ramirez, J.M. 2014. Voltage collapse detection based on local measurements. *Electric Power Systems Research*; vol. 107, pp. 77-84.
[256] Trudel, G., Bernard, S., Scott, G. 1999. Hydro-Quebec's defence plan against extreme contingencies. *IEEE Transactions on Power Systems,* vol. 14, no. 3, pp. 958-966.
[257] Tsai, S.J., Wong, K.H. 2008. Adaptive Undervoltage Load Shedding Relay design Using Thevenin Equivalent Estimation. *IEEE Power and Energy Society General Meeting-Conversion and Delivery of Electrical Energy in the 21st Century,* pp. 1-8.
[258] Tso, S.K., Zhu, T.X., Zeng, Q.Y., Lo, K.L. 1997. Evaluation of Load Shedding to Prevent Dynamic Voltage Instability Based on Extended Fuzzy Reasoning. *IEE Proceedings on Generation, Transmission & Distribution,* vol. 144, no. 2, pp. 81-86.
[259] Tuan, T.Q., Fandino, J., Subonnadiere, J.C., Vu, H. Heilbronn, B. 1993. Determination of Load Shed Using Linear Programming to Avoid Voltage Instability. *IEEE/NTUA Athens Power Tech Conference: "Planning, Operation and Control of Today's Electric Power Systems", Athens, Greece 5-8 Sept.,* pp. 553-557.
[260] Tuan, T.Q., Fandino, J., Hadjsaid, N., Sabonnadiere, J.C., Vu, H. 1994. Emergency Load Shedding to Avoid Risks of Voltage Instability Using Indicators. *IEEE Transactions on Power Systems*, vol. 9, no. 1, pp. 341-351.
[261] Van Cutsem, T., Wehenkel, L., Pavella, M., Heilbronn, B., Goubin, M. 1993. Decision tree approaches to voltage security assessment. *IEE Proc. on Generation, Transmission & Distribution*, vol. 140, no. 3, pp. 189-198.
[262] Van Cutsem, T. 1995. An Approach to Corrective Control of Voltage Instability using Simulation and Sensitivity. *IEEE Transactions on Power Systems*, vol. 10, no. 2, pp. 616-622.
[263] Van Cutsem, T., Moors, C., Lefebvre, D. 2002. Design of load shedding schemes against

voltage instability using combinatorial optimization. *Proceedings of IEEE Power Engineering Society Winter Meeting*, vol. 2, pp. 848-853.
[264] Van Cutsem T, Vournas C. Voltage Stability of Electric Power System, Springer, 2008.
[265] Van der Merwe, I.L., Cloete, J., Fischer, N. 2005. Implementation of an Unconventional Voltage Slide Scheme. *58th Annual Conference for Protective Relay Engineers*, pp. 96-111.
[266] Verbic, G., Gubina, F. 2004. A New Concept of Voltage-Collapse Protection Based on Local Phasors. *IEEE Transactions on Power Delivery*, vol. 19, no. 2, pp. 576-581.
[267] Vournas, C.D. 2002. On the Role of LTCs in Emergency and Preventive Voltage Stability Control. *IEEE Power Engineering Society Winter Meeting,* vol. 2, pp. 854-859.
[268] Vournas, C., Karystianos, M. 2004. Load Tap Changers in Emergency and Preventive Voltage Stability Control. *IEEE Transactions on Power Systems*, vol. 19, no. 1, pp. 492-498.
[269] Vournas, C.D., Sakellaridis, N.G. 2007. Tracking Maximum Loadability Conditions in Power Systems. *2007 iREP Symposium-Bulk Power System Dynamics and Control-VII Revitalizing Operational Reliability, 19-24 August, Charleston, USA,* pp. 1-12.
[270] Vournas, C., Lambrou, C., Glavic, M., Van Cutsem, T. 2010. An Integrated Autonomous Protection System against Voltage Instability based on Load Tap Changers. *2010 iREP Symposium-Bulk Power System Dynamics and Control-VIII, 1-6 August, Buzios, Brazil,* pp. 1-14.
[271] Vu, K.T., Liu, C.C. 1992. Shrinking stability regions and voltage collapse in power systems. *IEEE Transactions Circuit Systems*, vol. 39, no. 4, pp.271-289.
[272] Vu, K., Begovic, M., Novosel, D., Saha, M.M. 1999. Use of Local Measurements to Estimate Voltage-Stability Margin. *IEEE Transactions on Power Systems*, vol. 14, no. 3, pp. 1029-1035.
[273] Walker, J.H. 1954. Operating characteristics of salient-pole machines. *Proceedings of the IEE-Part II: Power Eng.,* vol. 100, no. 73, pp. 13-24.
[274] Wang, Y.J., Liu, C.W., Liu, Y.H. 2005. A PMU Based Special Protection Scheme: A Case Study of Taiwan Power System. *Electrical Power and Energy Systems,* vol. 27, pp. 215-223.
[275] Wang, Y., Li, W., Lu, J. 2009. A new node voltage stability index based on local voltage phasors. *Electric Power Systems Research,* vol. 79, pp. 265-271.
[276] Wang, Y., Pordanjani, I.R., Xu, W. 2011. An event-driven demand response scheme for power system security enhancement. *IEEE Transactions on Smart Grid*, vol. 2, no. 1, pp. 23-29.
[277] Warland, L., Holen, A.T. 2002. Estimation of Distance to Voltage Collapse: Testing and Algorithm Based on Local Measurements. *Proceedings of 14th Power System Computation Conference, Sevilla, Spain,* vol. 38, pp. 1-7.
[278] WECC Undervoltage Load Shedding Guidelines 1999. Undervoltage Load Shedding Taskforce, Technical Studies Subcommittee, Western Electricity Coordinating Council.
[279] WECC Reactive Reserve Working Group (RRWG) Guide to WECC/NERC Planning Standards I.D: Voltage Support and Reactive Power, 2006. Western Electricity Coordinating Council.
[280] Wehenkel, L., Van Cutsem, T., Pavella, M. 1989. An artificial intelligence framework for online transient stability assessment of electric power systems. *IEEE Transactions on Power Systems*, vol. 4, no. 2, pp. 789-800.
[281] Wei, J., Kundur, D., Butler-Purry, K.L. 2014. A Novel Bio-Inspired Technique for Rapid Real-Time Generator Coherency Identification, *IEEE Transactions on Smart Grid,* vol. 6, no. 1, pp. 178-188.
[282] Wester, C., Smith, T., Theron, J., McGinn, D. 2014. Developments in Fast Load Shedding. *Annual Pulp and Paper Industry Technical Conference,* pp. 28-33.
[283] Wolsey, L.A. 1998. *Integer Programming*, New York: Wiley.

[284] Xue, Y., Pavella, M. 1993. Critical-Cluster Identification in Transient Stability. *IEE Proceedings,* vol. 140, no. 6, pp. 481-489.
[285] Yang, D.Y., Cai, G.W., Jiang, Y.T., Liu, C. 2013. Centralized Adaptive Under Frequency Load Shedding Schemes for Smart Grid Using Synchronous Phase Measurement Unit. *J Electr Eng Technol,* vol. 8, no. 3, pp. 446-452.
[286] Yarza, J.M., Cimadevilla, R. 2014. Advanced Tap Changer Control of Parallel Transformers based on IEC 61850 GOOSE Service. *IEEE PES T&D Conference and Exposition,* pp. 1-5.
[287] Yorino, N., Danyoshi, M., Kitagawa, M. 1997. Interaction Among Multiple Controls in Tap Change Under load Transformers. *IEEE Transactions on Power Systems,* vol. 12, no. 1, pp. 430-436.
[288] Yuan, H., Li, F. 2015. Hybrid Voltage Stability Assessment (VSA) for N-1 Contingency. *Electric Power Systems Research,* vol. 122, pp. 65-75.
[289] Zaborszky, J., Whang, K.W., Huang, G.M., Chiang, L.J., Lin, S.Y. 1982. A Clustered Dynamic Model for a Class of Linear Autonomous Systems Using Simple Enumerative Sorting. *IEEE Transactions on Circuits and Systems, vol. CAS-29, no. 11,* pp. 748-758.
[290] Zad, B.B., Lobry, J., Vallee, F. 2013. Coordinated Control of On-Load Tap Changer and D-STATCOM for Voltage Regulation of Radial Distribution Systems with DG Units. *3rd International Conference on Electric Power and Energy Conversion Systems, 2-4 October,* pp. 1-4.
[291] Zambroni de Souza, A.C., Quintana, V.H. 1994. New Technique of Partitioning for Voltage Collapse Margin Calculations. *IEE Proceedings-Generation, Transmission, Distribution,* vol. 141, no. 6, pp. 630-636.
[292] Zambroni de Souza, A.C., Alves da Silva, A.P., Jardim, J.L.A., Silva Neto, C.A., Torres, G.L., Ferreira, C., Ferreira, L.C.A. 2005. A New Contingency Analysis Approach for Voltage Collapse Assessment. *Electrical Power and Energy Systems,* vol. 25, pp. 781-785.
[293] Zambroni de Souza, A.C., Monn, F., Borges, I.F. 2011. Using PV and QV Curves with the Meaning of Static Contingency Screening and planning. *Electric Power System Research,* vol. 81, pp. 1491-1498.
[294] Zhang, F., Sun, Y., Cheng, L., Li, X., Chow, J.H., Zhao, W. 2015. Measurement and Modeling of Delays in Wide-Area Closed-Loop Control Systems. *IEEE Transactions on Power Systems*, vol. 30, no. 5, pp. 2426-2433.

APPENDICES

APPENDIX A: Generator Over-Excitation Limiter and Transformer under Load Tap Changer

APPENDIX A1: Generator Over-Excitation Limiter

The OXLs at generators G2 and G3 of the New England 39-bus test system are calculated using recommendations from (IEEE Task Force On Excitation Limiters, 1995). Figure A1 shows the structure of the OXL used. The parameters used are given in Tables A1 and A2.

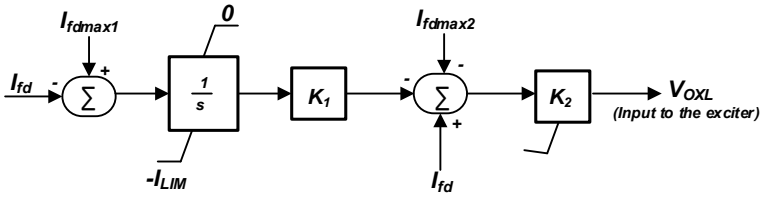

Figure A1: Block diagram of OXL used at generator 3 for case study 3

Table A1: Generator G2 OXL parameters

Ifdmax1 (p.u.)	Ifdmax1 (p.u.)	I_{LIM}(p.u.)	K_1	K_2
2.47695	3.7744	11	0.248	12.6

Table A2: Generator G3 OXL parameters

Ifdmax1 (p.u.)	Ifdmax1 (p.u.)	I_{LIM}(p.u.)	K_1	K_2
2.352	3.584	11	0.248	12.6

where I_{fd} is the generator field current at the current operating time, I_{fdmax1} and I_{fdmax2} are the maximum field current limits for stages 1 and 2 of the generator OXL respectively.

APPENDIX A2: Transformer Under-Load Tap Changer

The ULTC parameters used for the transformer between buses 11 and 12 are given in Table B1.

Table B1: Transformer ULTC Parameters

Dead Band (Vp.u.)	Tap Range (Steps)	Step Size (p.u.)	Time Delay for 1st Tap (s)	Time Delay for Subsequent Tap (s)
±1%	±16	0.00625	30.0	5.0

APPENDIX H: Test System-1 RSCAD Model
APPENDIX H1: RSCAD Draft Module for the 10-bus Multi-machine Test System

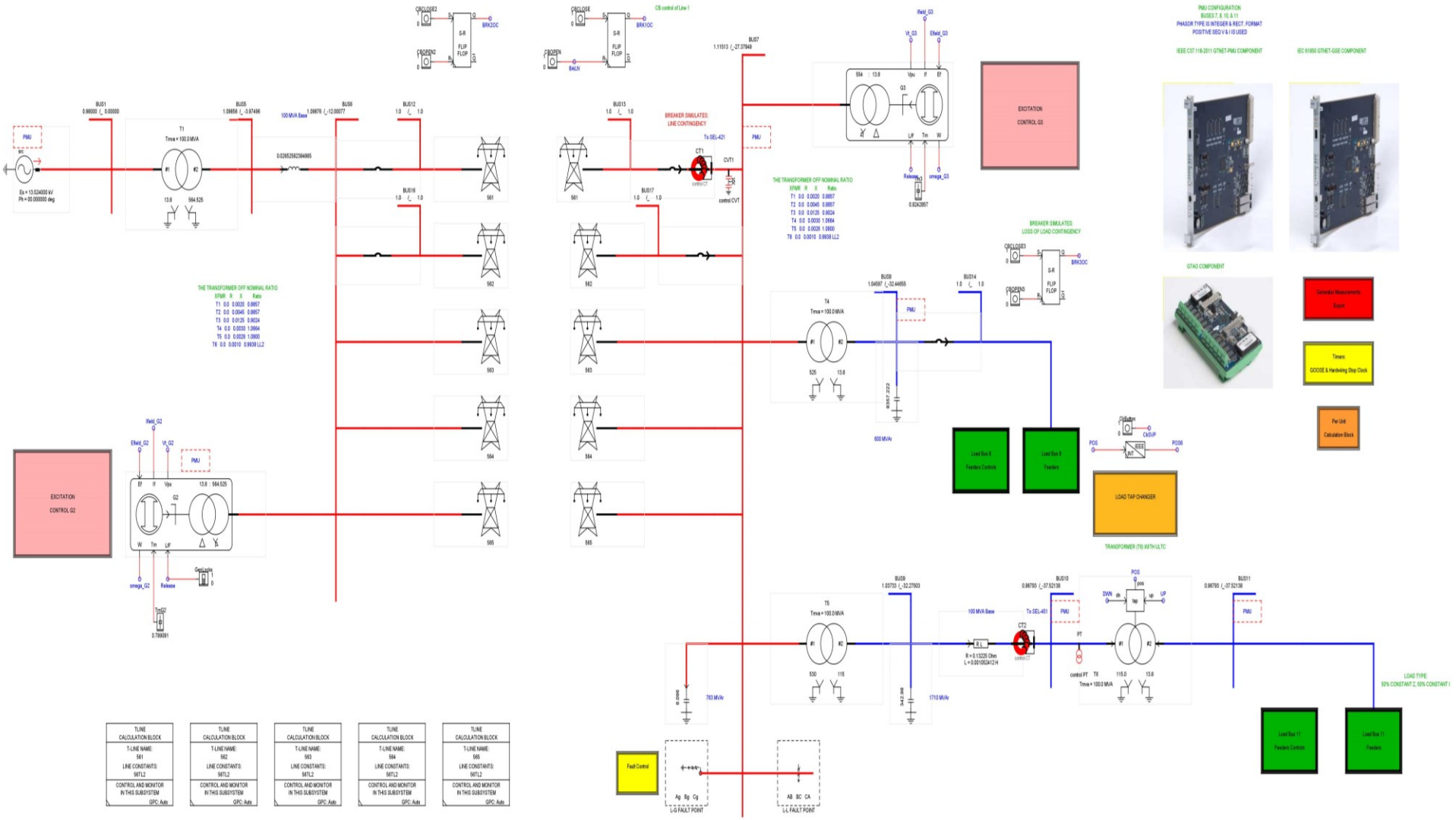

Figure H1: RSCAD draft model of the 10-bus multi-machine equivalent system

APPENDIX H2: RSCAD Runtime Module for the 10-bus Multi-machine Test System

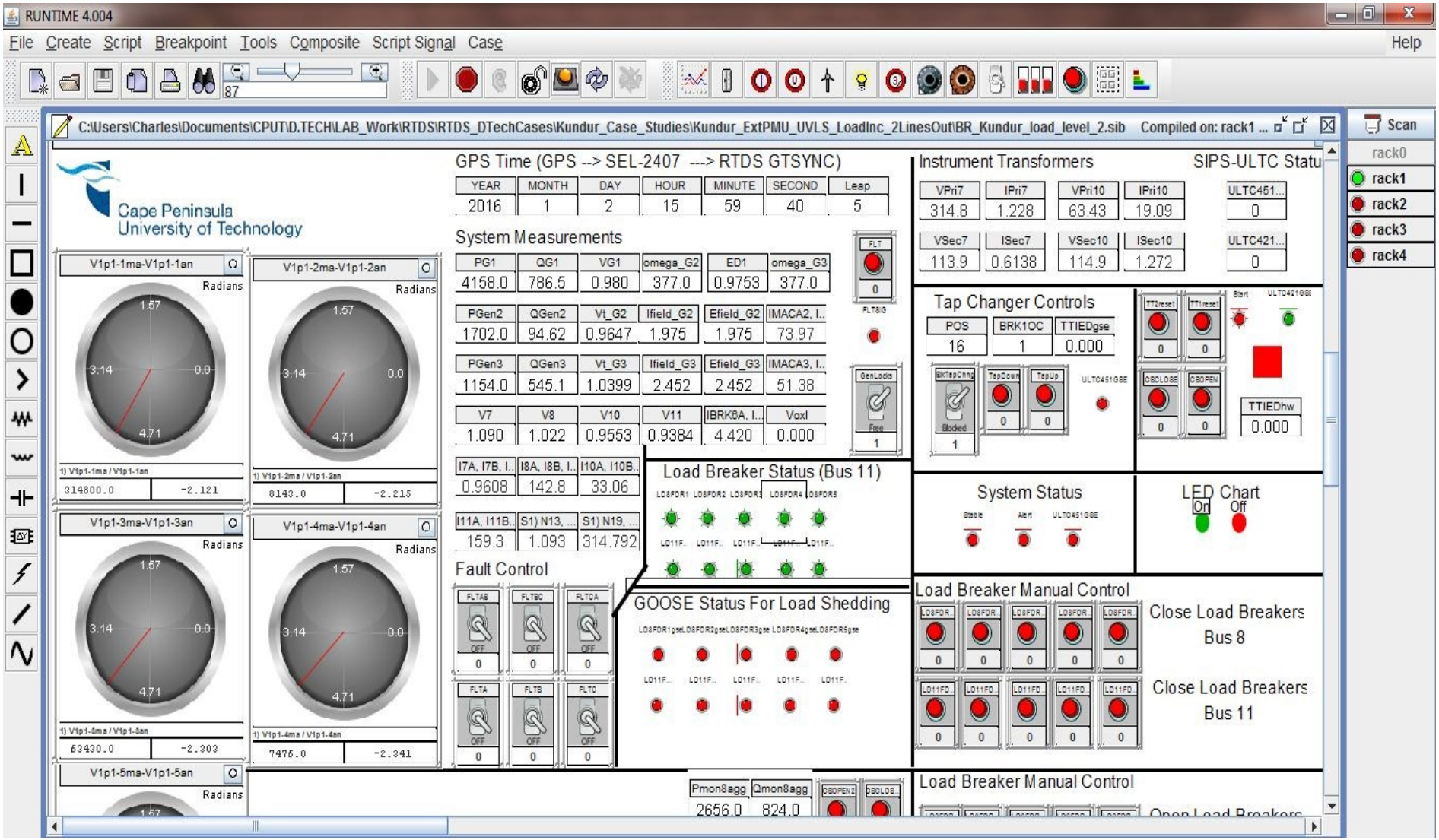

Figure H2: RSCAD Runtime designed for the 10-bus multi-machine equivalent system

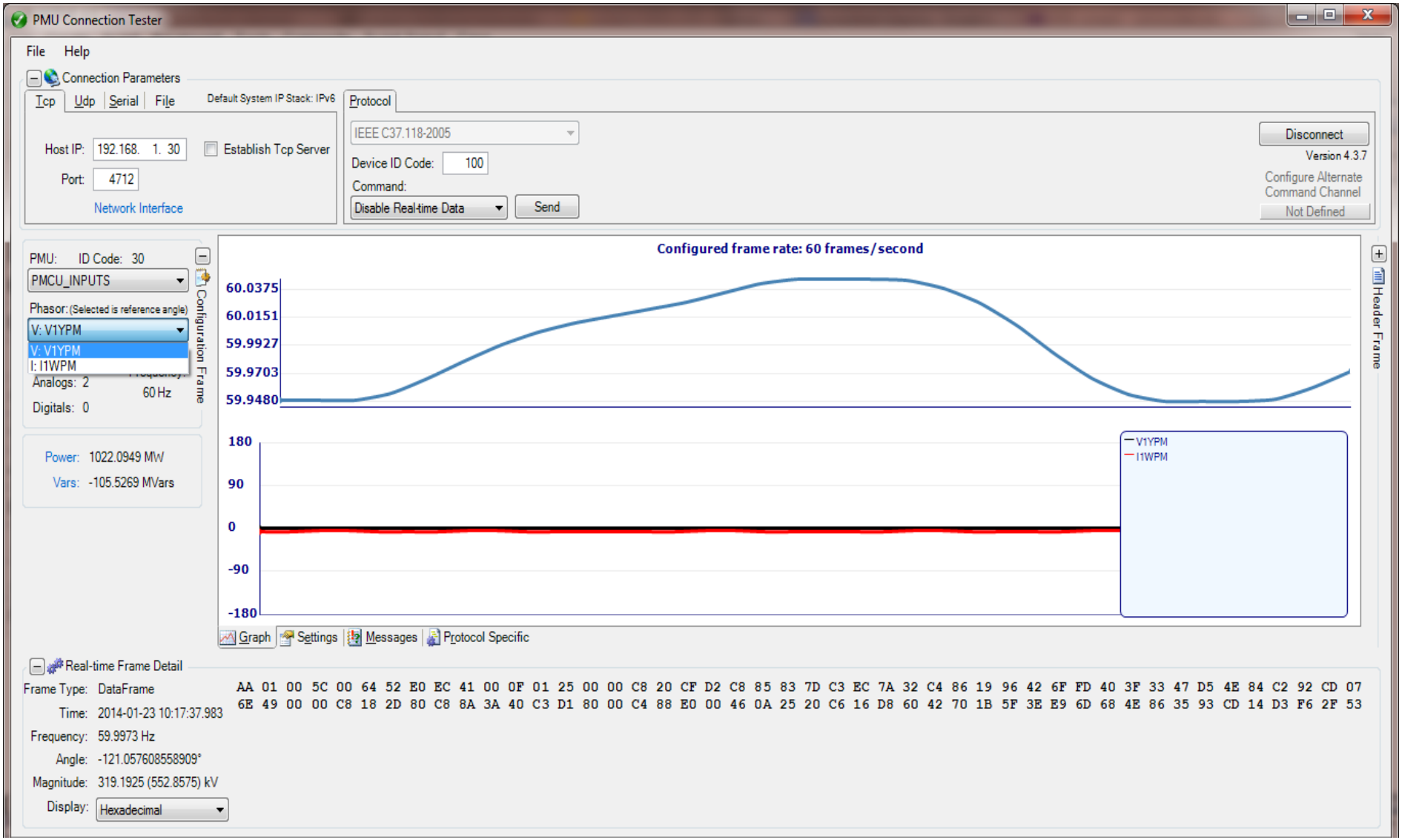

Figure I1: SEL-451 connection testing using the PMU Connection Tester

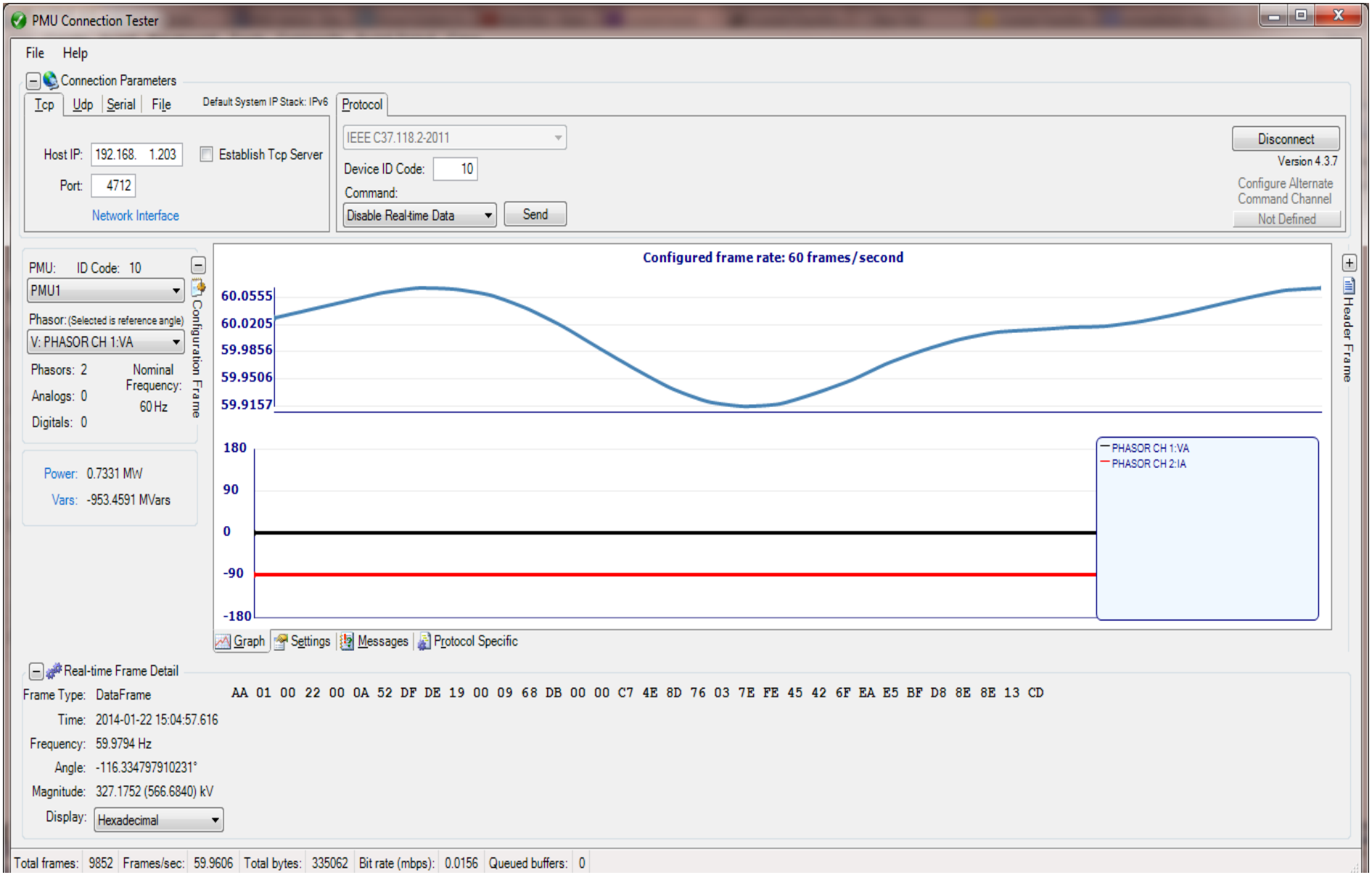

Figure I2: GTNET-PMU connection testing using the PMU Connection Tester

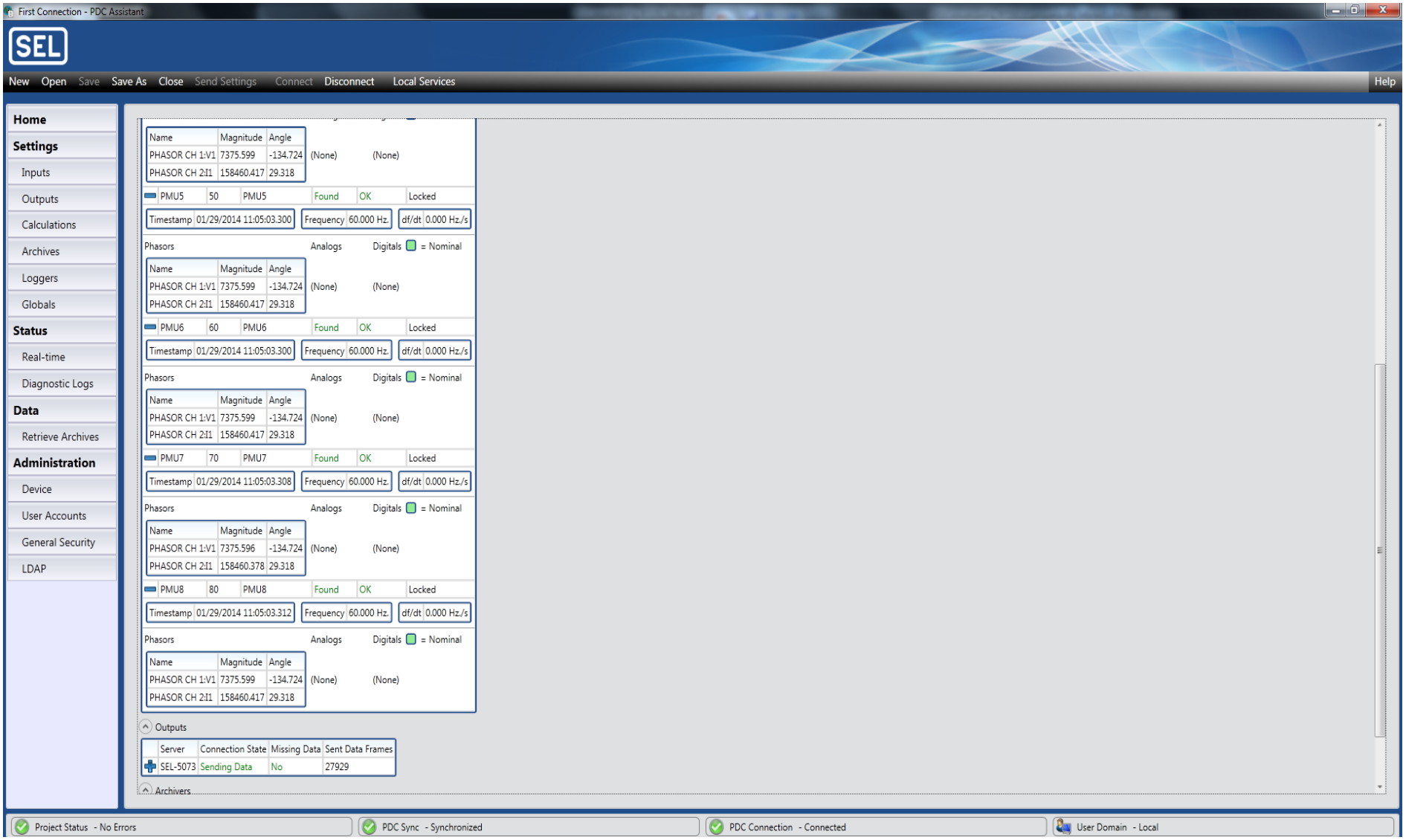

Figure I3: PMU measurements received by the PDC and displayed in real-time mode

APPENDIX J: Graphical User Interface (GUI) for the Measurement-Based Clustering Algorithm for RVSA

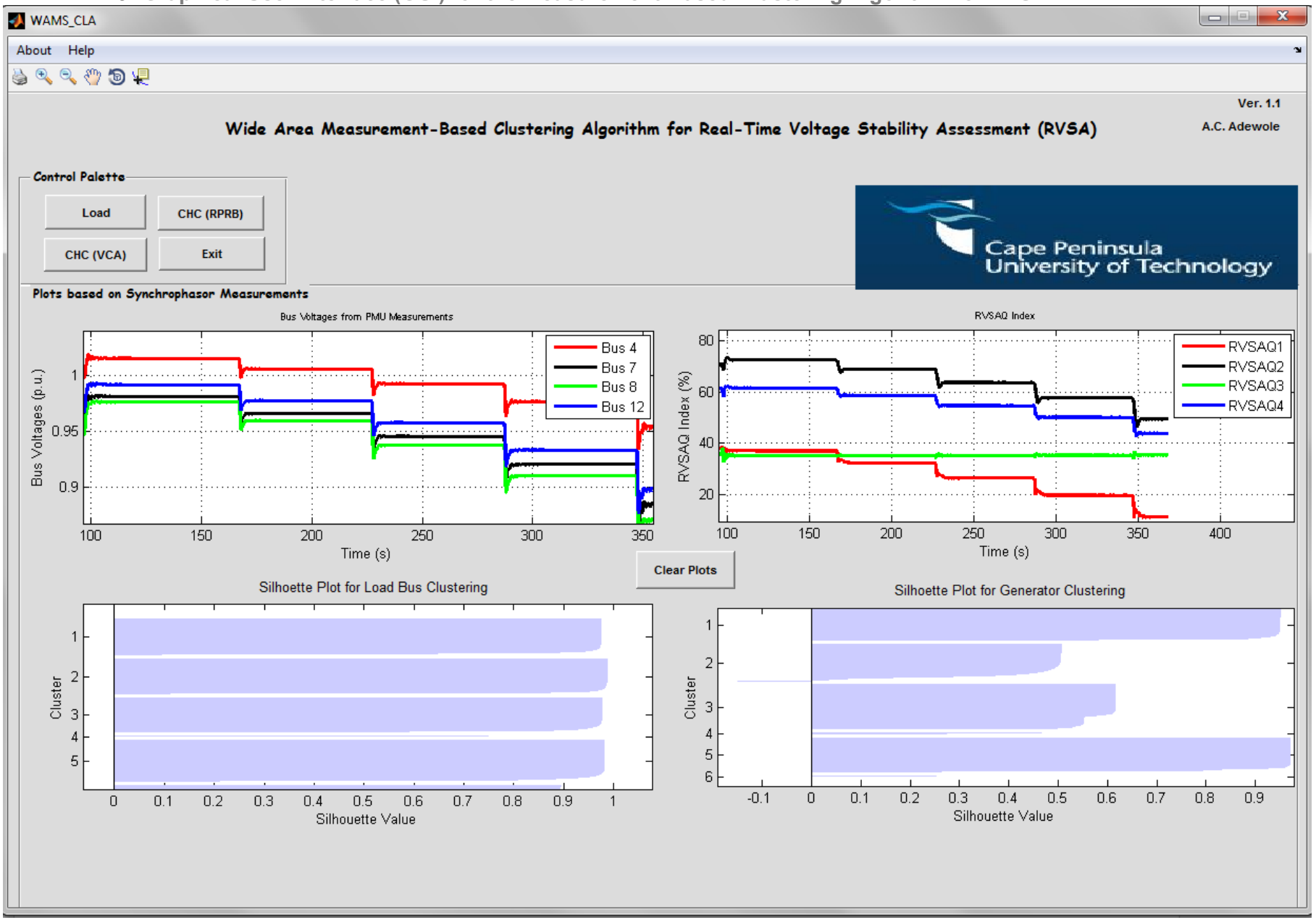

Figure J: Designed Graphical User Interface (GUI) for measurements-based clustering algorithm for RVSA